İZMİR KÂTİP ÇELEBİ ÜNİVERSİTESİ
2010
GRADUATE SCHOOL OF NATURAL AND APPLIED SCIENCES

Determination and Modeling of Shear Strength Behavior of Soil – Geosynthetic Interface

Submitted to the Graduate School of Natural and Applied Sciences
in partial fulfillment of the requirements for the degree of

Doctor of Philosophy

in Civil Engineering

by
İnci ERTAM

ORCID 0000-0001-6594-8095

June, 2023

This is to certify that we have read the thesis **Determination and Modeling of Shear Strength Behavior of Soil – Geosynthetic Interface** submitted by **İnci Ertam**, and it has been judged to be successful, in scope and in quality, at the defense exam and accepted by our jury as a DOCTORAL THESIS.

APPROVED BY:

Advisor: **Assoc. Prof. Dr. Hasan Fırat Pulat**
İzmir Kâtip Çelebi University

Committee Members:

Prof. Dr. Yeliz Yükselen Aksoy
Dokuz Eylül University

Prof. Dr. Ali Hakan Ören
Dokuz Eylül University

Assoc. Prof. Dr. Mehmet Rıfat Kahyaoğlu
Muğla Sıtkı Koçman University

Assoc. Prof. Dr. Tuğba Eskişar Tefçi
Ege University

Date of Defense: 22.06.2023

Declaration of Authorship

I, **İnci Ertam**, declare that this thesis titled **Determination and Modeling of Shear Strength Behavior of Soil – Geosynthetic Interface** and the work presented in it are my own. I confirm that:

- This work was done wholly or mainly while in candidature for the Doctoral degree at this university.
- Where any part of this thesis has previously been submitted for a degree or any other qualification at this university or any other institution, this has been clearly stated.
- Where I have consulted the published work of others, this is always clearly attributed.
- Where I have quoted from the work of others, the source is always given. This thesis is entirely my own work, with the exception of such quotations.
- I have acknowledged all major sources of assistance.
- Where the thesis is based on work done by myself jointly with others, I have made clear exactly what was done by others and what I have contributed myself.

Date: 22.06.2023

Determination and Modeling of Shear Strength Behavior of Soil – Geosynthetic Interface

Abstract

In this study, engineering parameters affecting the interfaces between different soils and geomembrane (GM) were examined under various conditions such as curing liquid, curing time, and normal stress level. Besides, in designs where multiple geosynthetics (GSs) are used together, such as landfill sites, potential shearing surfaces may occur in interfaces formed between GSs. For this reason, the study aimed to investigate the interface behaviors between GMs and geotextiles (GTXs). In the first stage, the engineering parameters of the GSs and soils to be used were determined by laboratory experiments. In the second stage, medium-scale direct shear experiments were carried out to determine the shear strength parameters of soils. In the third stage, the shearing behavior of soil samples with GM interfaces was examined under changing conditions. Most of the variables in here were related to the geotechnical properties of the soils and the physico-chemical properties of the GMs such as tensile strength, elongation at break, static puncture resistance, yield strength etc., and these variables included the effect of parameters not studied in the literature. These parameters were morphological properties, grain size, and normal stress levels. HDPE, LDPE, PVC, and TPO with different chemical properties are GMs that are commonly used in our country and their thicknesses were examined in experiments. To reflect the actual field conditions, tap water, salt water at 0.5 molarities, and synthetic waste leachate (acidic mine drainage leachate, coal combustion product leachate, municipal solid waste leachate) were used as pore liquid. GMs were kept in different pore liquids in the curing pool for 4, 8, and 16 months, and their aging effects were examined. In the fourth stage, interfaces between different GMs and geotextiles were created and the shear behavior of the surface was examined. The surface deformations and roughness of the geosynthetics used in the experiments were examined by Scanning Electron Microscope (SEM) and Optical Profilometer (OPM) analyses. So, the effect of soil properties, pore liquids, aging, and normal stress on the geosynthetic surface could be investigated. The experiments carried out in the last stage were modeled with a finite element software (Plaxis 2D) and the results were compared. As a result of the experiments, all interface friction angles were lower in terms of internal friction angle. The interface friction angle of more angular and coarser grain soils was higher. The interface friction angles decreased as the curing time increased for all curing liquids. The most damaging leachate of GMs to the interface friction angle was acidic mine drainage, while the minimal damage was the coal combustion product. The results of Plaxis 2D, OPM, and SEM analysis were compatible with the interface direct shear test results and the results from the experiments were supported by these analyzes.

Keywords: Geomembrane, geosynthetic, geotextile, interface shear strength, leachate curing

Zemin – Geosentetik Arayüzey Kayma Dayanımı Davranışının Belirlenmesi ve Modellenmesi

Öz

Bu çalışmada, farklı zeminler ve geomembranlar (GM) arasındaki arayüzleri etkileyen mühendislik parametreleri, kür sıvısı, kür süresi ve normal gerilme sınıfı gibi çeşitli koşullar altında incelenmiştir. Ayrıca depolama sahaları gibi birden çok geosentetiğin (GS) bir arada kullanıldığı tasarımlarda, GS'ler arasında oluşan arayüzeylerde de potansiyel kayma yüzeyleri oluşabilir. Bu nedenle, bu çalışmada aynı zamanda GM ve geotekstiller arasındaki arayüzeyler de araştırılmıştır. İlk aşamada, GS'lerin ve zeminlerin mühendislik parametreleri laboratuvar deneyleri ile belirlenmiştir. İkinci aşamada, zeminlerin kayma dayanımı parametrelerini belirlemek amacıyla orta ölçekli direkt kesme deneyleri gerçekleştirilmiştir. Üçüncü aşamada, değişen koşullar altında, zeminlerin GM'ler ile oluşturdukları arayüzeylerin kayma davranışı incelenmiştir. Buradaki değişkenlerin çoğu, zeminlerin geoteknik özellikleri ve GM'lerin fiziko-kimyasal özellikleri ile ilgilidir ve literatürde çalışılmayan parametreleri içerir. Bu parametreler morfolojik özellikler, dane boyu ve normal gerilme sınıfıdır. Farklı kimyasal özellikteki HDPE, LDPE, PVC ve TPO ülkemizde en çok kullanılan GM türleridir ve bu çalışmada aynı zaman kalınlıkları da incelenmiştir. Gerçek saha koşullarını yansıtabilmek amacıyla, direkt kesme deneylerinde boşluk suyu olarak çeşme suyu, 0.5 molaritede tuzlu ve laboratuvarda sentetik olarak hazırlanmış atık sızıntı sıvıları (asidik maden drenajı sızıntısı, kömür yanma ürünü sızıntısı, kentsel katı atık sızıntısı) kullanılmıştır.

GM’ler bu boşluk sıvıları içerisinde 4, 8 ve 16 ay bekletilmiş, böylece yaşlandırma etkisi incelenmiştir. Dördüncü aşamada GM – geotekstil arayüzeyleri oluşturulmuş ve kayma davranışları incelenmiştir. Geosentetiklerin yüzeyinde oluşan deformasyonlar ve pürüzlülükleri Taramalı Elektron Mikroskopu (SEM) ve Optik Profilometre (OPM) analizleri ile incelenmiştir. Böylece, GS arayüzeyleri üzerinde zemin özelliklerinin, boşluk sıvısının, yıllandırmanın ve normal gerilmenin etkileri belirlenmiştir. Son aşamada, deneyler, bir bilgisayar yazılımı olan Plaxis 2D ile modellenmiş ve elde edilen sonuçlar karşılaştırılmıştır. Deneylerin sonucunda, tüm arayüz sürtünme açılarının içsel sürtünme açılarında daha düşük olduğu tespit edilmiştir. Köşeli ve iri daneli zeminlerin arayüzey sürtünme açıları daha yüksek elde edilmiştir. Tüm kür sıvıları için kür süresi arttıkça arayüzey sürtünme açıları azalmıştır. GM'lerin arayüzey sürtünme açılarına en çok zarar veren sızıntı sıvısı asidik maden drenajı iken minimum hasar yaratan ise kömür yanma ürünüdür. Plaxis 2D, OPM ve SEM analizlerinin sonuçları arayüzey direkt kesme deneyleri sonuçları ile uyumludur ve deneylerden elde edilen sonuçlar bu analizlerle desteklenmiştir.

Anahtar Kelimeler: Arayüzey kayma dayanımın, geomembran, geosentetik, geotekstil, sızıntı sıvısı kürü

To my family,

Acknowledgment

I would like to thank my advisor Assoc. Prof. Dr. Hasan Fırat PULAT, who endlessly helped me on any issue from the very beginning of my thesis and my six year doctoral degree with his extensive knowledge and experience. I would like to thank Prof. Dr. Yeliz YÜKSELEN AKSOY and Prof. Dr. Ali Hakan ÖREN for their great support in the thesis monitoring committee.

I would like to thank my mother, Fatma DEVELİOĞLU, my father, Caner DEVELİOĞLU, my sister, İrem DEVELİOĞU, and my husband Yalım ERTAM, without their continuous support and encouragement I never would have been able to achieve my goals. Thanks for always being there for me, believing in me, and motivating me to set out on my own path.

I would like to thank my great friends for motivational contributions for this thesis project.

Lastly, we gratefully thank the companies of Geoplas Plastik Zemin Teknikleri ve Kimya San.Tic.Ltd.Şti., BTM Company, and Totomak Makina ve Yedek Parça Sanayi ve Ticaret A.Ş.

This thesis study was funded by Scientific Research Projects Coordination Unit of Izmir Katip Celebi University. Project number: 2020-TDR-FEBE-0006. This work was also supported by the TUBITAK 2211-A education scholarship program.

Table of Contents

List of Figures

List of Tables

List of Abbreviations

AMD	Acidic mine drainage
ASTM	American Society for Testing and Materials
CCP	Coal combustion product
CCR	Coal combustion residue
CCW	Coal combustion waste
CG	Crushed gravel
Co-GMX	Coextruded textured geomembrane
CS	Crushed sand
EC	Electrical conductivity
EPDM	Ethylene propylene diene monomer
EPRI	Electric Power Research Institute
FGD	Flue gas desulfurization
FPO	Flexible polyolefin
FS	Factor of safety
GCL	Geosynthetic clay liner
GM	Geomembrane
GS	Geosynthetic
GTX	Geotextile
HDPE	High density polyethylene
HDPE(S)	Smooth high density polyethylene geomembrane
HDPE(T)	Textured high density polyethylene geomembrane
IEA	International Energy Agency

Imp-GMX	Impingement textured geomembrane
Lam-GMX	Laminated textured geomembrane
LC	Low plasticity clay
LDPE	Low density polyethylene
LLDPE	Linear low density polyethylene
M	Molar
MC	Mohr-Coulomb
MSW	Municipal solid waste
OIT	Oxidative induction time
OPM	Optical profilometer
PE	Polyethylene
PET	Polyethylene terephthalate
PVC	Polyvinyl chloride
PVC(1.5)	1.5 mm polyvinyl chloride
PVC(3.0)	3.0 mm polyvinyl chloride
PVC(S)	Smooth polyvinyl chloride
PVC(T)	Textured polyvinyl chloride
RG	River gravel
RPP	Reinforced polypropylene
RS	River sand
SB	Sand/bentonite mixture
SEM	Scanning electron microscope
SWt	Salt water
TPO	Thermoplastic polyolefin
TRP	Reinforced polyethylene
USA	United States of America
USCS	Unified Soil Classification System

UV	Ultraviolet
VLDPE	Very low density polyethylene

List of Symbols

%	Percent
C_c	Coefficient of curvature
C_E	Curing effect
C_u	Coefficient of uniformity
E	Efficiency ratio
EA	Axial stiffness
e_{max}	Maximum void ratio
e_{min}	Minimum void ratio
G_s	Specific gravity of solid
G_w	Specific gravity of water
LL	Liquid limit
N	Normal force
PL	Plastic limit
R_a	Average roughness
R_{int}	Interface coefficient
R_{max}	Maximum roughness
w_{opt}	Optimum water content
W_s	Weight of dry soil
α	Adhesion
$\gamma_{dry,max}$	Maximum dry unit weight
δ	Interface friction angle
ε	Axial strain

μ	Friction coefficient
σ	Normal stress
τ	Shear stress
ϕ	Internal friction angle

Chapter 1

Introduction

Geosynthetics (GSs) are artificial synthetic materials in the form of sheets, strips, or three-dimensional structures made of natural or polymeric materials. They are easy to prepare and transport, and they help green construction projects. The use of GSs in civil engineering applications has been steadily increasing in recent years [1–5]. When used in construction, they serve five critical functions: separation, reinforcement, filtration, drainage, and containment [6]. GSs are divided into nine categories: Geotextile, Geonet, Geogrid, Geomembrane, Geocell, Geosynthetic Clay Liner, Geocomposite, Geopipes, and Geofoam [7]. Some geosynthetics can serve multiple functions simultaneously.

According to ASTM D4439, a geomembrane (GM) can be defined as "*A very low permeability synthetic membrane liner or barrier used with any geotechnical engineering related material to control fluid or gas migration in a human-made project, structure, or system*" [8]. GMs are used to ensure impermeability for many engineering branches such as geotechnical, hydraulic, environment, and transportation, which provide advantages in terms of operating speed, ease of access, and economy [9–12]. There are many different types of GMs according to the production method and polymer type. Some of these are high density polyethylene (HDPE), linear low density polyethylene (LLDPE), polyvinyl chloride (PVC), ethylene propylene diene monomer (EPDM), reinforced polypropylene (RPP), reinforced polyethylene (TRP), and thermoplastic polyolefin (TPO). The types of GMs used in this thesis are PVC, HDPE, and TPO. The reason for choosing these GM types is that PVC and HDPE are some of the most used GM types in the world. In Figure 1.1, the total number of GM types used in 237 dams in different parts of the world are shown [13]. The reason why TPO is preferred is that it is more environmentally friendly during its production than other GM types, although not much information is known about the new ones.

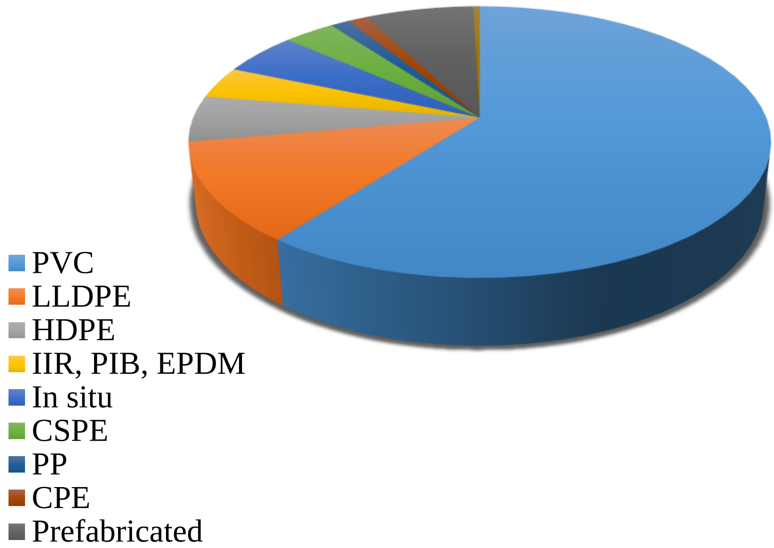

Figure 1.1: Type of geomembranes used in dam projects worldwide [13]

Polyvinyl chloride (PVC) GMs are used for bundling in the foundation base and insulation on roofs. High density polyethylene (HDPE) GMs are used for sealing in projects such as mine waste landfills, tank fields, municipal solid waste landfills, acid tanks, ponds, and irrigation canals. Thermoplastic polyolefin (TPO) GMs are synthetic waterproofing membrane reinforced with fiberglass felt, used in basic bundling, green roof, metal roof, and inverted roof insulation, which is resistant to atmospheric conditions and UV rays, does not age or harden over time. It is also called FPO (flexible polyolefin) in the literature. Since it does not contain PVC or plasticizer in its content, it does not emit harmful substances into the environment, so it is a very environmentally friendly product.

According to ASTM D4439, a geotextile (GTX) can be defined as "*A permeable GS comprised solely of textiles. GTXs are used with foundation, soil, rock, earth, or any other geotechnical engineering-related material as an integral part of human-made project, structure, or system*" [8]. GTXs are fabrics used in geotechnical applications such as road and rail embankments, earthen embankments, and coastal protection structures, designed to perform one or more essential functions such as filtration, drainage, separation of soil layers, reinforcement, or stabilization [14]. GTX fabrics come in three basic forms: non-woven GTXs, woven GTXs (needle punched), or heat bonded GTXs (structural woven). The type of GTX used in this study is nonwoven GTX. Nonwoven GTXs are permeable GSs made of nonwoven materials used with soil, rock, or other geotechnical-related material as an integral part of a civil engineering project, structure, or system [15].

The utilization of GTX and GM coatings in engineering structures serves as a robust shield against leakage and environmental elements, although the interaction with the soil may create a potential surface for shearing. Aside from the potential shearing plane, other drawbacks include the possibility of tears or ruptures occurring on the GM surfaces when subjected to high vertical stresses. To safeguard the GM surfaces from damage, they are covered with a different type of GS called GTX. Consequently, in addition to the soil – GM interface, new shear planes emerge between GM – GTX and soil – GTX. Therefore, while the proper application of GSs offers numerous advantages, neglecting the aforementioned factors can lead to adverse situations. To address these issues and ensure safe designs during the design phase, it is essential to have a thorough understanding of the shearing behavior at the interfaces of GS – soil and GS – GS.

1.1 Aim and Scope

The aim of this study is to examine the interface shear behavior between soils and GSs. In this context, six different soil types, three different GM types, and one GTX (nonwoven) type were used. The soil types are low plasticity clay (LC), sand/bentonite mixture (SB), crushed sand (CS), river sand (RS), crushed gravel (CG), and river gravel (RG). The GM types are polyvinyl chloride (PVC), high density polyethylene (HDPE), and thermoplastic polyolefin (TPO). Two different thicknesses of PVC, 1.5 and 3.0 mm, were used. HDPE with two different surface roughnesses, textured and smooth, was used. Interface friction parameters were determined by direct shear test under low, medium, and high normal stress levels. All these parameters reflect the aims of the thesis. These aims are used to investigate the effect of soil particle size, soil particle shape, GS type, GM roughness, GM thickness, and normal stress on the interface friction behavior.

In addition, the shear strength behavior between different GMs and non-woven GTXs and normal stress level effect was also investigated.

Another aim of the thesis is to investigate the interface friction behavior of GMs aged in certain liquids. For this purpose, for GMs used in areas close to the coastline, GMs were immersed in 0.5M salt water for 4, 8, and 16 months and then interface direct shear tests were performed. Also, GMs were kept in synthetically prepared acidic mine drainage for 4, 8, and 16 months in order to revive the mining exploration facilities or the storage facilities where metal wastes are collected. Likewise, GMs were cured for 4, 8, and 16 months in synthetically prepared coal combustion product leachate to revive the facilities where coal wastes are stored, and in the synthetically prepared municipal solid waste leachate to revive the municipal solid waste storage facilities.

Chapter 2

Previous Studies

There are some studies in the literature on the shear strength behavior of the interfaces formed between different GM types and different soils. In the literature, it has been observed that the number of studies on the shearing behavior of the interfaces between many different GMs and different soil types in this study is quite limited. In addition, there are no studies in which GMs are cured in salt water and leachates and then subjected to interface direct shear tests. The former studies are summarized in detail.

2.1 Effect of soil type on interface shear behavior of soil – geosynthetic

Numerous studies in the literature focus on investigating the impact of soil type on the shear strength behavior of the soil – GS interface. Fleming et al. (2006) conducted research on the interface shear behavior between soil and GM, specifically using smooth GM and unsaturated soil. The GM utilized was HDPE with a thickness of 1.5 mm. They employed three different soil types: Ottawa sand, Ottawa sand/bentonite mixture, and silty sand. To measure shear behavior, a modified direct shear test apparatus was used, with a miniature pore pressure transducer placed within the shear box. This allowed for the measurement of excess pore water pressure, and the results were interpreted in terms of both total and effective stresses. The test results revealed that the internal friction angles of Ottawa sand and silty sand were 35.5^{o} and 31.8^{o}, respectively. Lower interface friction angles were observed with higher water content during placement, while higher interface friction angles were obtained at higher dry densities during placement. Under saturated conditions, the interface friction angles for silty sand and sand/bentonite mixture were 14.1º and 21.0º for total stress, and 13.8º and 21.2º for effective stress. Under unsaturated conditions, the interface friction angles for silty sand and sand/bentonite mixture were 21.4º and 19.8º for total stress, and 23.6º and 21.5º for effective stress. The authors explained the decrease in friction angle by citing slide and scratch at low normal stress, as well as plowing at high normal stress [11]. Vangla and Gali (2016) investigated the influence of particle size and morphology on the interface shear behavior between soil and GM. They used three sandy soils with different particle sizes (fine, medium, coarse) but the same morphology to examine the particle size effect. Additionally, two sands with the same size but different morphologies (coarse sand, angular coarse angular sand) were used to determine the morphology effect. All soils were classified as poorly graded sand. The study also explored the influence of normal stress on the interface shear behavior. A smooth HDPE GM with a thickness of 1.5 mm was employed, and the experiments were conducted using a large-scale direct shear test apparatus with dimensions of 300x300x85 mm. The soil samples were prepared in a zero moisture state and at 70% relative density. The GM surface roughness was measured using a 3D optical profilometer, while the sand morphologies were analyzed through image analysis. The study concluded that the peak friction coefficient decreases as the normal stress increases until reaching a critical normal stress, which was determined to be approximately 53 kPa. Surface changes intensified gradually from a normal stress of 22 kPa to the critical normal stress of 53 kPa. Beyond this point, the normal stress was high enough to cause damage to the GM surface. The internal friction angles of the fine, medium, coarse, and angular coarse soils were measured at 40.4º, 40.7º, 40.8º, and 36.5º, respectively, while the interface friction angles were observed at 22º, 22.2º, 18.7º, and 27.1º, respectively. The coarse-grained sand exhibited the most negative effect, and it was determined that angularity had a positive impact on the interface friction angle [16].

2.2 Effect of geosynthetic type on interface shear behavior of soil – geosynthetic

In addition to the effect of the soil type on the interface shear strength behavior, studies investigating the effect of the GS type also exist in the literature. Feng and

Cheng (2014) conducted a series of laboratory experiments that were performed to obtain the interface shear strength between soil – GM and GM – GTX. These experiments were repeated more than once under various normal stresses. Nonwoven GTX with a mass per unit area of 400 g/m^2 and 1.5 mm thick textured HDPE GM was used. The soil used in this study was classified as silty clay with silty sand. The shear strength experiments were conducted with a large-scale direct shear apparatus whose dimensions are 400x600 mm and the shear rate was 1 mm/min. For GM – GTX interface experiments, three samples were tested three times under constant normal stress of 50, 100, and 200 kPa to determine the reduction of shear strength of the interface. One sample was tested under increasing normal stress with the order of 50, 100, and 200 kPa. For GM – soil interface experiments, five specimens were examined three times under constant normal stress of 20, 50, 100, 200, and 300 kPa. One sample was sheared three times at increasing normal stress from 50 to 100 and 200 kPa. The GM – GTX interface friction angle values were obtained 19.8º, 18.07º, and 17.45º for the 1st, the 2nd, and 3rd repeat, respectively. Generally, interface contacts reach maximum shear strength at a higher strain when they were sheared for the first time. The maximum shear strength was reached at a much smaller strain for the second and third time shearing tests. The GM – soil interface friction angle values were obtained 10.67º, 9.07º, and 9.00º for the 1st, 2nd, and 3rd repeat, respectively [17]. Also, the researchers investigated the effect of both GS type and thickness on the interface shear behavior. Chai and Saito (2016) investigated the interface shear strength parameters of clayey soil – GM using a large-scale direct shear test device. Bentonite and quartz powder were mixed with a clayey soil of 3/10. Three different types of GMs were used: polyethylene (PE), PVC, and HDPE. The dimension of the upper part of the large-scale direct shear device was 200x450x100 mm and the lower part was 200x200x70 mm. In the experiments, 50, 80, and 100 kPa normal stresses were applied. The test results showed that maximum adhesion value was obtained between a clayey mixture and PVC. The interface friction angles between bentonite and GMs were quite small (3 - 4º). For all specimens, the interface shear strength was achieved to approximately 55% smaller than the own shear strength of the soil [18]. Effendi (2011) presented the interface shear strength of various GMs and Ottawa sand. Smooth HDPE, smooth very LDPE, and PVC GMs were used. Their thicknesses were 2.03, 1.52, and 1.52 mm, respectively. The interface shear behavior was determined with the ring shear test.

The shear rate was 2.4 mm/min and the normal stresses changed between 50 kPa and 200 kPa. At the end of the tests, it was obtained that the efficiency ratio (E) was equal to $\tan\delta/\tan\phi$. The very stiff and smooth surface of the HDPE showed the lowest interface friction changing from 34 to 45% (E = 0.34 to 0.45) of the internal friction angle of the Ottawa sand ($\phi_{average}$ = 28.8°). A higher interface friction angle between 44 to 59% of that of the Ottawa sand was mobilized in the tests with the relatively softer surface VLDPE. For PVC, which was the softest material used in this study, the interface friction angle of 70 to 97% of the Ottawa sand at normal stress from 50 kPa to 223 kPa. In conclusion, the interface strength of these smooth GMs was found to be dependent on normal stress levels: the PVC was most dependent, and the smooth HDPE was the least dependent [19]. Stark and Santoyo (2017) investigated the interface shear strength behavior between ten GMs and two soils. Seven GMs are smooth, three are textured and their thickness varies between 0.75 and 1.5 mm. The types of GMs used are PVC, HDPE, LLDPE, coated woven polyethylene, and TPO. The types of soil used were clayey glacial till and Ottawa fine sand. The interface shear strength parameters were measured with a torsional ring shear apparatus and the shear rate was 0.015 mm/min. The results of the experimental study showed that textured GMs have a larger interface friction angle than smooth GMs. According to clayey glacial till soil tests, the maximum interface friction angle (46°) was obtained tenth GM (textured, 1.5 mm, HDPE). The minimum interface friction angle (14°) was obtained ninth GM (smooth, 1.5 mm, HDPE). According to the test on the Ottawa sand soil, the maximum interface friction angle (31°) was obtained tenth GM (textured, 1.5 mm, HDPE). The minimum interface friction angle (15°) was obtained second GM (smooth, 1.5 mm, LLDPE). Also, the glacial till – GM interfaces exhibited higher interface friction angles than the Ottawa Sand – GM interfaces [20].

2.3 Effect of both geosynthetic and soil type on interface shear behavior of soil – geosynthetic

When examining studies that investigate the combined effects of GS and soil type, Frost et al. (2012) explored the influence of soil angularity, GM surface roughness, and normal stress on the behavior of interface shear strength. The researchers conducted direct shear tests in multiple series. The first series involved testing rounded sand with three different levels of GM roughness under a normal stress of 100 kPa. The second series included testing angular sand with two different GM roughness levels under the same normal stress. Two additional series were carried out using rounded and angular sands under a normal stress of 300 kPa to study the effects of normal stress. The experiments utilized a modified direct shear test device with dimensions of 100x100x38 mm, and the shear rate was set at 0.25 mm/min. The soil specimens were placed into the shear box using the pluviated method with a relative density of 80%. The findings revealed that the displacement required for rough GM (1.5 mm) to reach the peak state was greater than that for smooth GM (0.3 mm). Additionally, the peak and residual interface friction angles exhibited significant increases with changes in roughness until reaching a critical roughness value (approximately 1.35), after which they remained constant. The interface friction angle increased as roughness increased. Normal stress did not have an impact, and angularity had a positive effect on the interface friction angle [21]. Punetha et al. (2017) aimed to comprehend the shearing mechanism at the soil – GS interface and investigate the effects of various parameters on interface behavior. They utilized two types of GS: smooth HDPE GM and nonwoven GTX. Two sands with different grain size distributions were employed as the soil. The parameters of the sand, including degree of saturation, mean particle size, relative density, as well as testing conditions such as shearing rate and normal stress, were examined. The experiments were conducted using a large-scale direct shear apparatus with dimensions of 300x300x300 mm. To interpret the test results, the authors determined the coefficient of friction (μ), which represents the ratio of shear strength to normal stress (τ/N). According to the test results, the coefficient of friction decreased as the normal stress increased for both GM and GTX. However, after reaching a specific value of normal stress (100 kPa), the coefficient of friction remained relatively constant. Three different degrees of saturation (0, 50, 100%) were considered to assess the saturation effect, and it was observed that the coefficient of friction decreased with increasing degree of saturation. The mean particle size (0.21 mm, 0.44 mm) was found to have a minimal effect on the coefficient of friction. As the relative density (40, 60, 80%) increased, the coefficient of friction also increased. Finally, the coefficient of friction decreased as the shearing rate increased (0.314 mm/min, 0.502 mm/min, 2.54 mm/min) [3].

2.4 Effect of other parameters on interface shear behavior of soil – geosynthetic

With the increasing use of GSs in many fields, studies examining the different parameters affecting the interface shear strength have also increased. Studies are investigating the effects of many parameters such as water content, aging, and different interface on the interface shear strength behavior. Vaid and Rinne (1995) examined the effect of the soil angularity and GM surface texture on the interface shear strength of the soil – GM. The medium quartz sand with rounded and angular grains was used as a soil specimen to investigate the angularity effect. The PVC, smooth, and rough HDPE were used to determine the texture effect. Their surface roughness (R_a) was 1.3, 1.1, and 2.3 μm, respectively. The interface friction angles were obtained with the ring shear test apparatus and the shear rate ranged between 5 and 8.3 mm/min. The soil specimen was placed in the box pluviated method, and the relative density was obtained from 30 to 35%. The interface friction angle of PVC and rough HDPE were very close to each other for rounded sand. The interface friction angle of the smooth HDPE was quite low compared to the others. The same was true for the angular sand sample, but this time the interface friction angle of the smooth HDPE was closer to the others [10]. Stark et al. (1996) analyzed the interface shear behavior of GM – GTX, and GM – geocomposite. Six different GMs were used: Coextruded textured GM (Co-GMX, Co-GMX1, Co-GMX2), laminated textured GM (Lam-GMX), impingement textured GM (Imp-GMX), smooth GM (GM). All these GMs had a thickness of 1.5 mm. A drainage geocomposite created by placing the HDPE between the heat bond and the two nonwoven GTXs was used. Five types of GTXs were used: 540 g/m^2 polypropylene staple filament (GT1), 540 g/m^2 polyester single filament (GT2), 270 g/m^2 polypropylene single filament (GT3), 540 g/m^2 polypropylene single filament (GT4), 540 g/m^2 polypropylene staple filament calendered (GT5). Torsional ring shear tests with a shear rate of 0.37 mm/min were conducted. The test results showed that textured HDPE GMs afford an increase in interface shear strength over smooth HDPE GMs. Nonwoven GTX – textured HDPE interface failure envelopes could be nonlinear. The nonwoven GTX – textured HDPE interface shear resistance showed to be independent of fiber type, mass per unit area, and fabric style. A nonwoven GTX mass per unit area of 270 g/m^2 showed to result in higher peak interface strengths than a 540 g/m^2 GTX at normal stresses greater than 100 kPa. If the texturing is not damaged from the laminated product, laminated, and coextruded textured GMs exhibit similar peak interface shear strength. Nonwoven GTX or drainage geocomposite – textured HDPE interfaces demonstrated a post-peak strength loss of 50 – 60% (22). Islam and Rowe (2007) predicted the antioxidant depletion time of GMs. Three HDPE GMs of 1.5, 2.0, and 2.5 mm thickness were used. GMs were aged in synthetic leachate at different temperatures (22, 55, 70, 85ºC) conditions. The antioxidant depletion time was measured with the oxidative induction time (OIT) test. The synthetic leachate was constituted by mixing surfactant, trace metals, and reducing agents in distilled water and was changed every two weeks. The test results showed that the predicted antioxidant depletion times of 1.5 mm GM were 47, 9.5, and 2.3 years for 20, 40, and 60ºC, respectively. The predicted antioxidant depletion times of 2.0 mm GM were 62, 13, and 3.1 years for 20, 40, and 60ºC, respectively. The predicted antioxidant depletion times of 2.5 mm GM were 71, 15, and 3.6 years for 20, 40, and 60ºC, respectively. So, the antioxidant depletion time decreased with temperature increasing and thickness decreasing [23]. Eid (2011) investigated the shear strength behavior of the composite liner and cover systems of the municipal solid waste landfill. The composite cover system occurred in textured GM, unreinforced geosynthetic clay liner (GCL), and sand, respectively. The composite liner system occurred in textured GM, reinforced GCL, and silty clay, respectively. The shear strength tests were performed with a torsional ring shear apparatus. The shear rate was 0.015 mm/min. The specimen was prepared at optimum moisture content and maximum dry unit weight. Liner system test results showed that failure occurred along the soil – GCL nonwoven GTX side at normal stresses of 17, 25, 50, and 75 kPa. The shear failure surface moved to the GM – GCL woven GTX side at normal stresses of 100, 150, 200, and 250 kPa. For specimens sheared at a normal stress of 300 kPa or higher, failure occurred through shearing the GCL internally. Their friction angles were obtained 24.5º, 22º, and 13º, respectively. Cover system test results showed that this occurred at the GCL smooth GM backing – sand interface for specimens with bentonite water contents of 11 and 34%. For specimens with higher water contents, the shear surface was located between the textured GM and the hydrated bentonite. Their friction angles were obtained at 26.9º and 16º, respectively [24]. Monteiro et al. (2013) studied the interface shear strength behavior of soil – GM for different types of GMs and degrees of saturation. Three types of GMs of the same thickness (1.0 mm) were used; PVC, smooth HDPE, and textured HDPE. Soil samples were prepared in eight different degree of saturation ranging from 5.5 to 66%. The interface friction angle values were determined with ramp and direct shear tests. The peak interface friction angles ranged from 55 to 65% of the internal friction angle for rounded sand, and from 65 to 90% for the angular sand. The peak interface friction angle was attributable directly to the resistance of the smooth HDPE surface to scouring. Rough HDPE and the much softer, smooth PVC GM both showed interface friction angles equal to the internal friction angle of the contacting sand. The normal stress values in the direct shear test were 25, 55, and 150 kPa. The results of the direct shear and ramp tests were very close. The highest interface friction angles were obtained in textured HDPE, while the lowest interface friction angles were obtained in smooth HDPE. It was also observed that as the degree of saturation increased, the interface friction angle also increased [25]. Cen et al. (2018) investigated the interface shear strength behavior of soil, concrete, and GSs. The interfaces examined in the study were GM – fine sand, GM – sandy gravel, GM – GTX, GM – ordinary concrete, and GM – no fine concrete. The tests were carried out with a large-scale direct shear test device (300x300x180 mm). Two different HDPE GMs, 2 mm thick, rough, and smooth, were used. When the experimental results are compared, it is determined that the interface friction angles of rough GMs for all interfaces are higher than those of smooths. Coarse grained soil has a larger interface friction angle than fine grained soil. Ordinary concrete gave higher results than no fine concrete. The maximum (32.72º) and minimum (11.61º) interface friction angles were obtained at the interface of GM (rough) – sandy gravel and GM (smooth) – GTX, respectively [26].

The soil type, GM thickness and type, test method, normal stress values, and shear rates used in the literature studies mentioned in Sections 2.1, 2.2, 2.3, and 2.4 are summarized in Table 2.1.

Table 2.1: Parameters used in the literature studies

Study	Soil type	GM type	Thickness	Normal stress (kPa)	Shear rate	Test device
Vaid and Rinne, 1995 [10]	Quartz sand (rounded and angular)	PVC, HDPE(S), HDPE(T)	-	-	5.0 mm/min	Torsional ring shear
Stark et al., 1996 [22]	-	HDPE(S), HDPE(T)	1.5mm	100-200-300	0.37 mm/min	Torsional ring shear
Fleming et al., 2006 [11]	Ottawa sand, Sand/bentonite, Silty	HDPE	1. mm	5-12-24-30	0.833 mm/min	Direct shear (100x100mm)
Effendi, 2011 [19]	Ottawa sand	HDPE, PVC, VLDPE	2.03-1.52-1.52mm	25-50-100-150-200-250-300-400	2.4 mm/min	Torsional ring shear
Eid, 2011 [24]	Bentonite	HDPE	1.5mm	17-25-50-75-100-150-200-250-300-350-400	0.015 mm/min	Torsional ring shear
Frost et al., 2012 [21]	Round and angular sand	HDPE(S), HDPE(T)	1.5mm	100-300	0.25 mm/min	Direct shear (100x100mm)
Monteiro et al., 2013 [25]	Sandy soil	PVC, HDPE(S), HDPE(T)	1.0mm	25-55-150	-	Direct shear (100x100mm)
Feng and Cheng, 2014 [17]	Clayey soil	PE, PVC, HDPE(S)	-	-	-	Direct shear (200x200mm)
Chai and Saito, 2016 [18]	Silty clay, silty sand	HDPE(T)	-	50-100-200-300	1.0 mm/min	Direct shear (400x600mm)
Vangla and Gali, 2016 [16]	Angular sand (fine, medium, coarse)	HDPE(S)	1.5mm	22-37-53-68	1.0 mm/min	Direct shear (300x300mm)
Punetha et al., 2017 [3]	River sand	HDPE(S)	1.5mm	50-100-150-200	0.2 mm/min	Direct shear (300x300mm)
Stark and Santoyo, 2017 [20]	Clayey glacial till, Ottawa fine sand	PVC(S), PVC(T), LLDPE, TPO, HDPE	0.75-1.0-1.5mm	17-50-100-200-400	0.015 mm/min	Torsional ring shear
Cen et al., 2018 [26]	Fine sand, sandy gravel	HDPE(S), HDPE(T)	2.0mm	50-100-150-200	1.0 mm/min	Direct shear (360x360mm)

2.5 Aging and surface roughness of geomembranes

Adamska (2019) conducted research to determine the shear strength at the interface between HDPE GMs and fly ash. The experiments utilized a conventional direct shear test device with a cylindrical box. Two HDPE GMs, one with a rough surface and the other with a smooth surface, both measuring 1.5 mm in thickness, were employed. The fly ash was placed into the box at the optimum moisture content and maximum dry unit weight according to the Standard Proctor energy. Additionally, the water content values (w_{opt}±2.5 and w_{opt}±5) were varied to assess the effect of water content on the interface shear strength. The test results revealed that water content had a negligible impact on the interface shear strength for smooth GMs. However, the lowest interface shear strength was observed at the highest water content for rough GMs. Furthermore, it was observed that rough GMs exhibited a larger interface friction angle compared to smooth GMs [27]. Abdelaal et al. (2014) investigated the effect of leachate constituents on the OIT and physical properties of GM. The leachate was obtained by mixing various chemicals in the laboratory to represent municipal solid waste leachate. The GMs were kept in glass pools containing these leachates for about 108 months at different temperatures (22, 40, 55, 70, 85ºC). Melt index, stress-crack resistance, and OIT tests were performed on the samples that completed the curing period. At the end of 4 months, the OIT value decreased by 98% at 85ºC and by 40% at 55ºC. There was a decrease in melting index at 55 ºC to reach almost 0.8 (from 1.0) after 25 months and then the values increase with time to the initial values after 75 months of incubation. Similar trends were obtained at other temperatures. On the other hand, a sharp decrease was observed in the stress-crack resistance at the end of 80 months at 55ºC, 40 months at 70ºC, and 12 months at 85ºC [28]. Rowe et al. (2010) performed accelerated aging tests to evaluate the depletion of antioxidants from an HDPE. The effects of high pressure, temperature, and continuous leachate circulation on the aging of GMs in composite liner systems were investigated. The antioxidant depletion rates (0.05, 0.19, and 0.41 month^{-1} at 55, 70, and 85°C, respectively) obtained for the simulated landfill liner under normal stress of 250 kPa are lower than those obtained from conventional leachate immersion tests on the same GM (0.12, 0.39, and 1.1 month^{-1} at 55, 70, and 85°C). This difference leads to a significant increase in antioxidant depletion times at a typical landfill temperature (35ºC), with an estimated 40 years based on data from landfill liner simulators tests compared to the 15 years predicted for the same GM based on leachate immersion tests. In these tests, the crystallinity and tensile yield stress of the GM increased during the early stages of aging and subsequently remained relatively constant throughout the test period. There was no significant change in other GM properties during the test period [29]. Gulec et al. (2005) examined the effect of acidic mine drainage (AMD) leachate on the mechanical properties of HDPE. The geosynthetic materials were immersed in tanks containing synthetic AMD at 20, 40, or 60°C over 22 months. According to mechanical test results, that is no temporal changes in wide-strip tensile, puncture, and tear strength are evident, regardless of the temperature or leachate [30]. Similar results have been reported by Mitchell (1990) and Grubb et al. (1999) for other GMs exposed to AMD [31,32]. Sun et al. (2019) analyzed the long-term behavior of HDPE GMs under field conditions using analytical and mechanical testing as well as geoelectric leak location. The aging information obtained together with site-specific meteorological and hydrogeological data and landfill design parameters was then used in LandSim and HELP models to make quantitative analyzes of environmental impacts on leachate production, emissions, and groundwater. The results showed that HDPE GMs reached their service life after 8 years of landfill operation, where the hydraulic performance started to decline rapidly. This resulted in an increase in leachate seepage from the initial 0.05 – 0.6 m^3/d to a long-term range of 27.4 – 37.6 m^3/d. This has been accompanied by changes in the impact on groundwater, with the impact scope expanding from 50 to 1000 m, and the probability of pollution increasing from "almost impossible" to "almost certain" [33].

Chapter 3

Geosynthetics

GSs are essential components of a system or structure used to fulfill various engineering designs or purposes. GS products are generally produced from polymeric materials. Many different polymers are used in the production of GSs. These are high-density polyethylene, linear low-density polyethylene, polypropylene, polyvinyl chloride, polyester, expanded polystyrene, chlorosulphonated polyethylene, ethylene propylene diene terpolymer, and thermoplastic polyolefin. There are many different types of GSs according to the production method and the type of polymer used. These are geotextiles, geogrids, geonets, geomembranes, geosynthetic clay liners, geopipe, geofoam, and geocomposites. Some of the uses of GSs are reinforcement, separation, filtration, drainage, and water barrier. GSs are mostly used in civil engineering applications related to highways, railways, dams, hydraulics, retaining walls, canals, marine structures, foundations, embankments, etc.

The soil **reinforcement** function makes the soil more stable against loading. Increases normal loading and reduces disturbing shear forces. As a result, steep slopes can be built, or a high embankment can be built on soft soil that would otherwise not be possible. For example, the geogrid element used for reinforcement in a retaining wall moves the shear wedge away from the wall, thus ensuring the stability of the wall (Figure 3.1).

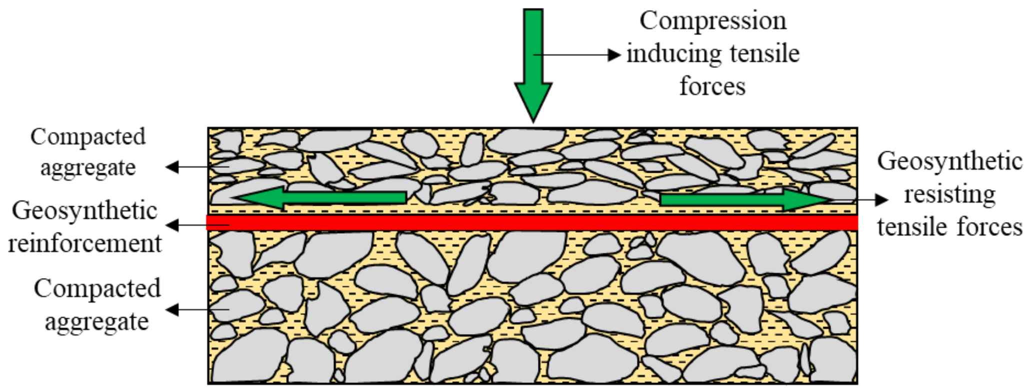

Figure 3.1: Reinforcement function of geosynthetics

GSs are useful for **separating** different types of soils. The separator helps prevent poor soil from mixing with quality granular materials when the structure is subjected to surface loading. It acts as a barrier against the migration of particles between two different soils, which is a necessity in many applications such as graded filters, pavements, linings in landfills, and clay covers [34] (Figure 3.2).

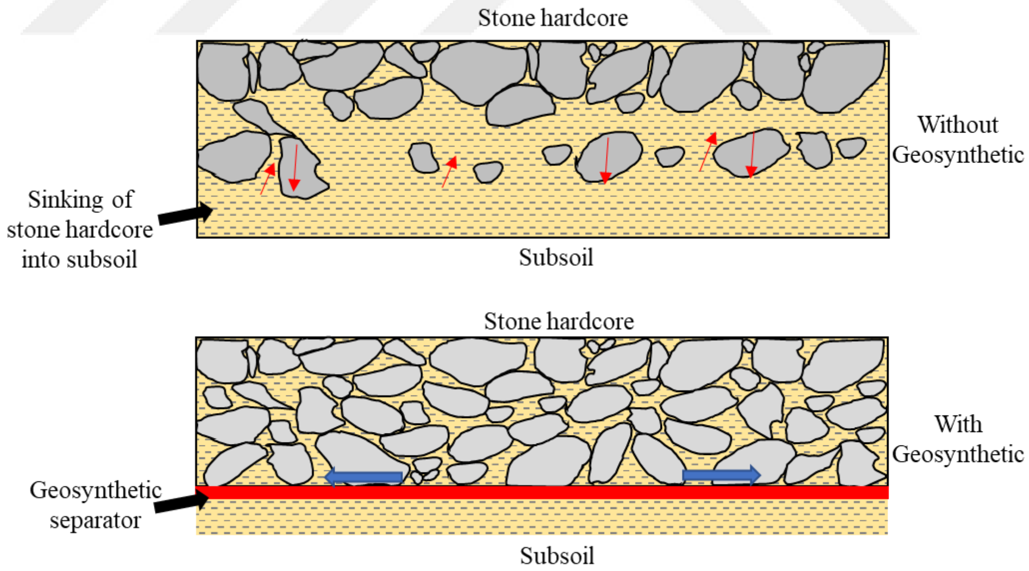

Figure 3.2: Separation function of geosynthetics

GSs, such as GTXs used for **filtration** purposes, hold the soil upward while allowing fluid to move along the plane of the GTX. To achieve this, the material must meet both adequate permeability, which requires an open fabric structure, and dirt retention, which requires a small aperture size. Long-term soil – GTX flow compatibility is also important, as the filter must not become excessively clogged during its lifetime. The filtration function of GTXs is widely used in geotechnical engineering. For example, GTXs are used to prevent soil particles from seeping and migrating into drainage aggregates or pipes while maintaining the normal operation of drainage systems; laying GTXs and other protective materials under the riprap protective layer can prevent soil erosion and riverbank subsidence (Figure 3.3).

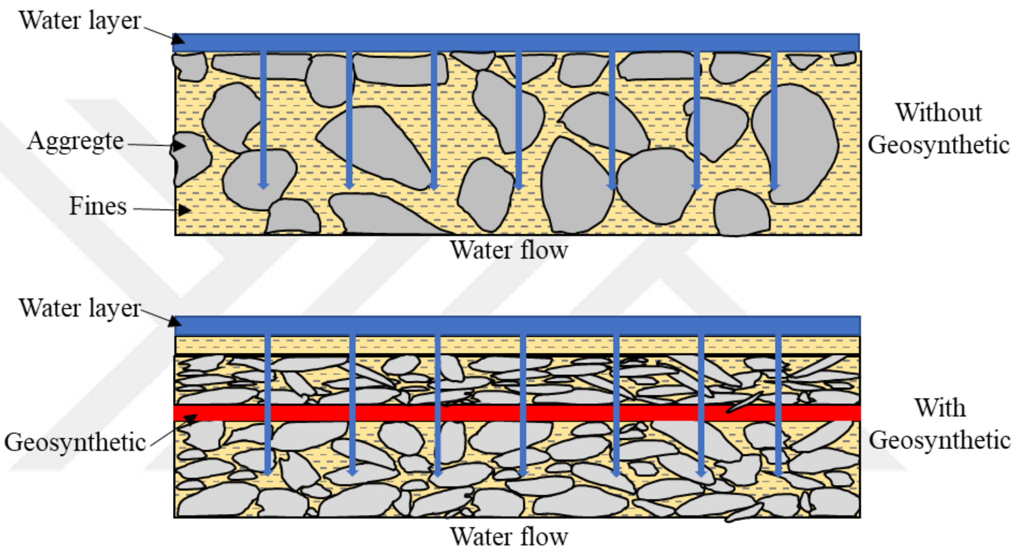

Figure 3.3: Filtration function of geosynthetics

The **drainage** function of GSs ensures the flow in the GS plane. GSs used as drainage channels must have water conductivity properties. Therefore, the most suitable GSs for drainage are GTXs, geonets, and drainage composites. In GTXs, the water in the soil structure can be collected and slowly discharged through the GTX (Figure 3.4).

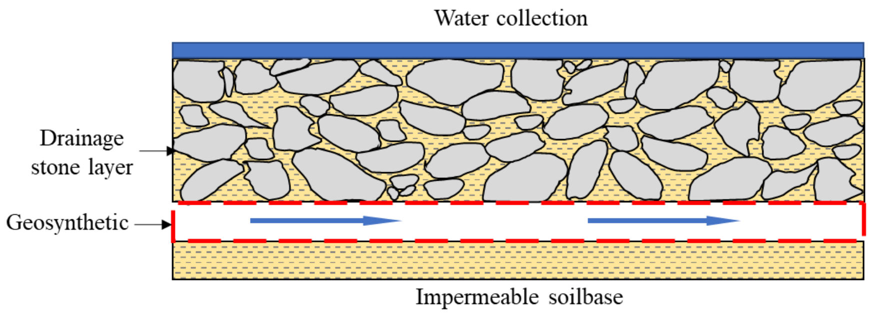

Figure 3.4: Drainage function of geosynthetics.

GMs and GTXs from GSs are used for **barrier** purposes. The barrier function of bitumen-coated GMs and GTXs is useful in many applications to minimize fluid and vapor flow. They are used in many applications such as canal linings, municipal waste landfills, dams, and liquid impoundment (Figure 3.5).

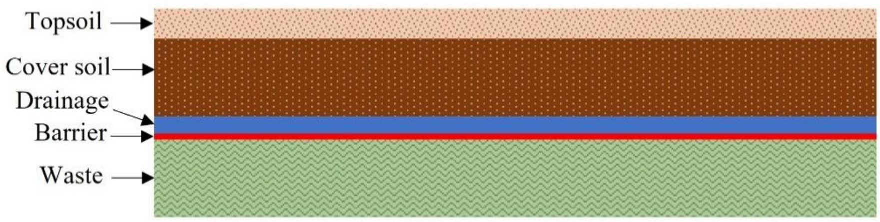

Figure 3.5: Barrier function of geosynthetics.

3.1 Geomembranes

GMs are impermeable GS materials composed of thin continuous polymer layers. As they are impermeable layers, they prevent the leakage of dangerous chemicals and harmful pollutants into the surrounding environment. It is also used as an anti-seepage barrier, conserving water for potable water and irrigation storage requirements. GMs, along with other GSs, are also used to control and contain fluid movement in projects related to sewage treatment, mining, and canal construction. GM production begins with the production of raw materials containing polymer resin and various additives. These raw materials are then formed into GM sheets of various widths and thicknesses by three different methods. These methods are extrusion, calendaring, and spreading coating. There are several different types of GMs, depending on the polymer resin and additives used. The commonly employed GMs include high-density polyethylene (HDPE), low-density polyethylene (LDPE), polyvinyl chloride (PVC), ethylene propylene diene monomer (EPDM), and thermoplastic polyolefin (TPO).

HDPE stands as the predominant choice among GMs, finding extensive usage across various applications. This thermoplastic polymer is derived from petroleum and possesses a generalized chemical formula $(C_2H_4)_n$. The formula of HDPE highlights its repeating monomer unit, ethylene, which forms a molecular chain of polyethylene. One notable distinction of HDPE from other polyethylene variants lies in its lower frequency of side chain branching. This particular GM garners preference for coating projects owing to its remarkable durability, robust UV resistance, and relatively affordable cost.

LDPE is produced from gaseous ethylene under very high pressures and high temperatures in the presence of oxide initiators. These processes yield a polymer structure with both long and short branches. LDPE is a very flexible material because the branches prevent the polyethylene molecules from being tightly packed in solid, rigid, crystalline arrangements. Since LDPE GMs are more flexible than HDPE, they are suitable for providing impermeability in plumbing projects. It is resistant to low temperatures and ultraviolet as it is made of untreated polyethylene resins.

TPO is a new technological product that offers a long service life thanks to its resistance to sun rays, atmospheric conditions, and plant roots as well as high puncture, tear, and abrasion resistance. It draws attention with its rapid growth potential, and economic and environmentally friendly nature in the roof and waterproofing sector. Olefin compound is composed of hydrogen and carbon-containing one or more pairs of carbon atoms bonded by a double bond. Olefins are examples of unsaturated hydrocarbons. They are classified in one or both of the following ways: as cyclic or acyclic olefins in which the double bond is located between the carbon atoms forming part of a cyclic or an open chain. As mono olefins, diolefins, triolefins, etc., where the number of double bonds per molecule is one, two, three, or any other number, respectively.

It is a thermoplastic waterproofing material made from **PVC**, vinyl, plasticizers, and stabilizers. Poly(vinyl chloride) (PVC) is a synthetic resin made from vinyl chloride and is a member of a large family of polymers commonly referred to as "vinyl". The chemical formula for vinyl chloride is $H_2C{=}CHCl$ and for PVC the formula is $(H_2C–CHCl)_n$, where n is the degree of polymerization. This polymer is one of the most widely used commercial thermoplastic materials. PVC is one of the oldest manufactured polymers and is currently one of the three most produced synthetic polymers.

EPDM is a copolymer of ethylene, propylene, and a small amount of unconjugated diene monomers (3 – 9%) and provides crosslinking sites for vulcanization (rubber curing). EPDM rubber is a class M synthetic rubber; an M classification consisting of elastomers with a saturated chain of the polyethylene type. It can withstand, as a GM, punctures, and extreme weather conditions. It has a rubber-like texture and is very resistant to UV rays.

3.2 Geotextiles

GTX consists of two terms, 'geo' and 'textile', the word 'Geo' means 'earth' in Greek. Therefore, GTXs can be defined as permeable textile materials used with soil or any other civil engineering material. It is a special type of polymer fabric with very small openings. GTXs are typically used to improve soil properties before constructing embankments, pipelines, roads, and soil retention structures. GTXs have various functions such as drainage, filtration, cushioning, reinforcement, waterproofing, and separation. Two types of fibers, natural and synthetic, are used in the production of GTXs. Natural fibers are obtained from plants (leaves, seeds, bark, etc.), animals, minerals, and similar natural structures. They have properties such as toughness, strength, durability, good covering ability, and biodegradability. However, natural fibers are no longer used as widely in GTX making. GTXs made using various polymers are synthetic. The most commonly used polymer types are polyester, polypropylene, polyethylene, polyamide, and PET. There are several different types of GTXs, depending on the type of polymer used and the method of manufacture. These are woven, nonwoven, knitted, spunbonded, and braided GTXs.

Woven GTXs are used for the separation process and to increase the strength of the soil. Since the yarn strength of its warps is very high, its tensile strength is high and thus it can carry much more load. There are different types of woven GTXs these are woven monofilament, woven multifilament, woven slit film monofilament, and slit film multifilament (Figure 3.6a).

The tensile strength is not very high in **nonwoven** GTXs, but the drainage, separation, and filtration properties are better than others. They are permeable GSs usually made of synthetic fibers and production methods are thermal and chemical bonding. There are various types of nonwoven GTXs these are continuous filament needle punched, continuous filament heat bonded, resin bonded, and staple needle punched (Figure 3.6b).

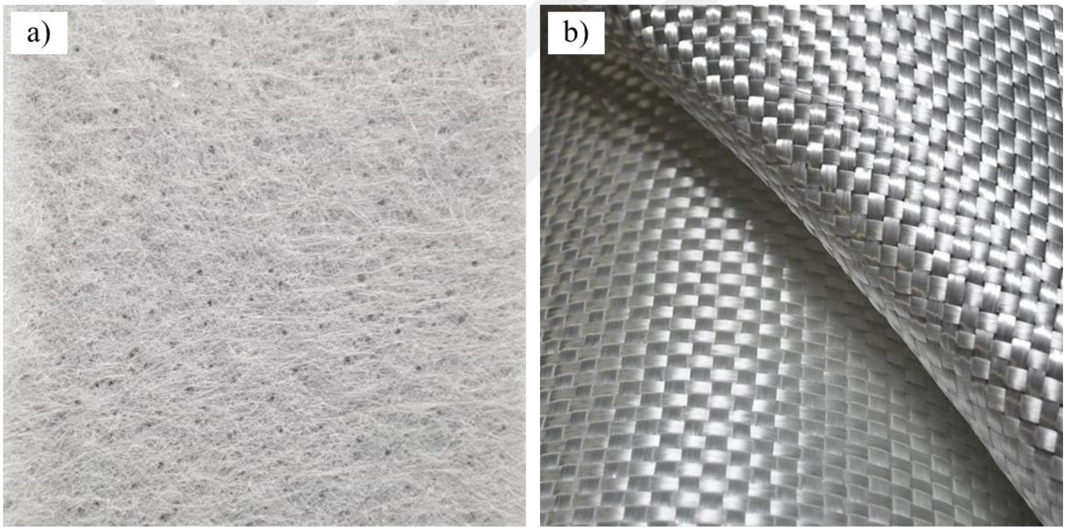

Figure 3.6: Physical appearances of GTX a) nonwoven, b) woven

Knitted GTXs have good flexibility and are more economical. Although its use is less, it is frequently used in drainage and soil erosion control. Knitted GTXs are made using knitting technology, while in some cases weaving is used to make these products.

The **spunbonded** process has the fastest production method among nonwovens. During the process, the extruded filaments are cut into belts, rolled, and the rolls are heated and held together. In the industrial sector, they are used as waterproofing rolls for the roof, reinforced material, polishing materials, filter materials, insulation materials, and cement bags.

Knitting is often used to crosswise interlace three or more bundles of fibers and threads to produce narrow thread-like materials. The topology of yarn helices in braided structures is like that of woven structures. It increases the bearing capacity of the soil in structures to be built on soft and weak soils. It is used as a reinforcement layer on roads due to its low elongation under high tensile force. It protects the bearing capacity by preventing the sub-base material from mixing with the soil. Especially geogrid reinforced structures are recommended for slope stability but knitted GTXs can also be used. This practice prevents soil loss during floods.

Chapter 4

Materials and Methods

4.1 Materials

4.1.1 Soils

Six types of soils, namely low plasticity clay (LC), sand/bentonite (SB) mixture, crushed sand (CS), river sand (RS), crushed gravel (CG), and river gravel (RG), have been used in this study. While LC was obtained during a reclamation study on the coastline of Mavişehir district in İzmir province, CS, CG, RS, RG, and SB were purchased commercially. Thus, a case study of the soil – GS interface shear strength parameters used in the structures built close to the Mavişehir coastline (Figure 4.1) was also carried out.

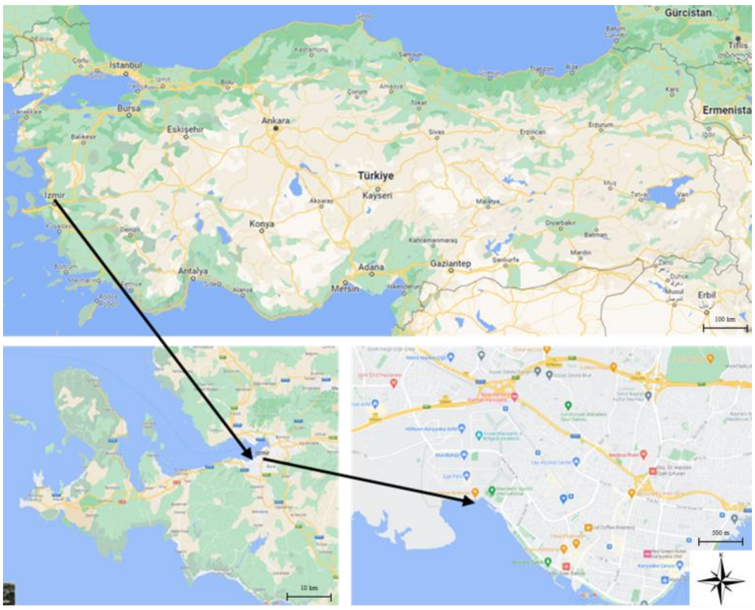

Figure 4.1: Location of Mavişehir district on the map

Crushed soils have angular particles and river soils have rounded particles, so the effect of morphology on soil – GS interface shear strength behavior was investigated. In addition, the particle size and plasticity effect was investigated on the shear strength parameters of soil – GS interface since soils with different grain sizes are used from bentonite to gravel. The minimum and maximum grain sizes of soils are listed in Table 4.1. The physical appearances of the soils used are shown in Figure 4.2.

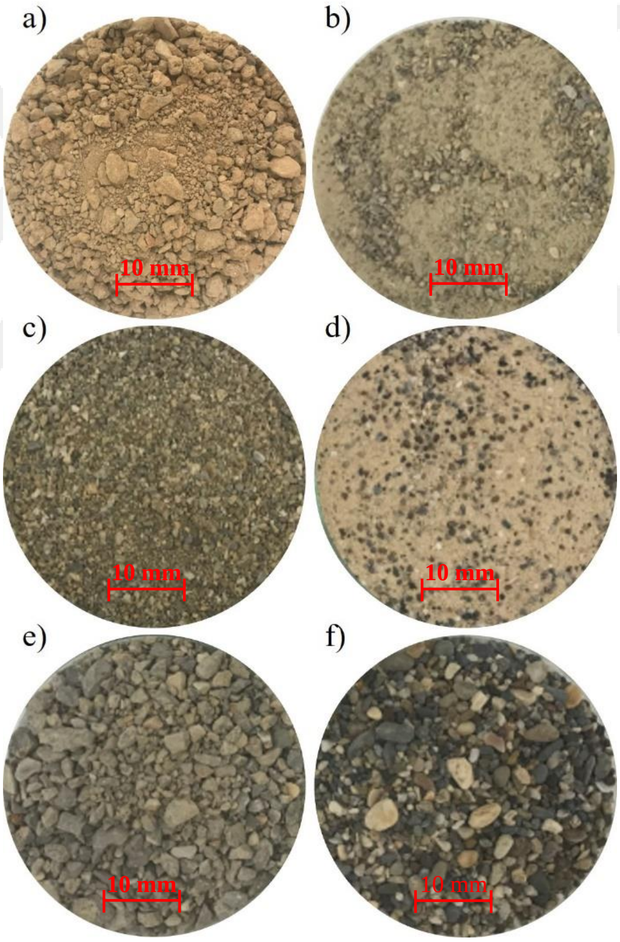

Figure 4.2: Physical appearance of soils; a) LC, b) SB, c) CS, d) RS, e) CG, f) RG

Table 4.1: Minimum and maximum grain size of soils

Soil	Minimum grain size (mm)	Maximum grain size (mm)
SB	0.002	2.0
LC	0.002	5.0
CS	0.075	2.0
RS	0.075	2.0
CG	0.425	10.0
RG	0.425	10.0

4.1.2 Geosynthetics

4.1.2.1 Geomembrane

In this study, three different types of GMs, PVC, HDPE, and TPO, were used. In order to examine the effect of GM thickness on the interface shear strength, PVC thicknesses of 1.5 and 3.0 mm were selected. The thicknesses of HDPE and TPO are 1.5 mm. A textured and smooth HDPE was chosen to examine the effect of GM roughness on the interface shear strength. The surfaces of PVC and TPO are smooth.

PVC is a protective layer made of synthetic raw materials and used for liquid and thermal insulation. PVC is a symbol created from the abbreviation of Poly-Vinyl-Cholride. It is a type of polymer produced from oil and salt in petrochemical plants. They are produced by mixing the PVC raw material with softeners, stabilizers (strengtheners), and various additives in a mixer, processing it with the help of an extrusion system at the appropriate temperature, and shaping it homogeneously. PVC GMs were supplied by the BTM company and technical features are given in Table 4.2.

Table 4.2: Technical features of PVC GM

Essential characteristics	Unit	Value	
Thickness	mm	1.5	3.0
Linearity	mm/m	75	75
Resistance to tearing	N	150	300
Shear resistance of joints	N/5cm*	800	1000
Tensile strength	N/mm^2	15	15
Elongation at break	%	250	250
Water tightness	-	Fully	Fully
Artificial aging – water tightness	-	Fully	Fully
Chemical resistance – water tightness	-	Fully	Fully
Resistance to impact	mm	1500	1500
Resistance to static loading	kg	20	20
Reaction to fire	-	Class E**	Class E**

*According to the results of the shear resistance of joints test performed with a 5 cm wide and 1 m long sample.
** Reaction to fire classifications; A1 No contribution to fire, A2 No noticeable contribution to fire, B Little or no contribution to fire, C Limited contribution to fire, D Contributes to fire, E Major contribution to fire, F Not within classes A1-E

HDPE is a GS liner that is formed as a result of the extrusion of high-density polyethylene and shaped homogenously by a calendar system. Polyethylene (PE) takes the name of ethylene which is in the form of a monomer. Ethylene becomes polyethylene with several methods of polymerization. It is used to ensure impermeability in projects such as municipal solid waste landfill sites, mine waste landfill sites, acid tanks, ponds, tank fields, and irrigation channels. HDPE was supplied by Geoplas company and technical features are given in Table 4.3.

Table 4.3: Technical features of HDPE GM

Essential characteristics	Unit	Value	
		Smooth	Textured
Thickness	mm	1.5	1.5
Tensile stress at break	N/mm^2	>26	>26
Elongation at yield	%	>12	>12
Elongation at break	%	>700	>700
Yield strength	N/mm^2	>16	>16
Static puncture resistance	N	3700	7200
Resistance to weathering	%	<25	<25
Oxidation strength	%	<25	<25
Stress crack resistance	h	>200	>200
Water permeability	m^3/m^2d	$<10^{-6}$	$<10^{-6}$

TPO is a technological waterproofing cover produced from thermoplastic polyolefin raw material and applied by sewing with hot air sources. This technology, which was developed in the 80s, is now the fastest-growing GM in the roofing and waterproofing industry. Compared to other GMs, TPO does not contain any toxic or harmful substances and therefore is an environmentally friendly product and has advantageous features that provide high energy saving thanks to its heat-retardant feature. In addition, TPO is recyclable, so their impact on the environment is very low, but one of the best features is that TPO does not use plasticizers to gain flexibility like PVC. It provides both very high durability and high elasticity advantages throughout its life, thanks to its polyolefin structure. TPO GMs were supplied by the BTM company and technical features are given in Table 4.4.

Table 4.4: Technical features of TPO GM

Essential characteristics	Unit	Value
Visible length	-	Excellent
Impermeability	-	Impermeable
Reaction to fire	-	E class
Peel the strength of the joints	N/50 mm	≥ 300
Shear strength of the joints	N/50 mm	≥ 800
Tensile strength	N/50 mm	≥ 1100
Breaking elongation	%	≥ 20
Impact strength	mm	≥ 700
Resistance to the static charge	kg	≥ 20
Resistance to tearing	N	≥ 300
Resistance to the plant toots	-	Resistant
Dimensional determination	%	≤ 1
Elasticity in cold	°C	≤ - 30
UV resistance	-	Resistant
Resistance to water and chemical liquids	-	Resistant
Resistance to hail stones	m/s	≥ 20

4.1.2.2 Geotextile

The GTX used in this study is a nonwoven polypropylene GTX with a density of 200 g/m^3. This GTX is resistant to chemical wastes and has the highest bearing capacity. It also has protection, separation, and filtration properties. The most important properties of GTXs are flexibility, permeability, and durability. The nonwoven GTX was supplied by Geoplas company and technical features are given in Table 4.5.

Table 4.5: Technical features of nonwoven GTX

Essential characteristics	Unit	Value
Thickness	mm	1.5
Weight	g/m^2	200
Tensile strength	kN/m	11 – 13
Elongation	5	50 – 80
Static puncture	N	250
Dynamic puncture	mm	24
Water tightness	m/s	0.07
Opening	mm	0.13

4.1.3 Synthetic leachates and saltwater

Since GMs are used for insulation purposes, they are exposed to various chemicals during their life. In order to reflect this condition, GMs are aged in 0.5M salt water and various leachates. Leachates were not taken from their natural environment and were synthetically prepared in the laboratory. The reason for this is to aim for the experiments to be performed with leachates with the same characteristics.

4.1.3.1 Acidic mine drainage leachate (AMD)

Mine drainage is a metal-rich fluid formed from the chemical reaction between water and sulfur-containing mineral rocks. The resulting runoff is usually acidic, occurring in areas where coal or ore mining activities have exposed rocks containing pyrite, a sulfur-containing mineral. Drainage may also occur in metal-rich mineralized areas without mining activities [35].

Acidic mine drainage (AMD) is the formation and movement of highly acidic water rich in heavy metals. This acidic water is formed by the chemical reaction of surface water (rainwater, snowmelt, pond water) and shallow groundwater with sulfur-containing mineral rocks. The resulting fluids can be highly toxic and have harmful effects on humans, animals, and plants when mixed with groundwater, surface waters, and soil [36–38].

The amount of AMD released depends on the volume of the ore, the exposed surface area, the concentration, and the type of sulfides it contains. The formation and discharge of AMD continue not only during the mining activity but also after the mining is stopped and poses serious dangers to the ecological systems. The most important source of AMD in the world comes from many abandoned mines that are left untreated. For example, Roman gold mine sites in Romania still cause acid mine drainage after over 2000 years (Rosia Montana mine, Figure 4.3) [39–41].

Figure 4.3: Rosia Montana gold mine sites, Romania

In mining waste storage facilities, HDPE GMs are used to prevent leachate from mixing with groundwater. In addition, the use of TPO GMs for insulation purposes has become widespread recently. Therefore, in this study, the HDPE and TPO GMs were kept in the AMD leachate for 4, 8, and 16 months, then the interface direct shear tests were carried out. The AMD leachate used in this study was produced synthetically in the laboratory by mixing various chemical compounds in distilled water (Table 4.6). The content of the AMD liquid was selected by reviewing the composition of the twelve AMDs for metallic mine waste mentioned in the literature. In this mixture, the most abundant metals (Fe, Zn, Cu, and Ca) in AMD, their relative concentrations, and their types were determined [42]. The pH measurements were taken on the day the leachate was prepared and at 4, 8, and 16 months. The measurements were 0.95, 0.97, 1.12, and 1.29, respectively. Electric potential and viscosity values were also measured, respectively, 308 mV and 2.02 centipoise (cP) were obtained.

Table 4.6: Chemical composition of AMD leachate

Chemical name	Chemical formula	Amount (mg/l)
Copper (II) sulfate	$CuSO_4$	88
Zinc Sulphate Heptahydrate	$ZnSO_4.7H_2O$	864
Sulfuric Acid	H_2SO_4	886
Iron (II) sulfate heptahydrate	$FeSO_4.H_2O$	4076
Calcium sulfate	$CaSO_4$	681

4.1.3.2 Coal combustion product leachate (CCP)

Coal is a non-renewable fossil fuel that has been used since ancient times and is still one of the most important energy sources today. Coal production and use cause various operational and environmental problems. One reason is that most of the high-quality coal has already been mined and the remaining coal contains high humidity and ash. In addition, the environmental problems associated with coal burning are multifaceted, threatening the sustainability of coal use, mostly in power generation and gasification [43].

Coal combustion products (CCPs), also called coal combustion residues (CCRs) or coal combustion wastes (CCWs), are categorized into four groups based on their physical and chemical forms, according to coal combustion methods and emission controls: Fly ash, flue-gas desulfurization, bottom ash, and boiler slag. These are generally used as the binder for cement, structural fills, land reclamation, grouts, and masonry product, while the unused portion is landfilled in solid waste disposal areas.

According to Coal 2022, the IEA's annual market report on the industry, global coal use increased by 1.2% in 2022 to exceed 8 billion tons [44]. Also, according the

2021 CCP Production & Use Survey Report of the American Coal Association, it has been shown that the coal combustion product released in a year in the world is 780 million tons. While this amount is 77 million tons in the USA, only 60% of them is reused and the rest is stored in landfills [45]. For this reason, the storage of these wastes is very important for the environment. If impermeability is not successfully achieved in landfills, it may cause various environmental damages. For example, at a landfill near the Gavin Power Plant in Ohio, USA, CCP leachates caused soil contamination (Figure 4.4).

Figure 4.4: Gavin Power Plant in Ohio, USA

In CCP waste storage facilities, HDPE GMs are used to prevent leachate from mixing with groundwater. In addition, the use of TPO GMs for insulation purposes has become widespread recently. Therefore, in this study, the HDPE and TPO GMs were kept in the CCP leachate for 4, 8, and 16 months, then the interface direct shear tests were carried out. The CCP leachates used in this study were identified through analysis of a database containing leachate data from 33 CCP disposal sites compiled by the Electric Power Research Institute (EPRI) [46]. The database includes concentrations of major cations and anions, ionic strength, the relative abundance of monovalent and polyvalent cations, pH, and electrical conductivity (EC). It was determined that CCP leachate was slightly alkaline (pH 7.67) as a result of pH measurements. The pH measurements were repeated at the 4th, 8th, and 16th months and the results were obtained as 7.67, 7.70, and 7.81. Electric potential and viscosity values were also measured, respectively, 26 mV and 1.68 cP were obtained. The chemical contents of the CCP leachate are listed in Table 4.7.

Table 4.7: Chemical composition of CCP leachate

Chemical name	Chemical formula	Amount (mg/l)
Potassium sulfate	K_2SO_4	161
Sodium chloride	$NaCl$	51
Calcium chloride	$CaCl_2$	58
Sodium sulfate	Na_2SO_4	722
Calcium sulfate	$CaSO_4$	987
Magnesium sulfate	$MgSO_4$	146

4.1.3.3 Municipal solid waste leachate (MSW)

Municipal solid waste (MSW), commonly known as garbage or rubbish, consists of everyday items that we use and then dispose of, such as product packaging, clippings, clothing, grass, leftovers, furniture, tools, bottles, paint, newspapers, batteries, and the like. According to the Global Waste Statistics of What a Waste 2.0, the world produced 2.01 billion tons of MSW in 2022 and this is expected to increase by roughly 70% to 3.4 billion tons by 2050. Worldwide, approximately 40% of MSW is disposed of in landfills, approximately 19% is recovered through composting and recycling, and 11% is processed through modern incineration (Figure 4.5:) [47].

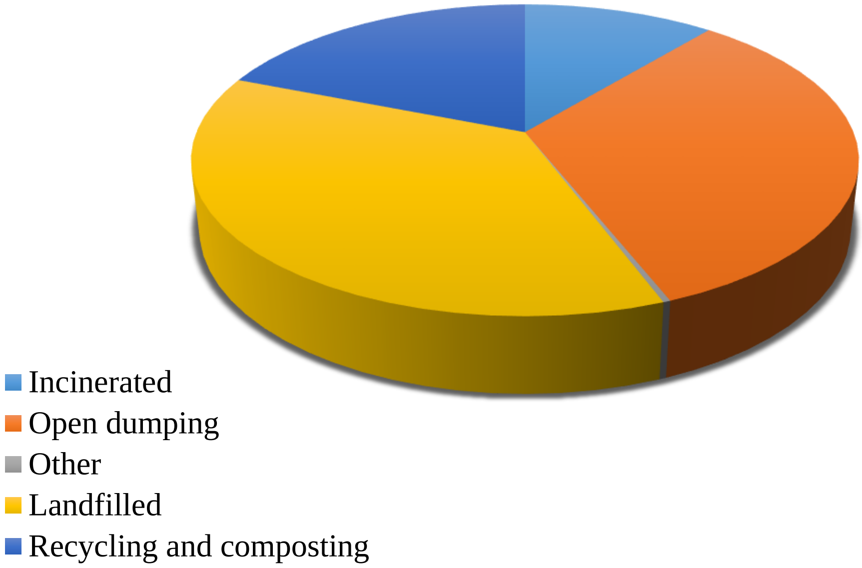

Figure 4.5: Global waste treatment and disposal [47]

HDPE GMs can be used in MSW landfills to ensure slope stability and prevent leakage of leachate from mixing with groundwater. In addition, the use of TPO GMs for insulation purposes has become widespread recently. However, in storage facilities designed to serve for many years, GMs may be damaged over time due to the chemicals in the leachate and become unable to function. Therefore, in this study, the HDPE and TPO GMs were kept in the MSW leachate for 4, 8, and 16 months, then the interface direct shear tests were carried out. The MSW leachate used in this study was produced synthetically in the laboratory by mixing various chemical compounds in distilled water (Table 4.8). The content of the MSW was taken from the study of Hrapovic and Rowe (2002) [48]. Prepared MSW leachate is a suitable medium for the growth and maintenance of acetogenic, methanogenic, and sulfidogenic bacteria involved in the mineralization stage of anaerobic degradation. Also, the mixture containing only three volatile fatty acids has been used as a very similar variation of possible storage leachate [48–51]. The pH measurements were taken on the day the leachate was prepared and at 4, 8, and 16 months. The measurements were 1.73, 1.76, 1.77, and 1.82, respectively. Electric potential and viscosity values were also measured, respectively, 280 mV and 1.89 cP were obtained.

Table 4.8: Chemical composition of MSW leachate

Chemical name	Chemical formula	Amount (per 1 L)
Acetic acid	CH_3COOH	7 mL
Propionic acid	$CH_3CH_2CO_2H$	5 mL
Butyric acid	$C_4H_8O_2$	1 mL
Dipotassium phosphate	K_2HPO_4	30 mg
Potassium bicarbonate	$KHCO_3$	312 mg
Potassium carbonate	K_2CO_3	324 mg
Sodium chloride	$NaCl$	1440 mg
Sodium nitrate	$NaNO_3$	50 mg
Bicarbonate of Soda	$NaHCO_3$	3012 mg
Calcium chloride	$CaCl_2$	2882 mg
Magnesium chloride hexahydrate	$MgCl_2.6H_2O$	3114 mg
Magnesium sulfate	$MgSO_4$	156 mg
Ammonium bicarbonate	NH_4HCO_3	2439 mg
Urea	$CO(NH_2)_2$	695 mg
Trace metal solution*	-	1 mL
Sodium sulfide nonahydrate	$Na_2S.9H_2O$	E_h-120-180 mV
Sodium hydroxide	$NaOH$	pH 5.8-6.0
Distilled water	H_2O	To make 1 L
*Chemical composition of trace metal solution		
Ferrous sulfate	$FeSO_4.7H_2O$	2000
Boric acid	H_3BO_3	50
Zinc sulfate heptahydrate	$ZnSO_4.7H_2O$	50
Cupric sulfate pentahydrate	$CuSO_4.5H_2O$	40
Manganous sulfate monohydrate	$MnSO_4.H_2O$	500
Ammonium molybdate tetrahydrate	$(NH_4)6Mo7O_{24}.4H_2O$	50
Aluminum sulfate 16-hydrate	$Al_2(SO_4)_3.16H_2O$	30
Cobaltous sulfate heptahydrate	$CoSO_4.7H_2O$	150
Nickel (II) sulfate	$NiSO_4.6H_2O$	500
Sulphuric acid	H_2SO_4	1

4.1.3.4 Saltwater (SWt)

In areas where the groundwater level is high, GM is laid under the foundations to prevent the foundation from being exposed to groundwater. If the built structures are close to coastal areas, there may be a significant amount of salt in the groundwater. This salt in the groundwater or seawater which is infiltrated from the sea to the foundation can damage the GM after many years, and this may cause the foundation to come into contact with water and lose its strength. A building whose foundation is damaged may collapse over time or as a result of an earthquake, which can cause many losses of life and property. Therefore, it is extremely important to have information about the behavior of GMs exposed to saltwater. In this study, PVC and TPO GMs were kept in 0.5 molar (M) salt water for 4, 8, and 16 months, and then they were subjected to the interface direct shear tests. The reason for the preparation of salt water 0.5 M is that the salt ratio of the Aegean Sea water, which is the region where LC soil is taken, is 0.5 M. The reason for using only TPO and PVC GMs is the use of these GM types for bundling in building foundations. The 0.5M saltwater was obtained by mixing 1 liter of distilled water with 29.22 g of NaCl. The pH measurements were taken on the day the salt water was prepared and at the 4th, 8th, and 16th months. The measurements were 8.12, 8,08, 8.07, and 8.06, respectively. Electric potential and viscosity values were also measured, respectively, -77 mV and 1.58 cP were obtained. In Figure 4.6, which GM is cured in which liquid is summarized.

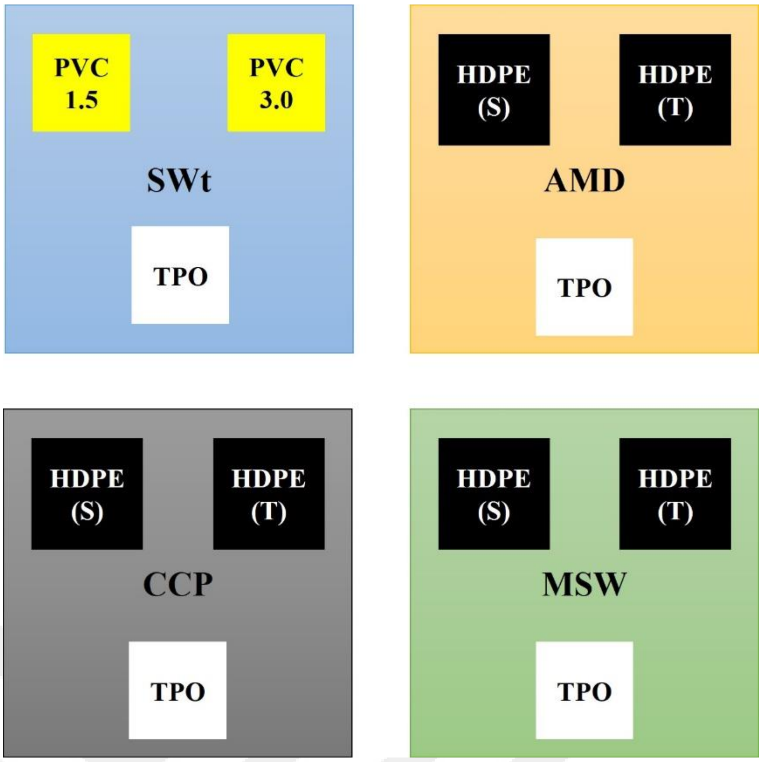

Figure 4.6: Schematic demonstration of the curing liquid information

4.2 Methods

In this section, laboratory tests performed to determine the geotechnical index properties and shear strength parameters of the soils used in the experiments are given. The method of direct shear tests with the soil – GM (uncured and cured) and GM – GTX interface is also given. In addition, the applied methods of microscopic image acquisition, image processing, surface roughness, and Plaxis 2D analyses are given in details.

4.2.1 Geotechnical index properties

In order to determine the geotechnical index properties of the soils, wet and dry sieve analyses, hydrometer analysis, specific gravity test, Standard Proctor test, pH meter test, and liquid and plastic limit tests were carried out. All experiments were performed in accordance with American Society for Testing and Materials (ASTM) standards (Table 4.9).

Table 4.9: ASTM standards used in laboratory experiments

Experiment	ASTM Standard
Sieve analysis	ASTM D422 [52]
Hydrometer analysis	ASTM D7928 [53]
Specific gravity test	ASTM D854 [54]/ASTM C127 [55]
Liquid and plastic limit test	ASTM D4318 [56]
Standard Proctor test	ASTM D698 [57]
pH measurement	ASTM D4972 [58]

4.2.1.1 Sieve analysis

In this study, wet and dry sieve analysis was performed according to the ASTM D422 standard to determine the grain size distribution of the soils [52]. Total 1 kg of sample was first washed through a No. 200 (0.074 mm) sieve and the sample remaining on the sieve was thrown into the oven and kept at 105°C for 24 hours and completely dried. The percentage of silt and clay was obtained by subtracting the weight of the sample dried after washing from the initial weight. Then, the grain size distribution graph was obtained by performing dry sieve analysis with the material remaining on the No.200 sieve. The sieve no and sieve openings used are shown in Figure 4.7. Experiments were carried out separately for all types of soils.

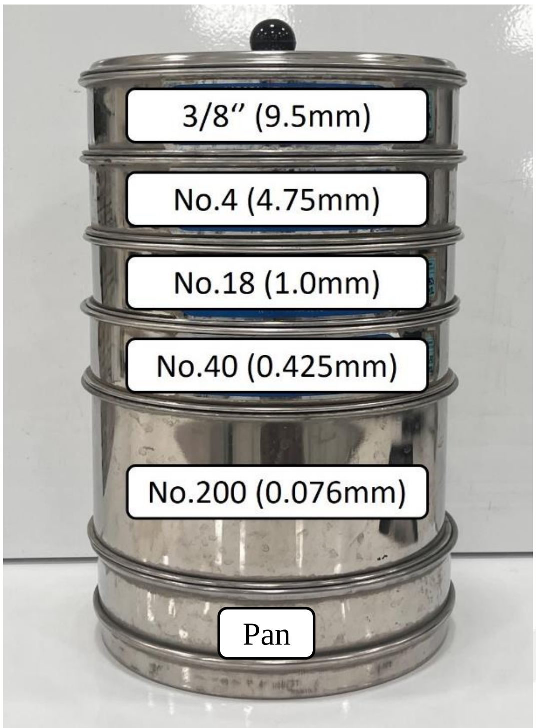

Figure 4.7: Number and sizes of sieves

4.2.1.2 Hydrometer analysis

Hydrometer analysis is an experiment to find the particle size distribution of fine grained soils (<0.074 mm). For silt and clay soils, approximately 50 g, and for soils with high sand content, approximately 100 g of completely dried sample is prepared. The dry sample is placed in a 250 ml glass container and 125 ml of sodium hexametaphosphate solution ($Na_8P_3O_{10}$) is poured over it. The solution is obtained by placing 40 g of sodium hexametaphosphate into 1.0 liter of distilled water. This chemical liquid is mixed with the soil and left to stand for 24 hours. The well-mixed suspension is poured into a graduated glass container containing approximately 100 ml of distilled water. On top of this, pure water is added to ensure that the suspension in the glass container is 1000 ml. Hydrometer is slowly placed into the hydrometer suspension with two fingers without creating turbulence. Insertion of the hydrometer should be done within 5-6 seconds. After the hydrometer is immersed in the suspension, readings are taken at the 15th, 30th, and 120th seconds without removing the hydrometer from the suspension. At the end of the first two minutes, the hydrometer is removed from the suspension and slowly placed in a measuring tape containing distilled water at the same temperature as the suspension. The temperature of the soil-water suspension is measured and recorded after each hydrometer reading. About 20 seconds before the reading times, the hydrometer is carefully placed into the suspension and the hydrometer readings are taken at the 5th, 10th, 15th, 30th, 60th, 240th, and 1440th minutes [53]. The graduated cylinder and type 151H hydrometer used are shown in Figure 4.8. After all the hydrometer analysis readings are taken, the suspension in the glass container is poured into a large porcelain container and placed in the oven. After drying for 24 hours, the dry weight of the soil is determined as W_s. The particle diameter distribution is determined using Equation 4.1 and Equation 4.2. In equations; R: hydrometer readings, t: time, N: viscosity of water at test temperature, G_s: specific gravity of soil, G_w: specific gravity of water, L: effective depth, a: ratio of soil specific gravity to constant 2.65.

$$Grain\ size\ (mm) = \sqrt{\frac{30 * N * L}{980 * (G_w - G_s) * t}} \tag{4.1}$$

$$Percent\ passing\ (\%) = \frac{a * R}{W_s} * 100 \tag{4.2}$$

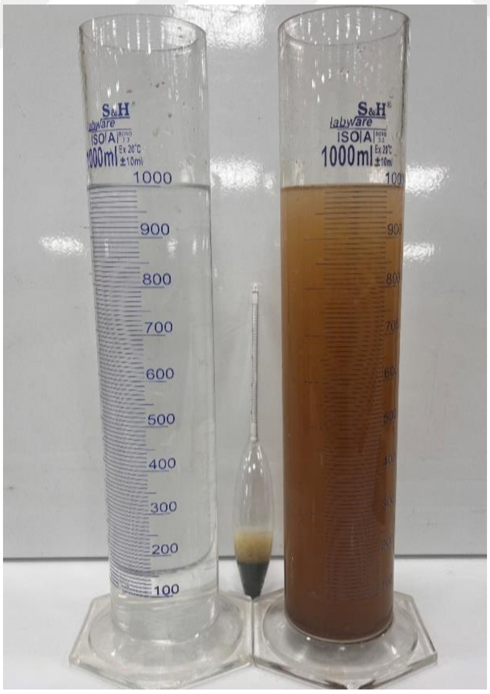

Figure 4.8: Graduated cylinder and type 151H hydrometer

4.2.1.3 Specific gravity test

Specific gravity is defined as the ratio of the weight of solid particles of soils to the weight of water as much as the volume of solid particles. In this study, the specific gravity value was determined according to the ASTM D854 standard for the soils of SB, LC, CS, and RS [54]. The 500 ml pycnometer was filled halfway with distilled water, and the vacuum was applied for 15 minutes (Figure 4.9a), then it was filled up to the meniscus line and the vacuum was applied with a vacuum pump for 15 minutes (Figure 4.9b). Thus, a pycnometer + weight of water was obtained (W_1). Then, 50 g of sample (W_2) was placed in an empty pycnometer, and pycnometer was filled halfway with distilled water, and the vacuum was applied for 15 minutes (Figure 4.9c), then it was filled up to the meniscus line and the vacuum was applied with a vacuum pump for 15 minutes (Figure 4.9d). Thus, the pycnometer + water + sample weight was found (W_3). Specific gravity value was obtained by substituting these values in Equation 4.3.

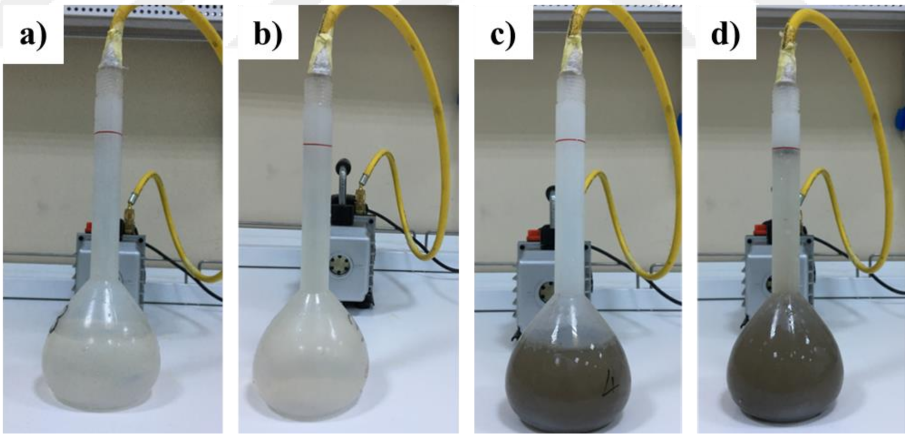

Figure 4.9: Steps of specific gravity test for LC, SB, CS, and RS

$$G_s = \frac{W_2}{W_2 + W_1 - W_3} \tag{4.3}$$

The specific gravity value was determined according to the ASTM C127 standard for the soils of CG and RG. Firstly, a 2 kg sample was completely dried in the oven (W_1). It was then wetted so that it was completely covered with water and left in this way for 3 hours. The water remaining on the surface was dried with a cloth and then weighed (W_2). A 4-liter glass beaker was filled with water and weighed (W_3) (Figure 4.10a). Then the wet sample was placed in the same beaker and was filled with water and weighed (W_4) (Figure 4.10b). Specific gravity value was obtained by substituting these values in Equation 4.4.

$$G_s = \frac{W_1}{W_2 + W_3 - W_4} \tag{4.4}$$

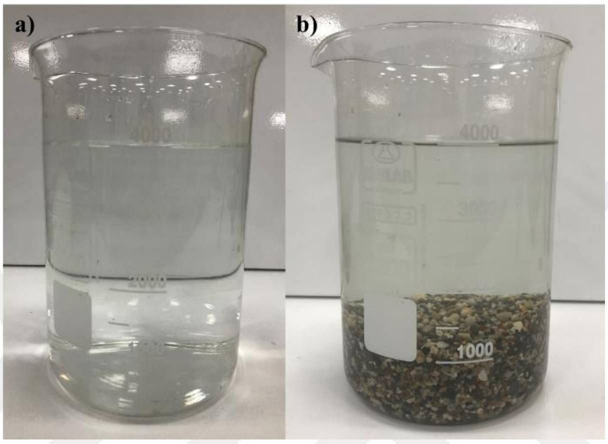

Figure 4.10: Steps of specific gravity test for CG and RG

4.2.1.4 Liquid and plastic limit test

Since only SB and LC are not nonplastic among the soil types used in the study, consistency limit tests were applied for these soil types. Liquid and plastic limits were determined according to ASTM D4318 [56]. The Casagrande test was conducted to obtain the liquid limit of SB and LC soil samples. For the test, the sample was sieved through a No.40 (0.425 mm) sieve. Samples were prepared in certain water contents and placed in the Casagrande mold. A slit was made in the middle of the sample with the help of a special spoon. Then, the device made two drops per second, and the number of drops where the closure in the slit was 13 mm was recorded. This process was repeated 5 times by adding water each time (Figure 4.11). A semi-logarithmic graph was drawn with the drop values and water contents obtained as a result of the experiment, and the water content corresponding to 25 drops on the line was found as the liquid limit value.

Figure 4.11: Casagrande liquid limit test device

For the plastic limit test, some water was added to the sample sieved through a No.40 (0.425 mm) sieve and mixed. Some of this mixture was taken and the sample was palm rolled on a smooth glass surface. The experiment was terminated when capillary cracks were observed when the sample reached 3 mm in diameter and the plastic limit value was determined by calculating the water content (Figure 4.12). This process was repeated two more times and the water content of the samples was determined. The average water content value obtained represents the plastic limit value of the soil.

Figure 4.12: Plastic limit determination with the hand-rolling method

4.2.1.5 Standard Proctor test

The Standard Proctor tests were conducted to determine the maximum dry unit weight and optimum moisture content of soil samples according to ASTM D698 [57]. Method A was applied for LC, SB, CS, and RS soil samples, method B was applied for CG and RG soil samples. A cylindrical Standard Proctor mold with a diameter of 101.6 mm and a 24.5 N hammer was used in both methods (Figure 4.13). Soil samples under a 4.75 mm sieve for method A and under a 9.5 mm sieve for method B were used. In both methods, the sample was placed in the mold in 3 layers and 25 blows to each layer. The experiment was repeated at least 5 times for different water contents and results were obtained. The results obtained were used when preparing samples for the medium scale direct shear experiment.

Figure 4.13: Standard Proctor mold and hammer

4.2.1.6 pH determination test

The pH measurements were made with Ohaus Starter 300 brand pH meter according to ASTM D4972 standard [58]. 40 g of sample, which was sieved through a No.10 (2.0 mm) sieve and completely dried, was mixed with 40 g of distilled water and left to stand for 1 hour. Then, the electrode of the pH meter was submerged in the upper liquid part in such a way that it would not touch the solids, and the pH measurement was taken (Figure 4.14). The same process was repeated 3 times and the average of the three measurements was determined as the pH value.

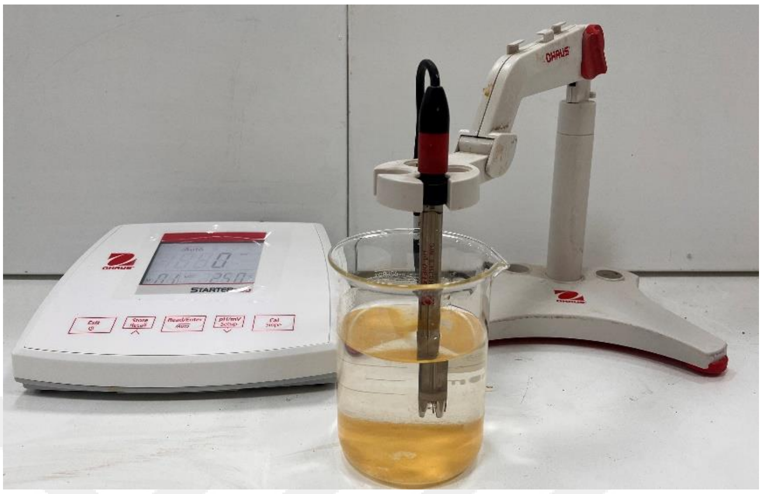

Figure 4.14: Measurement of pH with a digital pH meter

4.2.2 Direct shear test

Conventional direct shear tests were conducted to determine the internal friction angle and cohesion values of soil samples according to ASTM D3080 [59]. The dimensions of the medium scale shear box used in the experiments were 100x100x40 mm. The reason why the shear box is defined as the medium scale is that in previous studies in the literature, shear boxes with this and similar dimensions are called medium scale [60–63]. Direct shear tests were carried out with ELE brand computer-controlled fully automatic direct shear device (Figure 4.15). In order to prevent excess pore water pressure formation in fine grained soils (LC, SB), the shear rate was set as 0.1 mm/min. Because of the high permeability of coarse grained soils (CS, RS, CG, RG), the shear rate was determined as 0.5 mm/min. The samples were prepared at optimum water content and placed directly inside the shear box at maximum dry unit weight density. The experiment was carried out under three different levels of normal stress, these are low (12.25, 24.5, 49 kPa), medium (49, 98, 196 kPa), and high (196, 392, 784 kPa).

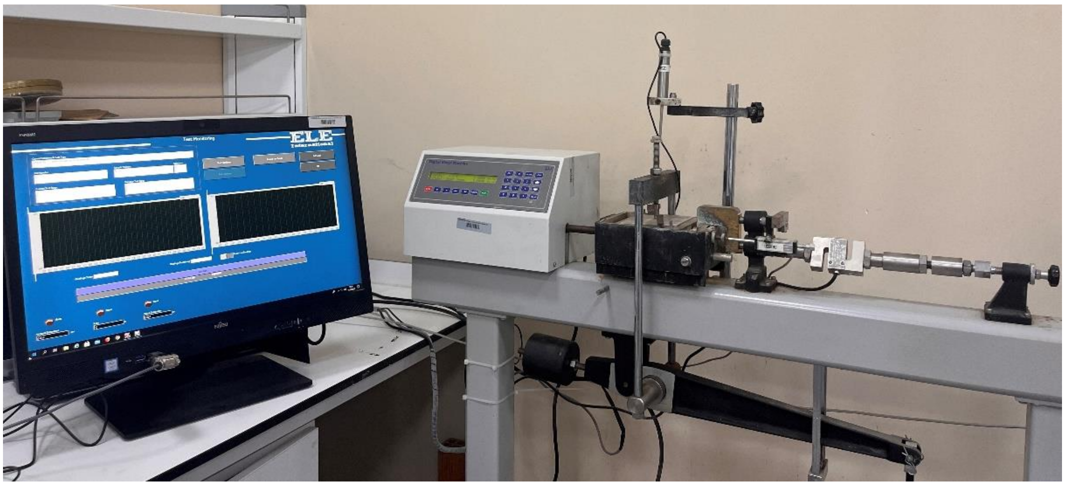

Figure 4.15: Computer-controlled automatic direct shear test device

4.2.3 Interface direct shear test of uncured GM and GTX

In order to obtain the interface shear strength parameters between GMs and GTXs, GM – GTX interface direct shear tests were carried out. Molds with the same dimensions as the lower and upper parts of the direct shear box were produced (Figure 4.16a). GM was placed at the bottom of the mold (Figure 4.16b), then the concrete prepared according to the C30 recipe was poured into the mold (Figure 4.16c). It was cured for 24 hours for the concrete to set. Then, GM adhered to the concrete block was placed at the bottom of the shear box and GTX was placed at the top of the GM, and soil was placed on the GTX (Figure 4.17a). In addition, in order to examine whether the soil at the top of the direct shear box affects the GM – GTX interface, the interface direct shear test was carried out by using concrete instead of the soil at the top (Figure 4.17b). Interface direct shear tests were carried out between nonwoven GTX and HDPE(T) under three different normal stress levels with a shear rate of 0.5 mm/min. A total of 18 experiments were carried out at this stage with six (five types of soils and concrete) interfaces and three normal stress levels. At the end of the tests interface friction angle (δ) values of GM – GTX interfaces.

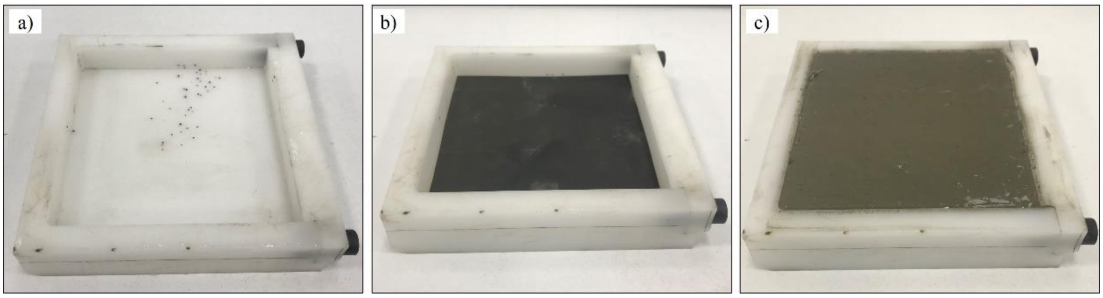

Figure 4.16: Concrete block production stages poured with geomembrane

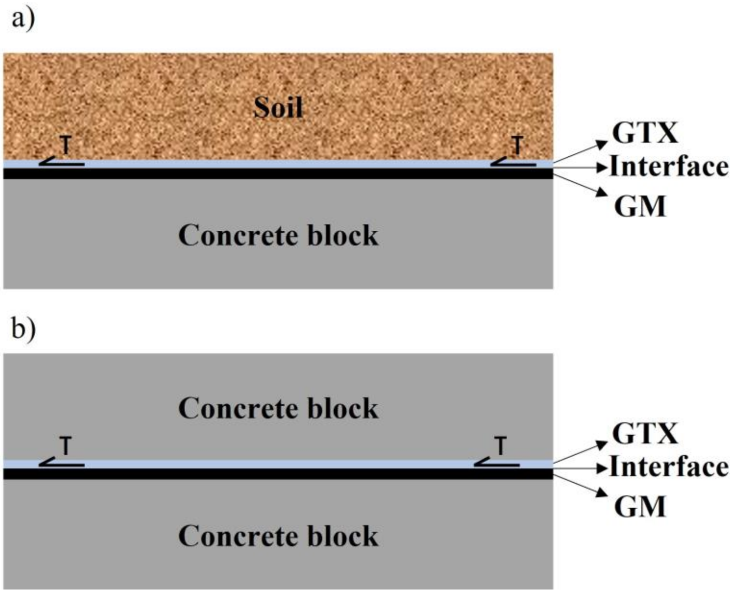

Figure 4.17: Schematic representation of interfaces a) GM – GTX interface with soil, b) GM – GTX interface without soil

As with the GM – GTX interface, first GM or GTX was placed under the mold, then concrete was poured on it and left to set for 24 hours (Figure 4.18a). Then, GM or GTX, which is attached to the concrete block, was placed on the lower part of the shear box (Figure 4.18b), and the soil was placed on the upper part (Figure 4.18c). The schematic representation of the interfaces is shown in Figure 4.19.

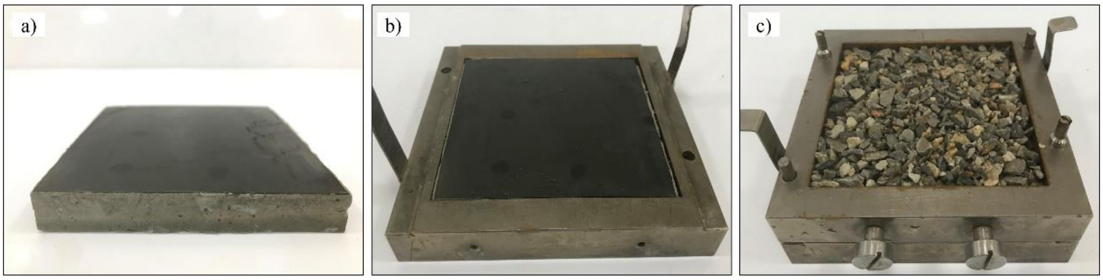

Figure 4.18: Interface direct shear test sample preparation steps

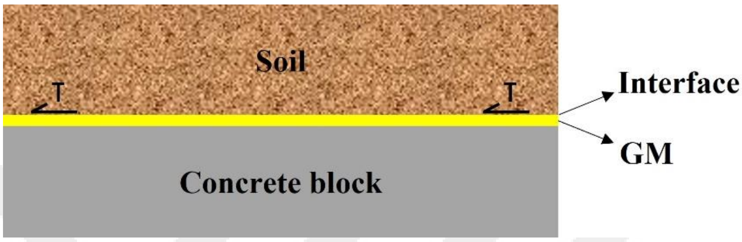

Figure 4.19: Schematic representation of soil – GM interface

To determine the interface shear strength parameters between GMs and soils, as well as GTXs and soils, interface direct shear tests were conducted following ASTM D5321 [64]. In all experiments, the soil was prepared at its optimum moisture content and placed inside the box at its maximum dry unit weight. Prior to each experiment, the samples were immersed in water for one hour to achieve 100% saturation. After each experiment, the water contents were checked, and it was observed that the saturation degree varied between 96 and 98%. Medium-scale direct shear tests were conducted under the influence of three different normal stress categories to investigate the behavior of GMs under varying normal stress values. These normal stress categories were classified as low (12.25 kPa, 24.5 kPa, 49 kPa), medium (49 kPa, 98 kPa, 196 kPa), and high (196 kPa, 392 kPa, 784 kPa). The shear rate applied was set at 0.5 mm/min for CS, CG, RS, RG interfaces, and 0.1 mm/min for LC and SB interfaces. At the conclusion of the tests, the interface friction angle (δ) values for uncured GM – soil and uncured GTX – soil interfaces were determined. A total of 36 interfaces and three normal stress categories resulted in a total of 108 medium-scale interface direct shear tests conducted at this stage. The interfaces established during this phase are summarized in Figure 4.20.

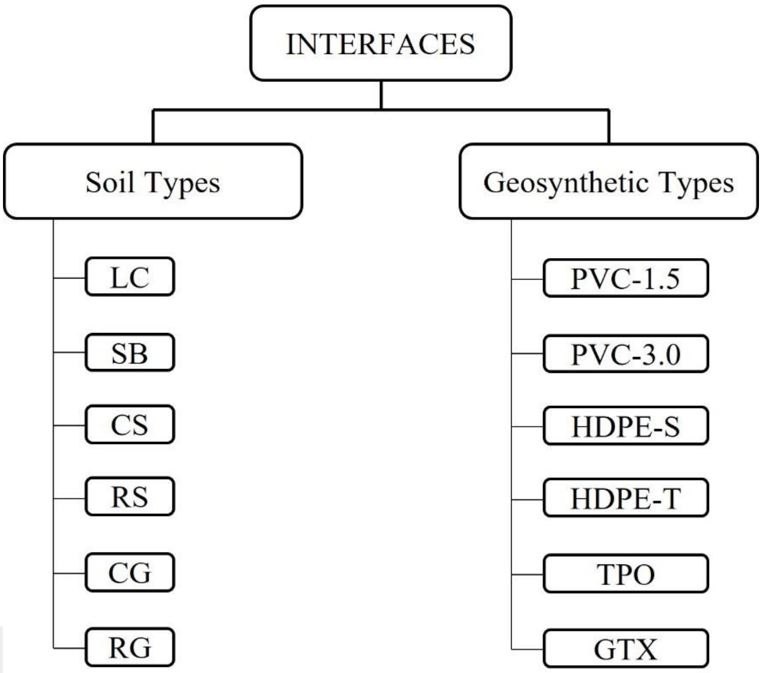

Figure 4.20: Interfaces of uncured direct shear experiments

4.2.4 Interface direct shear test of 4 months cured GM

In order to determine the effects of the curing liquid on the interface shear behavior of GM, PVC, and TPO were immersed in salt water (SWt), HDPE and TPO were immersed in leachates for 4 months. The curing process was carried out in airtight containers. It was cured by placing it on perforated platforms so that the GMs do not come into contact with each other, and the curing liquid contacts all parts of the GM. The curing liquid was re-prepared every month, and pH and electrical potential values were measured for control purposes. GMs that completed the curing process were removed from the liquid, dried, and subjected to the same procedures in the uncured interface direct shear tests. At this stage, the experiments were carried out only under the medium normal stress level (49, 98, 196 kPa). In addition, RG was excluded from the study as of the next part of the thesis, since the results obtained from the uncured tests were not sufficiently consistent and it was not a preferred soil type in the projects. Because HDPE is generally used in solid waste storage facilities to ensure the impermeability of leachate, SB, CS, RS, and CG soils were used with HPDE(S) and HDPE(T) GMs. Since PVC and TPO have more general usage areas, they were used with all soil types in interface direct shear tests. All interfaces created are summarized in Table 4.10. A total of 23 interfaces, four curing liquids, and one normal stress level, 54 medium scale interface direct shear tests were carried out at this stage.

Table 4.10: Interfaces used in the direct shear experiments for 4 months cured

Curing liquid	SWt		SWt, leachates	Leachates	Leachates
GM type	PVC(1.5)	PVC(3.0)	TPO	HDPE(S)	HDPE(T)
Soil type	Interfaces				
SB	x	x	x	x	x
CS	x	x	x	x	x
CG	x	x	x	x	x
RS	x	x	x	x	x
LS	x	x	x		

4.2.5 Interface direct shear test of 8 months cured GM

At this stage of the study, the GMs were cured for 8 months in SWt and leachates using the same method. However, this time, the interface direct shear tests were carried out under three normal stress levels (low, medium, high) in order to make comparisons with uncured samples. In addition, RS was excluded from the study as of the next part of the thesis, since the results obtained from the uncured and 4 months cured samples were not sufficiently consistent and it was not a preferred soil type in the projects. All interfaces created are summarized in Table 4.11. A total of 18 interfaces, four curing liquid and three normal stress level, 126 medium scale interface direct shear tests were carried out at this stage.

Table 4.11: Interfaces used in the direct shear experiments for 8 months cured

Curing liquid	SWt		SWt, leachates	Leachates	Leachates
GM type	PVC(1.5)	PVC(3.0)	TPO	HDPE(S)	HDPE(T)
Soil type	Interfaces				
SB	x	x	x	x	x
CS	x	x	x	x	x
CG	x	x	x	x	x
LS	x	x	x		

4.2.6 Interface direct shear test of 16 months cured GM

At this stage of the study, the GMs were cured for 16 months in SWt and leachates using the same method. Experiments were carried out only under the medium normal stress level, just like the samples cured for 4 months. All interfaces created are summarized in Table 4.12. A total of 18 interfaces, four curing liquid and one normal stress level, and 42 medium scale interface direct shear tests were carried out at this stage. With the completion of this stage, a total of 345 interface direct shear tests were conducted and this stage of the thesis was reached.

Table 4.12: Interfaces used in the direct shear experiments for 16 months cured

Curing liquid	SWt		SWt, leachates	Leachates	Leachates
GM type	PVC(1.5)	PVC(3.0)	TPO	HDPE(S)	HDPE(T)
Soil type	Interfaces				
SB	x	x	x	x	x
CS	x	x	x	x	x
CG	x	x	x	x	x
LS	x	x	x		

4.2.7 Surface properties

The situation of surface wear of GMs has been studied by many researchers [65–69]. Surface deformations, along with the fracture of GMs during interface shear experiments, are considered an indicator of post-peak strength reduction [70–73]. Therefore, measuring the surface roughness of GMs and explaining the deformation of the surface of the GM after peaking is very important to investigate the contribution of the GM – soil interface to the shear behavior. Previous studies have reported various methods to obtain GM surface profiles. One of them, Stylus profilometers, is used to obtain 2D interface information of the entire profile line [74,75]. But this method has the same problems such as limited vertical movement and possible damage to the surface of the GM by probe [76]. The other method is image analysis. Clear images were obtained by image analysis on the GM profile [71,77]. Another method is image analysis which is performed directly on the GM surface by non-contact digital imaging techniques such as optical microscopy, scanning electron microscopy, and atomic force microscopy. This method can avoid the limitations of the above measurement methods and different roughness parameters can be used to evaluate the surface roughness of interfaces between GM – soil [78–80].

In this study, the surface deformations of GMs, which were cured for 16 months and then subjected to interface direct shear tests, were investigated. Firstly, microscopic images (500x magnification) of the GM samples curing 16 months in SWt and leachates were taken from the Nikon Eclipse LV150N device (Figure 4.21) to prove this effect physically and images were processed with Clemex Vision Lite software. Microscopic images were analyzed with image processing techniques in ImageJ software (black and white treshold). The ratio of black areas to white areas was calculated using the ImageJ software. Black areas represent deformed areas, while white areas represent undeformed areas. In addition, the roundness of the deformed areas was calculated and thus it was aimed to establish a relation with the angularity of the soil particles.

Figure 4.21: Upright metallurgical LED microscope

Secondly, the surface roughness of the samples was measured with an optical profilometer (OPM) after direct shear tests to determine the damage caused by the leachates on the surface of the GMs. A profilometer is a measuring instrument used to measure a surface's profile, in order to quantify its roughness. Critical dimensions such as step, curvature, and flatness are computed from the surface topography. The OPM analysis was conducted in TOTOMAK A.Ş. with a Mahr profilometer device (Figure 4.22). The measurements were made by dividing the diagonal of the GM by three and the average of the three values obtained was taken. In the measurements, both maximum (R_{max}) and average (R_a) roughness values were obtained (Figure 4.23). The OPM analyzes were carried out with PVC(1.5), PVC(3.0), HDPE(S), HDPE(T), and TPO GMs cured for 16 months. Surface roughness measurements were made after the interface direct shear tests with LS, SB, CS, and CG soils.

Figure 4.22: Profilometer device

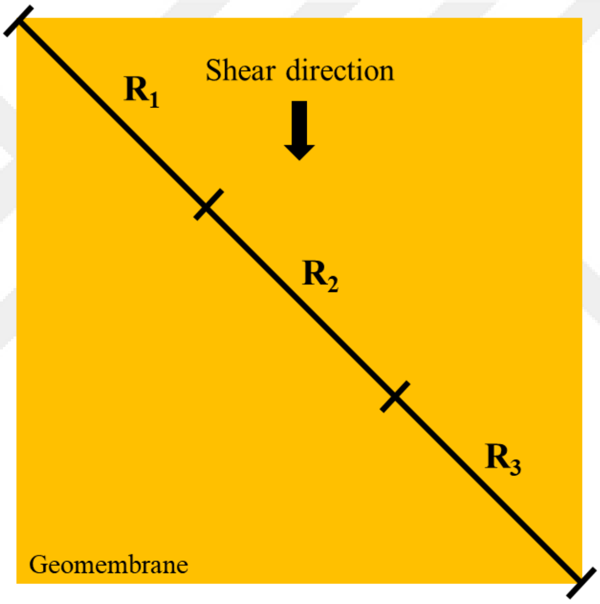

Figure 4.23: Area and direction of the profilometer measurement

4.2.8 Finite element method analysis

In the last stage of the thesis, it was desired to verify the results obtained from the interface direct shear experiments by establishing a numerical model. For this purpose, only experiments with 16 months of cured samples were modeled using Plaxis 2D software. The experiments were modeled as a slope stability analysis to represent solid waste storage facilities.

The interface direct shear tests were tried to be modeled as a slope stability analysis. For this purpose, a compactible clay liner was placed at the bottom, and the soils (LC, SB, CS, CG) used in this study was placed on the top. The cohesion of the compactible clay liner used is 35 kPa, the internal friction angle is 15° and the permeability is 10^{-6} mm/s. The properties of the soil on the GM were obtained from the soil – soil interface direct shear tests. Different GMs (PVC(1.5), PVC(3.0), HDPE(S), HDPE(T), TPO) were placed between the two soil layers created. Elastic behavior was selected as GM material and stiffness (EA) values obtained from factory data were entered. The EAs of TPO, HDPE, PVC(1.5), and PVC(3.0) are 3000, 3715, 6000, and 8000 kN/m, respectively. A positive interface assigned between the soil in the upper layer and the GM (Figure 4.24). A soil with the parameters (δ, α, R_{int}) obtained from the interface direct shear tests is assigned to this positive interface so that the experiment is exactly modeled. R_{int} is obtained by dividing the tangent of the interface friction angle by the tangent of the internal friction angle ($R_{int} = \tan\delta/\tan\phi$).

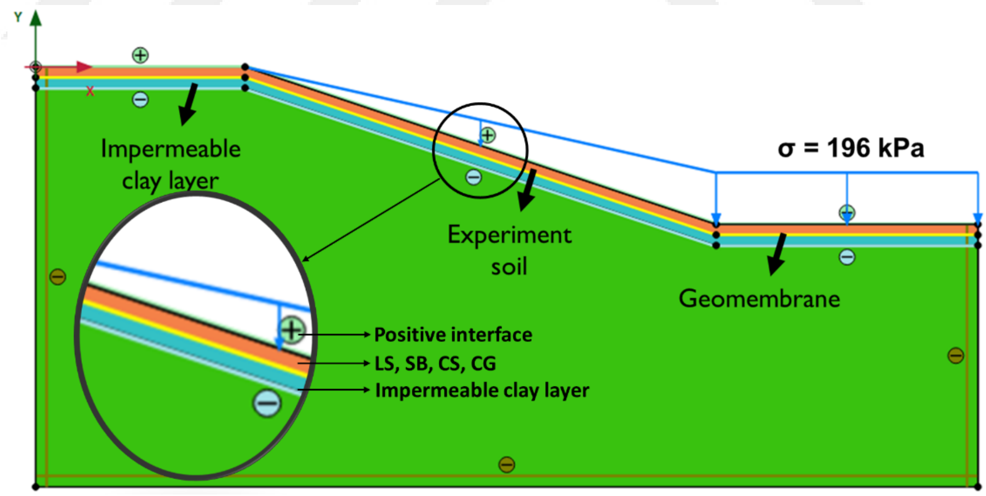

Figure 4.24: Plaxis 2D model of interface direct shear tests as a slope model

Figure 4.25 presents a summary of the parameters investigated in the thesis, including soil type, GS type, normal stress level, curing liquid, and curing time.

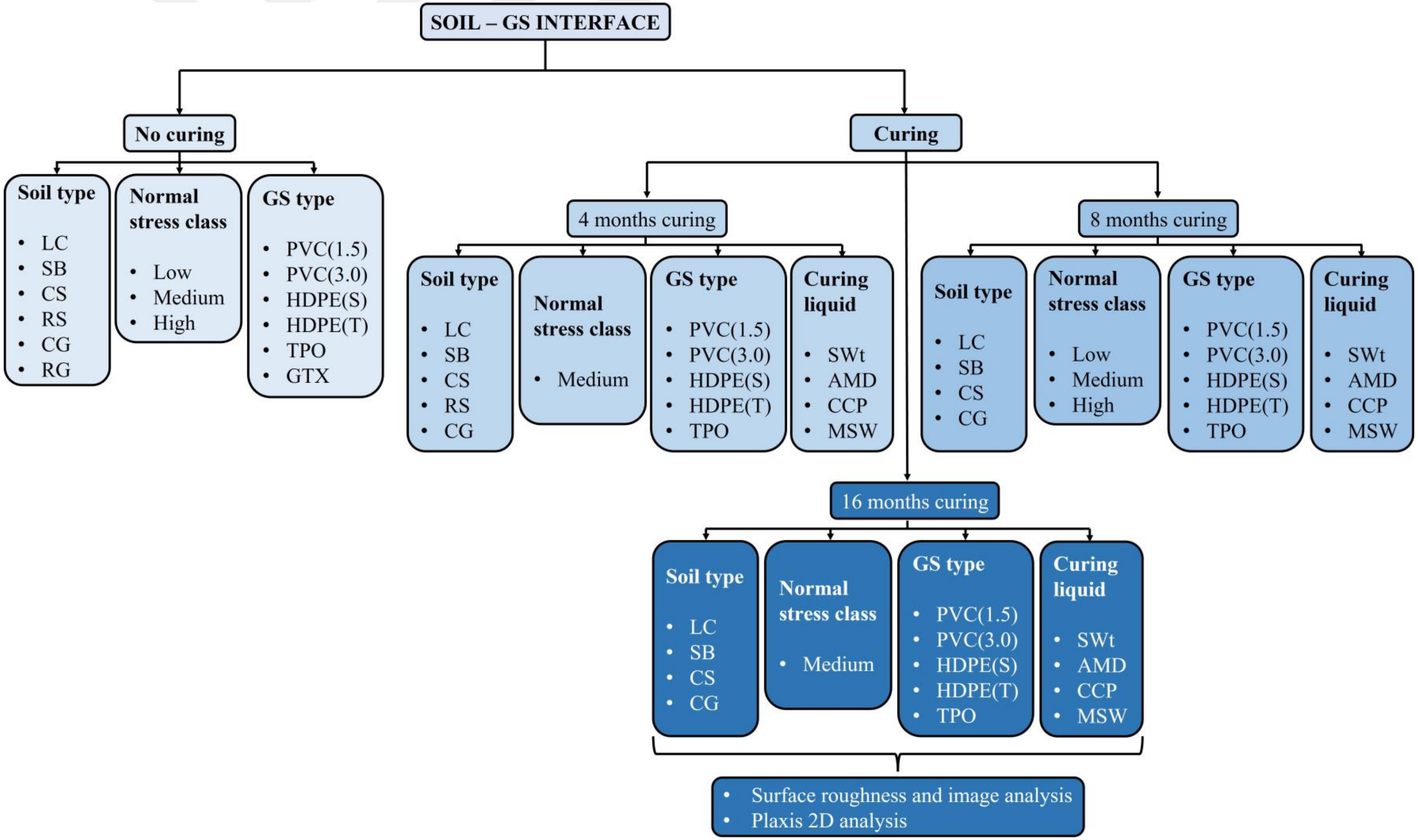

Figure 4.25: Summary of the parameters (soil type, GS type, normal stress level, curing liquid, curing time)

Chapter 5

Results and Discussions

5.1 Geotechnical index and shear strength properties

The grain size distributions of the soils obtained from sieve and hydrometer analysis are shown in Figure 5.1. While there was a uniform distribution in fine grained soils, there was no uniform distribution in coarse grained soils.

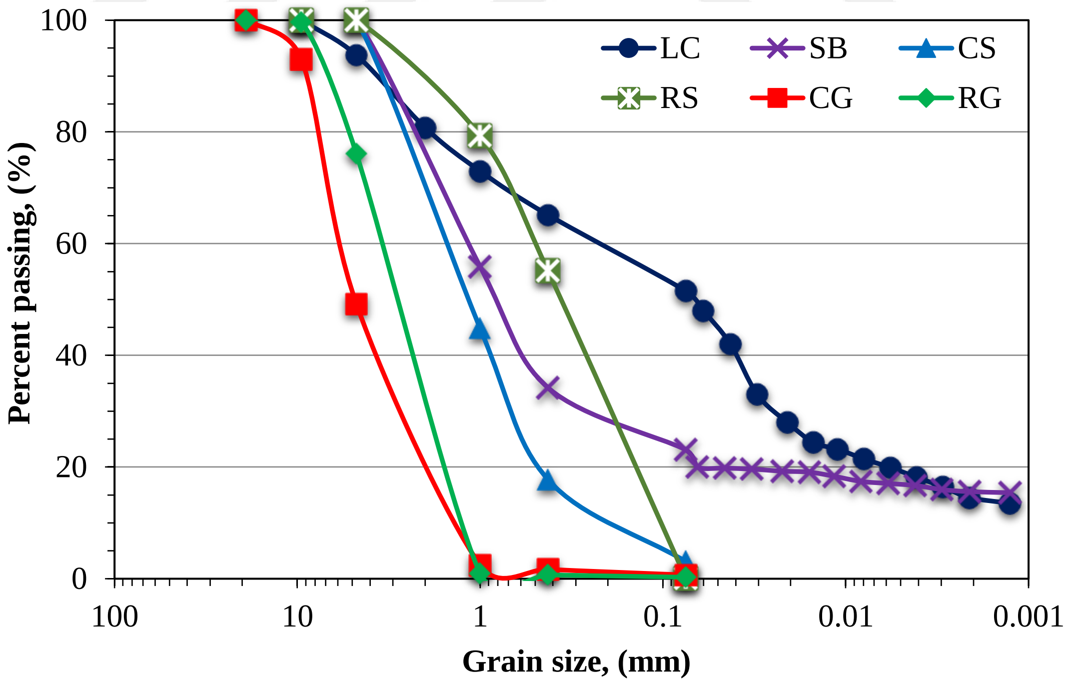

Figure 5.1: Grain size distributions of LC (Low plasticity clay), SB (Sand/Bentonite), CS (Crushed sand), RS (River sand), CG (Crushed gravel), and RG (River gravel)

The geotechnical index properties obtained from laboratory tests are listed in Table 5.1. The soil classes determined using the Unified Soil Classification System (USCS) system according to the ASTM D2487 [81] standard are also shown in Table 5.1.

Table 5.1: Geotechnical index parameters of soils

Property	LC*	SB*	CS*	RS*	CG*	RG*
Specific gravity, G_s	2.60	2.46	2.68	2.67	2.56	2.47
Liquid limit, LL (%)	30.7	60.7	-	-	-	-
Plastic limit, PL (%)	21.1	30.2	NP	NP	NP	NP
Max. dry unit weight, $\gamma_{dry,max}$ (kN/m^3)	19.0	17.5	17.3	17.2	17.1	17.0
Opt. moisture content, w_{opt} (%)	1.3	13.2	11.2	11.7	6.5	4.7
D_{10}	-	-	0.19	0.11	1.29	1.10
D_{30}	0.023	0.20	0.69	0.19	2.77	1.90
D_{60}	0.21	1.50	1.70	0.50	5.95	3.64
Coefficient of uniformity, C_u	-	-	8.95	4.55	4.61	3.31
Coefficient of curvature, C_c	-	-	1.47	0.66	1.00	0.90
USCS	CL	SC	SW	SP	GW	GP
pH	8.8	9.3	8.1	7.8	8.7	7.9

*LC: Low plasticity clay, SB: Sand/Bentonite, CS: Crushed sand, RS: River sand, CG: Crushed gravel, RG: River gravel

Mohr – Coulomb (MC) failure envelopes were drawn to determine the internal friction angles. MC envelopes were drawn separately for each normal stress level, as well as a single envelope for all normal stress levels. MC envelopes for all normal stress levels separately are shown in Figure 5.2. In addition, the internal friction angles obtained from all envelopes are listed in Table 5.2.

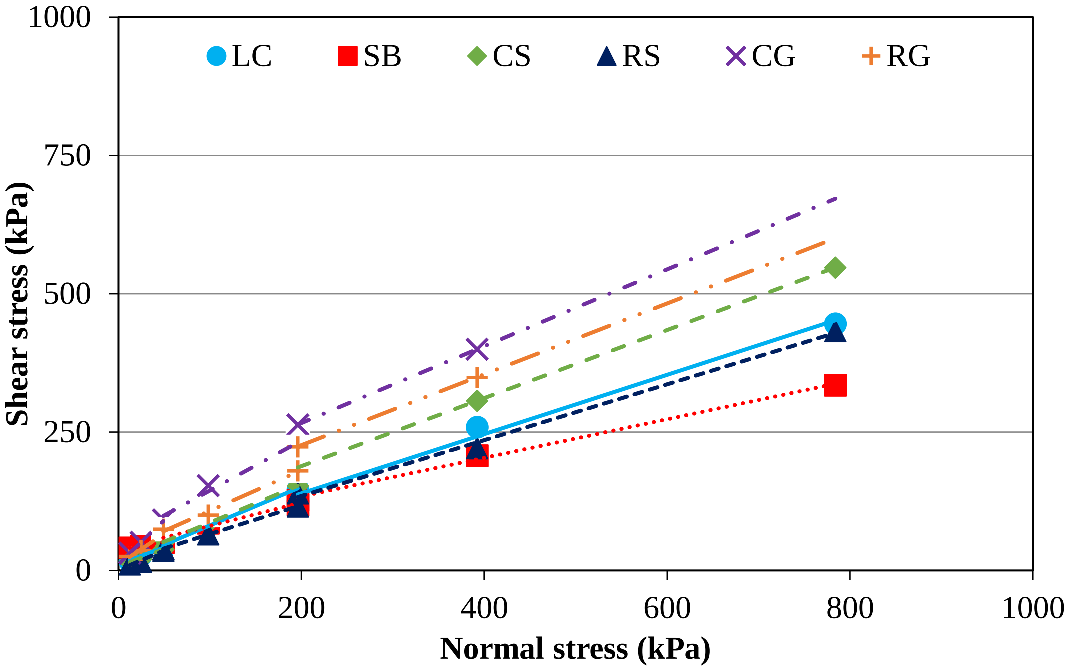

Figure 5.2: Mohr – Coulomb failure envelopes of soils

Table 5.2: Internal friction angles of soils

Soil	Normal stress level			One envelope
	Low	Medium	High	
LC	31.5	34.9	28.2	29.2
SB	15.7	22.8	19.2	22.6
CS	32.4	34.7	31.6	34.9
RS	35.3	27.6	26.8	33.5
CG	57.5	42.1	34.8	44.0
RG	48.0	36.2	32.6	40.6

Table 5.2 shows that soils with coarse and angular grains have higher internal friction angles than soils with fine and rounded grains. It is a known fact that the shear strength parameters of coarse and angular grained soils are higher than fine and rounded grained soils [82–84]. Simoni and Houlsby (2006) showed that the shear strength, constant volume strength, and maximum expansion ratio of the samples were higher even at low gravel fractions (10.2%) compared to 87 large-scale direct shear tests on sand – gravel mixtures for pure sand at the same density [83]. To the

same conclusion, Liu et al. (2006) have reached their conclusion by performing reverse direct shear, ring shear, and triaxial compression experiments with samples with gravel content ranging from 0 to 40% by weight [84]. Prakasha and Chandrasekaran (2005) found that sand particles in clay – sand mixtures reduce the void ratio, and increase friction and pore pressure response, resulting in a decrease in undrained shear strength [82]. Studies in the literature have also accepted that particle shape is an important factor affecting the shear strength behavior of soils [85–87]. Studies have shown that increasing angularity and decreasing roundness and sphericity lead to an increase in maximum (e_{max}) and minimum (e_{min}) void ratios [88,89]. Flat particles in soils, namely clay particles, cause a decrease in density, stiffness, and constant volume strength, while angular particles have the opposite effect [89–91]. Also, in coarse grained soils (CS, RS, and CG), the internal friction angle decreased as the normal stress level increased. The reason for this is that under high normal stresses, coarse grains break and break into finer grains, and also the grains are mobilized. In addition, it was determined that the internal friction angles increased as the grain size and angularity increased according to the single envelope internal friction angles. This is in parallel result with the previously mentioned shear strengths.

5.2 Direct shear test results of HDPE(T) – GTX interfaces

GTX is usually placed on the GMs used for sealing purposes in solid waste storage areas and as a drainage layer. The type of GTX used is usually nonwoven and textured HDPE is used as GM in order to better adhere to the GTX surface. In this section, direct shear test results of the HDPE(T) – GTX interface have been summarized. At the bottom of the direct shear box were the GM attached to the concrete block, the GTX at the top, and the soil above it (Figure 4.17a). In addition, in order to examine whether there was any effect of the soil on the upper part, an interface test was also carried out with the GM adhered to the concrete block at the bottom and this time with the GTX adhered to the concrete block at the upper part (Figure 4.17b). The shear stress – strain graphs of HDPE(T) – GTX interface with soils are shown in Figure 5.3. All results are very close to each other in HDPE(T) –

GTX(soil) interfaces. In other words, the conclusion drawn here is that the soil used on the GTX in such interfaces does not affect the interface shear behavior. However, the friction angle of the HDPE(T) – GTX(concrete) interface is quite high compared to the others (Table 5.3). The reason for this is that the concrete is much more rigid than the soil and increases the interface friction forces due to the pressure it exerts on the GTX with normal stress.

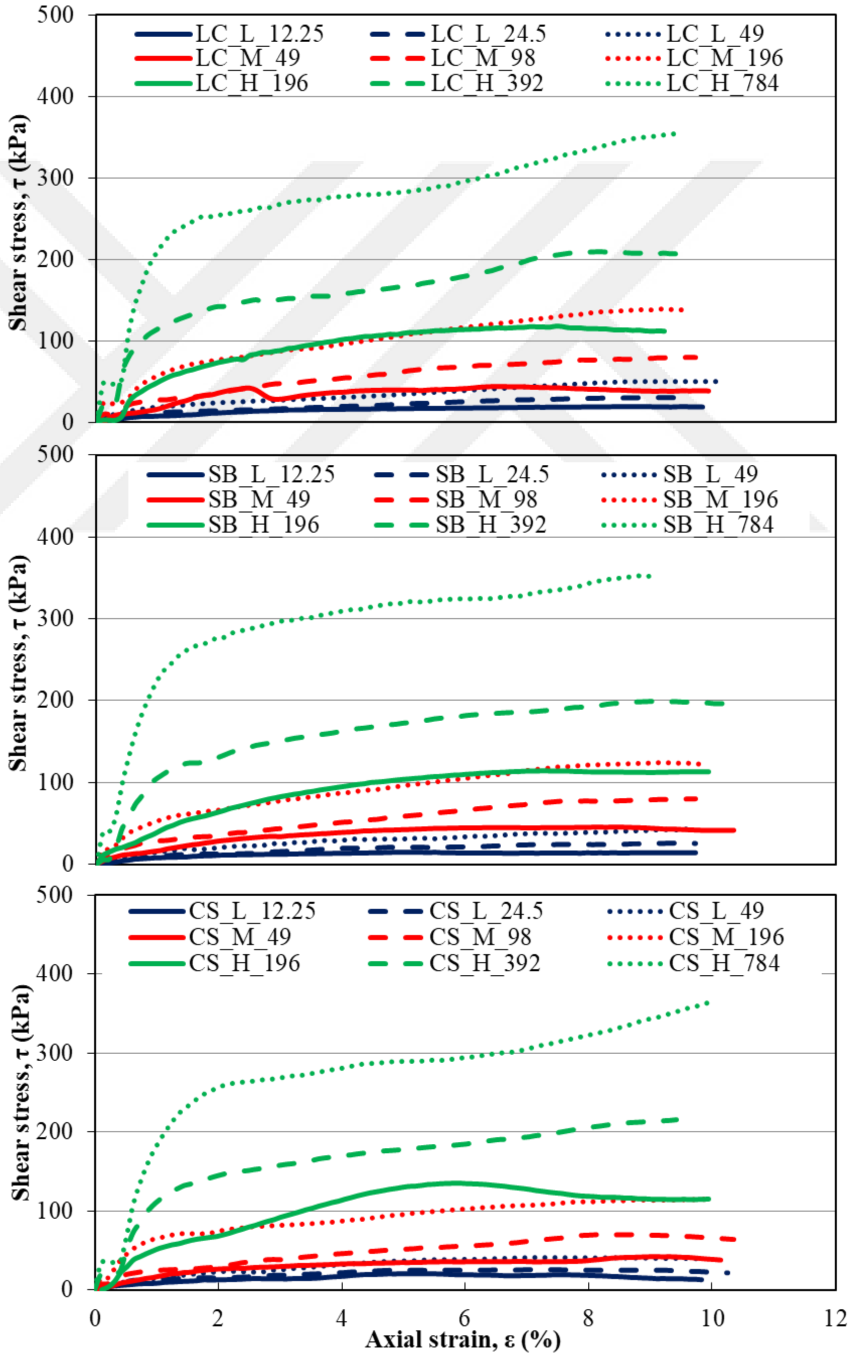

Figure 5.3: Shear stress (τ) – strain (ε) graphs of GM – GTX interface with soils

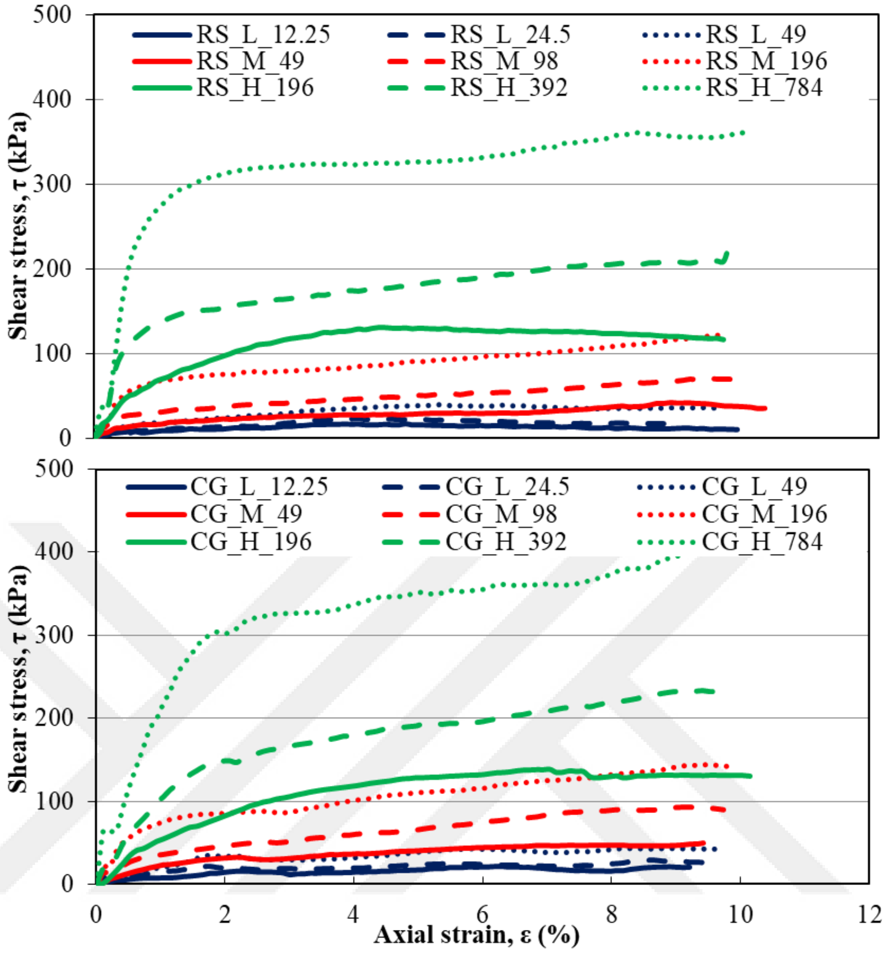

Figure 5.3 (continued): Shear stress (τ) – strain (ε) graphs of GM – GTX interface with soils

MC envelopes were drawn to determine the interface friction angles. MC envelopes for all normal stress levels separately are shown in Figure 5.4. In addition, the internal friction angle values obtained from the envelopes are listed in Table 5.3.

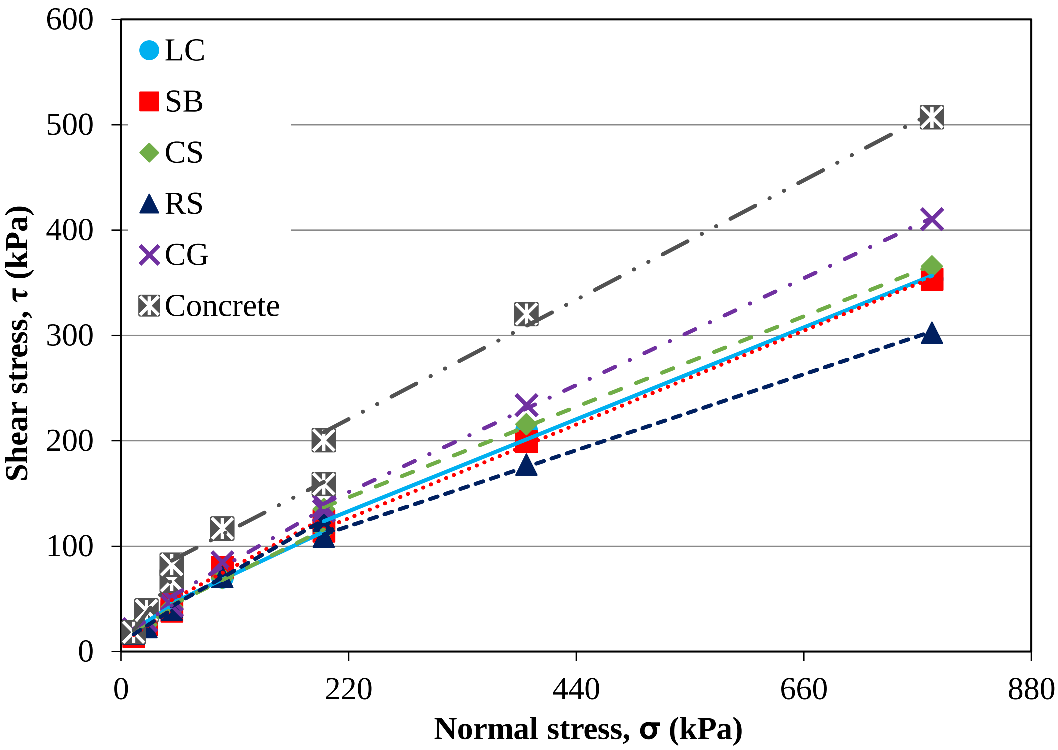

Figure 5.4: Mohr-Coulomb failure envelopes of GM – GTX

Table 5.3: Friction angles of GM – GTX interfaces

Interface	Normal stress level			One envelope
	Low	Medium	High	
GM – GTX(LC)	31.5	24.8	21.6	23.4
GM – GTX(SB)	32.4	27.9	22.0	23.3
GM – GTX(CS)	29.5	26.1	21.3	24.3
GM – GTX(RS)	32.4	29.1	18.1	20.1
GM – GTX(CG)	31.0	29.5	24.8	26.7
GM – GTX(Concrete)	31.5	26.9	27.3	31.9

As seen in both Figure 5.4 and Table 5.3, the friction angles of all interfaces were obtained very close to each other. This is because the upper soil does not affect the GM – GTX interface. The reason why the soil has no effect is that the density and thickness of the nonwoven GTX are high and dampen the effect of the soil from above on the GTX surface. However, since the density and stiffness of the concrete are very high compared to the soil and GTX, the concrete block placed on the GTX caused an increase in the interface friction angle. The reason why the interface friction angle decreases as the normal stress increases is that the notches of HDPE(T) GM adhere to the GTX surface without being damaged at low normal stresses, thus increasing the interface friction force. At high normal stress values, the notches on the surface of HDPE(T) GM are crushed and the GM becomes almost smooth.

5.3 Direct shear test results of uncured GM – soil interfaces

The shear stress – strain graphs of uncured PVC(1.5) – soil interface are shown in Figure 5.5. The maximum capacity of the load cell of the direct shear device used in the experiments is 5000 N. For this reason, the test was stopped manually in the samples whose shear force exceeded 5000 N during the test. The black crosses in the graphs are samples with this condition. When the shear strength values for all types of surfaces are arranged from lowest to highest, the situation is as follows: LC, SB, RS, CS, RG, and CG. Relatively larger particles require a greater amount of frictional force in order to reach a state of sliding and to continue rolling once the interlocking is released [59]. In comparison to fine and rounded grained soils, coarse and angular grained soils have less spherical, less rounded, and less regular particles. These angular particles are capable of forming deeper grooves and exerting a higher interface friction angle by plowing through the surface [16, 21, 26, 98]. Several studies conducted by Fleming et al. [11], and Adamska [27] have reported that higher values of interfacial friction angles are achieved at higher void ratios of soils. The void ratio values of LC, SB, RS, CS, RG, and CG are 0.218, 0.339, 0.437, 0.514, 0.549, and 0.562. This is attributed to the increased contact area between the soil grains and the surface of the GM (presumably a material or substrate), leading to enhanced interface shear strength. The findings of this study align with the aforementioned conclusions.

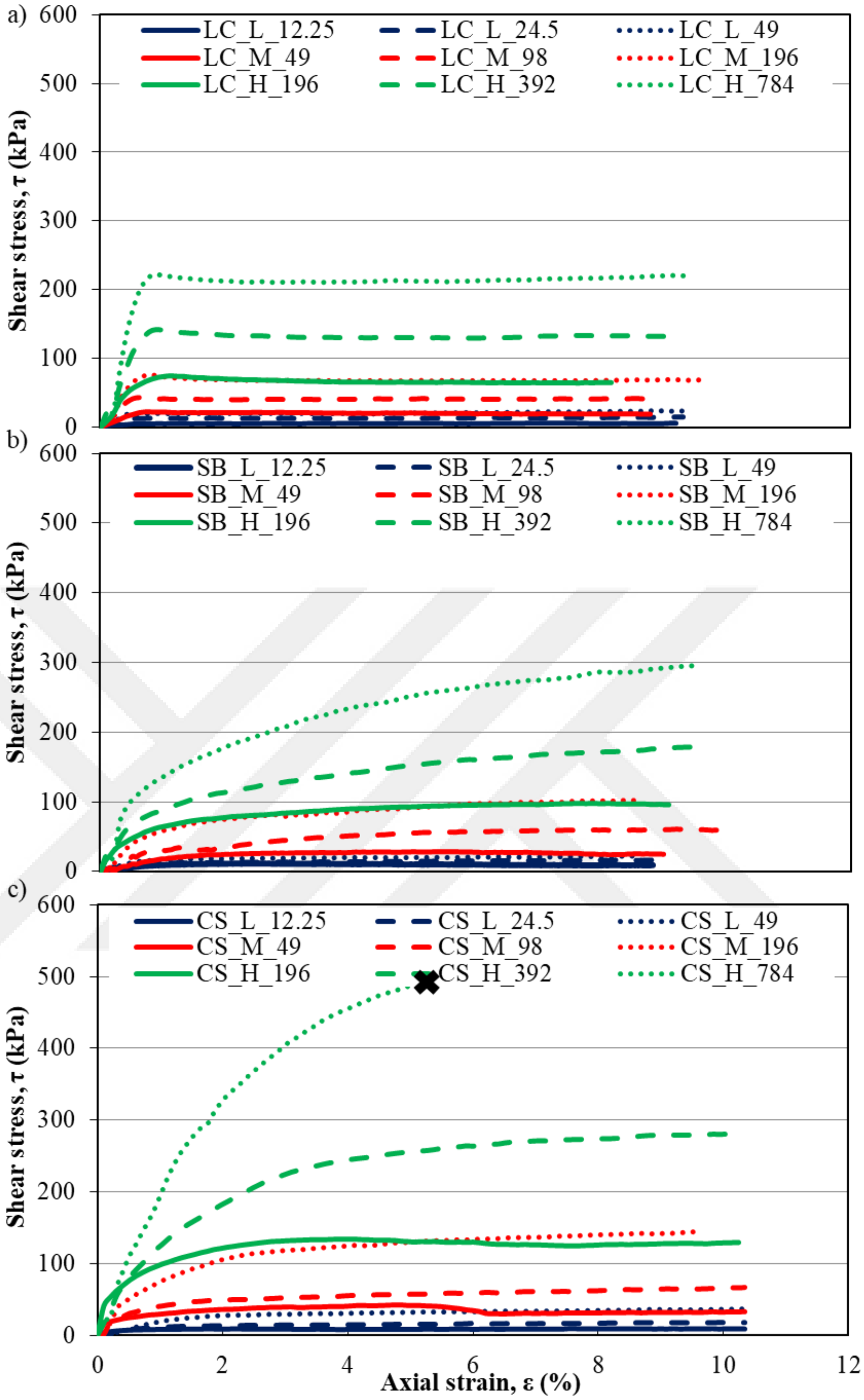

Figure 5.5: Shear stress (τ) – strain (ε) graphs of PVC(1.5) – soil interface

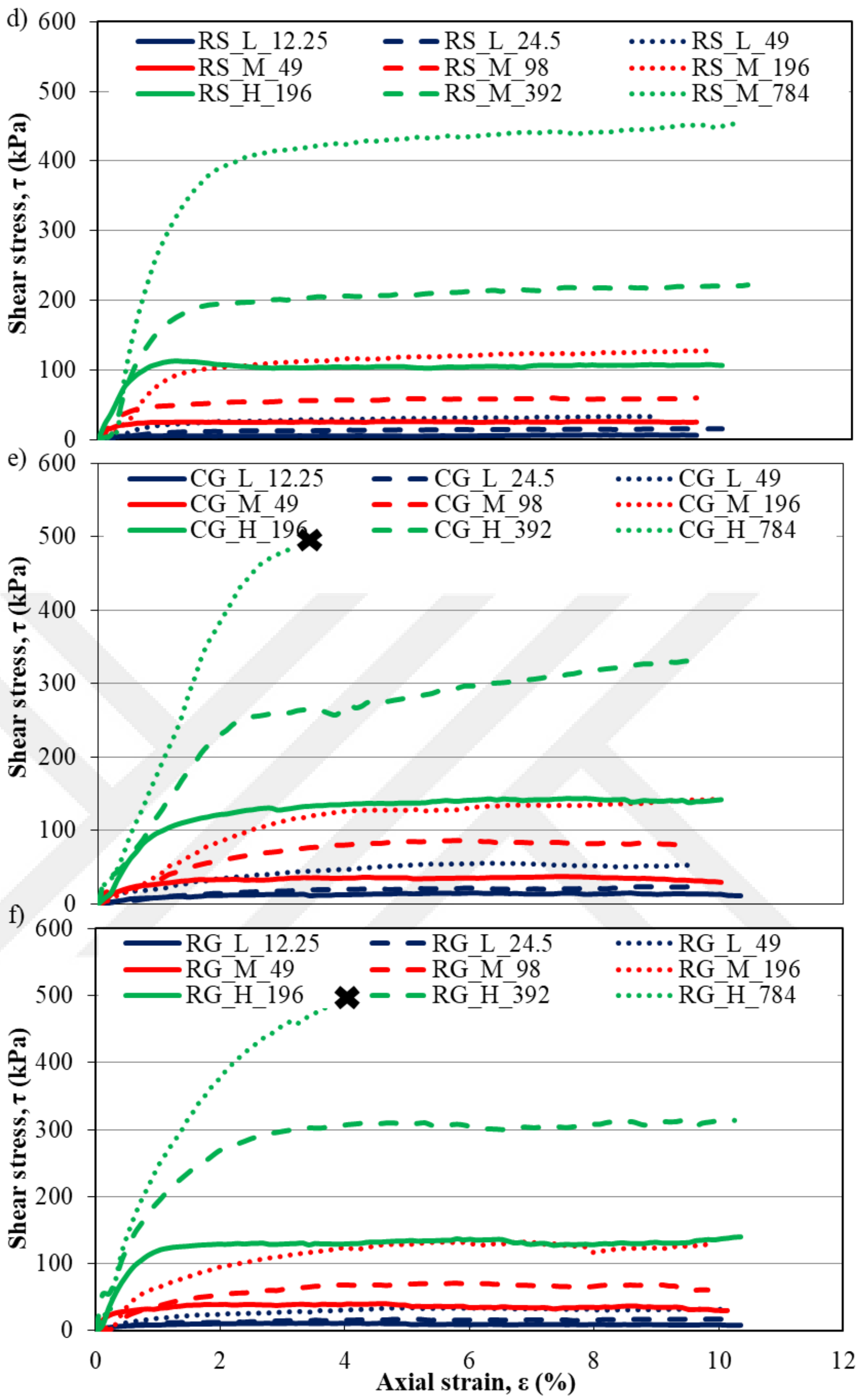

Figure 5.5 (continued): Shear stress (τ) – strain (ε) graphs of PVC(1.5) – soil interface

MC envelopes for all normal stress levels separately are shown in Figure 5.6. In addition, the interface friction angle values obtained from the envelopes are listed in Table 5.4

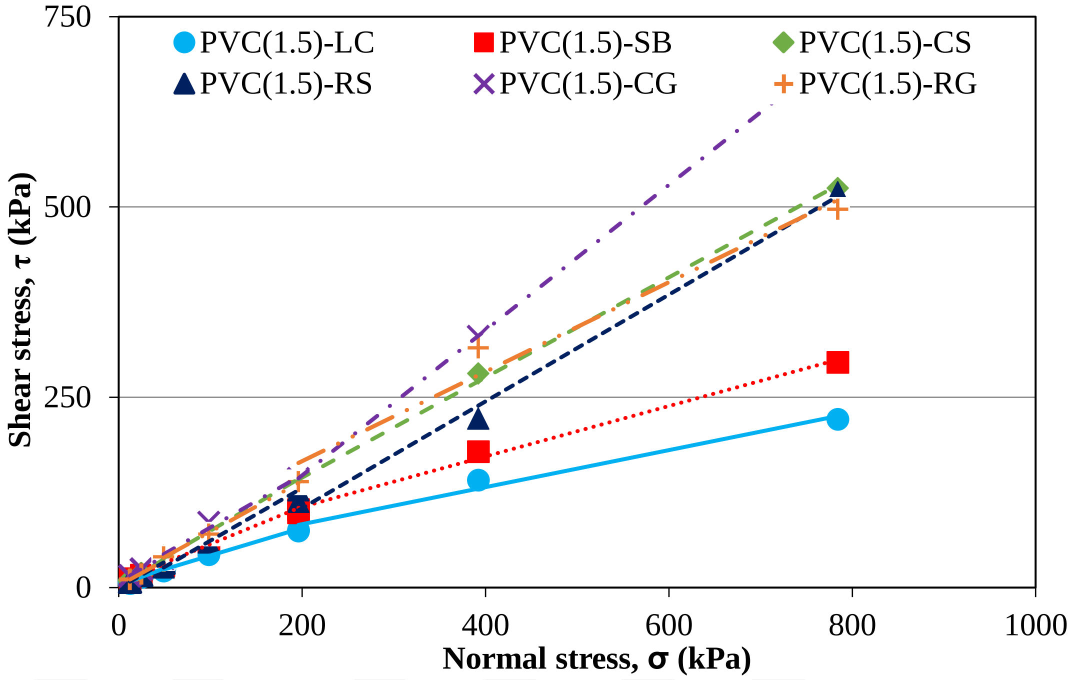

Figure 5.6: Mohr – Coulomb failure envelopes of PVC(1.5) – soil

Table 5.4: Friction angles of PVC(1.5) – soil interfaces

Interface	Normal stress level			One envelope
	Low	Medium	High	
PVC(1.5) – LC	34.2	19.9	13.7	15.7
PVC(1.5) – SB	27.4	26.3	18.3	20.4
PVC(1.5) – CS	37.0	35.3	33.3	33.9
PVC(1.5) – RS	34.3	34.6	35.0	33.1
PVC(1.5) – CG	34.2	34.7	43.7	39.0
PVC(1.5) – RG	33.4	33.6	41.9	33.1

The shear stress – strain graphs of uncured PVC(3.0) – soil interface are shown in Figure 5.7.

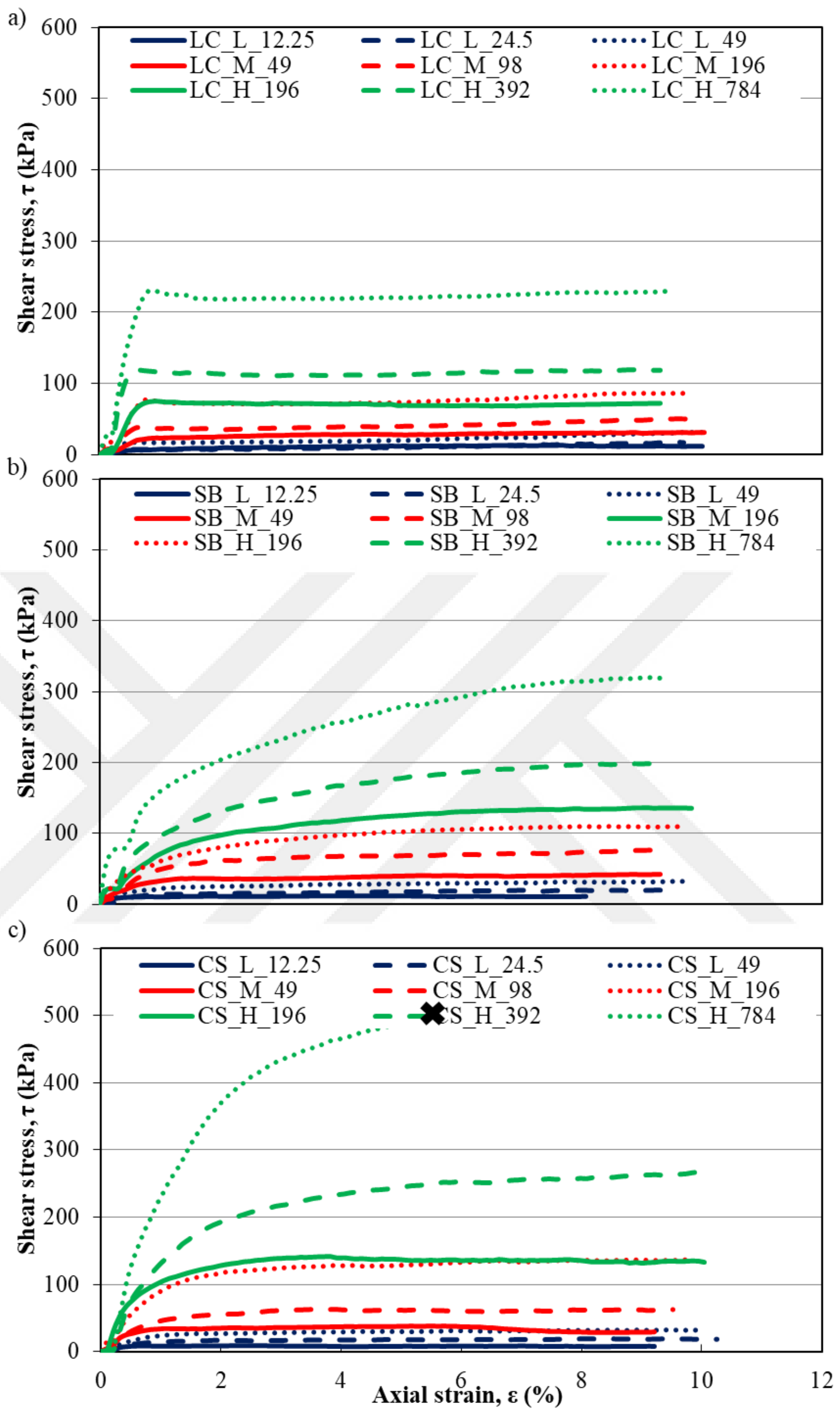

Figure 5.7: Shear stress (τ) – strain (ε) graphs of PVC(3.0) – soil interface

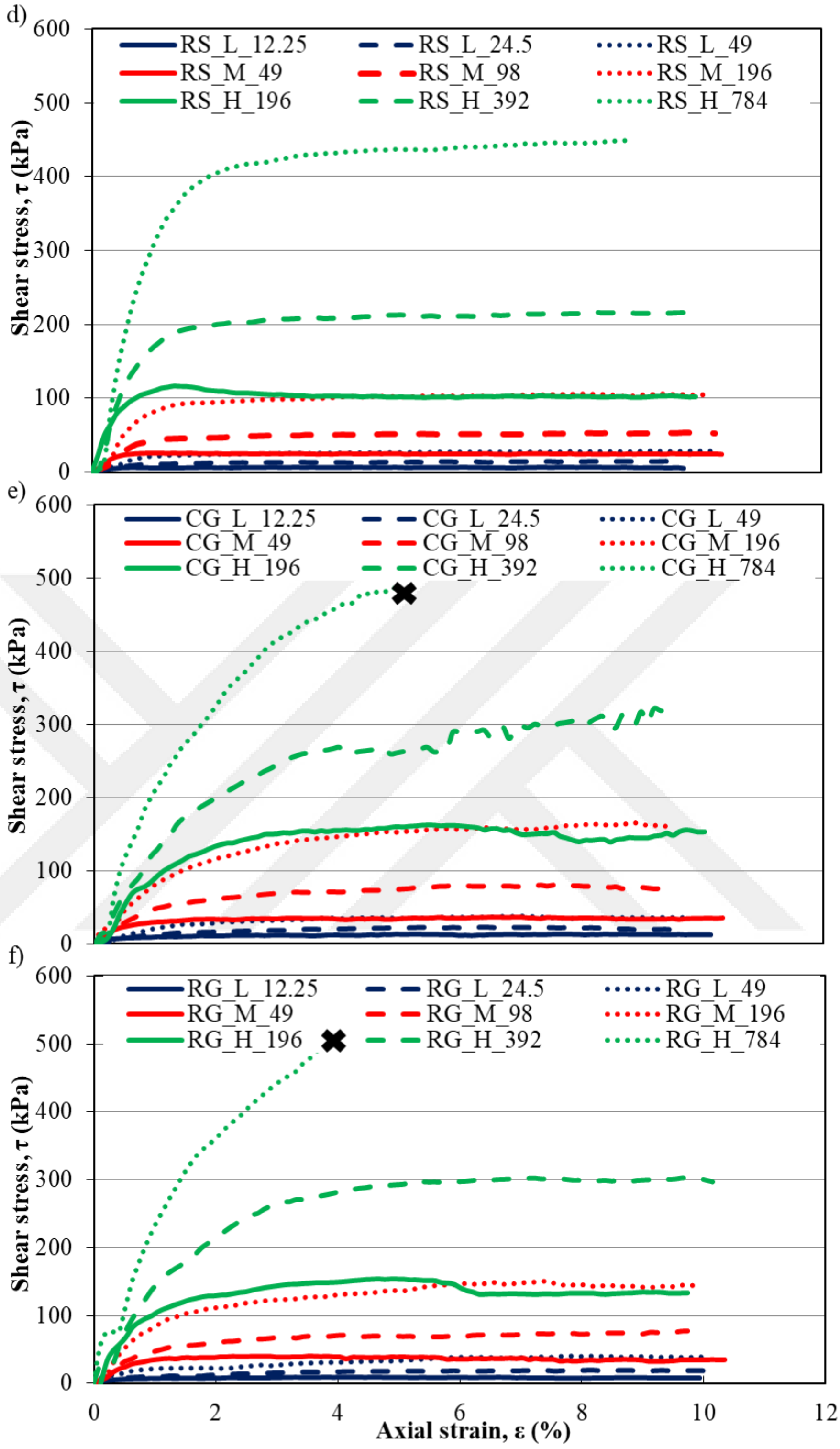

Figure 5.7 (continued): Shear stress (τ) – strain (ε) graphs of PVC(3.0) – soil interface

MC envelopes for all normal stress levels separately are shown in Figure 5.8. In addition, the interface friction angle values obtained from the envelopes are listed in Table 5.5.

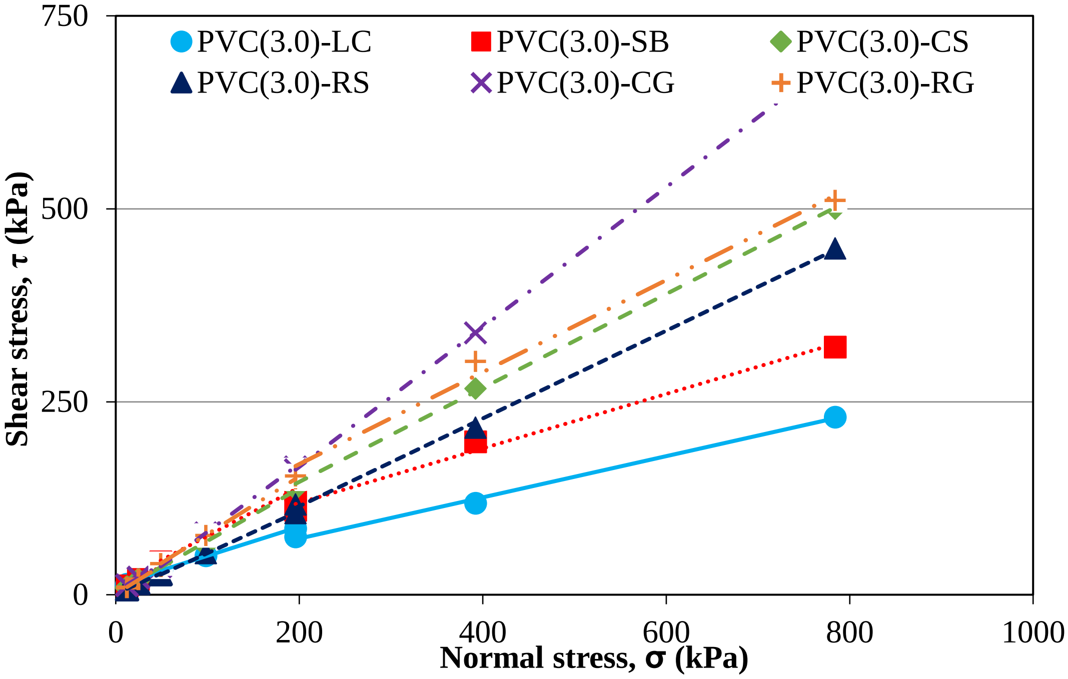

Figure 5.8: Mohr – Coulomb failure envelopes of PVC(1.5) – soil

Table 5.5: Friction angles of PVC(3.0) – soil interfaces

Interface	Normal stress level			One envelope
	Low	Medium	High	
PVC(3.0) – LC	28.1	20.6	14.9	15.3
PVC(3.0) – SB	33.8	32.2	19.4	21.7
PVC(3.0) – CS	35.3	34.2	32.9	32.6
PVC(3.0) – RS	28.2	28.7	29.6	29.7
PVC(3.0) – CG	34.8	41.3	42.2	40.8
PVC(3.0) – RG	36.4	36.7	37.2	33.5

The shear stress – strain graphs of the uncured HDPE(S) – soil interface are shown in Figure 5.9.

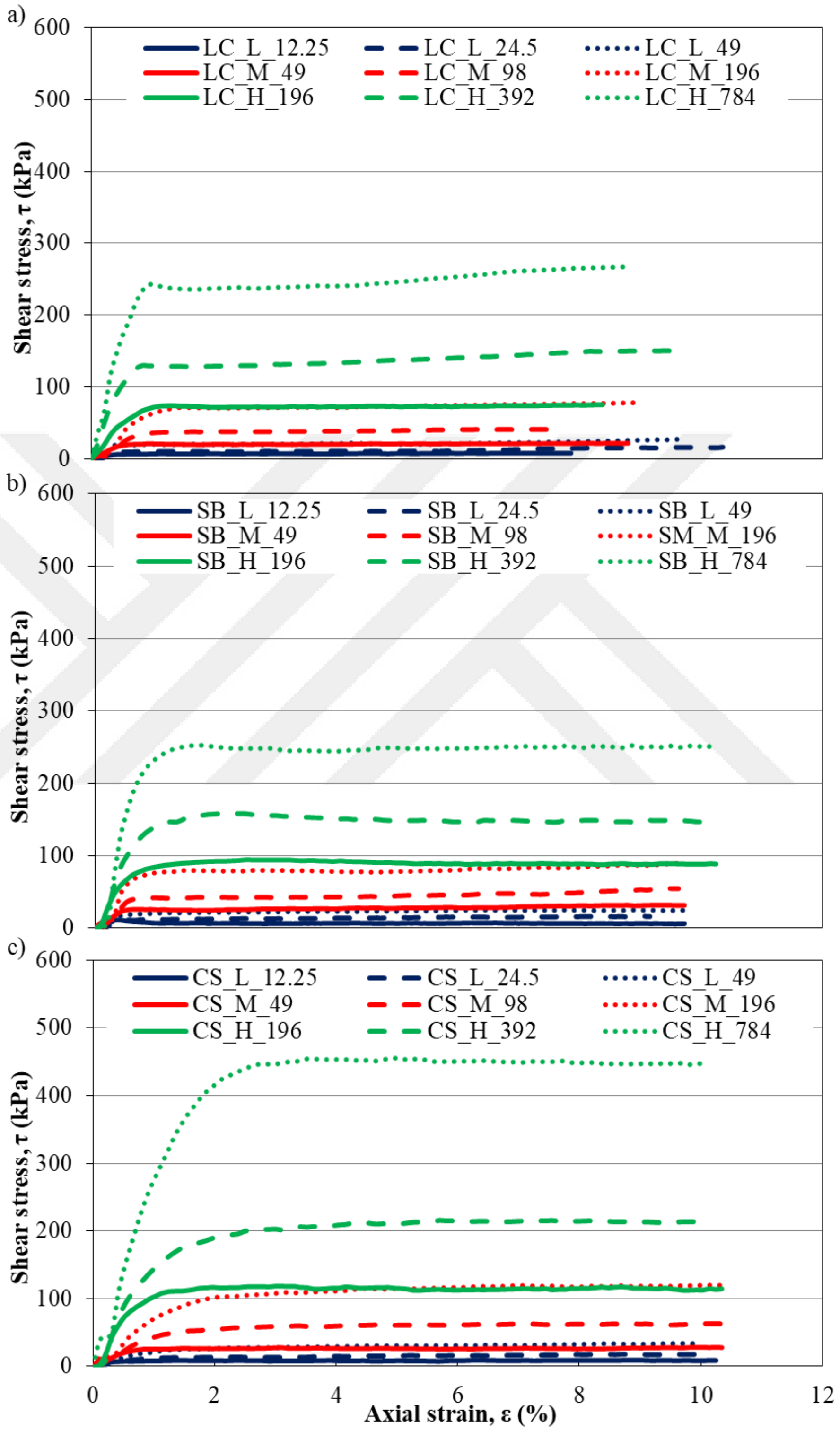

Figure 5.9: Shear stress (τ) – strain (ε) graphs of HDPE(S) – soil interface

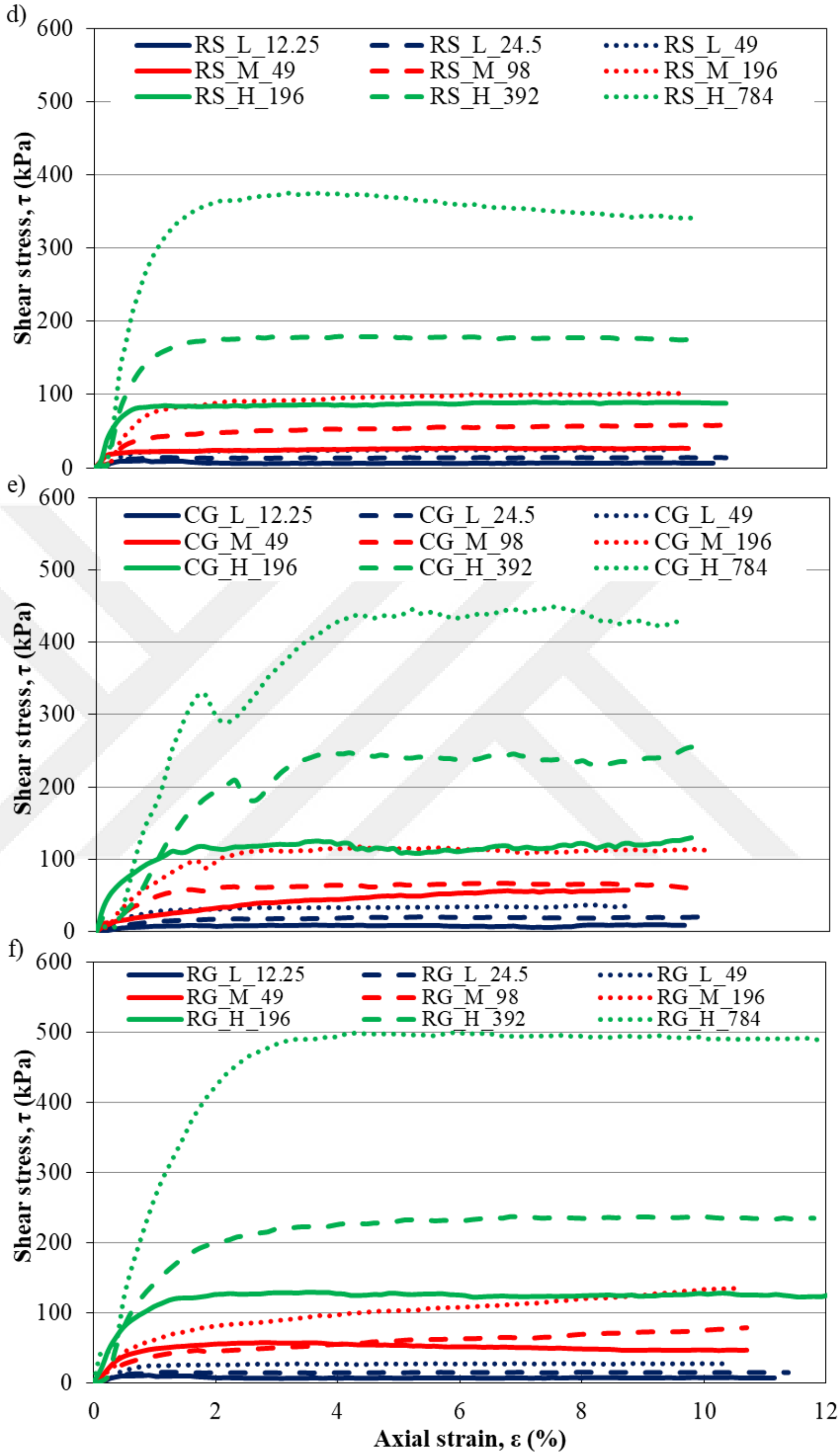

Figure 5.9 (continued): Shear stress (τ) – strain (ε) graphs of HDPE(S) – soil interface

MC envelopes for all normal stress levels separately are shown in Figure 5.10. In addition, the interface friction angle values obtained from the envelopes are listed in Table 5.6

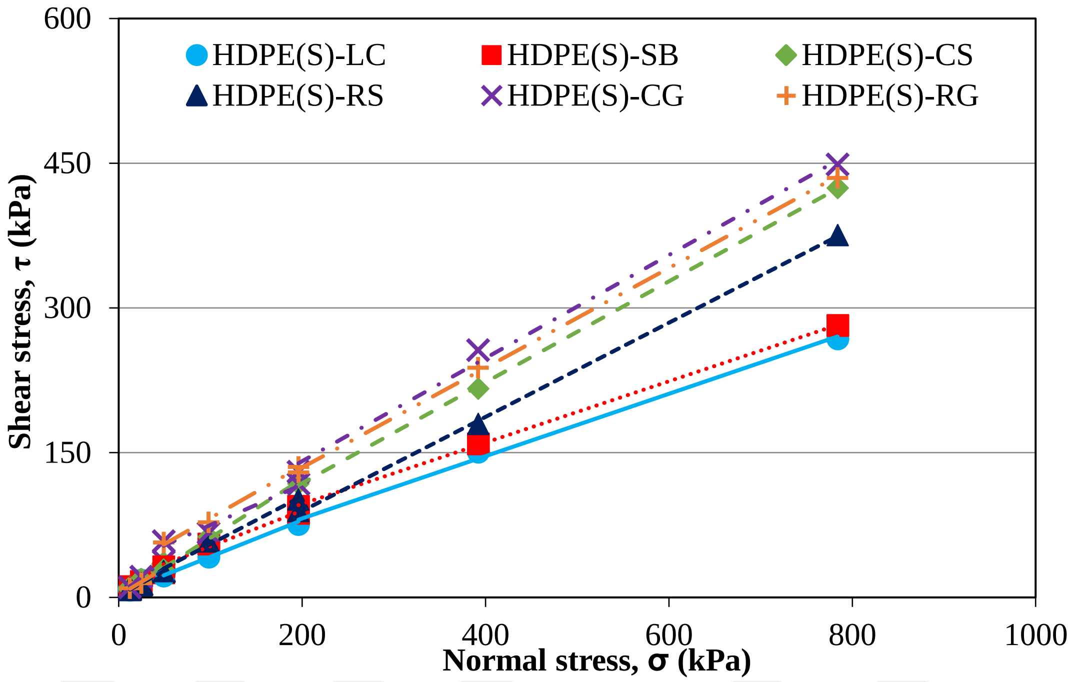

Figure 5.10: Mohr – Coulomb failure envelopes of HDPE(S) – soil

Table 5.6: Friction angles of HDPE(S) – soil interfaces

Interface	Normal stress level			One envelope
	Low	Medium	High	
HDPE(S) – LC	25.6	20.8	17.9	18.6
HDPE(S) – SB	21.0	20.3	17.6	19.3
HDPE(S) – CS	34.6	31.4	27.6	28.1
HDPE(S) – RS	27.5	26.4	26.0	25.1
HDPE(S) – CG	35.8	33.8	28.1	29.5
HDPE(S) – RG	29.4	28.3	27.3	28.6

The shear stress – strain graphs of the uncured HDPE(T) – soil interface are shown in Figure 5.11.

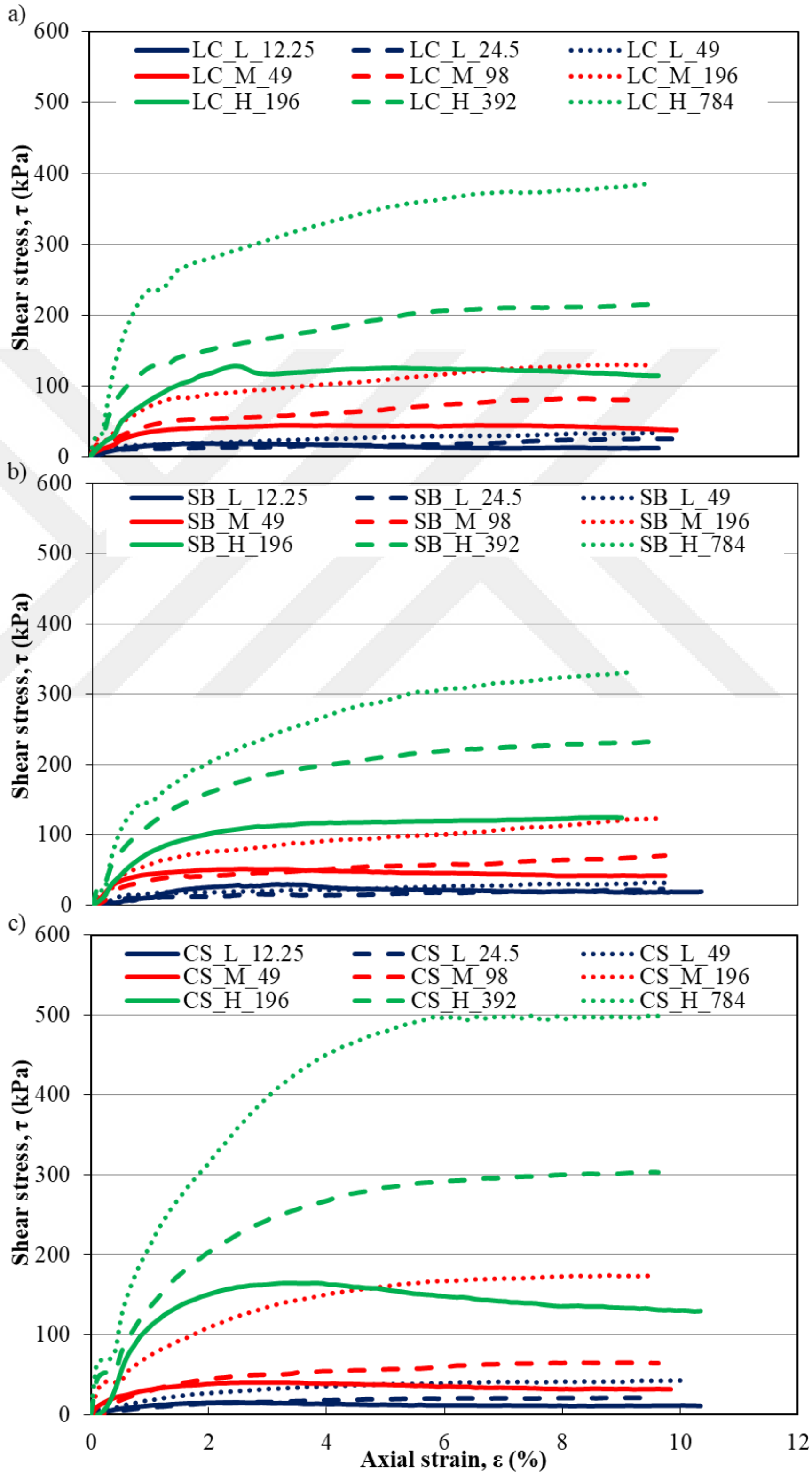

Figure 5.11: Shear stress (τ) – strain (ε) graphs of HDPE(T) – soil interface

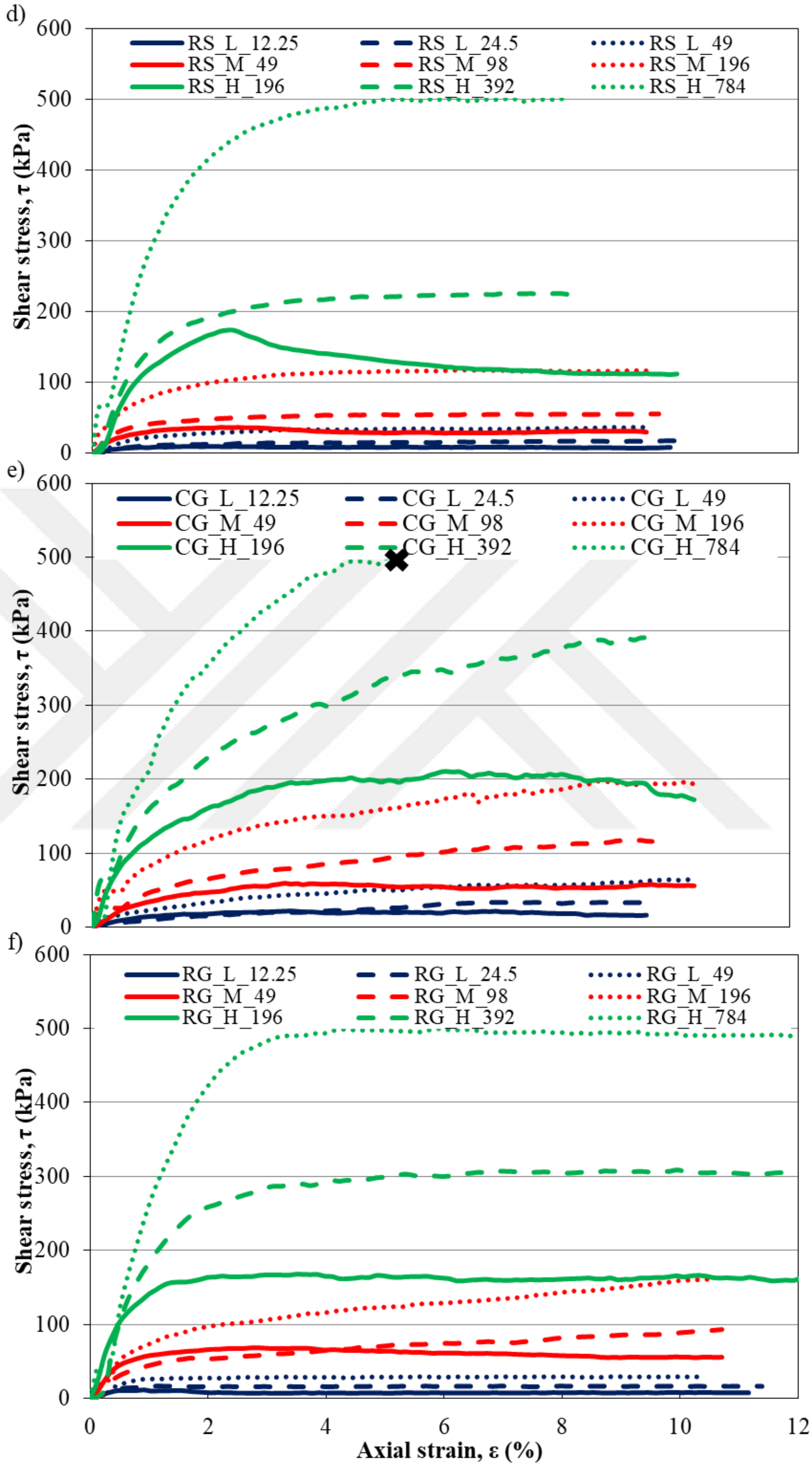

Figure 5.11 (continued): Shear stress (τ) – strain (ε) graphs of HDPE(T) – soil interface

MC envelopes for all normal stress levels separately are shown in Figure 5.12. In addition, the interface friction angle values obtained from the envelopes are listed in Table 5.7.

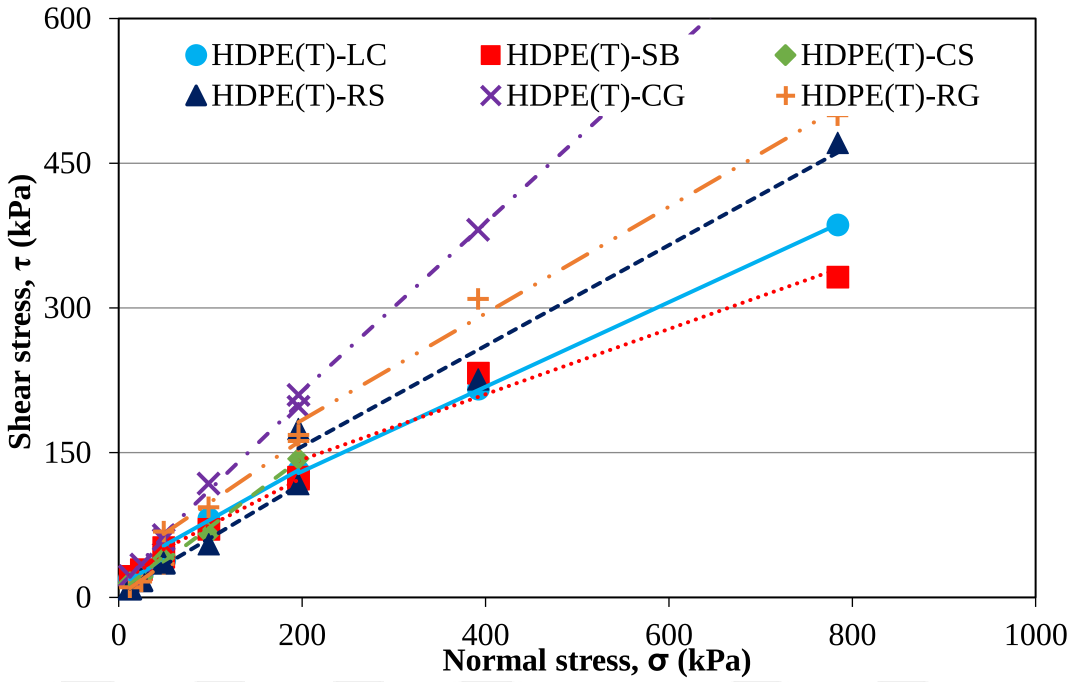

Figure 5.12: Mohr – Coulomb failure envelopes of HDPE(T) – soil

Table 5.7: Friction angles of HDPE(T) – soil interfaces

Interface	Normal stress level			One envelope
	Low	Medium	High	
HDPE(T) – LC	28.9	28.1	23.7	25.3
HDPE(T) – SB	28.5	26.1	18.7	22.5
HDPE(T) – CS	38.2	35.5	29.1	32.8
HDPE(T) – RS	36.3	29.4	27.5	30.6
HDPE(T) – CG	49.4	42.6	41.1	43.3
HDPE(T) – RG	33.8	32.9	30.0	32.1

The shear stress – strain graphs of the uncured TPO – soil interface are shown in Figure 5.13.

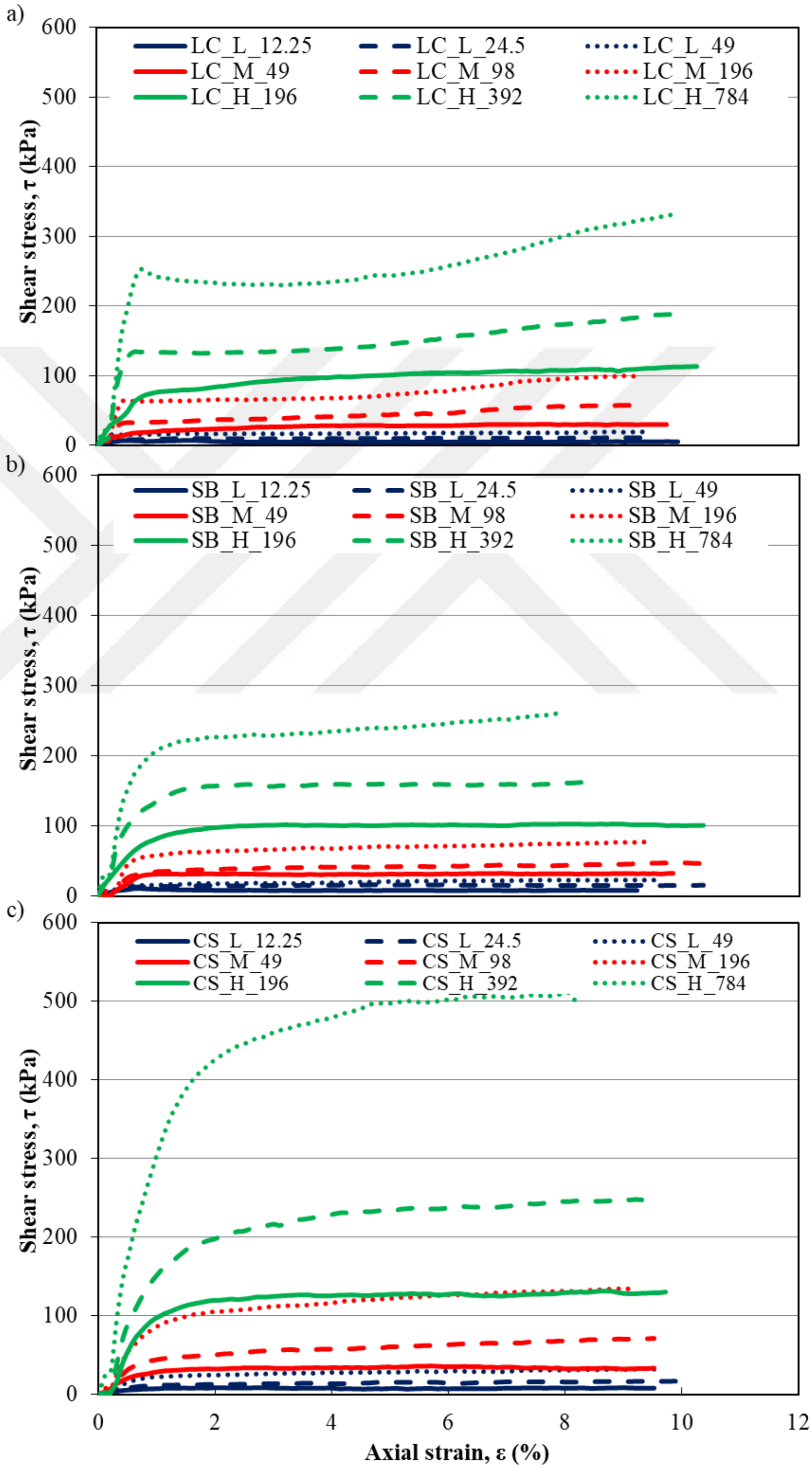

Figure 5.13: Shear stress (τ) – strain (ε) graphs of TPO – soil interface

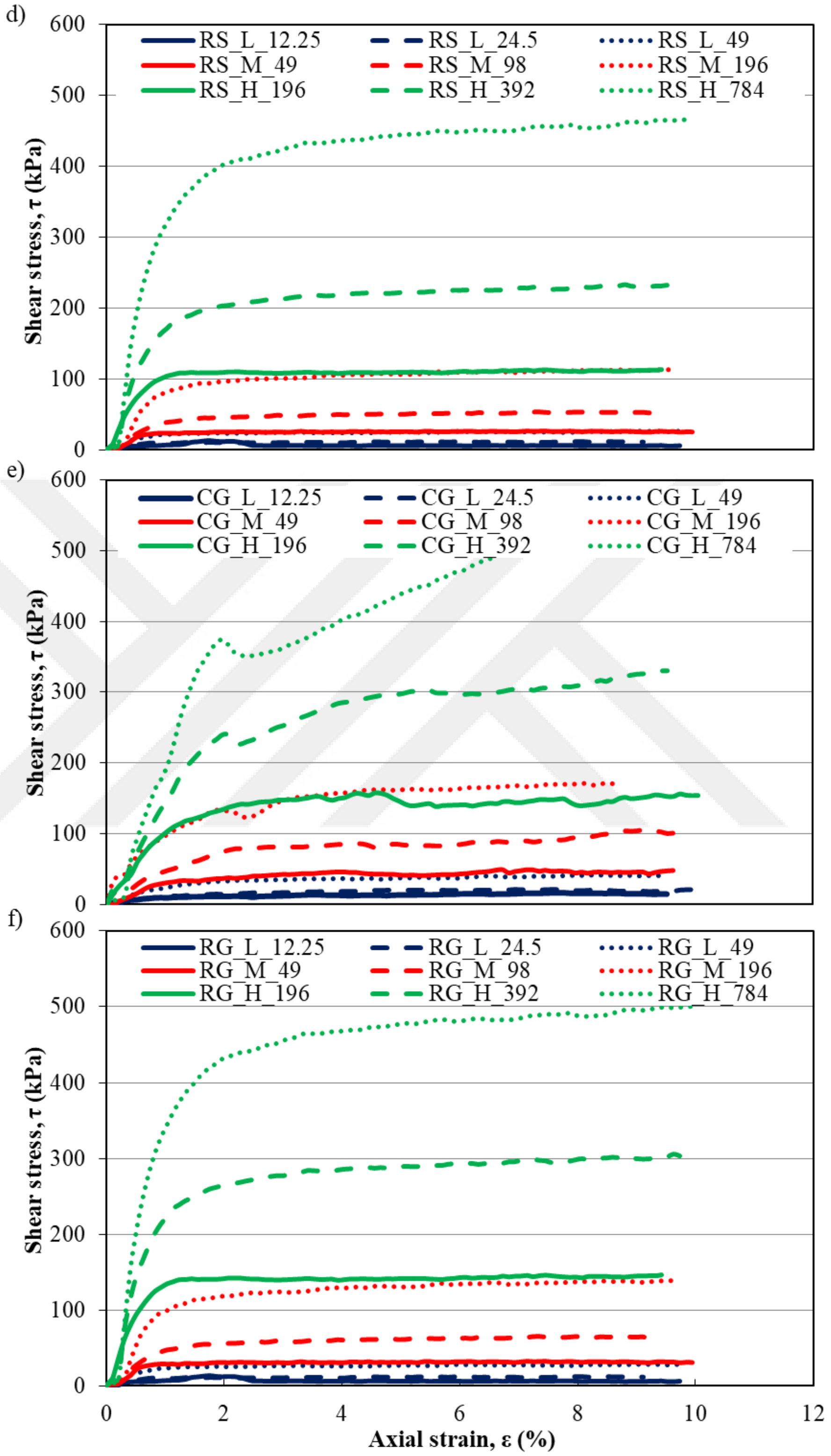

Figure 5.13 (continued): Shear stress (τ) – strain (ε) graphs of TPO – soil interface

MC envelopes for all normal stress levels separately are shown in Figure 5.14. In addition, the interface friction angle values obtained from the envelopes are listed in Table 5.8.

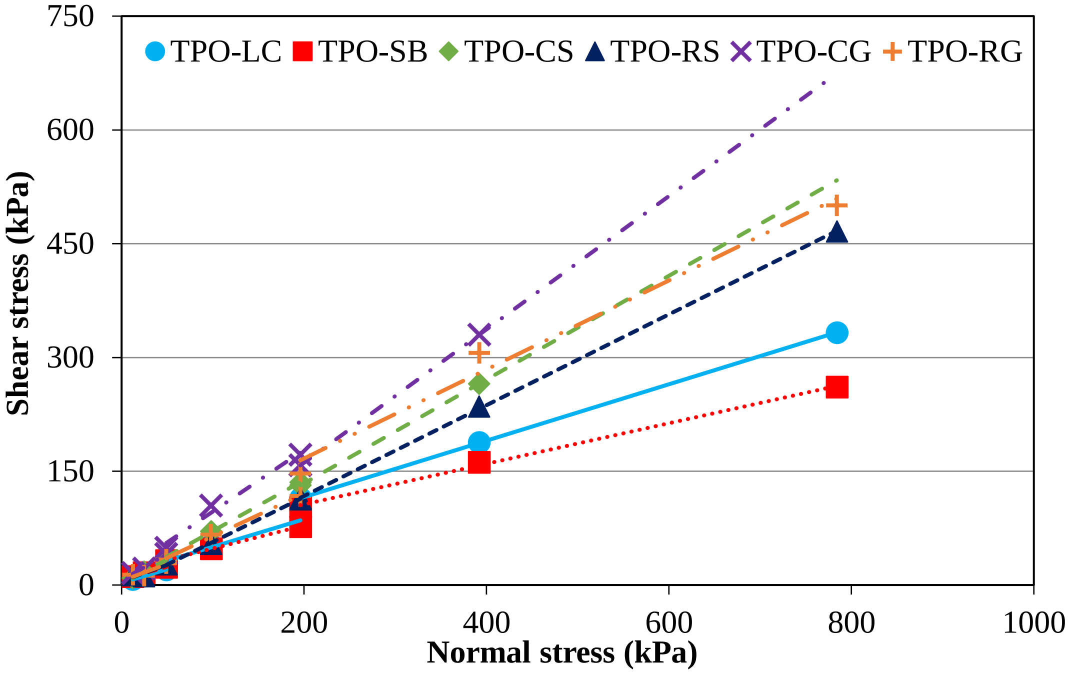

Figure 5.14: Mohr – Coulomb failure envelopes of TPO – soil

Table 5.8: Friction angles of TPO – soil interfaces

Interface	Normal stress level			One envelope
	Low	Medium	High	
TPO – LC	19.4	20.0	20.4	23.1
TPO – SB	18.7	21.8	15.0	18.2
TPO – CS	32.9	33.8	34.3	33.9
TPO – RS	23.1	30.7	30.9	30.8
TPO – CG	34.8	39.1	41.3	39.5
TPO – RG	24.1	29.5	30.4	33.4

When the shear stress – strain curves are examined, it is seen that the shear stresses peak at very small deformation values, then either increase very little or remain constant. While this situation is more prominent in coarse grained soils, fixation in fine grained soils is observed at larger displacement values. This is because, at low normal stresses, shear is the leading shear mechanism for the soil – GM interface [92]. At elevated normal stresses, the shear stress-strain curves exhibit a steep initial slope, which is subsequently followed by a reduction in slope leading up to the peak. Beyond the peak, there is a decline in shear stress that eventually reaches a constant value. The initial steep slope is attributed to the activation of friction between the coarser and angular grains in contact with the GM. Following the initial steep slope, the slope decreases due to both the mobilization of friction and the plastic indentation of particles on the GM surface. As the normal stress increases, the tension on each particle at the interface intensifies, reaching a point where this stress surpasses the yield stress of the polymer [93]. The augmentation of normal stress induces the formation of an indentation on the polymer surface. As a consequence of this indentation, a substantial shear force is necessary to initiate the shearing of the GM surface and facilitate the displacement of particles. The attainment of the peak shear stress value signifies the initiation of particle-induced movement on the GM surface. [21]. The alteration in shearing mechanism at higher normal stress levels gives rise to a corresponding variation in the shear stress response in relation to the normal stress [3]. In addition, while this situation is most evident in PVC, this situation is not so in HDPE. In TPO, on the other hand, there is a situation between the two. The reason for this is that the softest GM is PVC, and the hardest GM is HDPE. Because, in order for the above-mentioned mechanism to take place, the GM must be softer.

Furthermore, to examine the difference between the soil – GM interface and the soil – soil interface more effectively, an efficiency (E) value was obtained. The efficiency value is equal to the ratio of $\tan\delta/\tan\phi$. The E coefficients determined based on the angles obtained from a one envelope are listed in the Table 5.9. As seen, all E coefficients were obtained to be less than 1. This means that the soil – GM interface can potentially form a shearing surface. Additionally, the lowest E coefficient was obtained for the LC – PVC(3.0) interface, indicating that extra attention should be paid when using PVC GM in designs involving low plasticity clay.

Table 5.9: Efficiency coefficients of uncured GM – soil interfaces

Soil	PVC(1.5)	PVC(3.0)	HDPE(S)	HDPE(T)	TPO
LC	0.54	0.52	0.64	0.87	0.79
SB	0.90	0.96	0.85	1.00	0.81
CS	0.97	0.93	0.81	0.94	0.97
RS	0.99	0.89	0.75	0.91	0.92
CG	0.89	0.93	0.67	0.98	0.90
RG	0.82	0.83	0.70	0.79	0.82

5.4 Direct shear test results of cured GM – soil interfaces

In this section, the interface direct shear test results of GMs cured in SWt, AMD, CCP, and MSW synthetic liquids for 4, 8, and 16 months are summarized.

5.4.1 Direct shear test results of 4 months cured GM – soil interfaces

In this section, the interface direct shear test results of GMs cured in SWt, AMD, CCP, and MSW synthetic liquids for 4 months are summarized. MC failure envelopes of 4 months SWt cured PVC(1.5) – soil, PVC(3.0) – soil, and TPO – soil interfaces are shown in Figure 5.15, Figure 5.16, and Figure 5.17. In addition, the interface friction angle values obtained from the envelopes are listed in Table 5.10. In order to see the decrease in the δ with curing, the δ of the uncured GMs in the medium normal stress level are also given in Table 5.10.

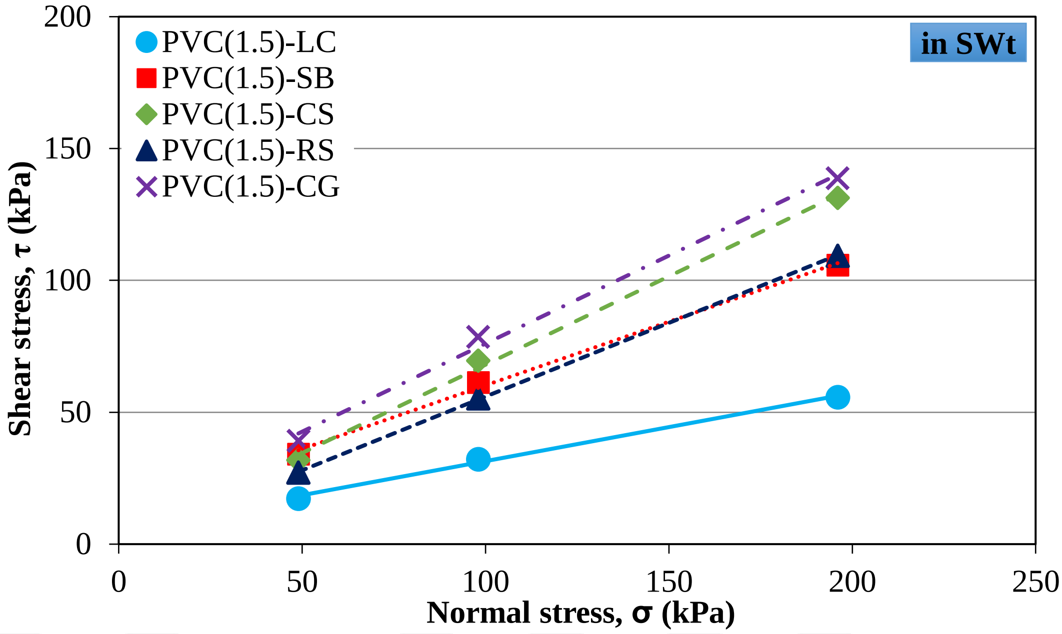

Figure 5.15: Mohr-Coulomb envelopes of 4 months SWt cured PVC(1.5) – soil

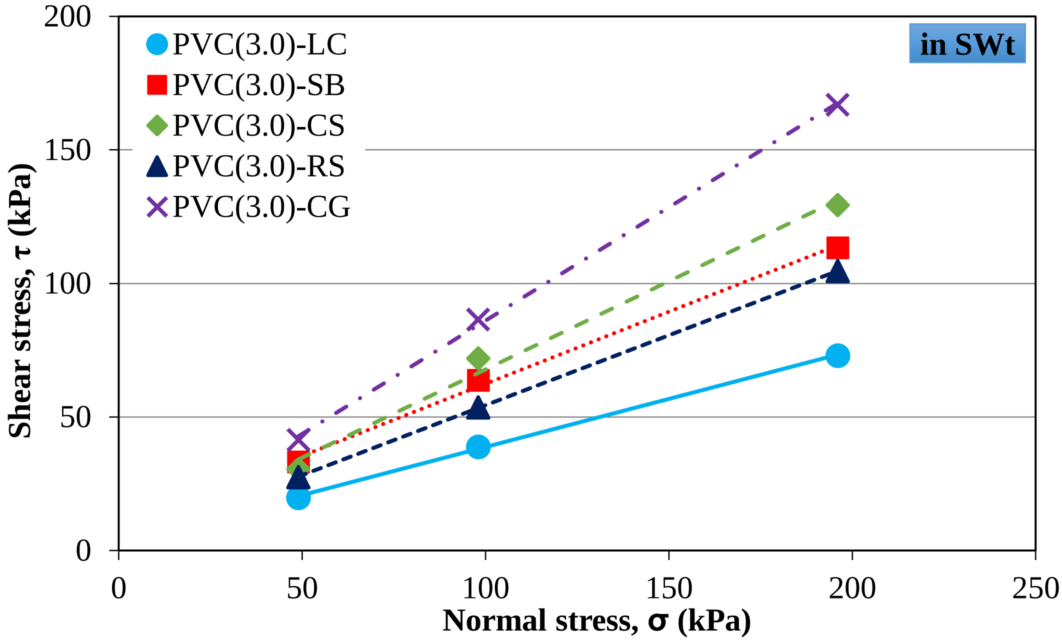

Figure 5.16: Mohr-Coulomb envelopes of 4 months SWt cured PVC(3.0) – soil

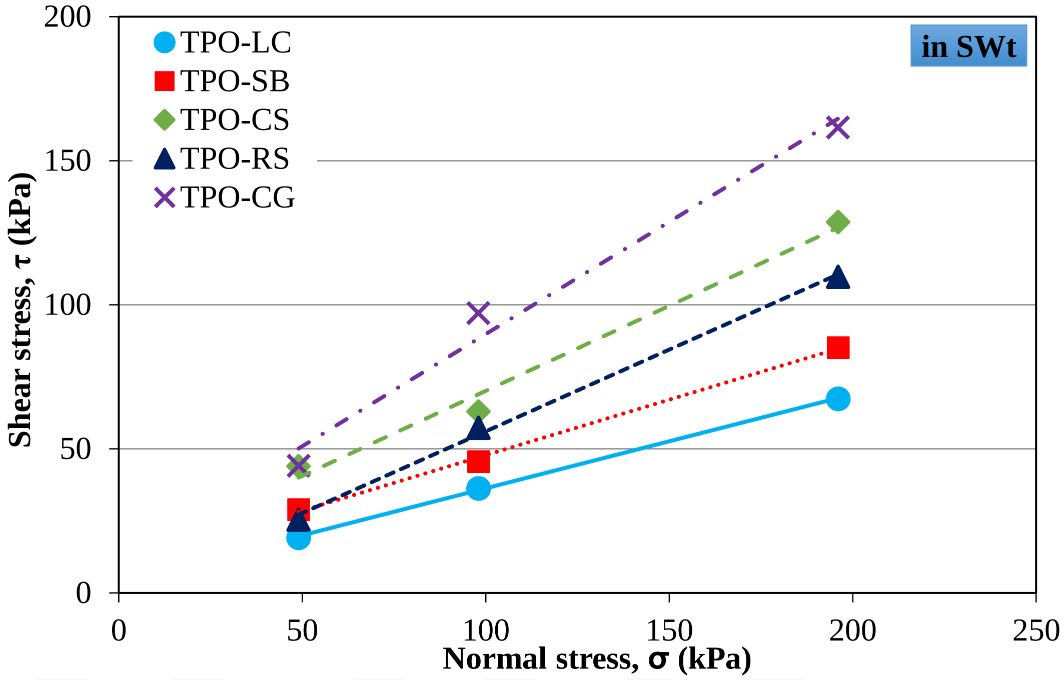

Figure 5.17: Mohr-Coulomb failure of 4 months SWt cured TPO – soil

Table 5.10: Friction angles of 4 months SWt cured PVC(1.5) – soil, PVC(3.0) – soil, and TPO – soil interfaces

Soil	SWt curing		
	PVC(1.5)	PVC(3.0)	TPO
LC	14.5	19.8	18.1
SB	25.6	28.4	21.0
CS	32.9	33.4	30.5
RS	29.2	27.7	29.6
CG	33.7	40.3	37.9

The reductions in the δ of PVC(1.5) cured in SWt for 4 months were 27.1, 1.9, 6.8, 15.6, and 2.9% for LC, SB, CS, RS, and CG, respectively. The average amount of decrease is 11%. The reductions in the δ of PVC(3.0) cured in SWt for 4 months were 3.9, 11.8, 2.3, 3.5, and 2.4% for LC, SB, CS, RS, and CG, respectively. The average amount of decrease is 4.8%. The reductions in the δ of TPO cured in SWt for 4 months were 9.5, 3.7, 9.8, 3.6, and 3.1% for LC, SB, CS, RS, and CG, respectively. The average amount of decrease is 5.9%. When the average decreases are compared, the highest decrease was in PVC(1.5), while the least decrease was in PVC(3.0). This is because PVC(3.0) is thicker than the other GMs. When TPO and PVC(1.5) are compared with the same thickness, TPO is harder and fibrous. While the highest amount of decrease was observed at the PVC(1.5) – LC interface, the lowest amount of decrease was observed at the PVC(3.0) – CS interface. That is, in areas that will be exposed to SWt, 4 months curing results have shown that 1.5 mm thick PVC GM and low plasticity clay are not suitable.

MC failure envelopes of 4 months AMD cured HDPE(S) – soil, HDPE(T) – soil, and TPO – soil interfaces are shown in Figure 5.18, Figure 5.19, and Figure 5.20. In addition, the interface friction angle values obtained from the envelopes are listed in Table 5.11.

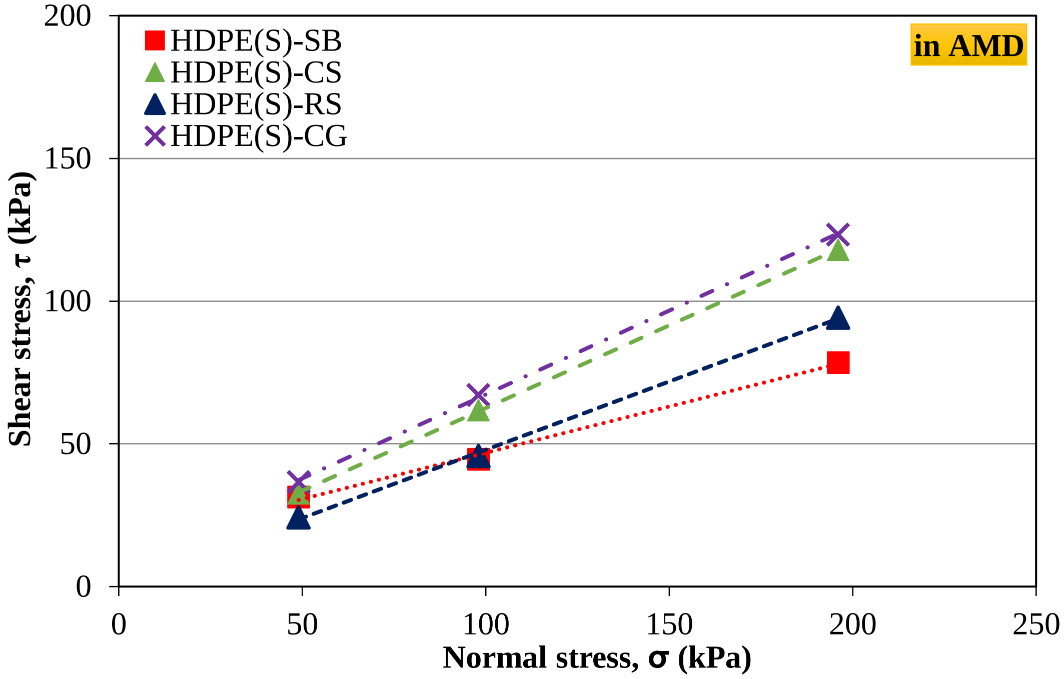

Figure 5.18: Mohr-Coulomb envelopes of 4 months AMD cured HDPE(S) – soil

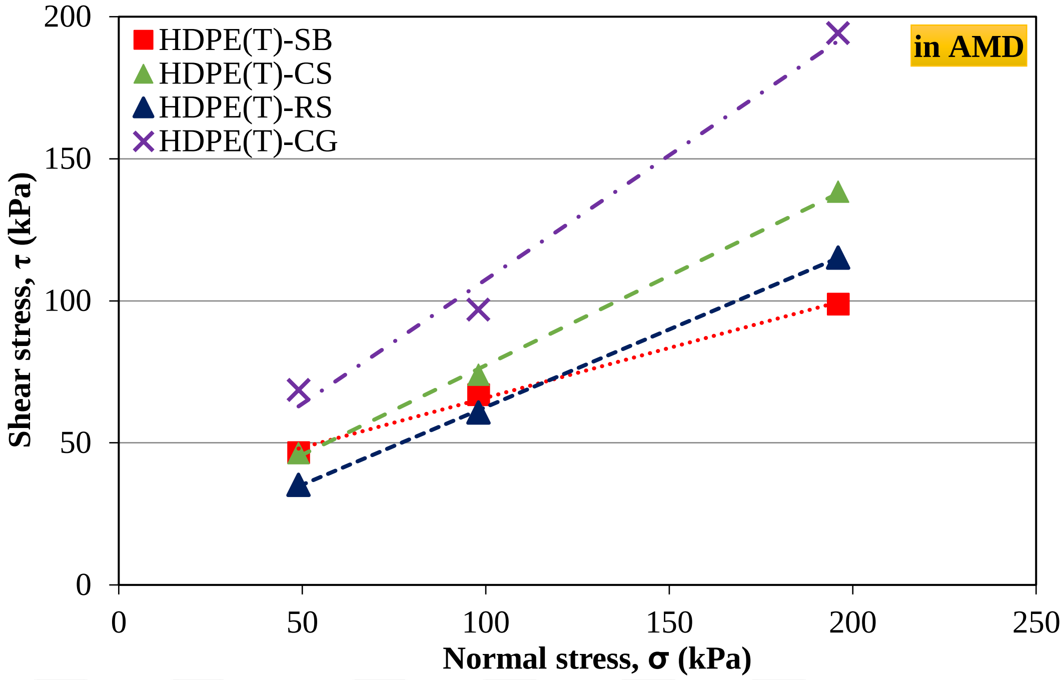

Figure 5.19: Mohr-Coulomb envelopes of 4 months AMD cured HDPE(T) – soil

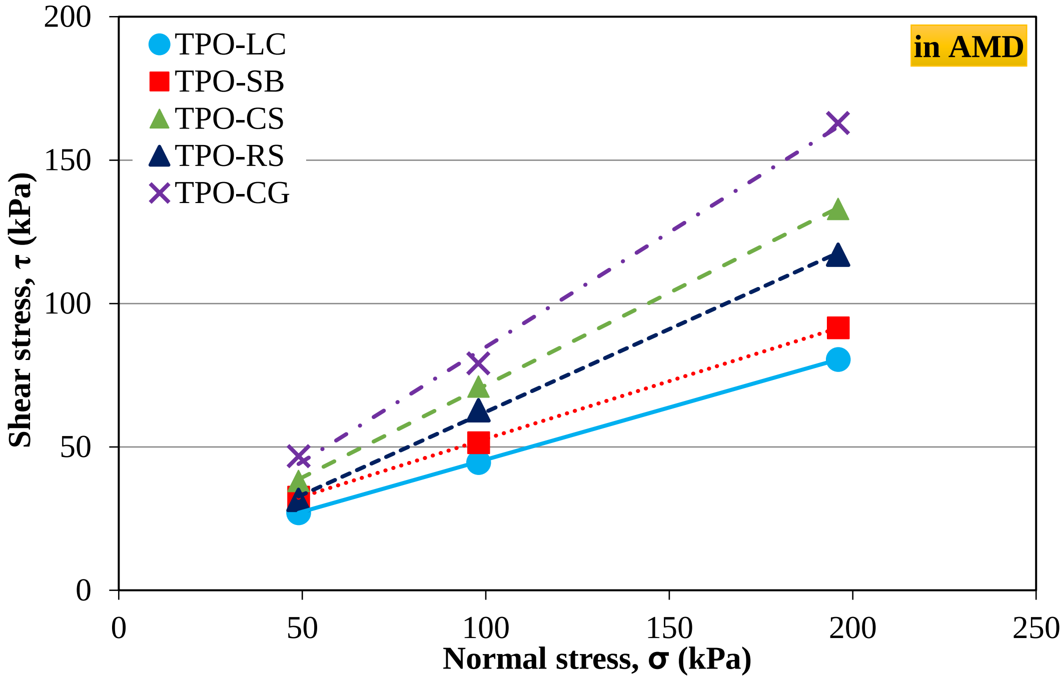

Figure 5.20: Mohr-Coulomb envelopes of 4 months AMD cured TPO – soil

Table 5.11: Friction angles of 4 months AMD cured HDPE(S) – soil, HDPE(T) – soil, and TPO – soil interfaces

Soil	AMD curing		
	HDPE(S)	HDPE(T)	TPO
LC	-	-	19.0
SB	18.0	19.3	21.9
CS	30.1	32.2	32.8
RS	25.6	28.7	29.0
CG	30.4	41.2	38.7

The reductions in the δ of HDPE(S) cured in AMD for 4 months were 11.3, 4.1, 3.0, and 10.1% for SB, CS, RS, and CG, respectively. The average amount of decrease is 7.1%. The reductions in the δ of HDPE(T) cured in AMD for 4 months were 26.1, 9.3, 2.4, and 3.3% for SB, CS, RS, and CG, respectively. The average amount of decrease is 10.3%. The reductions in the δ of TPO cured in AMD for 4 months were 5.0, -0.5, 3.0, 5.5, and 1.0% for LC, SB, CS, RS, and CG, respectively. The average amount of decrease is 2.8%. When the average decreases are compared, the highest decrease is in HDPE(T) while the least decrease is in TPO. This may be because AMD, with its high acid content, damaged the needle-like roughness of HDPE(T). While the highest amount of decrease was observed at the HDPE(T) – SB interface, the lowest amount of decrease was observed at the TPO – SB interface. That is, in areas that will be exposed to AMD leachate, 4 month curing results have shown that textured HDPE GM and sand/bentonite mixture are not suitable.

MC failure envelopes of 4 months CCP cured HDPE(S) – soil, HDPE(T) – soil, and TPO - soil interfaces are shown in Figure 5.21, Figure 5.22, and Figure 5.23. In addition, the interface friction angle values obtained from the envelopes are listed in Table 5.12.

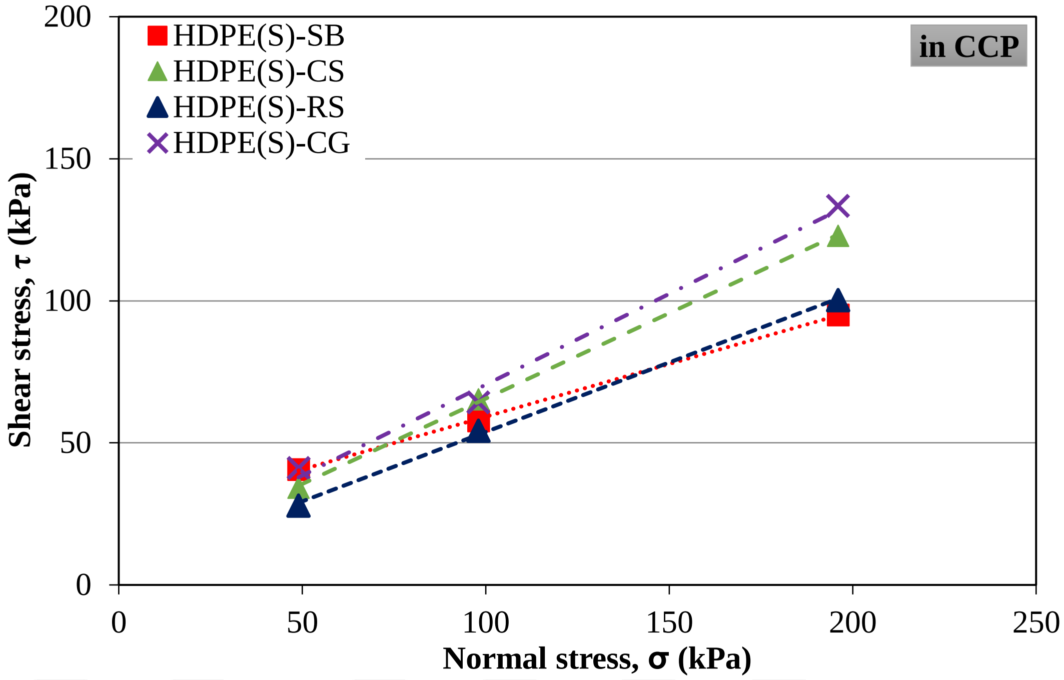

Figure 5.21: Mohr-Coulomb envelopes of 4 months CCP cured HDPE(S) – soil

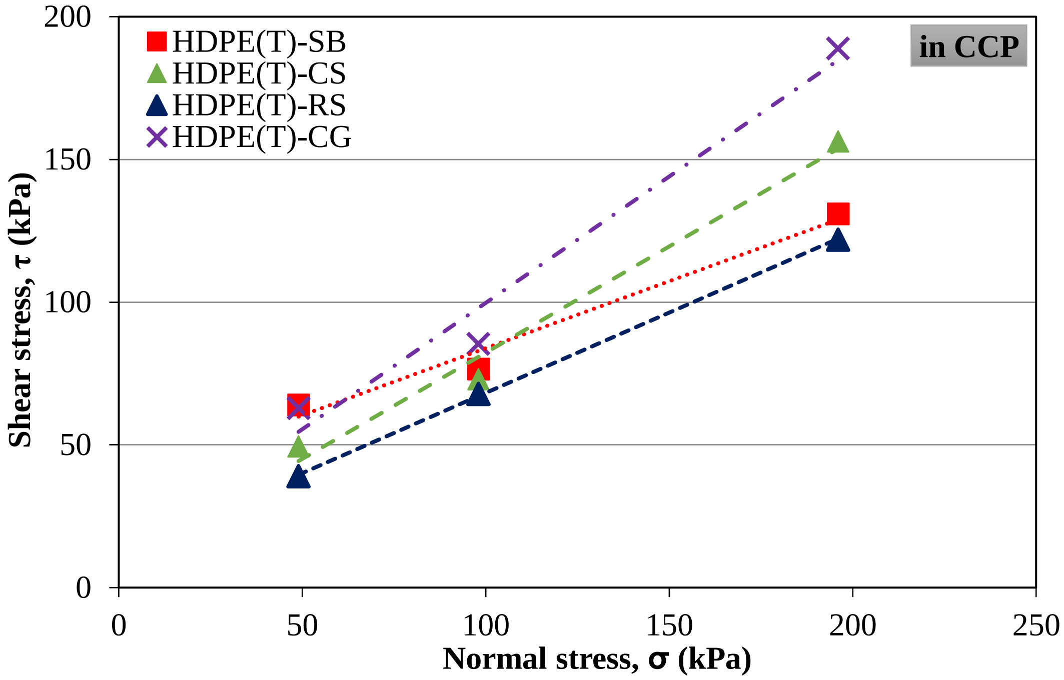

Figure 5.22: Mohr-Coulomb envelopes of 4 months CCP cured HDPE(T) – soil

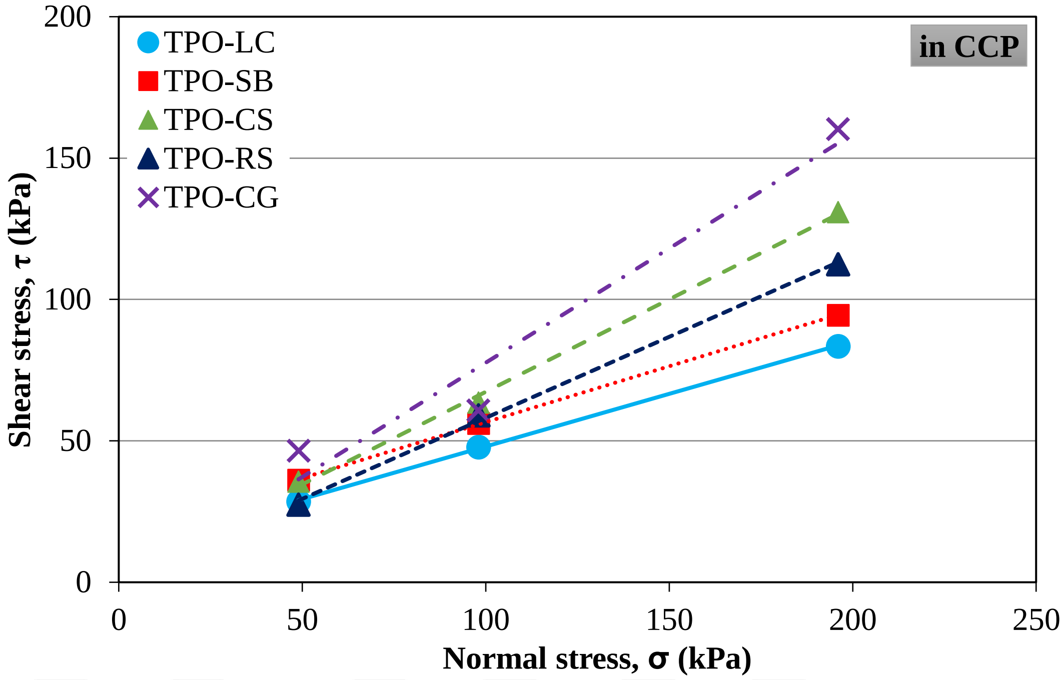

Figure 5.23: Mohr-Coulomb envelopes of 4 months CCP cured TPO – soil

Table 5.12: Friction angles of 4 months CCP cured HDPE(S) – soil, HDPE(T) – soil, and TPO – soil interfaces

Soil	CCP curing		
	HDPE(S)	HDPE(T)	TPO
LC	-	-	20.4
SB	20.4	25.1	21.6
CS	31.0	36.7	33.2
RS	26.1	29.3	29.8
CG	32.6	41.5	39.0

The reductions in the δ of HDPE(S) cured in CCP for 4 months were -0.5, 1.3, 1.1, and 3.6% for SB, CS, RS, and CG, respectively. The average amount of decrease is 1.4%. The reductions in the δ of HDPE(T) cured in CCP for 4 months were 3.8, -3.4, 0.3, and 2.6% for SB, CS, RS, and CG, respectively. The average amount of decrease is 0.8%. The reductions in the δ of TPO cured in CCP for 4 months were -2.0, 0.9, 1.8, 2.9, and 0.3% for LC, SB, CS, RS, and CG, respectively. The average amount of decrease is 0.8%. When the average decreases are compared, the highest decrease is in HDPE(S) while the least decrease is in TPO. While the highest amount of decrease was observed at the HDPE(T) – SB interface, the lowest amount of decrease was observed at the TPO – LC interface. That is, in areas that will be exposed to CCP leachate, 4 months curing results have shown that textured HDPE GM and sand/bentonite mixture are not suitable.

MC failure envelopes of 4 months MSW cured HDPE(S) – soil, HDPE(T) – soil, and TPO - soil interfaces are shown in Figure 5.24, Figure 5.25, and Figure 5.26. In addition, the interface friction angle values obtained from the envelopes are listed in Table 5.13.

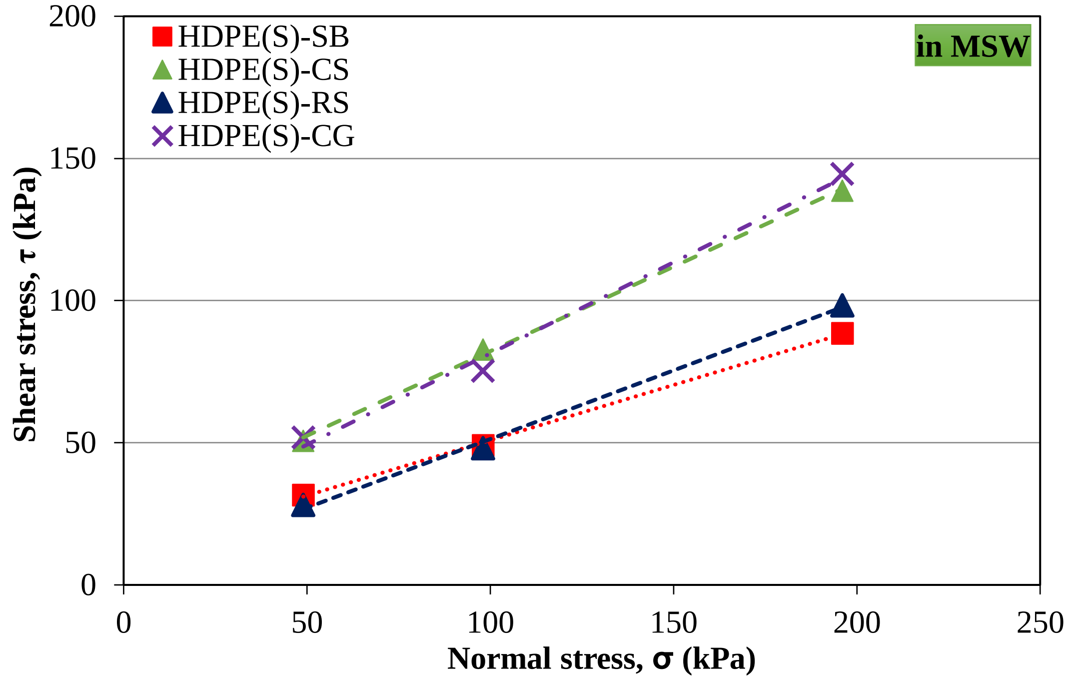

Figure 5.24: Mohr-Coulomb envelopes of 4 months MSW cured HDPE(S) – soil

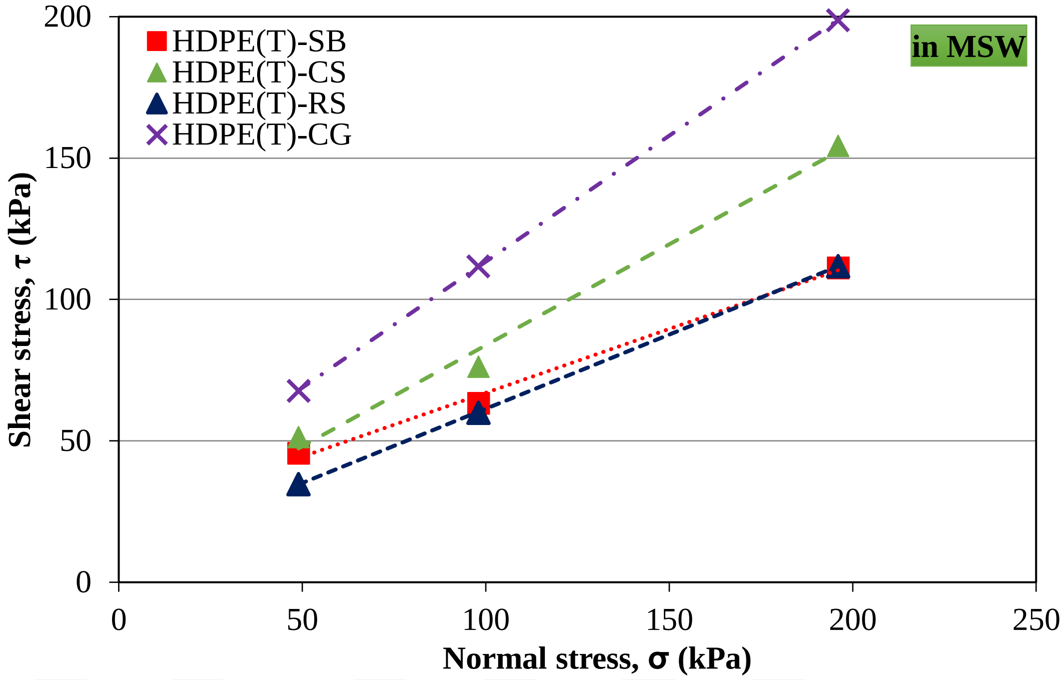

Figure 5.25: Mohr-Coulomb envelopes of 4 months MSW cured HDPE(T) – soil

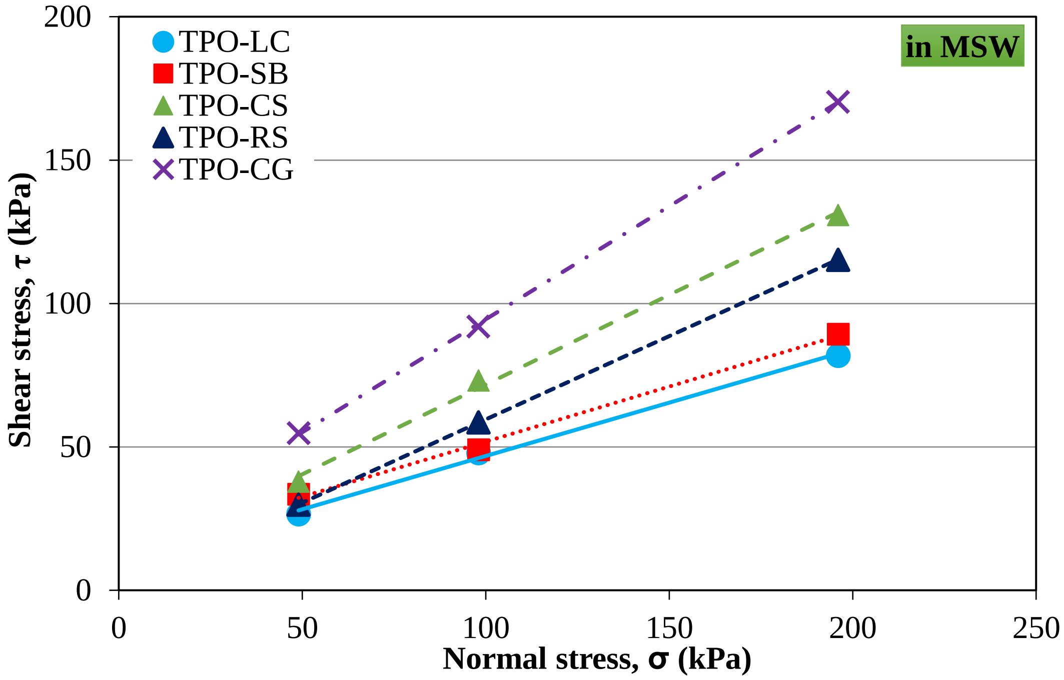

Figure 5.26: Mohr-Coulomb envelopes of 4 months MSW cured TPO – soil

Table 5.13: Friction angles of 4 months MSW cured HDPE(S) – soil, HDPE(T) – soil, and TPO – soil interfaces

Soil	MSW curing		
	HDPE(S)	HDPE(T)	TPO
LC	-	-	19.9
SB	21.2	24.3	21.0
CS	30.7	35.3	32.0
RS	25.8	27.7	30.2
CG	32.7	41.7	38.2

The reductions in the δ of HDPE(S) cured in MSW for 4 months were -4.4, 2.2, 2.3, and 3.3% for SB, CS, RS, and CG, respectively. The average amount of decrease is 0.8%. The reductions in the δ of HDPE(T) cured in MSW for 4 months were 6.6, 0.6, 5.8, and 2.1% for SB, CS, RS, and CG, respectively. The average amount of decrease is 3.8%. The reductions in the δ of TPO cured in MSW for 4 months were 0.5, 3.7, 5.3, 1.6, and 2.3% for LC, SB, CS, RS, and CG, respectively. The average amount of decrease is 2.7%. When the average decreases are compared, the highest decrease is in HDPE(T) while the least decrease is in HDPE(S). While the highest amount of decrease was observed at the HDPE(T) – SB interface, the lowest amount of decrease was observed at the HDPE(S) – SB interface. That is, in areas that will be exposed to MSW leachate, 4 months curing results have shown that textured HDPE GM and sand-bentonite mixture are not suitable.

5.4.2 Direct shear test results of 8 months cured GM – soil interfaces

MC envelopes were drawn separately for each normal stress level, as well as a single envelope for all normal stress levels. MC failure envelopes of 8 months SWt cured PVC(1.5) – soil, PVC(3.0) – soil, and TPO – soil interfaces for all normal stress levels separately are shown in Figure 5.27, Figure 5.28, and Figure 5.29. In addition, the interface friction angle values obtained from the envelopes are listed in Table 5.14. In order to see the decrease in the δ with curing, the δ of the uncured GMs in the medium normal stress level are also given in Table 5.14.

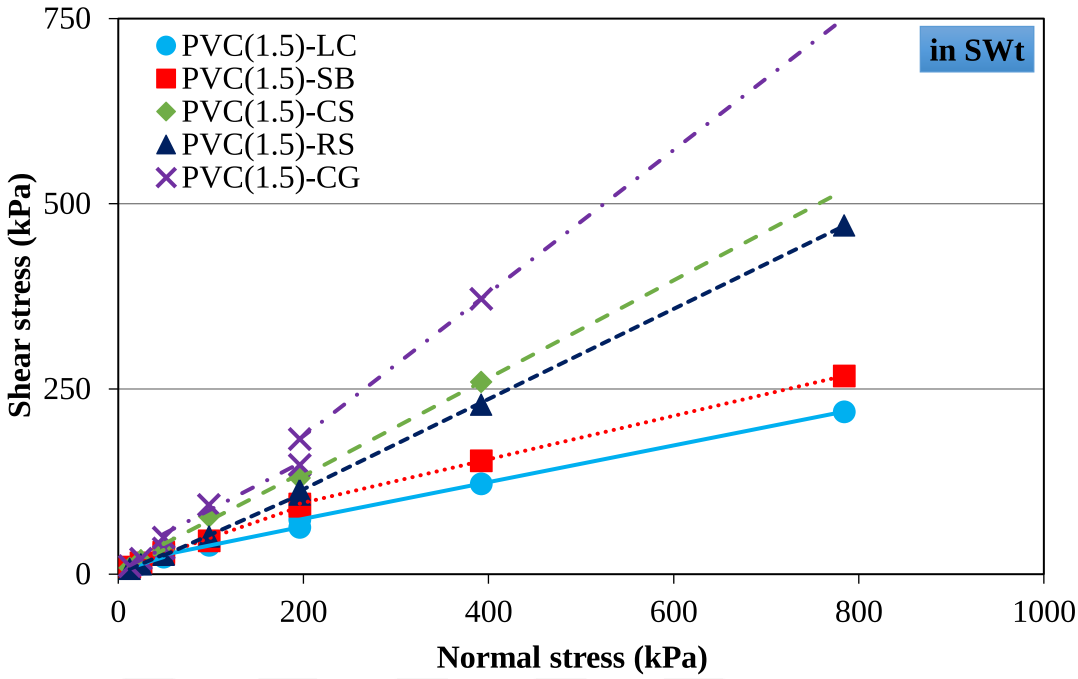

Figure 5.27: Mohr-Coulomb envelopes of 8 months SWt cured PVC(1.5) – soil

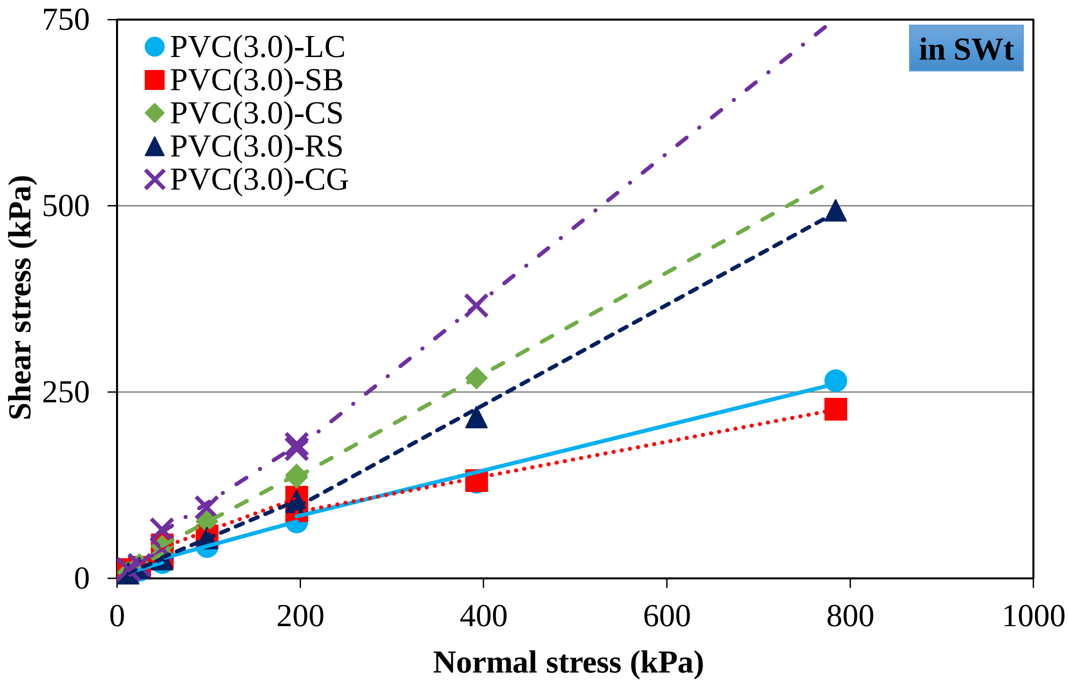

Figure 5.28: Mohr-Coulomb envelopes of 8 months SWt cured PVC(3.0) – soil

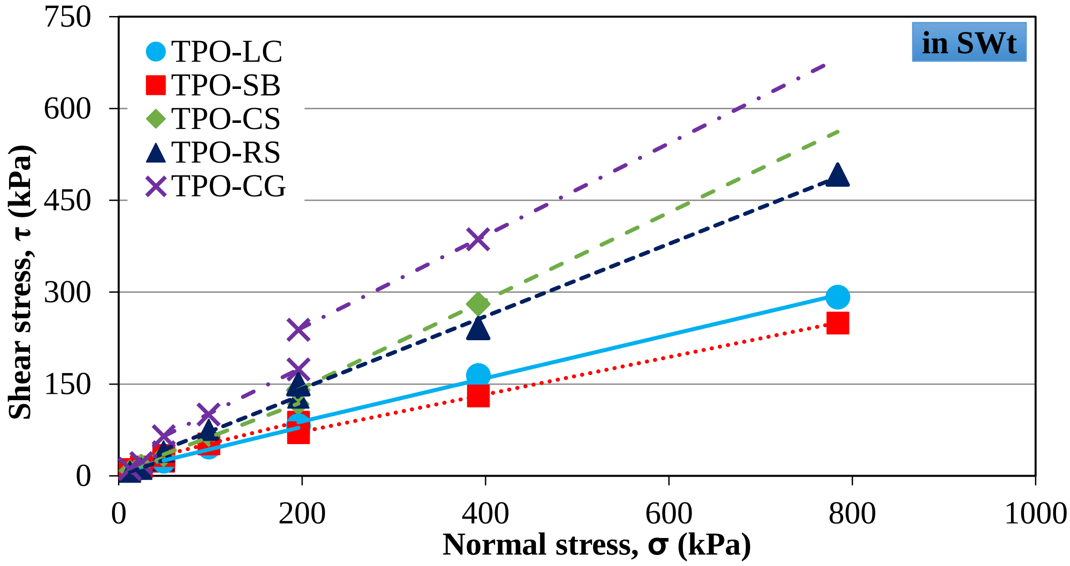

Figure 5.29: Mohr-Coulomb envelopes of 8 months SWt cured TPO – soil

Table 5.14: Friction angles of 8 months SWt cured PVC(1.5) – soil, PVC(3.0) – soil, and TPO – soil interfaces

Interface	Normal stress level			One envelope
	Low	Medium	High	
PVC(1.5) – LC	21.5	14.2	13.9	15.2
PVC(1.5) – SB	25.3	23.4	16.4	18.5
PVC(1.5) – CS	32.0	32.7	33.4	33.2
PVC(1.5) – RS	28.2	29.1	31.3	31.1
PVC(1.5) – CG	32.5	33.0	44.0	43.0
PVC(3.0) – LC	20.1	18.6	16.8	18.1
PVC(3.0) – SB	25.5	32.1	13.2	15.1
PVC(3.0) – CS	32.8	33.0	39.5	34.2
PVC(3.0) – RS	26.6	27.5	33.9	32.0
PVC(3.0) – CG	37.3	38.4	44.5	42.6
TPO – LC	26.8	18.0	19.5	20.4
TPO – SB	20.6	16.7	17.0	16.9
TPO – CS	28.1	29.5	34.0	35.4
TPO – RS	27.3	30.5	30.6	31.9
TPO – CG	36.2	36.6	37.0	45.0

The reductions in the δ of PVC(1.5) cured in SWt for 8 months were 28.6, 11.0, 7.4, 15.9, and 4.9% for LC, SB, CS, RS, and CG, respectively. The average amount of decrease is 13.6%. The reductions in the δ of PVC(3.0) cured in SWt for 8 months were 9.7, 0.3, 3.5, 4.2, and 7.0% for LC, SB, CS, RS, and CG, respectively. The average amount of decrease is 4.9%. The reductions in the δ of TPO cured in SWt for 8 months were 10.0, 23.4, 12.7, 0.7, and 6.4% for LC, SB, CS, RS, and CG, respectively. The average amount of decrease is 10.6%. When the average decreases are compared, the highest decrease is in PVC(1.5), while the least decrease is in PVC(3.0). While the highest amount of decrease was observed at the PVC(1.5) – LC interface, the lowest amount of decrease was observed at the PVC(3.0) – SB interface. That is, in areas that will be exposed to SWt, 8 months curing results have shown that 1.5 mm thick PVC GM and low plasticity clay are not suitable.

MC failure envelopes of 8 months AMD cured HDPE(S) – soil, HDPE(T) – soil, and TPO – soil interfaces for all normal stress levels separately are shown in Figure 5.30, Figure 5.31, and Figure 5.32. In addition, the interface friction angle values obtained from the envelopes are listed in Table 5.15.

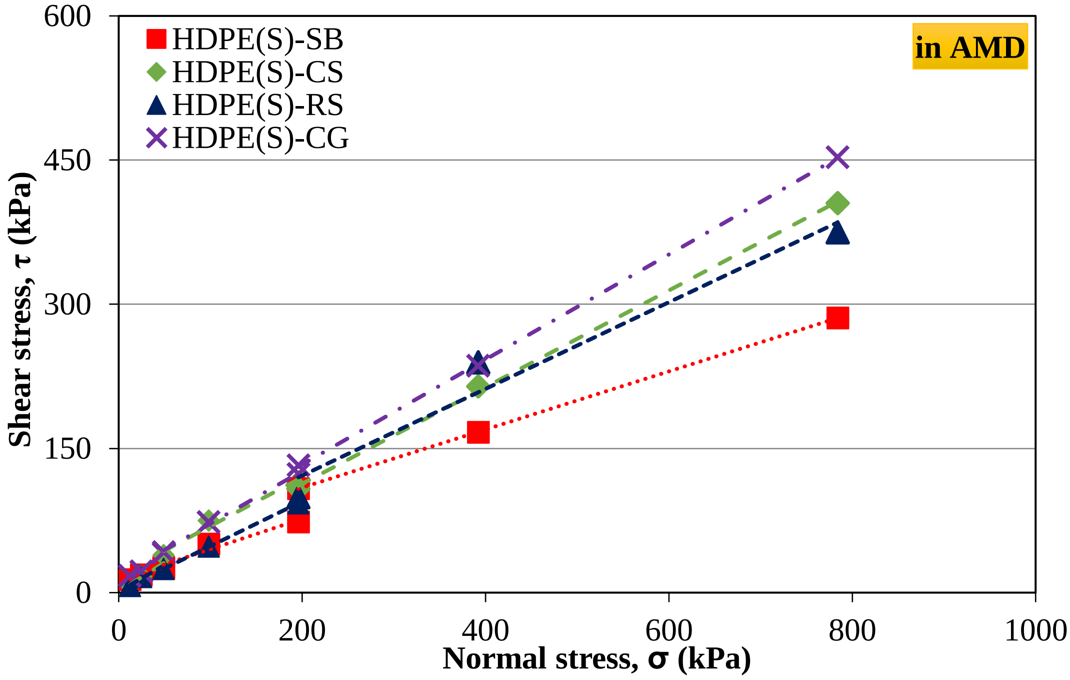

Figure 5.30: Mohr-Coulomb envelopes of 8 months AMD cured HDPE(S) – soil

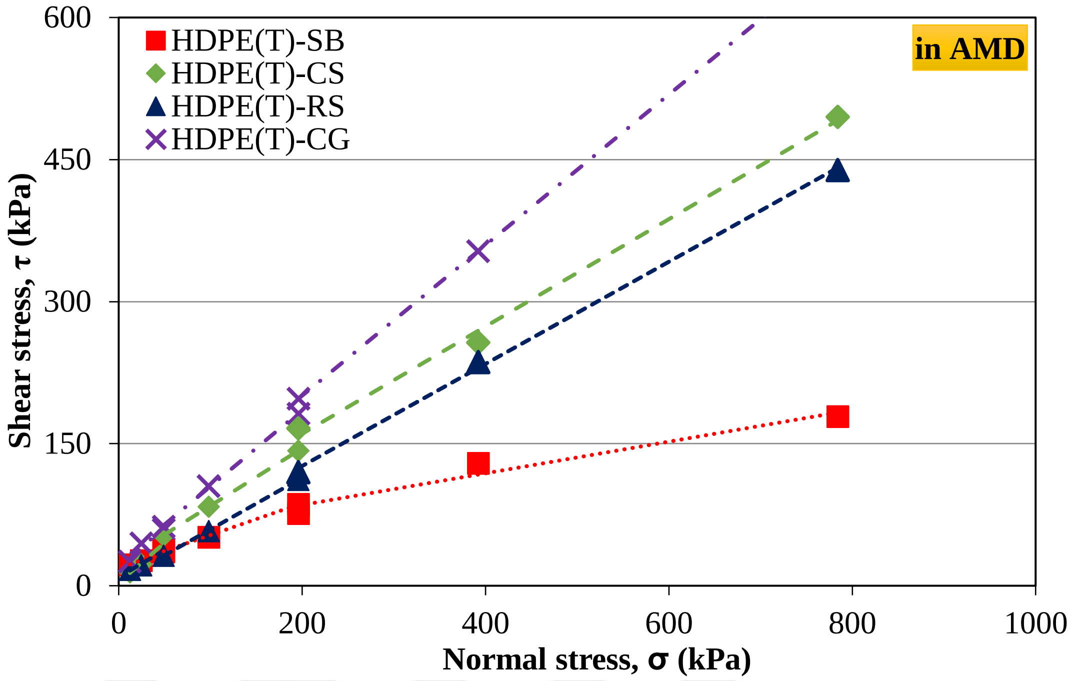

Figure 5.31: Mohr-Coulomb envelopes of 8 months AMD cured HDPE(T) – soil

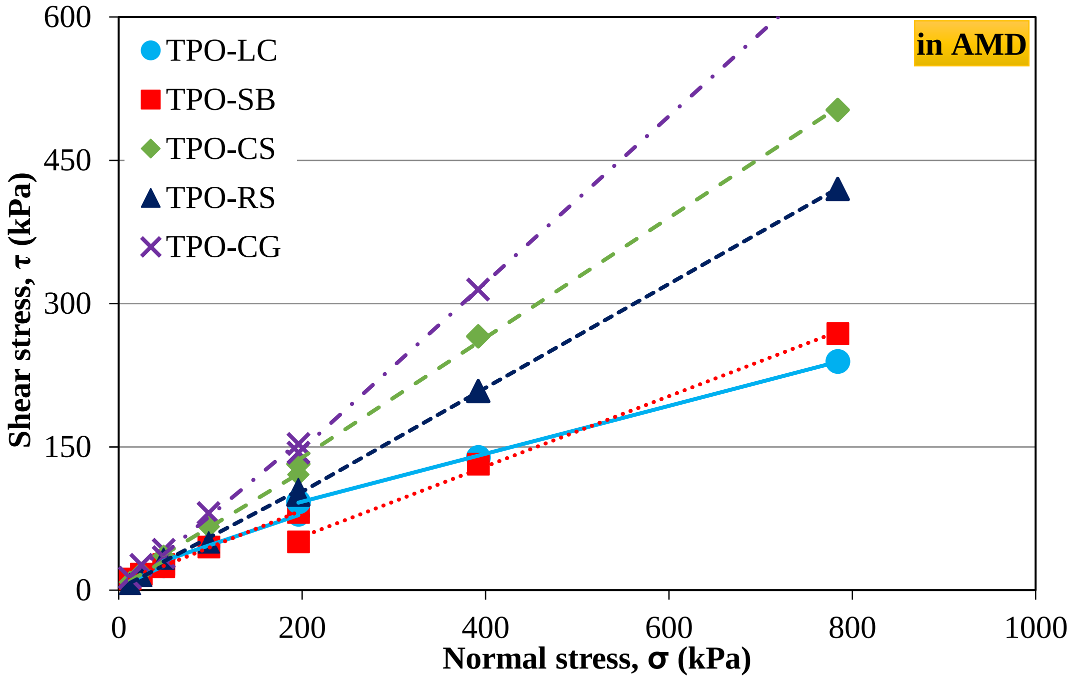

Figure 5.32: Mohr-Coulomb envelopes of 8 months AMD cured TPO – soil

Table 5.15: Friction angles of 8 months AMD cured HDPE(S) – soil, HDPE(T) – soil, and TPO – soil interfaces

Interface	Normal stress level			One envelope
	Low	Medium	High	
HDPE(S) – SB	18.9	17.5	16.8	19.7
HDPE(S) – CS	31.4	26.9	26.7	27.0
HDPE(S) – RS	28.7	24.9	24.3	26.3
HDPE(S) – CG	32.7	28.7	28.7	29.4
HDPE(T) – SB	20.0	18.6	9.2	11.7
HDPE(T) – CS	40.1	31.3	29.9	31.6
HDPE(T) – RS	29.6	28.6	28.3	29.0
HDPE(T) – CG	41.2	38.9	38.5	40.5
TPO – LC	24.1	18.0	14.1	16.5
TPO – SB	22.5	21.1	17.1	18.1
TPO – CS	29.5	30.0	32.1	32.8
TPO – RS	26.2	26.9	28.5	28.1
TPO – CG	37.5	38.6	41.1	38.1

The reductions in the δ of HDPE(S) cured in AMD for 8 months were 13.8, 14.3, 5.7, and 15.1% for SB, CS, RS, and CG, respectively. The average amount of decrease is 12.2%. The reductions in the δ of HDPE(T) cured in AMD for 8 months were 28.7, 11.8, 2.7, and 8.7% for SB, CS, RS, and CG, respectively. The average amount of decrease is 13.0%. The reductions in the δ of TPO cured in AMD for 8 months were 10.0, 3.2, 11.2, 12.4, and 1.3% for LC, SB, CS, RS, and CG, respectively. The average amount of decrease is 7.6%. When the average decreases are compared, the highest decrease is in HDPE(T) while the least decrease is in TPO. While the highest amount of decrease was observed at the HDPE(T) – SB interface, the lowest amount of decrease was observed at the TPO – CG interface. That is, in areas that will be exposed to AMD leachate, 8 months curing results have shown that textured HDPE GM and sand-bentonite mixture are not suitable.

MC failure envelopes of 8 months CCP cured HDPE(S) – soil, HDPE(T) – soil, and TPO – soil interfaces for all normal stress levels separately are shown in Figure 5.33, Figure 5.34, and Figure 5.35. In addition, the interface friction angle values obtained from the envelopes are listed in Table 5.16.

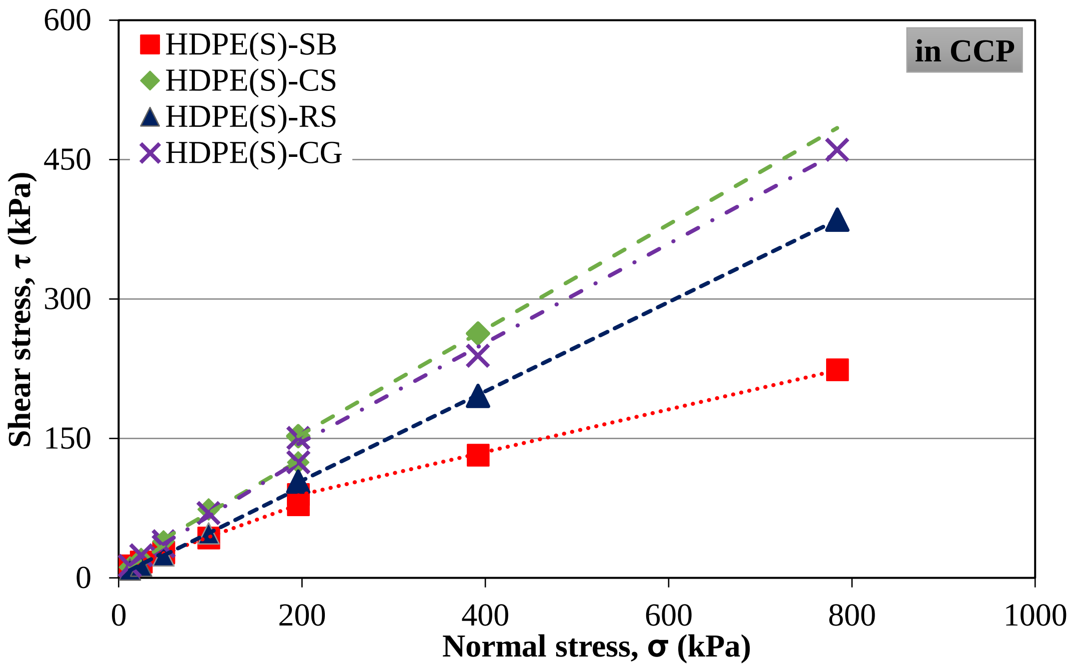

Figure 5.33: Mohr-Coulomb envelopes of 8 months CCP cured HDPE(S) – soil

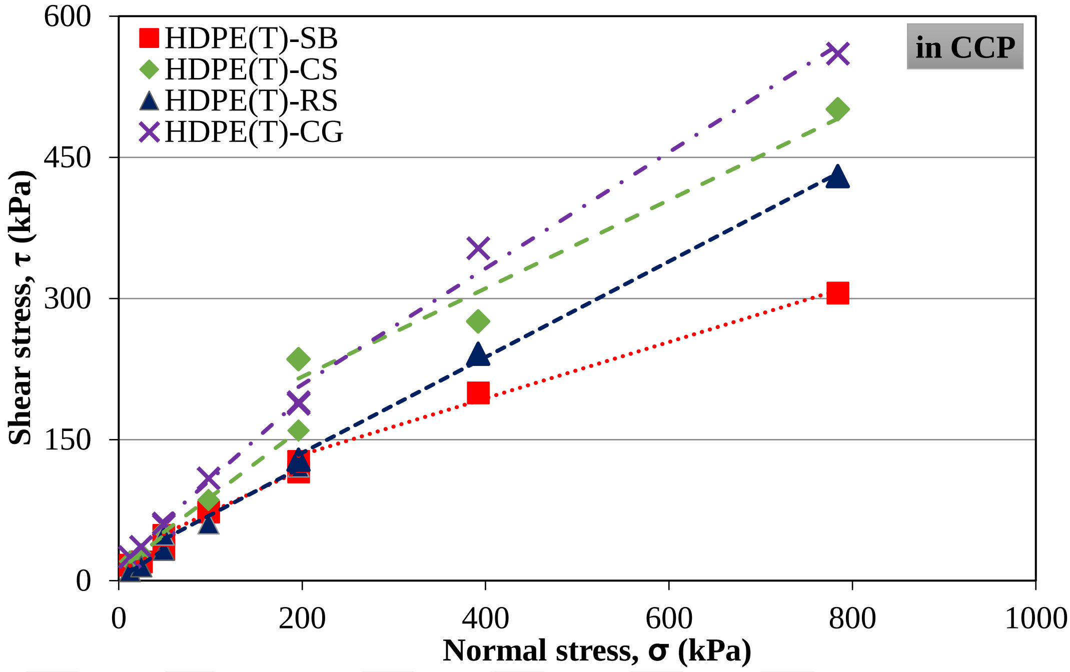

Figure 5.34: Mohr-Coulomb envelopes of 8 months CCP cured HDPE(T) – soil

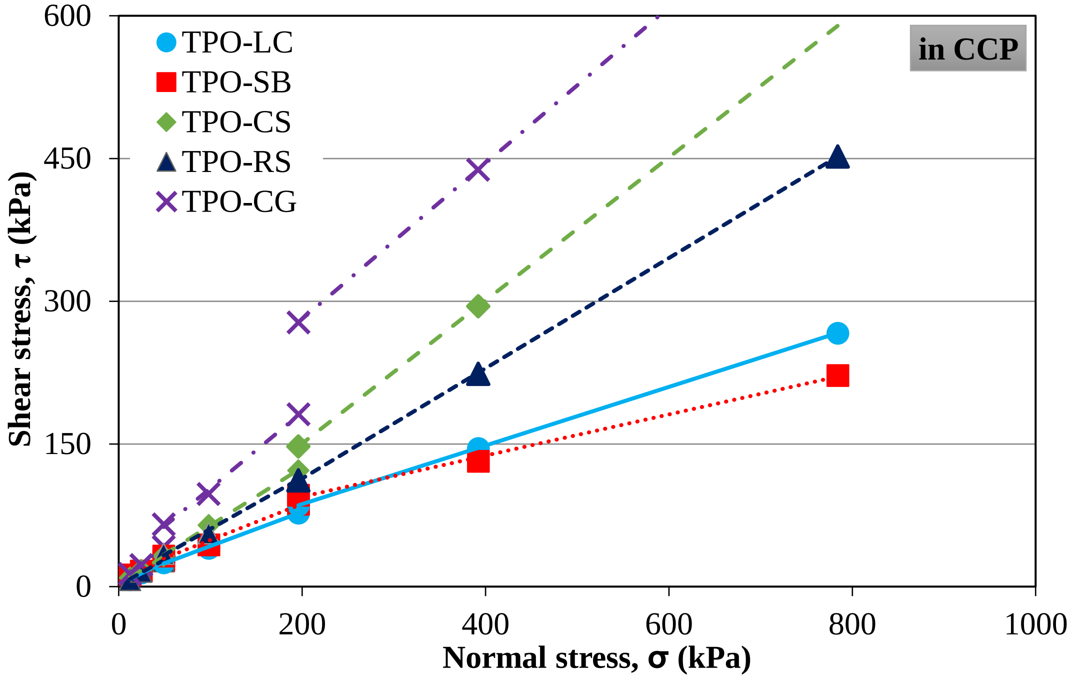

Figure 5.35: Mohr-Coulomb envelopes of 8 months CCP cured TPO – soil

Table 5.16: Friction angles of 8 months CCP cured HDPE(S) – soil, HDPE(T) – soil, and TPO – soil interfaces

Interface	Normal stress level			One envelope
	Low	Medium	High	
HDPE(S) – SB	21.0	19.6	14.7	15.4
HDPE(S) – CS	31.7	29.7	29.4	32.7
HDPE(S) – RS	27.2	26.0	25.6	26.1
HDPE(S) – CG	35.1	31.2	28.1	30.0
HDPE(T) – SB	25.1	24.4	16.7	20.8
HDPE(T) – CS	37.3	36.2	25.2	31.9
HDPE(T) – RS	32.4	27.1	27.0	28.7
HDPE(T) – CG	42.5	41.0	40.2	35.4
TPO – LC	25.7	19.7	17.1	18.5
TPO – SB	22.5	20.8	12.2	15.2
TPO – CS	30.4	31.3	36.9	36.7
TPO – RS	28.1	28.5	30.1	29.8
TPO – CG	38.0	38.6	39.2	48.7

The reductions in the δ of HDPE(S) cured in CCP for 8 months were 3.4, 5.4, 1.5, and 7.7% for SB, CS, RS, and CG, respectively. The average amount of decrease is 4.5%. The reductions in the δ of HDPE(T) cured in AMD for 8 months were 6.5, -2.0, 7.8, and 3.8% for SB, CS, RS, and CG, respectively. The average amount of decrease is 4.0%. The reductions in the δ of TPO cured in AMD for 8 months were 1.5, 4.6, 7.4, 7.2, and 1.3% for LC, SB, CS, RS, and CG, respectively. The average amount of decrease is 4.4%. When the average decreases are compared, the highest decrease is in HDPE(S) while the least decrease is in HDPE(T). While the highest amount of decrease was observed at the HDPE(T) – RS interface, the lowest amount of decrease was observed at the HDPE(T) – CS interface. That is, in areas that will be exposed to CCP leachate, 8 months curing results have shown that textured HDPE GM and round sand are not suitable.

MC failure envelopes of 8 months MSW cured HDPE(S) – soil, HDPE(T) – soil, and TPO – soil interfaces for all normal stress levels separately are shown in Figure 5.36, Figure 5.37, and Figure 5.38. In addition, the interface friction angle values obtained from the envelopes are listed in Table 5.17.

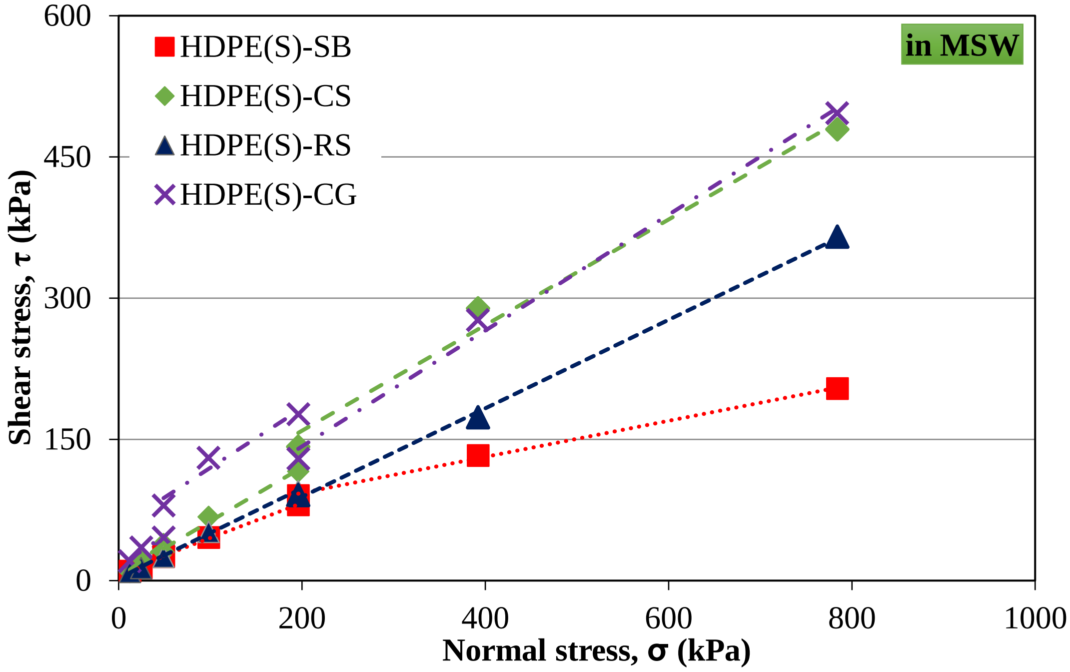

Figure 5.36: Mohr-Coulomb envelopes of 8 months MSW cured HDPE(S) – soil

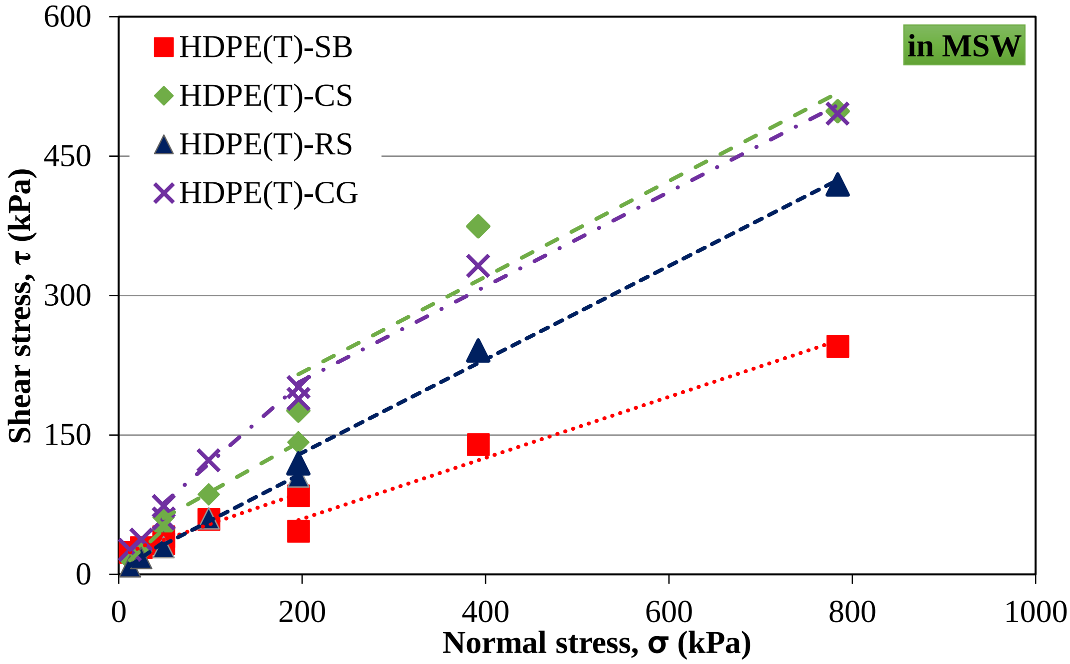

Figure 5.37: Mohr-Coulomb envelopes of 8 months MSW cured HDPE(T) – soil

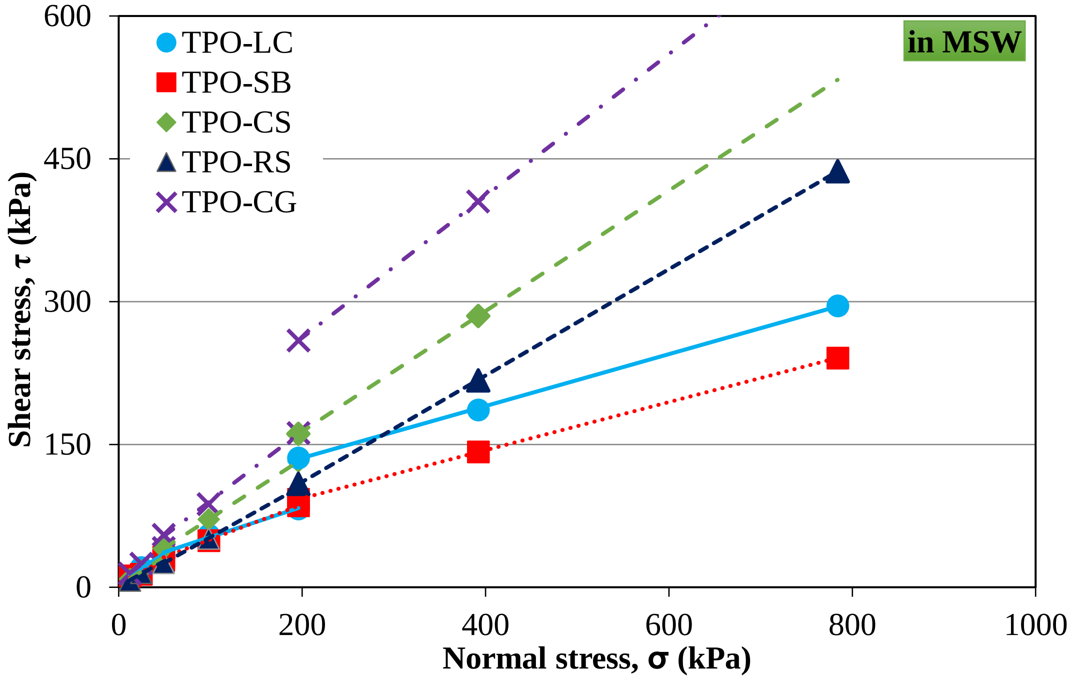

Figure 5.38: Mohr-Coulomb envelopes of 8 months MSW cured TPO – soil

Table 5.17: Friction angles of 8 months MSW cured HDPE(S) – soil, HDPE(T) – soil, and TPO – soil interfaces

Interface	MSW curing			
	Low	Medium	High	One envelope
HDPE(S) – SB	24.4	20.3	10.8	14.3
HDPE(S) – CS	37.6	29.7	29.3	31.9
HDPE(S) – RS	26.6	25.3	25.2	24.6
HDPE(S) – CG	33.1	32.3	32.1	30.9
HDPE(T) – SB	24.9	18.7	18.2	16.0
HDPE(T) – CS	42.3	28.9	27.2	33.3
HDPE(T) – RS	34.9	26.9	26.7	28.3
HDPE(T) – CG	42.5	40.8	36.1	31.6
TPO – LC	32.3	17.6	15.2	20.4
TPO – SB	25.2	20.2	14.2	16.5
TPO – CS	31.3	31.9	32.3	36.2
TPO – RS	28.1	28.3	29.2	29.2
TPO – CG	36.1	36.2	36.7	46.4

The reductions in the δ of HDPE(S) cured in MSW for 8 months were 0.0, 5.4, 4.2, and 4.4% for SB, CS, RS, and CG, respectively. The average amount of decrease is 3.5%. The reductions in the δ of HDPE(T) cured in MSW for 8 months were 28.4, 18.6, 8.5, and 4.2% for SB, CS, RS, and CG, respectively. The average amount of decrease is 14.9%. The reductions in the δ of TPO cured in MSW for 8 months were 12.0, 7.3, 5.6, 7.8, and 7.4% for LC, SB, CS, RS, and CG, respectively. The average amount of decrease is 8.0%. When the average decreases are compared, the highest decrease is in HDPE(T) while the least decrease is in HDPE(S). While the highest amount of decrease was observed at the HDPE(T) – SB interface, the lowest amount of decrease was observed at the HDPE(S) – SB interface. That is, in areas that will be exposed to MSW leachate, 8 month curing results have shown that textured HDPE GM and sand/bentonite mixture are not suitable.

5.4.3 Direct shear test results of 16 months cured GM – soil interfaces

MC failure envelopes of 16 months SWt cured PVC(1.5) – soil, PVC(3.0) – soil, and TPO – soil interfaces are shown in Figure 5.39, Figure 5.40, and Figure 5.41. In addition, the interface friction angle values obtained from the envelopes are listed in Table 5.18. In order to see the decrease in the δ with curing, the δ of the uncured GMs in the medium normal stress level are also given in Table 5.18.

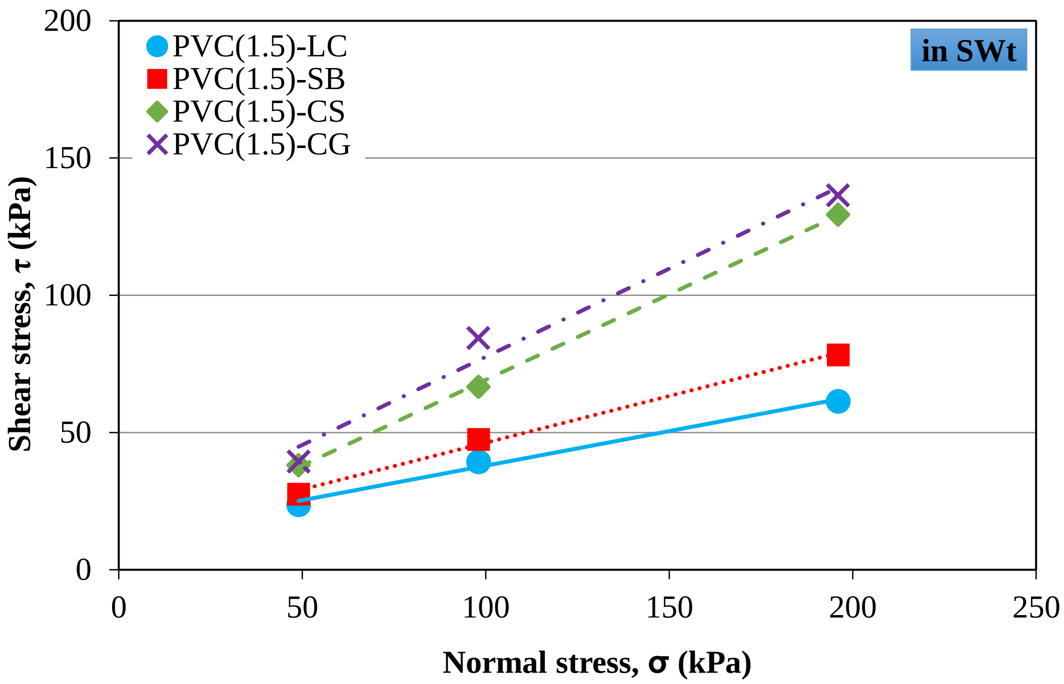

Figure 5.39: Mohr-Coulomb envelopes of 16 months SWt cured PVC(1.5) – soil

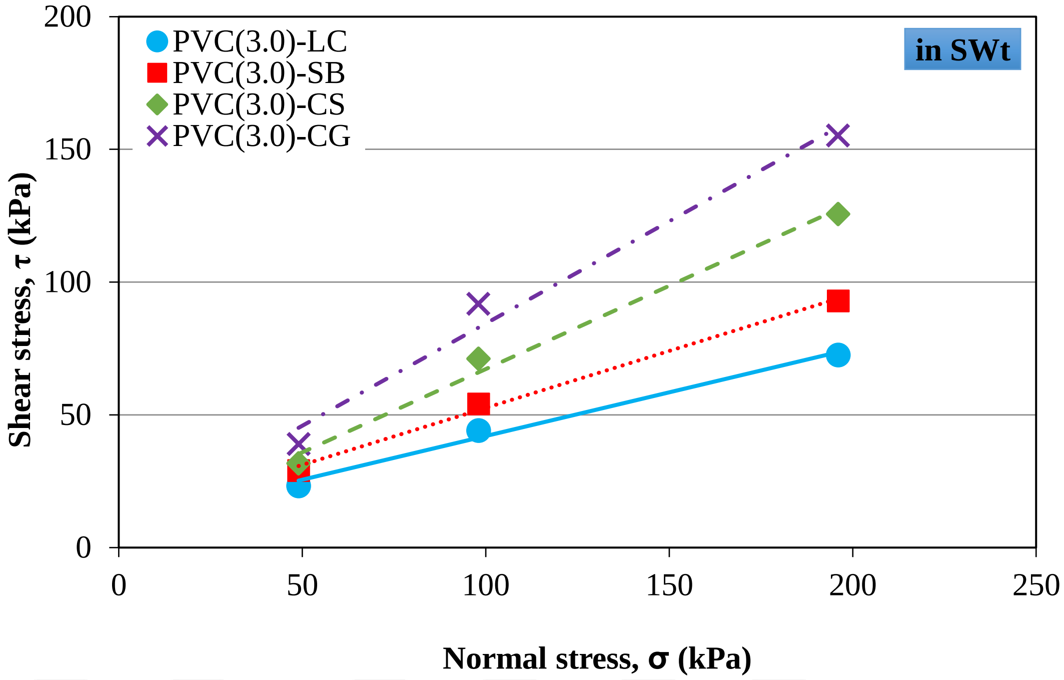

Figure 5.40: Mohr-Coulomb envelopes of 16 months SWt cured PVC(3.0) – soil

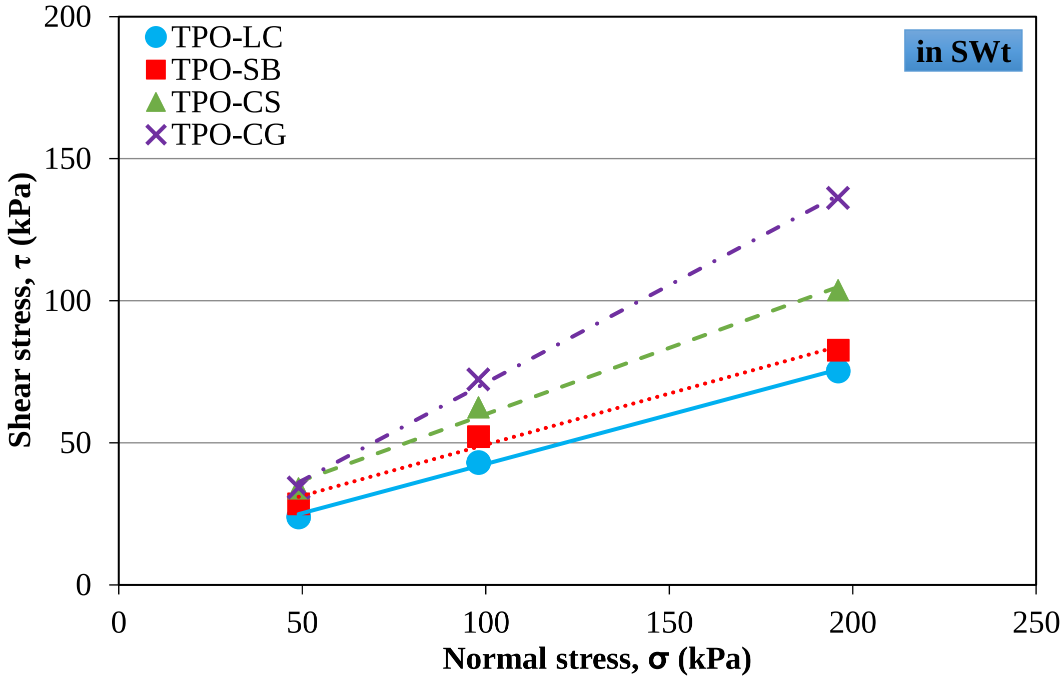

Figure 5.41: Mohr-Coulomb envelopes of 16 months SWt cured TPO – soil

Table 5.18: Friction angles of 16 months SWt cured PVC(1.5) – soil, PVC(3.0) – soil, and TPO – soil interfaces

Soil	No curing			SWt curing		
	PVC(1.5)	PVC(3.0)	TPO	PVC(1.5)	PVC(3.0)	TPO
LC	19.9	20.6	20	14.1	18.2	19.1
SB	26.3	32.2	21.8	18.8	23.2	19.8
CS	35.3	34.2	33.8	32.0	32.1	25.0
CG	34.7	41.3	39.1	32.7	37.6	34.5

The reductions in the δ of PVC(1.5) cured in SWt for 16 months were 29.1, 28.5, 9.3, and 5.8% for LC, SB, CS, and CG, respectively. The average amount of decrease is 18.2%. The reductions in the δ of PVC(3.0) cured in SWt for 8 months were 11.7, 28.0, 6.1, and 9.0% for LC, SB, CS, and CG, respectively. The average amount of decrease is 13.7%. The reductions in the δ of TPO cured in SWt for 16 months were 4.5, 9.2, 26.0, and 11.8% for LC, SB, CS, and CG, respectively. The average amount of decrease is 12.9%. When the average decreases are compared, the highest decrease is in PVC(1.5), while the least decrease is in TPO. While the highest amount of decrease was observed at the PVC(1.5) – LC interface, the lowest amount of decrease was observed at the TPO – LC interface. That is, in areas that will be exposed to SWt, 16 month curing results have shown that 1.5 mm thick PVC GM and low plasticity clay are not suitable.

MC failure envelopes of 16 months AMD cured HDPE(S) – soil, HDPE(T) – soil, and TPO – soil interfaces are shown in Figure 5.42, Figure 5.43, and Figure 5.44. In addition, the interface friction angle values obtained from the envelopes are listed in Table 5.19.

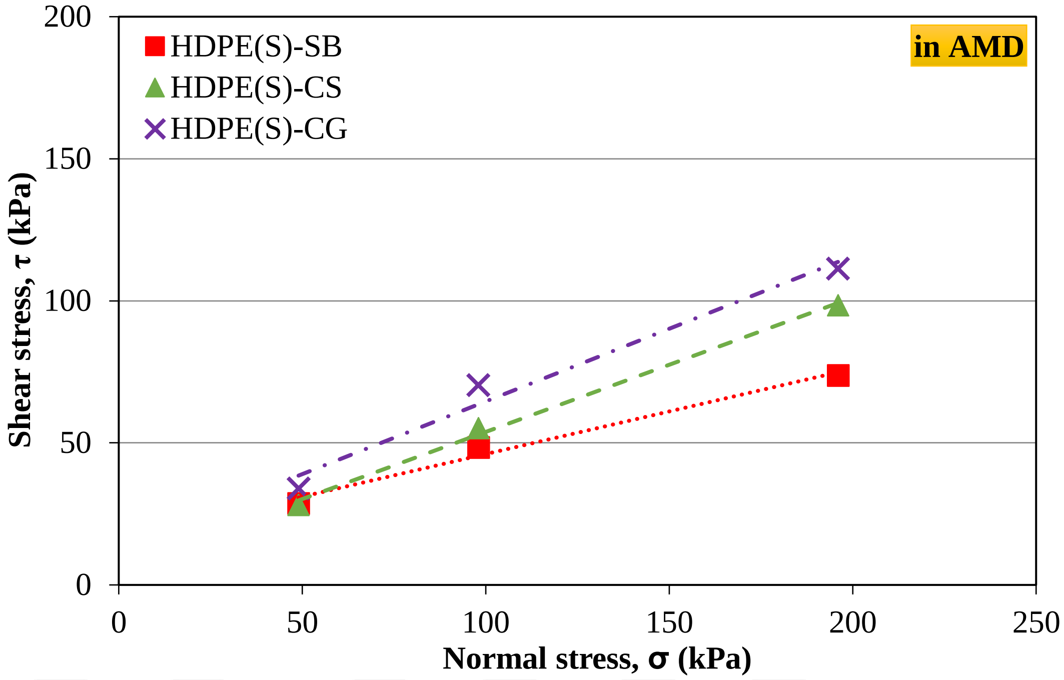

Figure 5.42: Mohr-Coulomb envelopes of 16 months AMD cured HDPE(S) – soil

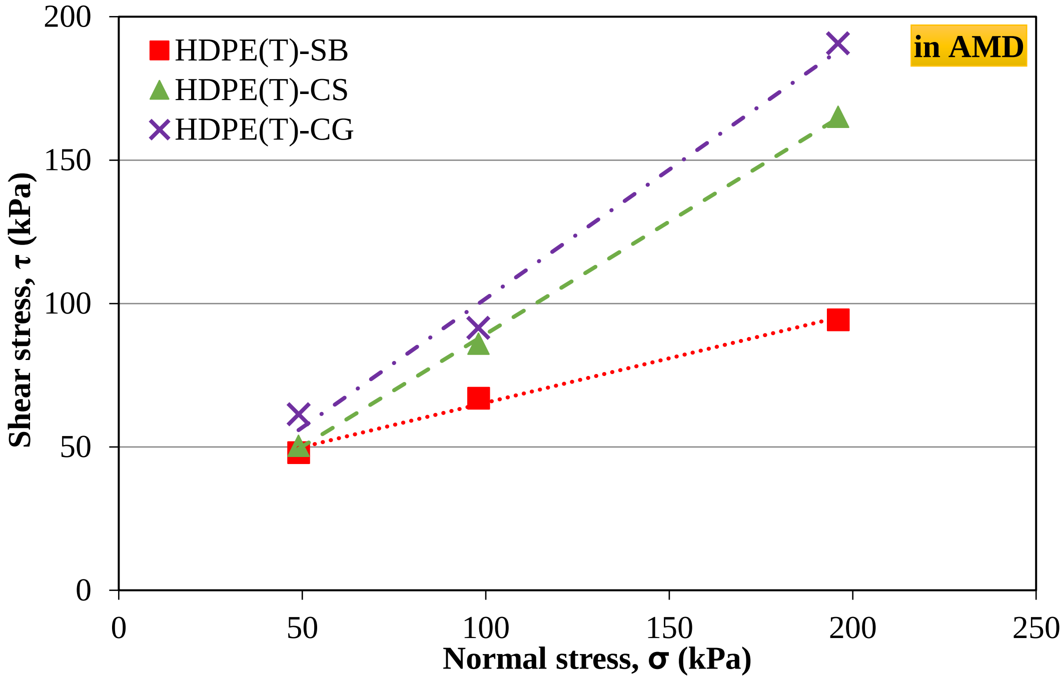

Figure 5.43: Mohr-Coulomb envelopes of 16 months AMD cured HDPE(T) – soil

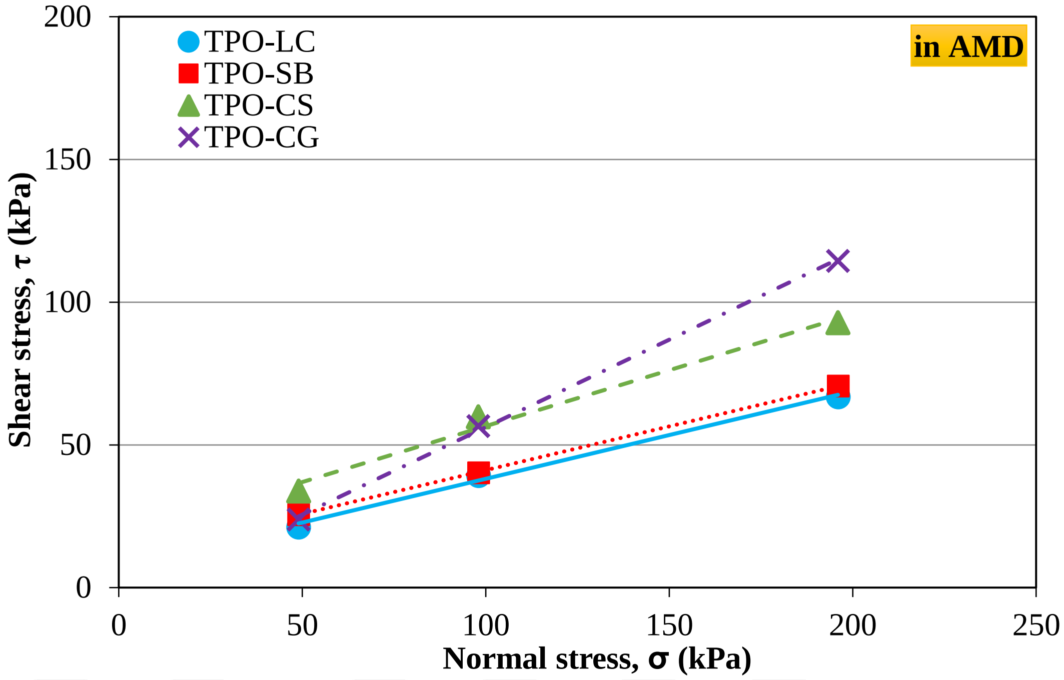

Figure 5.44: Mohr-Coulomb envelopes of 16 months AMD cured TPO – soil

Table 5.19: Friction angles of 16 months AMD cured HDPE(S) – soil, HDPE(T) – soil, and TPO – soil interfaces

Soil	No curing			AMD curing		
	HDPE(S)	HDPE(T)	TPO	HDPE(S)	HDPE(T)	TPO
LC	20.8	28.1	20	-	-	17.0
SB	20.3	26.1	21.8	16.7	17.2	17.1
CS	31.4	35.5	33.8	25.3	24.1	21.4
CG	33.8	42.6	39.1	27.1	38.1	31.5

The reductions in the δ of HDPE(S) cured in AMD for 16 months were 17.7, 19.4, and 19.8% for SB, CS, and CG, respectively. The average amount of decrease is 19.0%. The reductions in the δ of HDPE(T) cured in AMD for 16 months were 34.1, 32.1, and 10.6% for SB, CS, and CG, respectively. The average amount of decrease is 25.6%. The reductions in the δ of TPO cured in AMD for 16 months were 15.0, 21.6, 36.7, and 19.4% for LC, SB, CS, and CG, respectively. The average amount of decrease is 23.2%. When the average decreases are compared, the highest decrease is in HDPE(T), while the least decrease is in HDPE(S). While the highest amount of decrease was observed at the TPO – CS interface, the lowest amount of decrease was observed at the HDPE(T) – CG interface. That is, in areas that will be exposed to AMD, 16 month curing results have shown that TPO GM and angular sand are not suitable.

MC failure envelopes of 16 months CCP cured HDPE(S) – soil, HDPE(T) – soil, and TPO – soil interfaces are shown in Figure 5.45, Figure 5.46, and Figure 5.47. In addition, the interface friction angle values obtained from the envelopes are listed in Table 5.20.

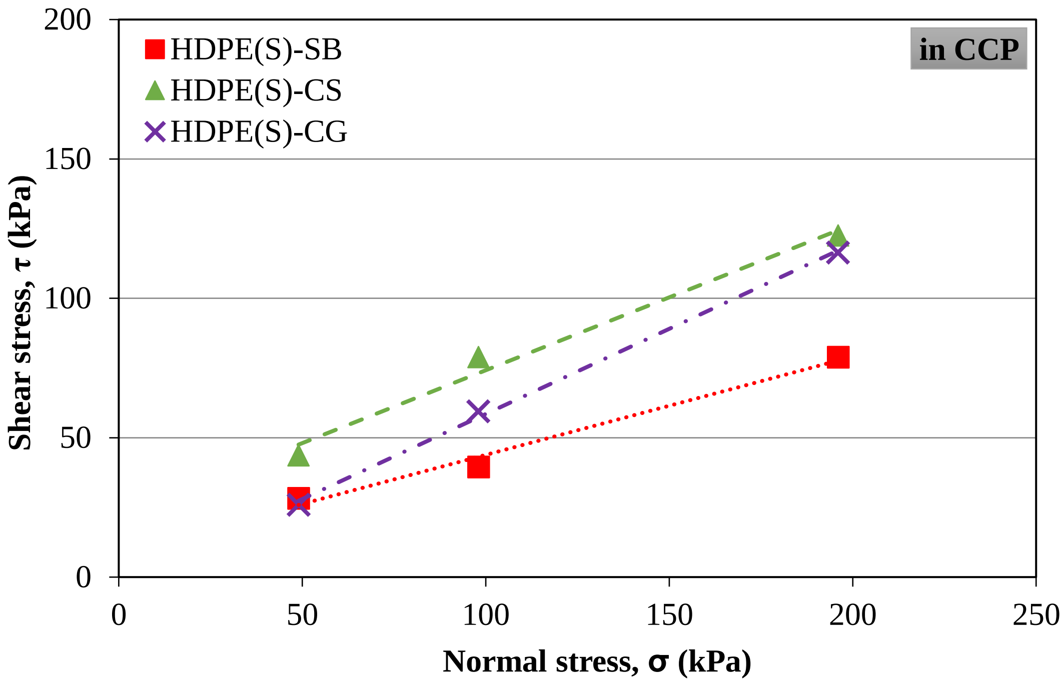

Figure 5.45: Mohr-Coulomb envelopes of 16 months CCP cured HDPE(S) – soil

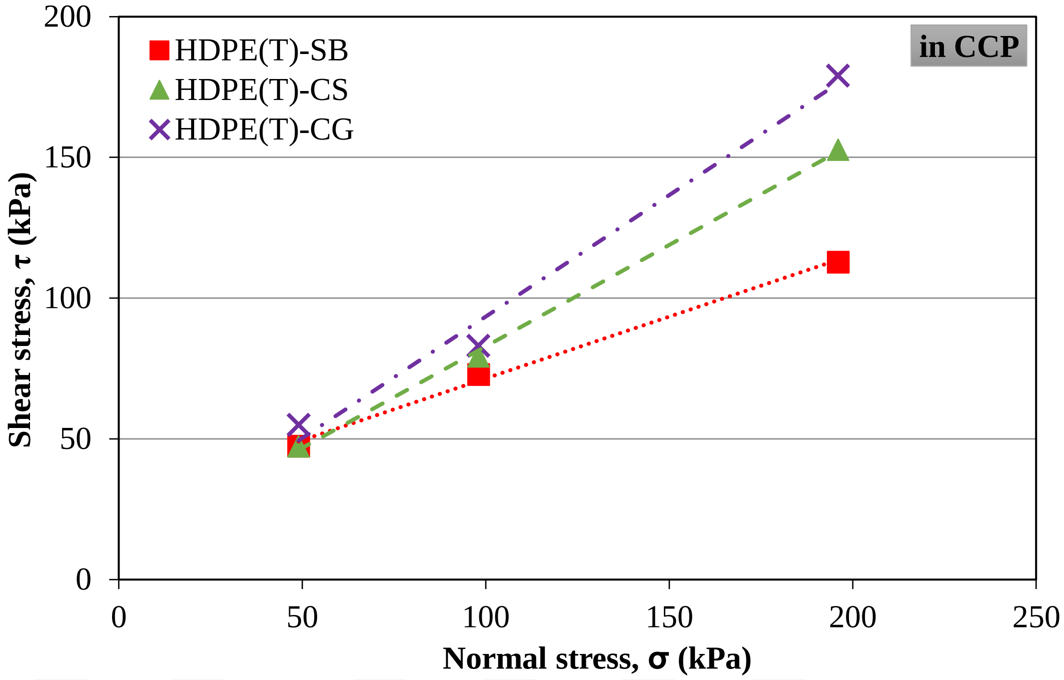

Figure 5.46: Mohr-Coulomb envelopes of 16 months CCP cured HDPE(T) – soil

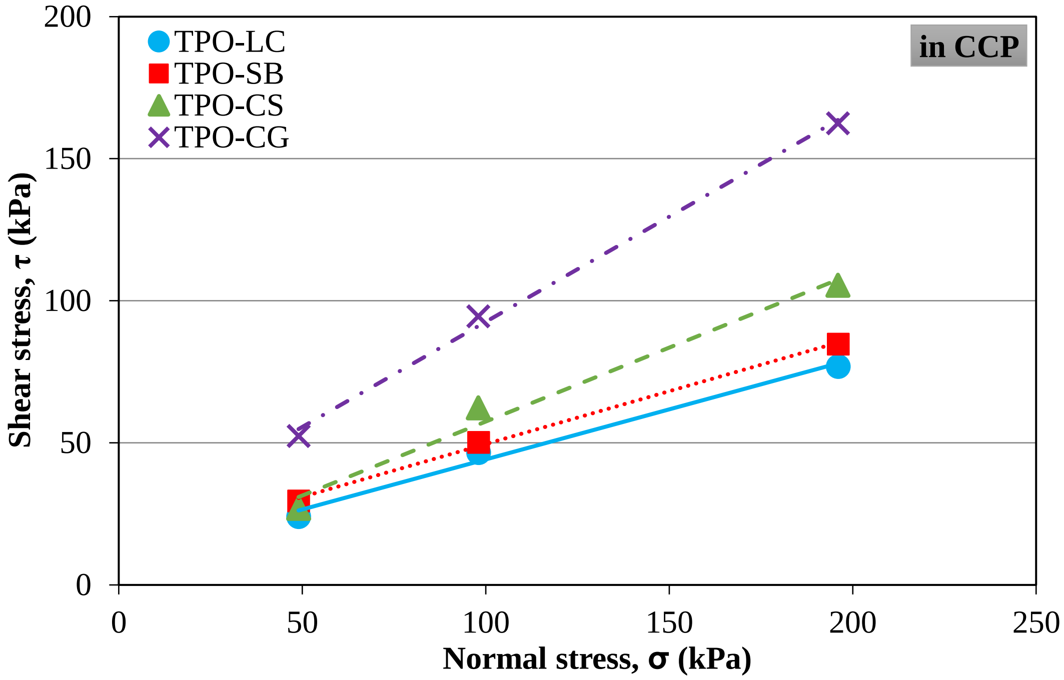

Figure 5.47: Mohr-Coulomb envelopes of 16 months CCP cured TPO – soil

Table 5.20: Friction angles of 16 months CCP cured HDPE(S) – soil, HDPE(T) – soil, and TPO – soil interfaces

Soil	No curing			CCP curing		
	HDPE(S)	HDPE(T)	TPO	HDPE(S)	HDPE(T)	TPO
LC	20.8	28.1	20	-	-	19.4
SB	20.3	26.1	21.8	19.4	23.7	20.4
CS	31.4	35.5	33.8	27.6	35.8	27.5
CG	33.8	42.6	39.1	31.4	40.8	36.5

The reductions in the δ of HDPE(S) cured in CCP for 16 months were 4.4, 12.1, and 7.1% for SB, CS, and CG, respectively. The average amount of decrease is 7.9%. The reductions in the δ of HDPE(T) cured in CCP for 16 months were 9.2, -0.8, and 4.2% for SB, CS, and CG, respectively. The average amount of decrease is 4.2%. The reductions in the δ of TPO cured in CCP for 16 months were 3.0, 6.4, 18.6, and 6.6% for LC, SB, CS, and CG, respectively. The average amount of decrease is 8.7%. When the average decreases are compared, the highest decrease is in TPO, while the least decrease is in HDPE(T). While the highest amount of decrease was observed at the TPO – CS interface, the lowest amount of decrease was observed at the HDPE(T) – CS interface. That is, in areas that will be exposed to CCP, 16 months curing results have shown that TPO GM and angular sand are not suitable.

MC failure envelopes of 16 months MSW cured HDPE(S) – soil, HDPE(T) – soil, and TPO – soil interfaces are shown in Figure 5.48, Figure 5.49, and Figure 5.50. In addition, the interface friction angle values obtained from the envelopes are listed in Table 5.21.

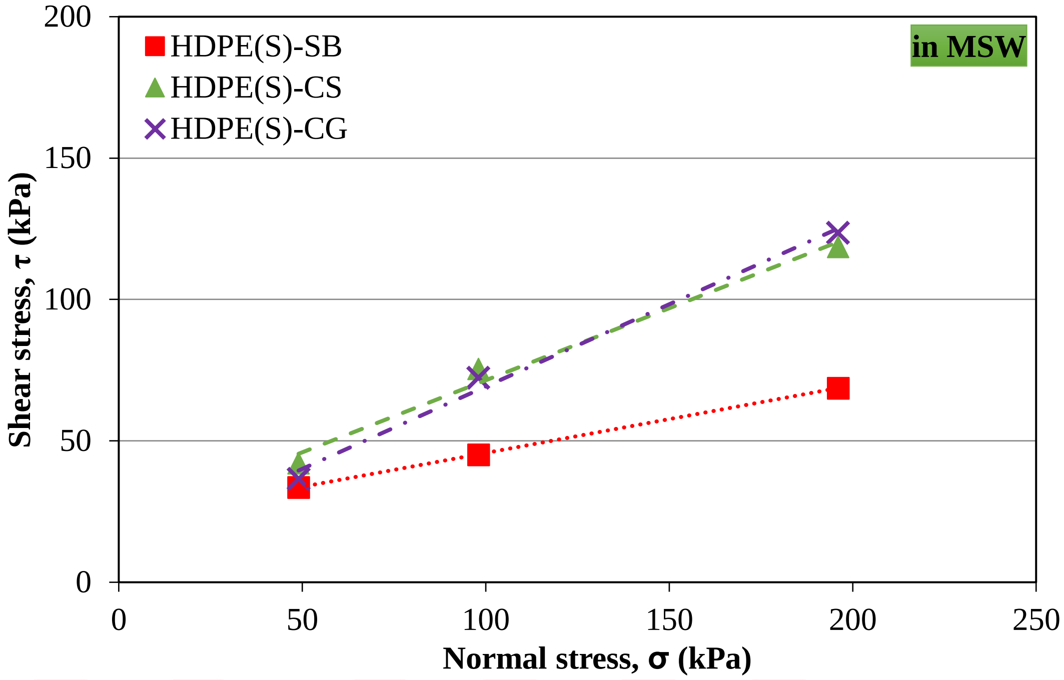

Figure 5.48: Mohr-Coulomb envelopes of 16 months MSW cured HDPE(S) – soil

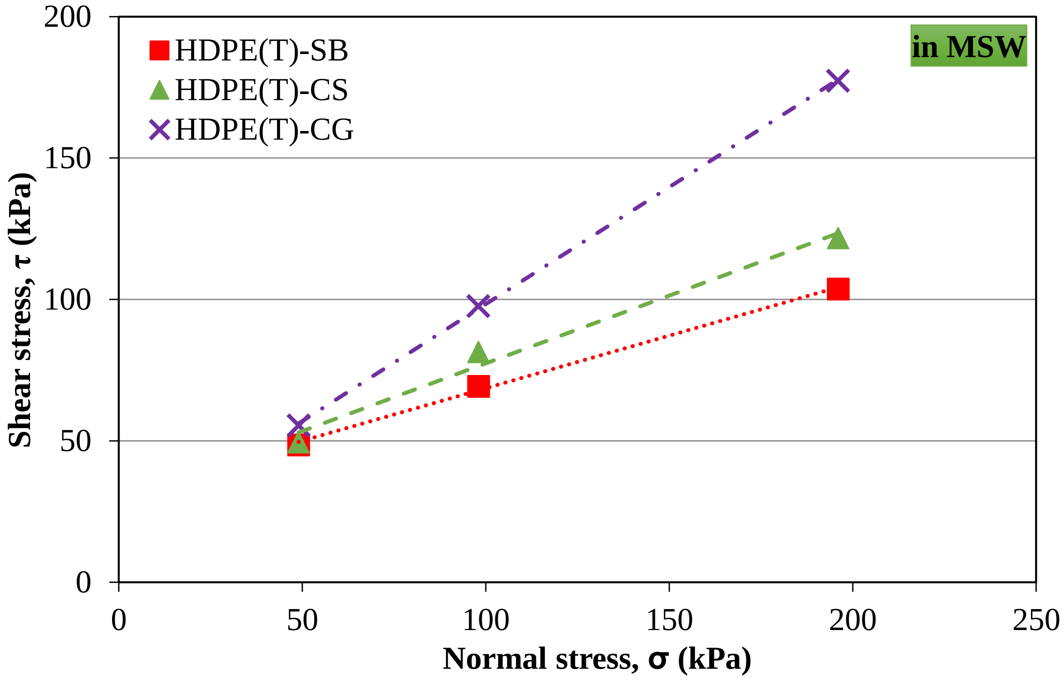

Figure 5.49: Mohr-Coulomb envelopes of 16 months MSW cured HDPE(T) – soil

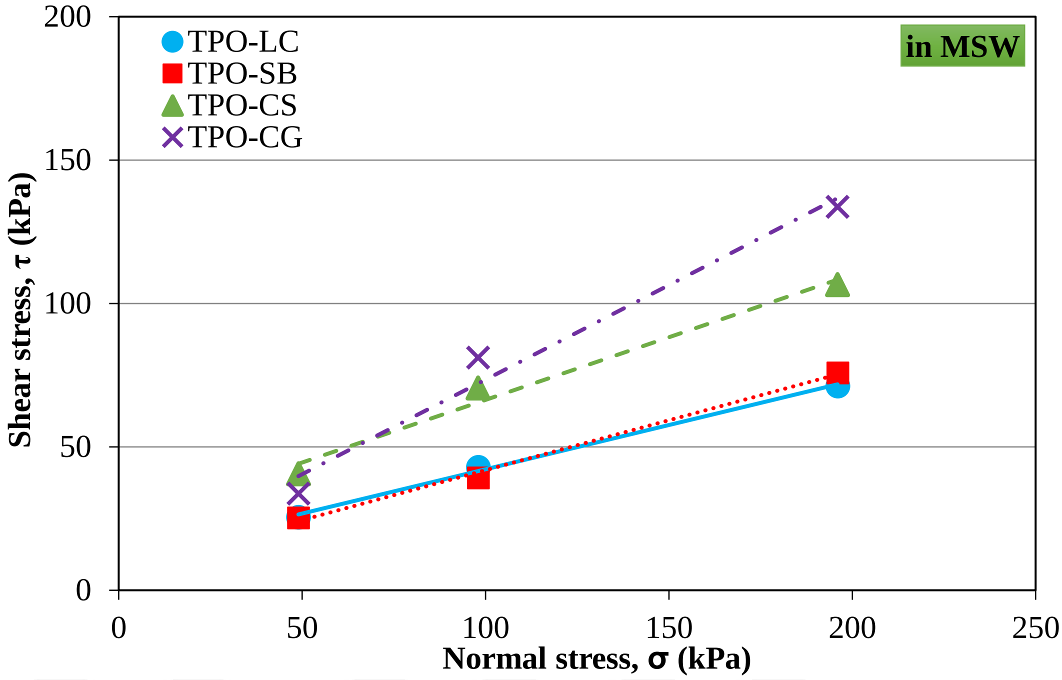

Figure 5.50: Mohr-Coulomb envelopes of 16 months MSW cured TPO – soil

Table 5.21: Friction angles of 16 months MSW cured HDPE(S) – soil, HDPE(T) – soil, and TPO – soil interfaces

Soil	No curing			MSW curing		
	HDPE(S)	HDPE(T)	TPO	HDPE(S)	HDPE(T)	TPO
LC	20.8	28.1	20	-	-	17.1
SB	20.3	26.1	21.8	18.2	20.4	19.2
CS	31.4	35.5	33.8	27.0	25.6	23.6
CG	33.8	42.6	39.1	30.2	39.6	33.4

The reductions in the δ of HDPE(S) cured in MSW for 16 months were 10.3, 14.0, and 10.7% for SB, CS, and CG, respectively. The average amount of decrease is 11.7%. The reductions in the δ of HDPE(T) cured in MSW for 16 months were 21.8, 27.9, and 7.0% for SB, CS, and CG, respectively. The average amount of decrease is 18.9%. The reductions in the δ of TPO cured in MSW for 16 months were 14.5, 11.9, 30.2, and 14.6% for LC, SB, CS, and CG, respectively. The average amount of decrease is 17.8%. When the average decreases are compared, the highest decrease is in HDPE(T) while the least decrease is in HDPE(S). While the highest amount of decrease was observed at the TPO – CS interface, the lowest amount of decrease was observed at the HDPE(T) – CG interface. That is, in areas that will be exposed to MSW, 16 month curing results have shown that TPO GM and angular sand are not suitable.

In order to learn more about the shear behaviors of the interfaces, the shear stress – axial strain graphs were examined under normal stress of 196 kPa (medium normal stress level). For this purpose, the strain value (ε_{50}) in which fifty percent of the shear strength, which occurs under 196 kPa normal stress for each interface, was determined as the percentage of the total strain (100%). The ε_{50} values of the SWt cured soil – PVC(1.5), soil – PVC(3.0), and soil – TPO interfaces are shown in Figure 5.51, Figure 5.52, and Figure 5.53. The ε_{50} values of the AMD cured soil – HDPE(S), soil – HDPE(T), and soil – TPO interfaces are shown in Figure 5.54, Figure 5.55, and Figure 5.56. The ε_{50} values of the CCP cured soil – HDPE(S), soil – HDPE(T), and soil – TPO interfaces are shown in Figure 5.57, Figure 5.58, and Figure 5.59. The ε_{50} values of the MSW cured soil – HDPE(S), soil – HDPE(T), and soil – TPO interfaces are shown in Figure 5.60, Figure 5.61, and Figure 5.62.

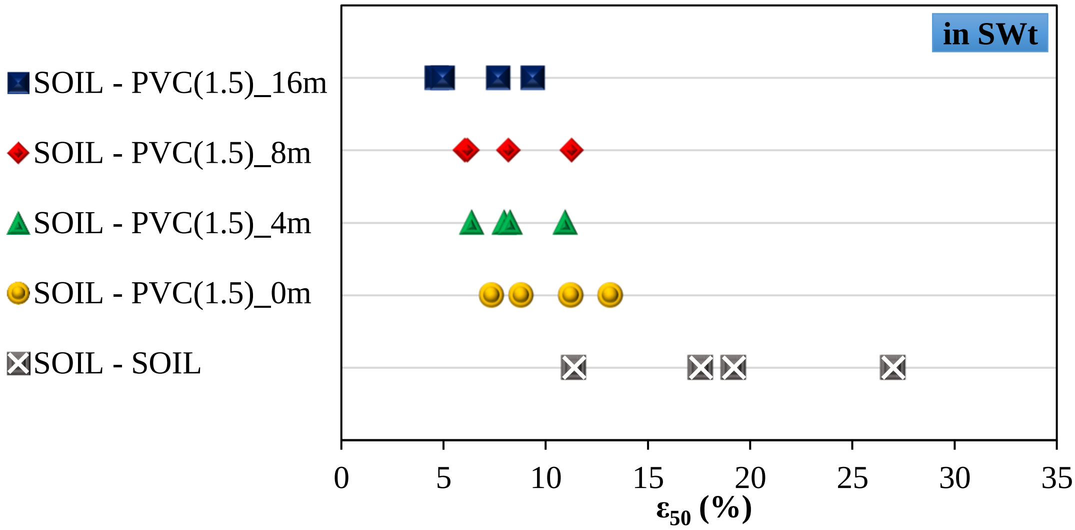

Figure 5.51: The ε_{50} values of the SWt cured soil – PVC(1.5) interface

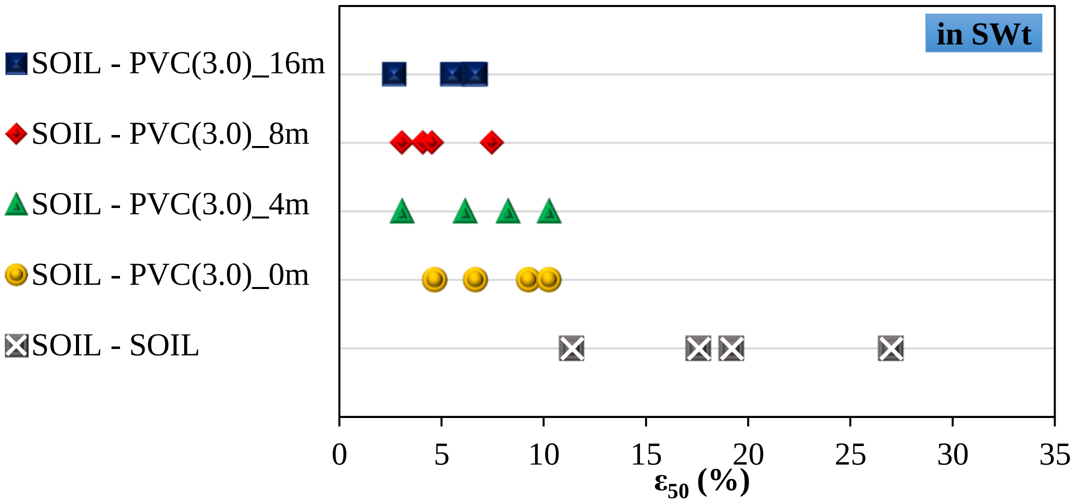

Figure 5.52: The ε_{50} values of the SWt cured soil – PVC(3.0) interface

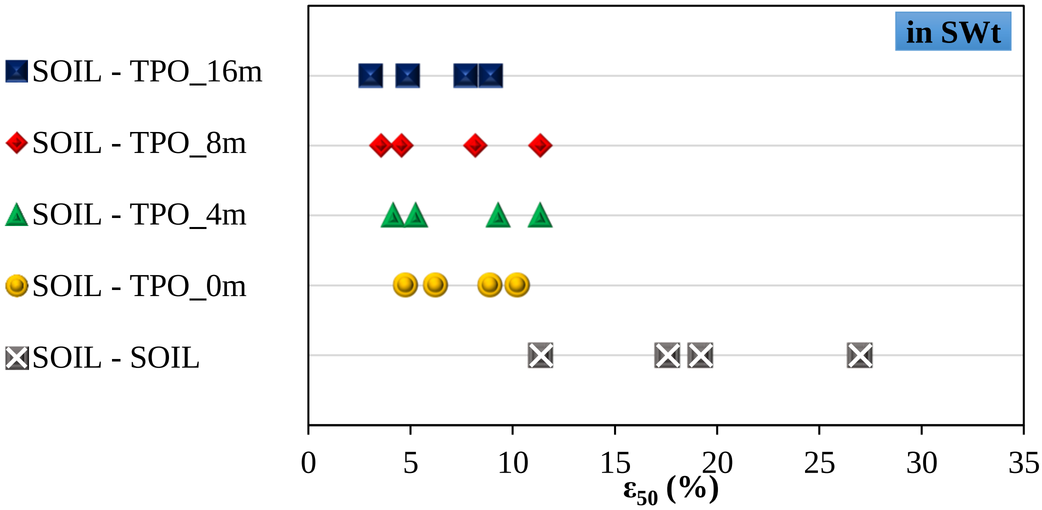

Figure 5.53: The ε_{50} values of the SWt cured soil – TPO interface

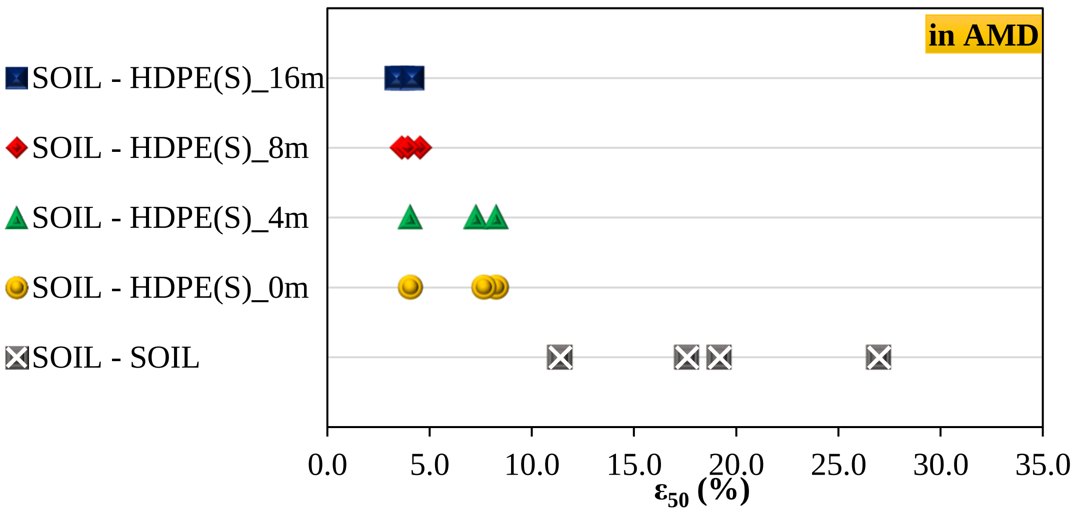

Figure 5.54: The ε_{50} values of the AMD cured soil – HDPE(S) interface

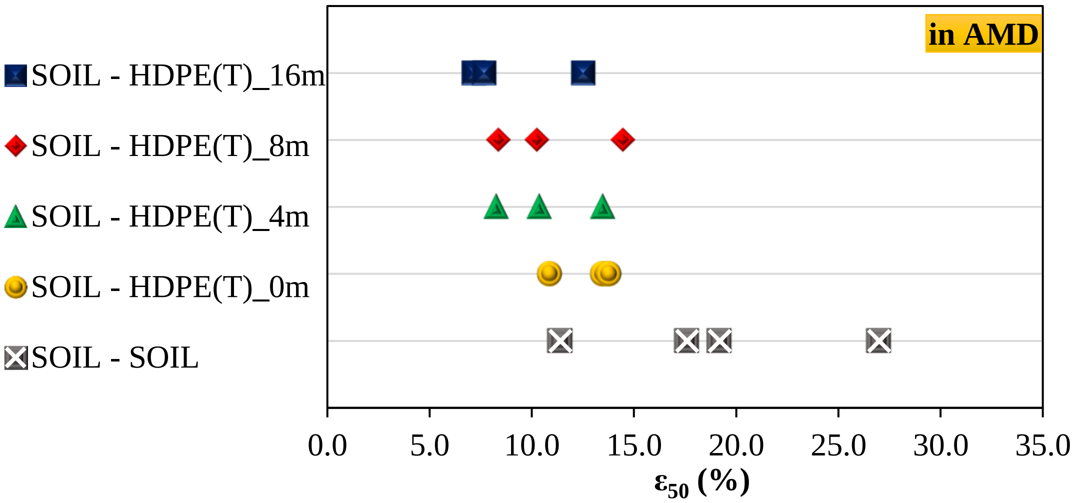

Figure 5.55: The ε_{50} values of the AMD cured soil – HDPE(T) interface

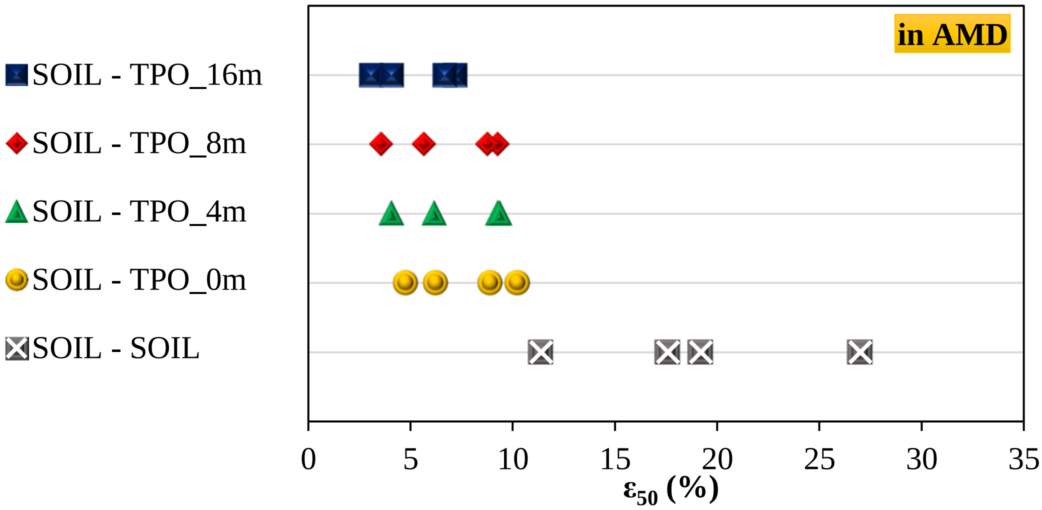

Figure 5.56: The ε_{50} values of the AMD cured soil – TPO interface

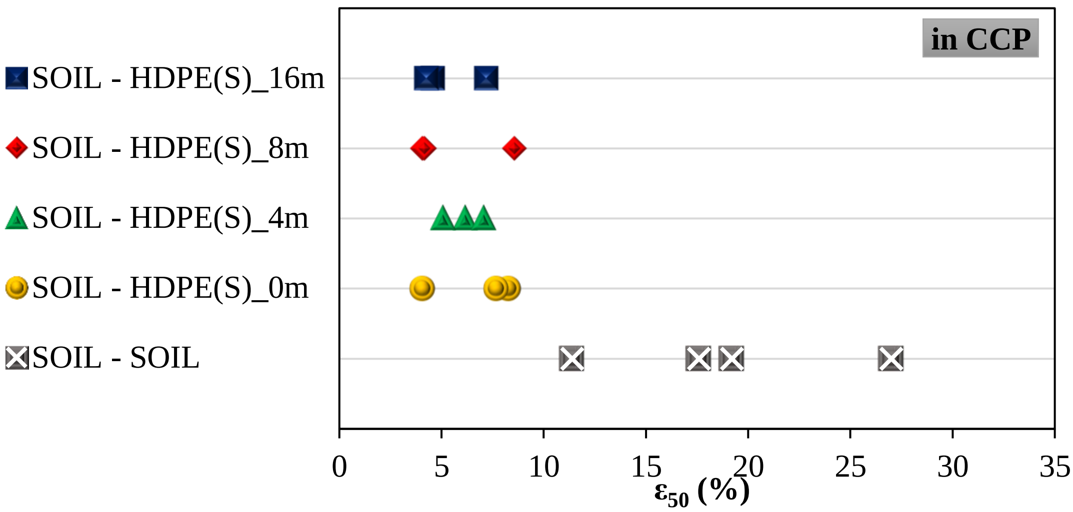

Figure 5.57: The ε_{50} values of the CCP cured soil – HDPE(S) interface

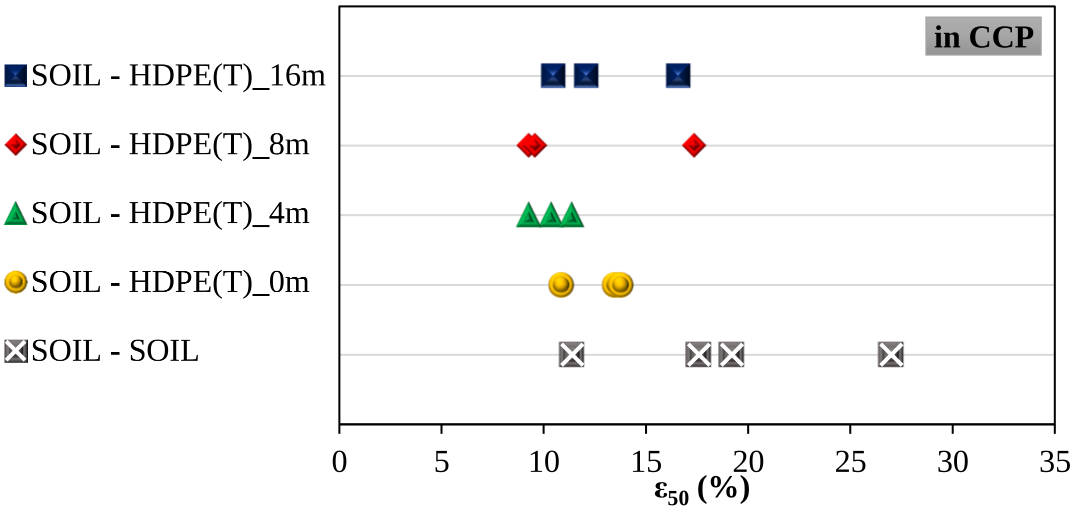

Figure 5.58: The ε_{50} values of the CCP cured soil – HDPE(T) interface

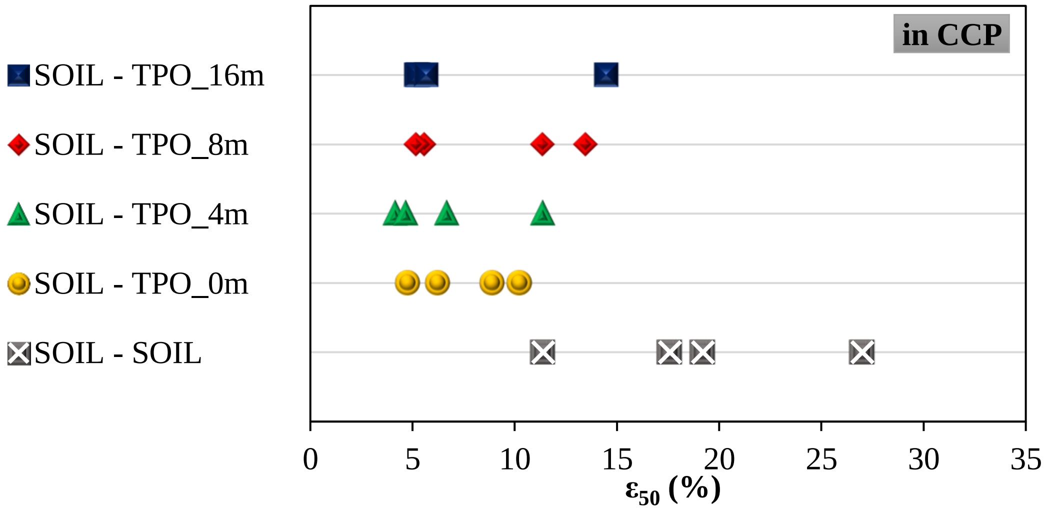

Figure 5.59: The ε_{50} values of the CCP cured soil – TPO interface

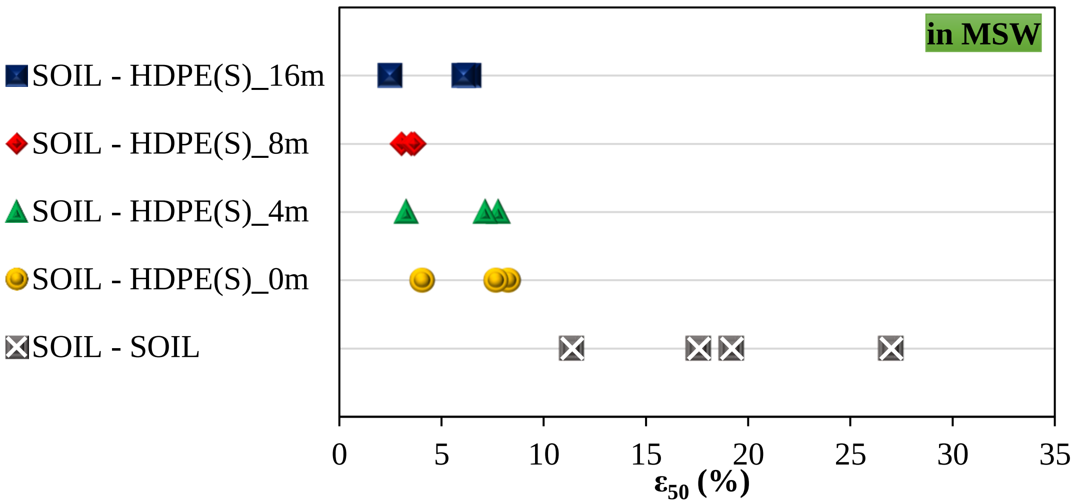

Figure 5.60: The ε_{50} values of the MSW cured soil – HDPE(S) interface

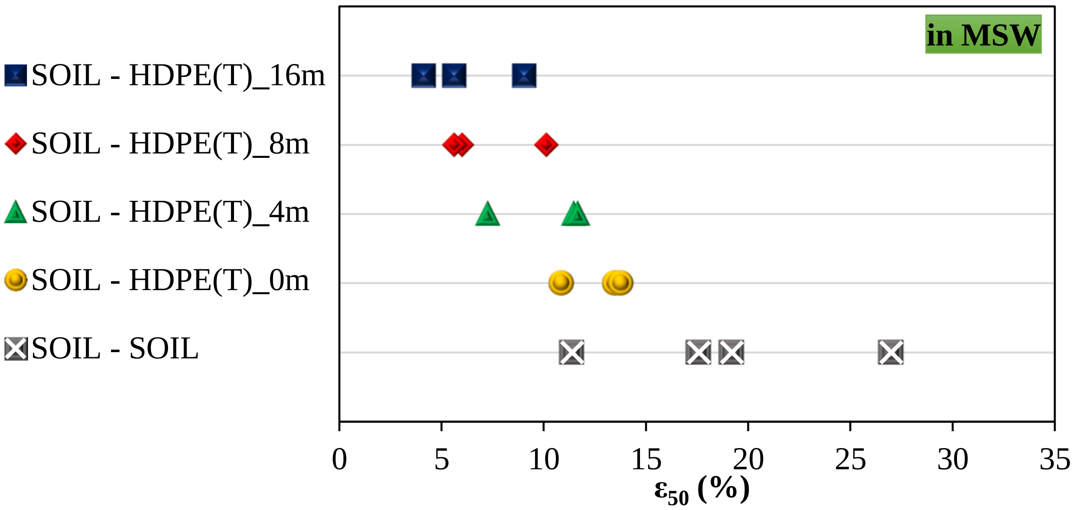

Figure 5.61: The ε_{50} values of the MSW cured soil – HDPE(T) interface

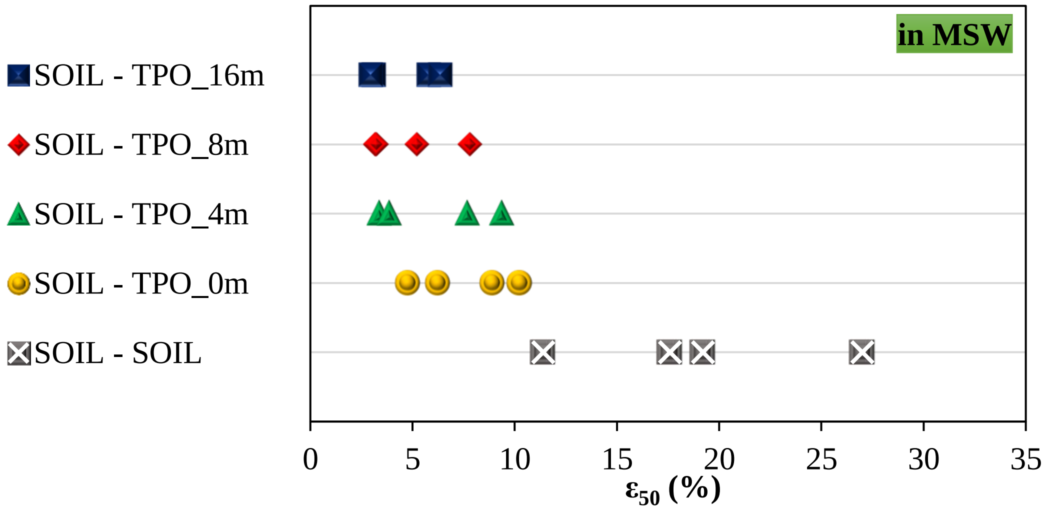

Figure 5.62: The ε_{50} values of the MSW cured soil – TPO interface

When all interfaces are examined, the soil – soil reached fifty percent of the shear strength (τ_{50}) in higher strains, while the soil – GM reached lower strains. This means the soil – GM interface has brittle behavior, and the soil – soil interface has ductile behavior. In other words, the soil – soil has a higher toughness, while the soil – GM interfaces have a lower toughness [94–96]. This is another indication of why the soil – GM interface is quite dangerous compared to the soil itself. For those who are cured in SWT, it is observed that the interfaces exhibit more brittle behavior as the curing time increases. This situation is more obvious in PVC, while it is not obvious in TPO. It can be interpreted that SWt curing reduces the toughness of the soil – PVC interface. It is seen that the ε_{50} values decrease as the curing time increases in the

AMD and MSW cured samples. So, AMD and MSW curing reduces the toughness of the soil – HDPE and soil – TPO interfaces.

5.5 Image analysis and surface roughness

The OPM analyses were carried out with PVC(1.5), PVC(3.0), HDPE(S), and TPO GMs cured for 16 months. Surface roughness measurements were made after the interface direct shear tests with LC, SB, CS, and CG soils. Average (R_a) and maximum (R_{max}) roughness values of PVC(1.5), PVC(3.0), and TPO cured in SWt are shown in Figure 5.63 and Figure 5.64. When Figure 5.63 and Figure 5.64 were examined, it was seen that R_a and R_{max} values increase as the grain size and grain angularity increase. This proves that angular and coarse grains are embedded in the GM surface and increase the interface friction angle. In addition, it was observed that the surface roughness after the direct shear test of TPO was higher than PVC. The reason for this is that PVC with a soft surface exhibits elastoplastic behavior and some of the deformations that occur are not permanent. TPO, on the other hand, showed plastic behavior and its deformations were permanent.

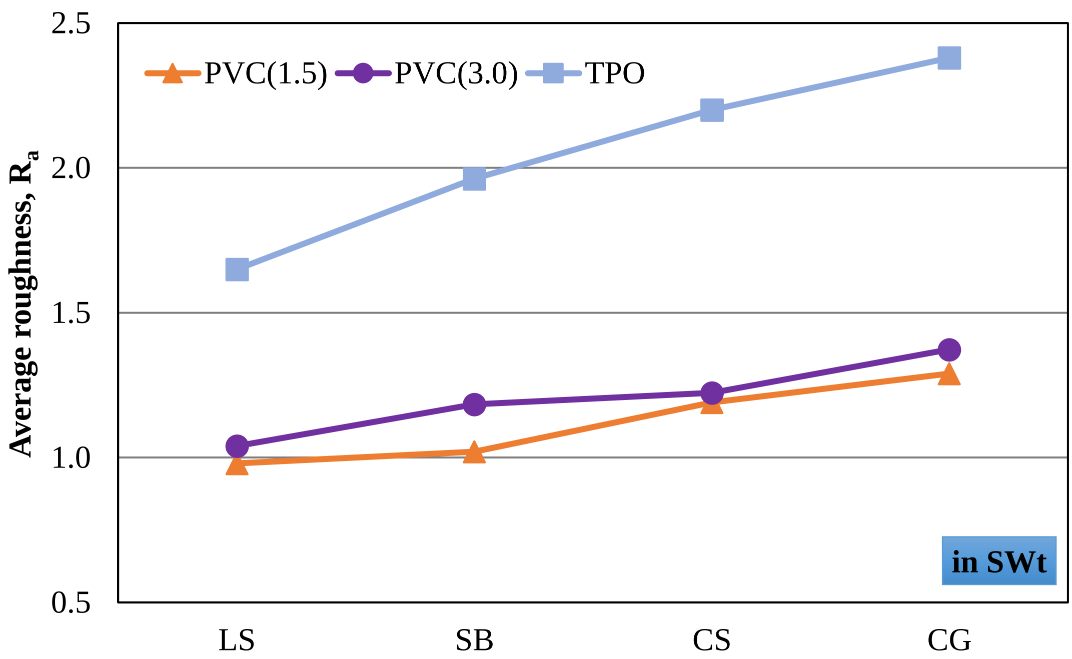

Figure 5.63: Average roughness values of 16 months SWt cured GM – soil interfaces after direct shear tests

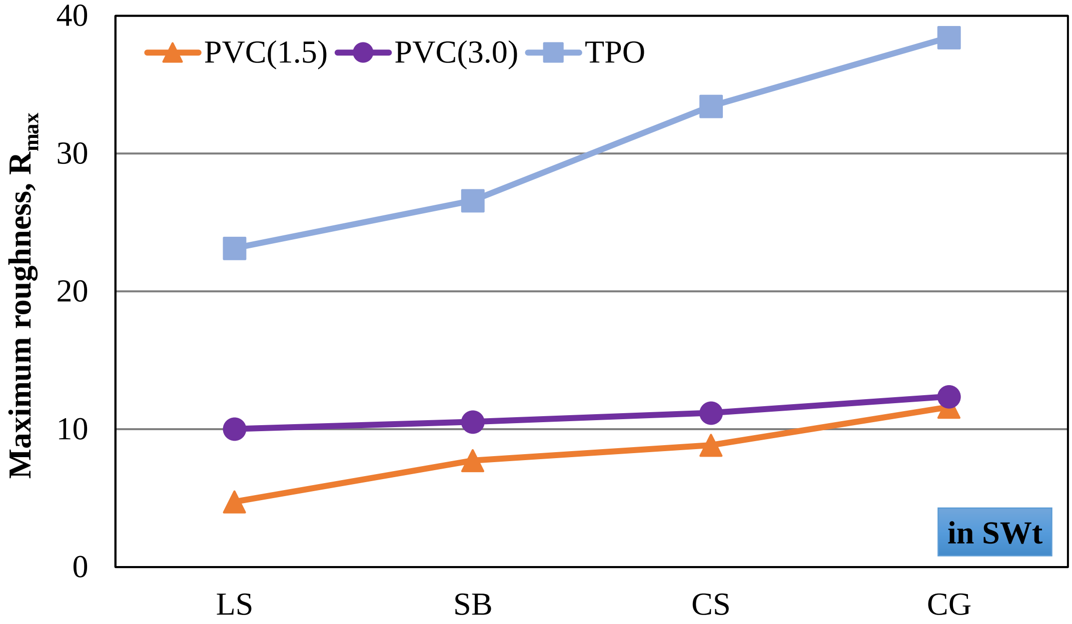

Figure 5.64: Maximum roughness values of 16 months SWt cured GM – soil interfaces after direct shear tests

R_a and R_{max} values of HDPE(S) cured in leachates are shown in Figure 5.65 and Figure 5.66. Also, R_a and R_{max} values of TPO cured in leachates and SWt are shown in Figure 5.67 and Figure 5.68. Again, it was seen that R_a and R_{max} values increase as the grain size and grain angularity increase. In addition, it was observed that the R_a and R_{max} values of GMs cured in AMD were the highest, and the R_a and R_{max} values of GMs cured in CCP were the lowest.

The reason why soil – GM interfaces with higher grain size and grain angularity have higher surface roughness after the test, the shearing resistance of the interface is caused by sliding and rolling of soil particles, adhesion, interlocking of soil particles with the GM surface, or embedding of soil particles into the GM surface. The combination of influencing factors can vary with the applied normal stress, and soil conditions and is sometimes a function of the horizontal deflection of the moving shear box [97]. At any normal stress, one or any of the above mechanisms can contribute to the total frictional force. For granular soil – GM interfaces, the cohesive force corresponds to the force required to allow soil particles to slide across the interface. As the normal stress increases, so does the ability of soil particles to plow the GM. Therefore, both sliding and plowing can contribute to the overall frictional force when shearing granular soil – GM interfaces [98]. However, the same is not true for cohesive soils. Even under high normal stresses, they only slide, not plow. Therefore, the R_a and R_{max} values of CS and CG soils are higher than that of LC and SB soils.

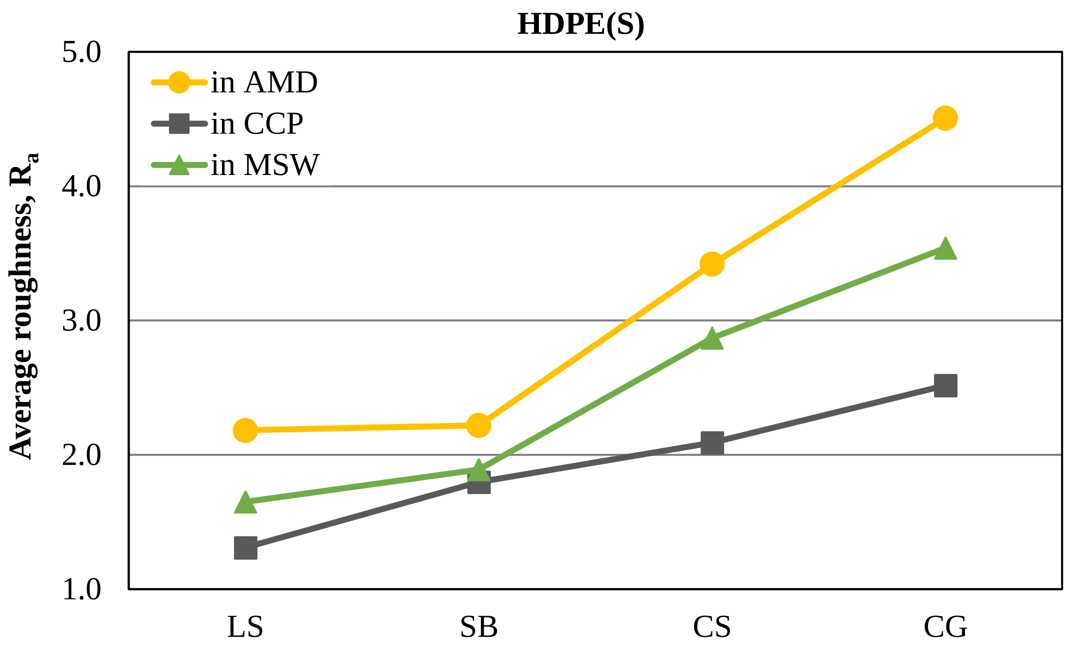

Figure 5.65: Average roughness values of 16 months leachate cured HDPE(S) – soil interfaces after direct shear tests

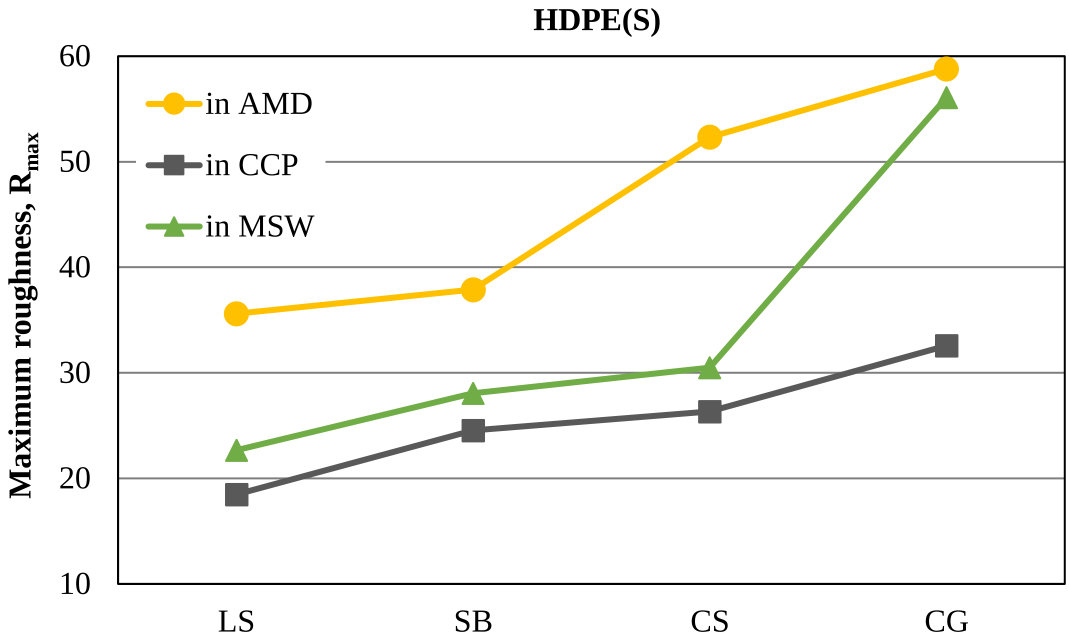

Figure 5.66: Maximum roughness values of 16 months leachate cured HDPE(S) – soil interfaces after direct shear tests

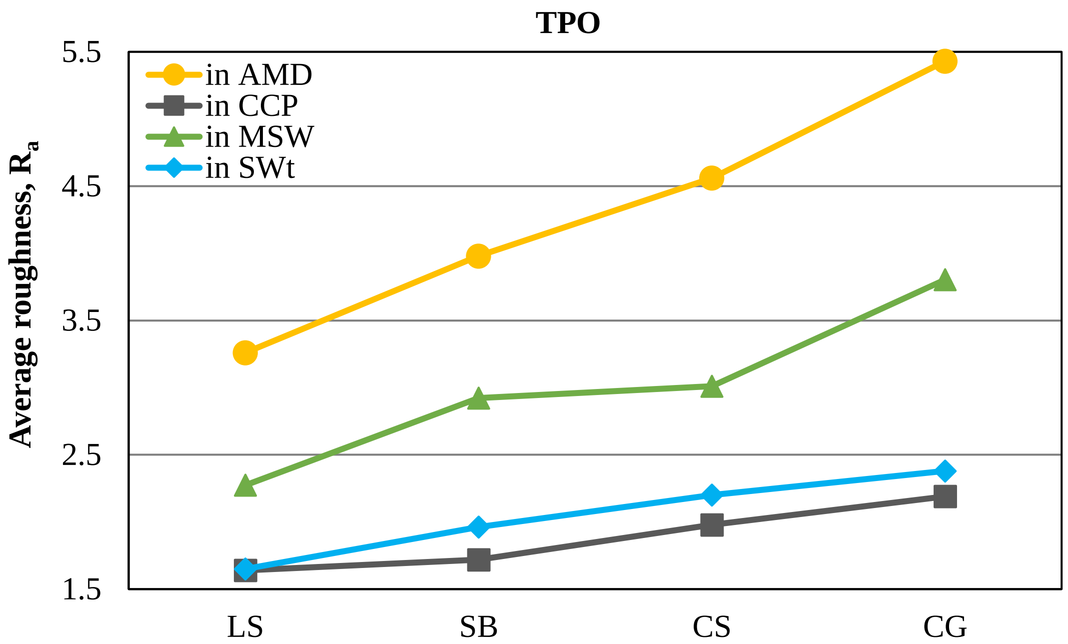

Figure 5.67: Average roughness values of 16 months leachate cured TPO – soil interfaces after direct shear tests

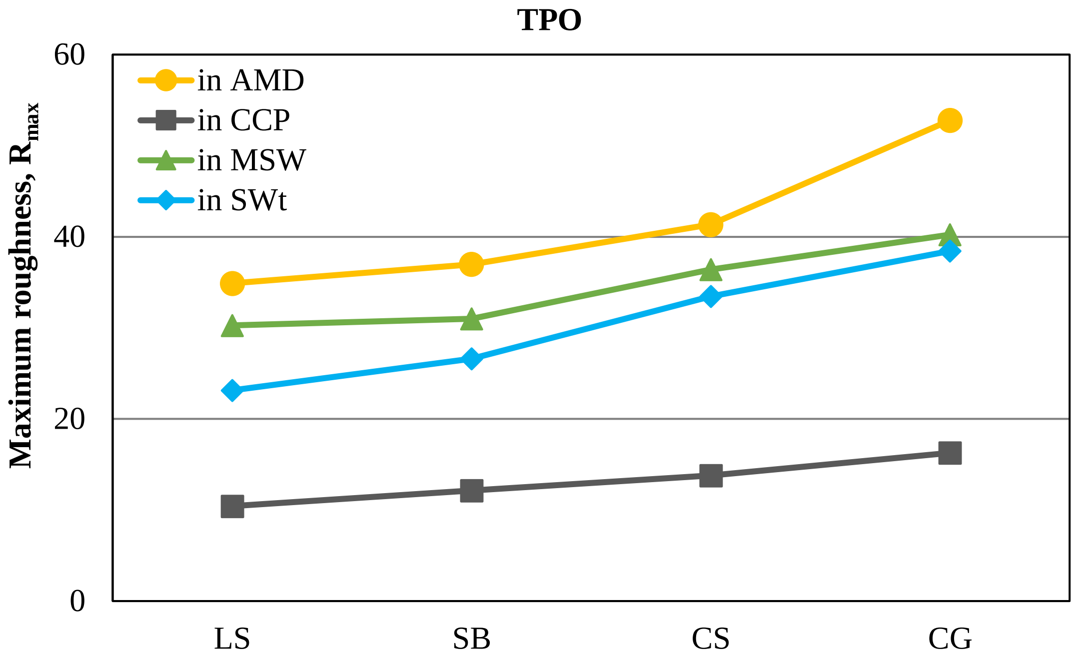

Figure 5.68: Maximum roughness values of 16 months leachate cured TPO – soil interfaces after direct shear tests

Microscopic images (500x magnification) of the GM samples cured for 16 months in SWt and leachates were taken from the Nikon Eclipse LV150N device to prove this effect physically and images were processed with Clemex Vision Lite software. Microscopic images were analyzed with image processing techniques in ImageJ software. The black areas in the images are the deformed areas, and the white areas are the undeformed areas. The black/white ratio is obtained by dividing the area size of the black areas by the area size of the white areas, and this ratio is called the "deformed area". In addition, the roundness of the black areas was determined so that it was compared with the particle shape of soils. A comparison of deformed areas with roundness values and microscopic images for PVC(1.5) and PVC(3.0) cured for 16 months in SWt is shown in Figure 5.69 and Figure 5.70. It was observed that as the grain size and grain angularity increased, the deformed area increased, and roundness decreased. These results are of the nature of proving the accuracy of the interface friction angles obtained from the direct shear tests and their relationship with the soil type. Also, the deformed area of PVC(3.0) was lower than the deformed area of PVC(1.5). This is due to the fact that the particles can be embedded in PVC(1.5) more easily.

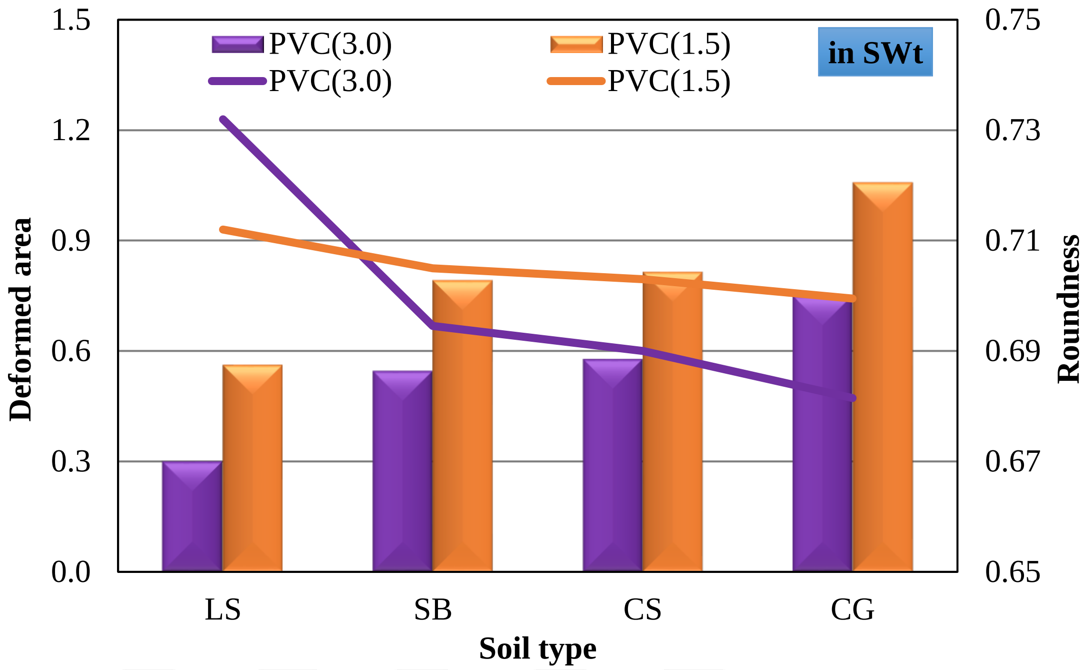

Figure 5.69: Deformed area and roundness of 16 months SWt cured PVC after direct shear tests

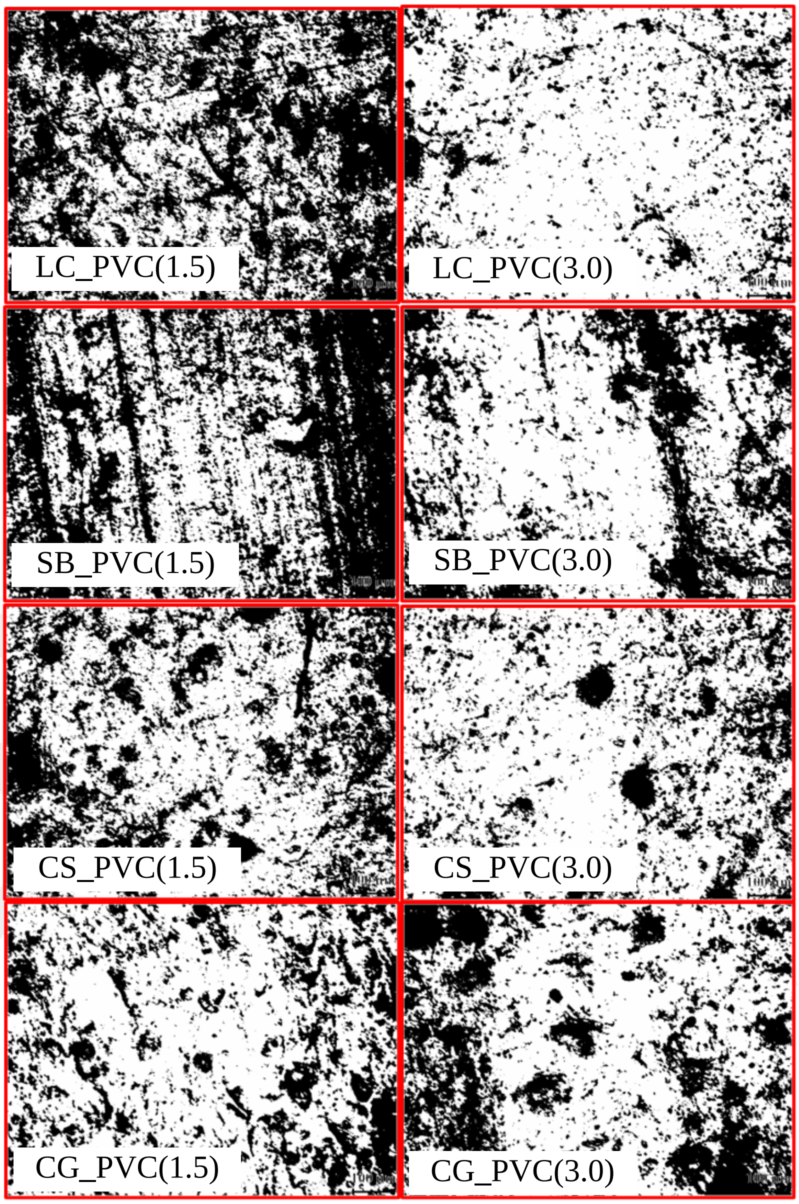

Figure 5.70: Microscopic images of 16 months SWt cured PVC after direct shear tests

A comparison of deformed areas with roundness values and microscopic images for HDPE(S) cured for 16 months in leachates (AMD, MSW, CCP) are shown in Figure 5.71 and Figure 5.72. The highest deformed area and lowest roundness were obtained with AMD cured GMs. The lowest deformed area and the highest roundness were obtained with GMs cured in CCP. This result proves that AMD is the most damaging leachate to GMs and CCP is the least damaging leachate to GMs. In addition, when Figure 5.70 and Figure 5.72 are compared, it is seen that the deformations on the PVC surface are round and the deformations on the HDPE surface are lines. The reason for this is the embedding of the particles on the soft surface of PVC, and the sliding movement of the particles on the hard surface of HDPE without embedding.

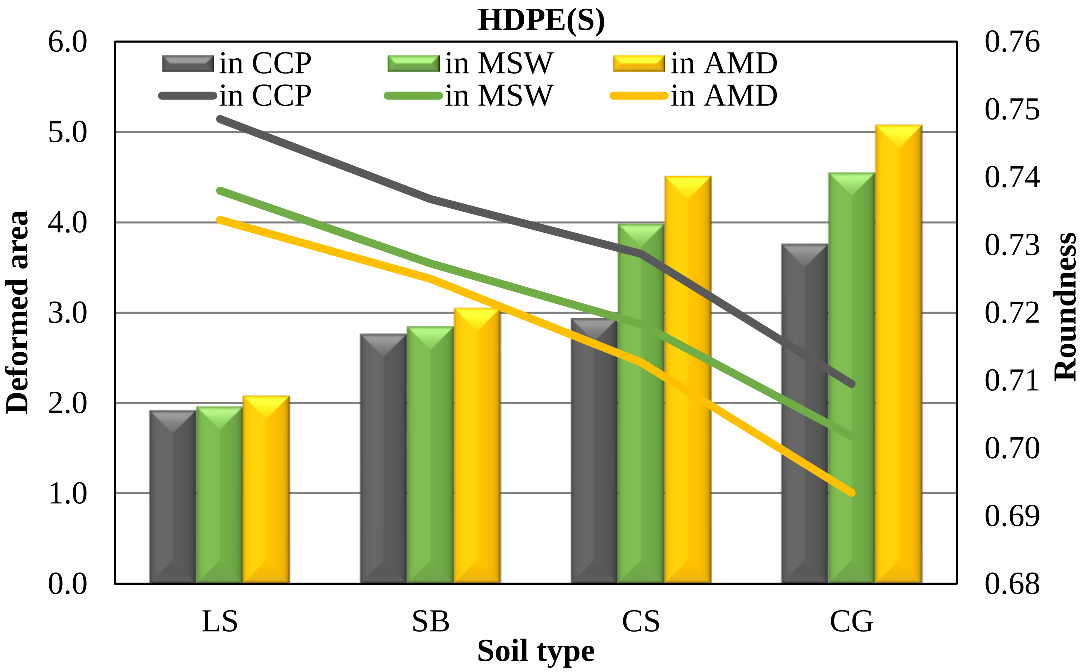

Figure 5.71: Deformed area and roundness of 16 months leachate cured HDPE(S) after direct shear tests

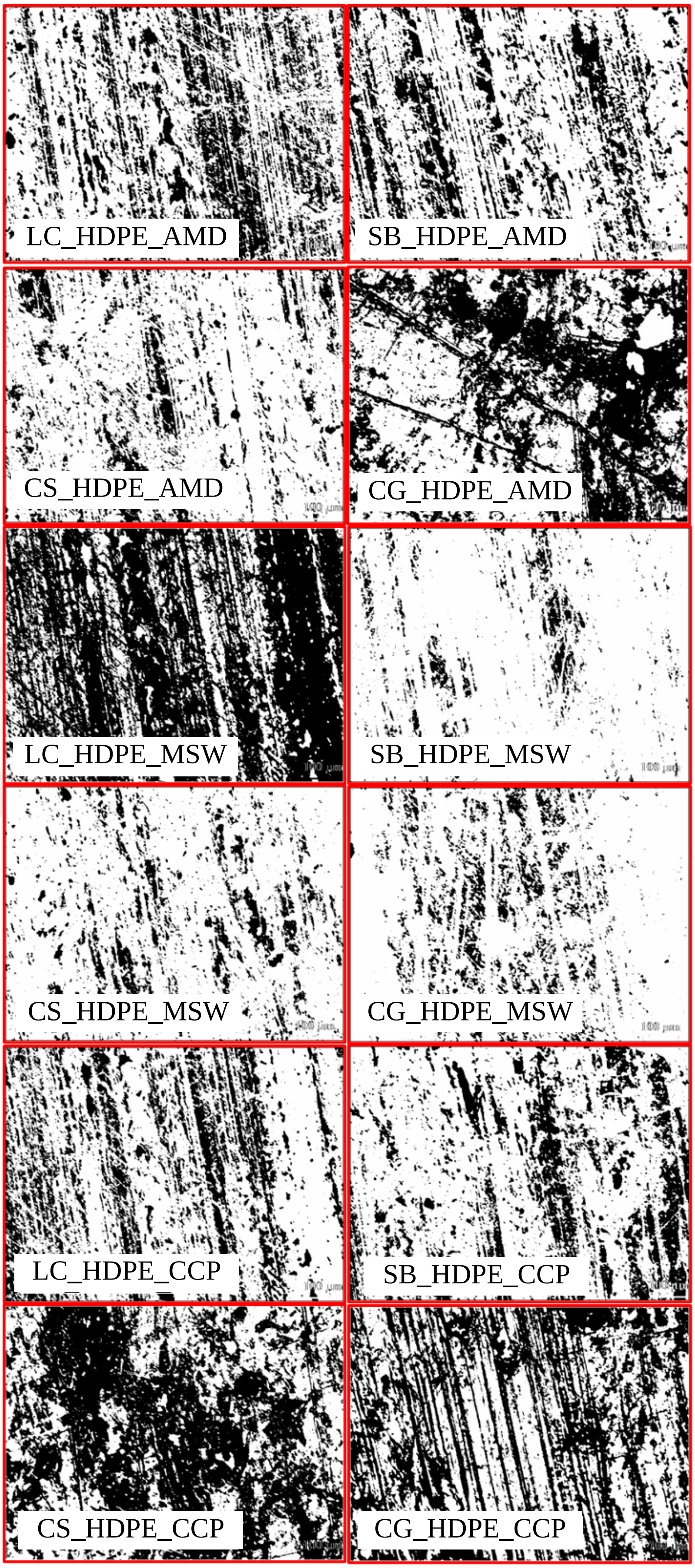
LC_HDPE_AMD
SB_HDPE_AMD
CS_HDPE_AMD
CG_HDPE_AMD
LC_HDPE_MSW
SB_HDPE_MSW
CS_HDPE_MSW
CG_HDPE_MSW
LC_HDPE_CCP
SB_HDPE_CCP
CS_HDPE_CCP
CG_HDPE_CCP

Figure 5.72: Microscopic images of 16 months leachate cured HDEP(S) after direct shear tests

A comparison of deformed areas with roundness values and microscopic images for TPO cured for 16 months in leachates (AMD, MSW, CCP) and SWt are shown in Figure 5.73 and Figure 5.74. When microscopic images were examined, fine grained soils created scratches on the GM surface, while coarse grained soils formed deep cavities on the GM surface. The cavities are more pronounced in PVC and TPO, which are relatively soft on the surface, while less pronounced in HDPE, which has a hard surface.

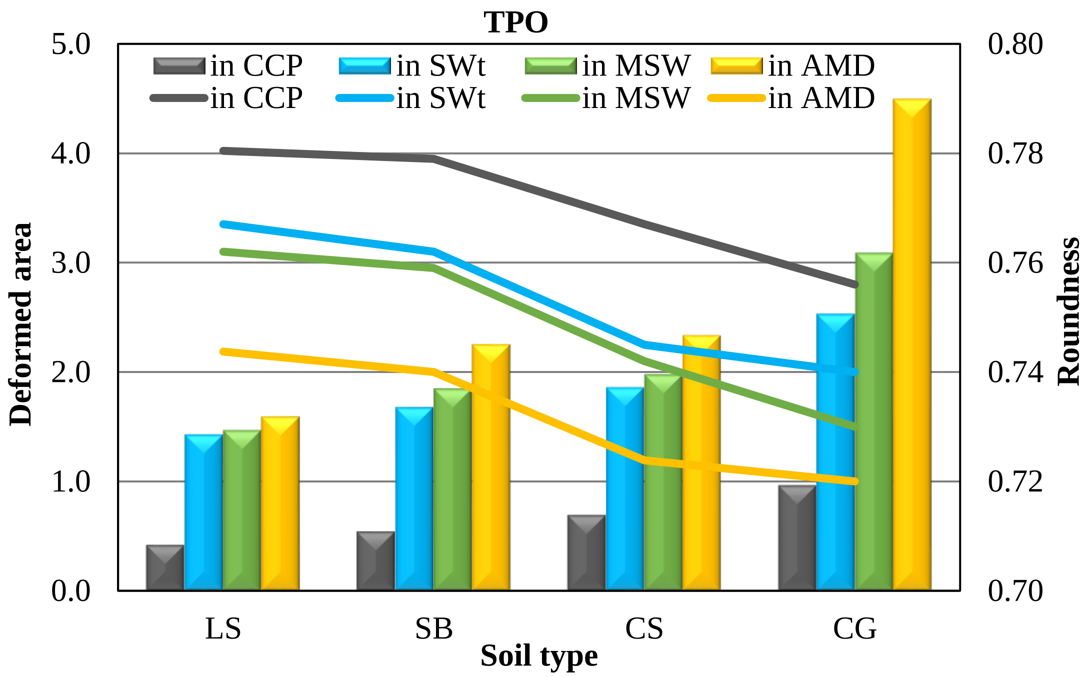

Figure 5.73: Deformed area and roundness of 16 months leachate and SWt cured TPO after direct shear tests

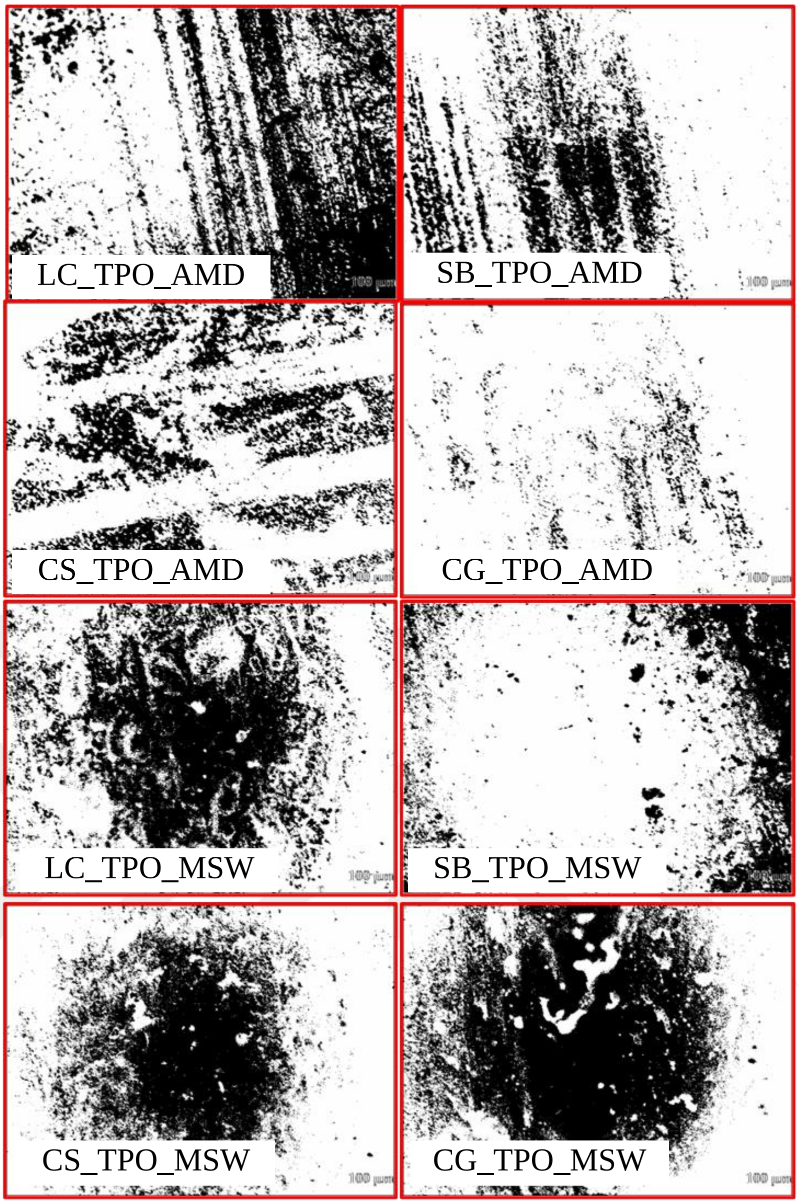

Figure 5.74: Microscopic images of 16 months leachate and SWt cured TPO after direct shear tests

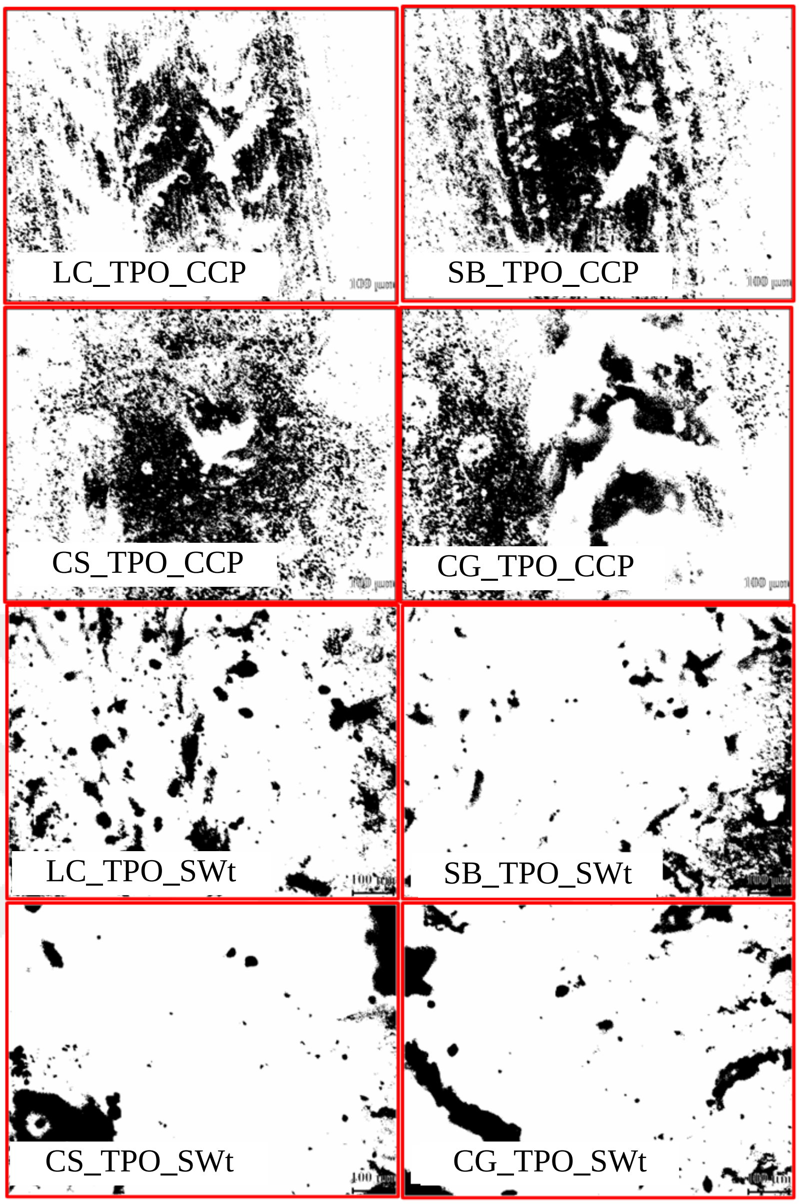

Figure 5.74 (continued): Microscopic images of 16 months leachate and SWt cured TPO after direct shear tests

5.6 Finite element method analysis

In the last stage of the thesis, in order to verify the results obtained from the interface direct shear tests, a numerical model was established, and the same interfaces were modeled as the slope of a solid waste landfill. For this purpose, only experiments with 16 months of cured samples were modeled using Plaxis 2D software. As a result of the analyses, the factor of safety (FS) values were obtained as 1.93, 1.84, 1.99, and 2.13 in the slope stability analysis without GM for LC, SB, CS, and CG, respectively. The analysis results of the soil – PVC(1.5), soil – PVC(3.0), and soil – TPO interfaces cured in SWt are shown in Figure 5.75, Figure 5.76, and Figure 5.77.

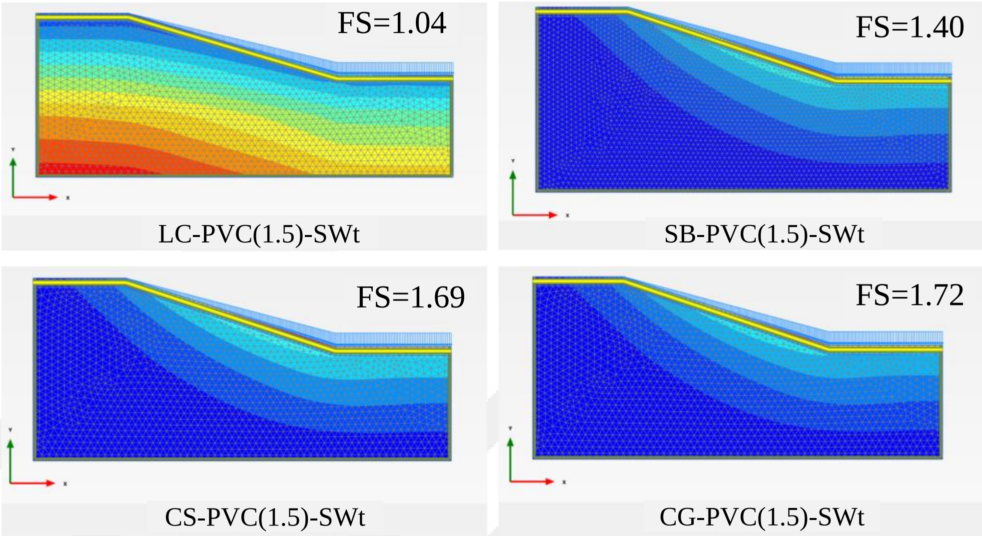

Figure 5.75: The Plaxis 2D analysis results of the 16 months SWt cured PVC(1.5) – soil interface

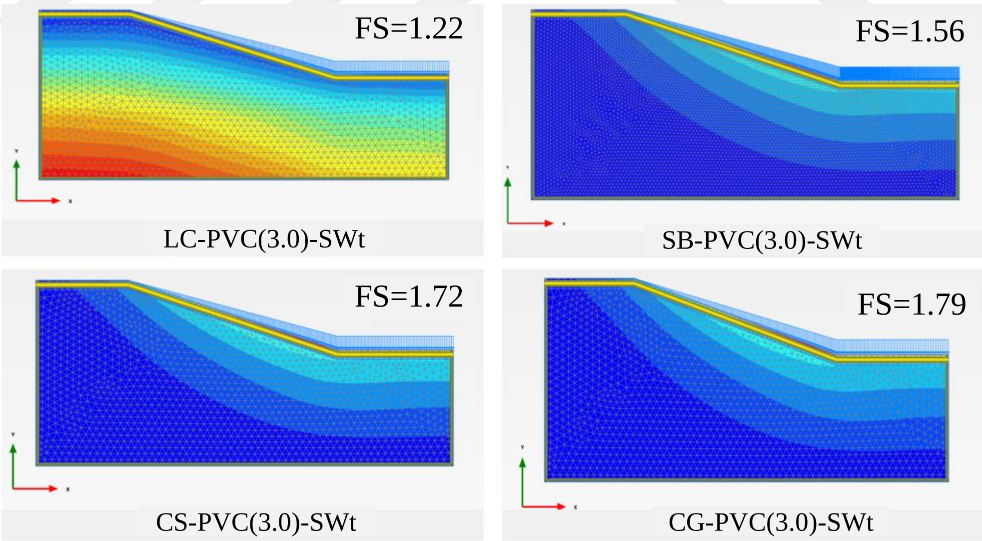

Figure 5.76: The Plaxis 2D analysis results of the 16 months SWt cured PVC(3.0) – soil interface

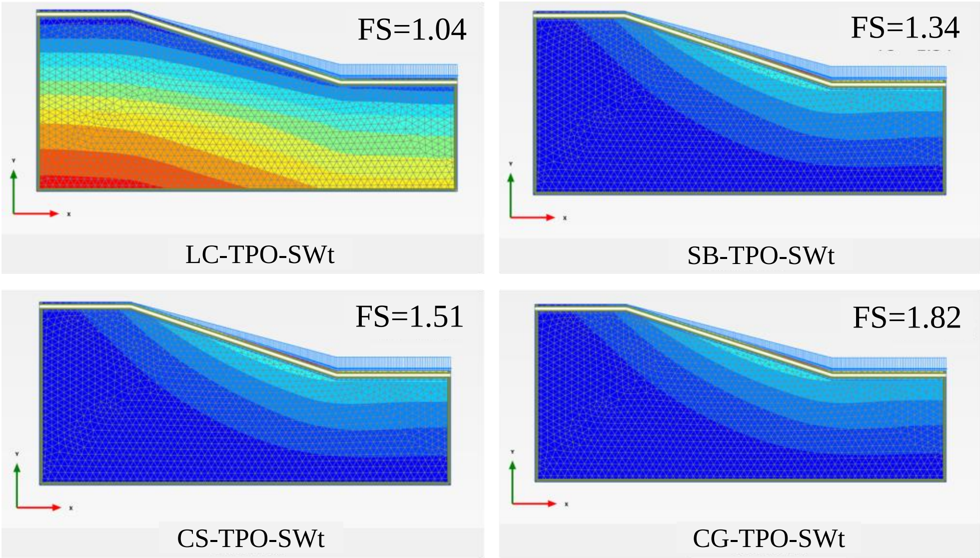

Figure 5.77: The Plaxis 2D analysis results of the 16 months SWt cured TPO – soil interface

The analysis results of the soil – HDPE(S) and soil – TPO interfaces cured in AMD are shown in Figure 5.78 and Figure 5.79.

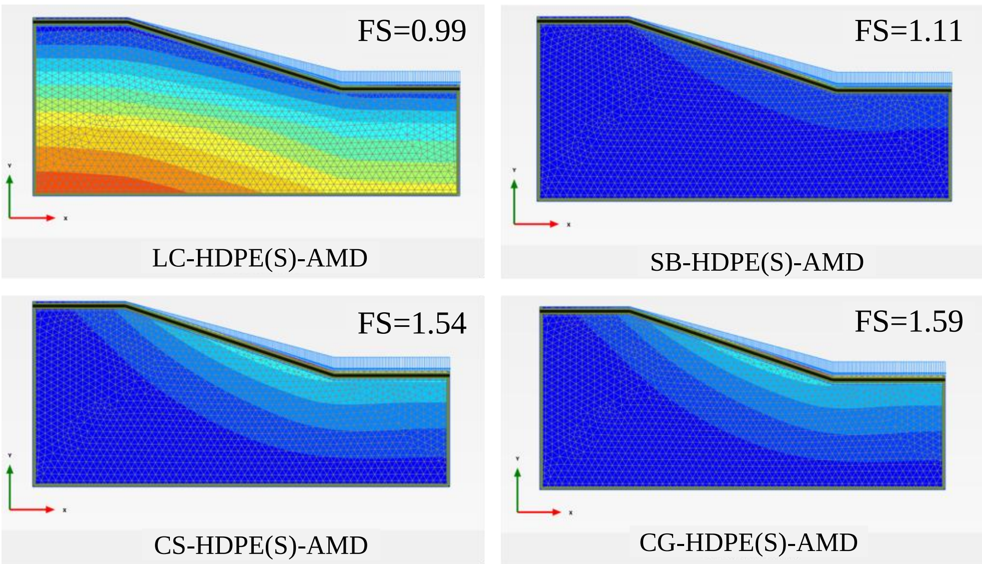

Figure 5.78: The Plaxis 2D analysis results of the 16 months AMD cured HDPE(S) – soil interface

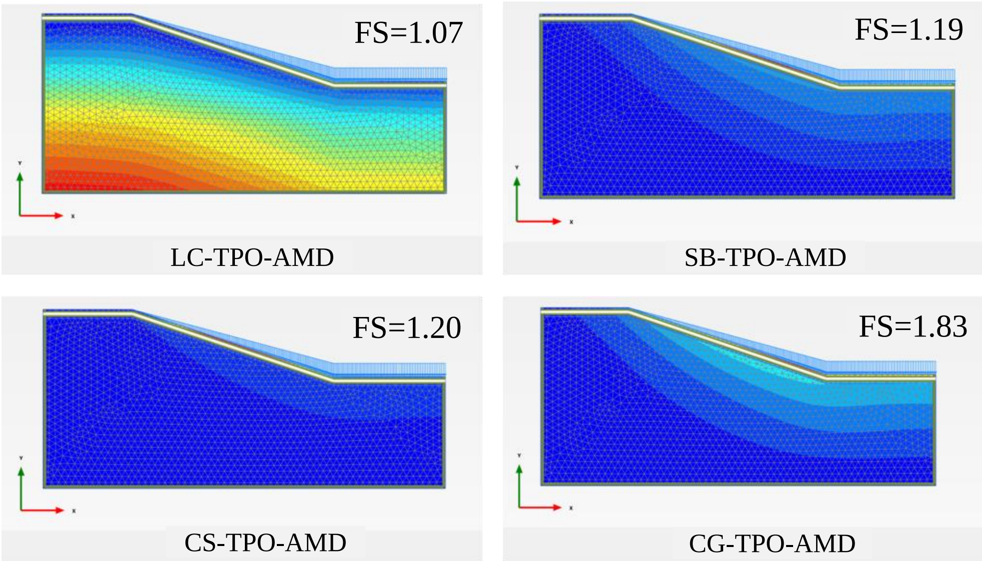

Figure 5.79: The Plaxis 2D analysis results of the 16 months AMD cured TPO – soil interface

The analysis results of the soil – HDPE(S) and soil – TPO interfaces cured in CCP are shown in Figure 5.80 and Figure 5.81.

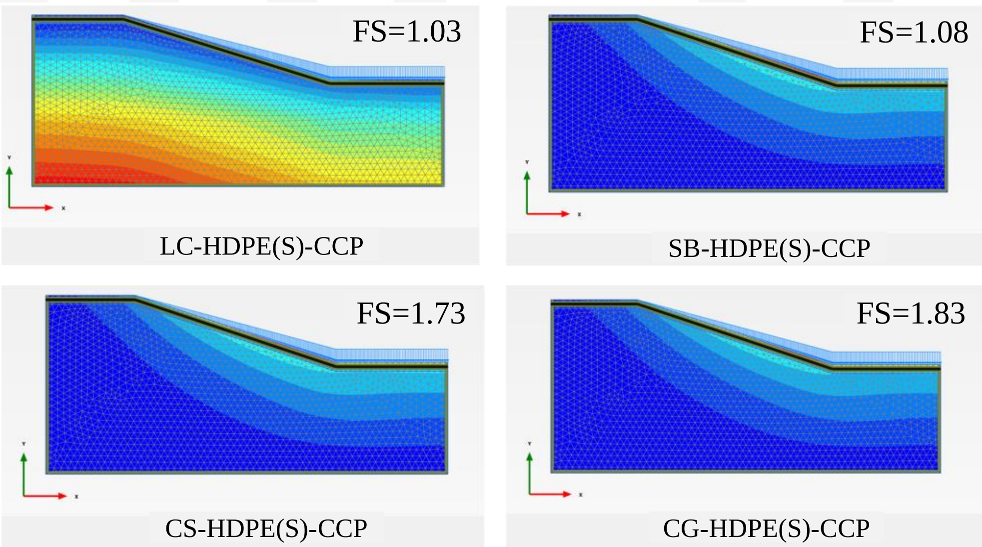

Figure 5.80: The Plaxis 2D analysis results of the 16 months CCP cured HDPE(S) – soil interface

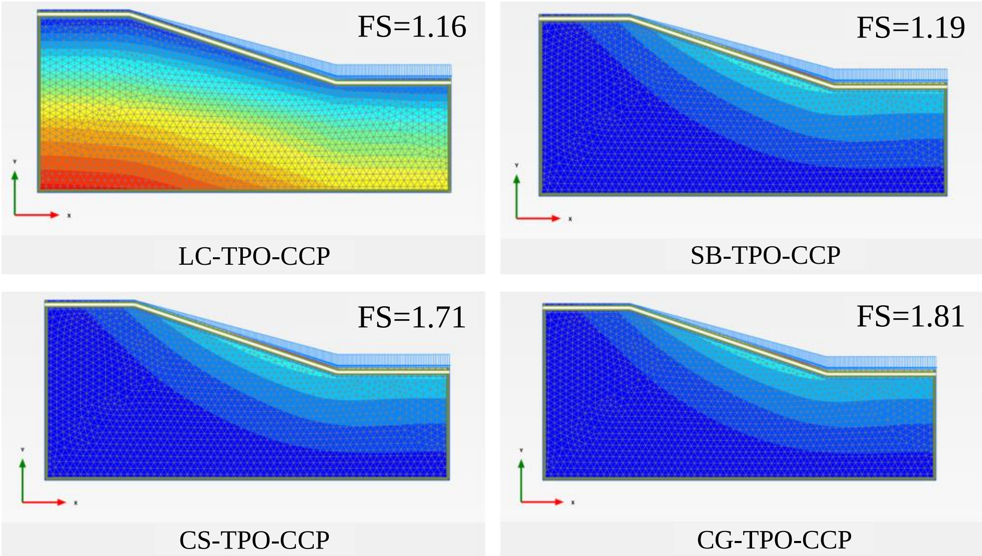

Figure 5.81: The Plaxis 2D analysis results of the 16 months CCP cured TPO – soil interface

The analysis results of the soil – HDPE(S) and soil – TPO interfaces cured in MSW are shown in Figure 5.80 and Figure 5.81.

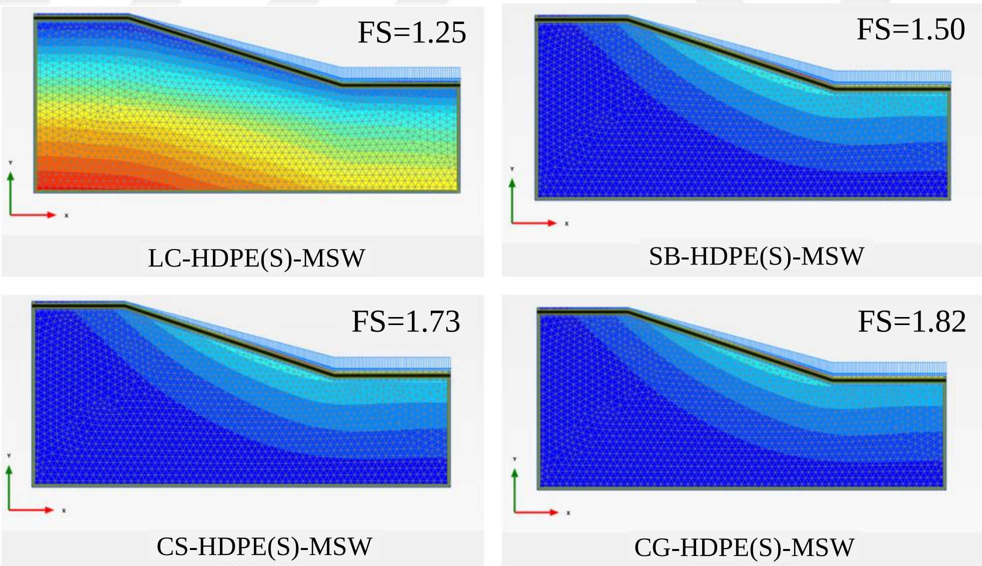

Figure 5.82: The Plaxis 2D analysis results of the 16 months MSW cured HDPE(S) – soil interface

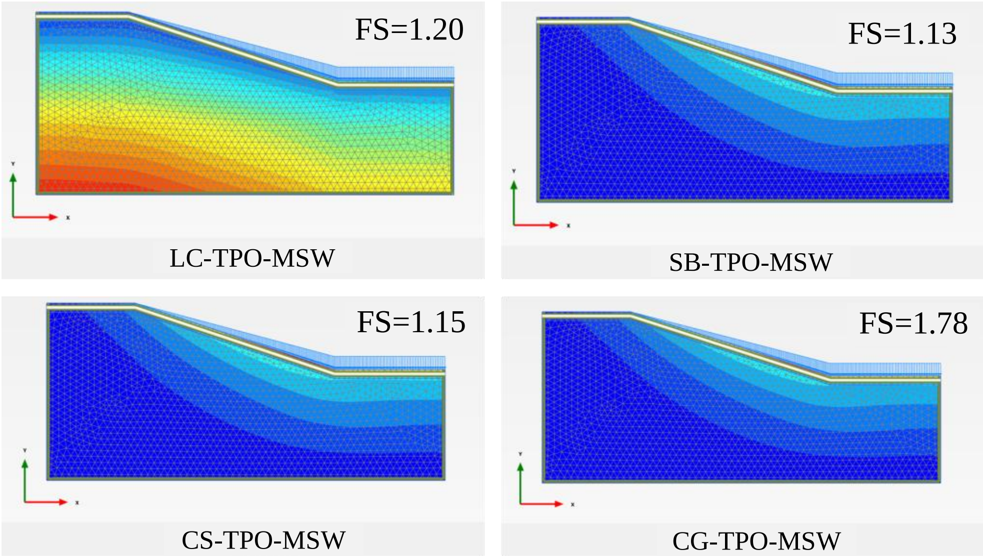

Figure 5.83: The Plaxis 2D analysis results of the 16 months MSW cured TPO – soil interface

From Figure 5.75 through Figure 5.83, the FS values of all slopes with GM interface are lower than the FS values of the slopes without GM. This result showed that when designing a waste storage facility when only the shear strength parameters of the soil are used, a very risky structure can be built. Therefore, not only the shear strength parameters of the soil but also the shear strength parameters of the interface formed between the soil and the GM should be considered. All FS values from Plaxis 2D analyses are listed in Table 5.22.

Table 5.22: FS values of all interfaces obtained from Plaxis 2D analysis

Soil type	AMD		CCP		MSW		SWt		
	HDPE(S)	TPO	HDPE(S)	TPO	HDPE(S)	TPO	PVC(1.5)	PVC(3.0)	TPO
LC	0.99	1.07	1.25	1.20	1.05	1.22	1.04	1.03	1.16
SB	1.11	1.19	1.50	1.13	1.40	1.56	1.34	1.08	1.19
CS	1.54	1.20	1.73	1.15	1.69	1.72	1.51	1.73	1.71
CG	1.59	1.83	1.82	1.78	1.72	1.79	1.82	1.83	1.81

According to the Plaxis 2D analysis results, in AMD cured samples, LC – HDPE(S) has the lowest FS value, while CG – TPO has the highest FS value. That is, it would be risky to use smooth HDPE GM with a low plasticity clay in mine waste storage facilities. It may be recommended to use TPO GM with crushed gravel instead. In MSW cured samples, SB – TPO has the lowest FS value, while CG – HDPE(S) has the highest FS value. That is, it would be risky to use TPO GM with a sand-bentonite mixture in municipal solid waste facilities. It may be recommended to use smooth HDPE GM with crushed gravel instead. In CCP cured samples, LC – HDPE(S) has the lowest FS value, while CG – HDPE(S) has the highest FS value. That is, it would be risky to use smooth HDPE GM with a low plasticity clay in coal waste storage facilities. It may be recommended to use smooth HDPE GM with crushed gravel instead. In SWt cured samples, LC – TPO has the lowest FS value, while CG – TPO has the highest FS value. That is, it would be risky to use TPO GM with a low plasticity clay in areas close to the coastline. It may be recommended to use TPO GM with crushed gravel instead.

5.7 Parameters affecting the interface friction angle

In this study, the most important parameters whose effects on the interface friction angle were investigated are the curing liquid type and curing time. Therefore, a more detailed and clear examination and comparison of these effects is made in this section. In addition, a discussion was made on the effect of curing time and the type of curing liquid.

5.7.1 Effect of curing period

The effects of the SWt curing period on the interface friction angles of soil – PVC(1.5), soil – PVC(3.0), and soil – TPO is shown in Figure 5.84, Figure 5.85, and Figure 5.86. It was seen that the interface friction angle decreased as the curing time increased. A curing effect (C_E) coefficient was derived as the ratio of the 16 months cured interface friction angle to the uncured interface friction angle to compare the results. When the average C_E values of the samples were compared, 0.783, 0.827, and 0.864 were obtained for TPO, PVC(1.5), and PVC(3.0), respectively. Based on this, it has been determined that SWt has more damaging effects on the TPO.

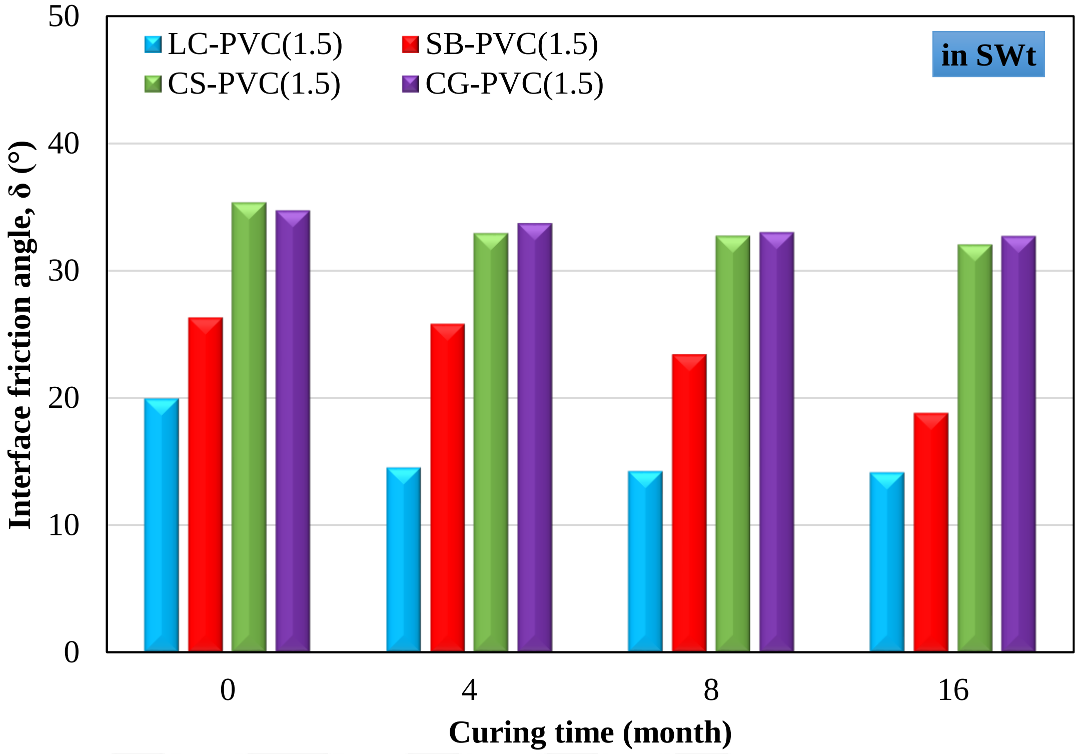

Figure 5.84: Friction angle values of no cured and SWt cured PVC(1.5) – soil interface

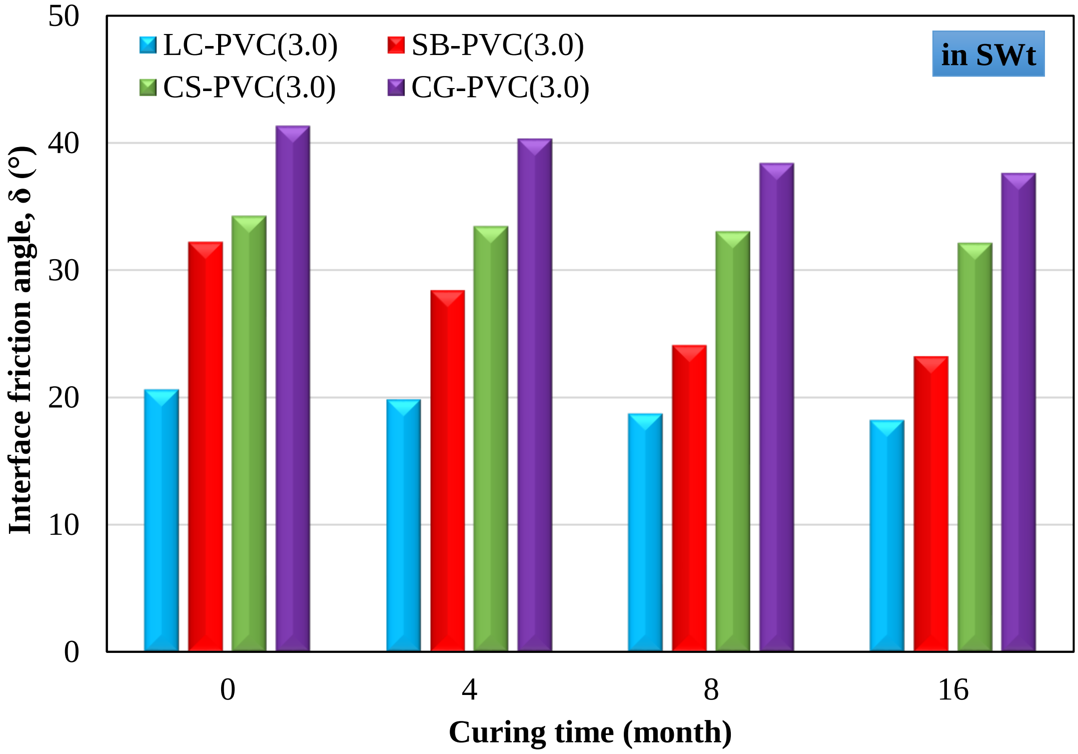

Figure 5.85: Friction angle values of no cured and SWt cured PVC(3.0) – soil interface

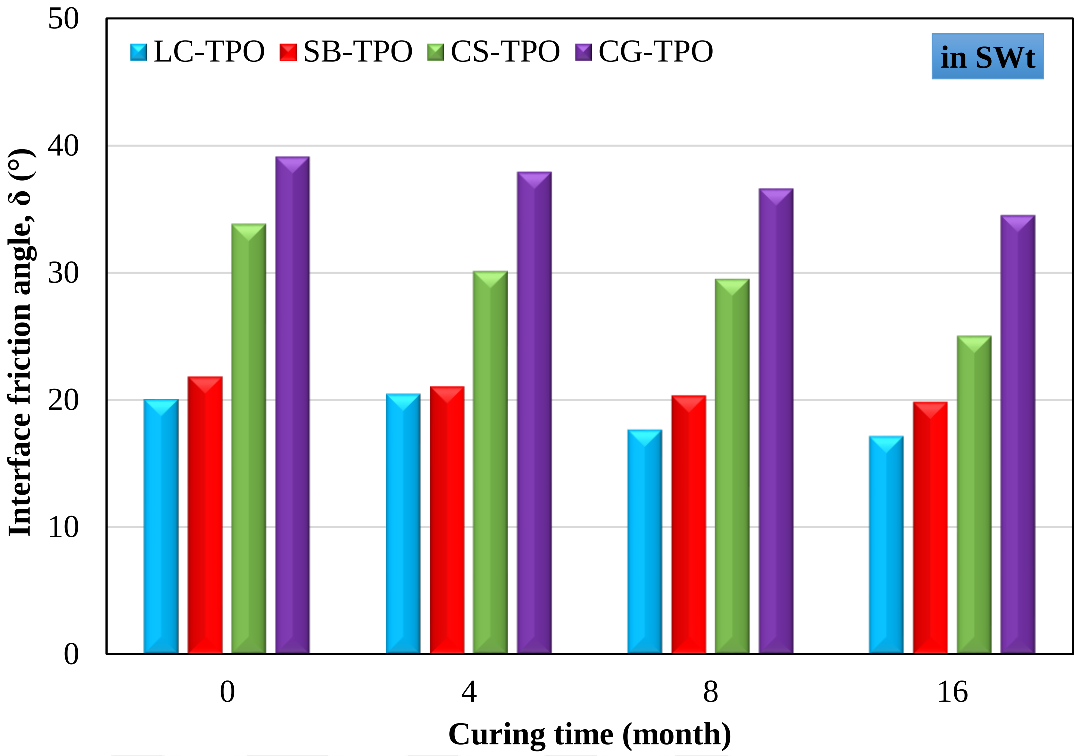

Figure 5.86: Friction angle values of no cured and SWt cured TPO – soil interface

The effect of the AMD curing period on the interface friction angles of soil – HDPE(S), soil – HDPE(T), and soil – TPO is shown in Figure 5.87, Figure 5.88, and Figure 5.89. It was seen that the interface friction angle decreased as the curing time increased. When the average C_E values of the samples cured for 16 months were compared, 0.690, 0.756, and 0.674 were obtained for TPO, HDPE(S), and HDPE(T), respectively. Based on this, it has been determined that AMD has more damaging effects on the HDPE(T). Within the scope of the Regulation on the Waste Landfills [99]. During the storage of wastes, the slope of the lot and the slope of the waste pool are a maximum of 1/3 in order to ensure slope stability and easy maneuvering of vehicles and machines. The lines indicated by the red dash in the graphs show the slope angle corresponding to the tangent of the 1/3 slope (18°). The samples cured for 8 and 16 months at the SB – HDPE(S) interface, the samples cured for 16 months at the SB – HDPE(T) interface, and the samples cured for 16 months at the LC – TPO and SB – TPO interfaces remained below this red line. Therefore, it is not recommended to use HDPE(S), HDPE(T), and TPO with SB and LC together in mine tailing storage facilities according to these results. The soil – GM couple recommended to be used in mine tailing storage facilities is CG – HDPE(T), which has the highest interface friction angle.

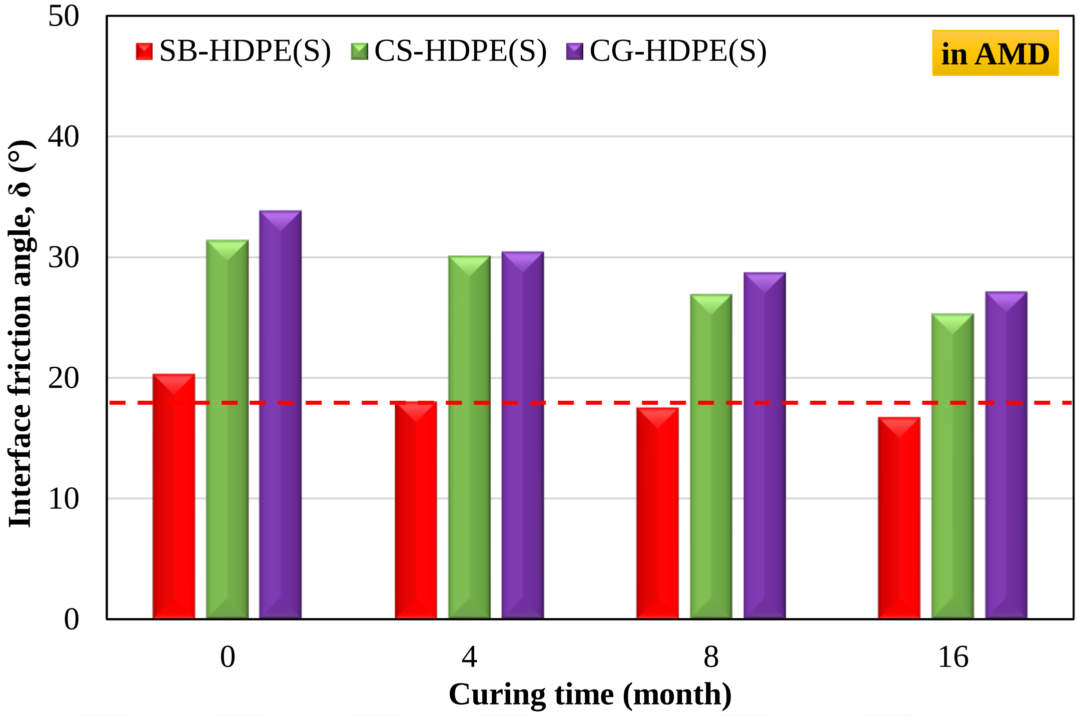

Figure 5.87: Friction angle values of no cured and AMD cured HDPE(S) – soil interface

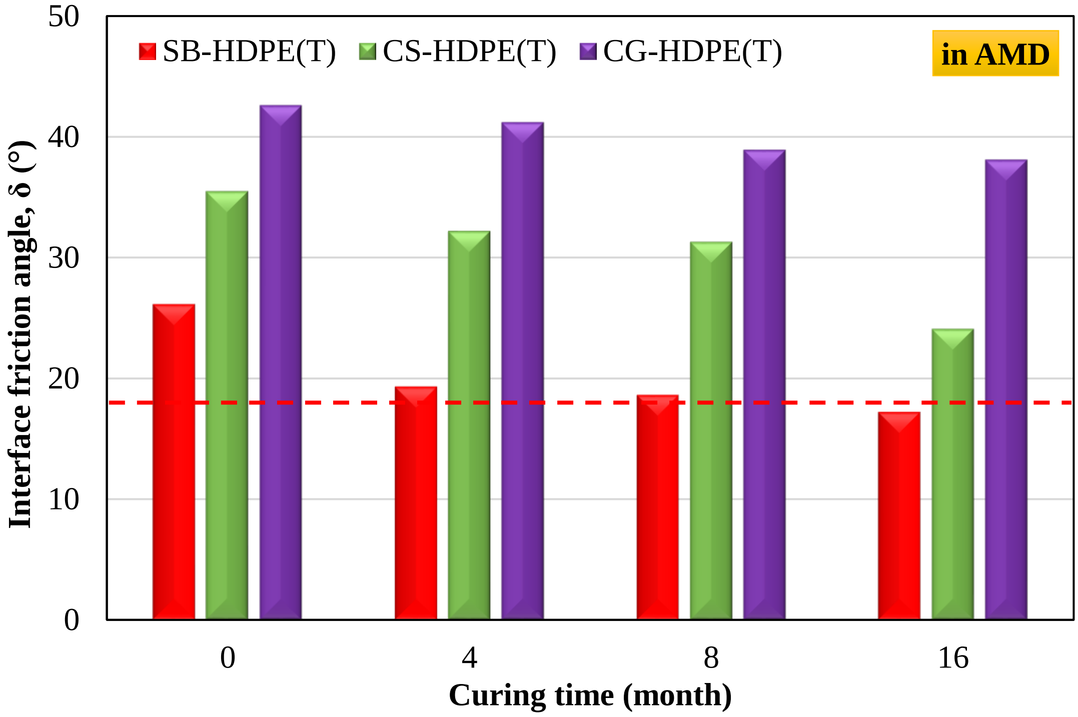

Figure 5.88: Friction angle values of no cured and AMD cured HDPE(T) – soil interface

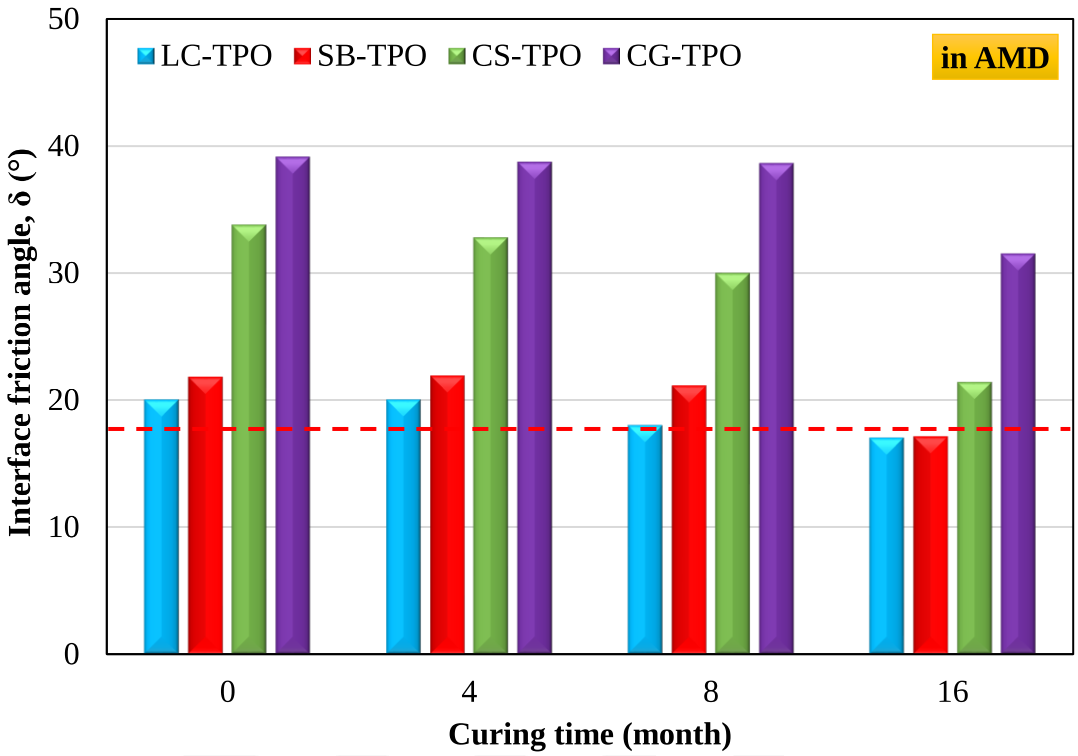

Figure 5.89: Friction angle values of no cured and AMD cured TPO – soil interface

The effect of the CCP leachate curing period on the soil – HDPE(S), soil – HDPE(T), and soil – TPO interfaces friction angles are shown in Figure 5.90, Figure 5.91, and Figure 5.92. Contrary to AMD, CCP did not cause a significant decrease in the interface friction angle of the GM after 16 months of curing. Because AMD encountered in mine tailing storage systems have acidic contents and low pH, coal combustion leachate can have extreme pH and high ionic strength [100,101]. When the average C_E values of the samples cured for 16 months were compared, 0.822, 0.855, and 0.906 were obtained for TPO, HDPE(S), and HDPE(T), respectively. Based on this, it has been determined that CCP has more damaging effects on the TPO. As a result of the experiment, it was observed that all samples remained above the red line. In other words, all soil – GM pairs are suitable for use in coal combustion waste storage facilities. But also, CG gave the best results with HDPE(T). So, it may be recommended to use CG soil type in coal combustion waste storages with the HDPE(T).

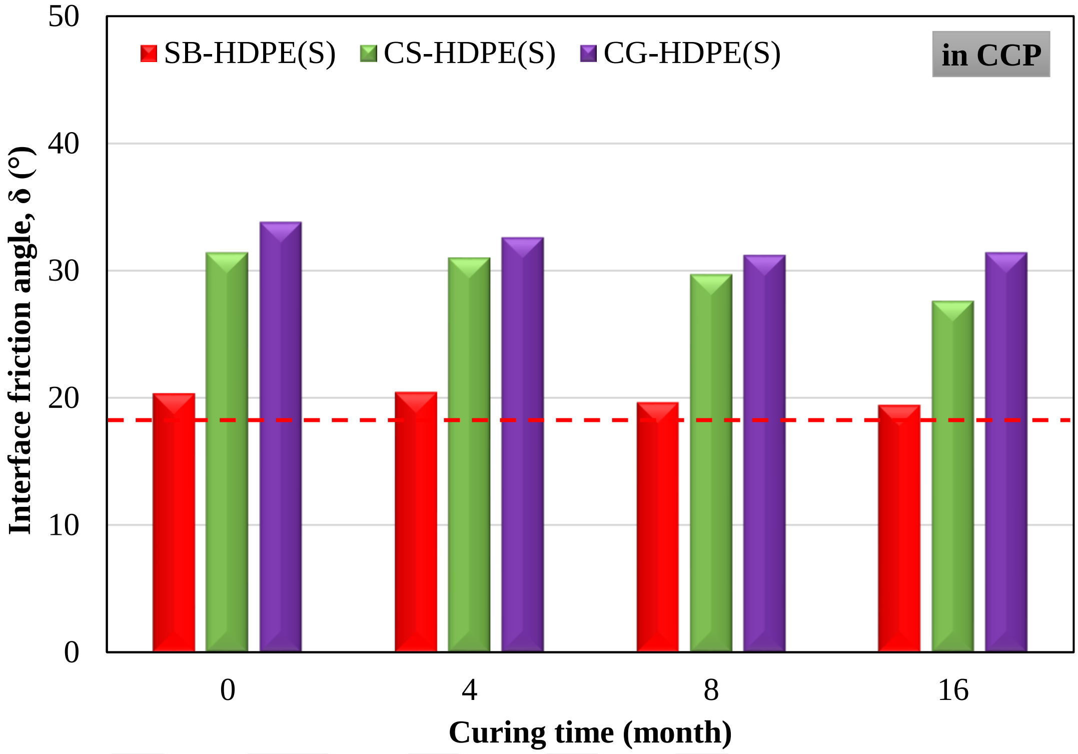

Figure 5.90: Friction angle values of no cured and CCP cured HDPE(S) – soil interface

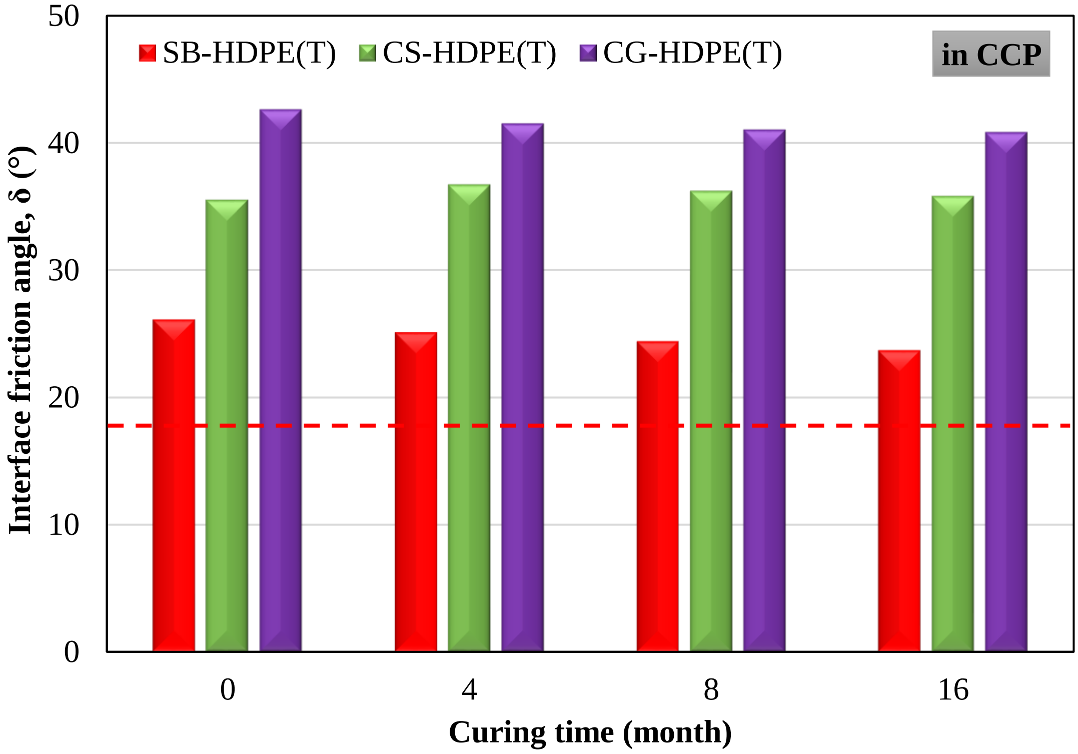

Figure 5.91: Friction angle values of no cured and CCP cured HDPE(T) – soil interface

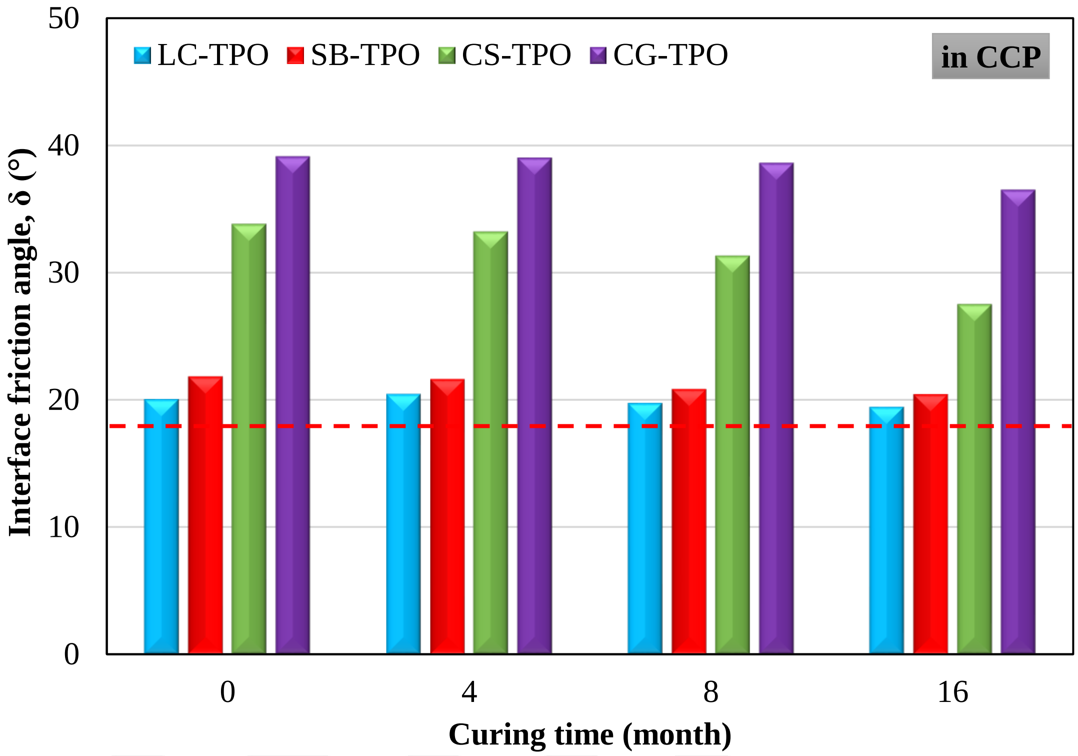

Figure 5.92: Friction angle values of no cured and CCP cured TPO – soil interface

The effect of the MSW leachate curing period on the soil – HDPE(S), soil – HDPE(T), and soil – TPO interface friction angle is shown in Figure 5.93, Figure 5.94, and Figure 5.95. It was determined that the effect of MSW on the friction angle of the GM was not as high as AMD and not as low as CCP. When the average C_E values of the samples cured for 16 months were compared, 0.740, 0.809, and 0.769 were obtained for TPO, HDPE(S), and HDPE(T), respectively. Based on this, it has been determined that MSW has more damaging effects on the TPO. As a result of accelerated aging experiments in the laboratory, Rowe et al. (2010) determined that the oxidative time was 35% reduced after 16 months in MSW, even at 50ºC [29]. Therefore, the decrease in friction angles of the samples cured for 16 months at room temperature is in accordance with the results obtained in the literature. The samples cured for 8 and 16 months at the SB – TPO interfaces remained below the red line. That is the use of LC – TPO couple in municipal solid waste storage facilities should be avoided. Also, it has been determined that CG – HDPE(T) couple is the most suitable GM – soil couple for municipal solid waste storage facilities.

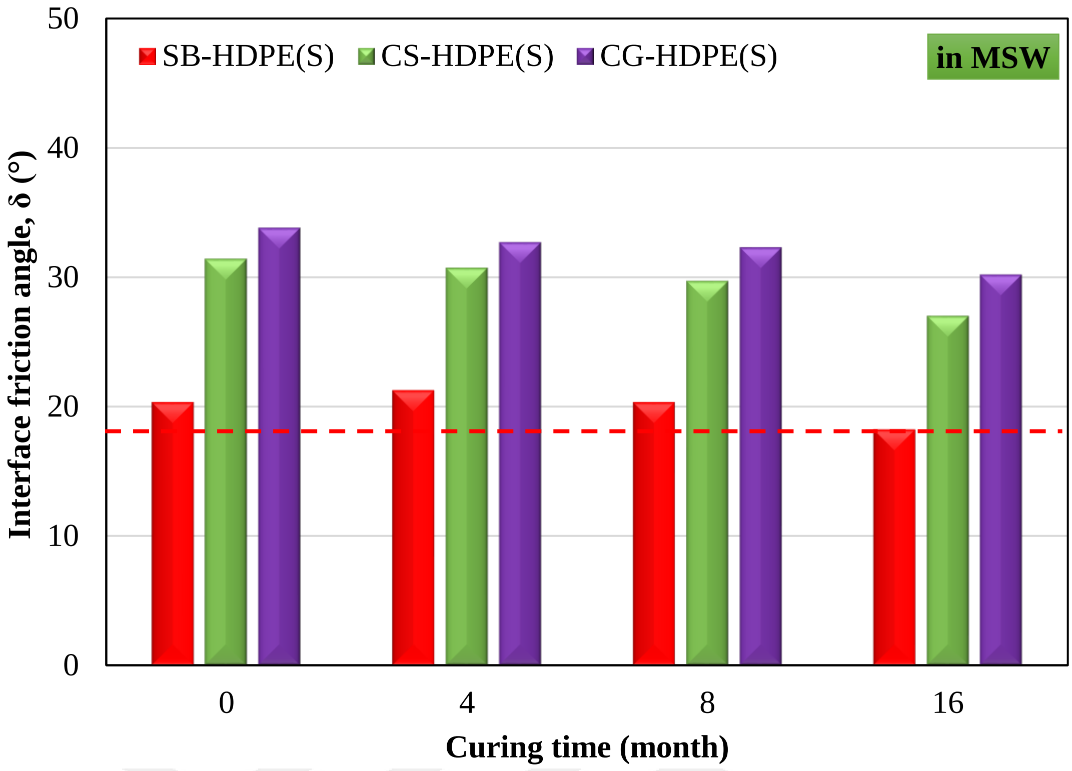

Figure 5.93: Friction angle values of no cured and MSW cured HDPE(S) – soil interface

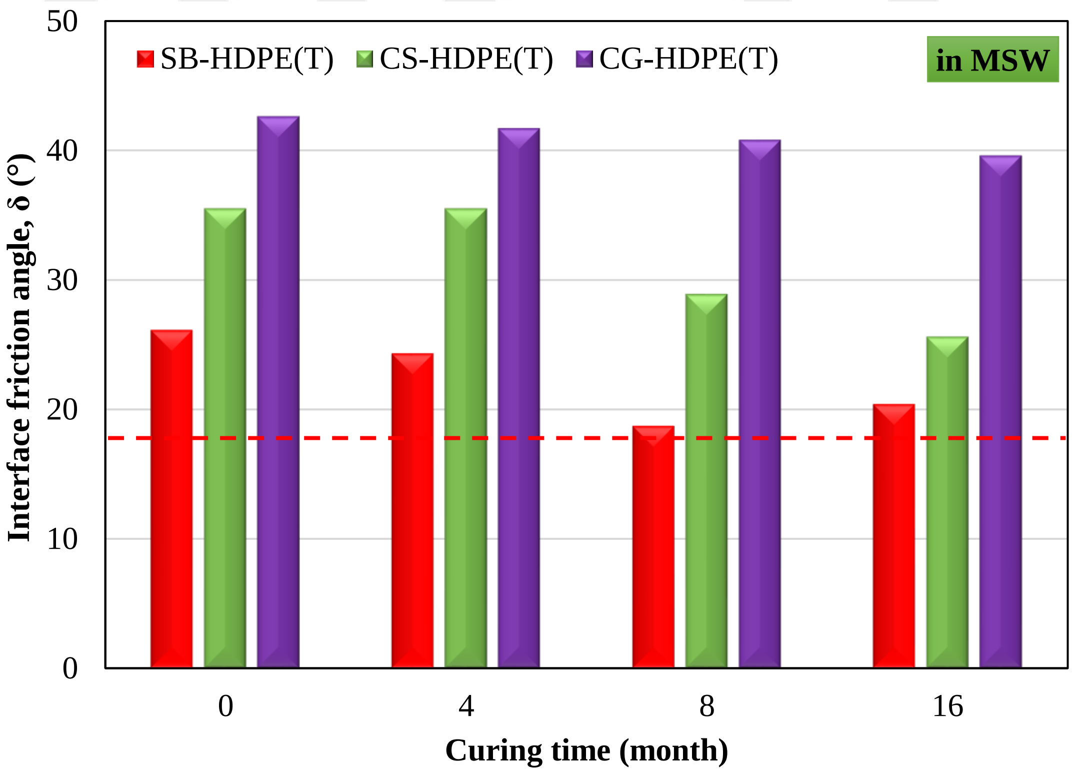

Figure 5.94: Friction angle values of no cured and MSW cured HDPE(T) – soil interface

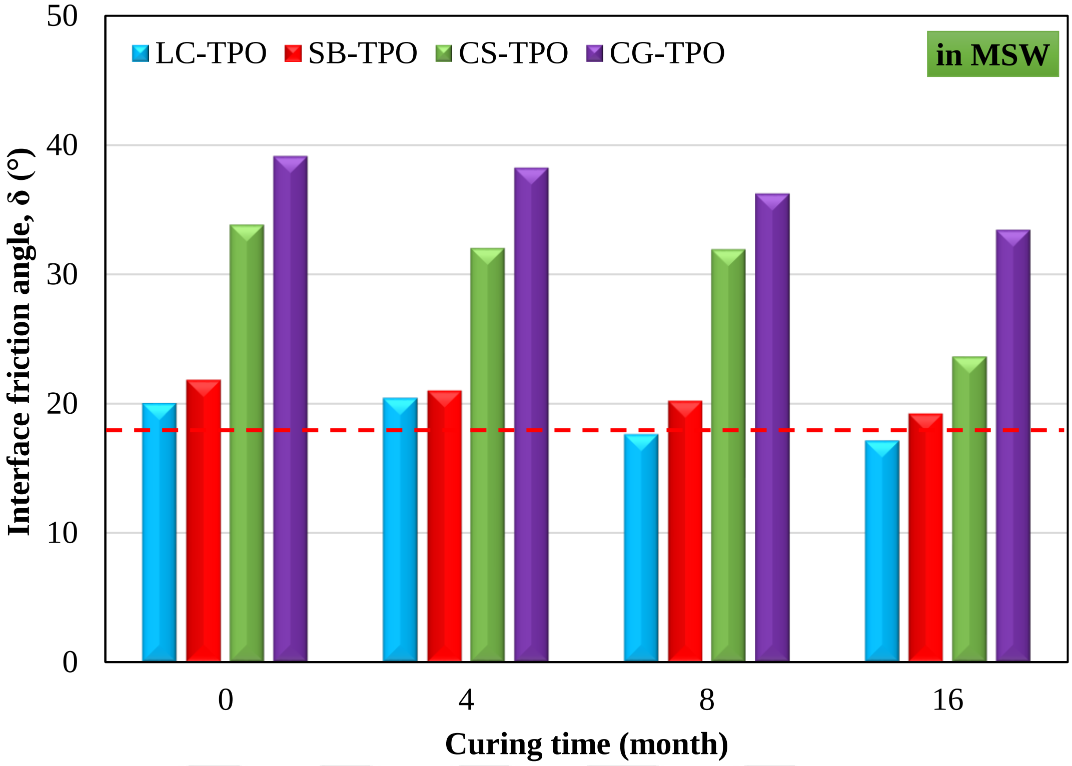

Figure 5.95: Friction angle values of no cured and MSW cured TPO – soil interface

5.7.2 Effect of curing liquid type

In order to compare the effect of different leachates on the friction angles of GMs, the correlation between D_{50} values and interface friction angles of 16 months cured samples under medium normal stress level are shown in Figure 5.96, Figure 5.97, and Figure 5.98.

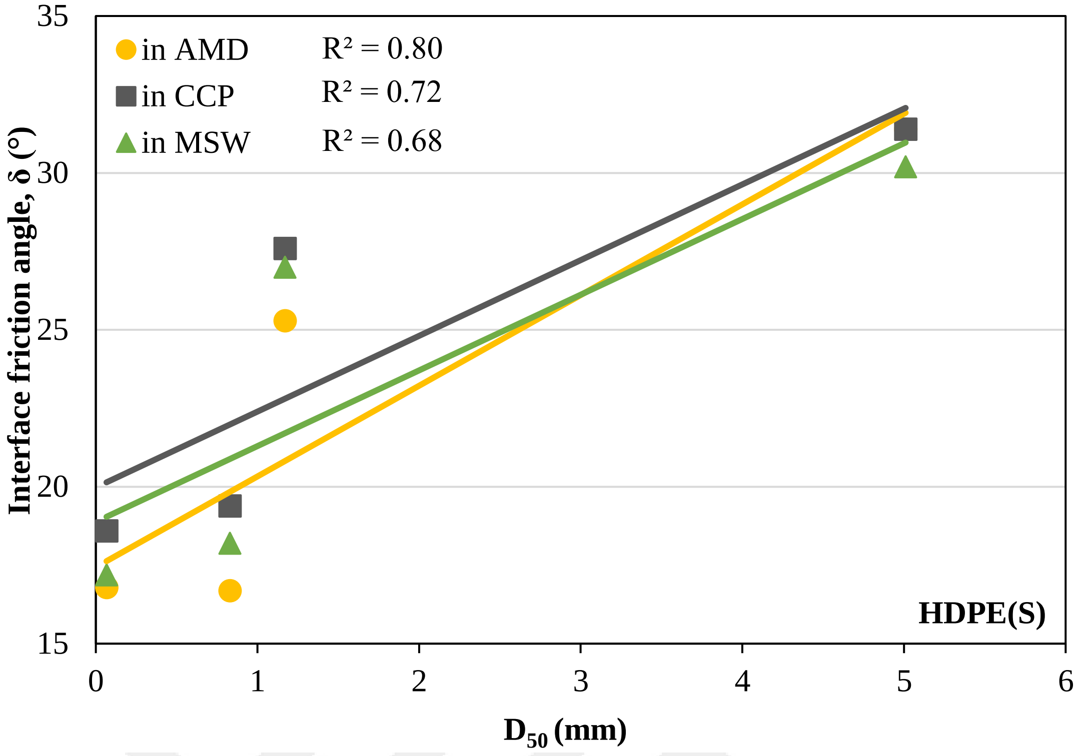

Figure 5.96: Correlation between interface friction angle values of 16 months leachates cured HDPE(S) – soil interface and D_{50}

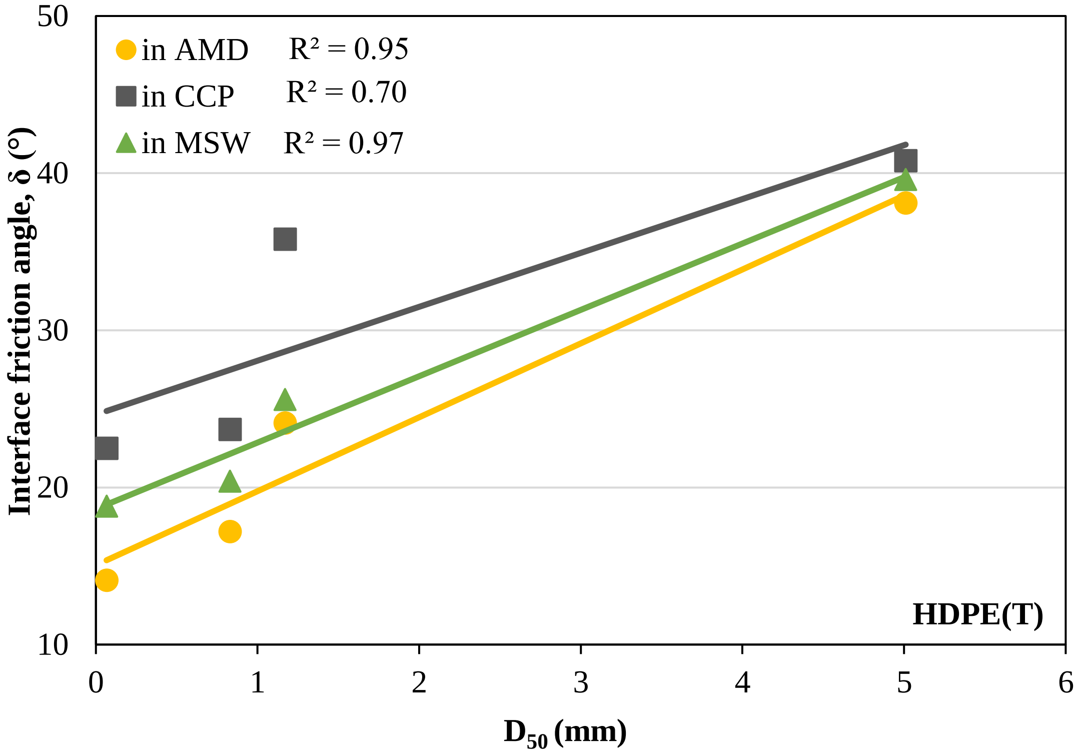

Figure 5.97: Correlation between interface friction angle values of 16 months leachates cured HDPE(T) – soil interface and D_{50}

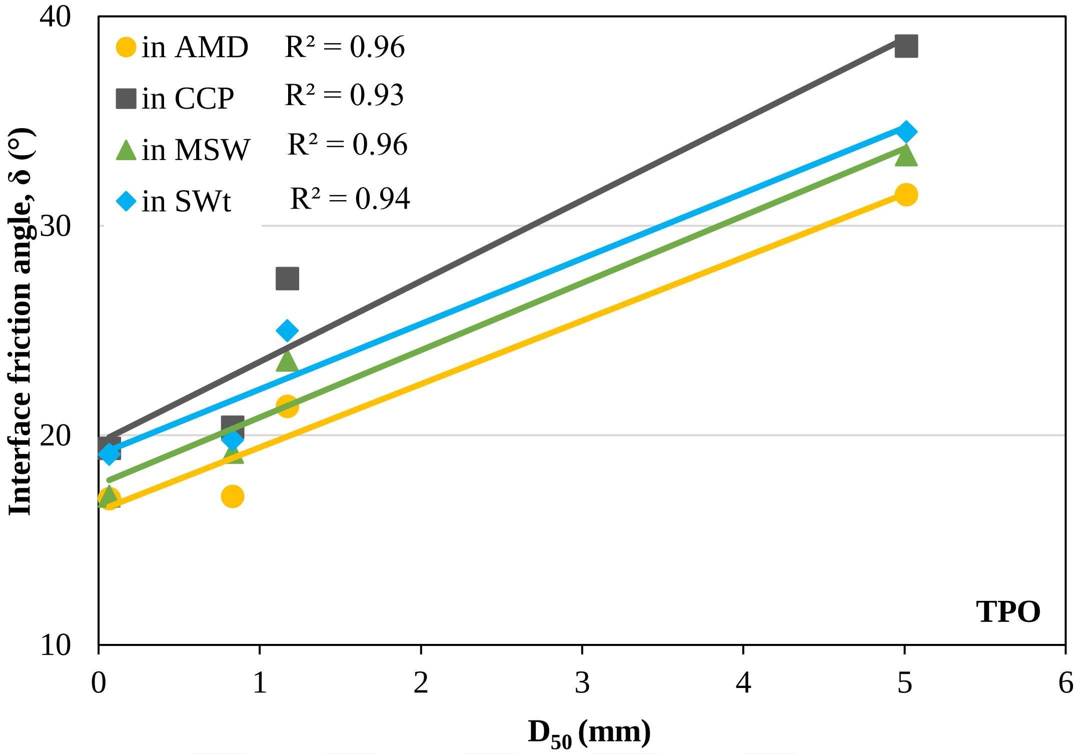

Figure 5.98: Correlation between interface friction angle values of 16 months leachates cured TPO – soil interface and D_{50}

When the graphs are examined, as the D_{50} value increased, the interface friction angle also increased. Also, it was seen that the most damaging to GMs, in other words, the leachate that reduces the interface friction angle the most, was AMD, and the least damaging leachate was CCP. In the Regulation on the Waste Landfills [99], AMD is classified as a 1st class storage facility because the Zn content is more than 20 mg/l and Cu is more than 10 mg/l. MSW has been also classified as a 1st class storage facility due to the Cl^- content of more than 2500 mg/l. CCP, on the other hand, is classified as a 2nd class storage facility due to its SO_4 content of more than 100 mg/l.

When geosynthetics are exposed to AMD, chemical degradation generally begins with a change in the polymer structure and ends with a change in the engineering properties of geosynthetics [102]. Diffuse changes in the polymer; decrease or increase in molecular weight, embrittlement, loss of additives and plasticizers, formation of free radicals, and deterioration of transparency [103]. The reason for these changes may be the acidic conditions and high metal concentration of AMD. Previous studies have shown that acidic conditions cause slight strength losses in polymers in the structure of geosynthetics [104–106].

When GMs are exposed to MSW for a long time, oxidative degradation begins. Viebke et al. (1994) and Hsuan and Koerner (1998) described oxidative degradation as a three-step process [102,107]. In stage I, there is no significant change in the engineering properties of the GM. Stage II is an induction time for degradation to begin and begins after the antioxidants are depleted. The end of the 2nd stage coincides with the time when the oxidation begins. In stage III, there are significant changes in physical and mechanical properties due to oxidation, which eventually leads to GM failure. Failure in this context refers to the reduction of an engineering property, e.g., stress-crack resistance and tensile-breaking stress, to a certain value [29].

Coal combustion products (CCP) are coal ash/residues and are produced when coal is burned to produce electricity or steam. CCPs include fly ash, bottom ash, flue gas desulfurization (FGD) materials, spray dryer ash, etc. is found [108]. CCP leachates are inorganic and can have a greater preponderance of polyvalent cations and higher ionic strength than MSW leachates [100,109]. It also has a much higher pH value than AMD. Therefore, the effect of CCP to damage the mechanical properties of the GM is very low compared to AMD and MSW.

5.8 Comparison with the literature studies

In order to determine whether the interface friction angles obtained in this study are compatible with previous studies in the literature, the friction angles obtained from many studies are summarized in Table 5.23 according to the GM and soil types used. As can be seen, both the friction angles obtained from the studies in the literature and the experiments obtained in this study are compatible with each other according to the interface types.

Table 5.23: The interface friction angle values from the literature studies

Study	Interface	Interface friction angle, δ (°)
Martin et al., 1984 [110]	HDPE(S) – Ottawa sand	20.0
	HDPE(S) – Concrete sand	24.0
	PVC – Ottawa sand	27.0
	PVC – Concrete sand	25.0
Saxena and Wong, 1984 [111]	HDPE(S) – Ottawa sand	21.0
Akber et al., 1985 [112]	HDPE(S) – Sand	25.0
	PVC - Sand	34.0
Weiss and Batereau, 1987 [113]	PVC – Sand	27.0
Williams and Houlihan, 1987 [114]	HDPE(S) – Ottawa sand	19.0
	HDPE(S) – Concrete sand	27.0
	PVC – Concrete sand	26.0
Negussey et al., 1989 [115]	HDPE(S) – Ottawa sand	18.0
	HDPE(S) – Concrete sand	24.0
O’Rourke et al., 1990 [92]	HDPE(S) – Ottawa sand	19.0
	PVC – Ottawa sand	30.0
Lam and Tape, 1991 [116]	PVC – Sand	42.0
Lauwers, 1991 [117]	PVC – Ottawa sand	24.1
Izgin and Wasti, 1998 [118]	HDPE(S) – Ottawa sand	16.5
	HDPE(S) – Crushed stone	23.5
	HDPE(T) – Ottawa sand	28.0
	HDPE(T) – Crushed stone	30.0
Welker and Josten, 2005 [119]	HDPE(S) – Clayey sand	19.0
Fleming et al., 2006 [11]	HDPE(S) – Ottawa sand	21.0
	HDPE(S) – Silty sand	15.4
	HDPE(S) – Sand/bentonite	21.1
Bagci, 2007 [120]	Geotextile – Silt	28.0
Sharma et al., 2007 [121]	HDPE(S) – Sand	14.1

Effendi, 2012 [19]	HDPE(S) – Ottawa sand	13.6
	PVC – Ottawa sand	30.0
Frost et al., 2012 [21]	HDPE(S) – Ottawa sand	24.5
	HDPE(S) – Blasting	25.5
	HDPE(T) – Ottawa sand	38.0
	HDPE(T) – Blasting	37.2
Monteiro et al., 2013 [25]	HDPE(S) – Sand	29.6
	HDPE(T) – Sand	34.6
	PVC – Sand	32.6
Feng and Cheng, 2014 [17]	HDPE(T) – Geotextile	19.8
	HDPE(T) – Clay	10.7
Bhowmik et al., 2016 [122]	HDPE(T) – Clay	18.0
	HDPE(T) – Sand	30.0
Vangla and Gali, 2016 [16]	HDPE(S) – Angular sand	27.1
	HDPE(S) – Rounded sand	18.7
Punetha et al., 2017 [3]	HDPE(S) – River sand	23.7
	HDPE(S) – River sand	20.8
	Geotextile – River sand	33.8
	Geotextile – River sand	34.6
Stark and Santoyo, 2017 [20]	HDPE(S) – Glacial till	13.0
	HDPE(S) – Ottawa sand	20.0
	HDPE(T) – Glacial till	31.0
	HDPE(T) – Ottawa sand	32.0
	PVC – Glacial till	28.0
	PVC – Ottawa sand	26.0
	TPO – Glacial till	15.0
	TPO – Ottawa sand	25.0
Cen et al., 2018 [26]	HDPE(S) – Fine sand	29.0
	HDPE(S) – Sandy gravel	30.6
	HDPE(S) – Geotextile	11.6

	HDPE(T) – Fine sand	32.7
	HDPE(T) – Sandy gravel	36.8
	HDPE(T) – Geotextile	20.9
Markou and Evangelou, 2018 [123]	HDPE(S) – Rounded sand	17.0
	HDPE(S) – Sub-angular sand	32.5
	HDPE(T) – Rounded sand	25.6
	HDPE(T) – Sub-angular sand	36.6
	PVC – Rounded sand	28.1
	PVC – Sub-angular sand	39.8
	TPO – Rounded sand	26.3
	TPO – Sub-angular sand	33.8
Ari, 2020 [124]	HDPE(S) – River sand	22.0
	HDPE(S) – Crushed sand	25.0
	HDPE(S) – Crushed stone	31.0
	HDPE(T) – River sand	37.0
	HDPE(T) – Crushed sand	41.0
	HDPE(T) – Crushed stone	47.0
Stoltz et al., 2020 [67]	HDPE(S) – Geotextile	14.0
	PVC – Geotextile	16.7
Zhou et al., 2020 [125]	HDPE(S) – Sand	24.2
	HDPE(S) – Clay	18.8
	HDPE(T) – Sand	37.6
	HDPE(T) – Clay	25.2
Araujo et al., 2022 [126]	HDPE(S) – Angular sand	24.2
	HDPE(T) – Angular sand	30.3
Rashed et al., 2022 [127]	HDPE(S) – Sand	15.2 – 20.2
Junior et al., 2023 [128]	HDPE(T) – Silt-clay sand-1	30.2
	HDPE(T) – Silt-clay sand-2	40.2

Chapter 6

Conclusions

In this thesis, the shear strength parameters of soil – GM interfaces were examined. The interface direct shear parameters were determined with a medium scale direct shear apparatus. The experiments were conducted under three normal stress levels (low, medium, high) to designate the effect of the normal stress on the interface shear behavior. Six types of soils were used in the experiments to investigate the effect of particle size and particle angularity. To determine the effect of the GM type, thickness, and roughness, 1.5 and 3.0 mm PVC, 1.5 mm TPO, and 1.5 mm smooth and textured HDPE GM were used. Also, the GMs were cured in 0.5m SWt, AMD, CCP, and MSW for 4, 8, and 16 months to determine the effect of curing type and curing time on the interface shear strength behavior. Lastly, to support the results obtained from the experiments, the surface roughness of the GMs cured for 16 months was measured and their microscopic images were taken after the direct shear test. In addition, the interface was modeled as a slope stability problem in the Plaxis 2D software by direct shear experiment, and the FS values of each interface were obtained and compared with the test results. The results of the examination and analysis are interpreted, and the results are summarized below:

For uncured GM – soil interfaces;

1. It was determined that the interface friction angle increased as the grain size and angularity increased for all GM types.
2. For PVC and TPO, the interface friction angle decreased as the normal stress increased in relatively fine grained soils (LC and SB), while the interface friction angle increased as the normal stress increased in coarse grained soils (CS, RS, CG, and RG).

3. For HDPE(S) and HDPE(T), the interface friction angle increased as the normal stress increased in all soil types.

For SWt cured GM – soil interfaces;

1. It was observed that the interface friction angle decreased as the curing time increased for all GMs.
2. In PVC(1.5) – soil interface tests, the C_E coefficients were obtained for LC, SB, CS, and CG, respectively, of 0.71, 0.71, 0.91, and 0.94.
3. In PVC(3.0) – soil interface tests, the C_E coefficients were obtained for LC, SB, CS, and CG, respectively, of 0.88, 0.72, 0.94, and 0.91.
4. In TPO – soil interface tests, the C_E coefficients were obtained for LC, SB, CS, and CG, respectively, of 0.86, 0.91, 0.74, and 0.88.
5. In general, the most adversely affected GM from the SWt cure was PVC(1.5), and the least adversely affected GM was PVC(3.0). This is because the thickness of PVC(1.5) and TPO is 1.5 mm, while the thickness of PVC(3.0) is 3.0 mm.
6. As for the interface, the most damaged is the LC – PVC(1.5) interface. Therefore, the use of PVC(1.5) GM for foundation insulation in structures to be built on a low plasticity clay soil in settlements **close to coastal areas** will be risky in terms of life and property safety. Instead, **PVC(3.0) or TPO GM** should be preferred.

For AMD cured GM – soil interfaces;

1. It was observed that the interface friction angle decreased as the curing time increased for all GMs.
2. In HDPE(S) – soil interface tests, the C_E coefficients were obtained for LC, SB, CS, and CG, respectively, of 0.82, 0.81, and 0.80.
3. In HDPE(T) – soil interface tests, the C_E coefficients were obtained for LC, SB, CS, and CG, respectively, of 0.66, 0.68, and 0.89.

4. In TPO – soil interface tests, the C_E coefficients were obtained for LC, SB, CS, and CG, respectively, of 0.85, 0.78, 0.63, and 0.81.
5. In general, HDPE(T) was the most adversely affected GM from AMD cure, and HDPE(S) was the least adversely affected GM. This is because HDPE(T) has fine needle-shaped roughnesses and highly acidic AMD can easily damage these roughnesses.
6. As for the interface, it is the CS – TPO interface that is most adversely affected. For this reason, if crushed sand is to be used as a drainage layer when creating **a waste pond in metal waste storage or mining exploration sites**, the use of TPO as an insulation GM may pose a great risk to the environment. According to the results of this study, the optimum soil – GM pair suitable for use in such fields is textured **HDPE GM with crushed gravel**.

For CCP cured GM – soil interfaces;

1. It was observed that the interface friction angle decreased as the curing time increased for all GMs.
2. In HDPE(S) – soil interface tests, the C_E coefficients were obtained for LC, SB, CS, and CG, respectively, of 0.96, 0.88, and 0.93.
3. In HDPE(T) – soil interface tests, the C_E coefficients were obtained for LC, SB, CS, and CG, respectively, of 0.91, 0.99, and 0.96.
4. In TPO – soil interface tests, the C_E coefficients were obtained for LC, SB, CS, and CG, respectively, of 0.97, 0.94, 0.81, and 0.94.
5. When examined in general, it was determined that the GM that was adversely affected by the CCP cure the most was TPO, and the GM that was least affected was HDPE(T). This is because polyolefin is a monomer composed of small alkenes, while polyethylene is an ethylene composed of these monomers. That is, while it is easier to damage the chemical bonds of TPO, polyethylene is easier. The reason why HDPE(T) does not damage its roughness as in other leachates is that CCP is not acidic.
6. In the interface, the most damaged is the CS – TPO interface. Therefore, if crushed sand is to be used as a drainage layer in **coal mine waste storage**

facilities, it would be very dangerous to use TPO GM. The conclusion drawn from this study is that the optimum soil – GM pair in this type of facility is **crushed sand and textured HDPE GM**.

For MSW cured GM – soil interfaces;

1. It was observed that the interface friction angle decreased as the curing time increased for all GMs.
2. In HDPE(S) – soil interface tests, the C_E coefficients were obtained for LC, SB, CS, and CG, respectively, of 0.90, 0.86, and 0.89.
3. In HDPE(T) – soil interface tests, the C_E coefficients were obtained for LC, SB, CS, and CG, respectively, of 0.78, 0.72, and 0.93.
4. In TPO – soil interface tests, the C_E coefficients were obtained for LC, SB, CS, and CG, respectively, of 0.86, 0.88, 0.70, and 0.85.
5. When examined in general, HDPE(T) is the most adversely affected GM due to MSW cure, and HDPE(S) is the least affected GM. This is because, just like AMD, the needle-shaped roughness of HDPE(T) is sensitive and easily damaged due to the high acid content of MSW.
6. In particular, the interface that is most damaged from MSW curing is CS – TPO. Therefore, if crushed sand is used as a drainage layer in **municipal solid waste landfills**, TPO should not be used as an insulation GM. Instead, the optimum soil – GM pair to be used in such storage facilities is **crushed gravel – textured HDPE**.

The most important conclusion to be drawn from this study is that the use of certain values as interface friction coefficient, for example, 2/3 (0.67), in projects designed with GM all over the world, presents quite risky situations. Because the results showed that a reduction of 0.67 in the internal friction angle is insufficient at some interfaces. For this reason, when designing with GMs that will be exposed to leachates, especially in landfills, the damages that will occur over time should also be considered and the design parameters should be selected accordingly. Otherwise, disasters that will lead to loss of life and property may occur.

References

1. Wasti Y, Özdüzgün ZB. Geomembrane–geotextile interface shear properties as determined by inclined board and direct shear box tests. Geotextiles and Geomembranes. 2001;19(1):45–57.

2. Bannour H, Barral C, Touze-Foltz N. Altered geosynthetic clay liners: effect on the hydraulic performance of composite liners. European Journal of Environmental and Civil Engineering. 2015;19(9):1155–76.

3. Punetha P, Mohanty P, Samanta M. Microstructural investigation on mechanical behavior of soil-geosynthetic interface in direct shear test. Geotextiles and Geomembranes. 2017;45(3):197–210.

4. Sabiri NE, Caylet A, Montillet A, Le Coq L, Durkheim Y. Performance of nonwoven geotextiles on soil drainage and filtration. European Journal of Environmental and Civil Engineering. 2020;24(5):670–88.

5. Chen WB, Xu T, Zhou WH. Microanalysis of smooth Geomembrane–Sand interface using FDM–DEM coupling simulation. Geotextiles and Geomembranes. 2021;49(1):276–88.

6. Koerner RM. Designing with geosynthetics-Vol. 1. Vol. 1. Xlibris Corporation; 2012.

7. Bathurst RJ, Ezzein FM. Geogrid pullout load–strain behaviour and modelling using a transparent granular soil. Geosynthetics International. 2016;23(4):271–86.

8. ASTM D4439 Standard Terminology for Geosynthetics [Internet]. [cited 2023 May 5]. Available from: https://www.astm.org/d4439-23a.html

9. Seed RB, Mitchell JK, Seed HB. Slope Stability Failure Investigation: Kettleman Hills Repository Landfill Unit B-19, Phase I A. Berkeley, California: University of California. 1988;

10. Vaid YP, Rinne N. Geomembrane coefficients of interface friction. Geosynthetics International. 1995;2(1):309–25.

11. Fleming IR, Sharma JS, Jogi MB. Shear strength of geomembrane–soil interface under unsaturated conditions. Geotextiles and Geomembranes. 2006;24(5):274–84.

12. Ghazizadeh S, Bareither CA. Failure mechanisms of geosynthetic clay liner and textured geomembrane composite systems. Geotextiles and Geomembranes. 2021;49(3):789–803.

13. Manan S, Pitroda J, Bhavsar JJ. HDPE geomembranes: A liner material for reservoirs. In: International Conference on:"Engineering: Issues, opportunities and Challenges for Development", 11th April, 2015, SN Patel Institute of Technolgoy & Research Centre, Umrakh, Bardoli. 2015.

14. Zangani D, Fuggini C, Loriga G. Electronic textiles for geotechnical and civil engineering. In: Electronic Textiles. Elsevier; 2015. p. 275–300.

15. Mao N. Methods for characterisation of nonwoven structure, property, and performance. In: Advances in technical nonwovens. Elsevier; 2016. p. 155–211.

16. Vangla P, Gali ML. Shear behavior of sand-smooth geomembrane interfaces through micro-topographical analysis. Geotextiles and Geomembranes. 2016;44(4):592–603.

17. Feng SJ, Cheng D. Shear strength between soil/geomembrane and geotextile/geomembrane interfaces. In: Tunneling and Underground Construction. 2014. p. 558–69.

18. Chai JC, Saito A. Interface shear strengths between geosynthetics and clayey soils. International Journal of Geosynthetics and Ground Engineering. 2016;2:1–9.

19. Effendi R. Interface friction of smooth geomembranes and Ottawa sand. INFO-TEKNIK. 2011;12(1):61–72.

20. Stark TD, Santoyo RF. Soil/geosynthetic interface strengths from torsional ring shear tests. In: Geotechnical Frontiers 2017. 2017. p. 260–8.

21. Frost JD, Evans TM, Hebeler GL, Giroud JP. Influence of wear mechanisms on geosynthetic interface strengths. In: Geosynthetics: state of the art-recent developments proceedings of the seventh international conference on geosynthetics, 7-icg, held 22-27 September 2002, Nice, France Volume 4. 2002.

22. Stark TD, Williamson TA, Eid HT. HDPE geomembrane/geotextile interface shear strength. Journal of Geotechnical Engineering. 1996;122(3):197–203.

23. Islam MZ, Rowe RK. Effect of HDPE geomembrane thickness on the depletion of antioxidants. In: 60th Canadian Geotechnical Conference. Citeseer; 2007. p. 2129–34.

24. Eid HT. Shear strength of geosynthetic composite systems for design of landfill liner and cover slopes. Geotextiles and Geomembranes. 2011;29(3):335–44.

25. Monteiro CB, Araújo GLS, Palmeira EM, Neto MPC. Soil-geosynthetic interface strength on smooth and texturized geomembranes under different test conditions. In: Proceedings of the 18th international conference on soil mechanics and geotechnical engineering, Paris. 2013. p. 3053–6.

26. Cen WJ, Wang H, Sun YJ. Laboratory investigation of shear behavior of high-density polyethylene geomembrane interfaces. Polymers (Basel). 2018;10(7):734.

27. Zabielska-Adamska K. Water content–density criteria for determining geomembrane–fly ash interface shear strength. In: MATEC Web of Conferences. EDP Sciences; 2019. p. 04005.

28. Abdelaal FB, Rowe RK, Brachman RWI. Brittle rupture of an aged HPDE geomembrane at local gravel indentations under simulated field conditions. Geosynthetics International. 2014;21(1):1–23.

29. Rowe RK, Islam MZ, Hsuan YG. Effects of thickness on the aging of HDPE geomembranes. Journal of Geotechnical and Geoenvironmental Engineering. 2010;136(2):299–309.

30. Gulec SB, Benson CH, Edil TB. Effect of acidic mine drainage on the mechanical and hydraulic properties of three geosynthetics. Journal of Geotechnical and Geoenvironmental Engineering. 2005;131(8):937–50.

31. Mitchell JK, Seed RB, Seed HB. Kettleman Hills waste landfill slope failure. I: Liner-system properties. Journal of geotechnical engineering. 1990;116(4):647–68.

32. Grubb DG, Diesing III WE, Cheng SCJ. High altitude exposure testing of geotextiles in the Peruvian Andes. Geosynthetics International. 1999;6(2):119–44.

33. Sun X chen, Xu Y, Liu Y qiang, Nai C xin, Dong L, Liu J cai, et al. Evolution of geomembrane degradation and defects in a landfill: Impacts on long-term leachate leakage and groundwater quality. Journal of Clean Productions. 2019;224:335–45.

34. Koerner RM, Hsuan YG, Koerner GR. Lifetime predictions of exposed geotextiles and geomembranes. Geosynthetics International. 2017;24(2):198–212.

35. Abandoned Mine Drainage | US EPA [Internet]. [cited 2023 May 5]. Available from: https://www.epa.gov/nps/abandoned-mine-drainage.

36. Dhir B. Biotechnological tools for remediation of acid mine drainage (removal of metals from wastewater and leachate). In: Bio-Geotechnologies for Mine Site Rehabilitation. Elsevier; 2018. p. 67–82.

37. Bergerson J, Lave L. Life cycle analysis of power generation systems. 2004;

38. Prasad MN V, Nakbanpote W, Phadermrod C, Rose D, Suthari S. Mulberry and vetiver for phytostabilization of mine overburden: cogeneration of economic products. In: Bioremediation and bioeconomy. Elsevier; 2016. p. 295–328.

39. Iatan EL. Gold mining industry influence on the environment and possible phytoremediation applications. In: Phytorestoration of abandoned mining and oil drilling sites. Elsevier; 2021. p. 373–408.

40. Jouini M, Benzaazoua M, Neculita CM. Stabilization/solidification of acid mine drainage treatment sludge. In: Low Carbon Stabilization and Solidification of Hazardous Wastes. Elsevier; 2022. p. 175–99.

41. Dalu T, Mwedzi T, Wasserman RJ. Phytoplankton dynamics. In: Fundamentals of Tropical Freshwater Wetlands. Elsevier; 2022. p. 189–219.

42. Gulec S. Effect of acid mine drainage on the properties of geosynthetics. Madison, Wis: Univ of Wisconsin-Madison. 2003;

43. Pudasainee D, Kurian V, Gupta R. Coal: Past, present, and future sustainable use. Future Energy. 2020;21–48.

44. Coal 2022 Analysis and forecast to 2025. 2022.

45. Production & Use Reports – ACAA [Internet]. [cited 2023 May 5]. Available from: https://acaa-usa.org/publications/production-use-reports/

46. Benson CH, Chen JN, Edil TB, Likos WJ. Hydraulic conductivity of compacted soil liners permeated with coal combustion product leachates. Journal of Geotechnical and Geoenvironmental Engineering. 2018;144(4):04018011.

47. What a Waste [Internet]. [cited 2023 May 5]. Available from: https://datatopics.worldbank.org/what-a-waste/

48. Hrapovic L, Rowe RK. Intrinsic degradation of volatile fatty acids in laboratory-compacted clayey soil. Journal of Contaminant Hydrology. 2002;58(3–4):221–42.

49. Rowe RK, Islam MZ, Hsuan YG. Leachate chemical composition effects on OIT depletion in an HDPE geomembrane. Geosynthetics International. 2008;15(2):136–51.

50. Rowe RK, Rimal S, Sangam H. Ageing of HDPE geomembrane exposed to air, water and leachate at different temperatures. Geotextiles and Geomembranes. 2009;27(2):137–51.

51. Xie H, Lou Z, Chen Y, Jin A, Zhan TL, Tang X. An analytical solution to organic contaminant diffusion through composite liners considering the effect of degradation. Geotextiles and Geomembranes. 2013;36:10–8.

52. ASTM D422 Standard Test Method for Particle-Size Analysis (Standard Withdrawn) -- eLearning Course [Internet]. [cited 2023 May 5]. Available from: https://www.astm.org/astm-tpt-156.html

53. ASTM D7928 Standard Test Method for Particle-Size Distribution (Gradation) of Fine-Grained Soils Using the Sedimentation (Hydrometer) Analysis [Internet]. [cited 2023 May 5]. Available from: https://www.astm.org/d7928-21e01.html

54. ASTM D854 Standard Test Methods for Specific Gravity of Soil Solids by Water Pycnometer [Internet]. [cited 2023 May 5]. Available from: https://www.astm.org/d0854-14.html

55. ASTM C127 Standard Test Method for Relative Density (Specific Gravity) and Absorption of Coarse Aggregate [Internet]. [cited 2023 May 5]. Available from: https://www.astm.org/c0127-15.html

56. ASTM D4318 Standard Test Methods for Liquid Limit, Plastic Limit, and Plasticity Index of Soils [Internet]. [cited 2023 May 5]. Available from: https://www.astm.org/d4318-17e01.html

57. ASTM D698 Standard Test Methods for Laboratory Compaction Characteristics of Soil Using Standard Effort (12,400 ft-lbf/ft3 (600 kN-m/m3)) [Internet]. [cited 2023 May 5]. Available from: https://www.astm.org/d0698-12r21.html

58. ASTM D4972 Standard Test Methods for pH of Soils [Internet]. [cited 2023 May 5]. Available from: https://www.astm.org/d4972-19.html

59. ASTM D3080/D3080M Standard Test Method for Direct Shear Test of Soils Under Consolidated Drained Conditions (Withdrawn 2020) [Internet]. [cited 2023 May 5]. Available from: https://www.astm.org/d3080_d3080m-11.html

60. Dadkhah R, Ghafoori M, Ajalloeian R, Lashkaripour GR. The effect of Scale Direct Shear Tests on The Strength parameters of Clayey Sand in Isfahan city, Iran. Journal of Applied Sciences. 2010;18.

61. Soból E, Sas W, Szymański A. Scale effect in direct shear tests on recycled concrete aggregate. Studia Geotechnica et Mechanica. 2015;37(2):45–9.

62. Mohapatra SR, Mishra SR, Nithin S, Rajagopal K, Sharma J. Effect of box size on dilative behaviour of sand in direct shear test. In: Geotechnical Characterisation and Geoenvironmental Engineering: IGC 2016 Volume 1. Springer; 2019. p. 111–8.

63. Zahran K, Naggar H El. Effect of sample size on TDA shear strength parameters in direct shear tests. Transportation Research Record. 2020;2674(9):1110–9.

64. ASTM D5321/D5321M Standard Test Method for Determining the Shear Strength of Soil-Geosynthetic and Geosynthetic-Geosynthetic Interfaces by Direct Shear [Internet]. [cited 2023 May 5]. Available from: https://www.astm.org/d5321_d5321m-21.html

65. Reyes Ramirez R, Gourc JP. Use of the inclined plane test in measuring geosynthetic interface friction relationship. Geosynthetics International. 2003;10(5):165–75.

66. Kim J, Riemer M, Bray JD. Dynamic properties of geosynthetic interfaces. ASTM geotechnical testing journal. 2005;28(3):288–96.

67. Stoltz G, Nicaise S, Veylon G, Poulain D. Determination of geomembrane–Protective geotextile friction angle: An insight into the shear rate effect. Geotextiles and Geomembranes. 2020;48(2):176–89.

68. Chang JY, Feng SJ. Dynamic shear behaviors of textured geomembrane/nonwoven geotextile interface under cyclic loading. Geotextiles and Geomembranes. 2021;49(2):388–98.

69. Pavanello P, Carrubba P, Moraci N. The characterisation of geosynthetic interface friction by means of the inclined plane test. Geotextiles and Geomembranes. 2021;49(1):257–75.

70. Triplett EJ, Fox PJ. Shear strength of HDPE geomembrane/geosynthetic clay liner interfaces. Journal of Geotechnical and Geoenvironmental Engineering. 2001;127(6):543–52.

71. Hebeler GL, Frost JD, Myers AT. Quantifying hook and loop interaction in textured geomembrane–geotextile systems. Geotextiles and Geomembranes. 2005;23(1):77–105.

72. Li MH, Gilbert RB. Mechanism of post-peak strength reduction for textured geomembrane–nonwoven geotextile interfaces. Geosynthetics International. 2006;13(5):206–9.

73. Bacas BM, Cañizal J, Konietzky H. Shear strength behavior of geotextile/geomembrane interfaces. Journal of Rock Mechanics and Geotechnical Engineering. 2015;7(6):638–45.

74. Dove JE, Harpring JC. Geometric and spatial parameters for analysis of geomembrane/soil interface behavior. In: Proceedings of Geosynthetics. 1999. p. 575–88.

75. Karademir T, Frost JD. Elevated Temperature Effects on Geotextile–Geomembrane Interface Shear Behavior. Journal of Geotechnical and Geoenvironmental Engineering. 2021 Dec;147(12).

76. Dove JE, Frost JD, Dove PM. Geomembrane microtopography by atomic force microscopy. Geosynthetics International. 1996;3(2):227–45.

77. Frost JD, Lee SW. Microscale study of geomembrane-geotextile interactions. Geosynthetics International. 2001;8(6):577–97.

78. Hanson JL, Chrysovergis TS, Yesiller N, Manheim DC. Temperature and moisture effects on GCL and textured geomembrane interface shear strength. Geosynthetics International. 2015;22(1):110–24.

79. Manheim DC, Yesiller N, Hanson JL, Gourc JP, Carbone L, Moraci N, et al. Investigation of Post-Shear Surface Texture Characteristics of Geomembranes. In: Geosynthetics 2015. 2015.

80. Afzali-Nejad A, Lashkari A, Martinez A. Stress-displacement response of sand–geosynthetic interfaces under different volume change boundary conditions. Journal of Geotechnical and Geoenvironmental Engineering. 2021;147(8):04021062.

81. ASTM D2487 Standard Practice for Classification of Soils for Engineering Purposes (Unified Soil Classification System) [Internet]. [cited 2023 May 5]. Available from: https://www.astm.org/d2487-17e01.html

82. Prakasha KS, Chandrasekaran VS. Behavior of marine sand-clay mixtures under static and cyclic triaxial shear. Journal of Geotechnical and Geoenvironmental Engineering. 2005;131(2):213–22.

83. Simoni A, Houlsby GT. The direct shear strength and dilatancy of sand–gravel mixtures. Geotechnical & Geological Engineering. 2006;24:523–49.

84. Liu XL, Loo H, Min H, Deng JH, Tham LG, Lee CF. Shear strength of slip soils containing coarse particles of Xietan landslide. In: Advances in Earth Structures: Research to Practice. 2006. p. 142–59.

85. Shimobe S. A new classification chart for sand liquefaction. In: Proc 1st International Conference on Earthquake Geotechnical Engineering, Tokyo. 1995. p. 315–20.

86. Miura K, Maeda K, Furukawa M, Toki S. Mechanical characteristics of sands with different primary properties. Soils and Foundations. 1998;38(4):159–72.

87. Dyskin A V, Estrin Y, Kanel-Belov AJ, Pasternak E. Toughening by fragmentation—how topology helps. Advances in Engineering Materials. 2001;3(11):885–8.

88. Santamarina JC. Soil Behavior at the Microscale: Particle Forces. In: Soil Behavior and Soft Ground Construction. Reston, VA: American Society of Civil Engineers; 2003. p. 25–56.

89. Cho GC, Dodds J, Santamarina CJ. Particle shape effects on packing density, stiffness, and strength: natural and crushed sands. Journal of Geotechnical and Geoenvironmental 132 (5): 591–602. 2006.

90. Cubrinovski M, Ishihara K. Maximum and minimum void ratio characteristics of sands. Soils and Foundations. 2002;42(6):65–78.

91. Guimaraes MS. Crushed stone fines and ion removal from clay slurries: Fundamental studies. Georgia Institute of Technology; 2002.

92. O'rourke TD, Druschel SJ, Netravali AN. Shear strength characteristics of sand-polymer interfaces. Journal of Geotechnical Engineering. 1990;116(3):451–69.

93. Dove JE, Frost JD. Peak friction behavior of smooth geomembrane-particle interfaces. Journal of Geotechnical and Geoenvironmental Engineering. 1999;125(7):544–55.

94. Da Silva LFM, De Magalhães FACRG, Chaves FJP, De Moura MFSF. Mode II Fracture Toughness of a Brittle and a Ductile Adhesive as a Function of the Adhesive Thickness. https://doi.org/101080/002184642010506155 [Internet]. 2010 [cited 2023 May 5];86(9):891–905. Available from: https://www.tandfonline.com/doi/abs/10.1080/00218464.2010.506155

95. Brostow W, Hagg Lobland HE, Khoja S. Brittleness and toughness of polymers and other materials. Materials Letter. 2015 Nov 15;159:478–80.

96. Li L, Zhang J, Xiao H, Hu Z, Wang Z. Experimental investigation of mechanical behaviors of fiber-reinforced fly ash-soil mixture. Advances in Materials Science and Engineering. 2019;2019.

97. Bove JA. Direct shear friction testing for geosynthetics in waste containment. In: Geosynthetic testing for waste containment applications. ASTM International; 1990.

98. Zettler TE, Frost JD, DeJong JT. Shear-induced changes in smooth HDPE geomembrane surface topography. Geosynthetics International. 2000;7(3):243–67.

99. Başbakanlık Mevzuatı Geliştirme ve Yayın Genel Müdürlüğü [Internet]. [cited 2023 May 5]. Available from: https://www.resmigazete.gov.tr/eskiler/2010/03/20100326-13.htm

100. Salihoglu H, Chen JN, Likos WJ, Benson CH. Hydraulic conductivity of bentonite-polymer geosynthetic clay liners in coal combustion product leachates. In: Geo-Chicago 2016. 2016. p. 438–47.

101. Chen JF, Li LY, Xue JF, Feng SZ. Failure mechanism of geosynthetic-encased stone columns in soft soils under embankment. Geotextiles and Geomembranes. 2015;43(5):424–31.

102. Hsuan YG, Koerner RM. Antioxidant depletion lifetime in high density polyethylene geomembranes. Journal of Geotechnical and Geoenvironmental Engineering. 1998;124(6):532–41.

103. Kulshreshtha AK. Chemical degradation. Handbook of Polymer Degradation Marcel Dekker, New York, USA. 1992;55–94.

104. Risseuw P, Schmidt HM. Geotextiles, Geomembranes and Related Products. Rotterdam, The Netherlands. 1990;

105. Jailloux JM, Anderson PL, Thomas RW. Chemical-compatibility studies of polyester filaments and yarns to be used in geocomposites. Phase 1: Tests at 95° C. Geotextiles and Geomembranes. 1992;11(3):277–90.

106. Salman A, Elias V, Juran I, Lu S, Pearce E. Durability of geosynthetics based on accelerated laboratory testing. 1997;

107. Viebke J, Elble E, Ifwarson M, Gedde UW. Degradation of unstabilized medium-density polyethylene pipes in hot-water applications. Polymer Engineering Science. 1994;34(17):1354–61.

108. Zainab B, Wireko C, Li D, Tian K, Abichou T. Hydraulic conductivity of bentonite-polymer geosynthetic clay liners to coal combustion product leachates. Geotextiles and Geomembranes. 2021 Oct;49(5):1129–38.

109. Benson C, Chen J, Edil T. Engineering properties of geosynthetic clay liners permeated with coal combustion product leachates. Rep No 3002003770, Electric Power Research Institute, Palo Alto, CA. 2014;

110. Martin JP, Koerner RM, Whitty JE. Experimental friction evaluation of slippage between geomembranes, geotextiles and soils. In: Proceedings of the International Conference on Geomembranes. IFAI Denver, CO, USA; 1984. p. 191–6.

111. Saxena SK, Wong YT. Friction characteristics of a geomembrane. In: Proceedings of International Conference on Geomembranes, Denver, CO. 1984. p. 187–90.

112. Akber SZ, Hammanji Y, Lafleur J. Frictional characteristics of geomembranes, geotextiles and geomembrane-geotextiles composites. In: Proc 2nd Canadian Symp on Geotextiles and Geomembranes Canadian Geotechnical Society, Edmonton, Alberta. 1985. p. 209–17.

113. Weiss W, Batereau C. A note on planar shear between geosynthetics and construction materials. Geotextiles and Geomembranes. 1987;5(1):63–7.

114. Williams ND, Houlihan MF. Evaluation of interface friction properties between geosynthetics and soils. In: Proceedings of Geosynthetics. 1987. p. 616–27.

115. Negussey D, Wijewickreme WKD, Vaid YP. Geomembrane interface friction. Canadian Geotechnical Journal. 1989;26(1):165–9.

116. Lam DJS, Tape RT. Geosynthetics: Design and Performance, Sixth Annual Symposium. In: Geomembrane Interface Strength Tests. Vancouver : Vancouver Geotechnical Society; 1991.

117. Lauwers DC. PVC geocomposite for improved friction and performance properties. In: Geosynthetics’ 91Industrial Fabrics Association; North American Geosynthetics Society; International Geotextile Society. 1991.

118. Izgin M, Wasti Y. Geomembrane–sand interface frictional properties as determined by inclined board and shear box tests. Geotextiles and Geomembranes. 1998;16(4):207–19.

119. Welker AL, Josten N. Interface friction of a geomembrane with a fiber reinforced soil. In: Slopes and retaining structures under seismic and static conditions. 2005. p. 1–8.

120. Bağcı F. Geosentetiklerle projelendirme ve zemin–geosentetik arayüzey sürtünme açilarinin değişik geosentetik ve zemin türleri için araştirilmasi [Master Science]. [Izmir]: Ege University Natural and Applied Science; 2007.

121. Sharma JS, Fleming IR, Jogi MB. Measurement of unsaturated soil–geomembrane interface shear-strength parameters. Canadian Geotechnical Journal. 2007;44(1):78–88.

122. Bhowmik R, Sukumar R, Datta M, Shahu JT. The use of geosynthetic reinforcement for enhancing the stability of the geomembrane–soil interface along the slopes of cover systems of MSW landfills. In: Geo-Chicago 2016. 2016. p. 307–18.

123. Markou IN, Evangelou ED. Shear Resistance Characteristics of Soil–Geomembrane Interfaces. International Journal of Geosynthetics and Ground Engineering. 2018 Dec 8;4(4):29.

124. Ari A. Kum-geosentetik arayüzeyi kayma direncine fraktal boyutun etkisinin araştirilmasi [Master Science]. [Istanbul]: Yıldız Teknik University Natural and Applied Science; 2020.

125. Zhou L, Zhu Z, Yu Z, Zhang C. Shear testing of the interfacial friction between an HDPE geomembrane and solid waste. Materials. 2020;13(7):1672.

126. Araújo GLS, Sánchez NP, Palmeira EM, Almeida M das GG de. Influence of micro and macroroughness of geomembrane surfaces on soil-geomembrane

and geotextile-geomembrane interface strength. Geotextiles and Geomembranes. 2022 Aug 1;50(4):751–63.

127. Rashed AS, Sorour TM, Elsayed AN. Study of the Effect of Geomembranes on the Interaction between the Soil and Underground Structures. Vol. 6, Journal of Engineering Research. 2022.

128. Junior SL da C, Aparicio-Ardila MA, Palomino CF, Lins da Silva J. Analysis of Textured Geomembrane–Soil Interface Strength to Mining Applications. International Journal of Geosynthetics and Ground Engineering. 2023 Feb 1;9(1).

Appendices

Appendix A

Graphical Representation of Interface Direct Shear Test Results

Direct Shear Test Results of Soils

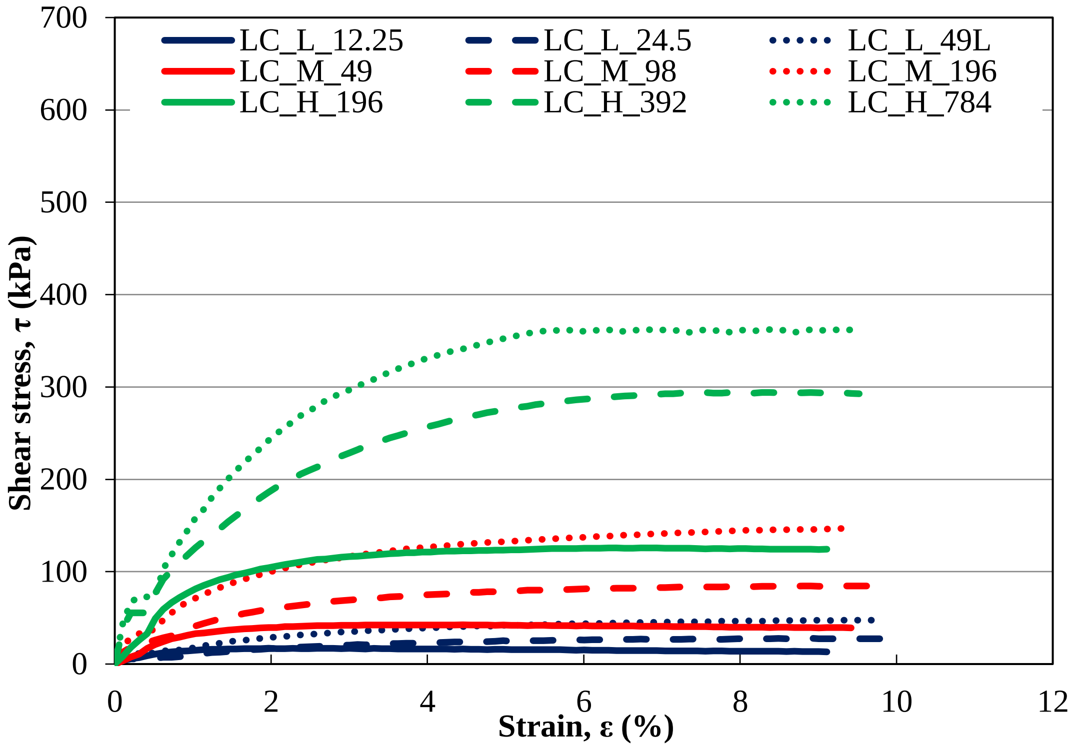

Figure A. 1: Shear stress (τ) – strain (ε) graphs of LC

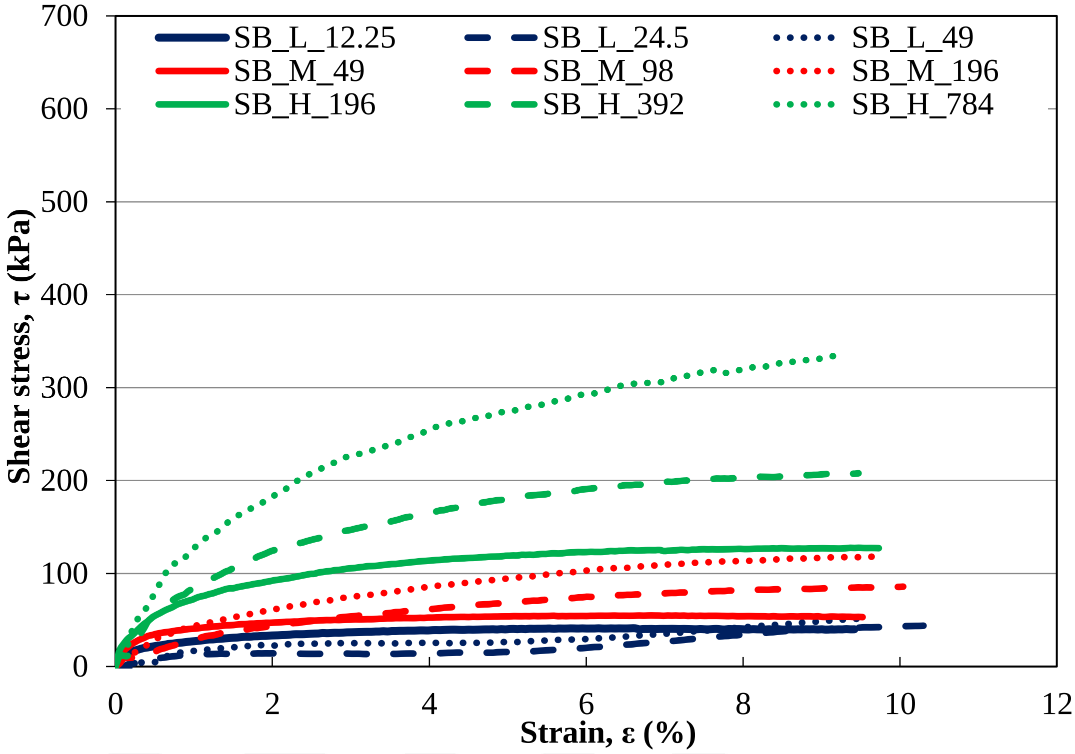

Figure A. 2: Shear stress (τ) – strain (ε) graphs of SB

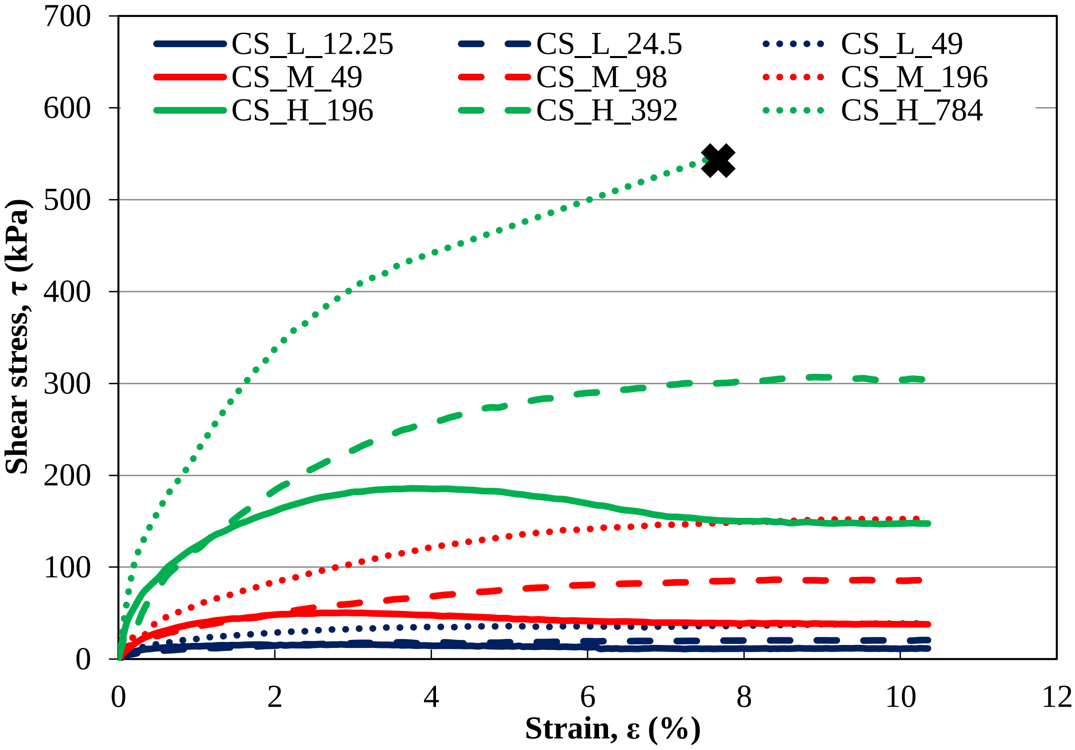

Figure A. 3: Shear stress (τ) – strain (ε) graphs of CS

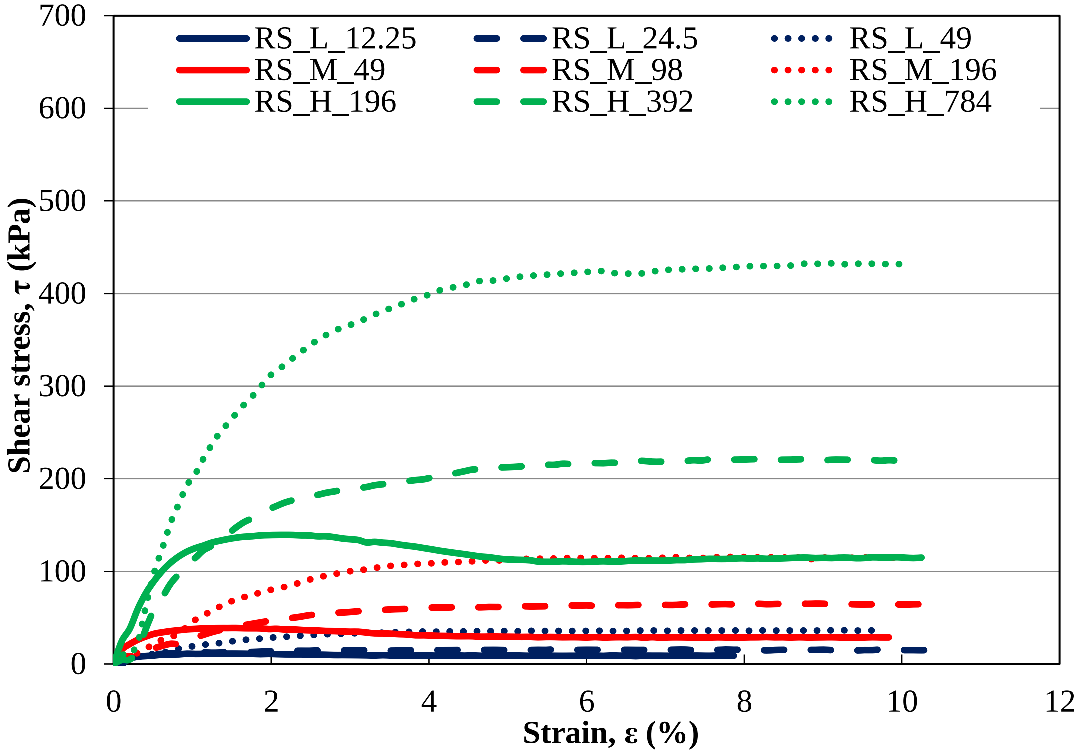

Figure A. 4: Shear stress (τ) – strain (ε) graphs of RS

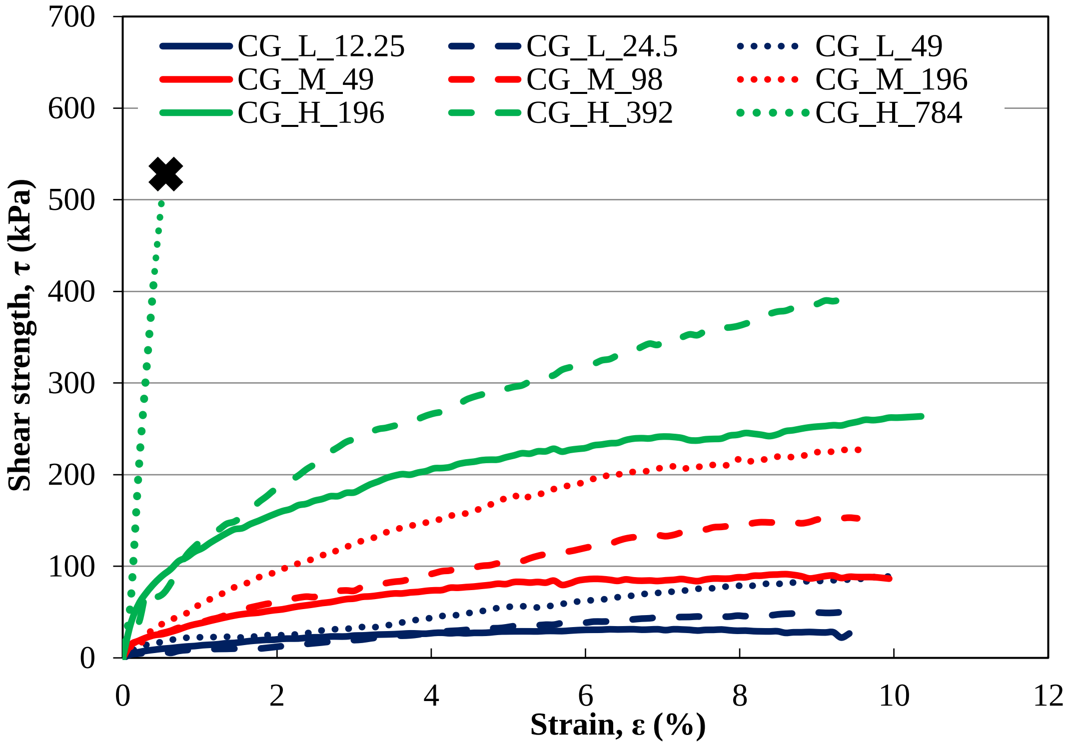

Figure A. 5: Shear stress (τ) – strain (ε) graphs of CG

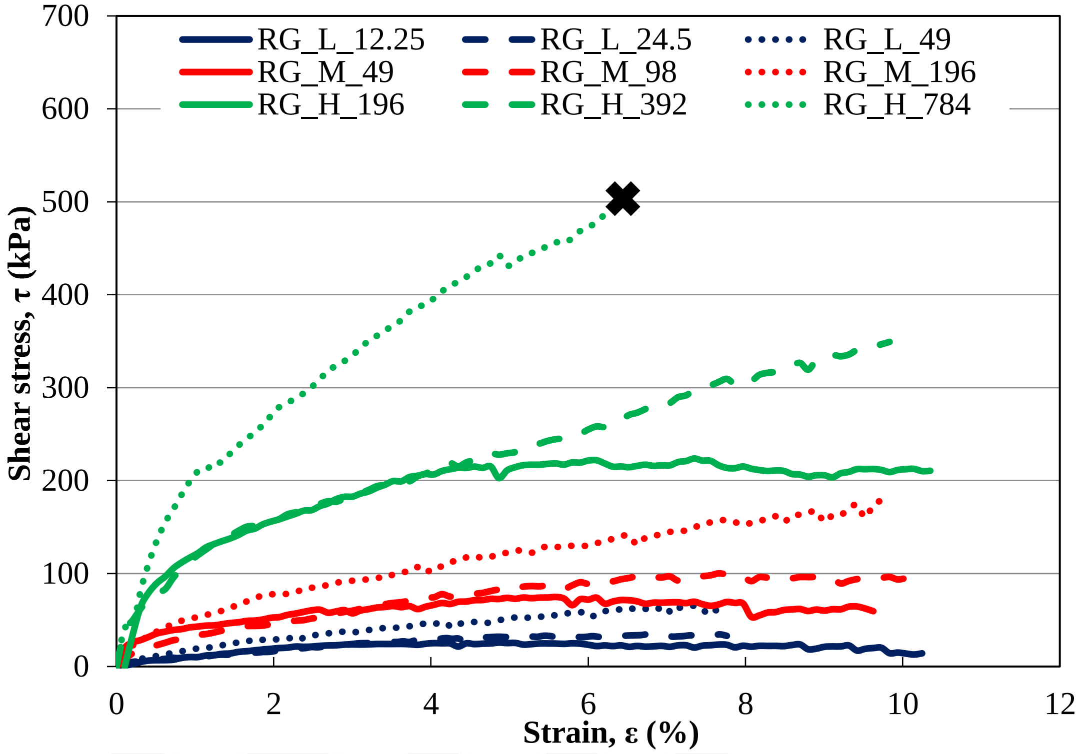

Figure A. 6: Shear stress (τ) – strain (ε) graphs of RG

Interface Direct Shear Test Results for 4 Months SWt Curing

PVC(1.5) – soil interfaces

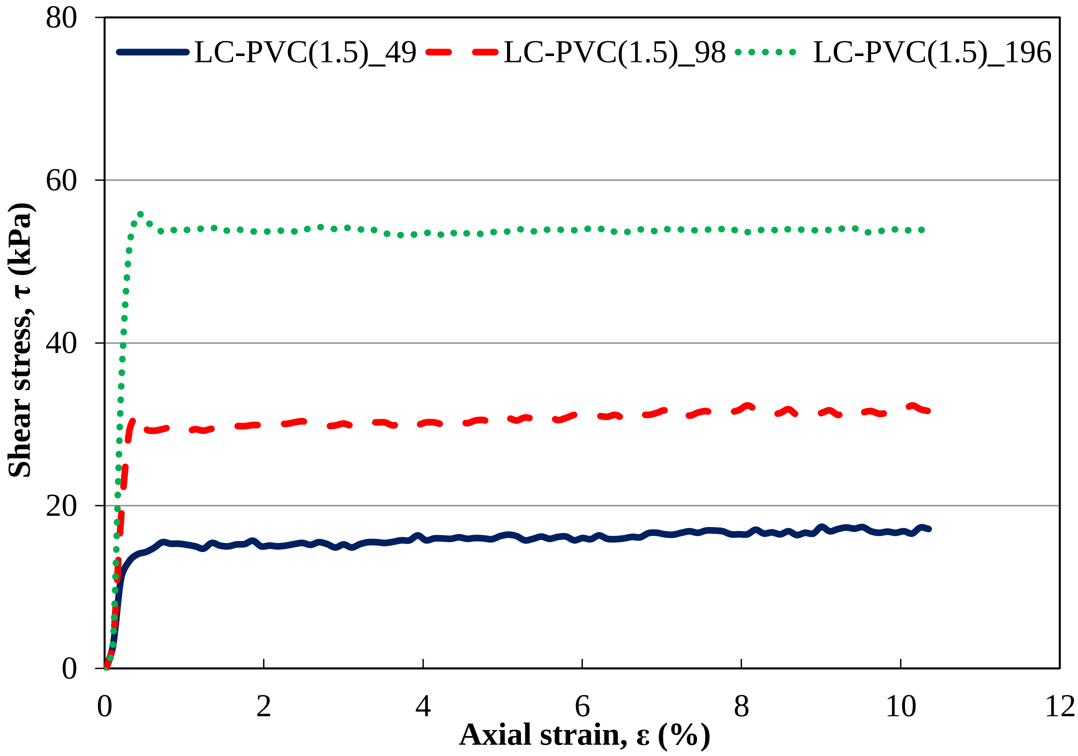

Figure A. 7: Shear stress (τ) – strain (ε) graphs of 4 months SWt cured PVC(1.5) – LC interface

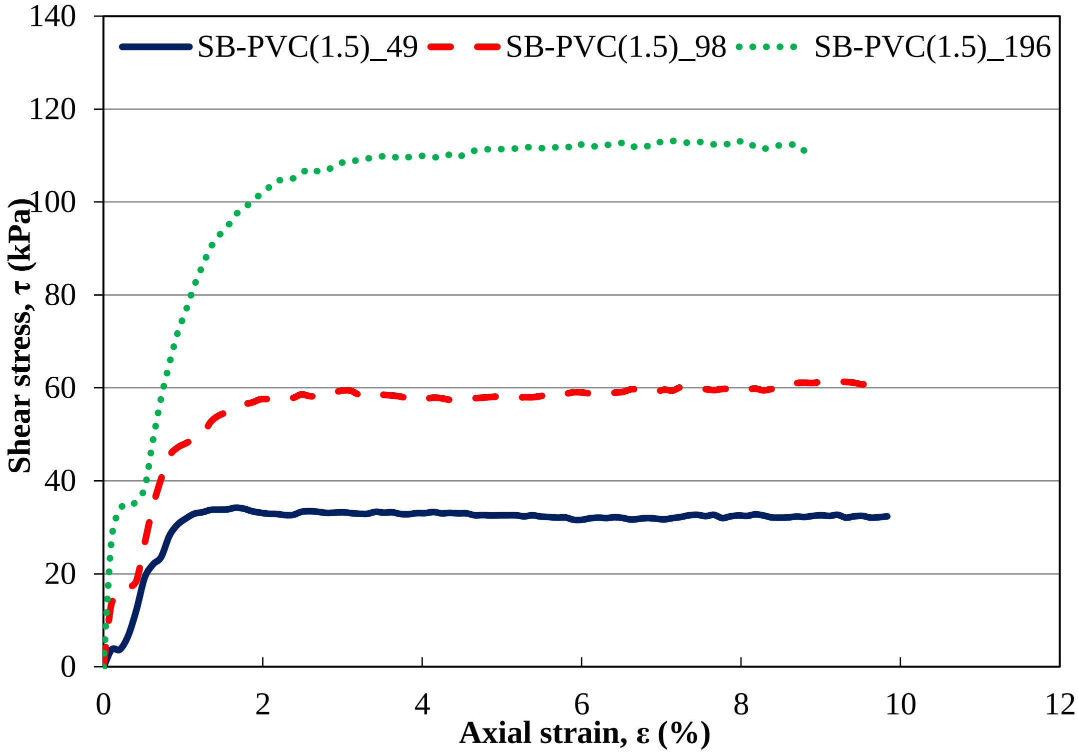

Figure A. 8: Shear stress (τ) – strain (ε) graphs of 4 months SWt cured PVC(1.5) – SB interface

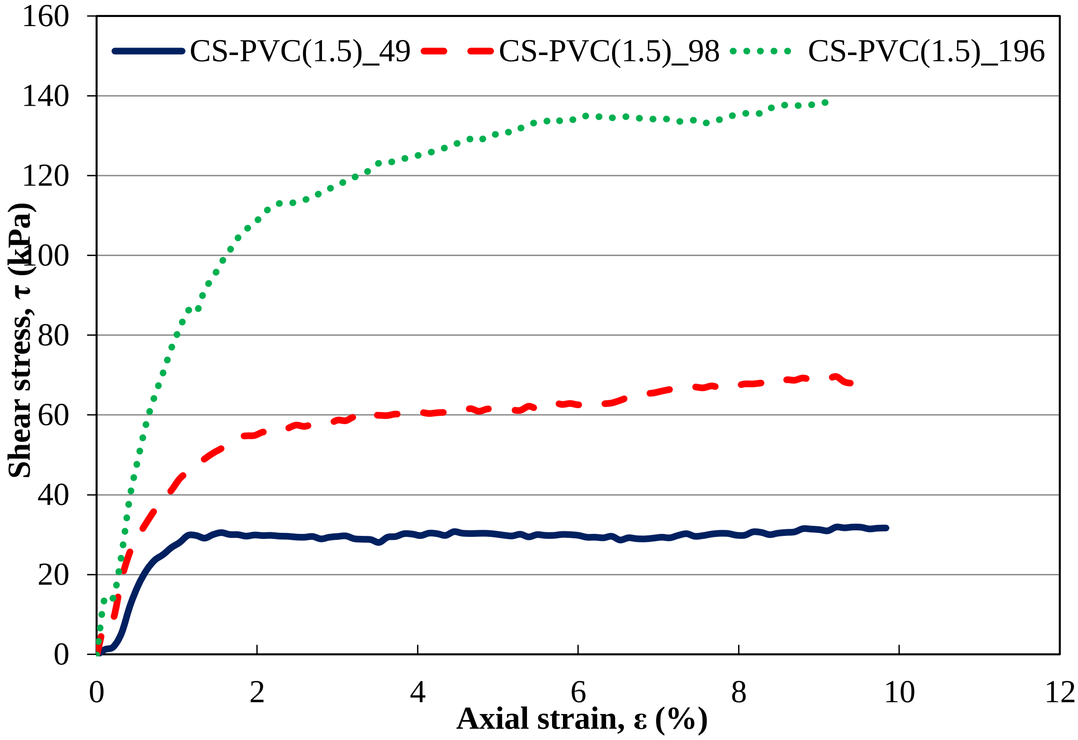

Figure A. 9: Shear stress (τ) – strain (ε) graphs of 4 months SWt cured PVC(1.5) – CS interface

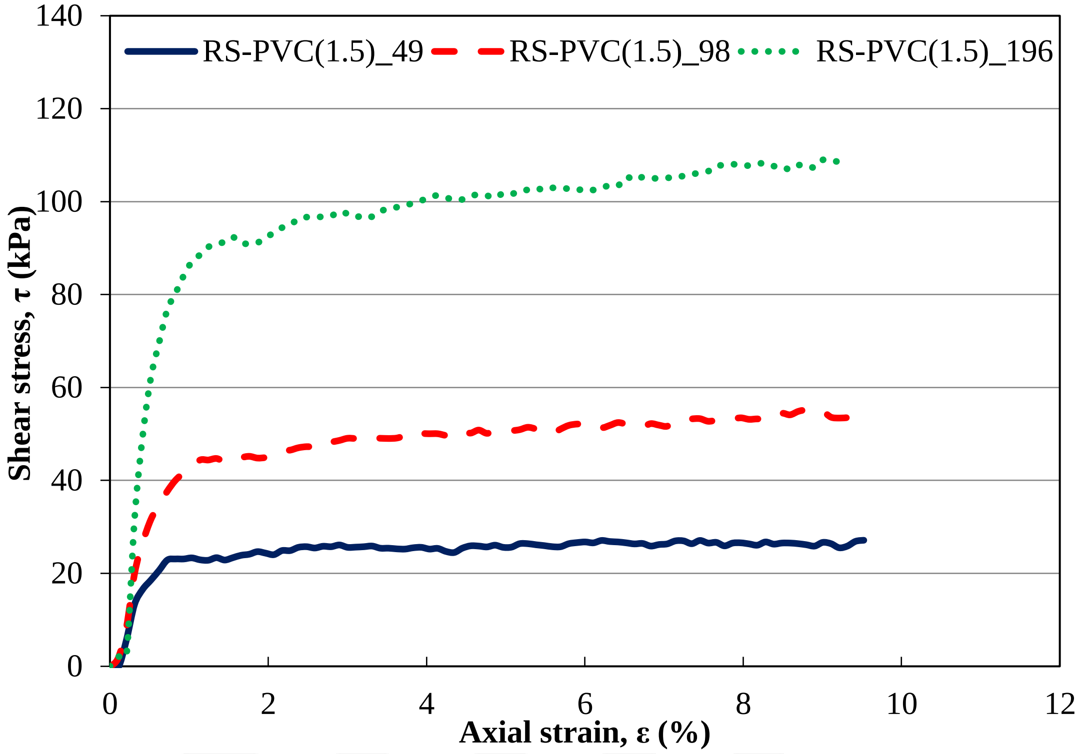

Figure A. 10: Shear stress (τ) – strain (ε) graphs of 4 months SWt cured PVC(1.5) – RS interface

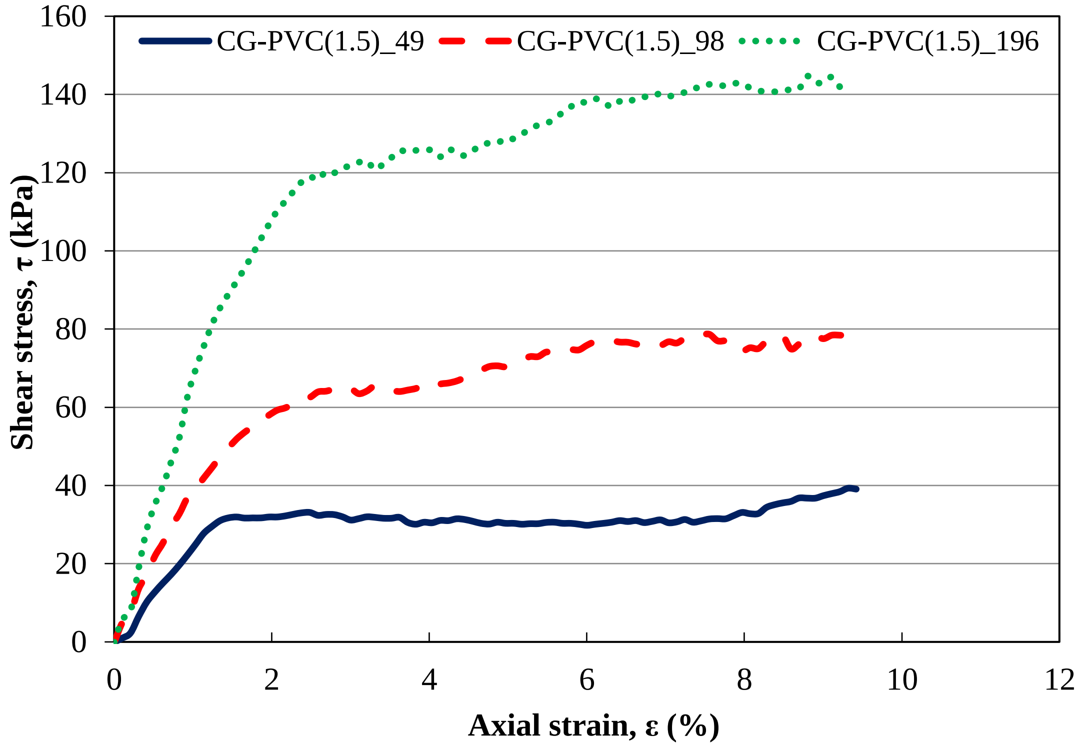

Figure A. 11: Shear stress (τ) – strain (ε) graphs of 4 months SWt cured PVC(1.5) – CG interface

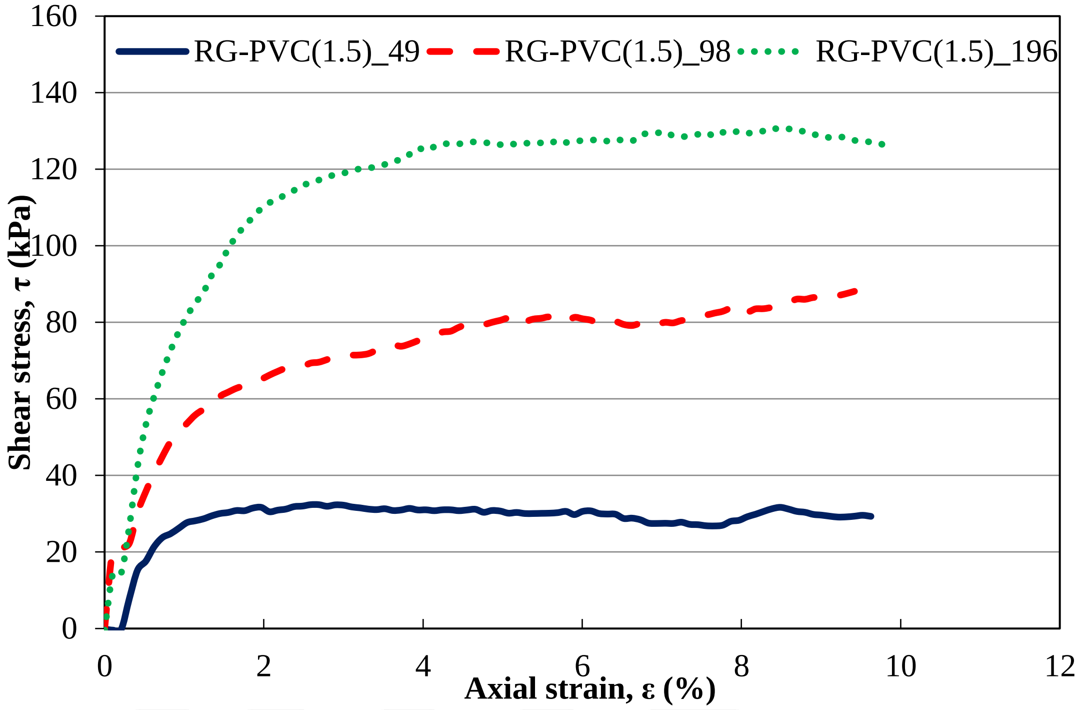

Figure A. 12: Shear stress (τ) – strain (ε) graphs of 4 months SWt cured PVC(1.5) – RG interface

PVC(3.0) – soil interfaces

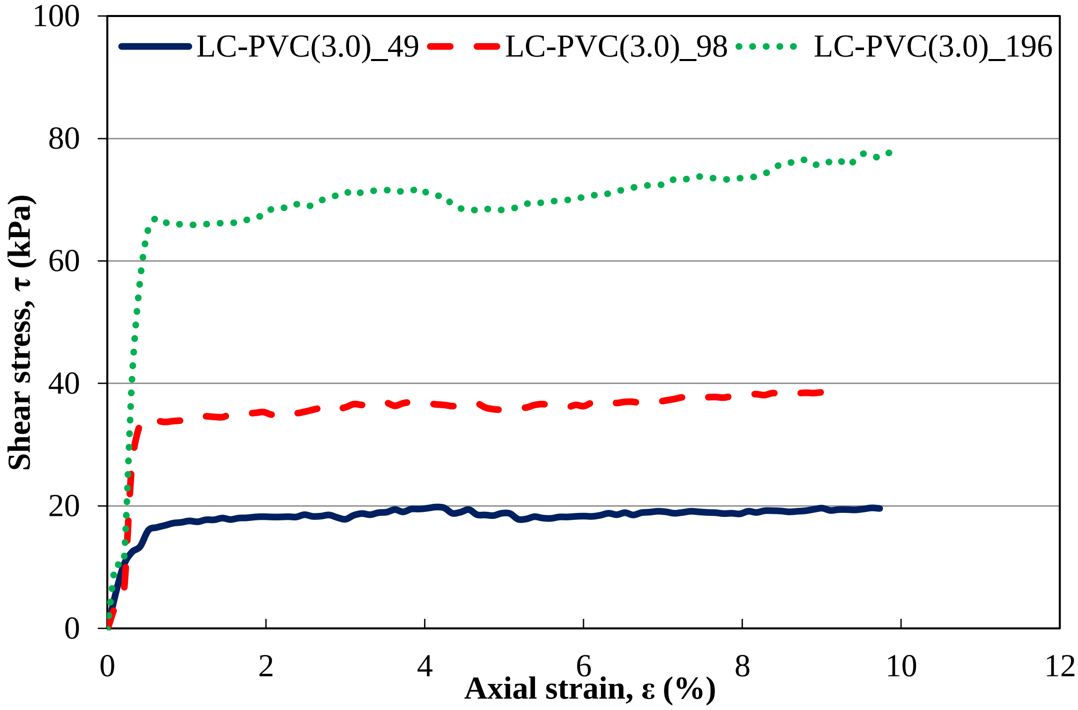

Figure A. 13: Shear stress (τ) – strain (ε) graphs of 4 months SWt cured PVC(3.0) – LC interface

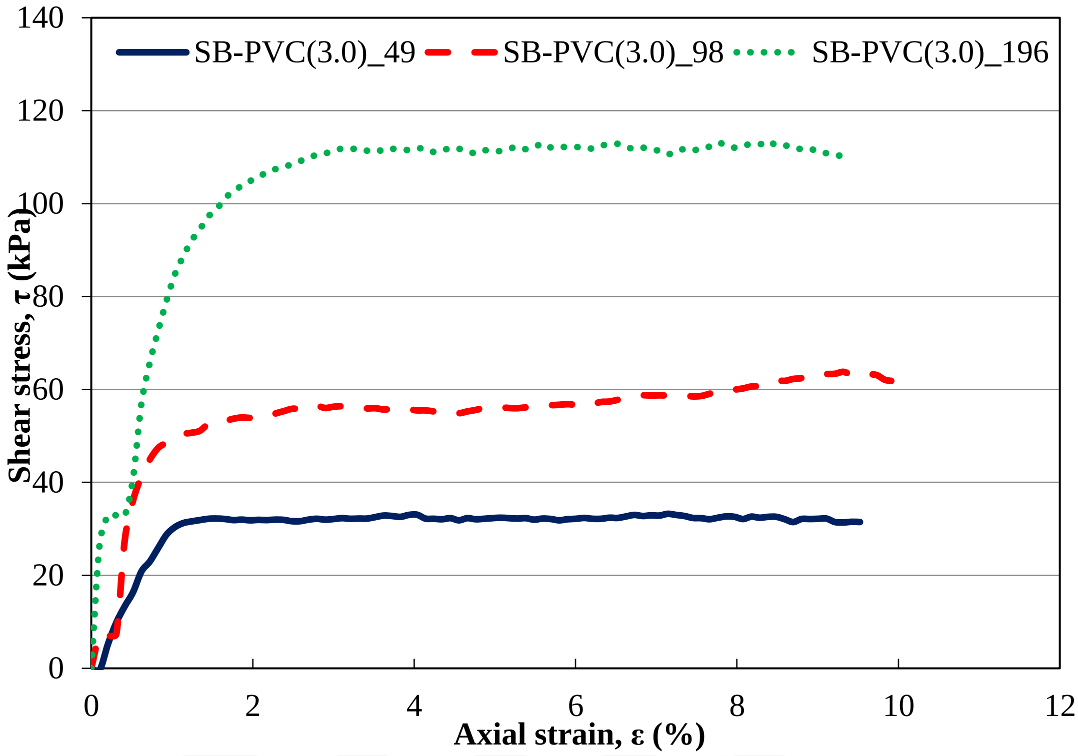

Figure A. 14: Shear stress (τ) – strain (ε) graphs of 4 months SWt cured PVC(3.0) – SB interface

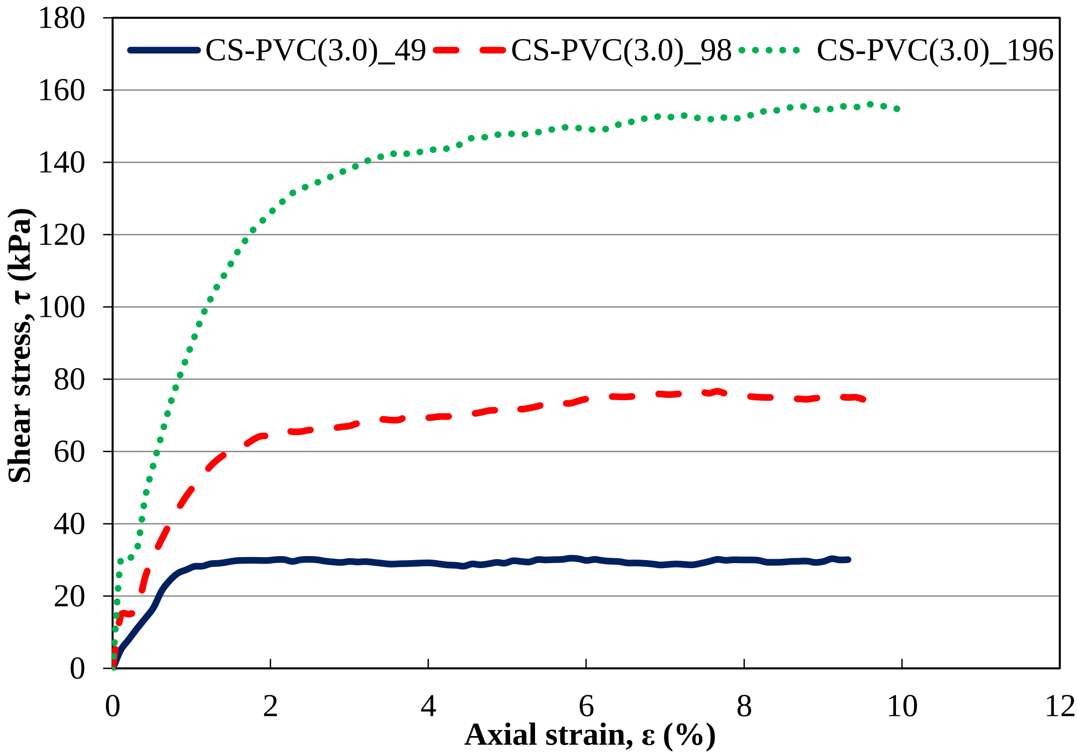

Figure A. 15: Shear stress (τ) – strain (ε) graphs of 4 months SWt cured PVC(3.0) – CS interface

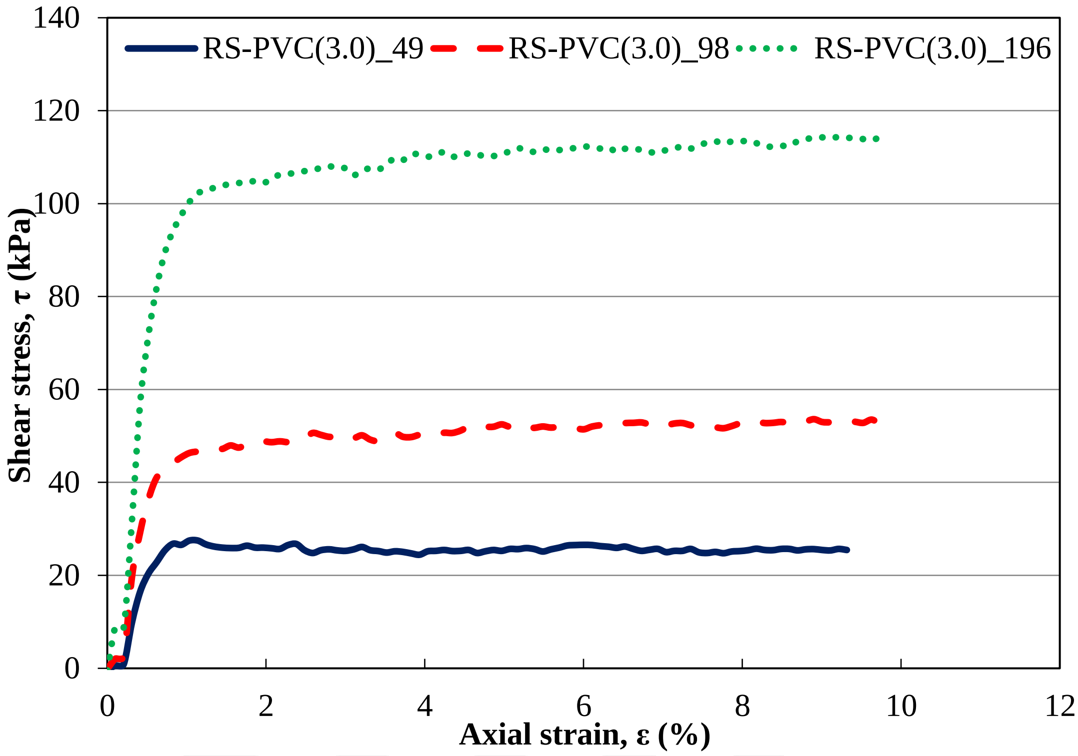

Figure A. 16: Shear stress (τ) – strain (ε) graphs of 4 months SWt cured PVC(3.0) – RS interface

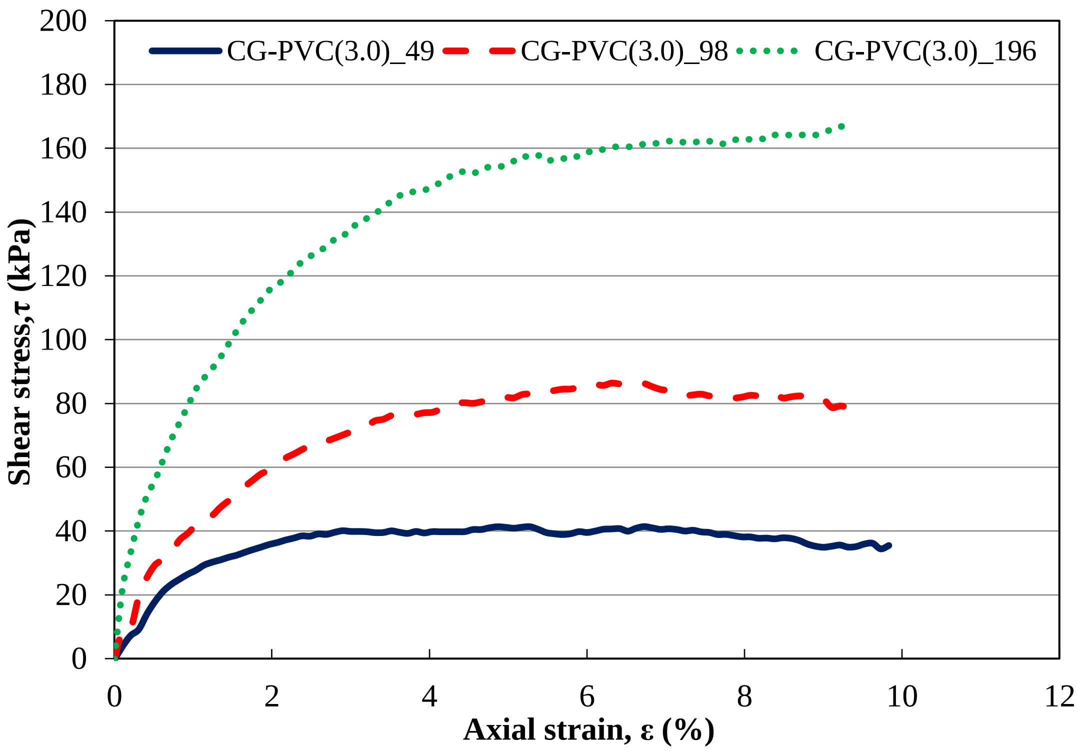

Figure A. 17: Shear stress (τ) – strain (ε) graphs of 4 months SWt cured PVC(3.0) – CG interface

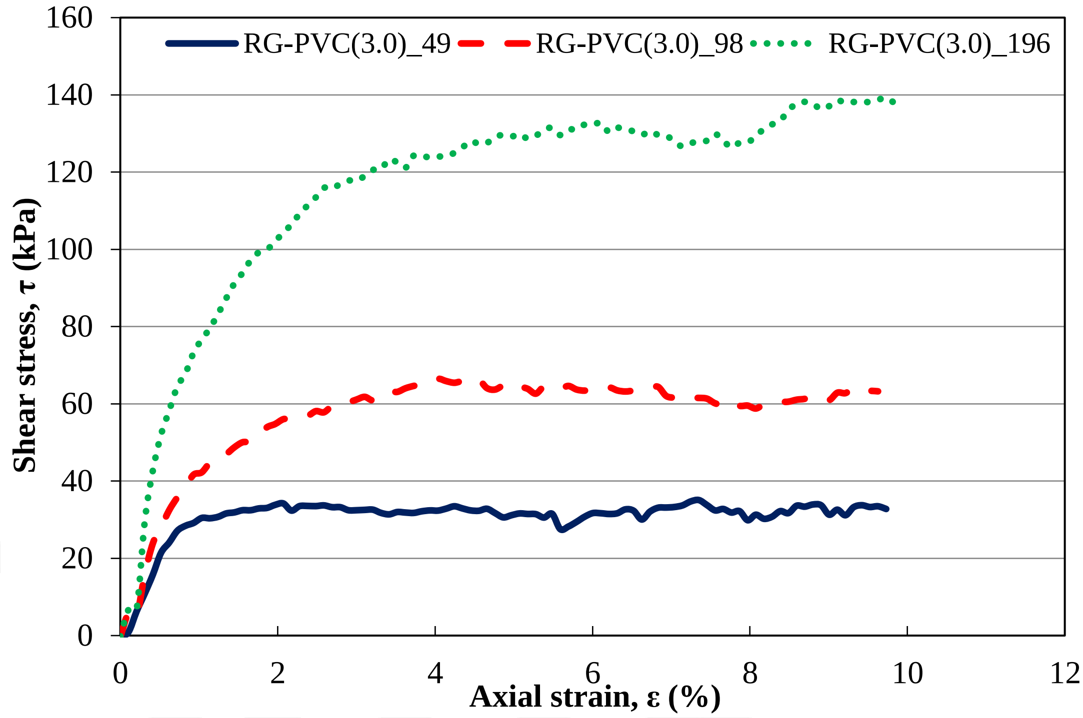

Figure A. 18: Shear stress (τ) – strain (ε) graphs of 4 months SWt cured PVC(3.0) – RG interface

TPO – soil interfaces

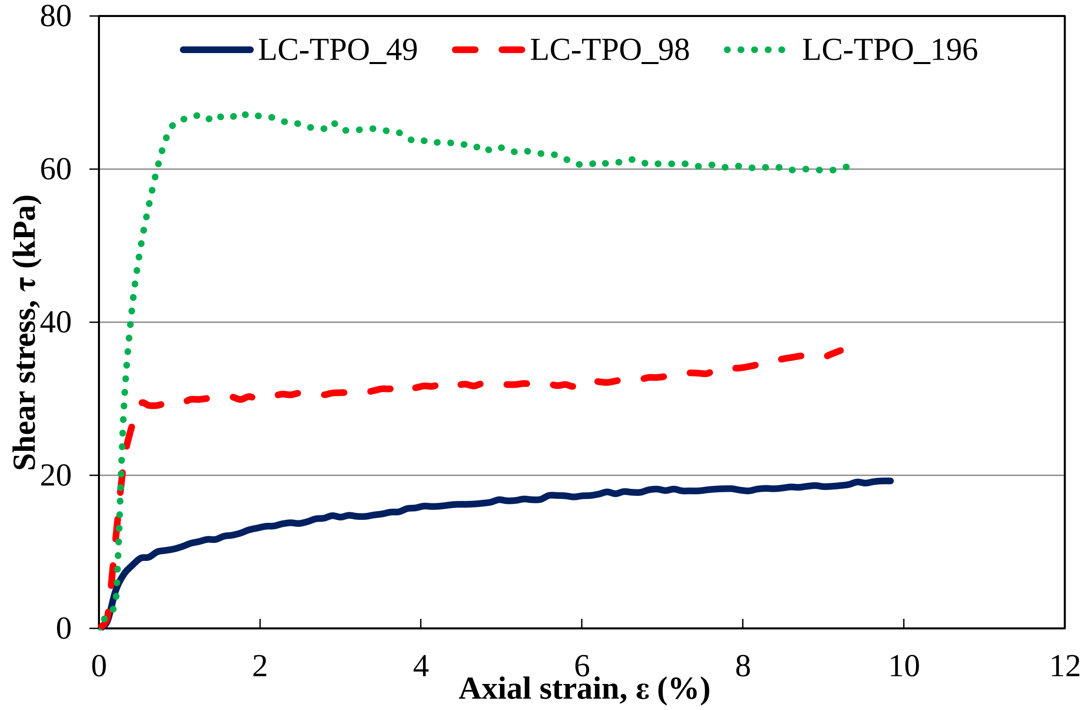

Figure A. 19: Shear stress (τ) – strain (ε) graphs of 4 months SWt cured TPO – LC interface

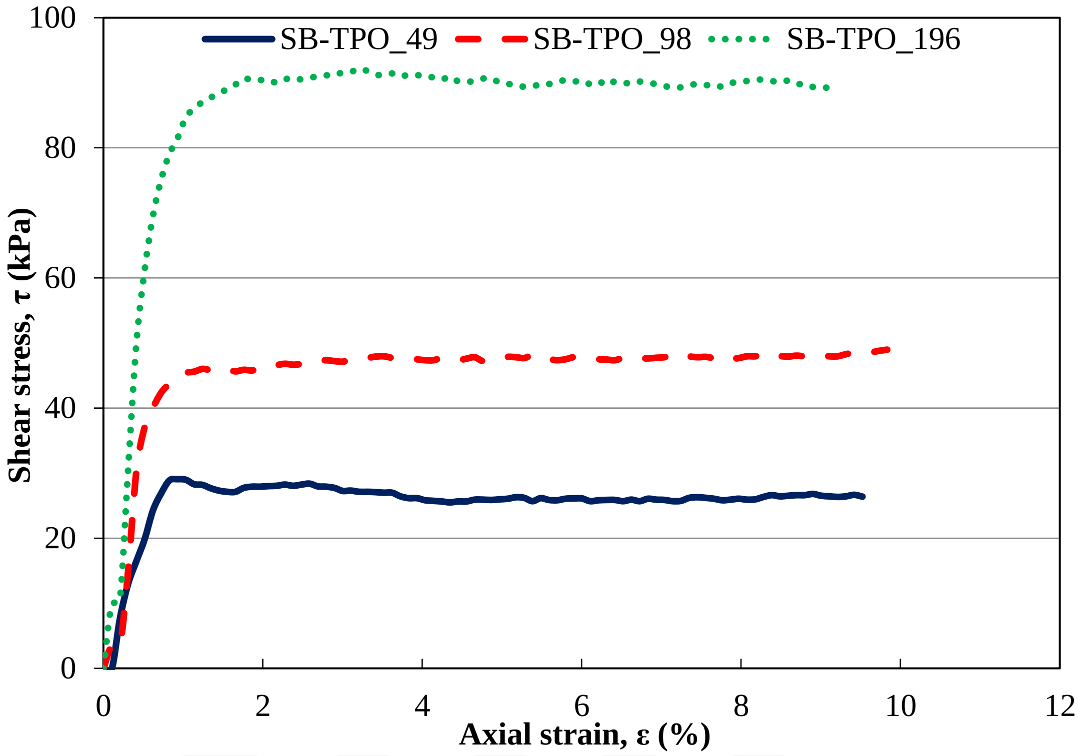

Figure A. 20: Shear stress (τ) – strain (ε) graphs of 4 months SWt cured TPO – SB interface

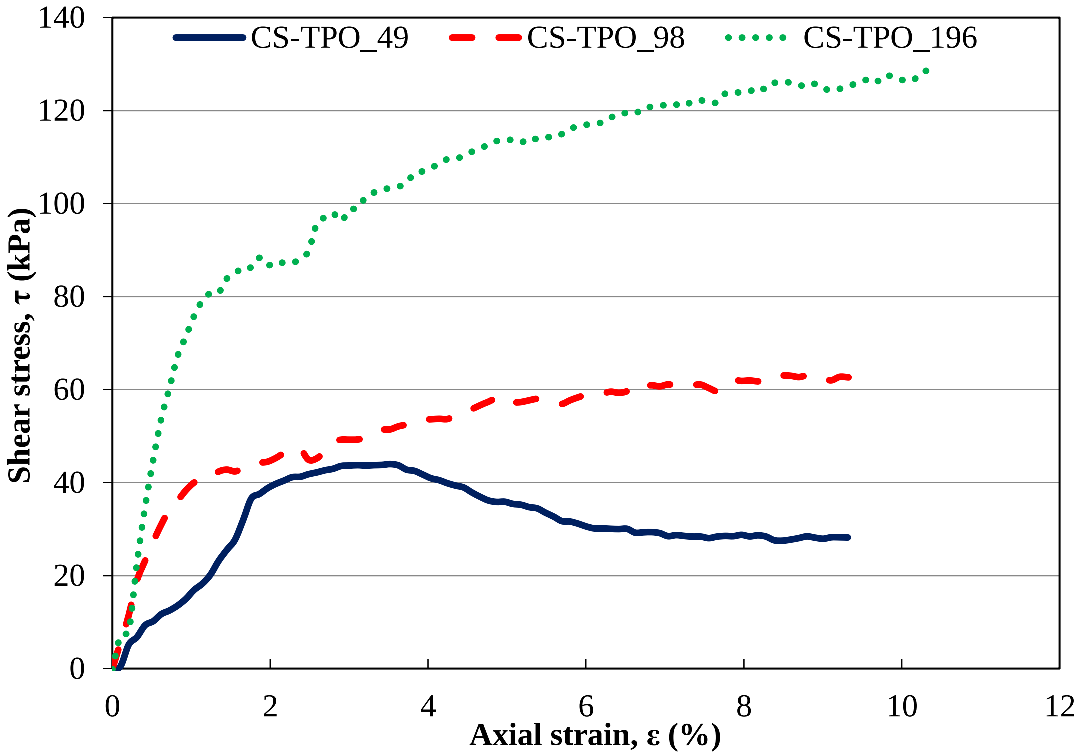

Figure A. 21: Shear stress (τ) – strain (ε) graphs of 4 months SWt cured TPO – CS interface

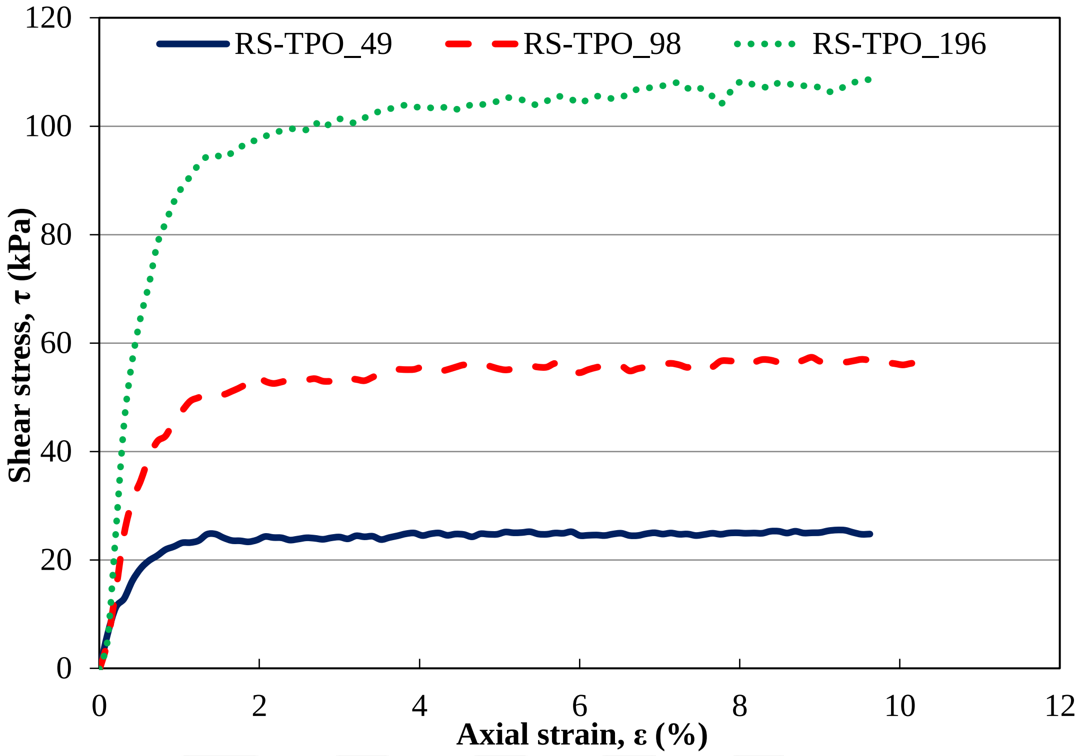

Figure A. 22: Shear stress (τ) – strain (ε) graphs of 4 months SWt cured TPO – RS interface

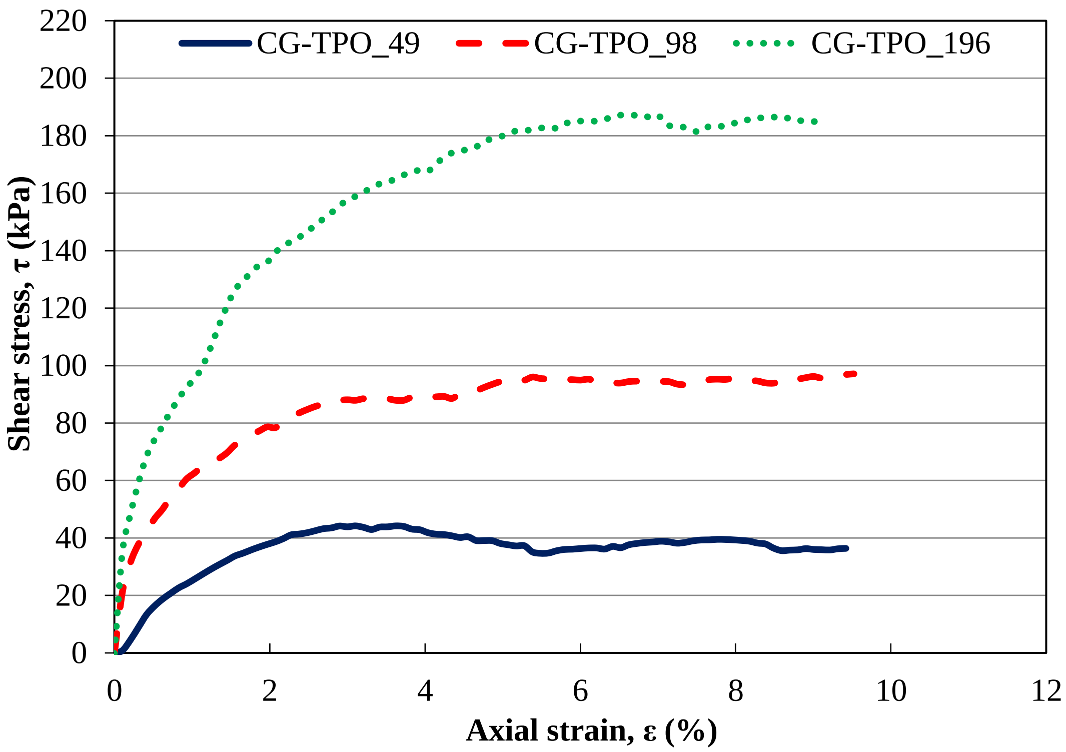

Figure A. 23: Shear stress (τ) – strain (ε) graphs of 4 months SWt cured TPO –CG interface

Interface Direct Shear Test Results for 4 Months AMD Curing

HDPE(S) – soil interfaces

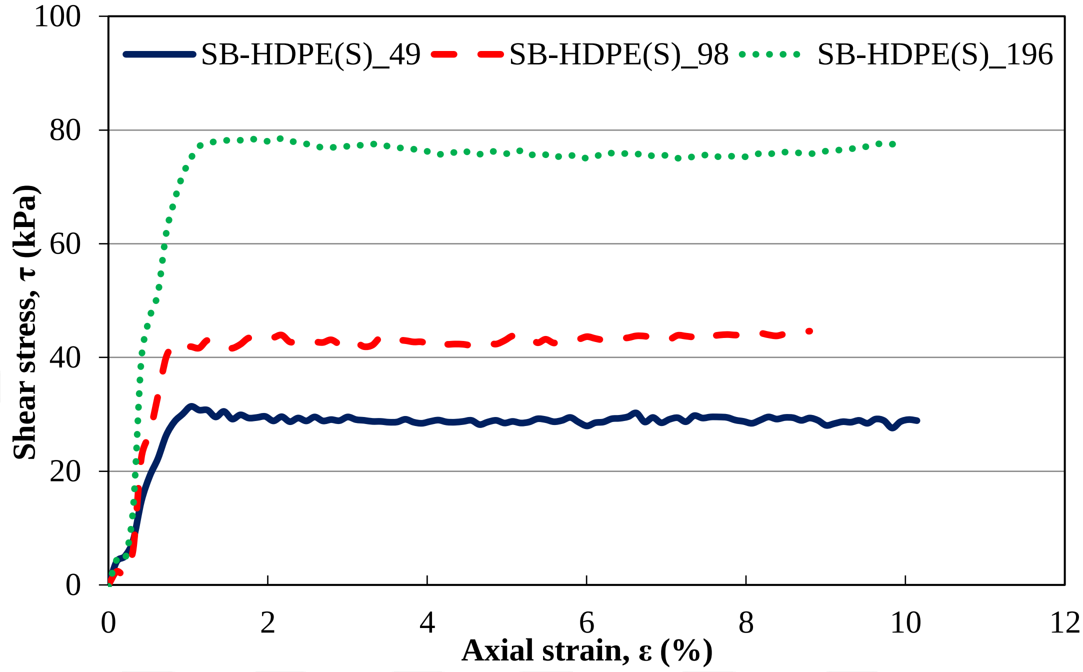

Figure A. 24: Shear stress (τ) – strain (ε) graphs of 4 months AMD cured HDPE(S) – SB interface

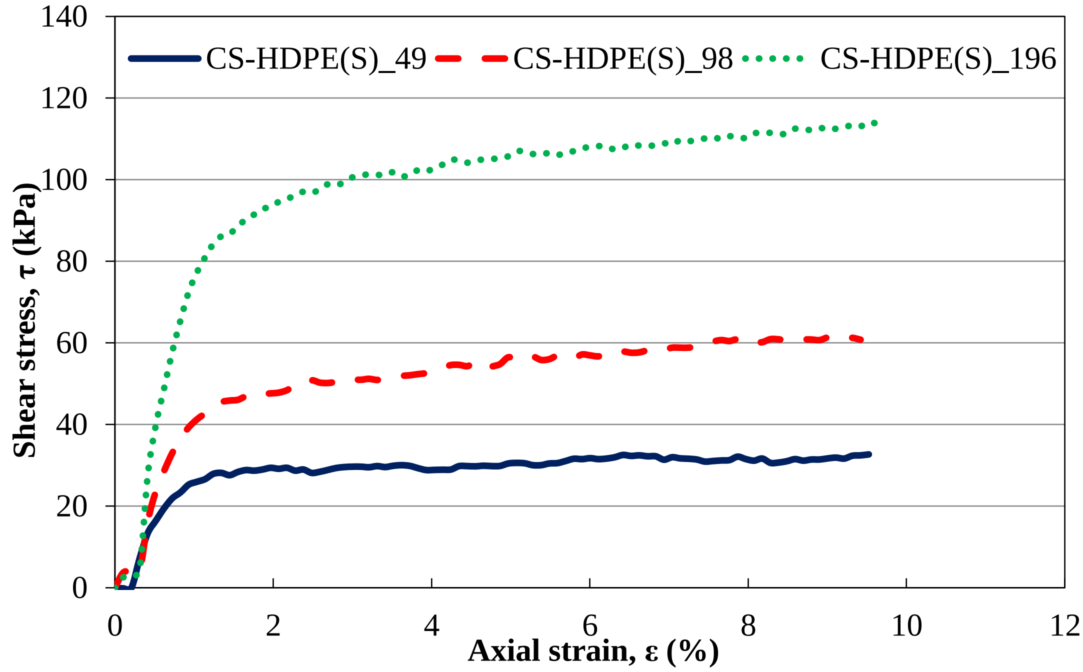

Figure A. 25: Shear stress (τ) – strain (ε) graphs of 4 months AMD cured HDPE(S) – CS interface

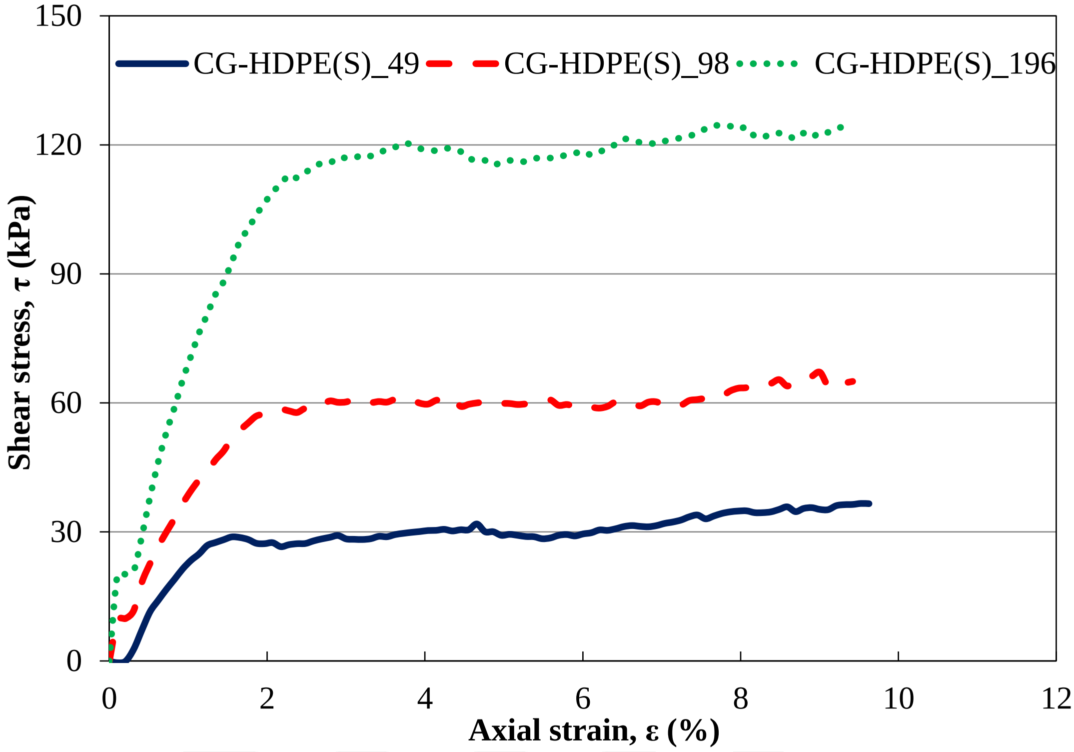

Figure A. 26: Shear stress (τ) – strain (ε) graphs of 4 months AMD cured HDPE(S) – CG interface

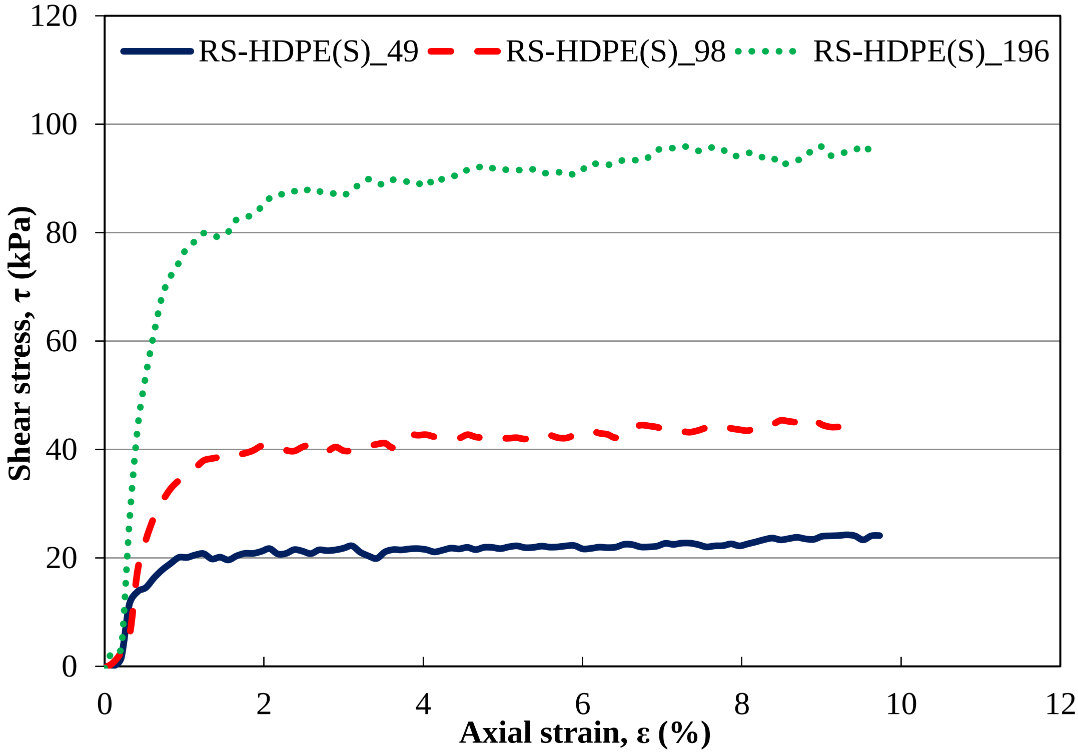

Figure A. 27: Shear stress (τ) – strain (ε) graphs of 4 months AMD cured HDPE(S) – RS interface

HDPE(T) – soil interfaces

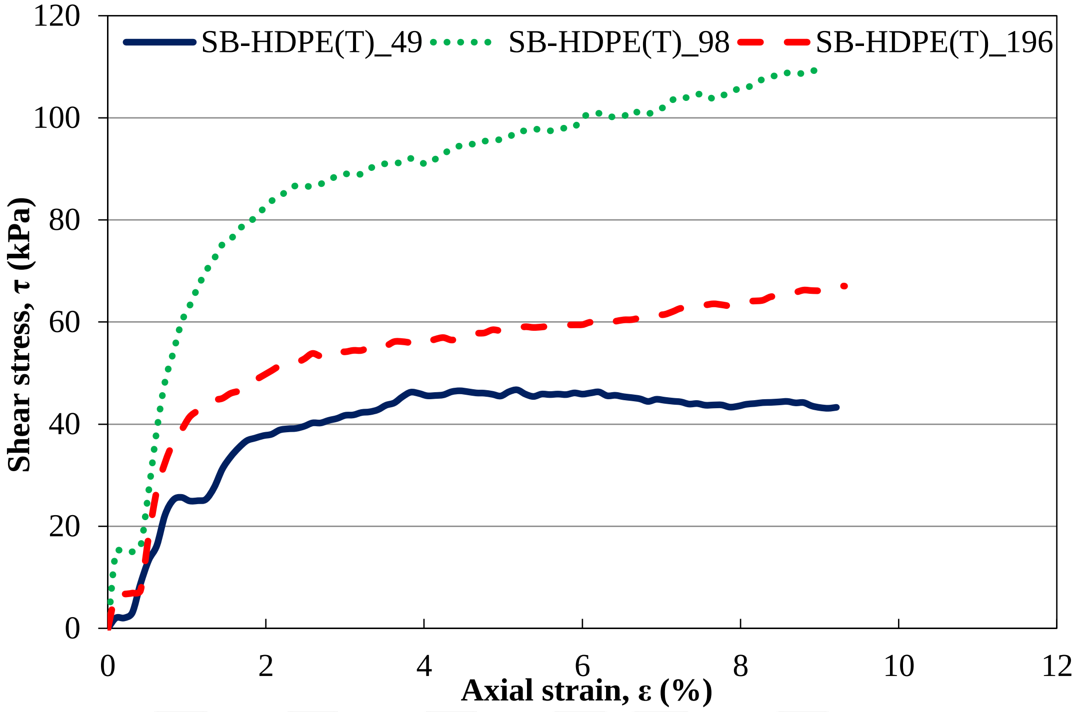

Figure A. 28: Shear stress (τ) – strain (ε) graphs of 4 months AMD cured HDPE(T) – SB interface

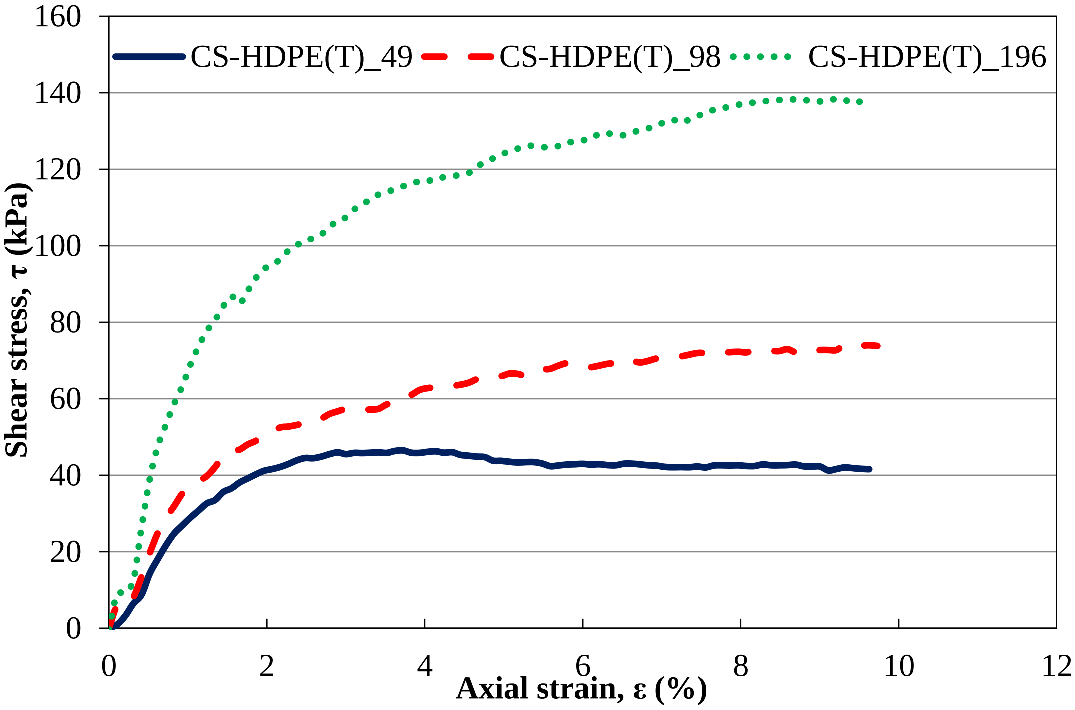

Figure A. 29: Shear stress (τ) – strain (ε) graphs of 4 months AMD cured HDPE(T) – CS interface

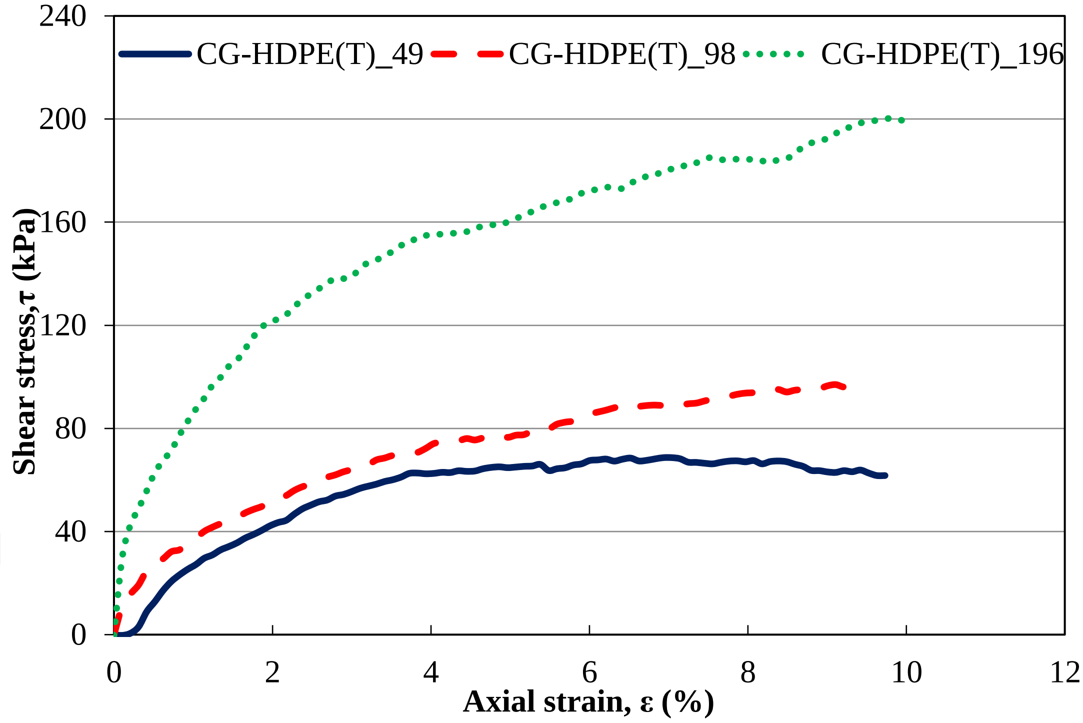

Figure A. 30: Shear stress (τ) – strain (ε) graphs of 4 months AMD cured HDPE(T) – CG interface

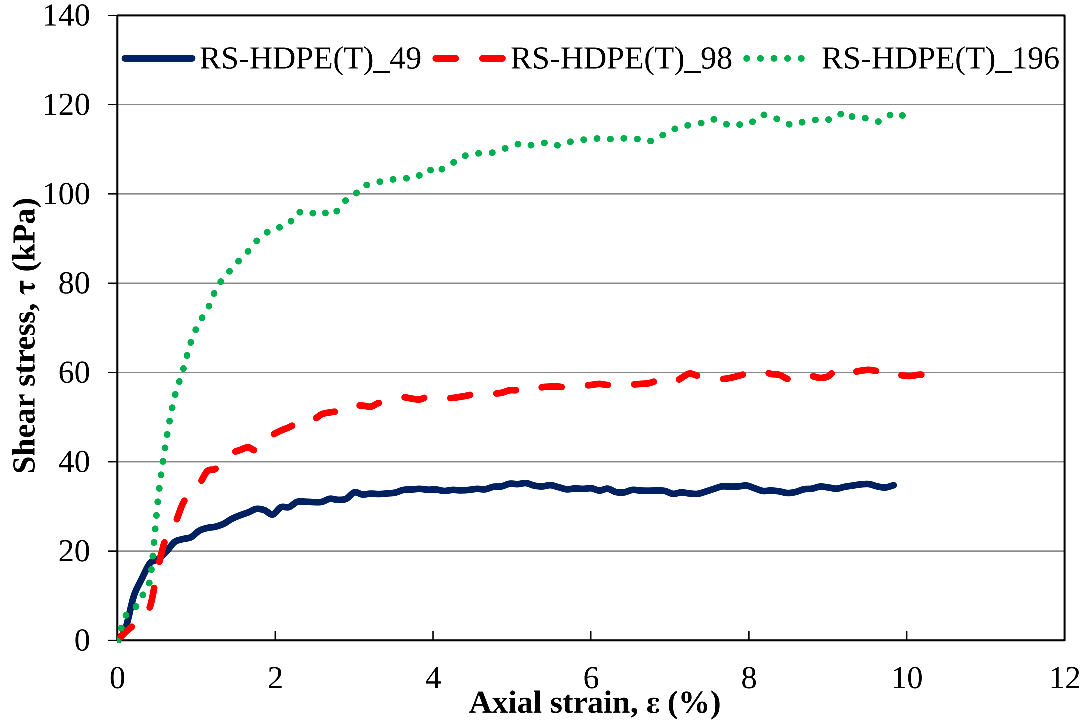

Figure A. 31: Shear stress (τ) – strain (ε) graphs of 4 months AMD cured HDPE(T) – RS interface

TPO – soil interfaces

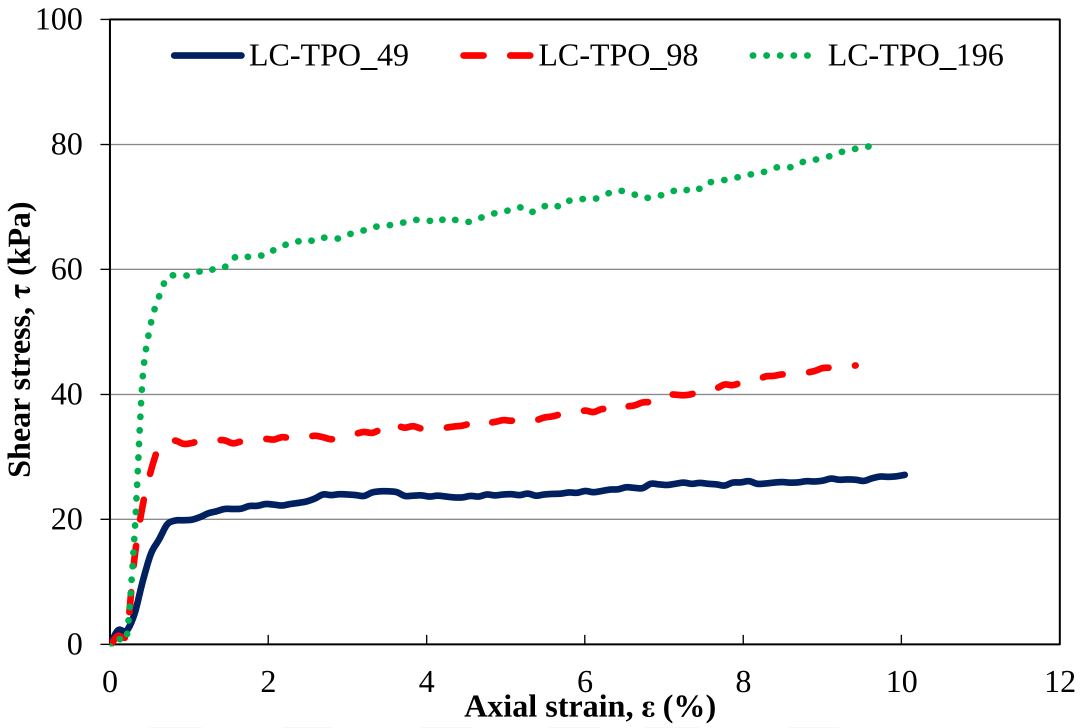

Figure A. 32: Shear stress (τ) – strain (ε) graphs of 4 months AMD cured TPO – LC interface

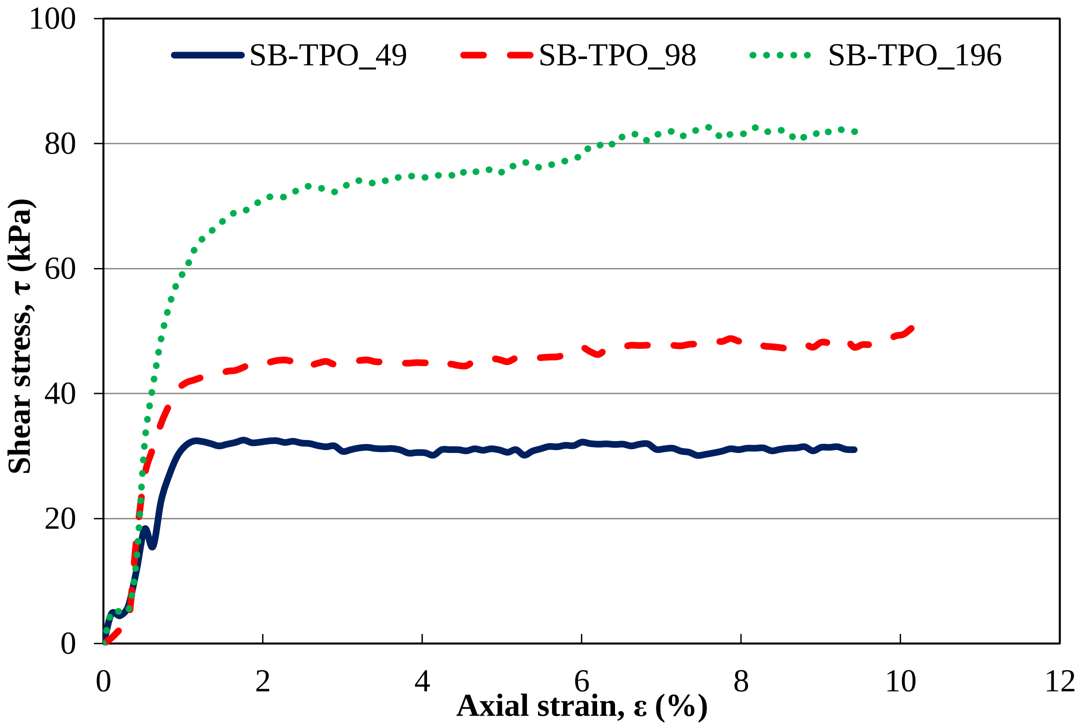

Figure A. 33: Shear stress (τ) – strain (ε) graphs of 4 months AMD cured TPO – SB interface

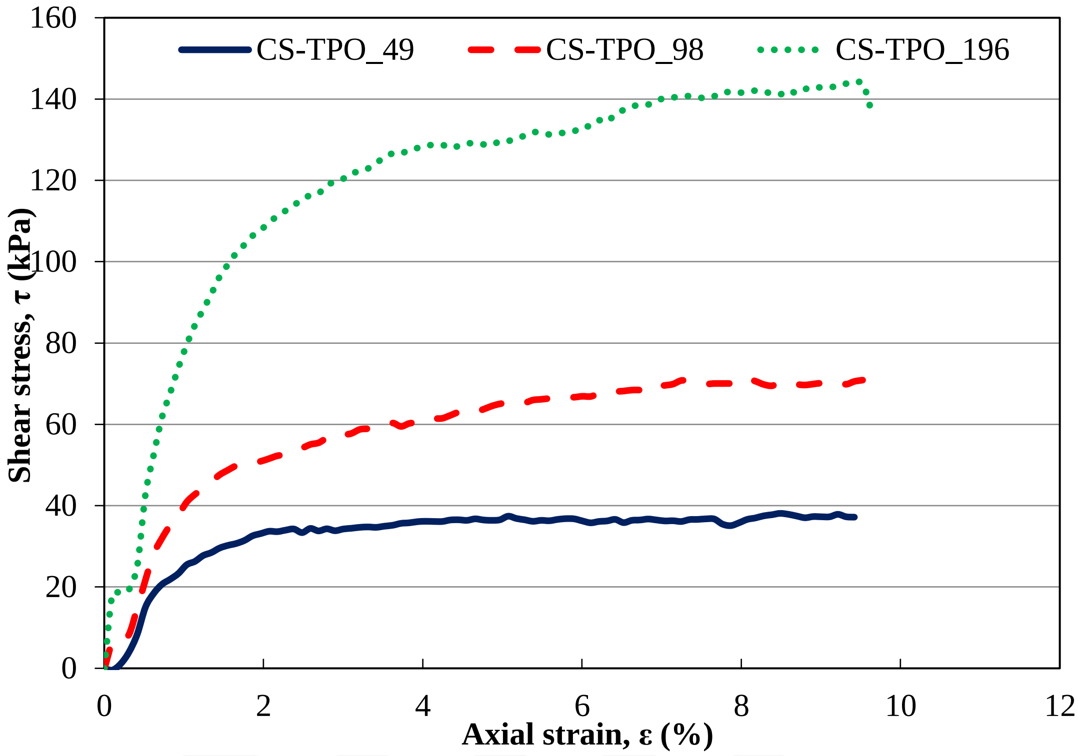

Figure A. 34: Shear stress (τ) – strain (ε) graphs of 4 months AMD cured TPO – CS interface

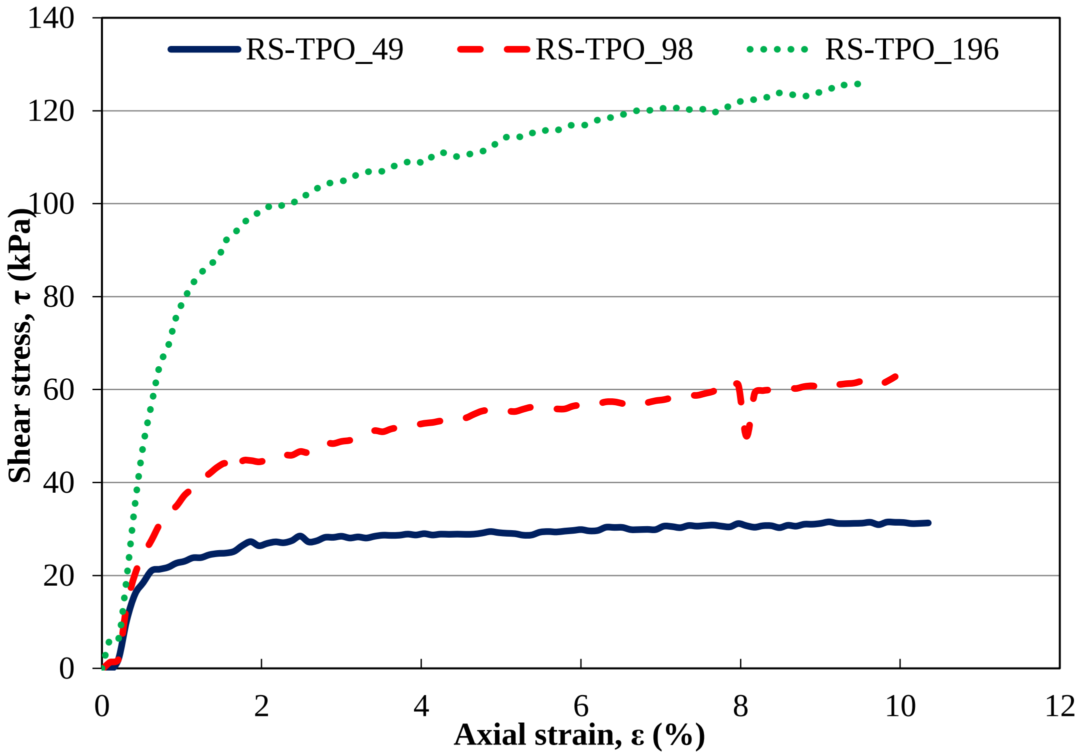

Figure A. 35: Shear stress (τ) – strain (ε) graphs of 4 months AMD cured TPO – RS interface

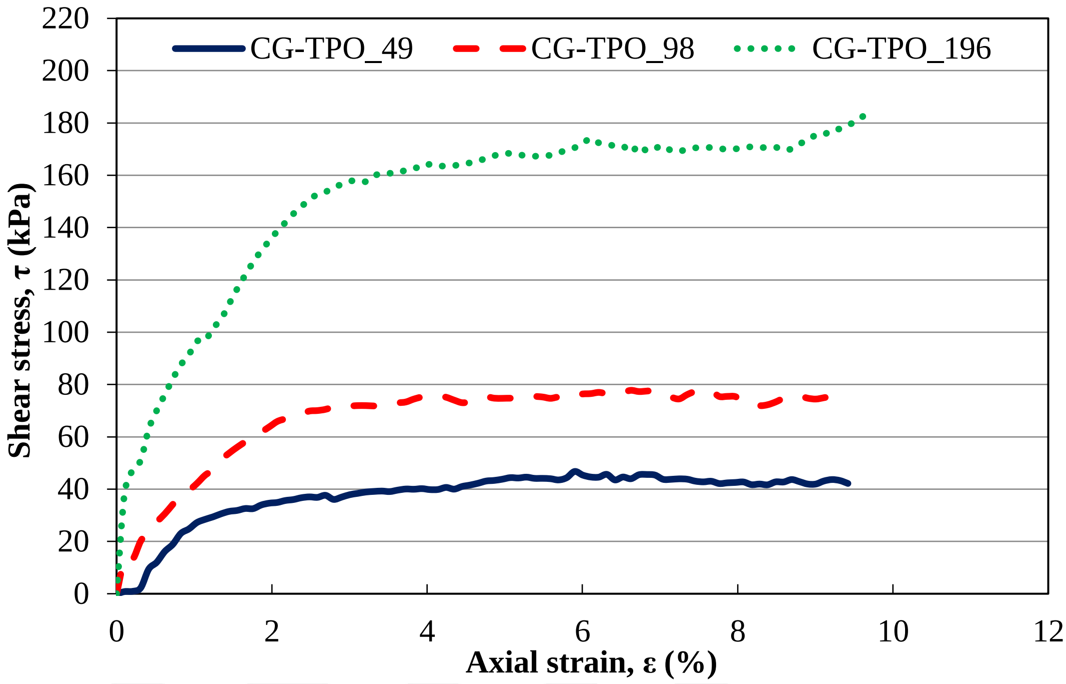

Figure A. 36: Shear stress (τ) – strain (ε) graphs of 4 months AMD cured TPO – CG interface

Interface Direct Shear Test Results for 4 Months CCP Curing

HDPE(S) – soil interfaces

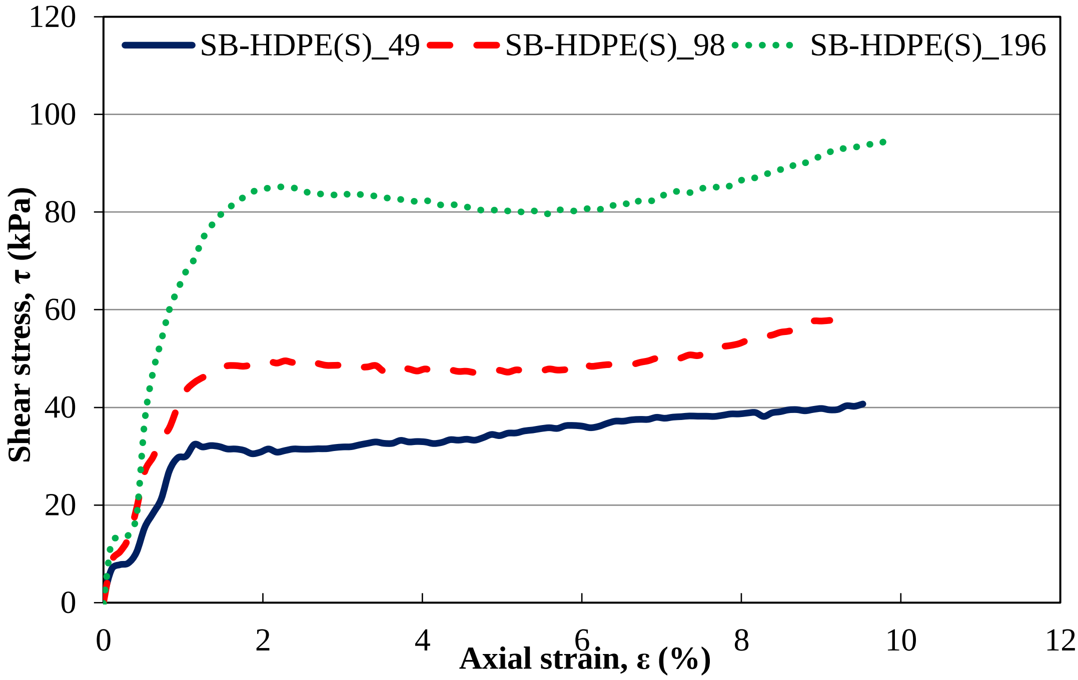

Figure A. 37: Shear stress (τ) – strain (ε) graphs of 4 months CCP cured HDPE(S) – SB interface

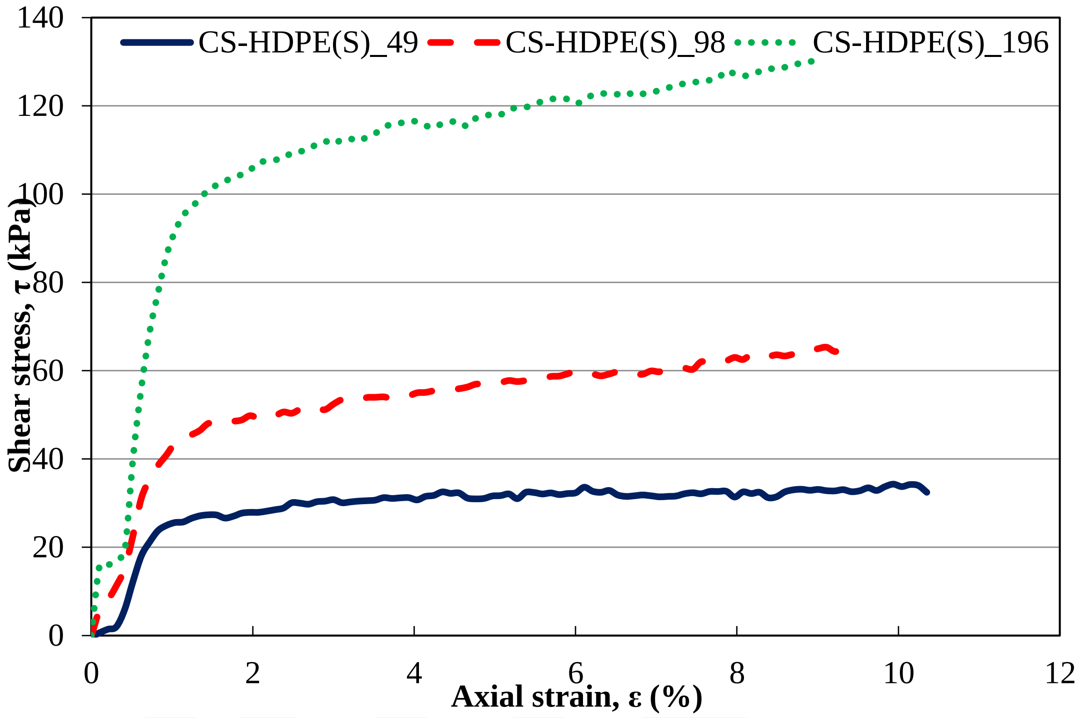

Figure A. 38: Shear stress (τ) – strain (ε) graphs of 4 months CCP cured HDPE(S) – CS interface

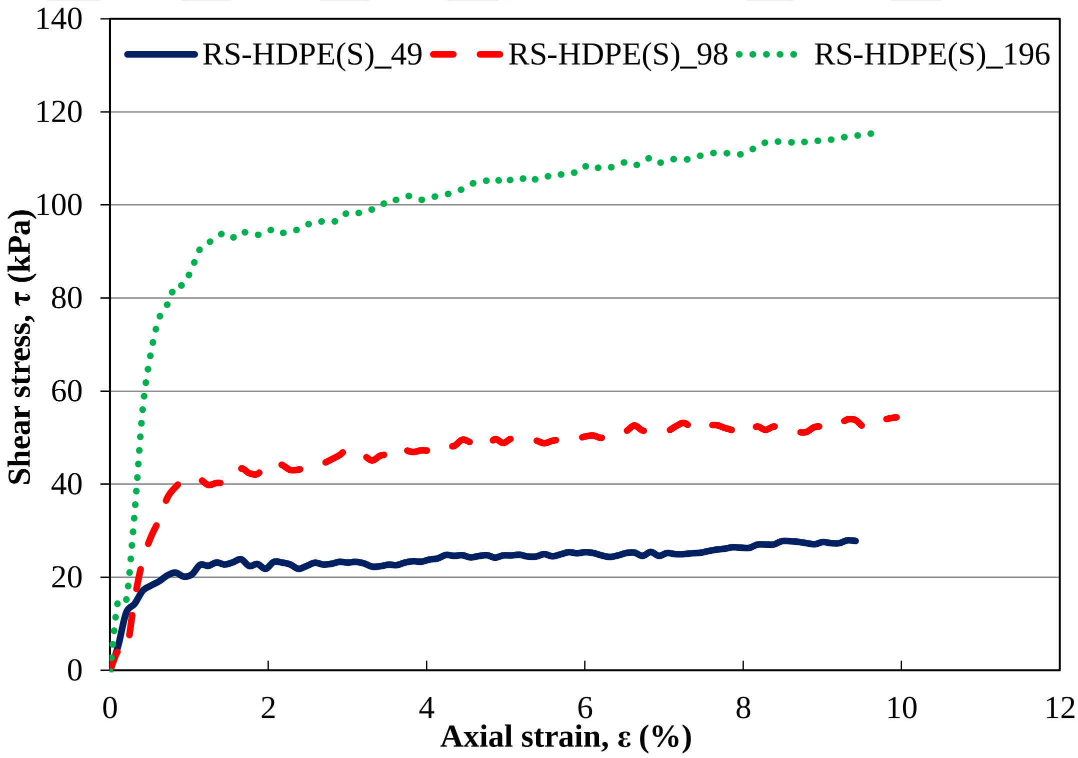

Figure A. 39: Shear stress (τ) – strain (ε) graphs of 4 months CCP cured HDPE(S) – RS interface

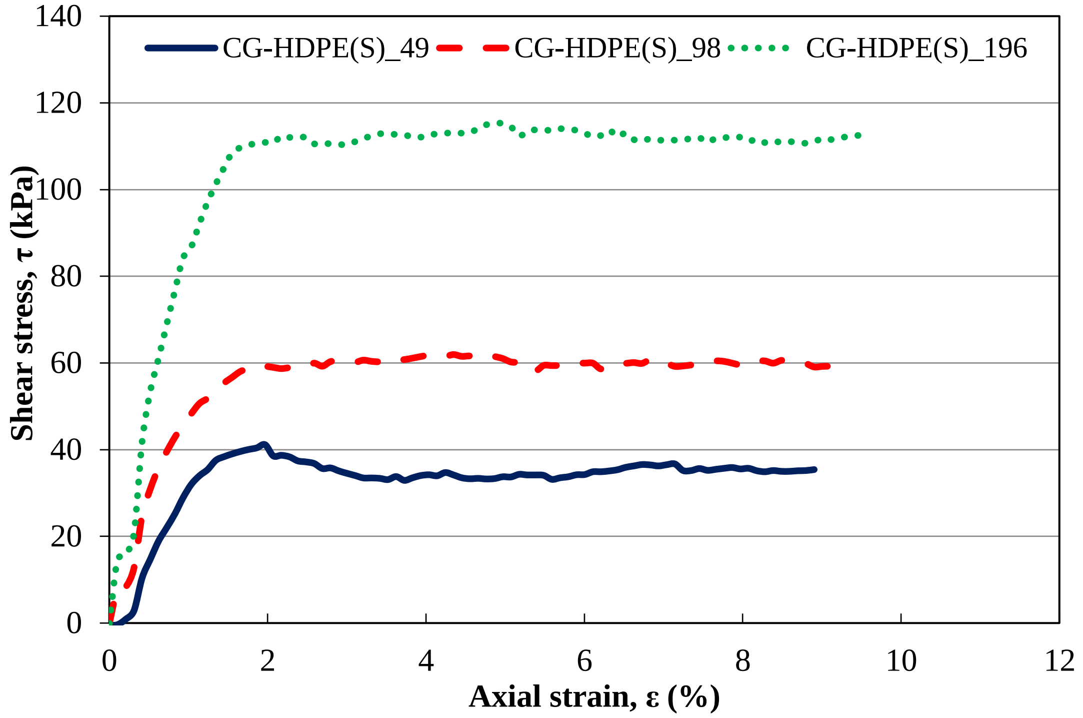

Figure A. 40: Shear stress (τ) – strain (ε) graphs of 4 months CCP cured HDPE(S) – CG interface

HDPE(T) – soil interfaces

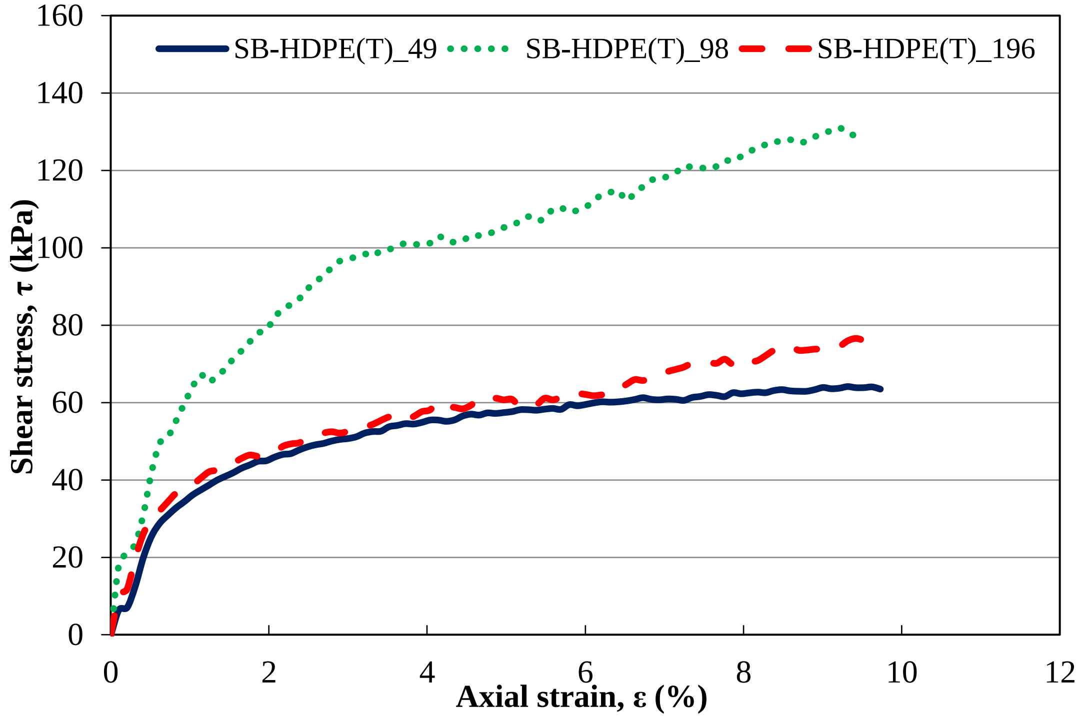

Figure A. 41: Shear stress (τ) – strain (ε) graphs of 4 months CCP cured HDPE(T) – SB interface

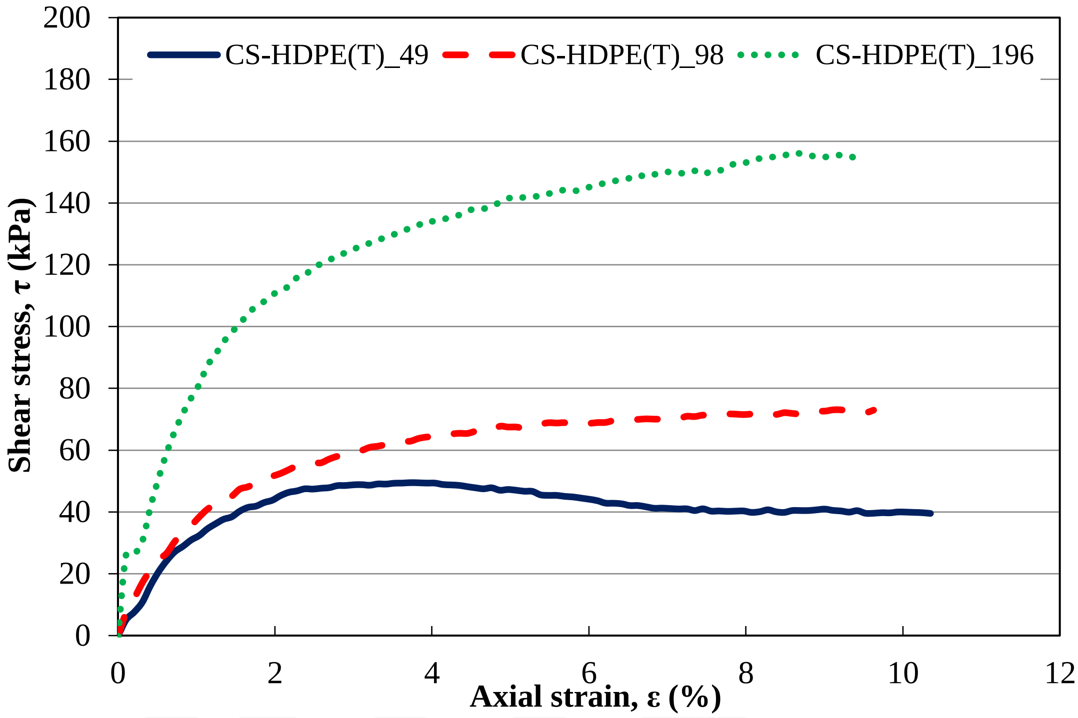

Figure A. 42: Shear stress (τ) – strain (ε) graphs of 4 months CCP cured HDPE(T) – CS interface

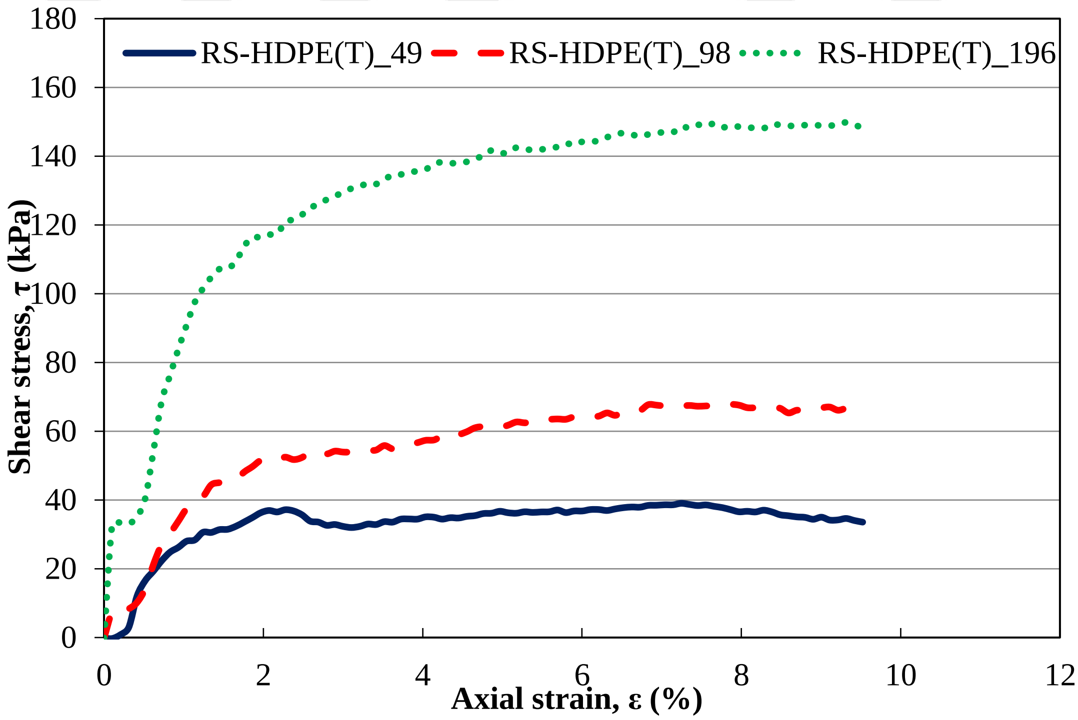

Figure A. 43: Shear stress (τ) – strain (ε) graphs of 4 months CCP cured HDPE(T) – RS interface

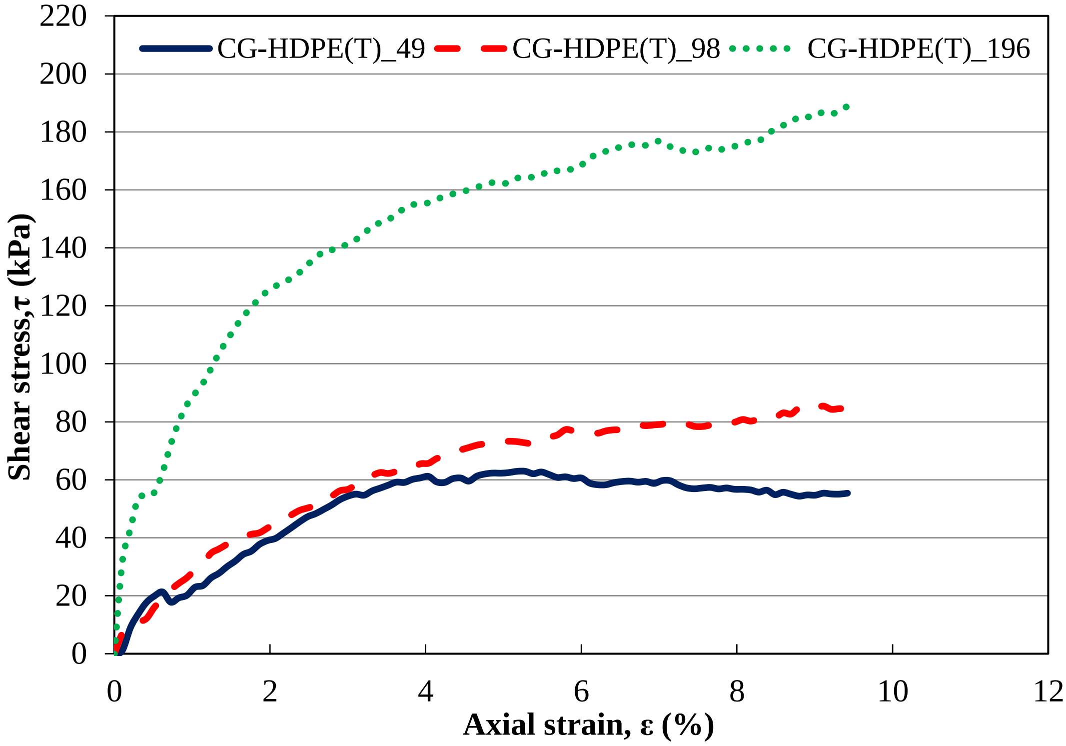

Figure A. 44: Shear stress (τ) – strain (ε) graphs of 4 months CCP cured HDPE(T) – CG interface

TPO – soil interfaces

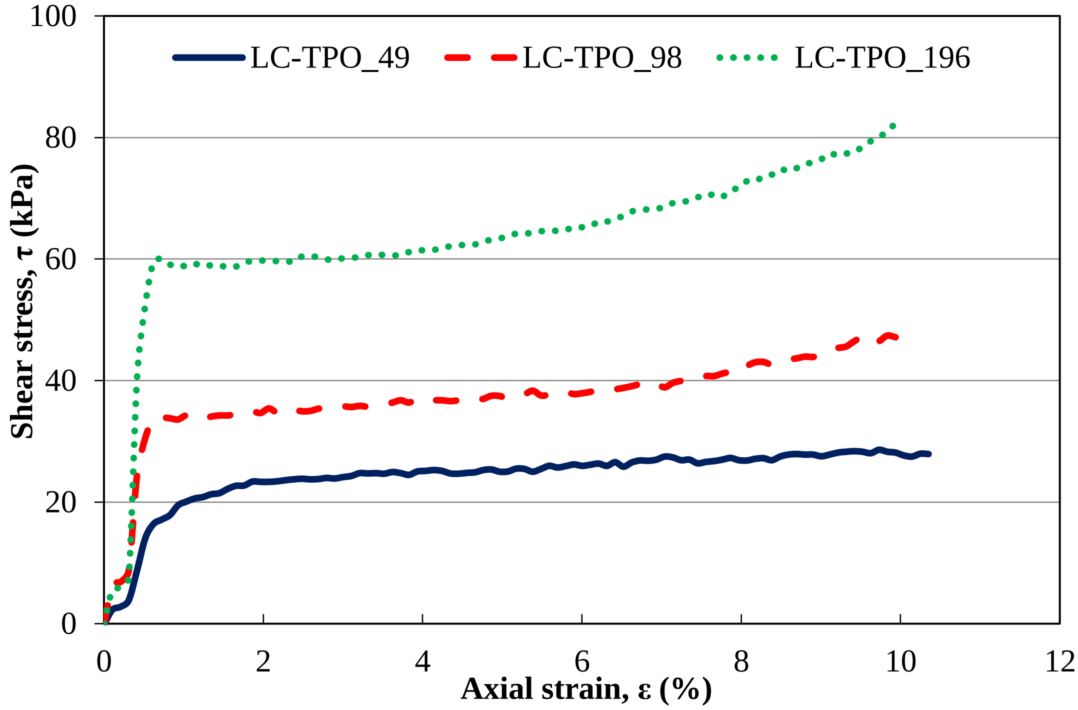

Figure A. 45: Shear stress (τ) – strain (ε) graphs of 4 months CCP cured TPO – LC interface

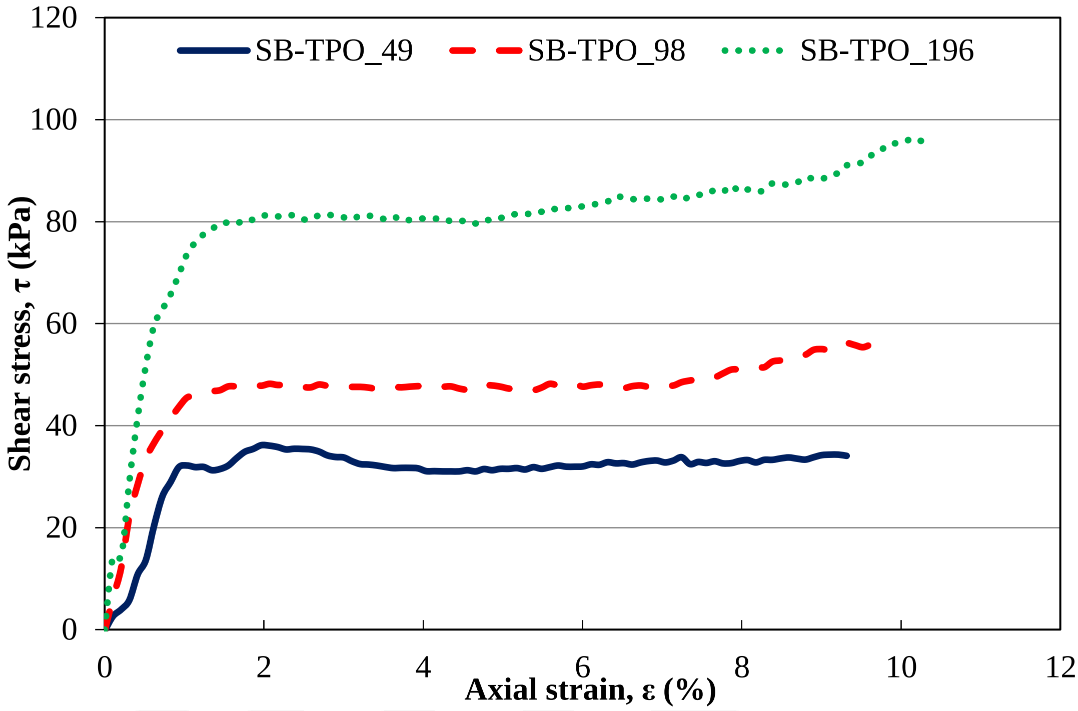

Figure A. 46: Shear stress (τ) – strain (ε) graphs of 4 months CCP cured TPO – SB interface

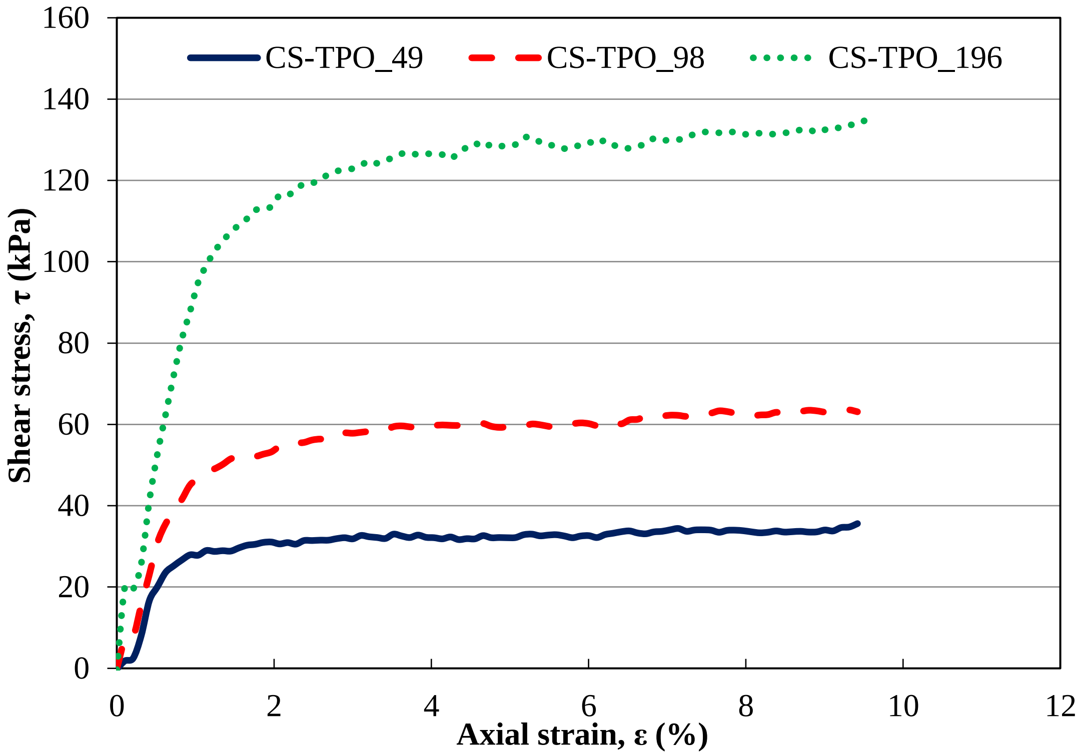

Figure A. 47: Shear stress (τ) – strain (ε) graphs of 4 months CCP cured TPO – CS interface

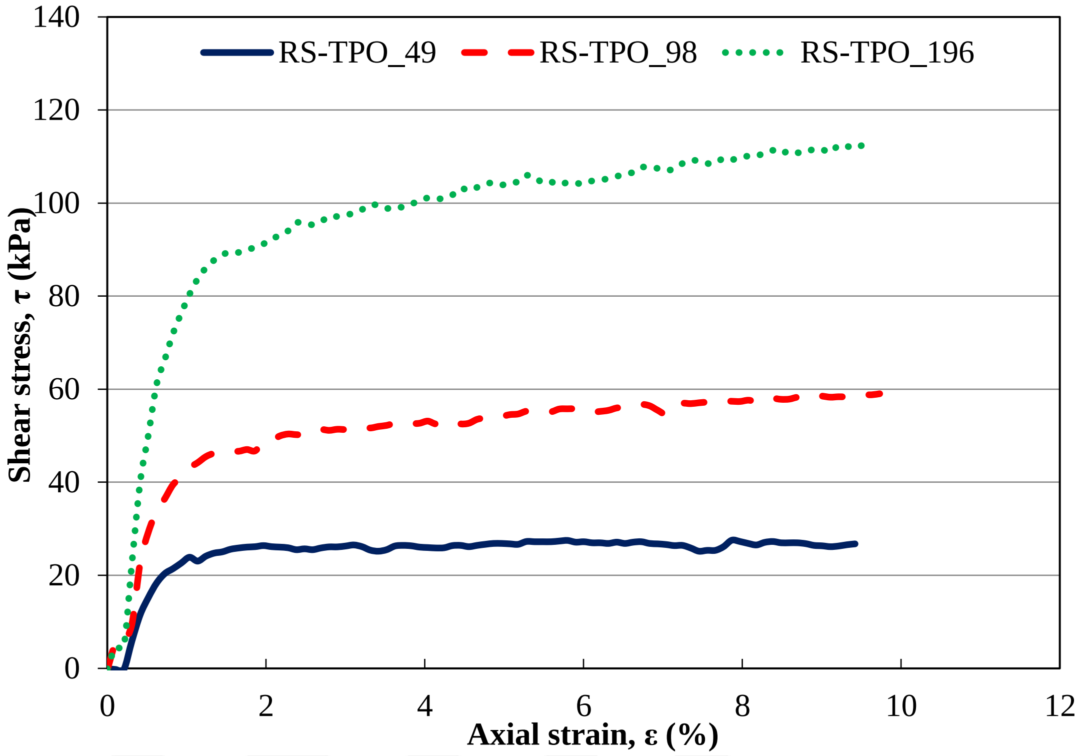

Figure A. 48: Shear stress (τ) – strain (ε) graphs of 4 months CCP cured TPO – RS interface

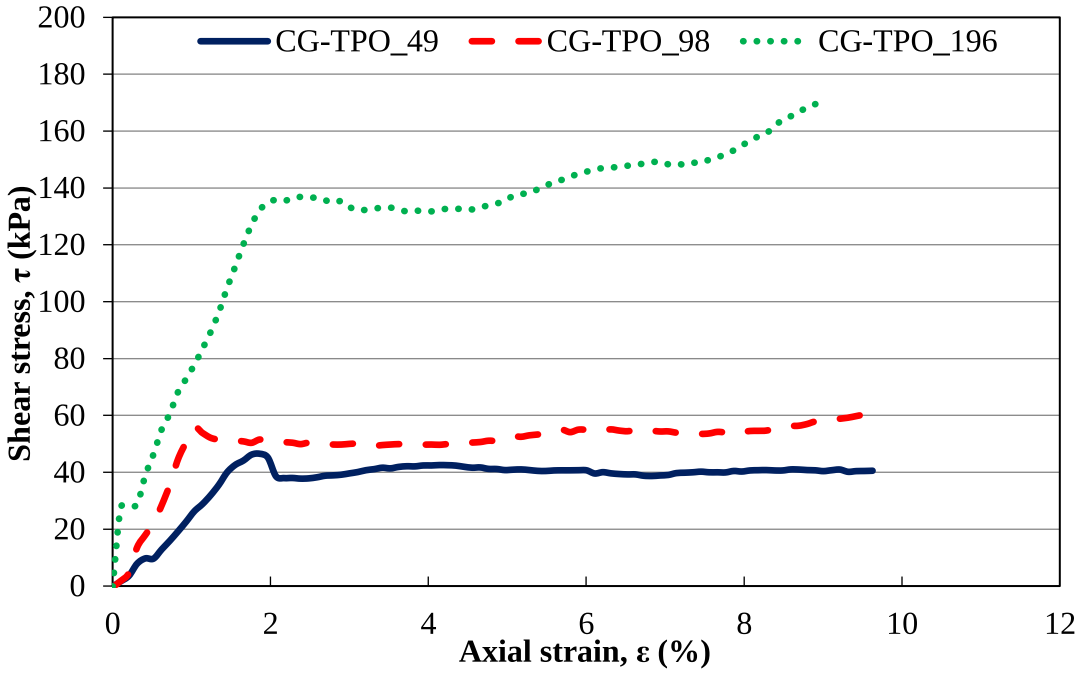

Figure A. 49: Shear stress (τ) – strain (ε) graphs of 4 months CCP cured TPO – CG interface

Interface Direct Shear Test Results for 4 Months MSW Curing

HDPE(S) – soil interfaces

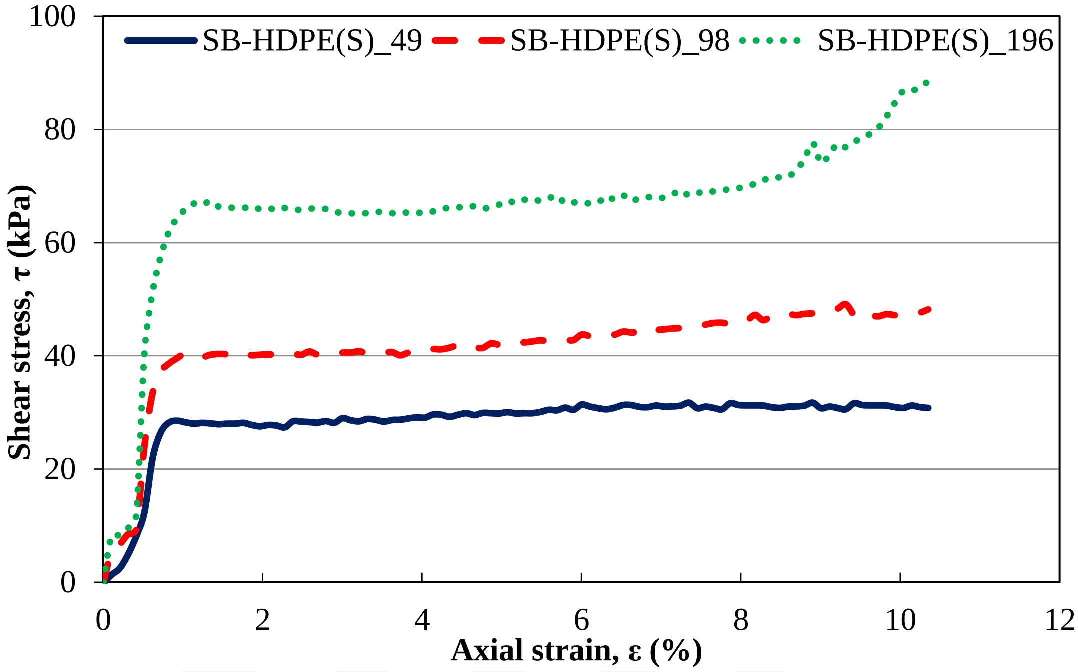

Figure A. 50: Shear stress (τ) – strain (ε) graphs of 4 months MSW cured HDPE(S) – SB interface

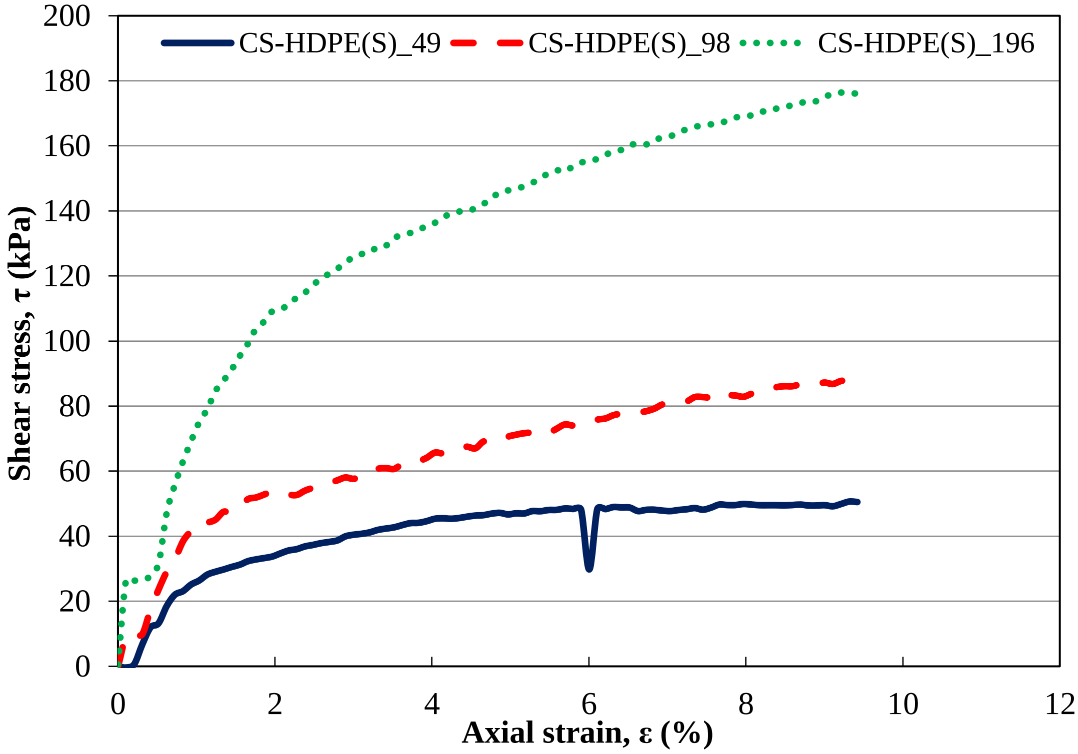

Figure A. 51: Shear stress (τ) – strain (ε) graphs of 4 months MSW cured HDPE(S) – CS interface

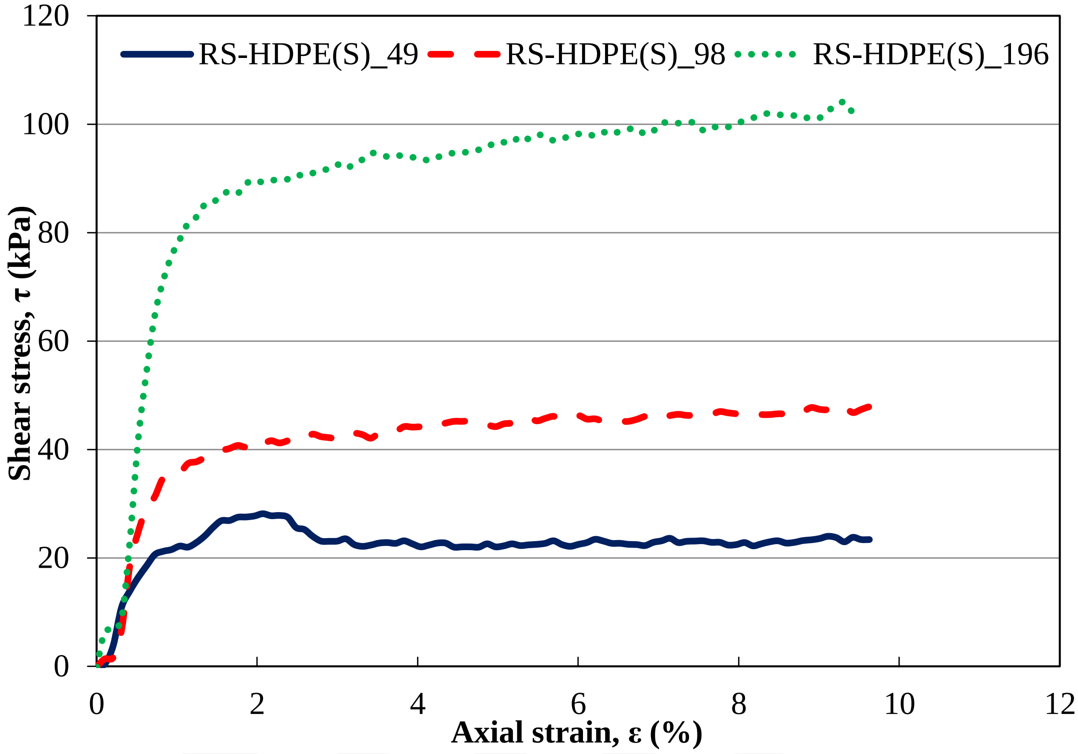

Figure A. 52: Shear stress (τ) – strain (ε) graphs of 4 months MSW cured HDPE(S) – RS interface

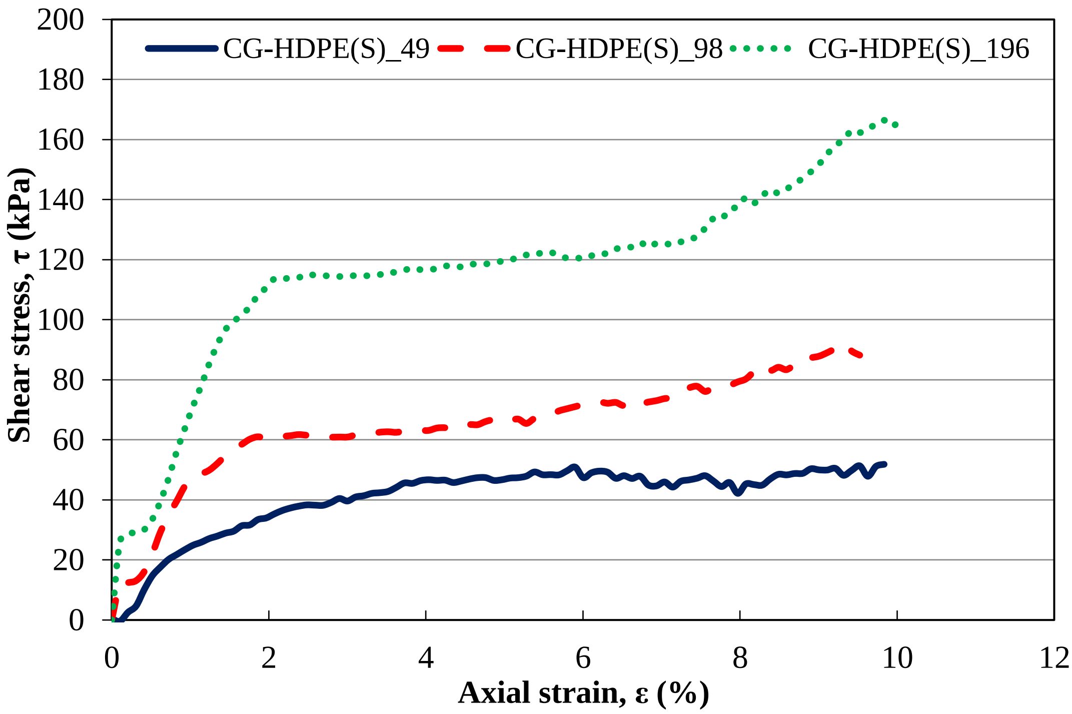

Figure A. 53: Shear stress (τ) – strain (ε) graphs of 4 months MSW cured HDPE(S) – CG interface

HDPE(T) – soil interfaces

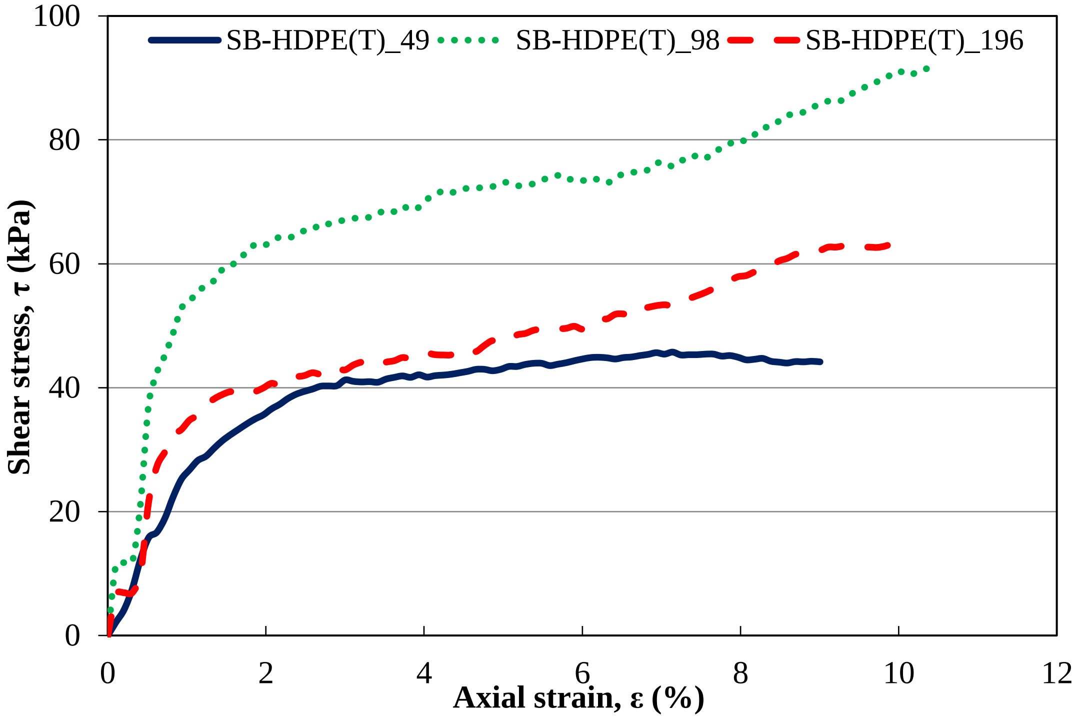

Figure A. 54: Shear stress (τ) – strain (ε) graphs of 4 months MSW cured HDPE(T) – SB interface

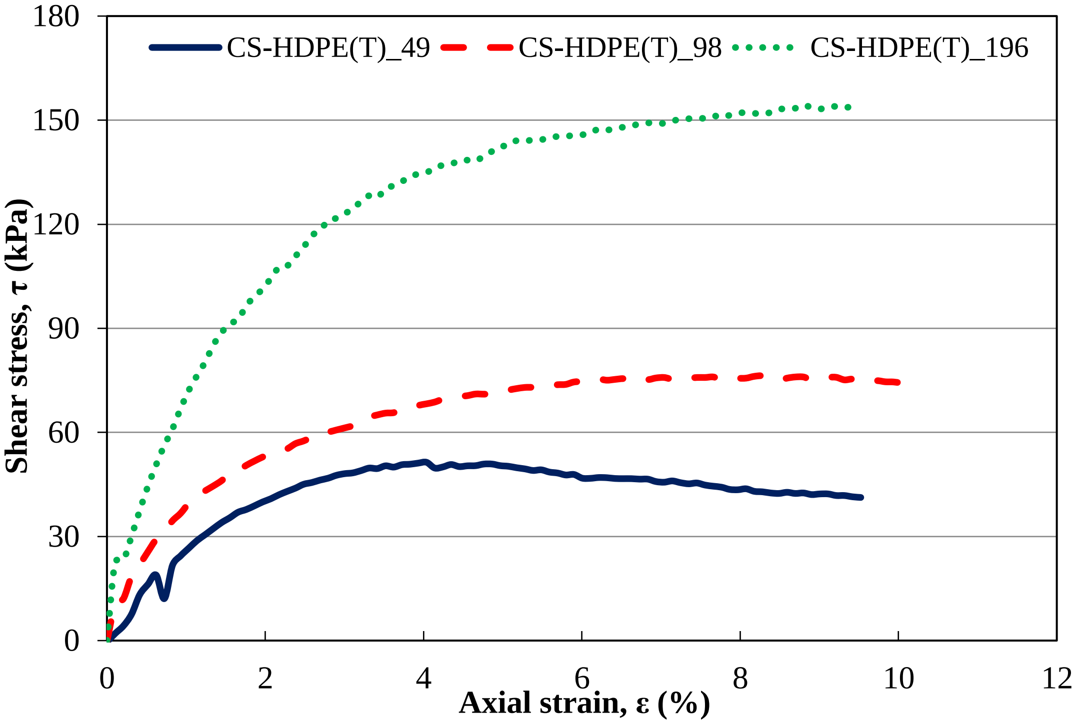

Figure A. 55: Shear stress (τ) – strain (ε) graphs of 4 months MSW cured HDPE(T) – CS interface

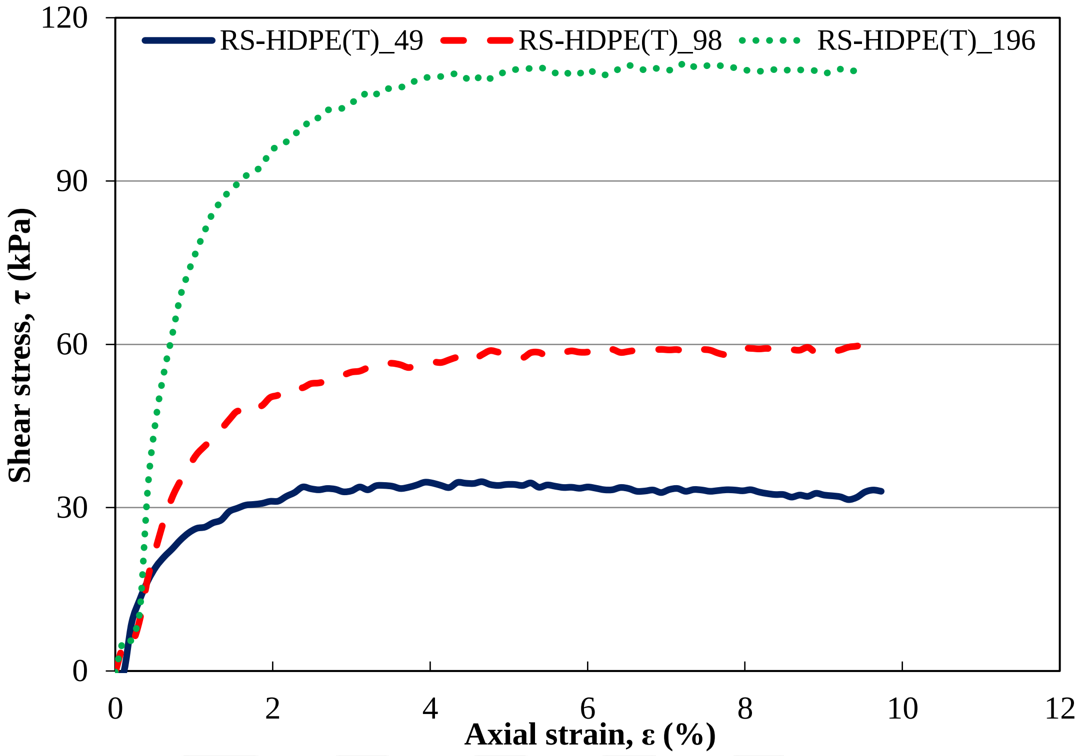

Figure A. 56: Shear stress (τ) – strain (ε) graphs of 4 months MSW cured HDPE(T) – RS interface

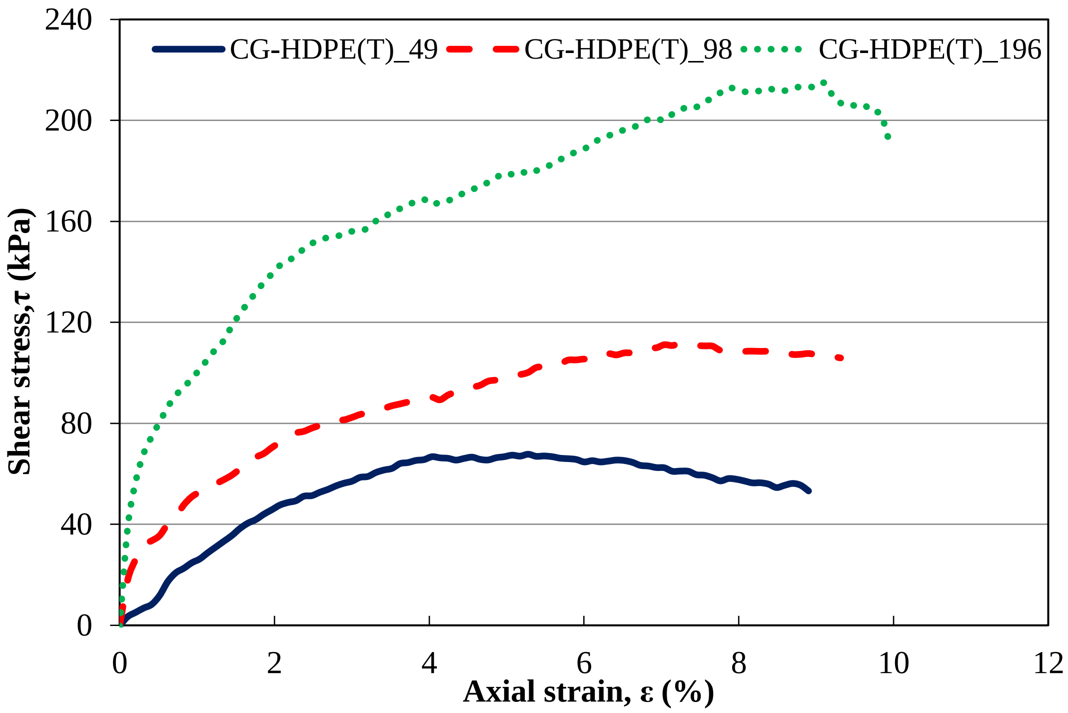

Figure A. 57: Shear stress (τ) – strain (ε) graphs of 4 months MSW cured HDPE(T) – CG interface

TPO – soil interfaces

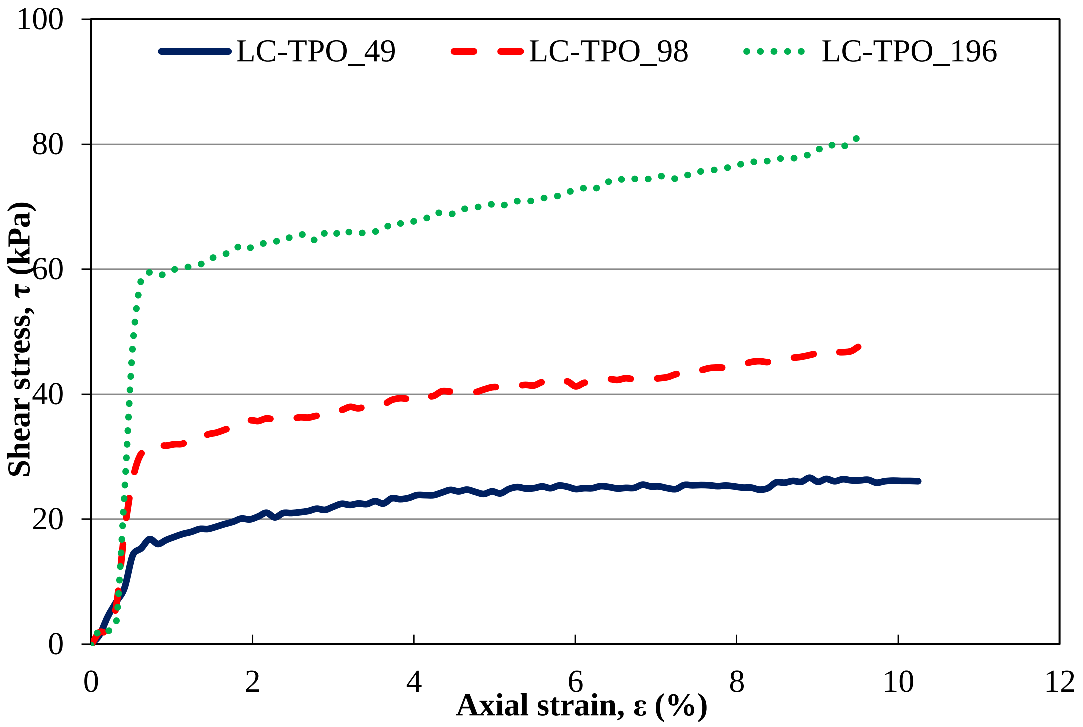

Figure A. 58: Shear stress (τ) – strain (ε) graphs of 4 months MSW cured TPO – LC interface

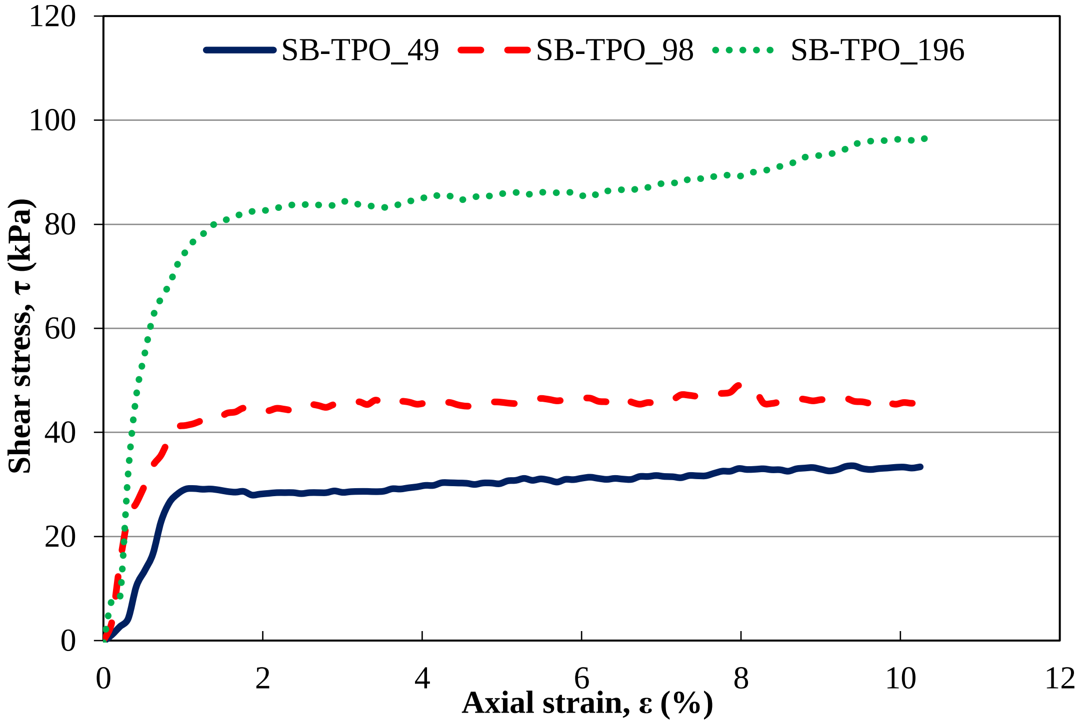

Figure A. 59: Shear stress (τ) – strain (ε) graphs of 4 months MSW cured TPO – SB interface

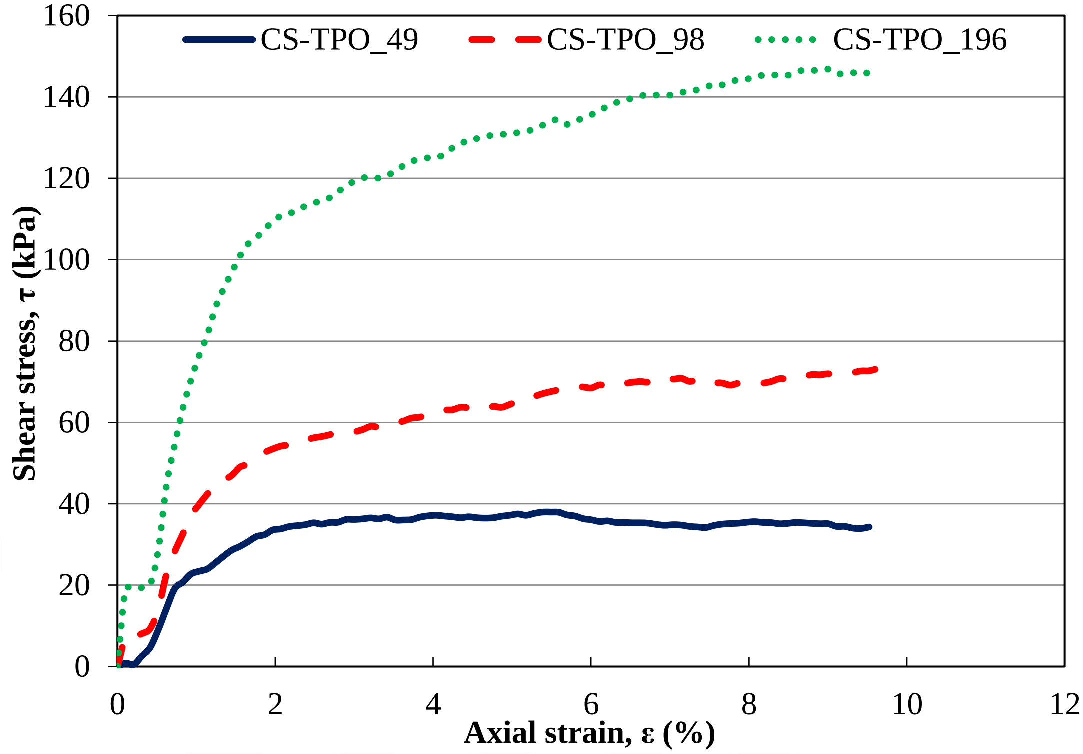

Figure A. 60: Shear stress (τ) – strain (ε) graphs of 4 months MSW cured TPO – CS interface

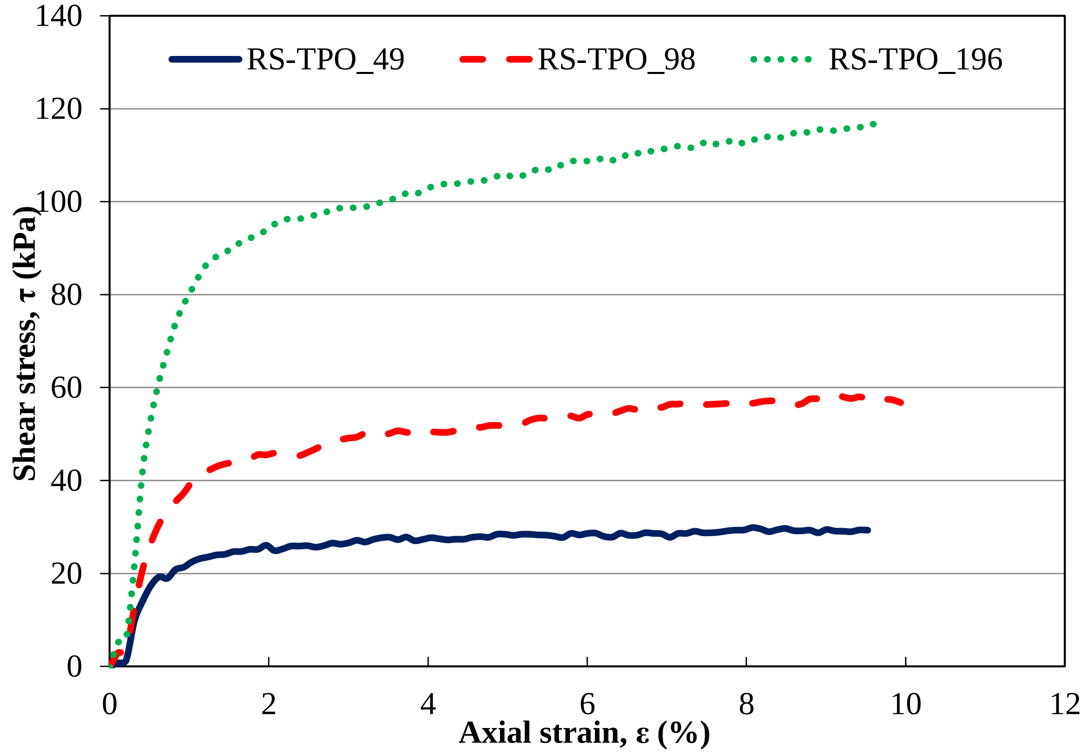

Figure A. 61: Shear stress (τ) – strain (ε) graphs of 4 months MSW cured TPO – RS interface

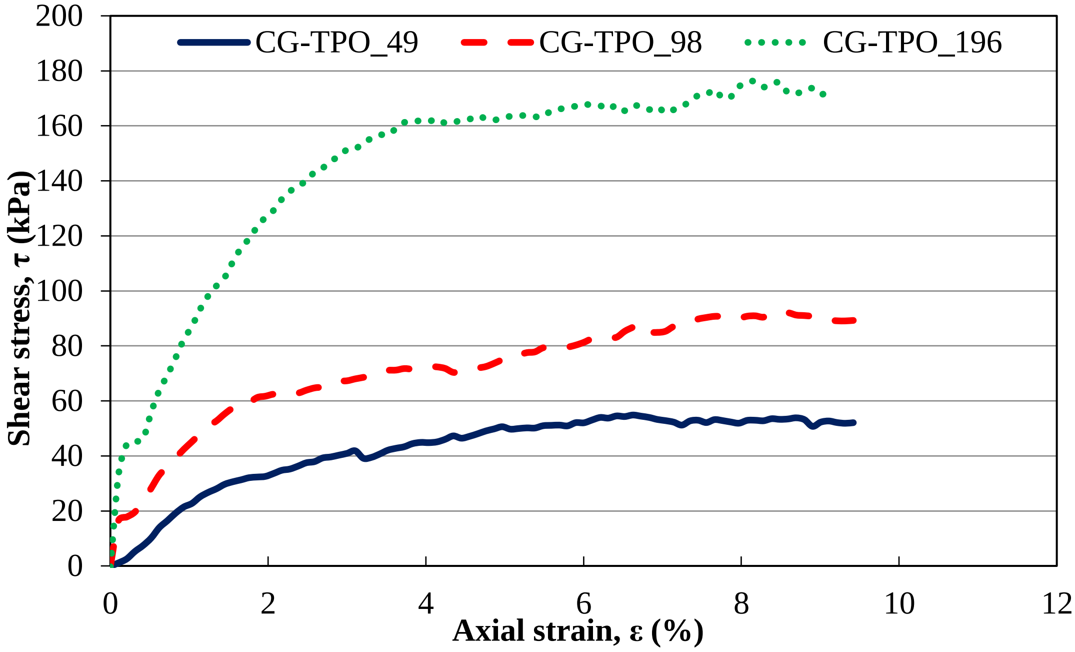

Figure A. 62: Shear stress (τ) – strain (ε) graphs of 4 months MSW cured TPO – CG interface

Interface Direct Shear Test Results for 8 Months SWt Curing

PVC(1.5) – soil interfaces

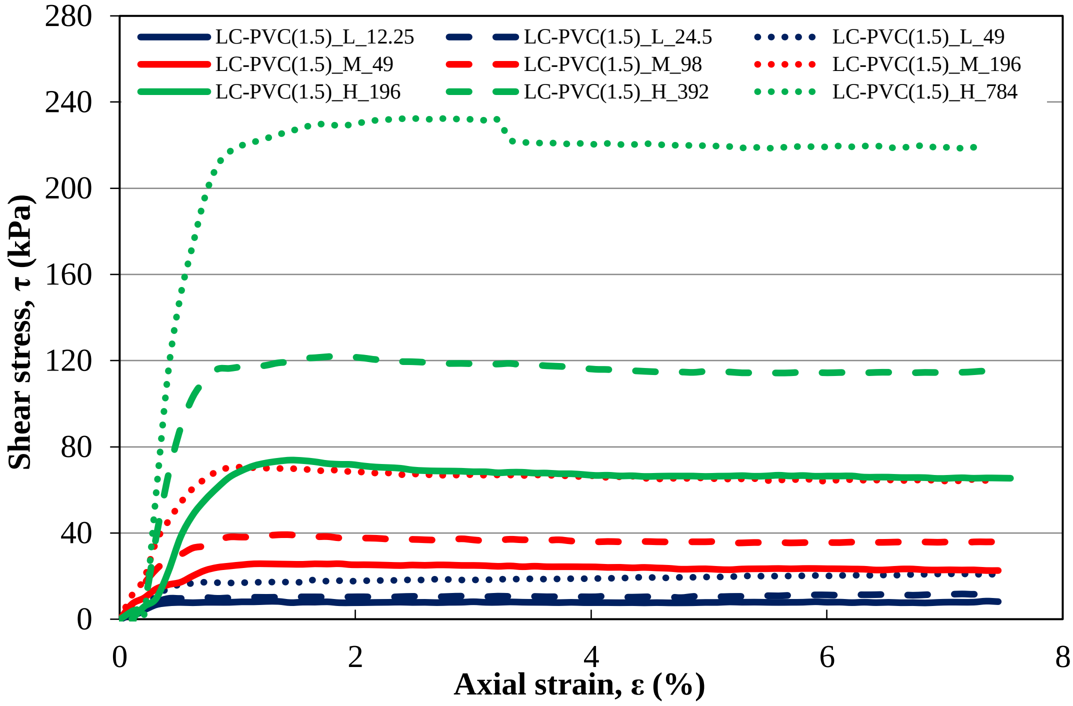

Figure A. 63: Shear stress (τ) – strain (ε) graphs of 8 months SWt cured PVC(1.5) – LC interface

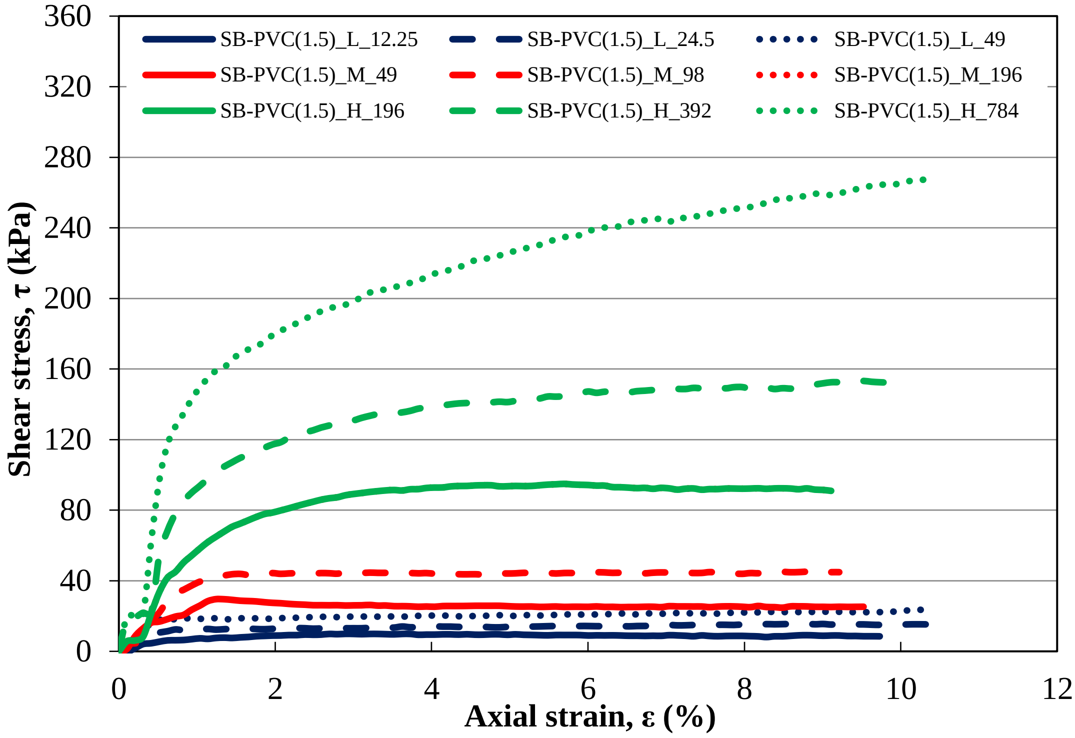

Figure A. 64: Shear stress (τ) – strain (ε) graphs of 8 months SWt cured PVC(1.5) – SB interface

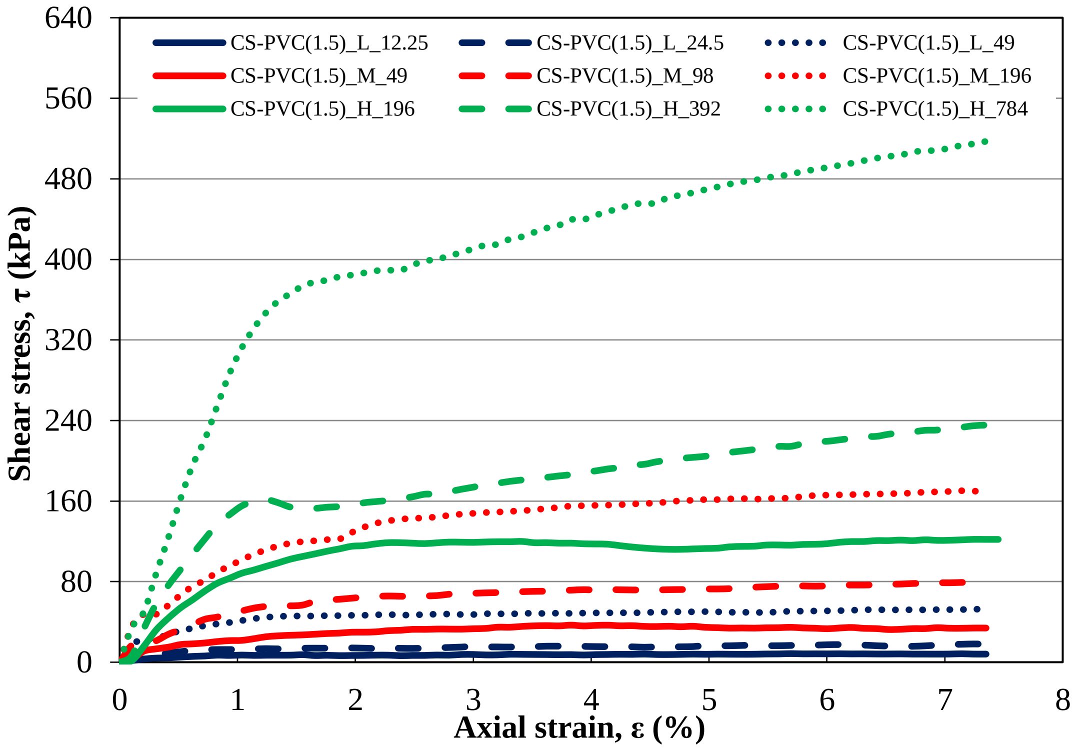

Figure A. 65: Shear stress (τ) – strain (ε) graphs of 8 months SWt cured PVC(1.5) – CS interface

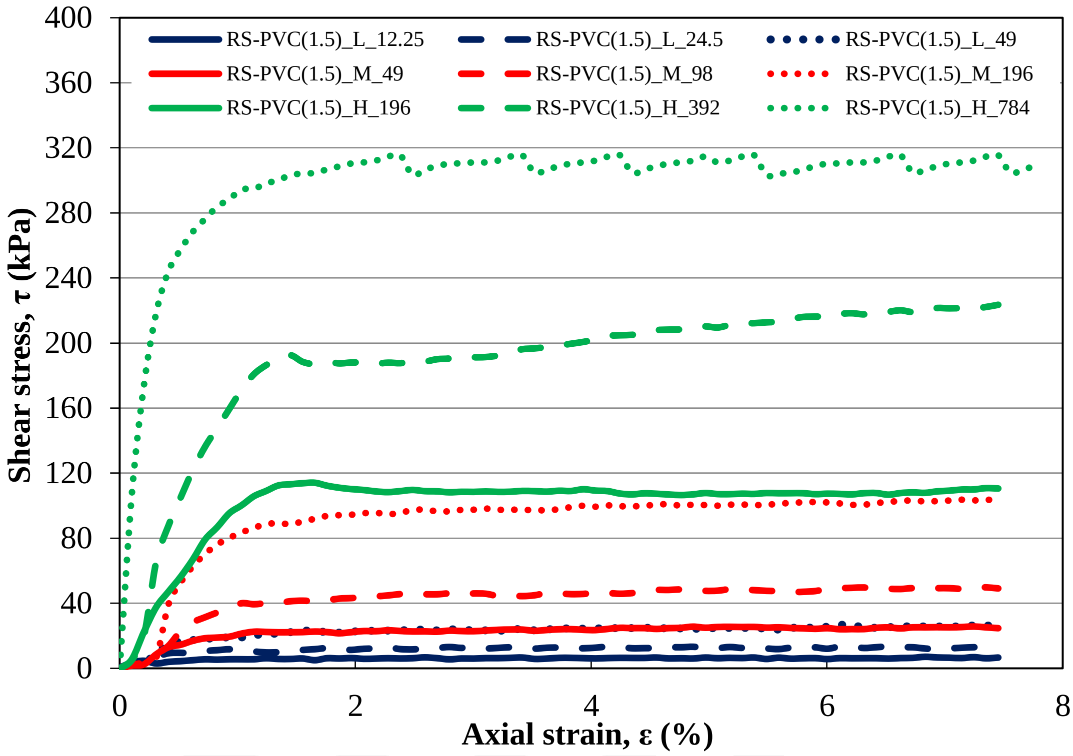

Figure A. 66: Shear stress (τ) – strain (ε) graphs of 8 months SWt cured PVC(1.5) – RS interface

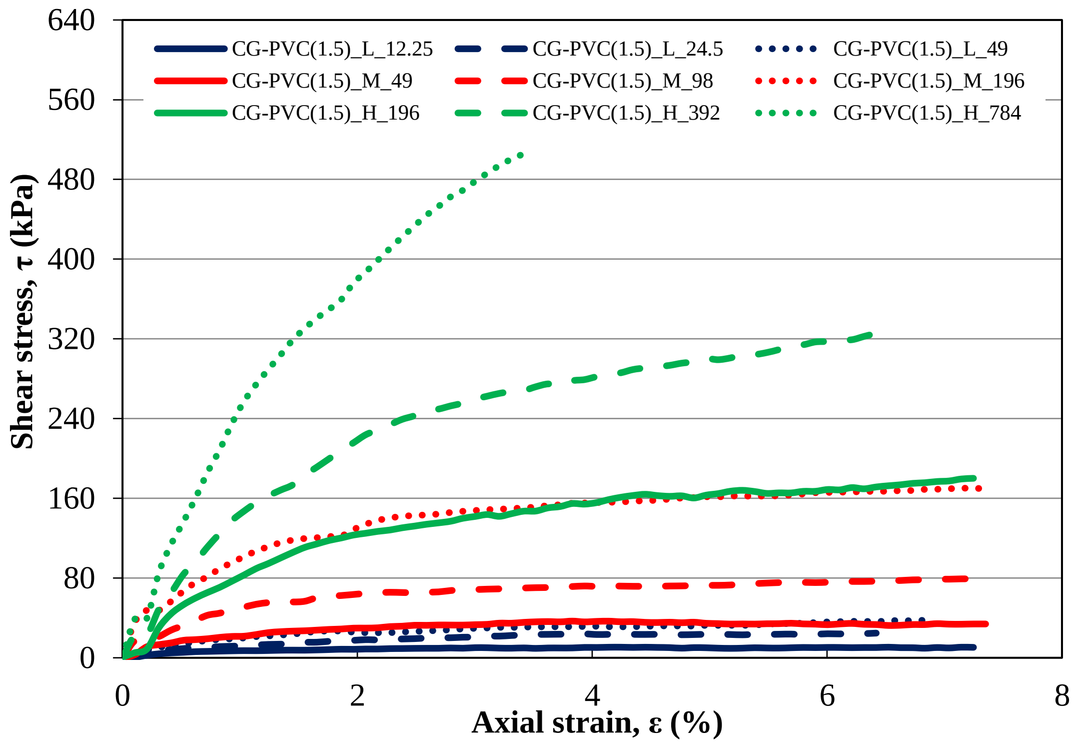

Figure A. 67: Shear stress (τ) – strain (ε) graphs of 8 months SWt cured PVC(1.5) – CG interface

PVC(3.0) – soil interfaces

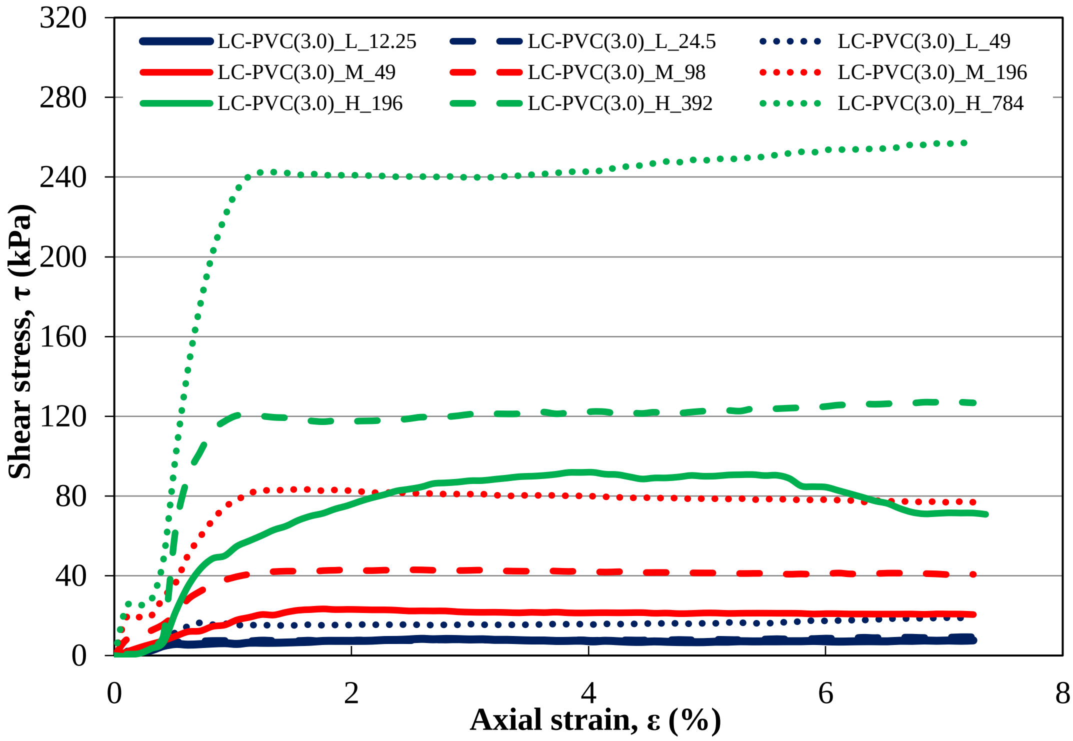

Figure A. 68: Shear stress (τ) – strain (ε) graphs of 8 months SWt cured PVC(3.0) – LC interface

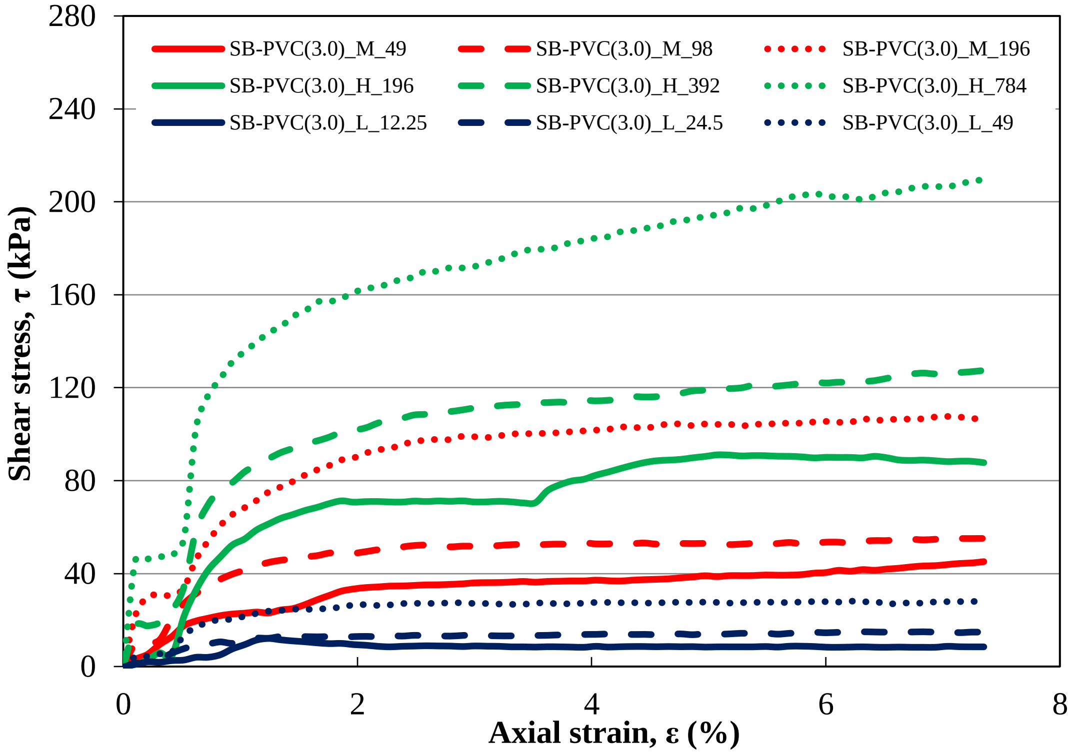

Figure A. 69: Shear stress (τ) – strain (ε) graphs of 8 months SWt cured PVC(3.0) – SB interface

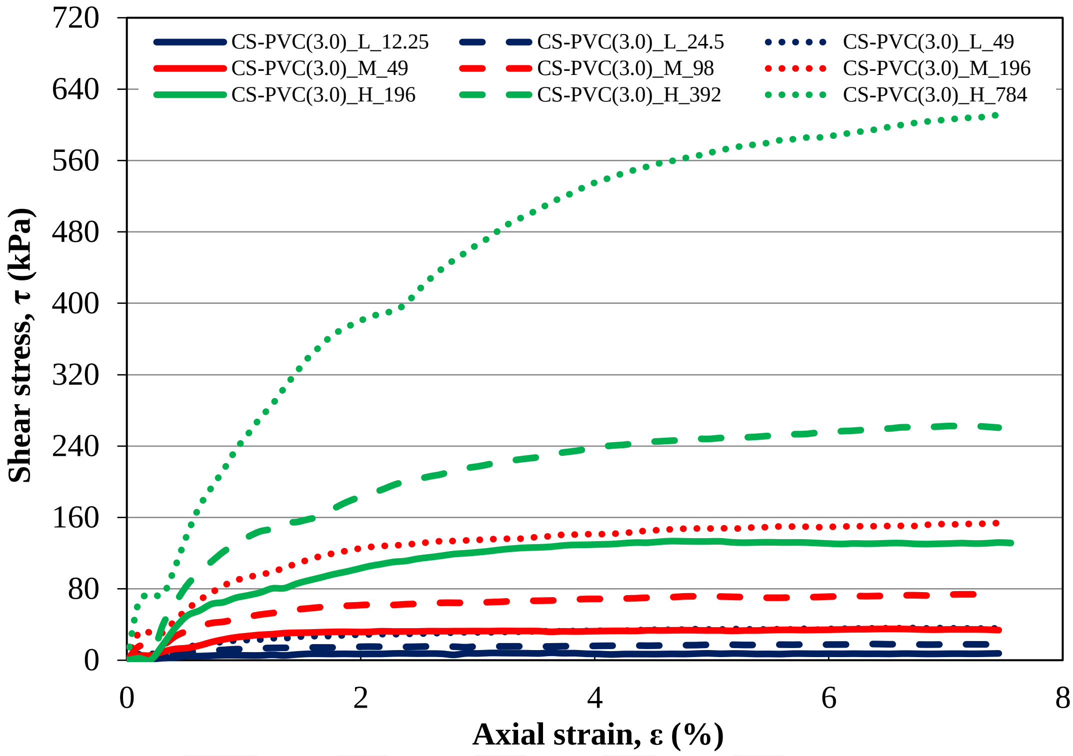

Figure A. 70: Shear stress (τ) – strain (ε) graphs of 8 months SWt cured PVC(3.0) – CS interface

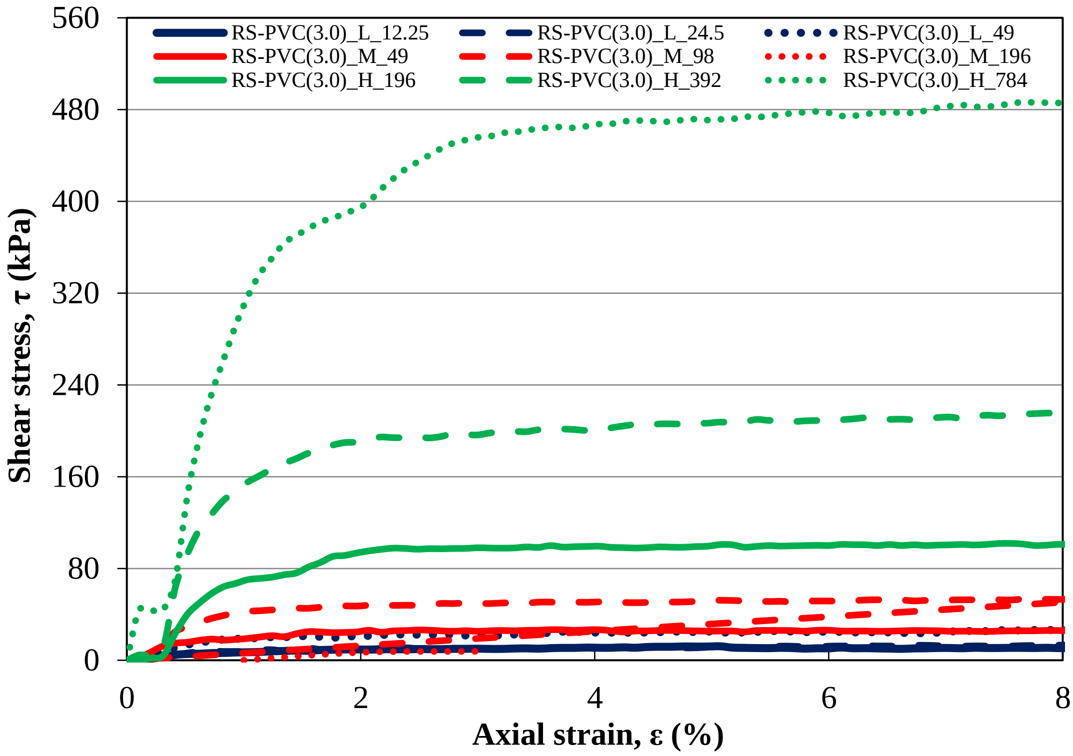

Figure A. 71: Shear stress (τ) – strain (ε) graphs of 8 months SWt cured PVC(3.0) – RS interface

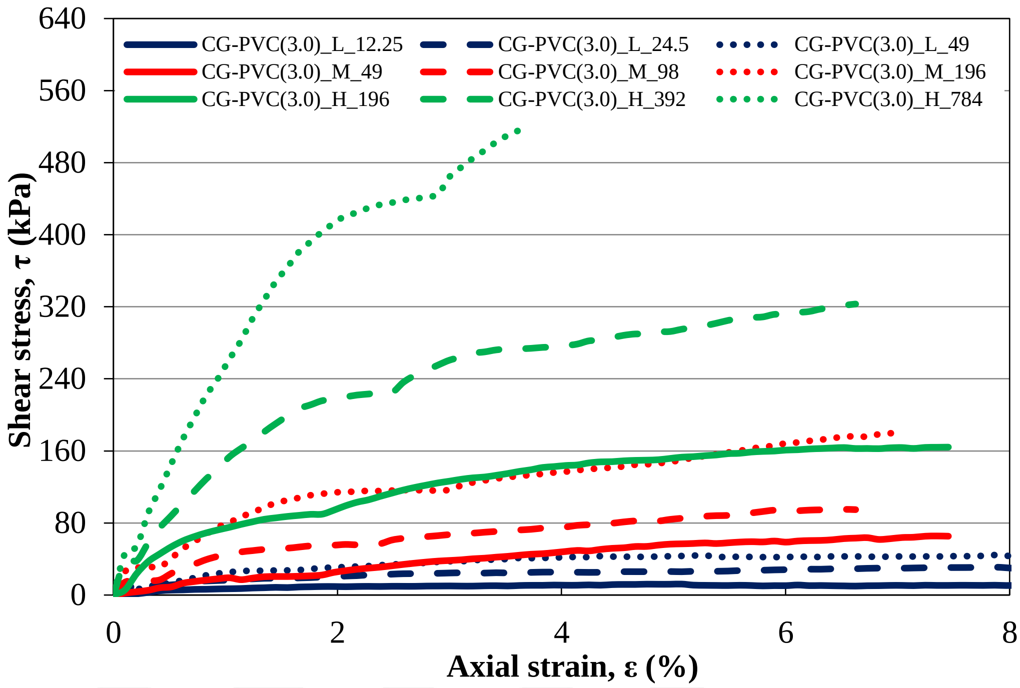

Figure A. 72: Shear stress (τ) – strain (ε) graphs of 8 months SWt cured PVC(3.0) – CG interface

TPO – soil interfaces

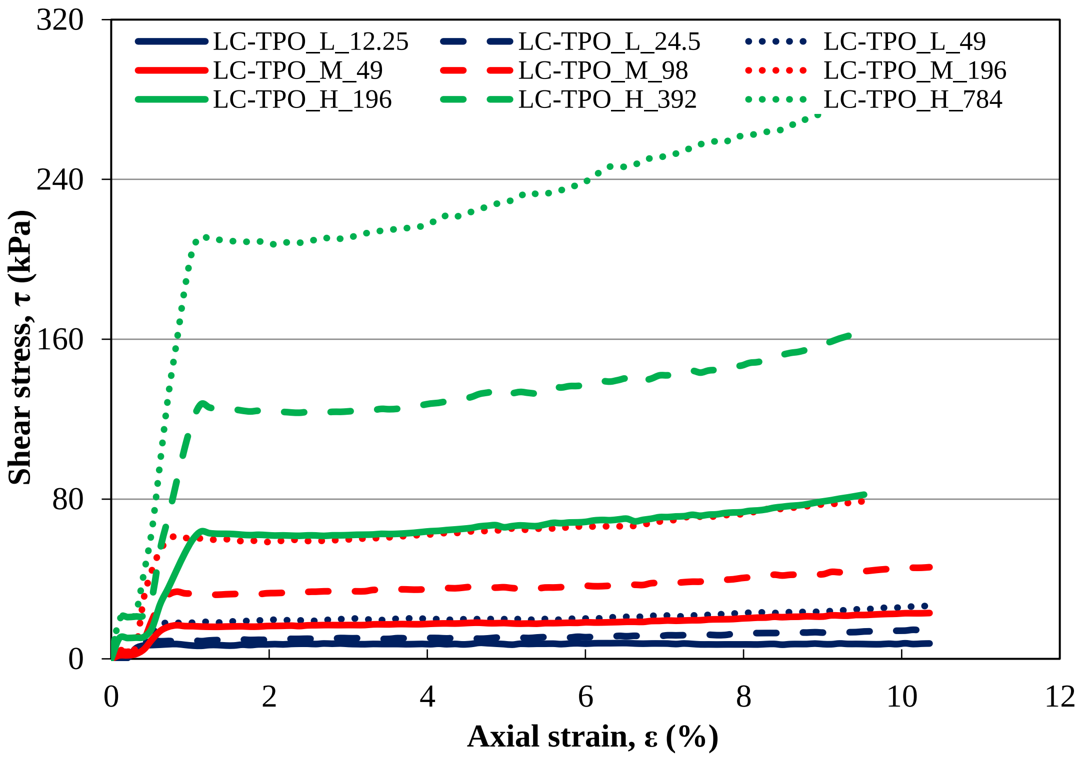

Figure A. 73: Shear stress (τ) – strain (ε) graphs of 8 months SWt cured TPO – LC interface

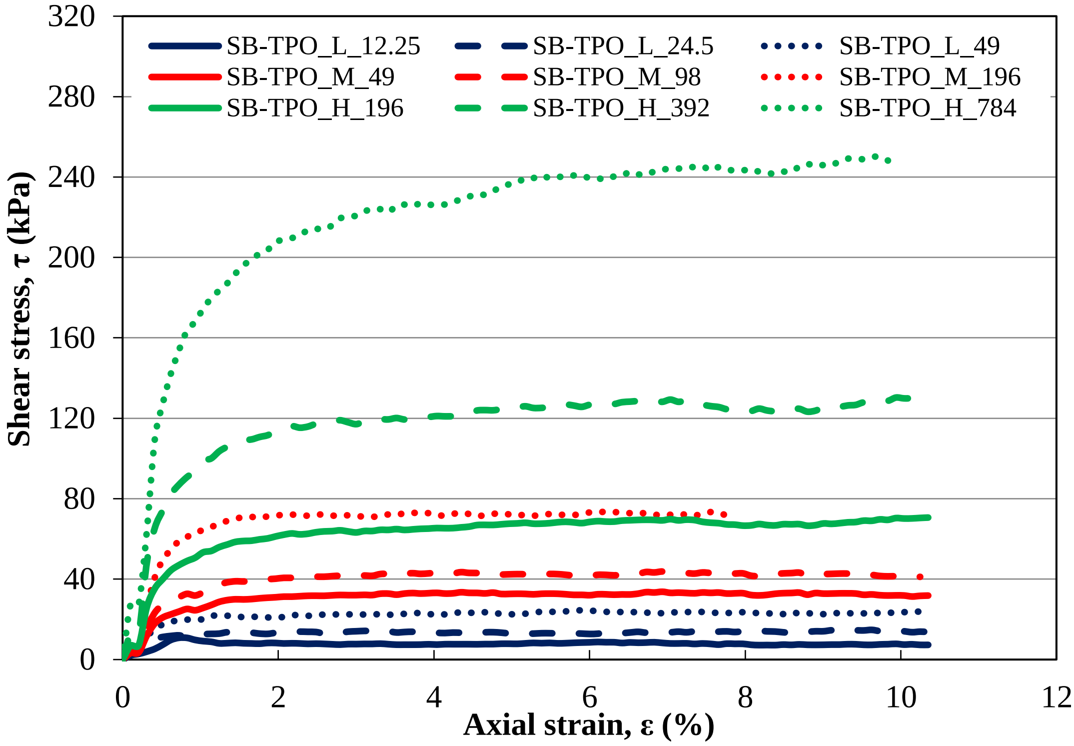

Figure A. 74: Shear stress (τ) – strain (ε) graphs of 8 months SWt cured TPO – SB interface

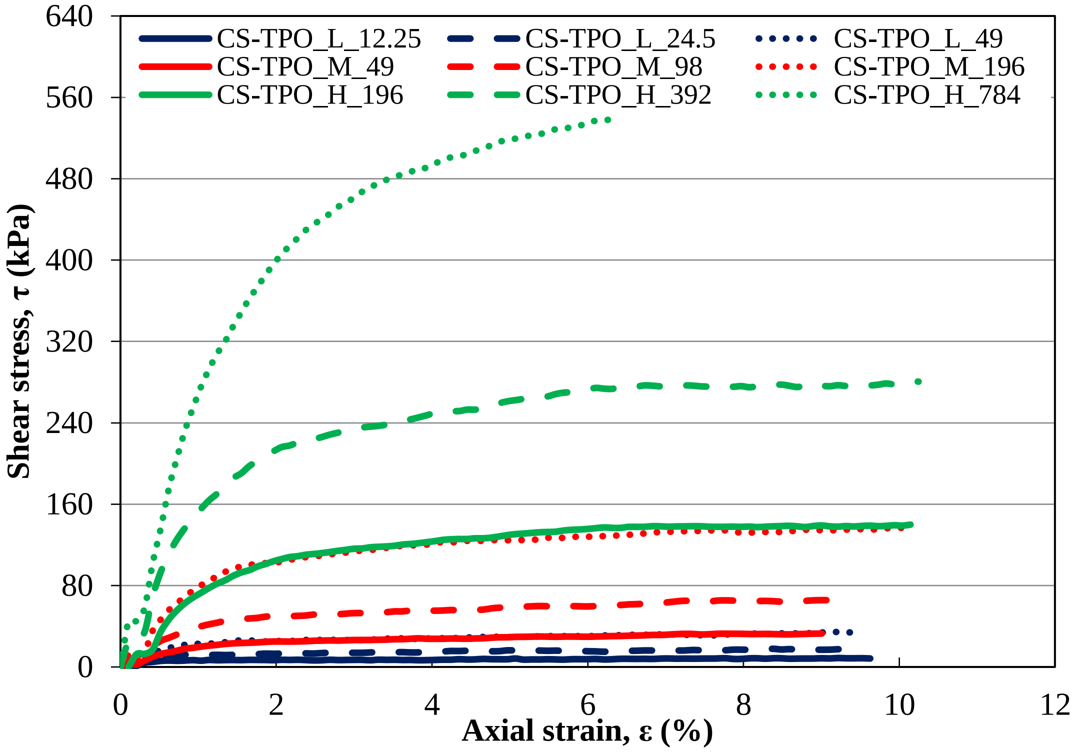

Figure A. 75: Shear stress (τ) – strain (ε) graphs of 8 months SWt cured TPO – CS interface

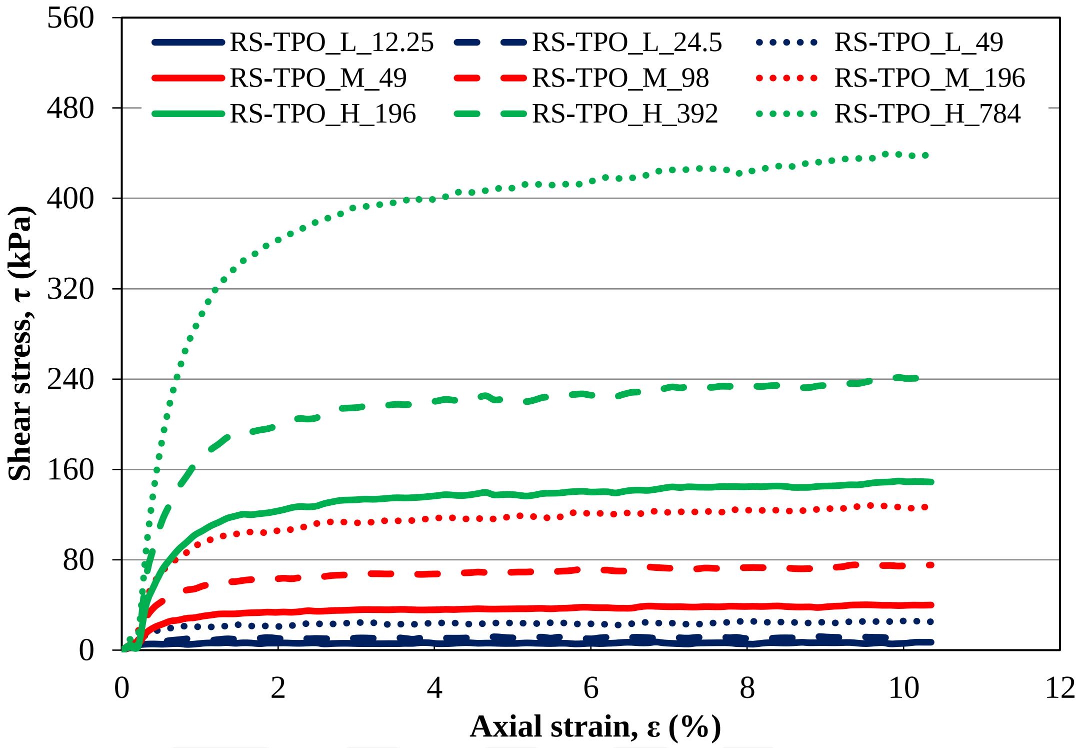

Figure A. 76: Shear stress (τ) – strain (ε) graphs of 8 months SWt cured TPO – RS interface

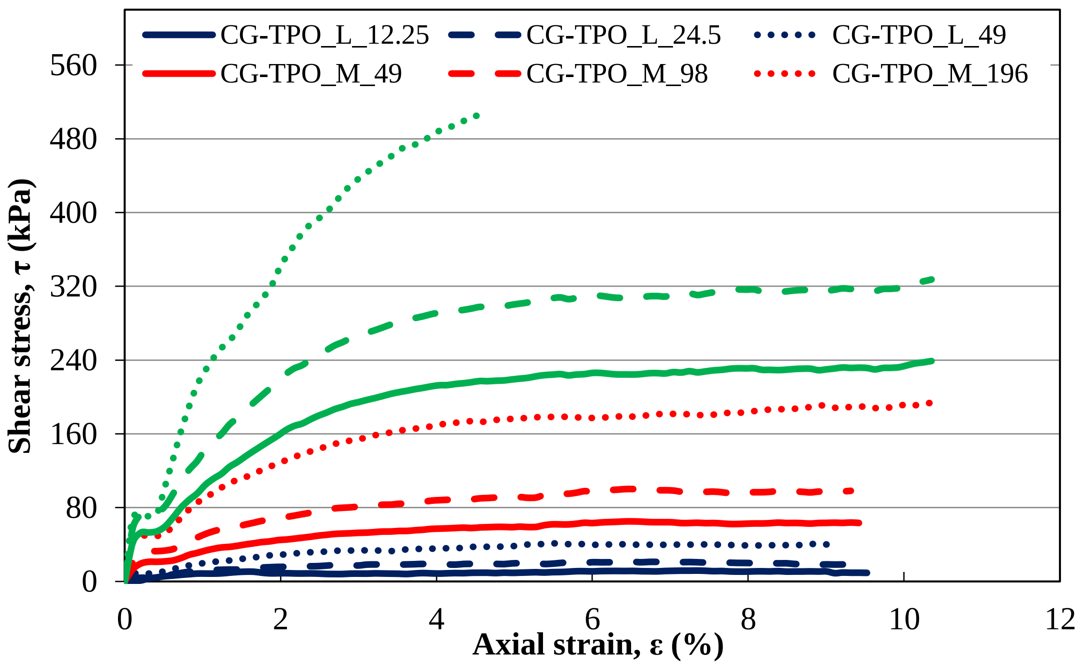

Figure A. 77: Shear stress (τ) – strain (ε) graphs of 8 months SWt cured TPO – CG interface

Interface Direct Shear Test Results for 8 Months AMD Curing

HDPE(S) – soil interfaces

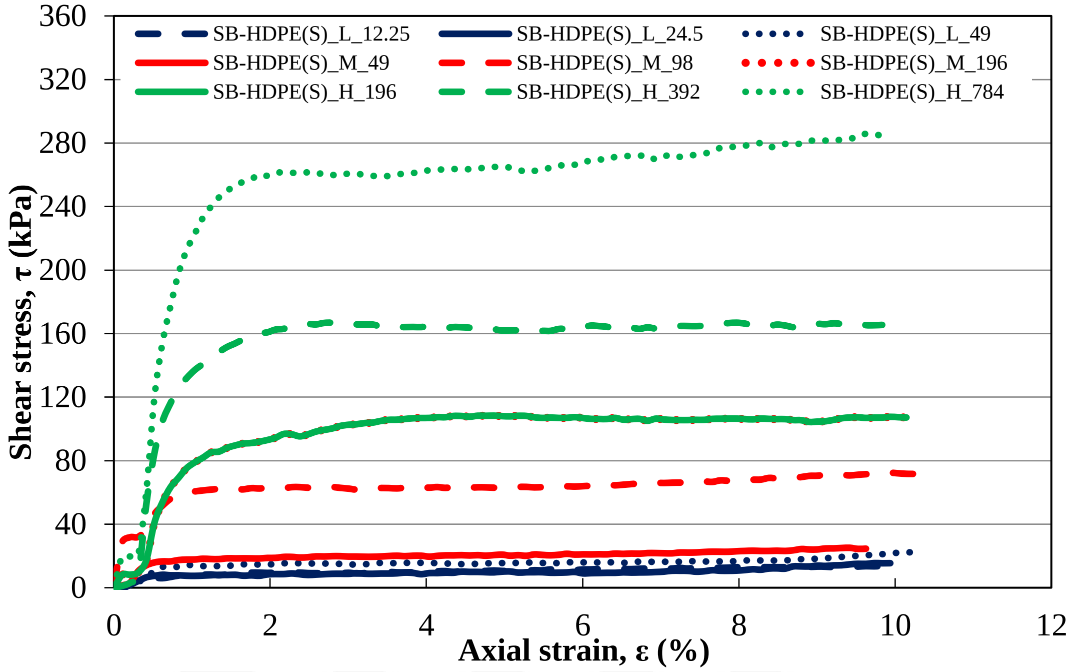

Figure A. 78: Shear stress (τ) – strain (ε) graphs of 8 months AMD cured HDPE(S) – SB interface

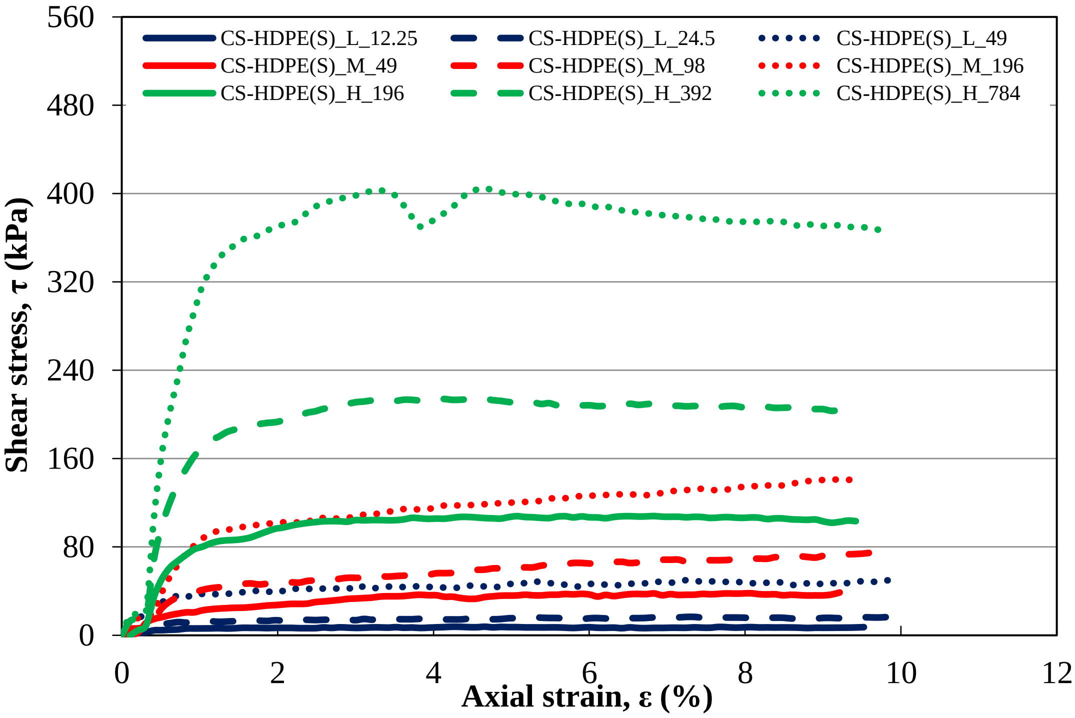

Figure A. 79: Shear stress (τ) – strain (ε) graphs of 8 months AMD cured HDPE(S) – CS interface

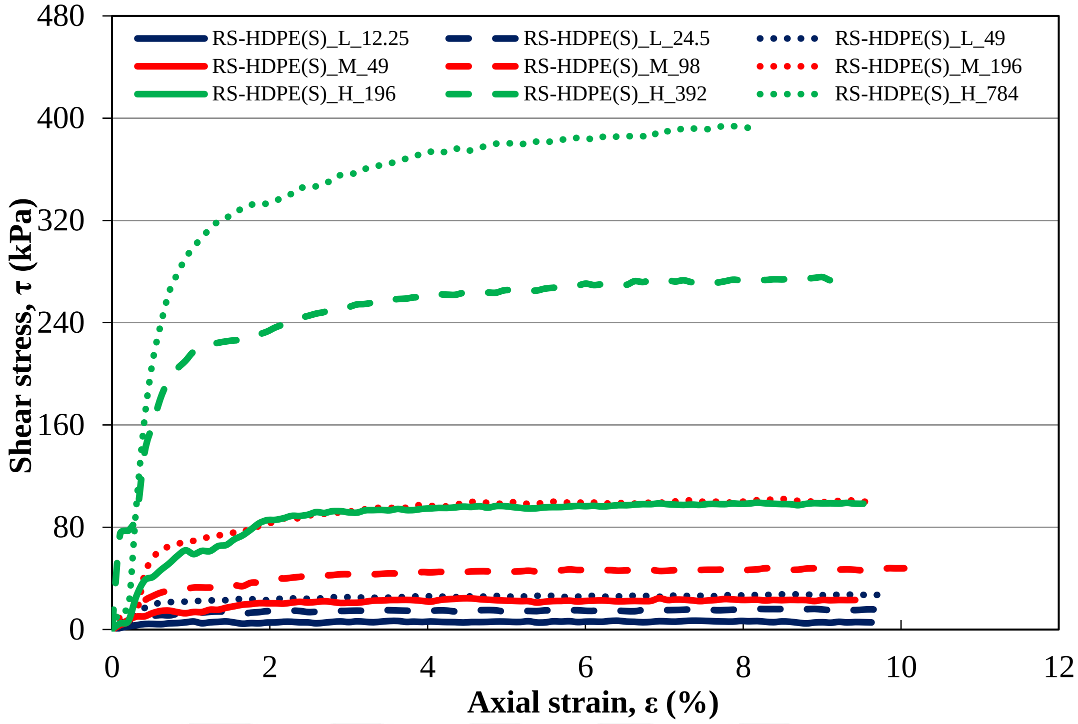

Figure A. 80: Shear stress (τ) – strain (ε) graphs of 8 months AMD cured HDPE(S) – RS interface

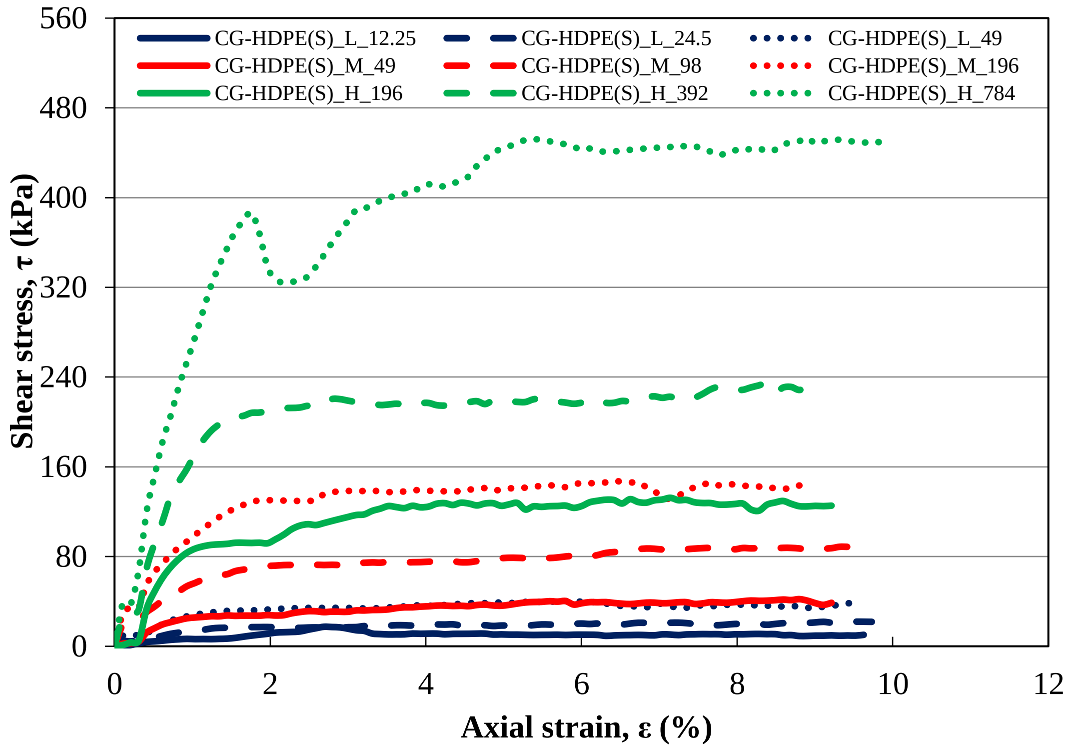

Figure A. 81: Shear stress (τ) – strain (ε) graphs of 8 months AMD cured HDPE(S) – CG interface

HDPE(T) – soil interfaces

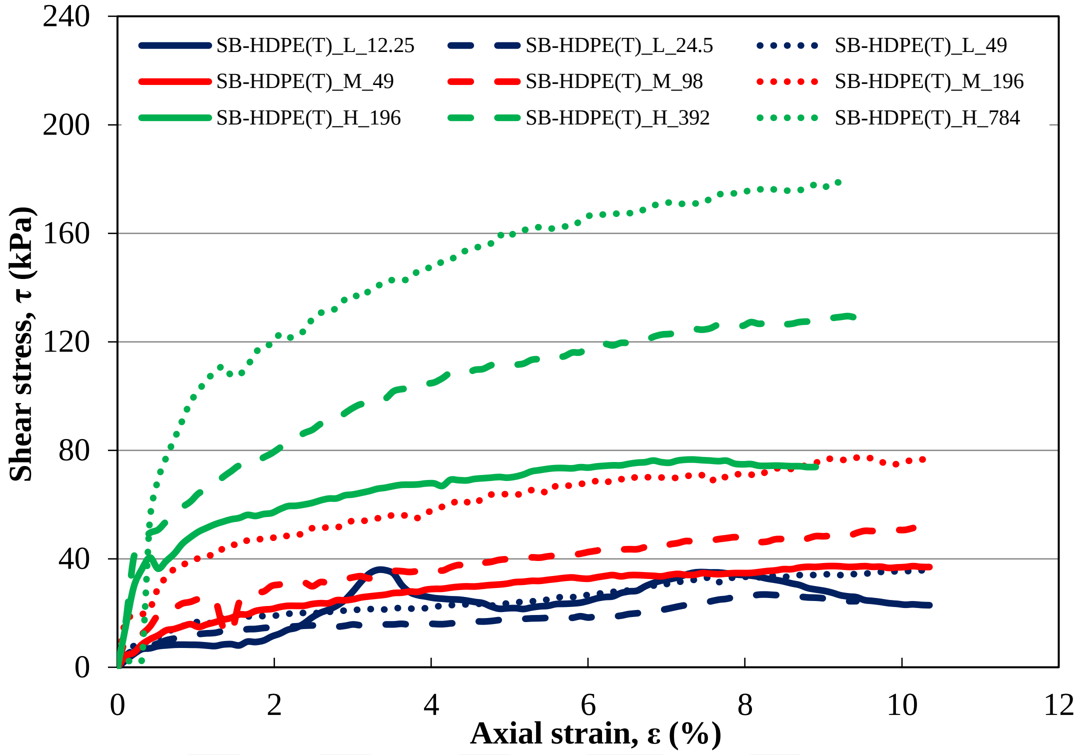

Figure A. 82: Shear stress (τ) – strain (ε) graphs of 8 months AMD cured HDPE(T) – SB interface

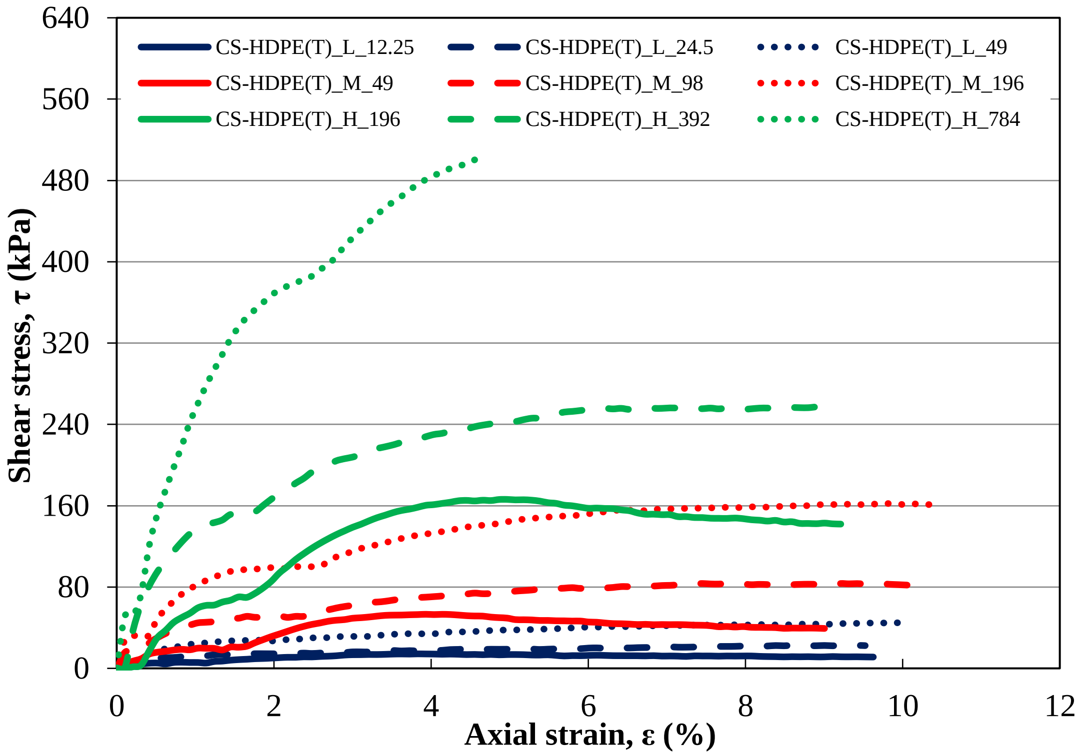

Figure A. 83: Shear stress (τ) – strain (ε) graphs of 8 months AMD cured HDPE(T) – CS interface

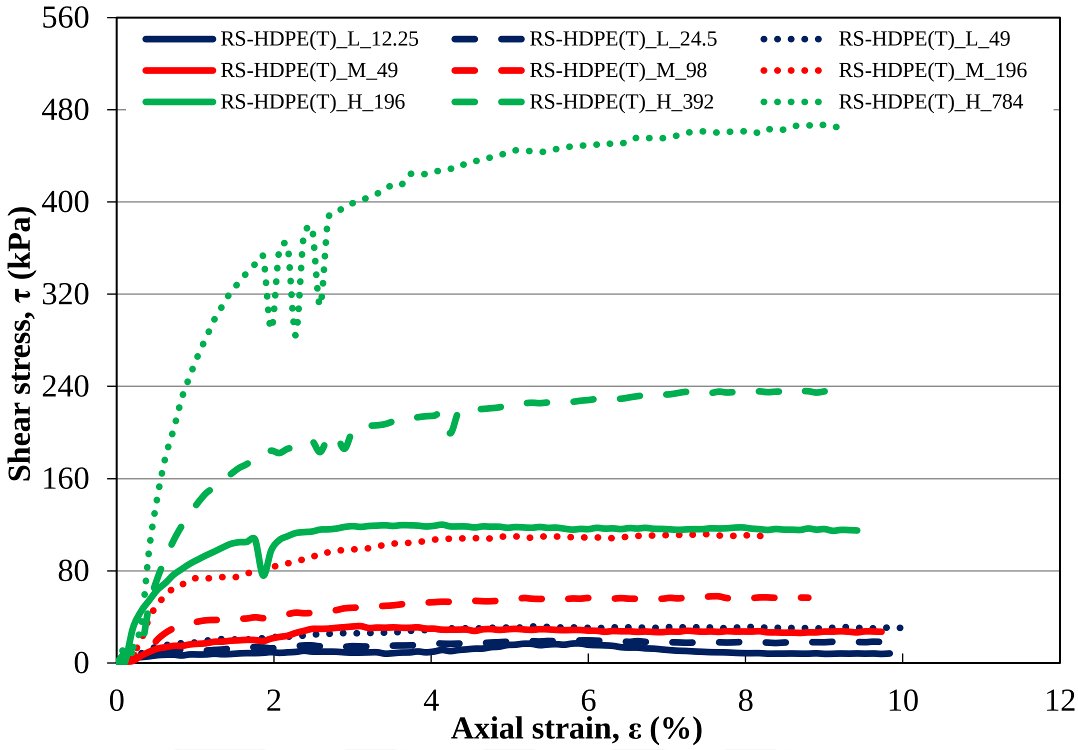

Figure A. 84 : Shear stress (τ) – strain (ε) graphs of 8 months AMD cured HDPE(T) – RS interface

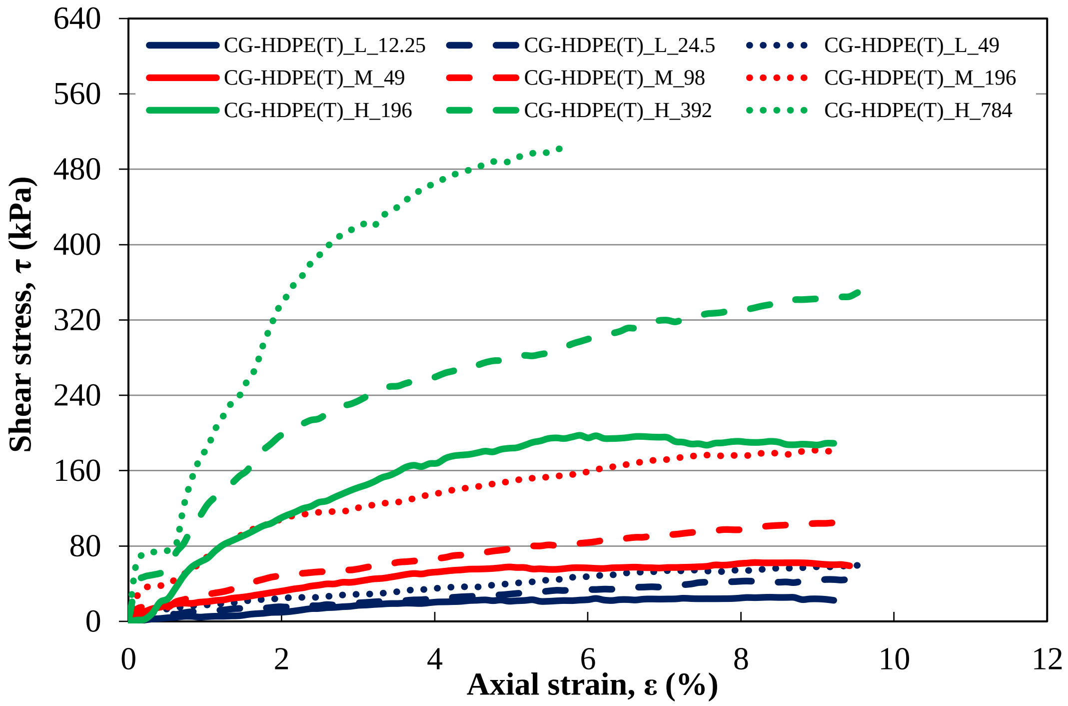

Figure A. 85: Shear stress (τ) – strain (ε) graphs of 8 months AMD cured HDPE(T) – CG interface

TPO – soil interfaces

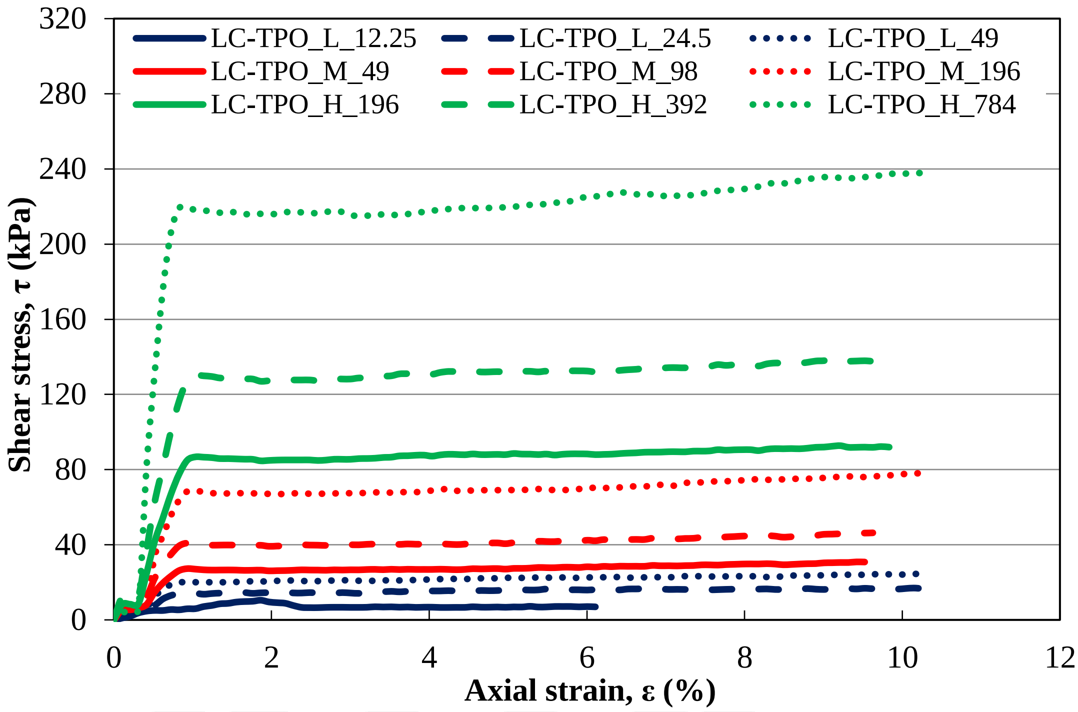

Figure A. 86: Shear stress (τ) – strain (ε) graphs of 8 months AMD cured TPO – LC interface

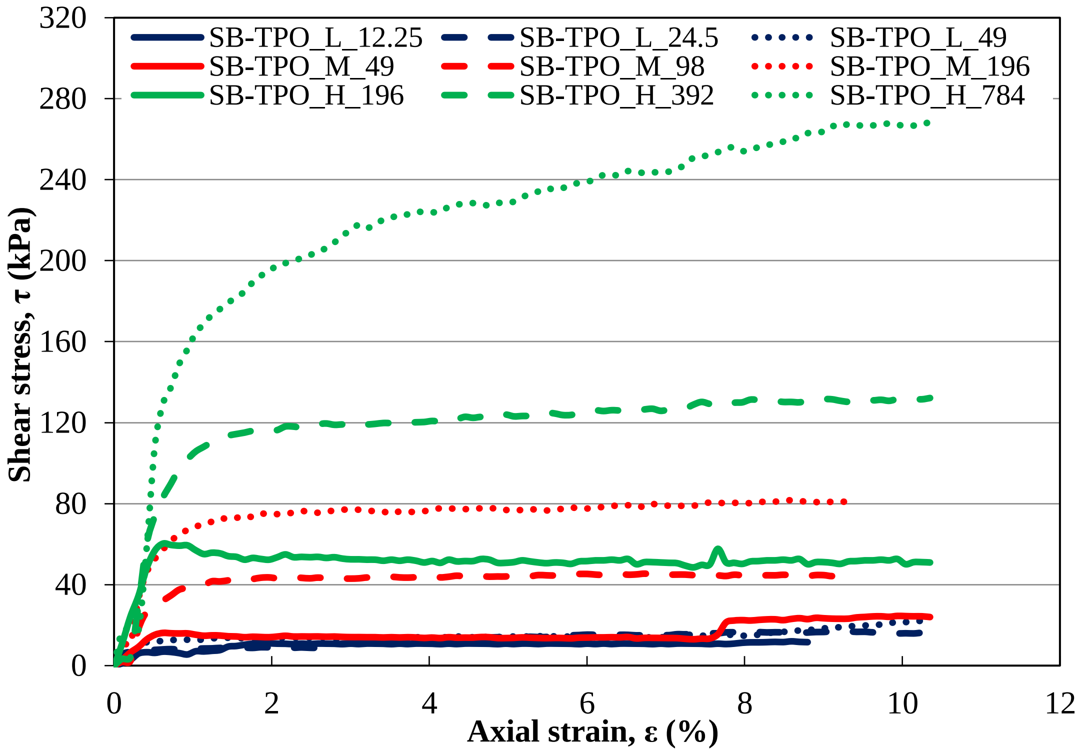

Figure A. 87: Shear stress (τ) – strain (ε) graphs of 8 months AMD cured TPO – SB interface

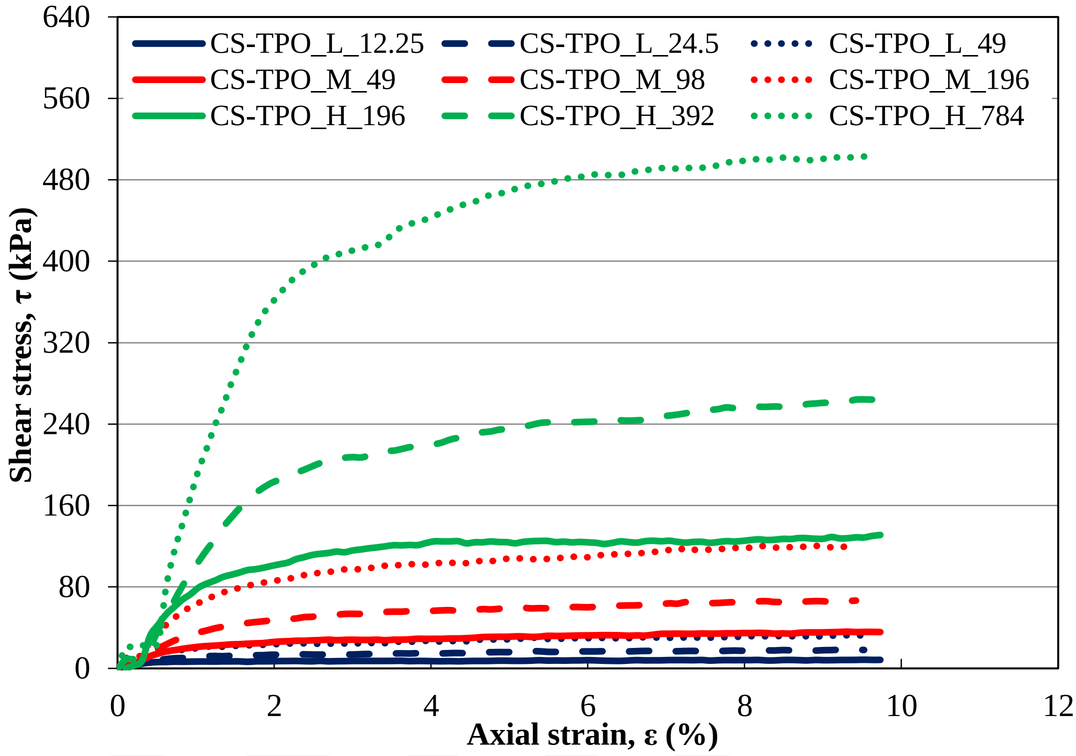

Figure A. 88: Shear stress (τ) – strain (ε) graphs of 8 months AMD cured TPO – CS interface

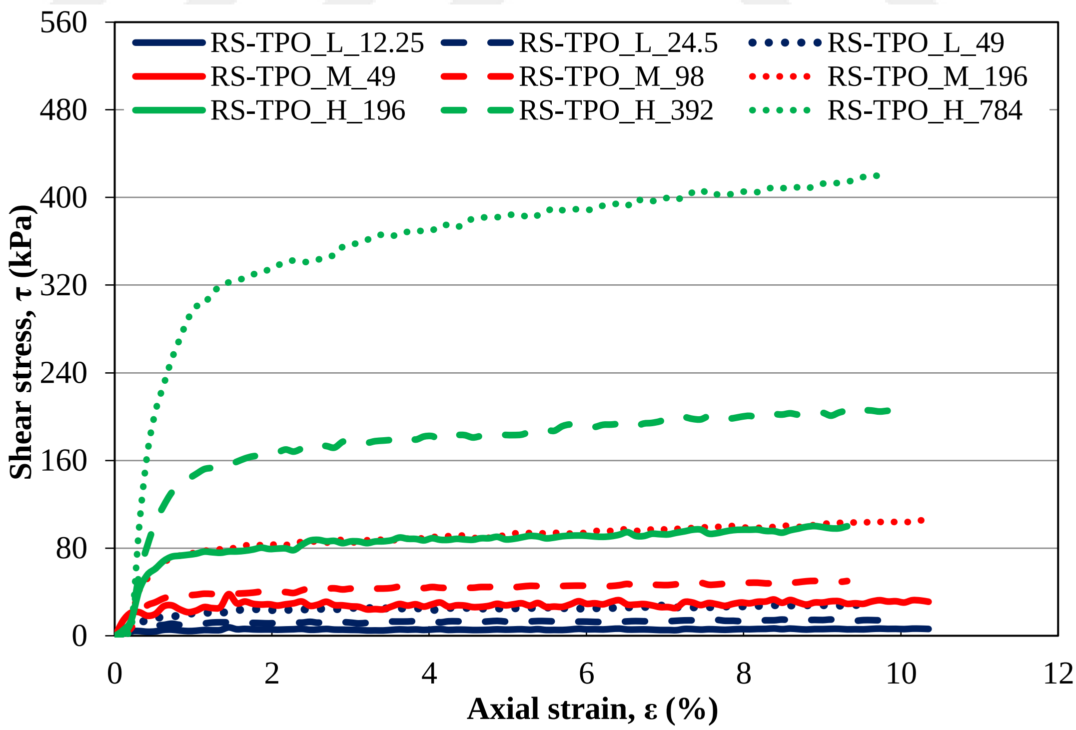

Figure A. 89: Shear stress (τ) – strain (ε) graphs of 8 months AMD cured TPO – RS interface

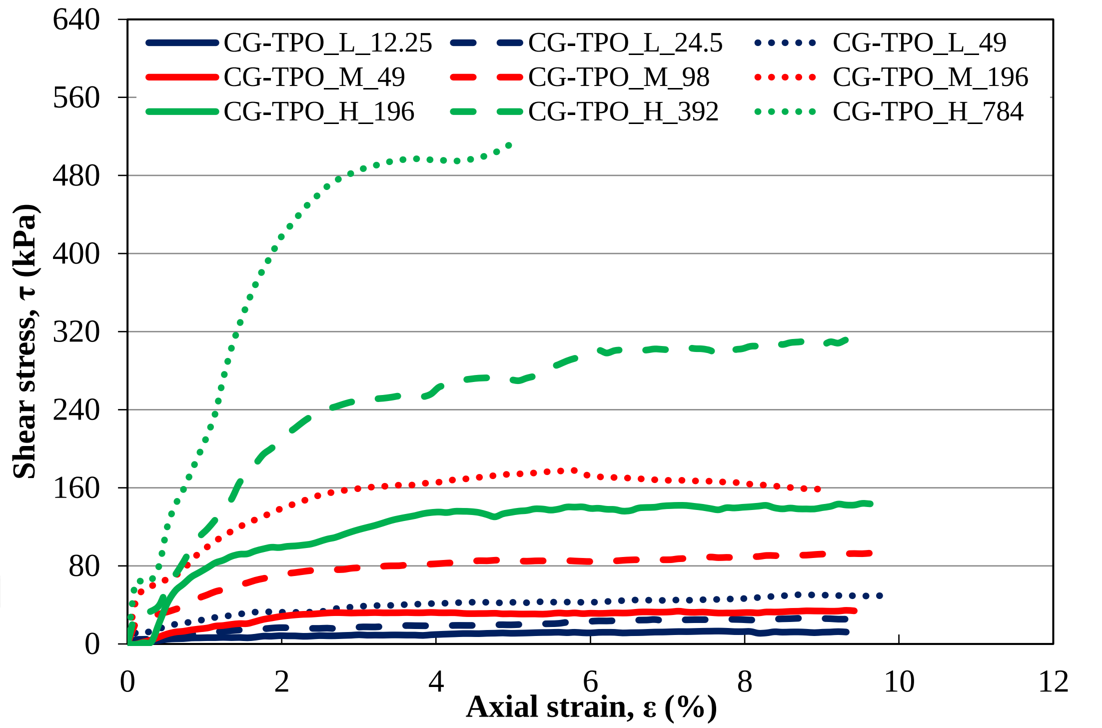

Figure A. 90: Shear stress (τ) – strain (ε) graphs of 8 months AMD cured TPO – CG interface

Interface Direct Shear Test Results for 8 Months CCP Curing

HDPE(S) – soil interfaces

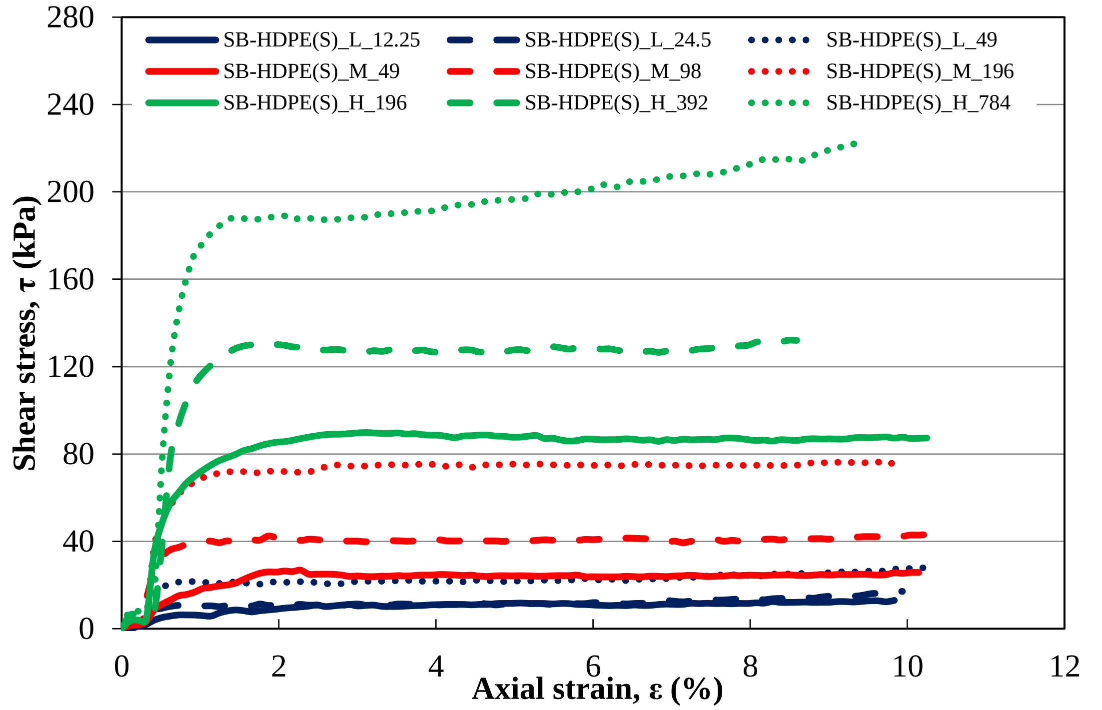

Figure A. 91: Shear stress (τ) – strain (ε) graphs of 8 months CCP cured HDPE(S) – SB interface

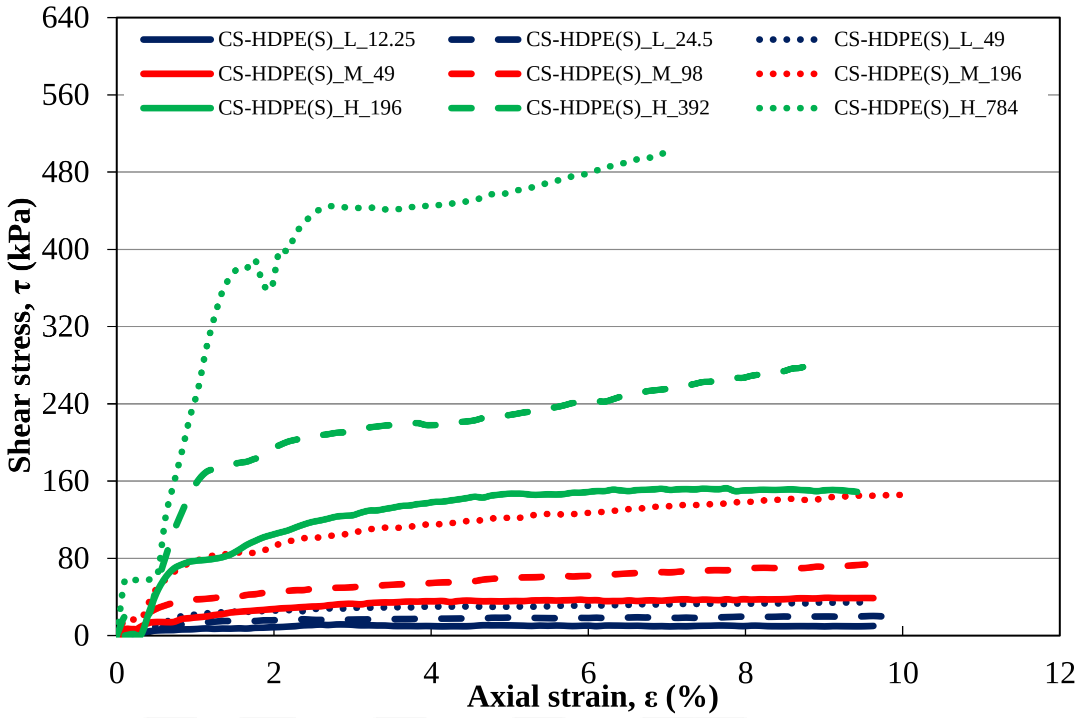

Figure A. 92: Shear stress (τ) – strain (ε) graphs of 8 months CCP cured HDPE(S) – CS interface

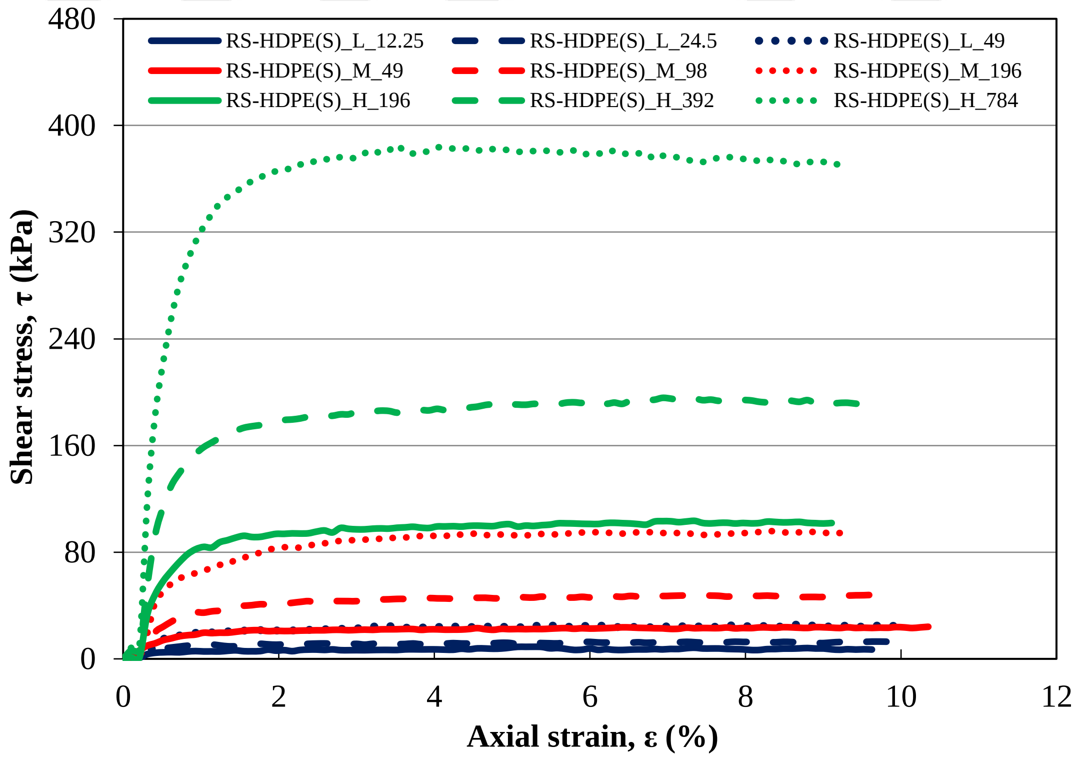

Figure A. 93: Shear stress (τ) – strain (ε) graphs of 8 months CCP cured HDPE(S) – RS interface

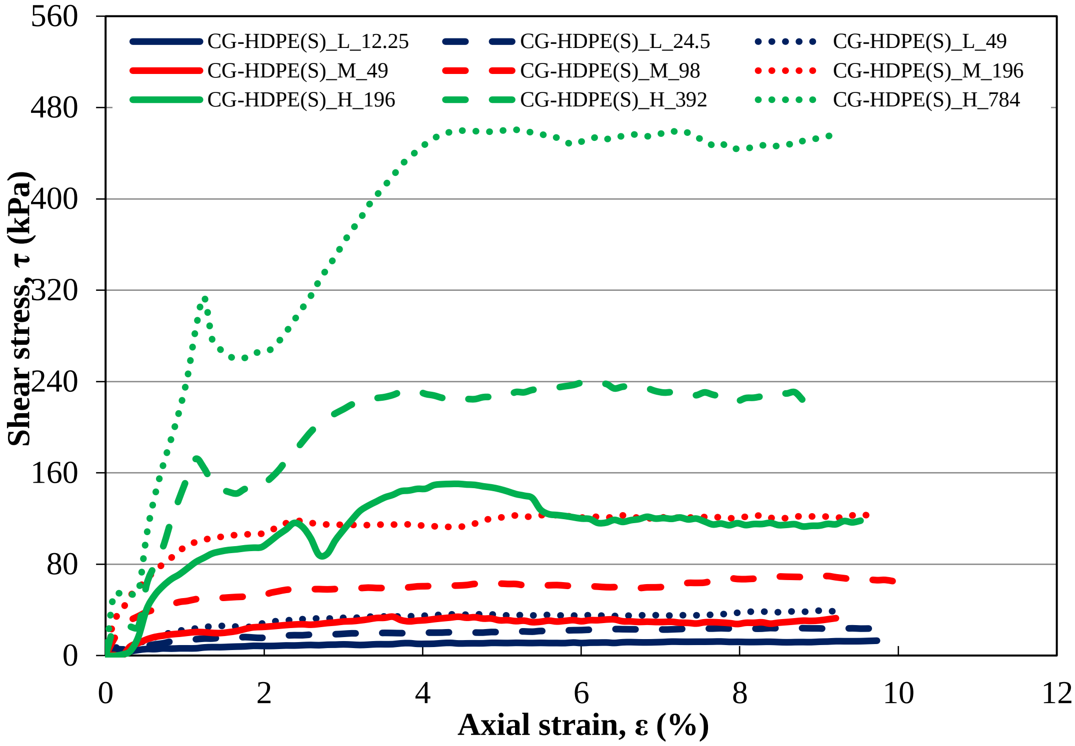

Figure A. 94: Shear stress (τ) – strain (ε) graphs of 8 months CCP cured HDPE(S) – CG interface

HDPE(T) – soil interfaces

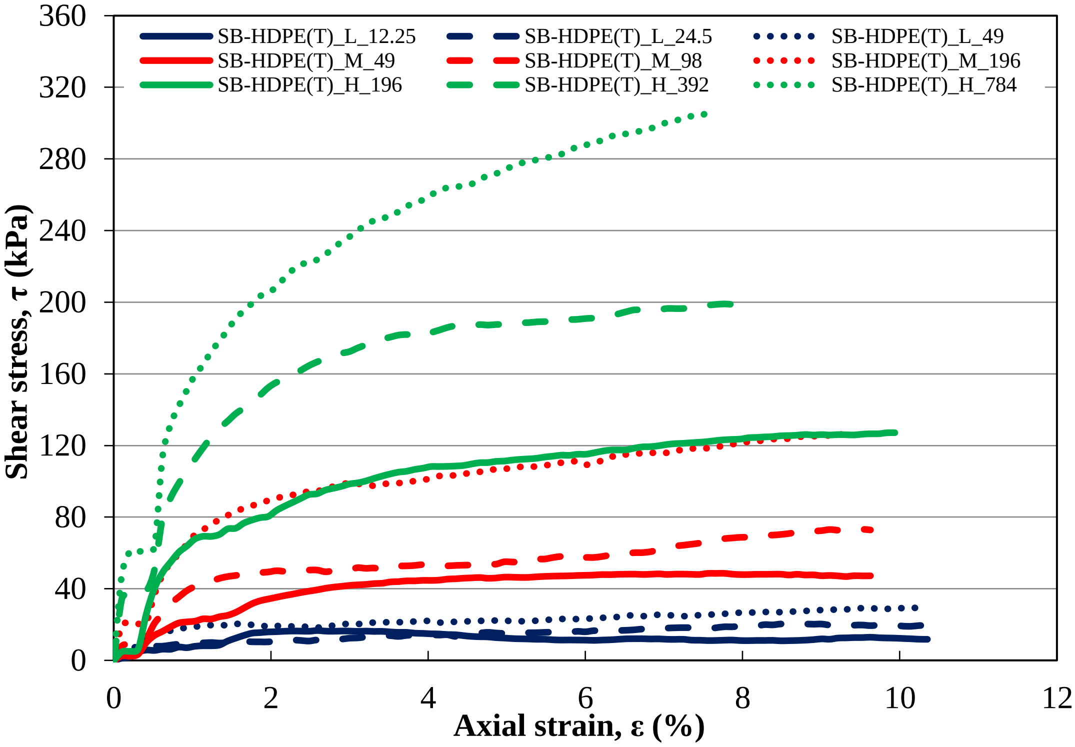

Figure A. 95: Shear stress (τ) – strain (ε) graphs of 8 months CCP cured HDPE(T) – SB interface

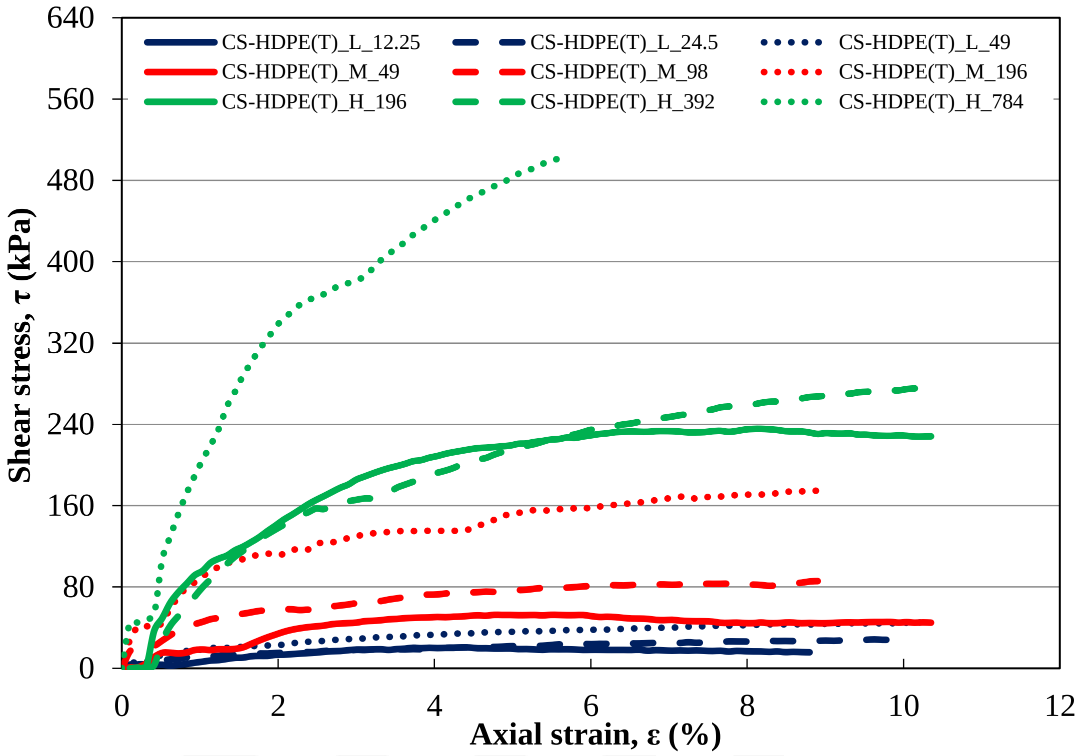

Figure A. 96: Shear stress (τ) – strain (ε) graphs of 8 months CCP cured HDPE(T) – CS interface

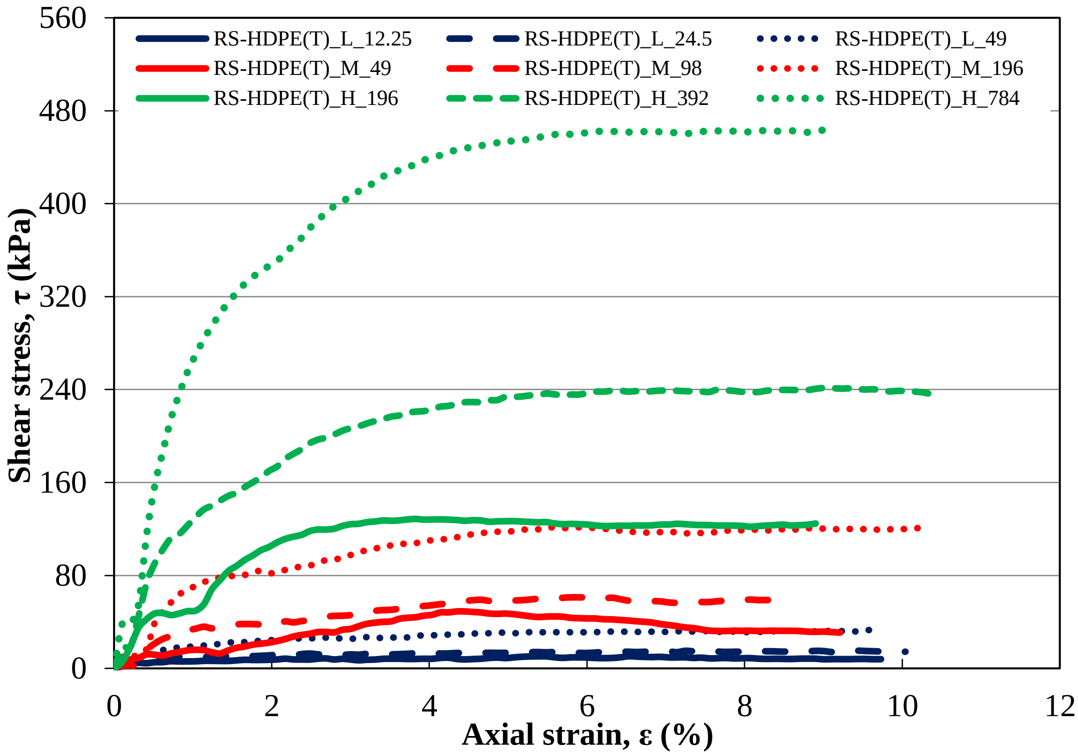

Figure A. 97: Shear stress (τ) – strain (ε) graphs of 8 months CCP cured HDPE(T) – RS interface

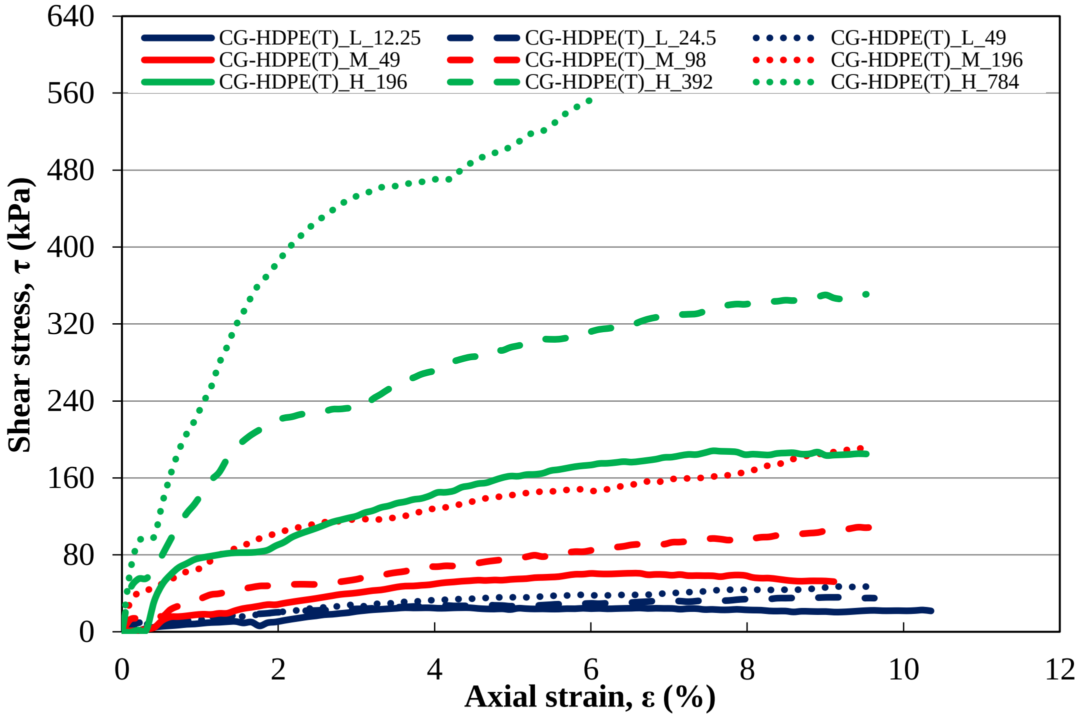

Figure A. 98: Shear stress (τ) – strain (ε) graphs of 8 months CCP cured HDPE(T) – CG interface

TPO – soil interfaces

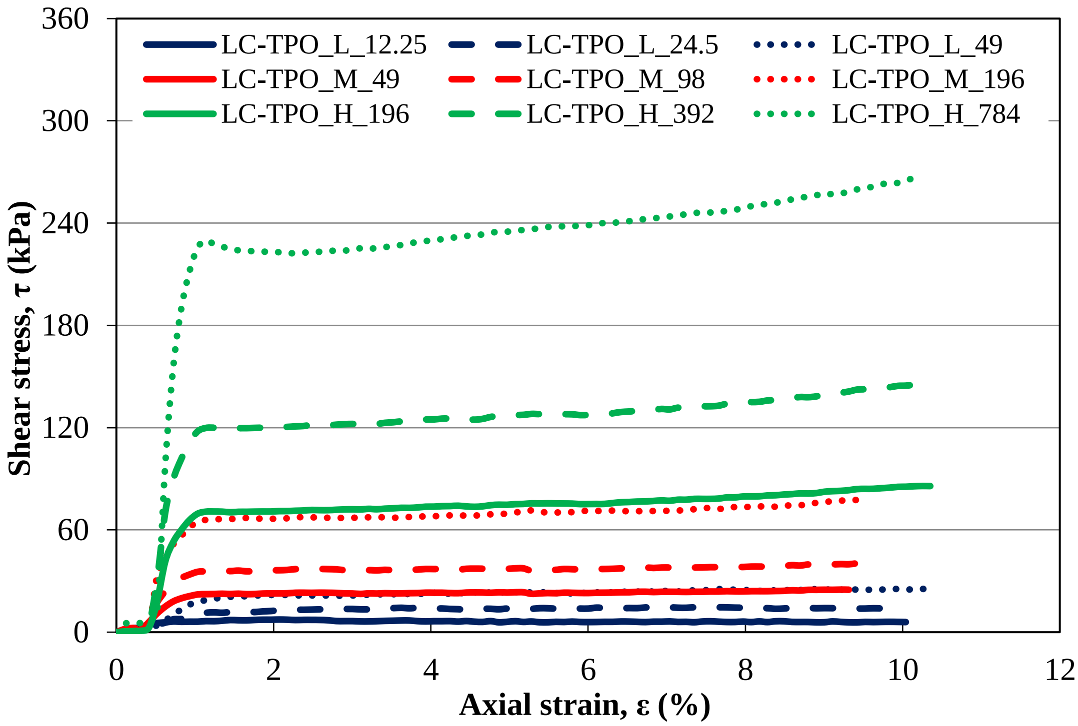

Figure A. 99: Shear stress (τ) – strain (ε) graphs of 8 months CCP cured TPO – LC interface

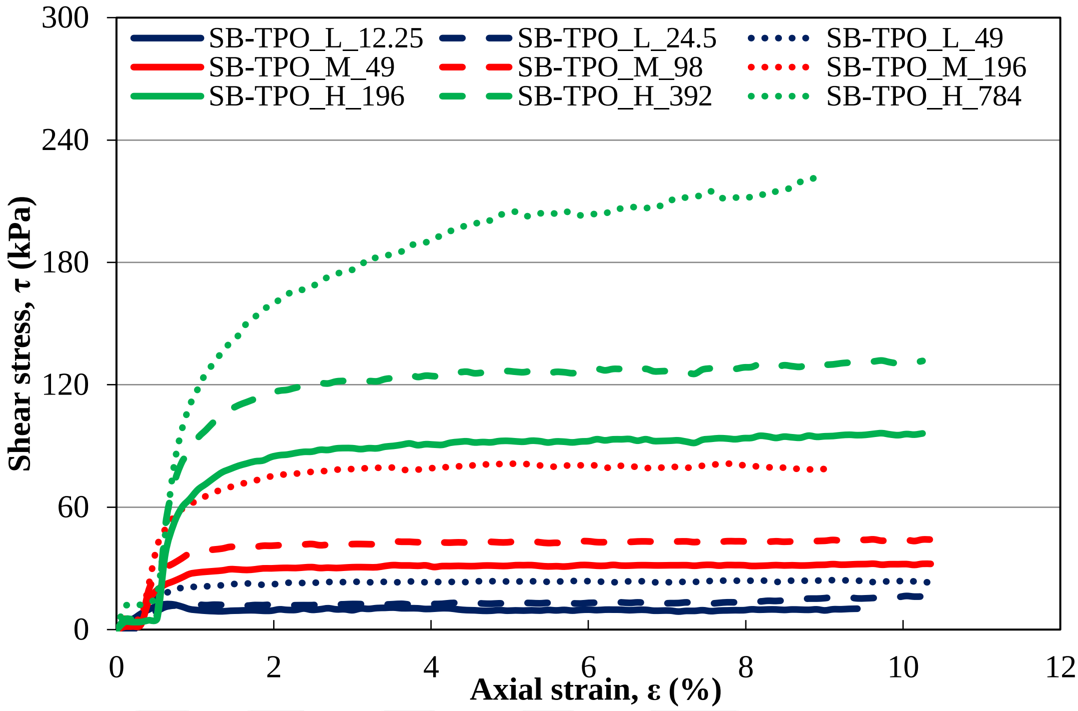

Figure A. 100: Shear stress (τ) – strain (ε) graphs of 8 months CCP cured TPO – SB interface

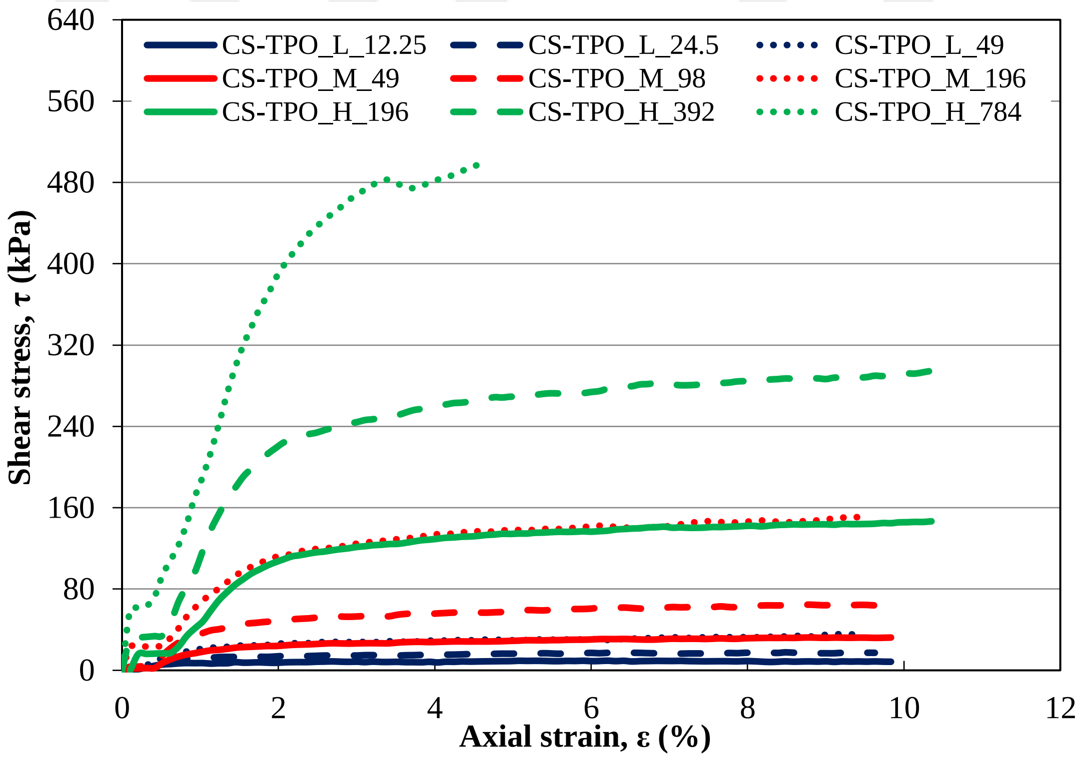

Figure A. 101: Shear stress (τ) – strain (ε) graphs of 8 months CCP cured TPO – CS interface

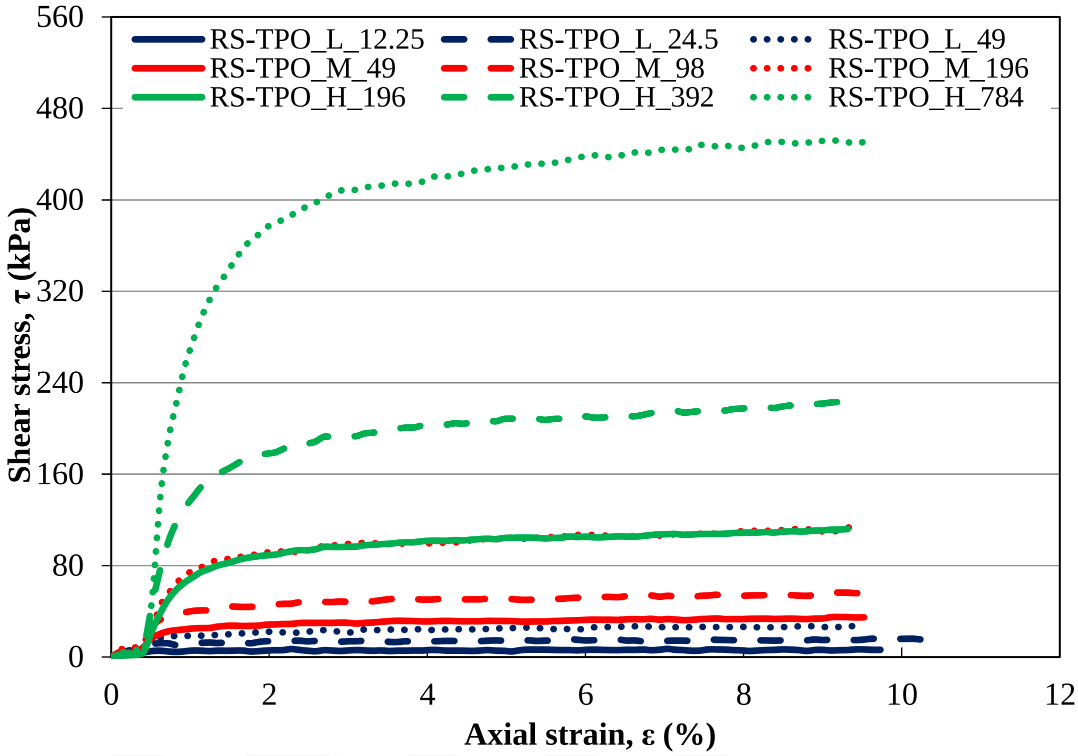

Figure A. 102: Shear stress (τ) – strain (ε) graphs of 8 months CCP cured TPO – RS interface

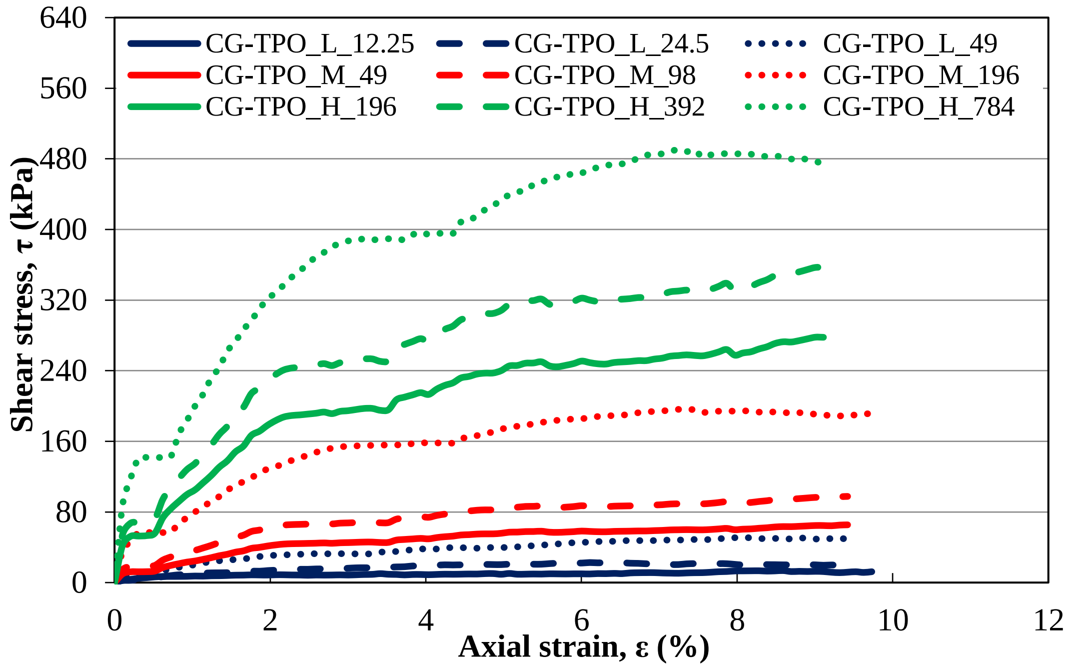

Figure A. 103: Shear stress (τ) – strain (ε) graphs of 8 months CCP cured TPO – CG interface

Interface Direct Shear Test Results for 8 Months MSW Curing

HDPE(S) – soil interfaces

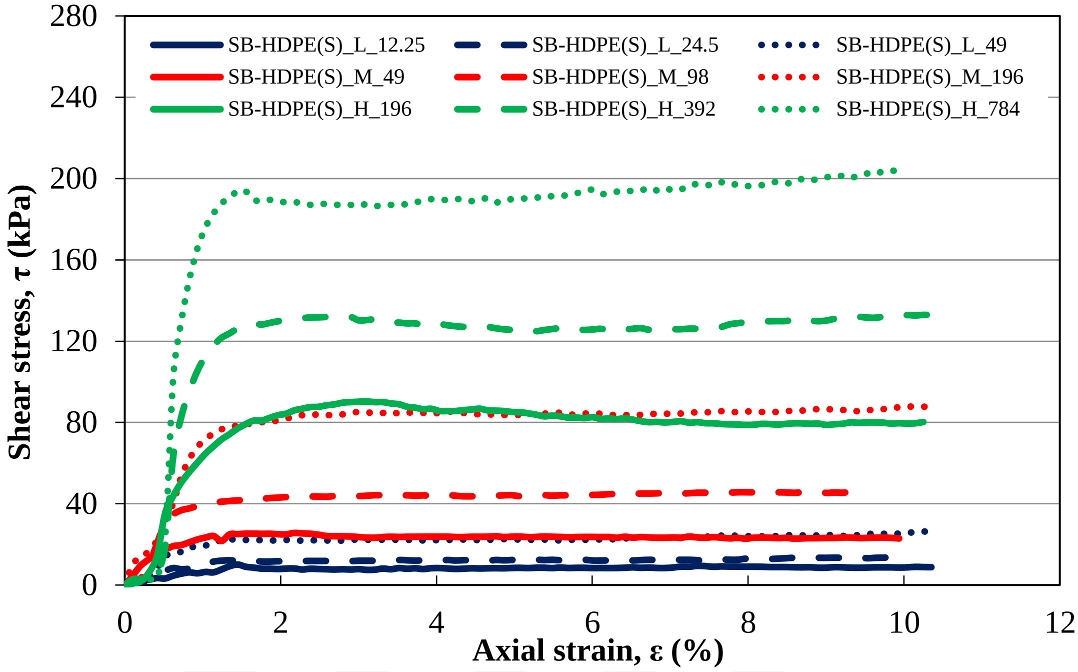

Figure A. 104 : Shear stress (τ) – strain (ε) graphs of 8 months MSW cured HDPE(S) – SB interface

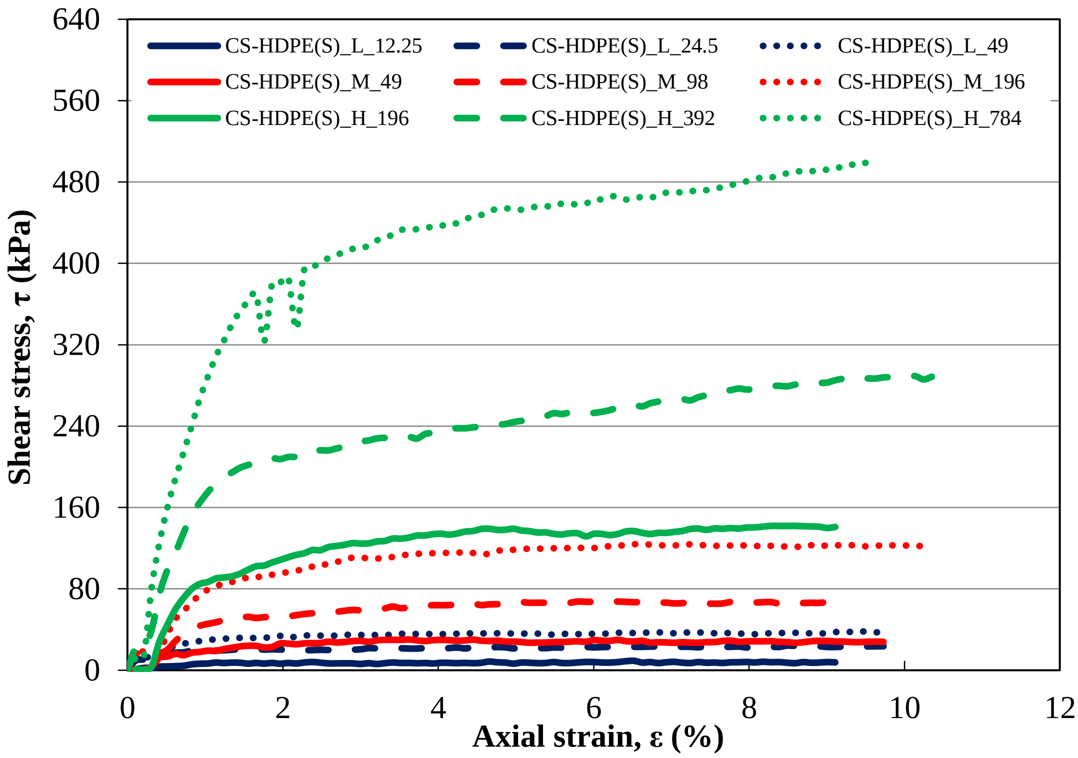

Figure A. 105: Shear stress (τ) – strain (ε) graphs of 8 months MSW cured HDPE(S) – CS interface

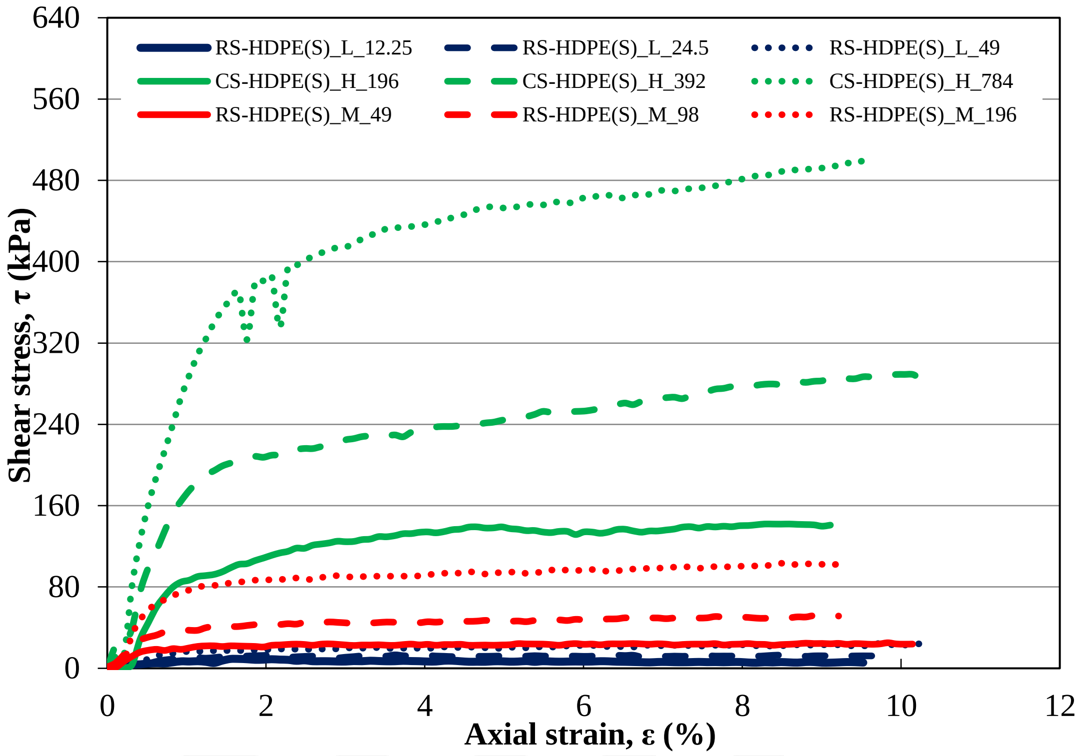

Figure A. 106: Shear stress (τ) – strain (ε) graphs of 8 months MSW cured HDPE(S) – RS interface

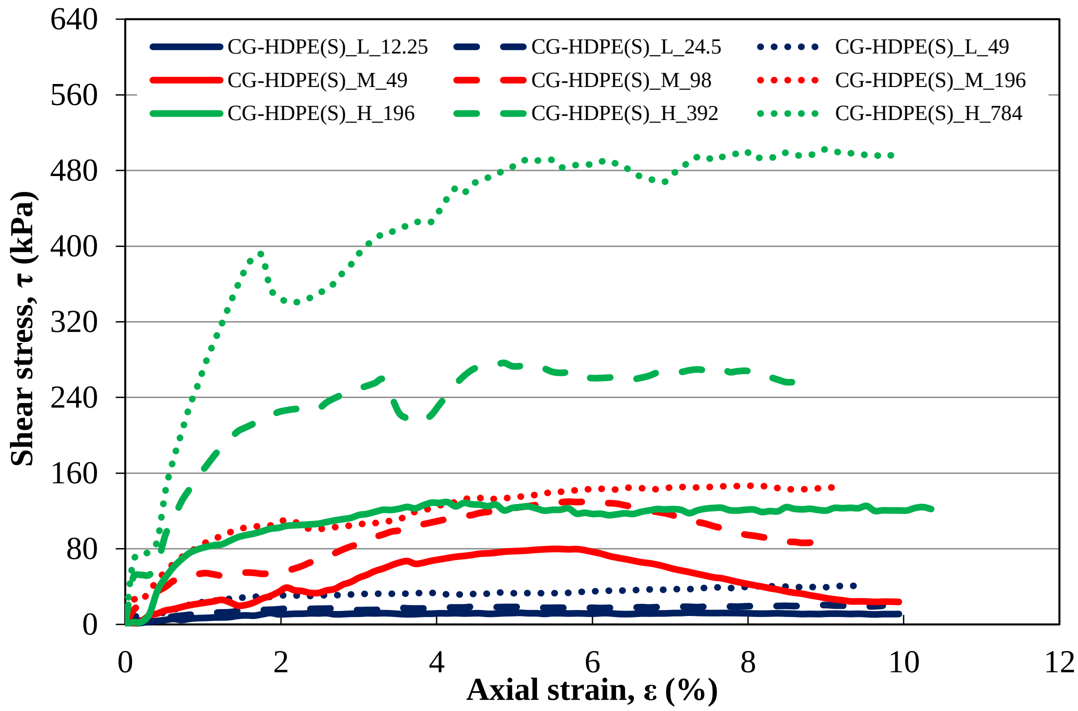

Figure A. 107: Shear stress (τ) – strain (ε) graphs of 8 months MSW cured HDPE(S) – CG interface

HDPE(T) – soil interfaces

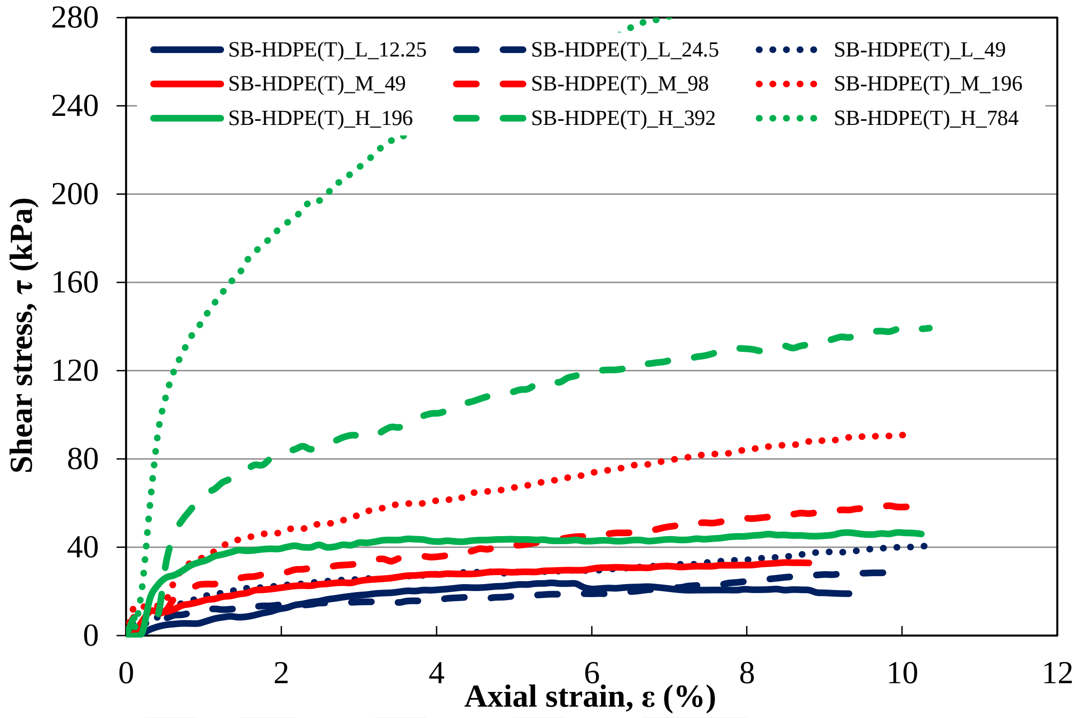

Figure A. 108: Shear stress (τ) – strain (ε) graphs of 8 months MSW cured HDPE(T) – SB interface

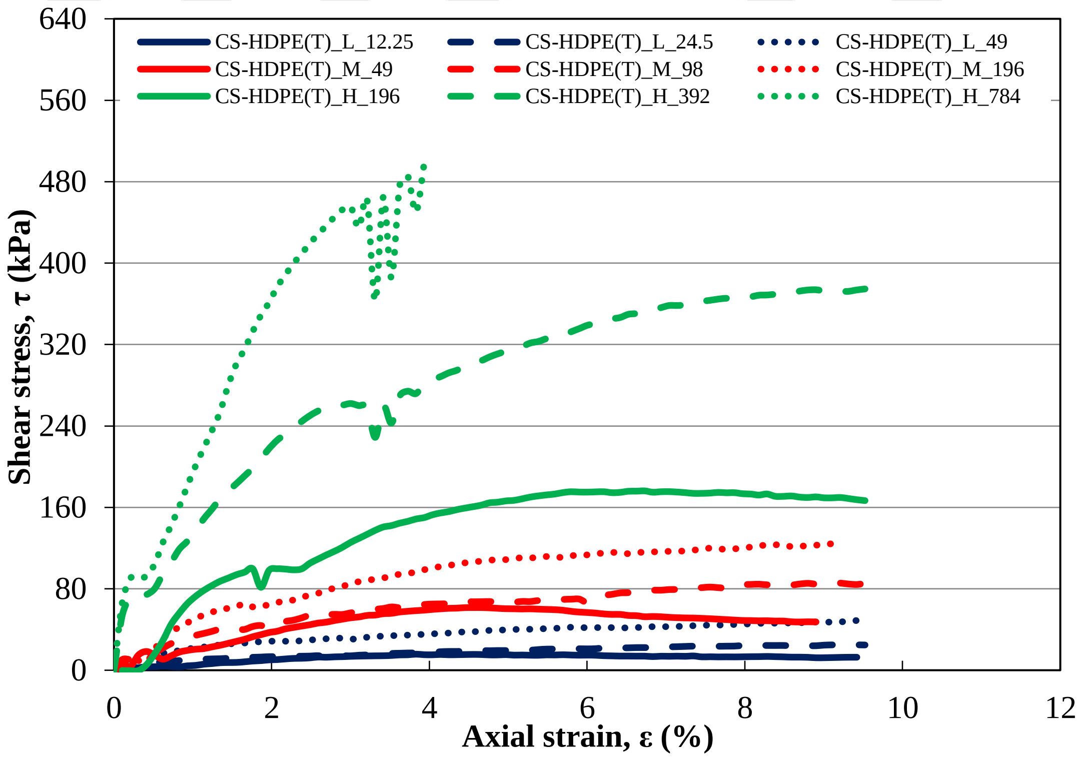

Figure A. 109: Shear stress (τ) – strain (ε) graphs of 8 months MSW cured HDPE(T) – CS interface

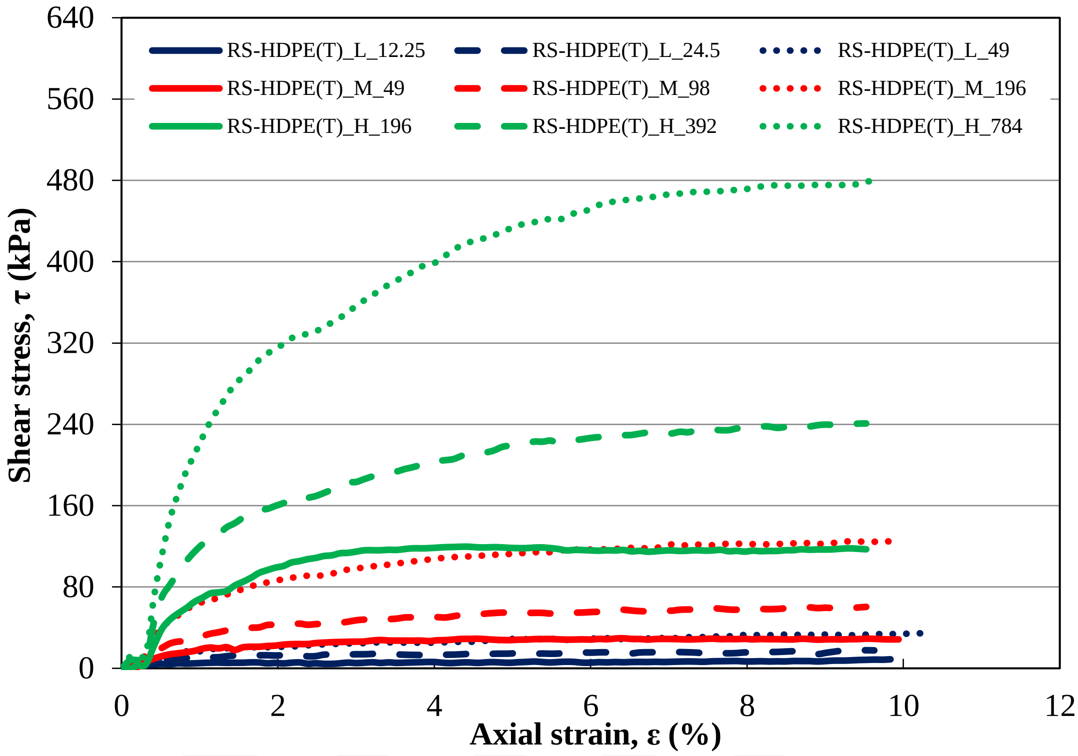

Figure A. 110: Shear stress (τ) – strain (ε) graphs of 8 months MSW cured HDPE(T) – RS interface

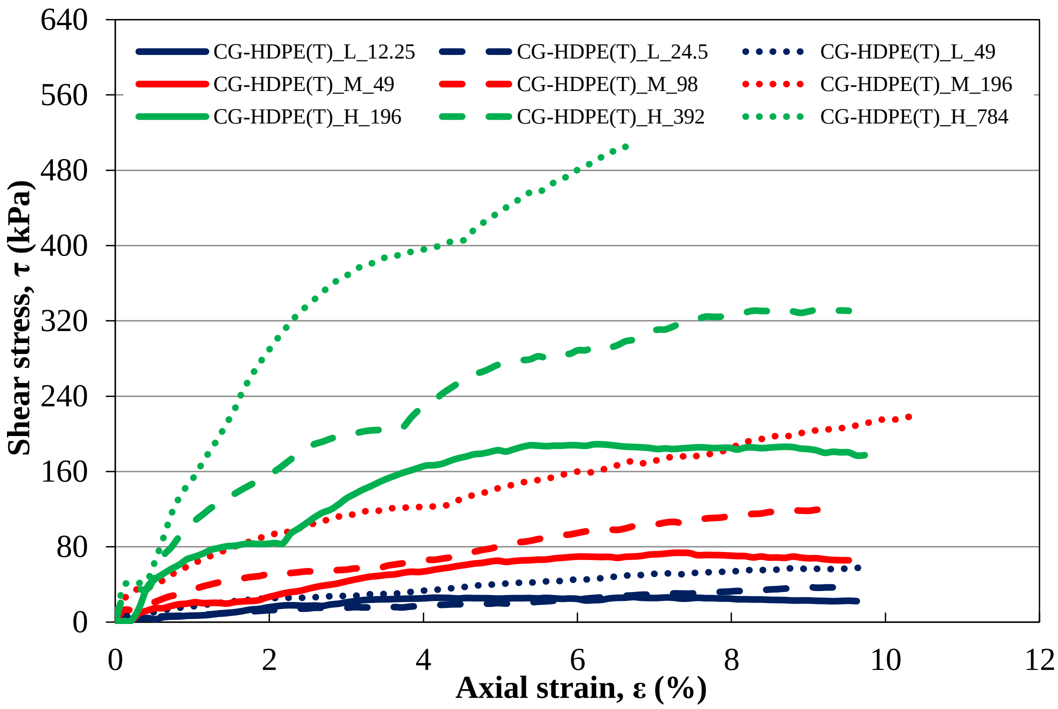

Figure A. 111: Shear stress (τ) – strain (ε) graphs of 8 months MSW cured HDPE(T) – CG interface

TPO – soil interfaces

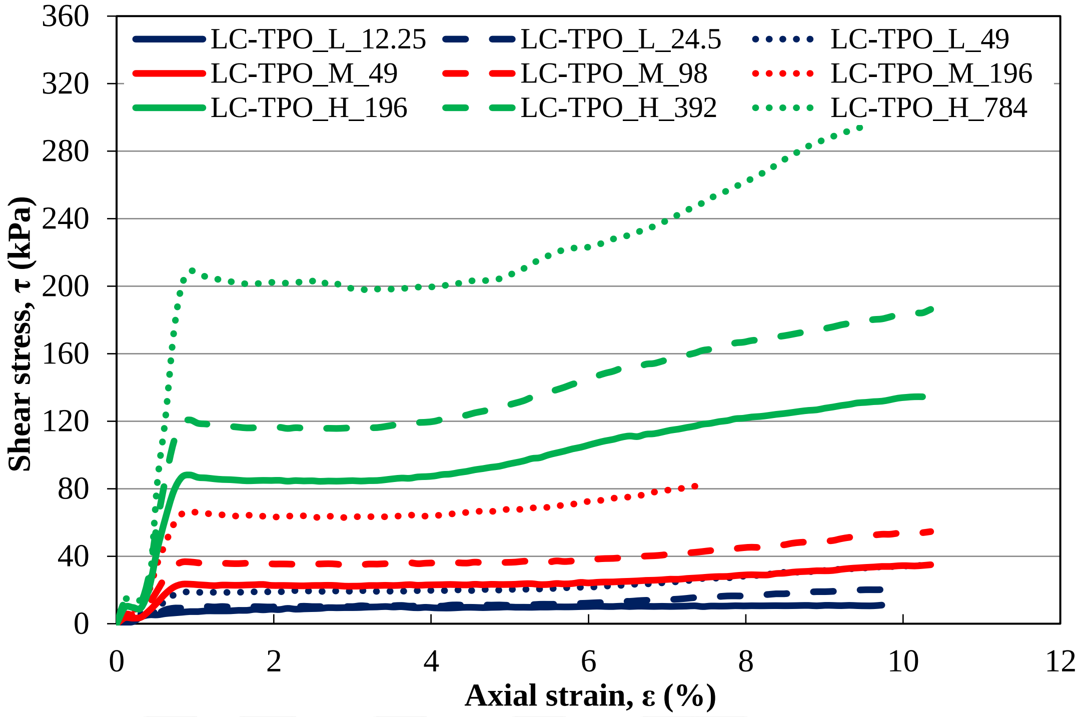

Figure A. 112: Shear stress (τ) – strain (ε) graphs of 8 months MSW cured TPO – LC interface

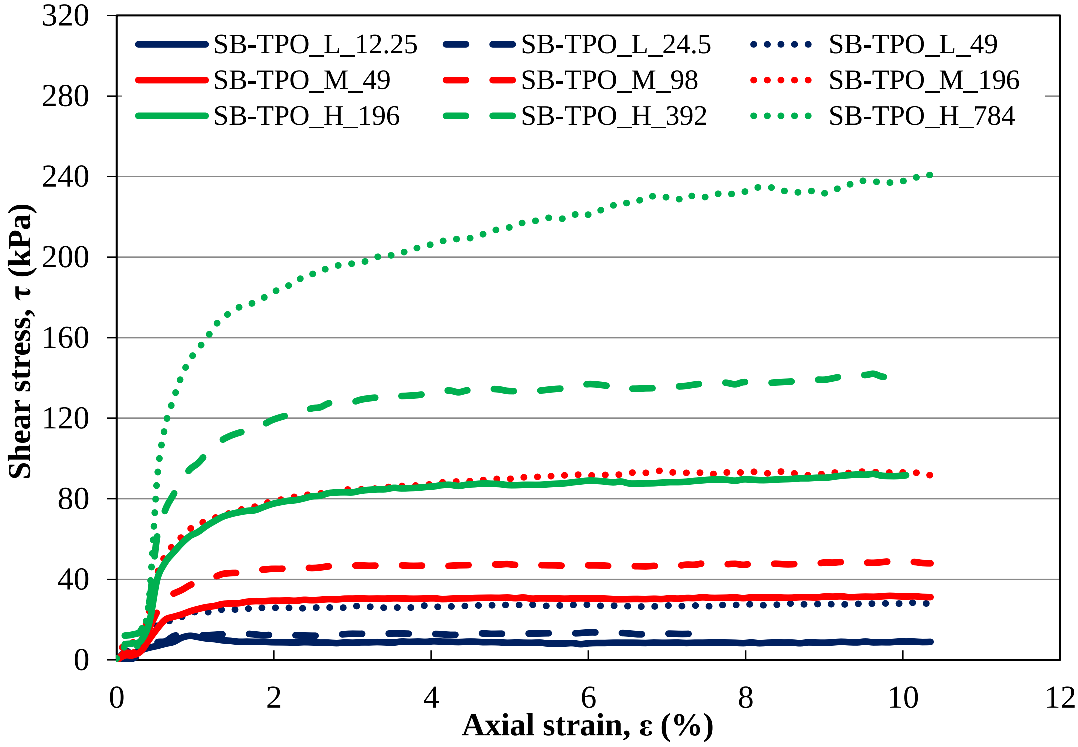

Figure A. 113: Shear stress (τ) – strain (ε) graphs of 8 months MSW cured TPO – SB interface

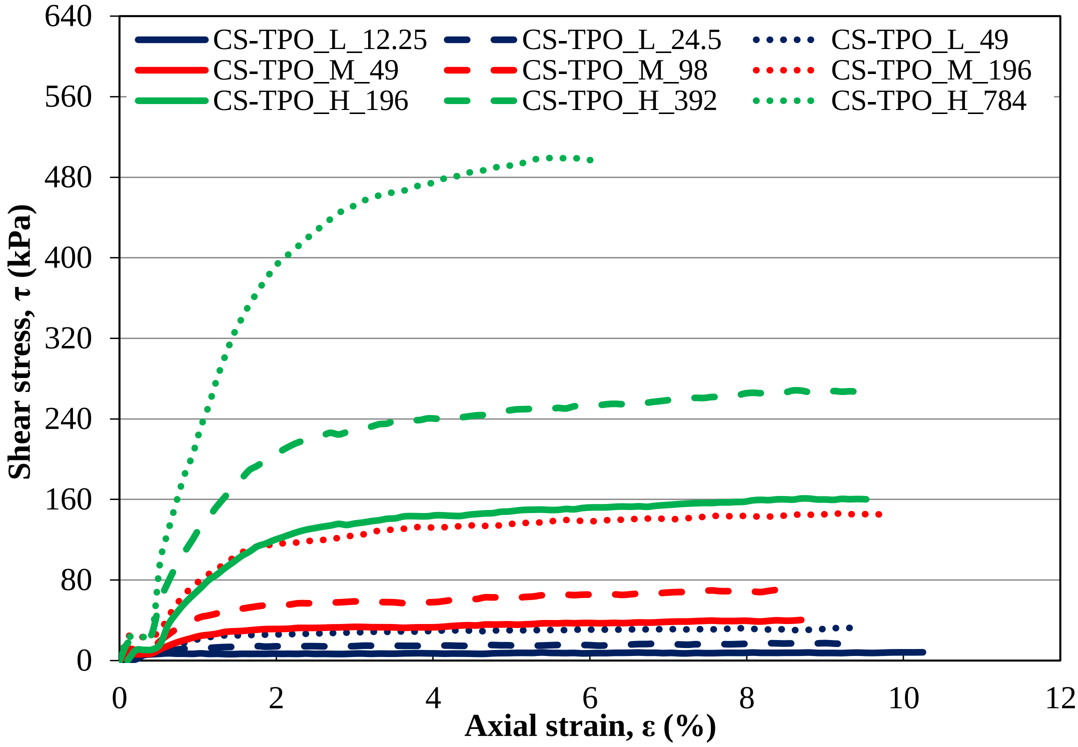

Figure A. 114: Shear stress (τ) – strain (ε) graphs of 8 months MSW cured TPO – CS interface

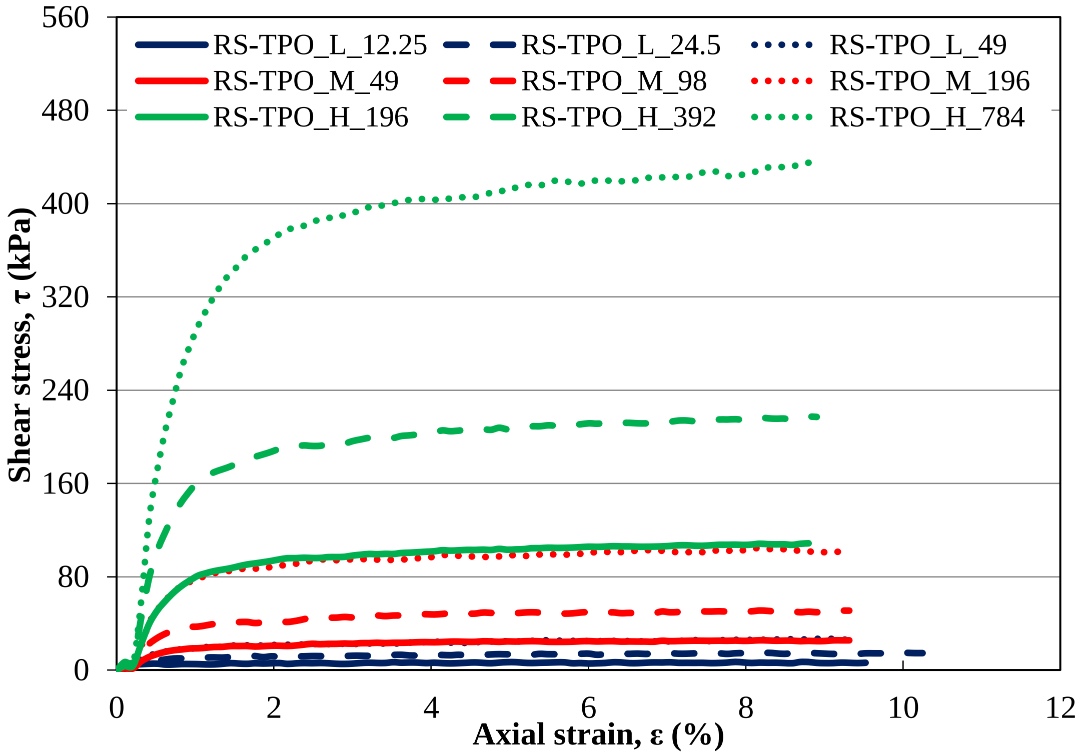

Figure A. 115: Shear stress (τ) – strain (ε) graphs of 8 months MSW cured TPO – RS interface

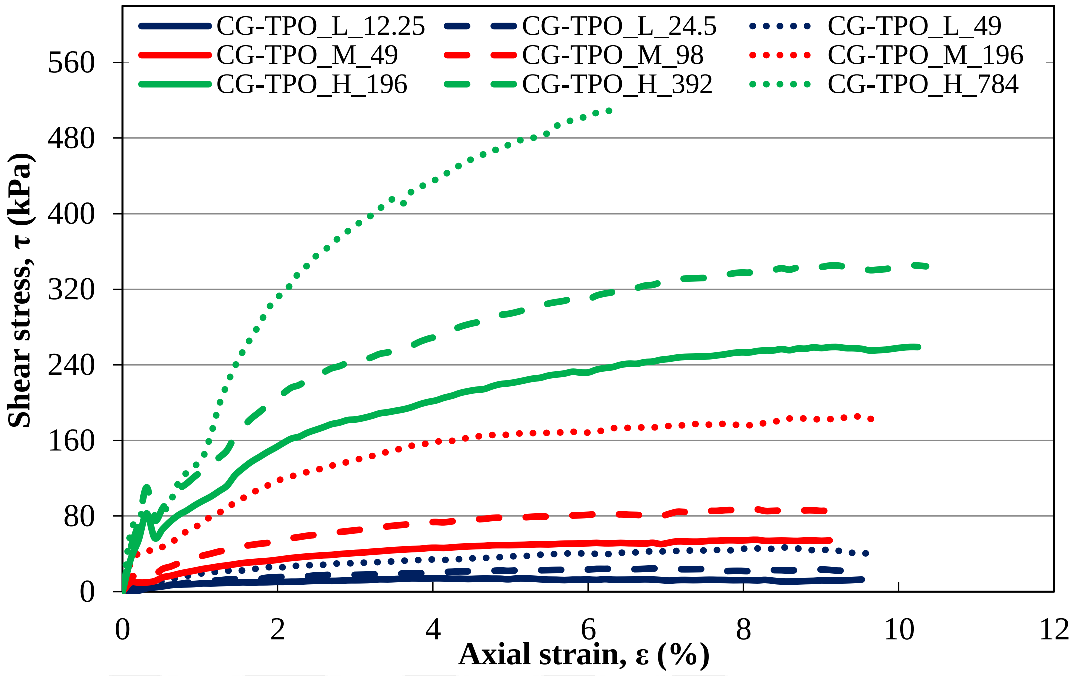

Figure A. 116: Shear stress (τ) – strain (ε) graphs of 8 months MSW cured TPO – CG interface

Interface Direct Shear Test Results for 16 Months SWt Curing

PVC(1.5) – soil interfaces

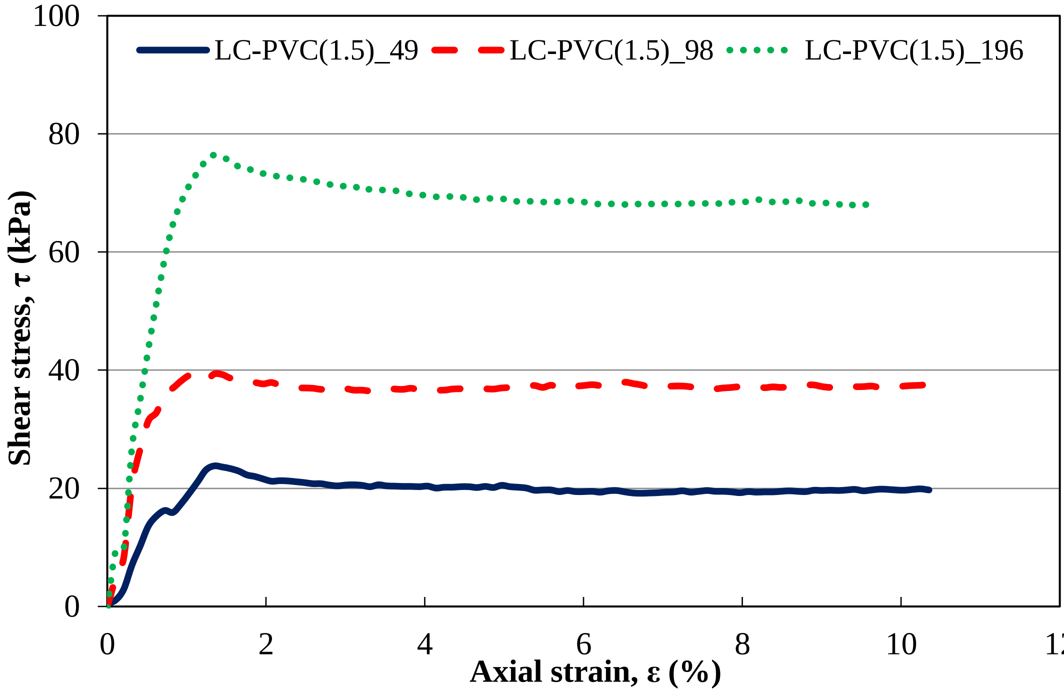

Figure A. 117: Shear stress (τ) – strain (ε) graphs of 16 months SWt cured PVC(1.5) – LC interface

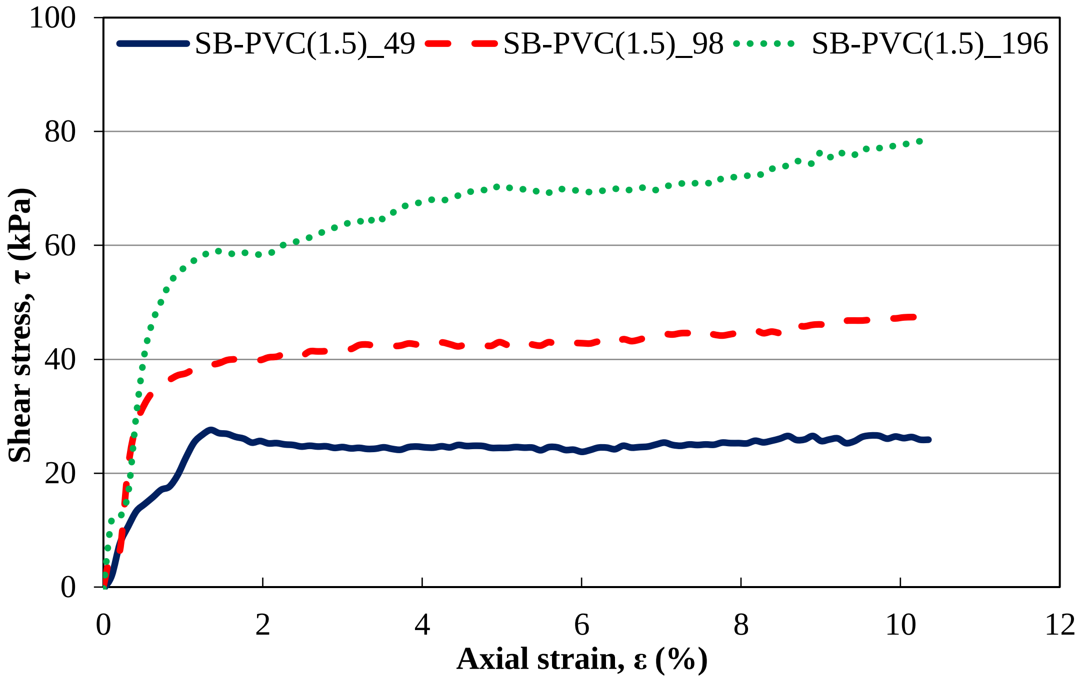

Figure A. 118: Shear stress (τ) – strain (ε) graphs of 16 months SWt cured PVC(1.5) – SB interface

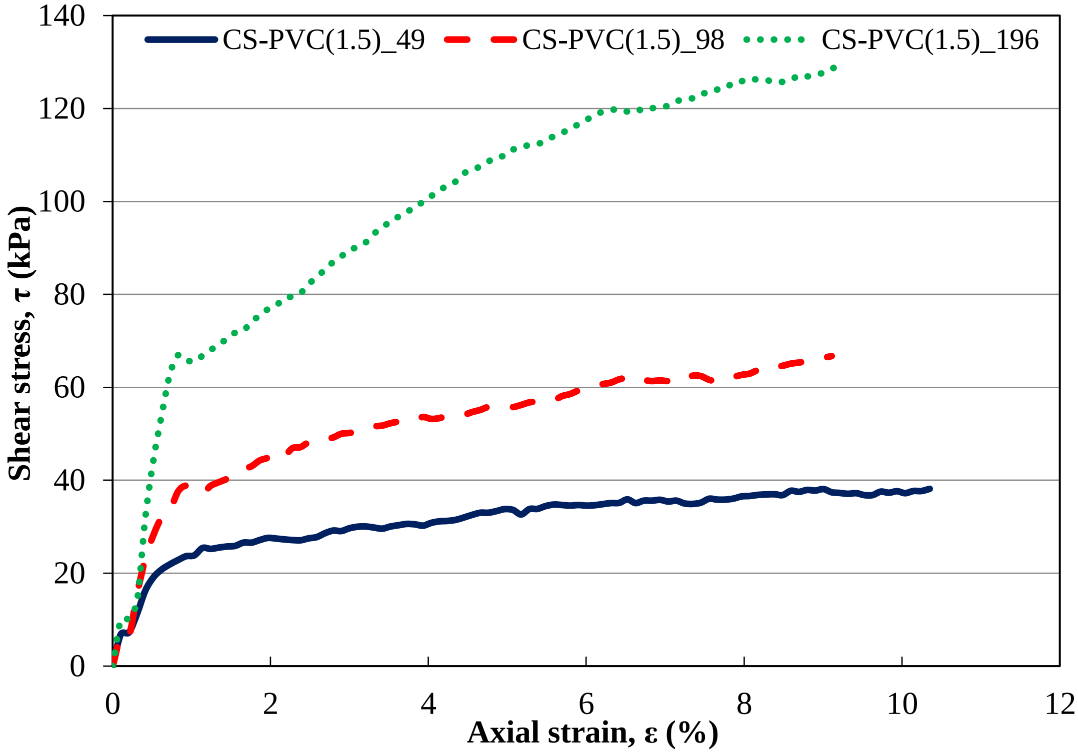

Figure A. 119: Shear stress (τ) – strain (ε) graphs of 16 months SWt cured PVC(1.5) – CS interface

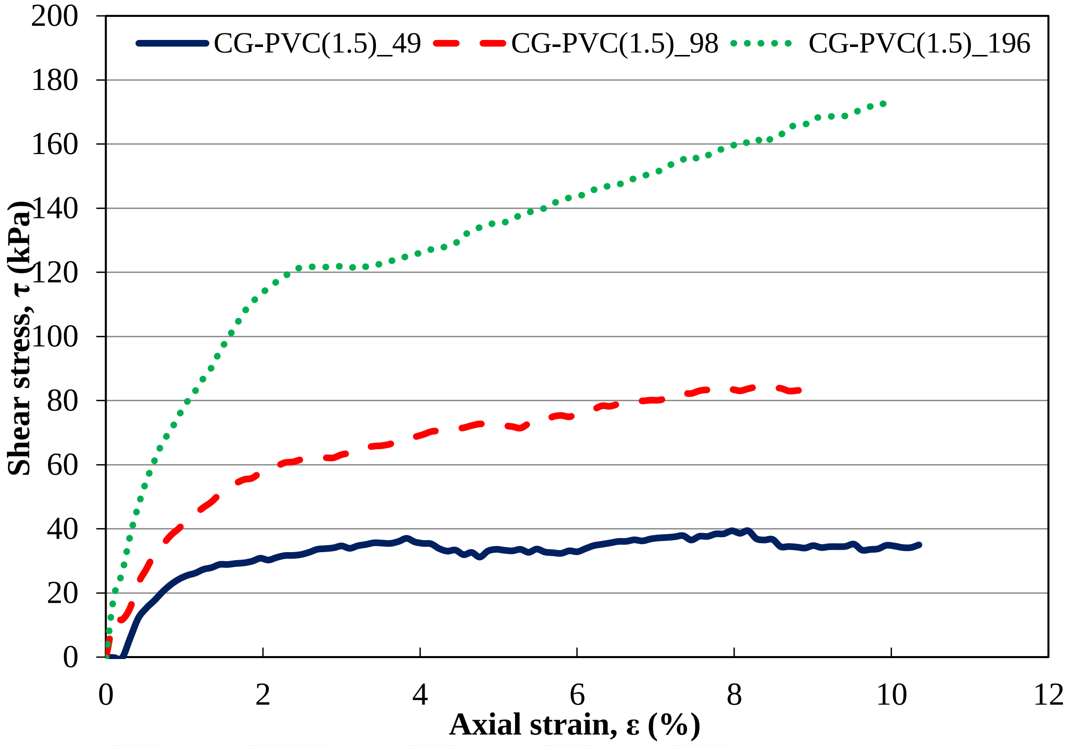

Figure A. 120: Shear stress (τ) – strain (ε) graphs of 16 months SWt cured PVC(1.5) – CG interface

PVC(3.0) – soil interfaces

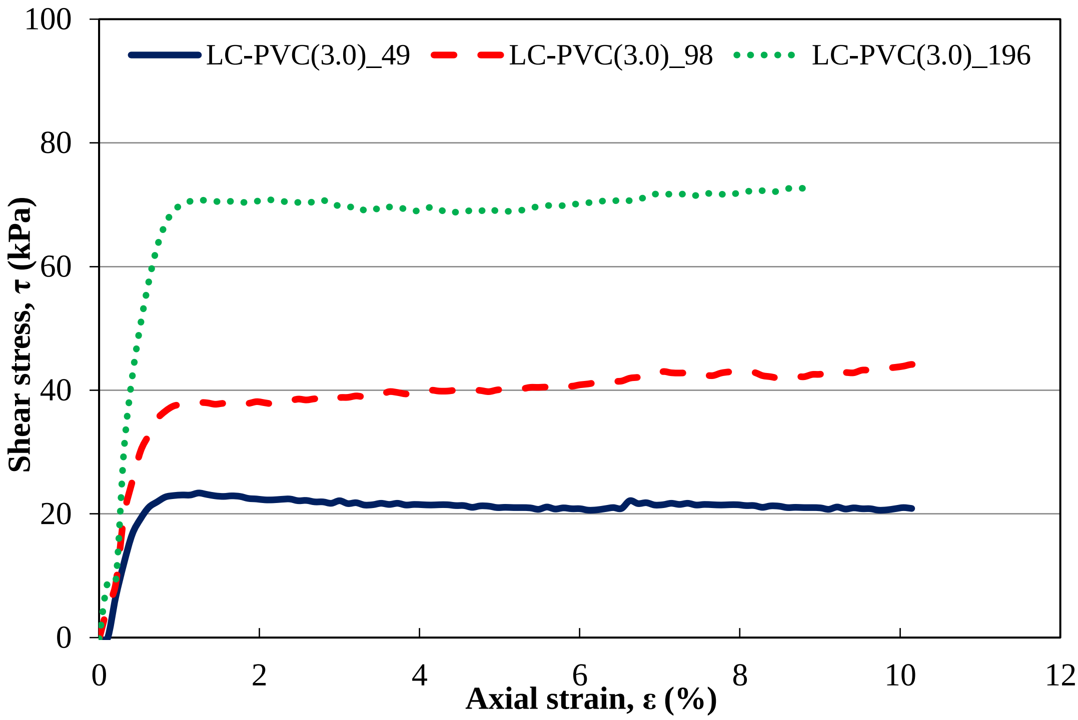

Figure A. 121: Shear stress (τ) – strain (ε) graphs of 16 months SWt cured PVC(3.0) – LC interface

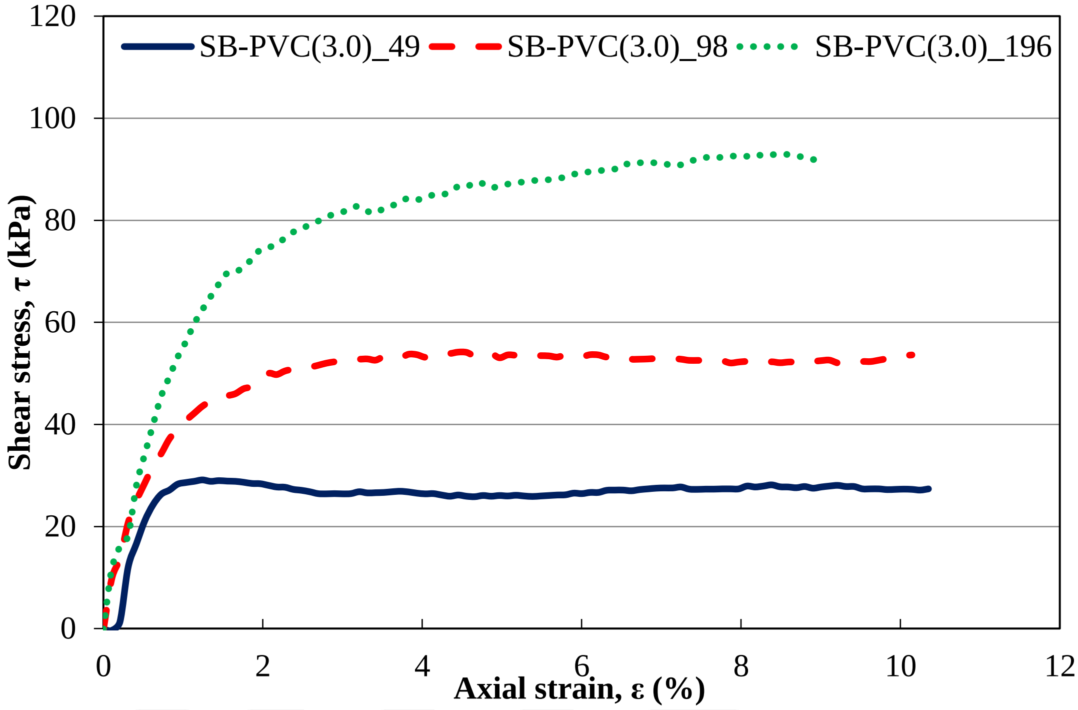

Figure A. 122: Shear stress (τ) – strain (ε) graphs of 16 months SWt cured PVC(3.0) – SB interface

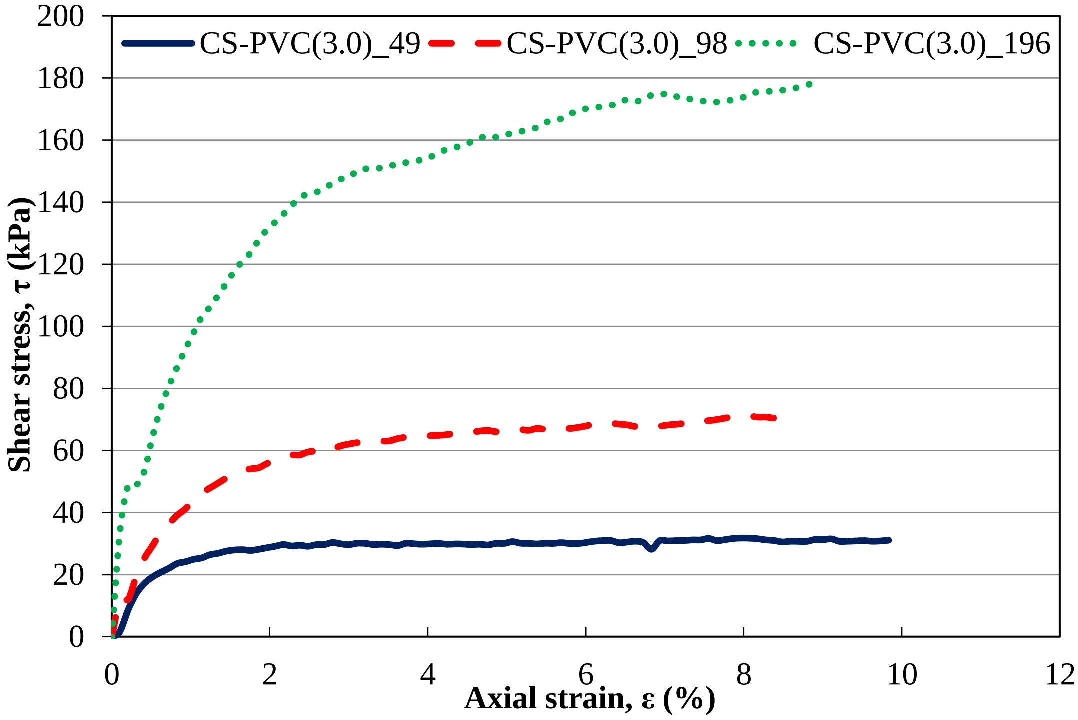

Figure A. 123: Shear stress (τ) – strain (ε) graphs of 16 months SWt cured PVC(3.0) – CS interface

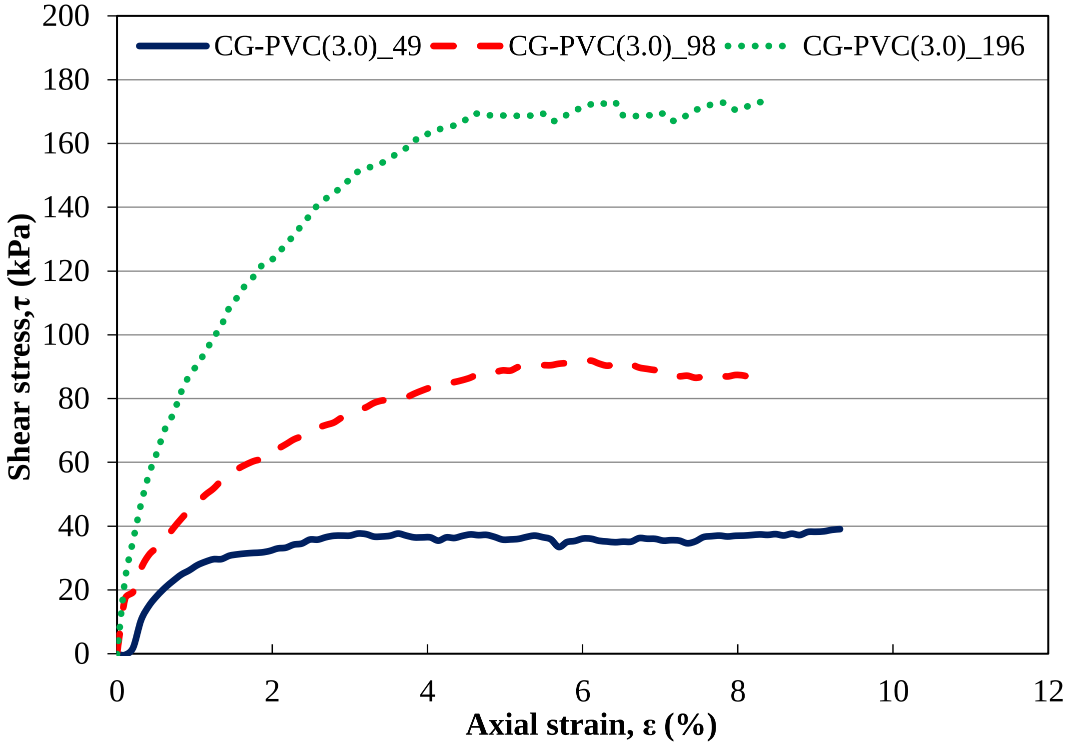

Figure A. 124: Shear stress (τ) – strain (ε) graphs of 16 months SWt cured PVC(3.0) – CG interface

TPO – soil interfaces

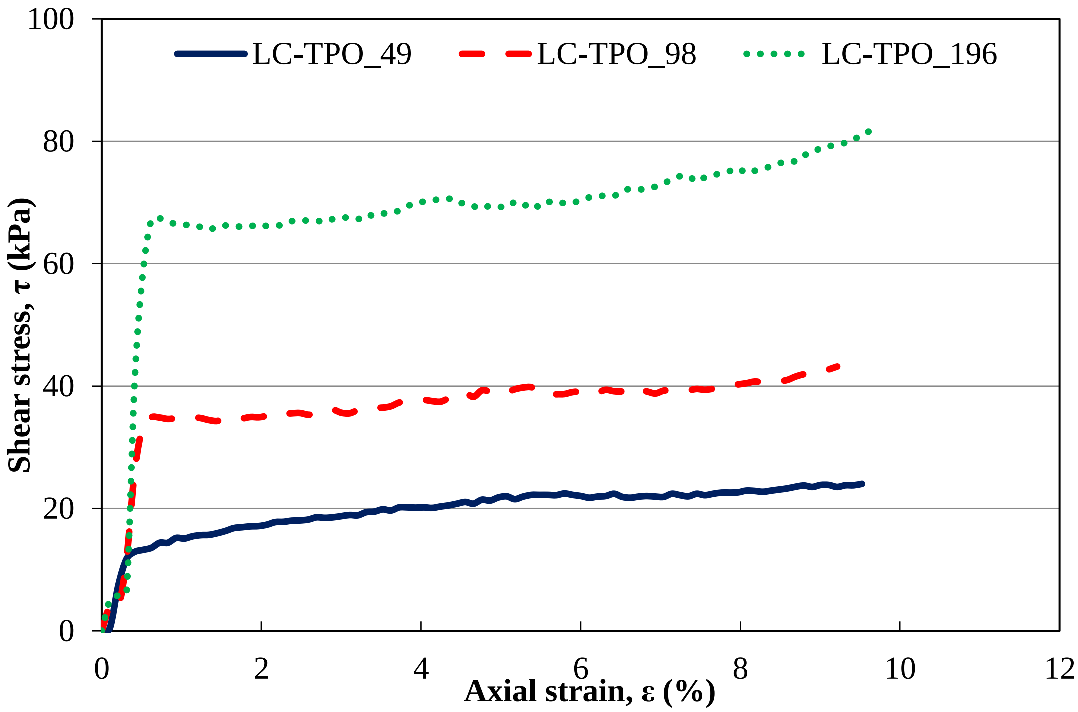

Figure A. 125: Shear stress (τ) – strain (ε) graphs of 16 months SWt cured TPO – LC interface

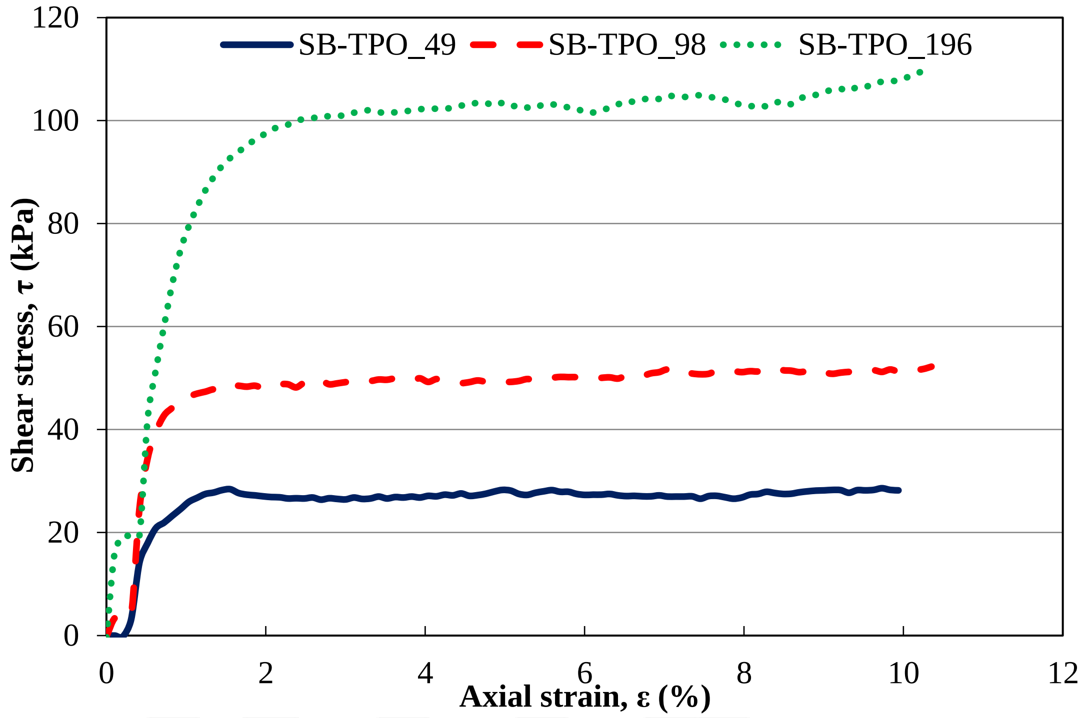

Figure A. 126: Shear stress (τ) – strain (ε) graphs of 16 months SWt cured TPO – SB interface

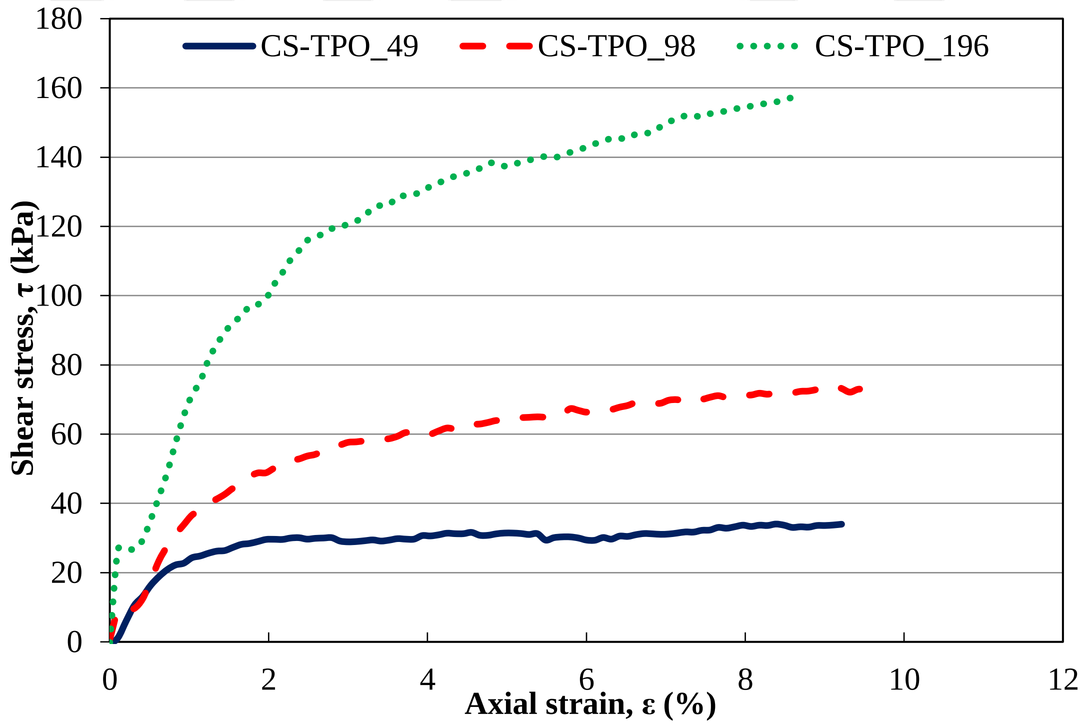

Figure A. 127: Shear stress (τ) – strain (ε) graphs of 16 months SWt cured TPO – CS interface

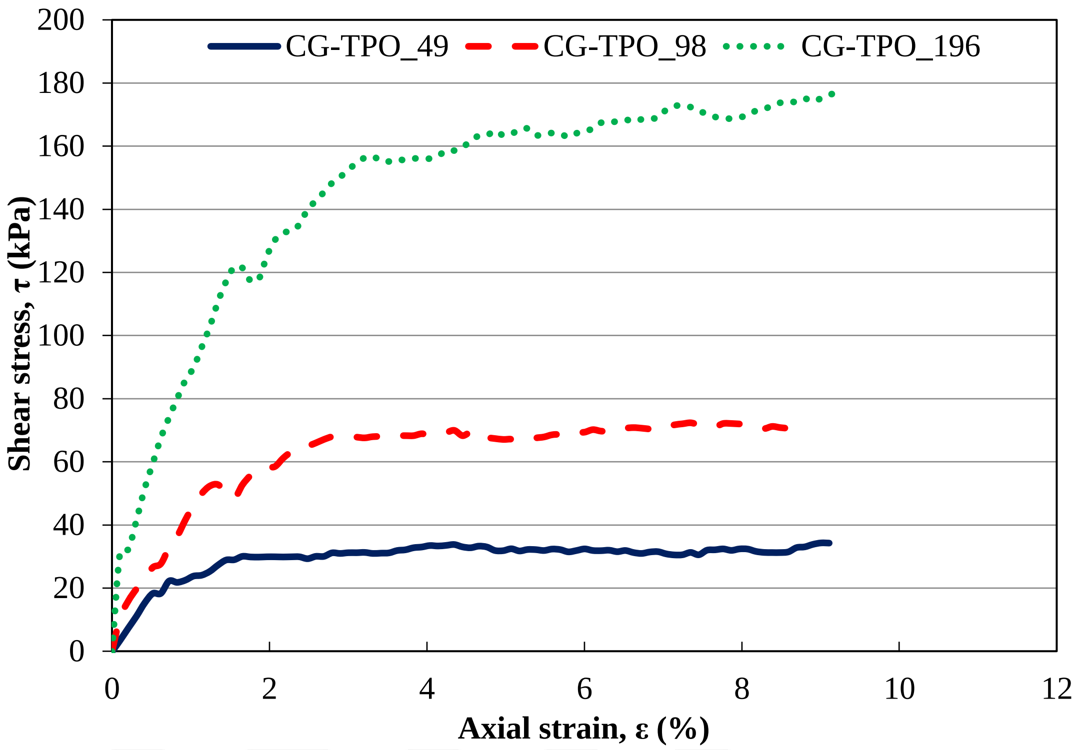

Figure A. 128: Shear stress (τ) – strain (ε) graphs of 16 months SWt cured TPO – CG interface

Interface Direct Shear Test Results for 16 Months AMD Curing

HDPE(S) – soil interfaces

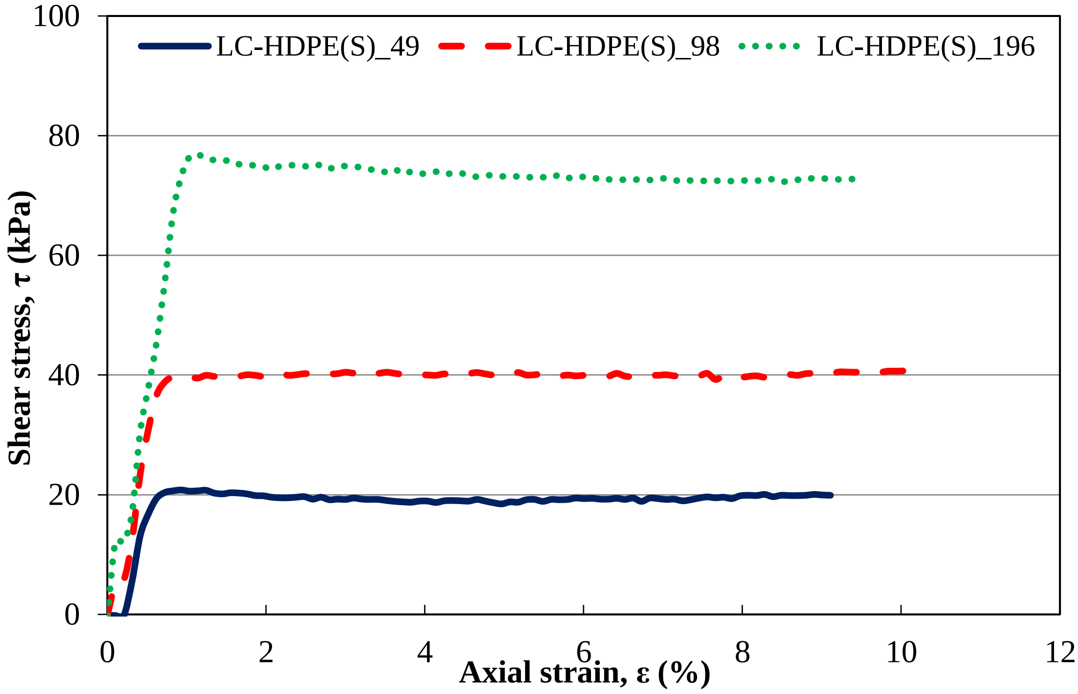

Figure A. 129: Shear stress (τ) – strain (ε) graphs of 16 months AMD cured HDPE(S) – LC interface

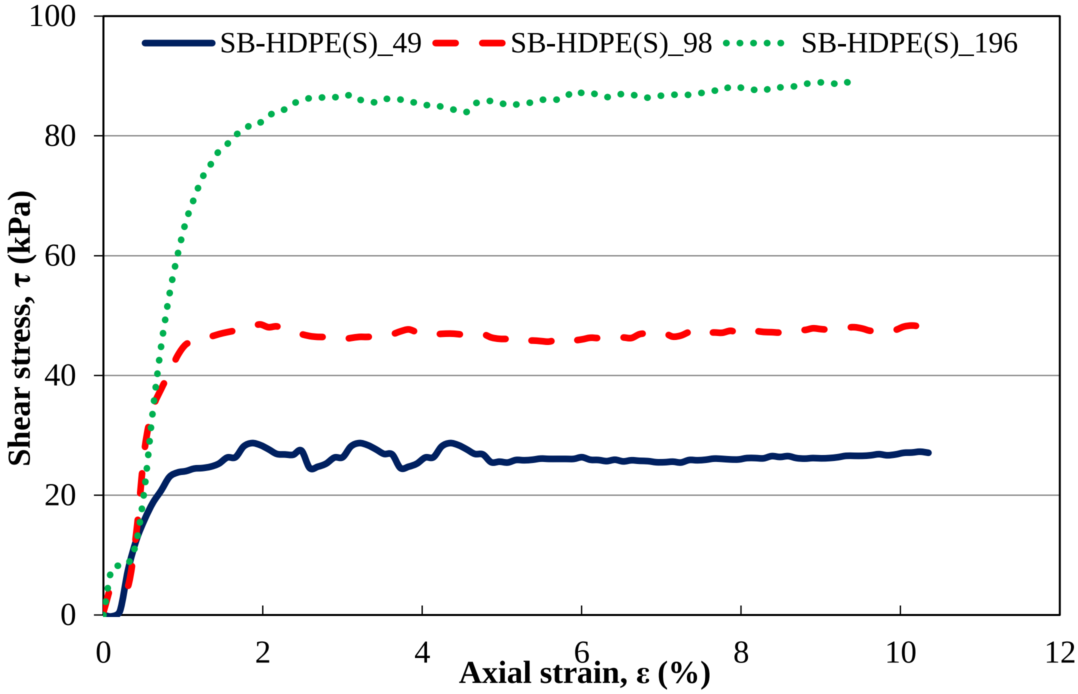

Figure A. 130: Shear stress (τ) – strain (ε) graphs of 16 months AMD cured HDPE(S) – SB interface

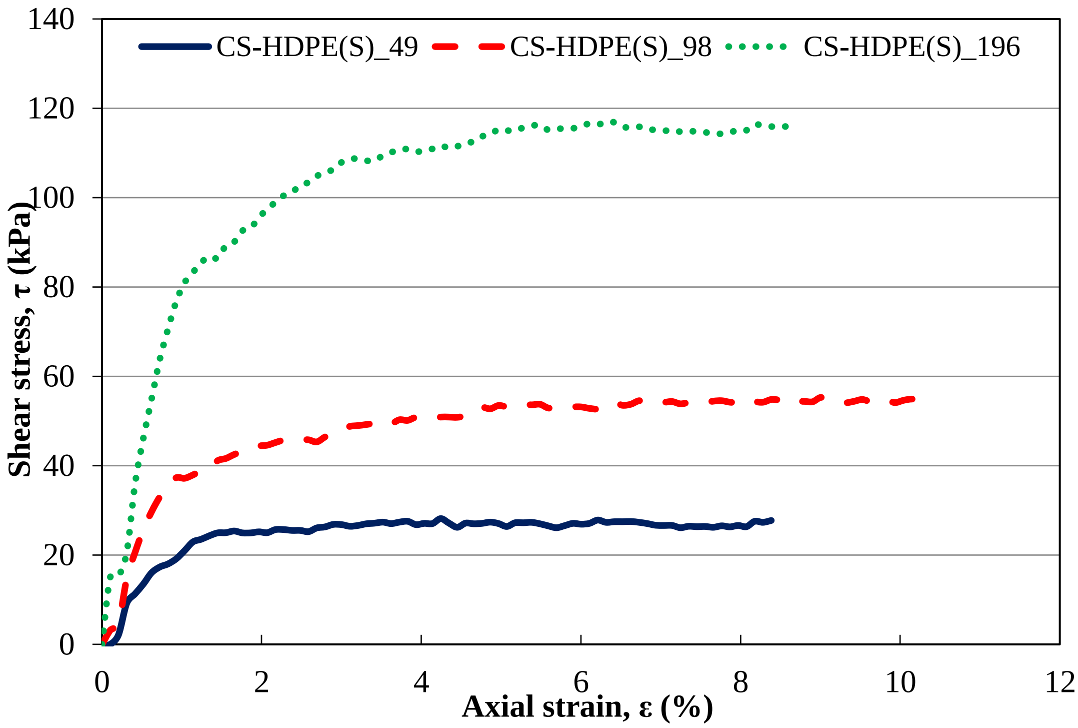

Figure A. 131: Shear stress (τ) – strain (ε) graphs of 16 months AMD cured HDPE(S) – CS interface

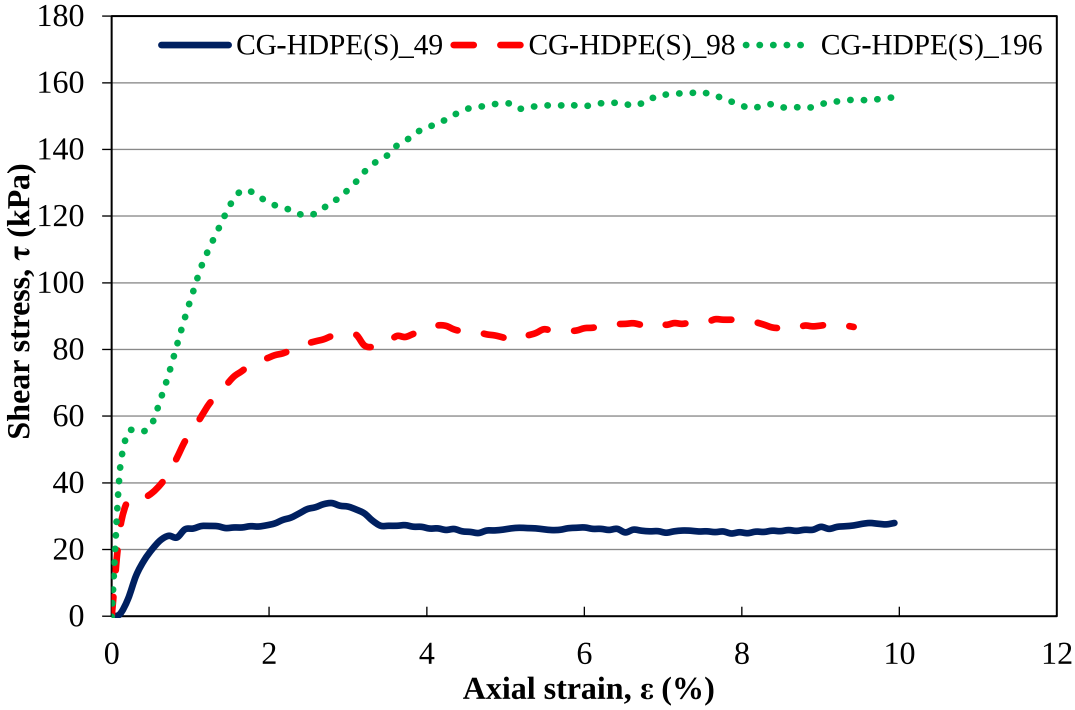

Figure A. 132: Shear stress (τ) – strain (ε) graphs of 16 months AMD cured HDPE(S) – CG interface

HDPE(T) – soil interfaces

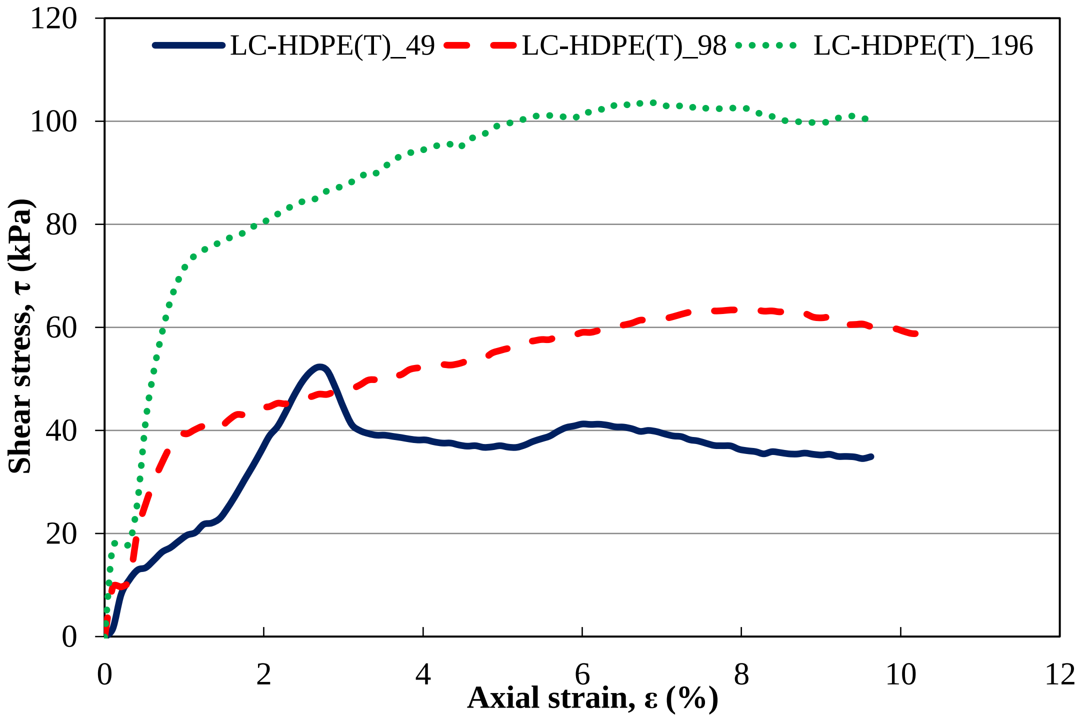

Figure A. 133: Shear stress (τ) – strain (ε) graphs of 16 months AMD cured HDPE(T) – LC interface

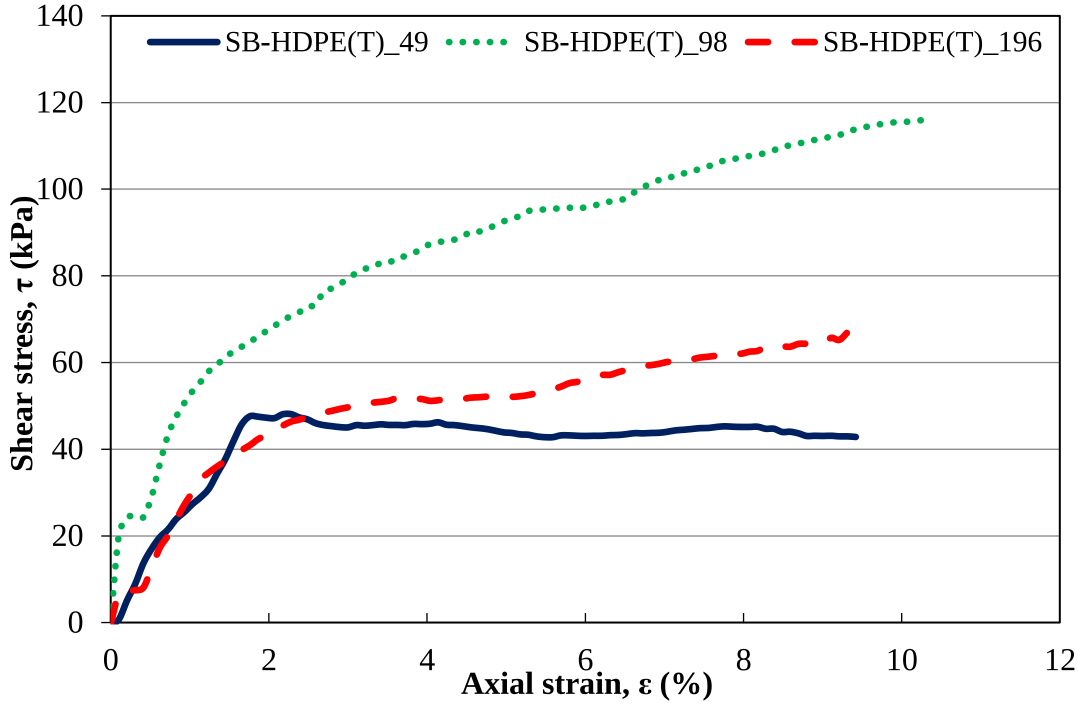

Figure A. 134: Shear stress (τ) – strain (ε) graphs of 16 months AMD cured HDPE(T) – SB interface

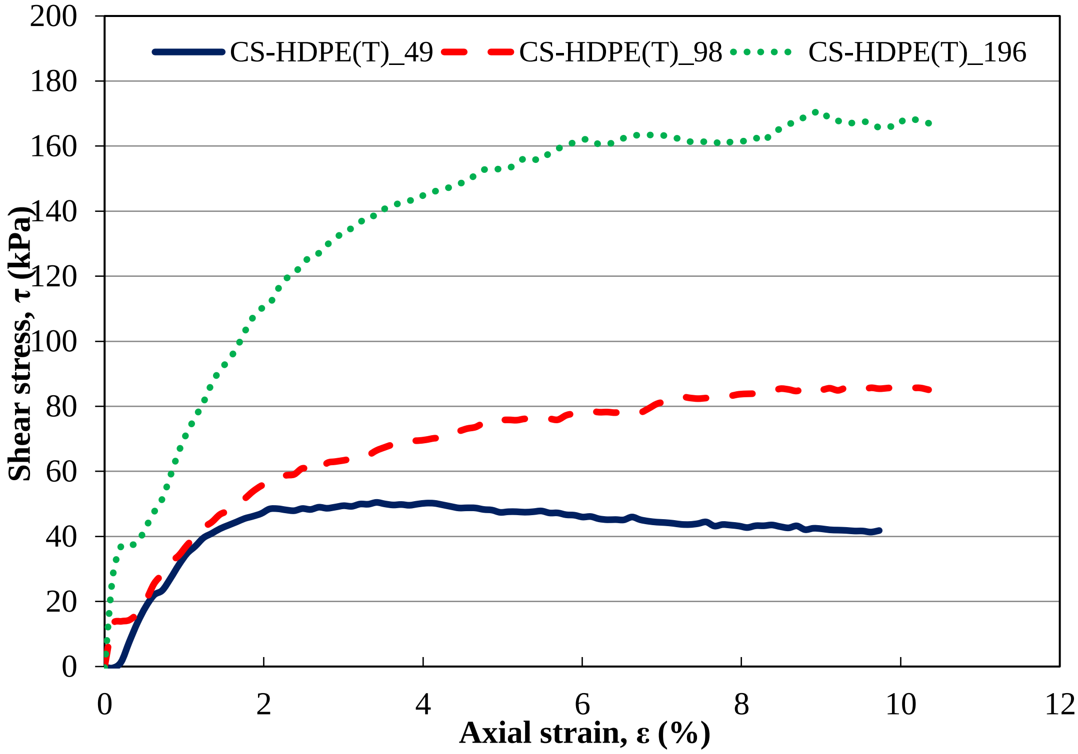

Figure A. 135: Shear stress (τ) – strain (ε) graphs of 16 months AMD cured HDPE(T) – CS interface

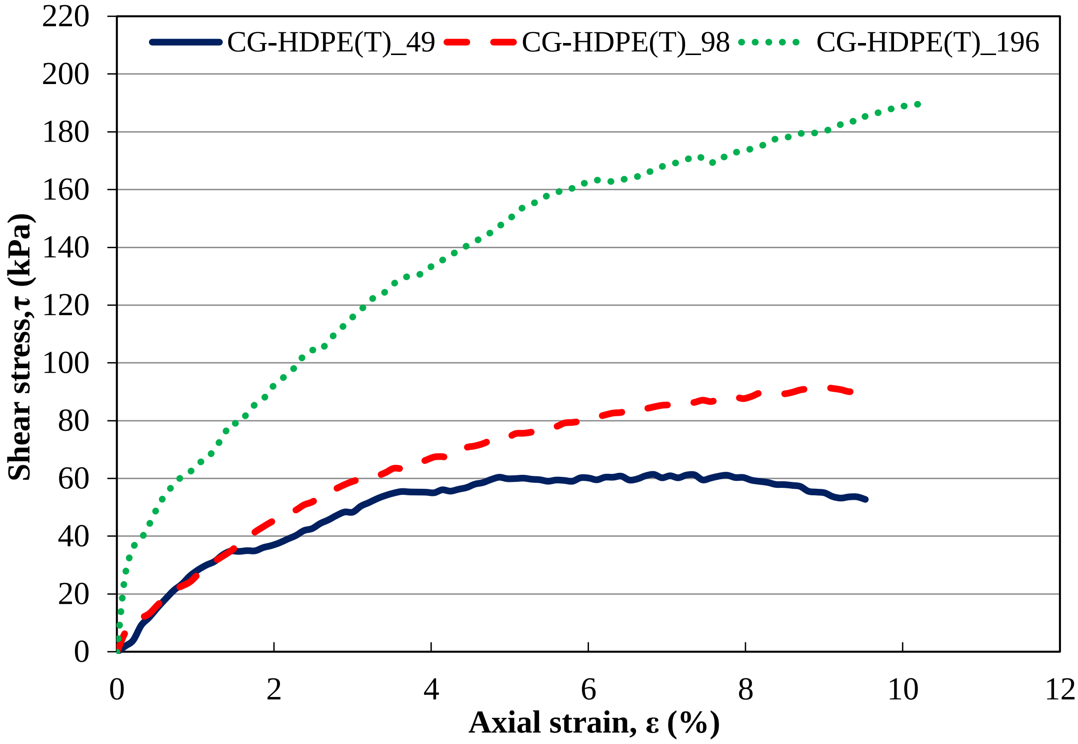

Figure A. 136: Shear stress (τ) – strain (ε) graphs of 16 months AMD cured HDPE(T) – CG interface

TPO – soil interfaces

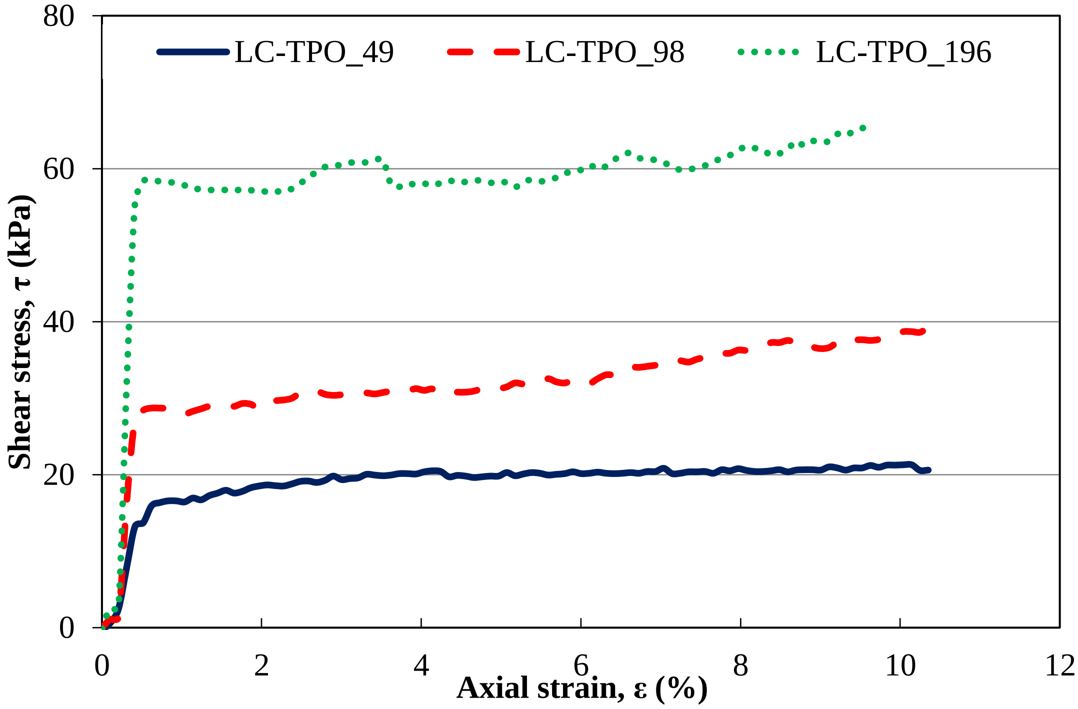

Figure A. 137: Shear stress (τ) – strain (ε) graphs of 16 months AMD cured TPO – LC interface

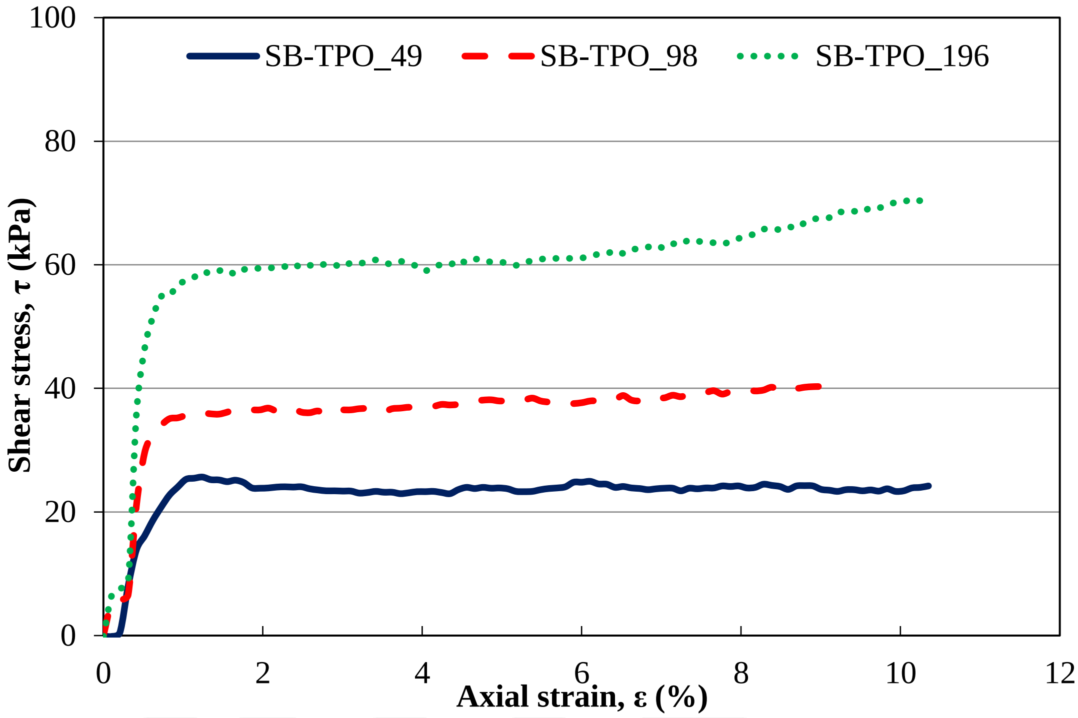

Figure A. 138: Shear stress (τ) – strain (ε) graphs of 16 months AMD cured TPO – SB interface

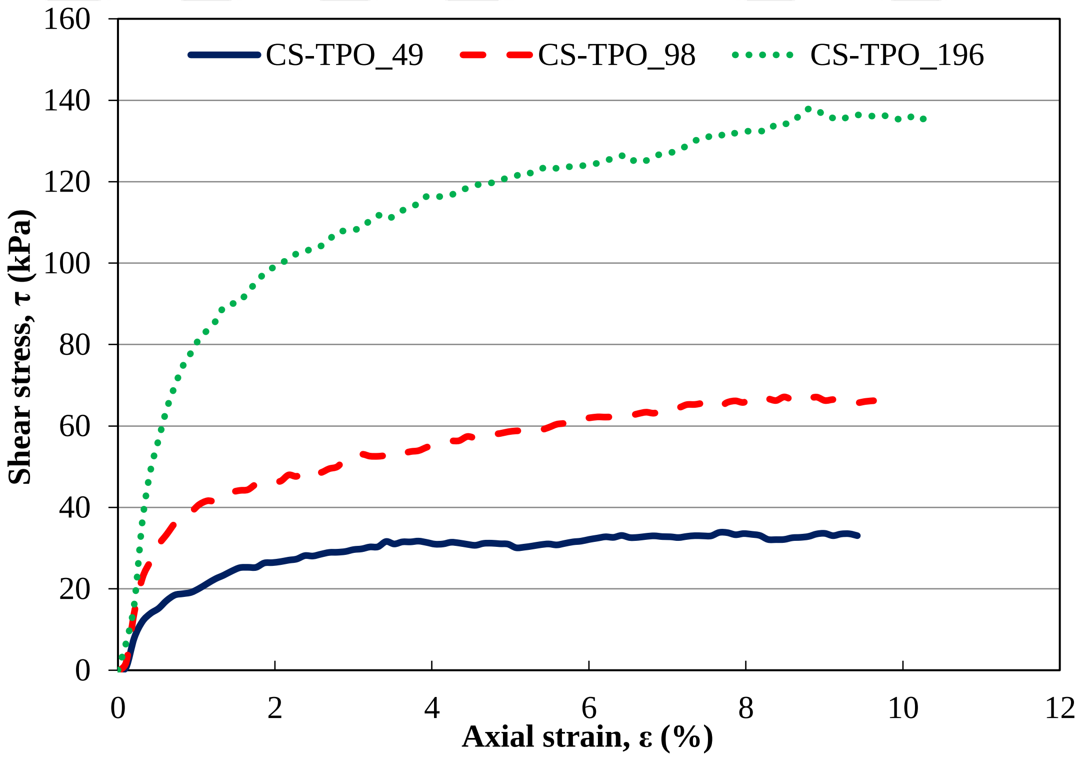

Figure A. 139: Shear stress (τ) – strain (ε) graphs of 16 months AMD cured TPO – CS interface

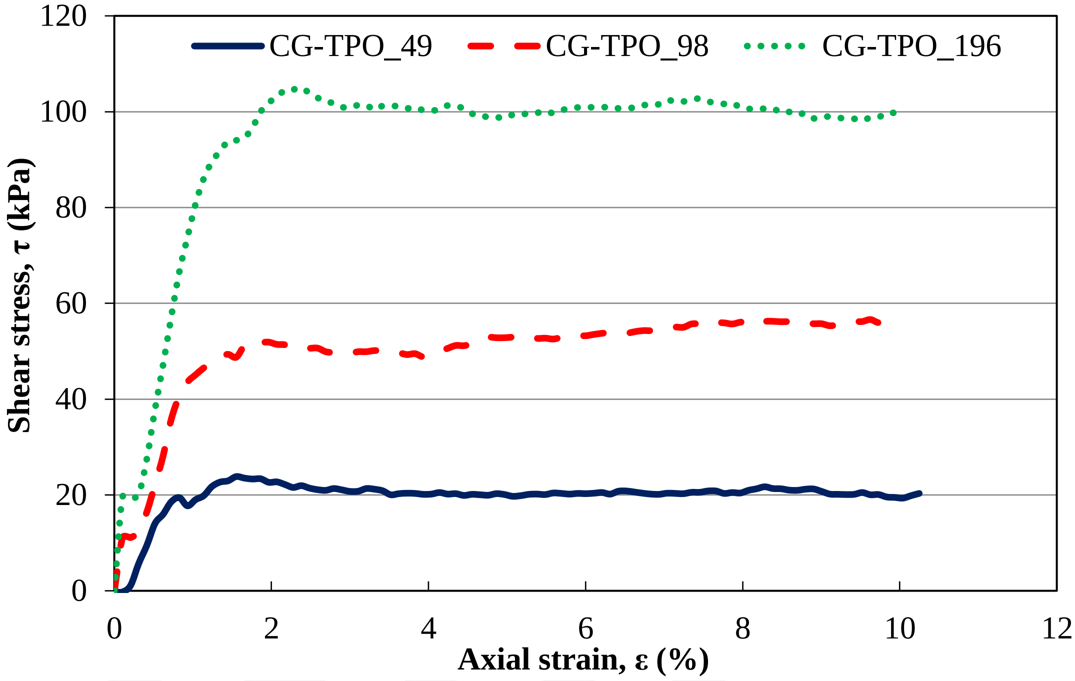

Figure A. 140: Shear stress (τ) – strain (ε) graphs of 16 months AMD cured TPO – CG interface

Interface Direct Shear Test Results for 16 Months CCP Curing

HDPE(S) – soil interfaces

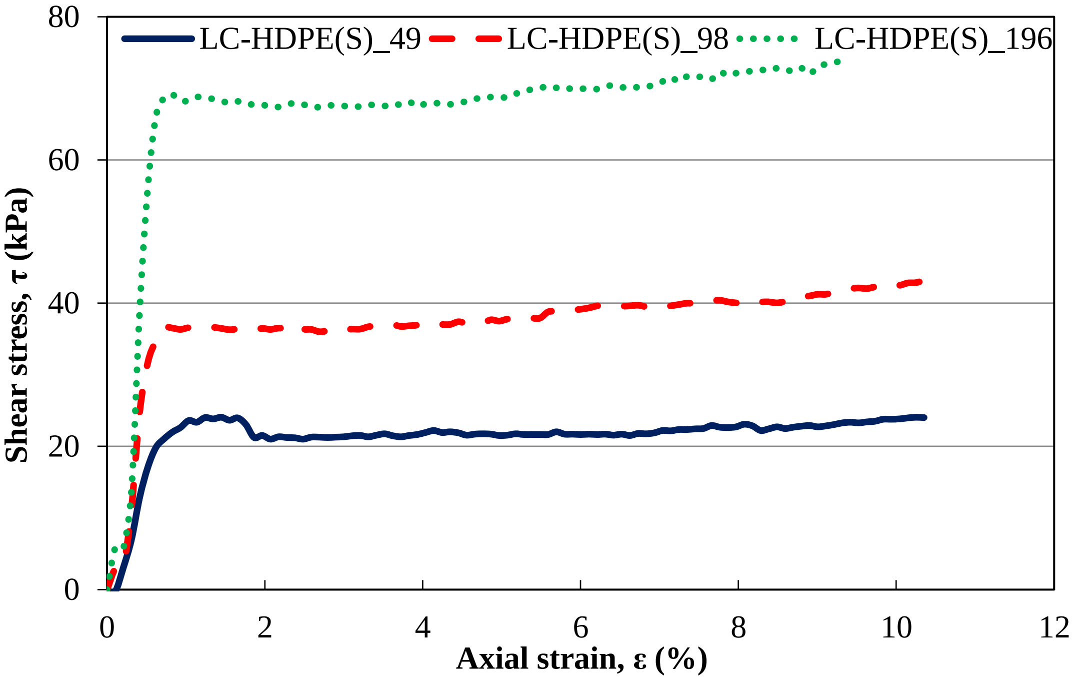

Figure A. 141: Shear stress (τ) – strain (ε) graphs of 16 months CCP cured HDPE(S) – LC interface

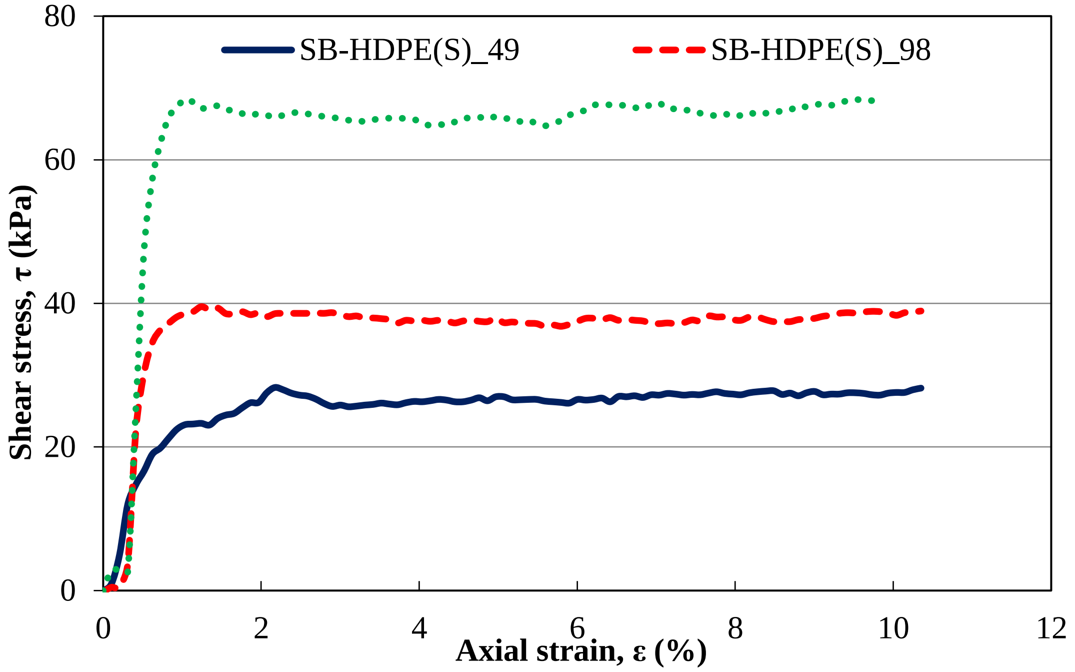

Figure A. 142: Shear stress (τ) – strain (ε) graphs of 16 months CCP cured HDPE(S) – SB interface

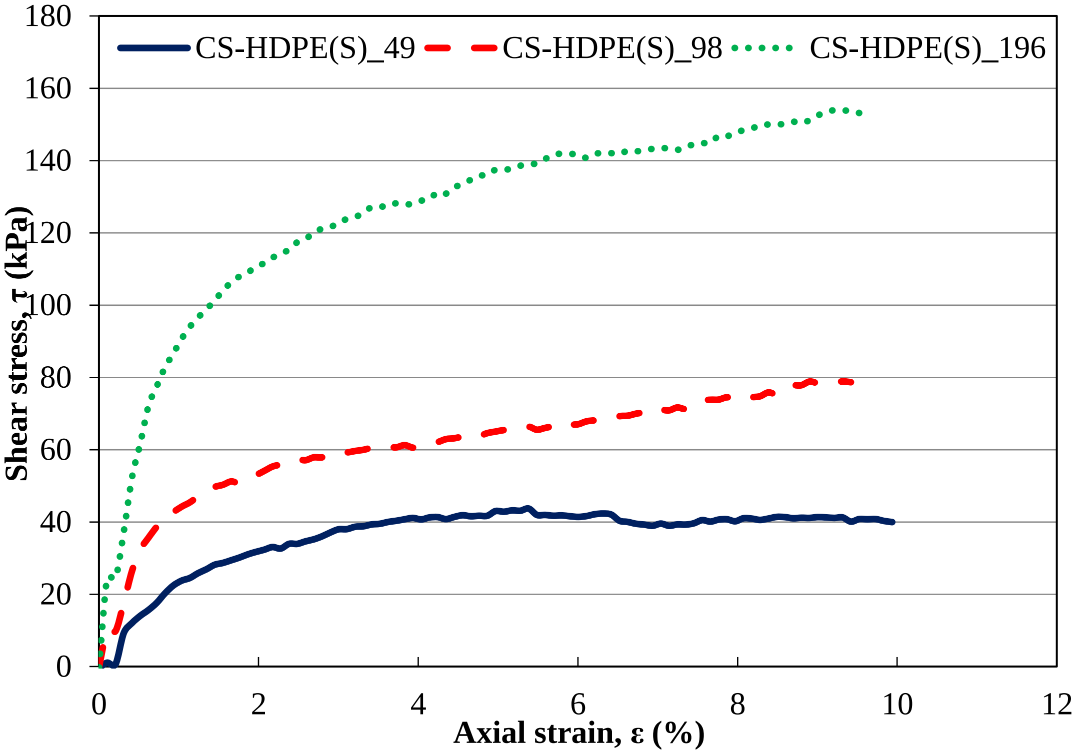

Figure A. 143: Shear stress (τ) – strain (ε) graphs of 16 months CCP cured HDPE(S) – CS interface

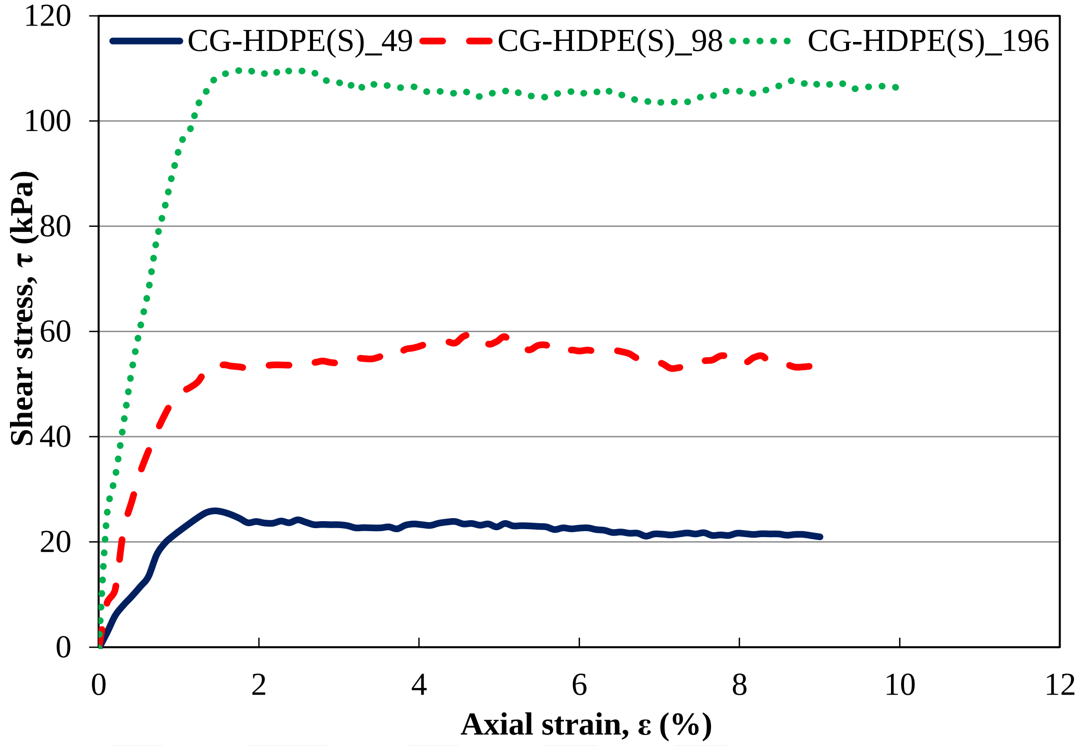

Figure A. 144: Shear stress (τ) – strain (ε) graphs of 16 months CCP cured HDPE(S) – CG interface

HDPE(T) – soil interfaces

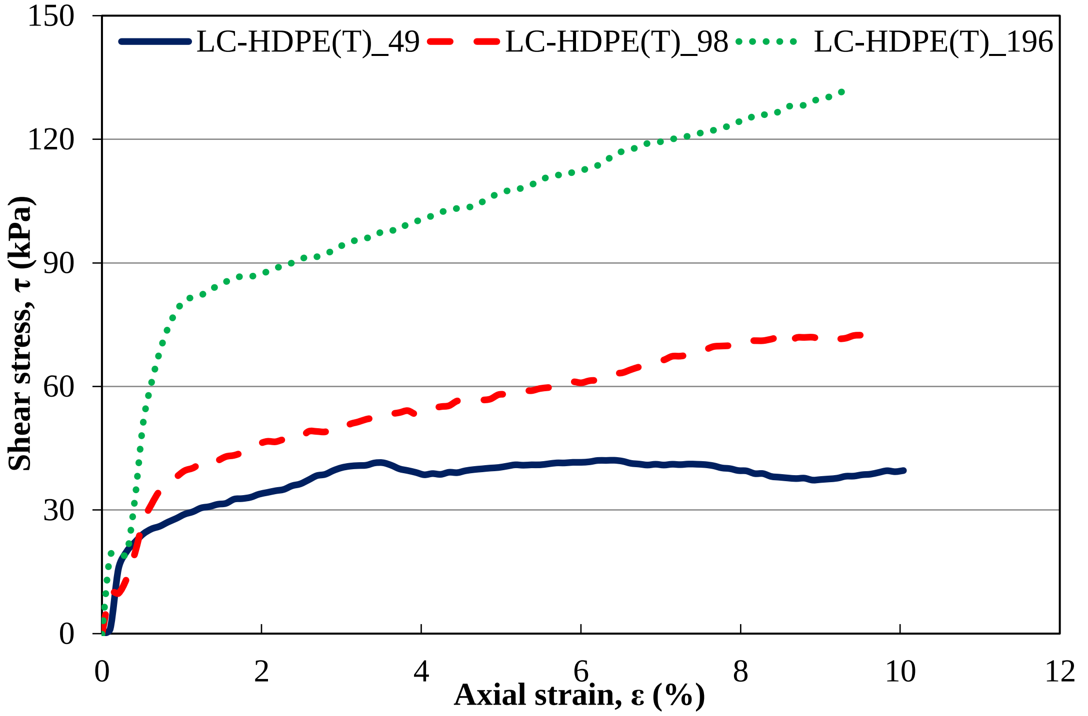

Figure A. 145: Shear stress (τ) – strain (ε) graphs of 16 months CCP cured HDPE(T) – LC interface

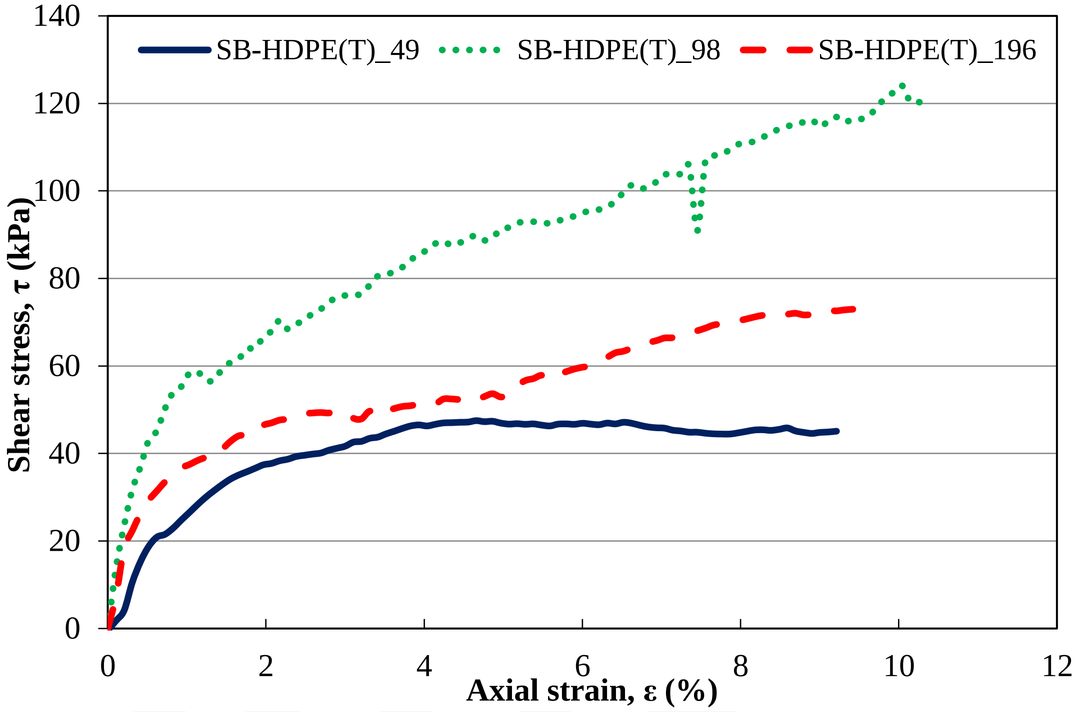

Figure A. 146: Shear stress (τ) – strain (ε) graphs of 16 months CCP cured HDPE(T) – SB interface

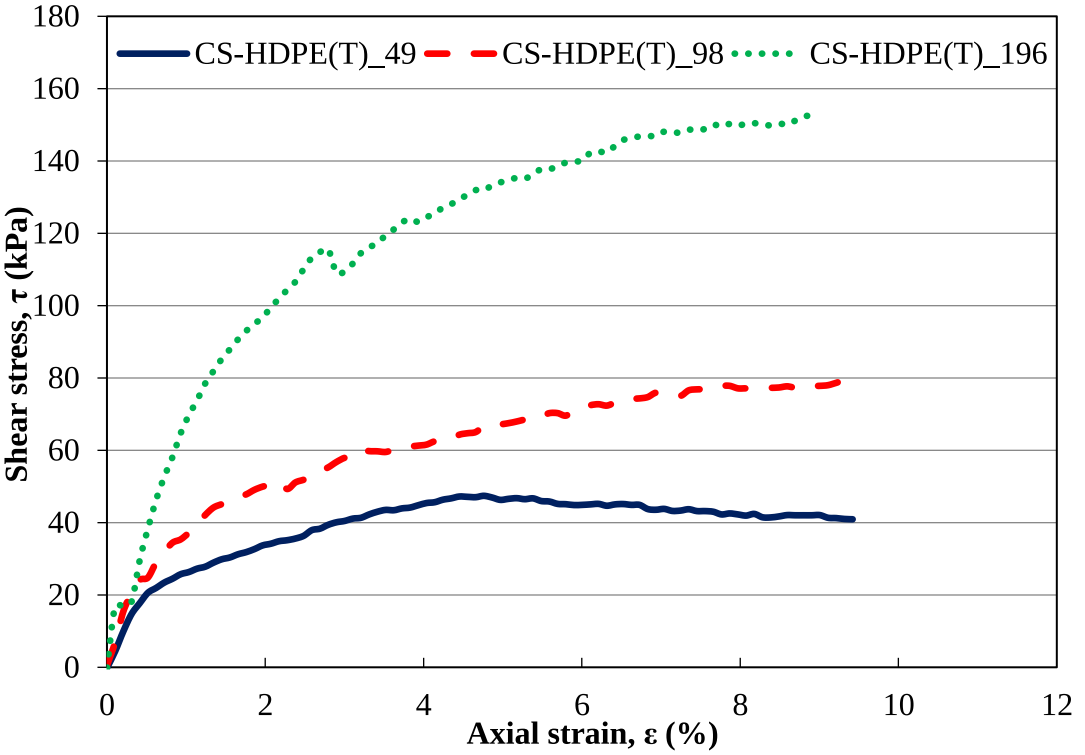

Figure A. 147: Shear stress (τ) – strain (ε) graphs of 16 months CCP cured HDPE(T) – CS interface

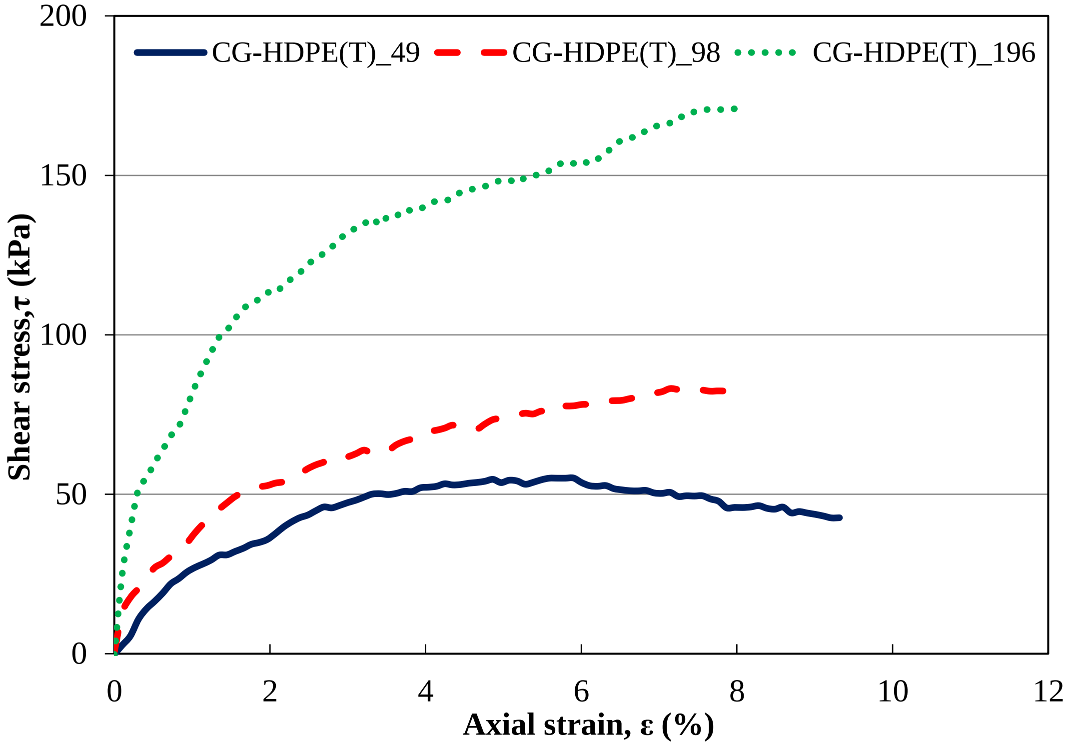

Figure A. 148: Shear stress (τ) – strain (ε) graphs of 16 months CCP cured HDPE(T) – CG interface

TPO – soil interfaces

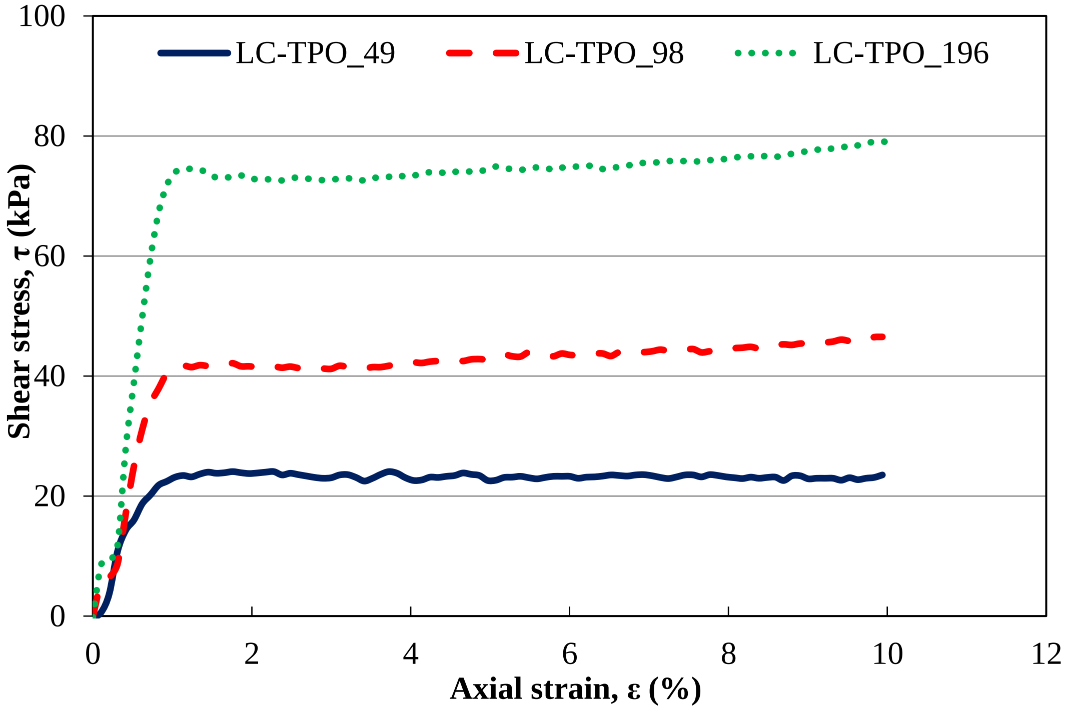

Figure A. 149: Shear stress (τ) – strain (ε) graphs of 16 months CCP cured TPO – LC interface

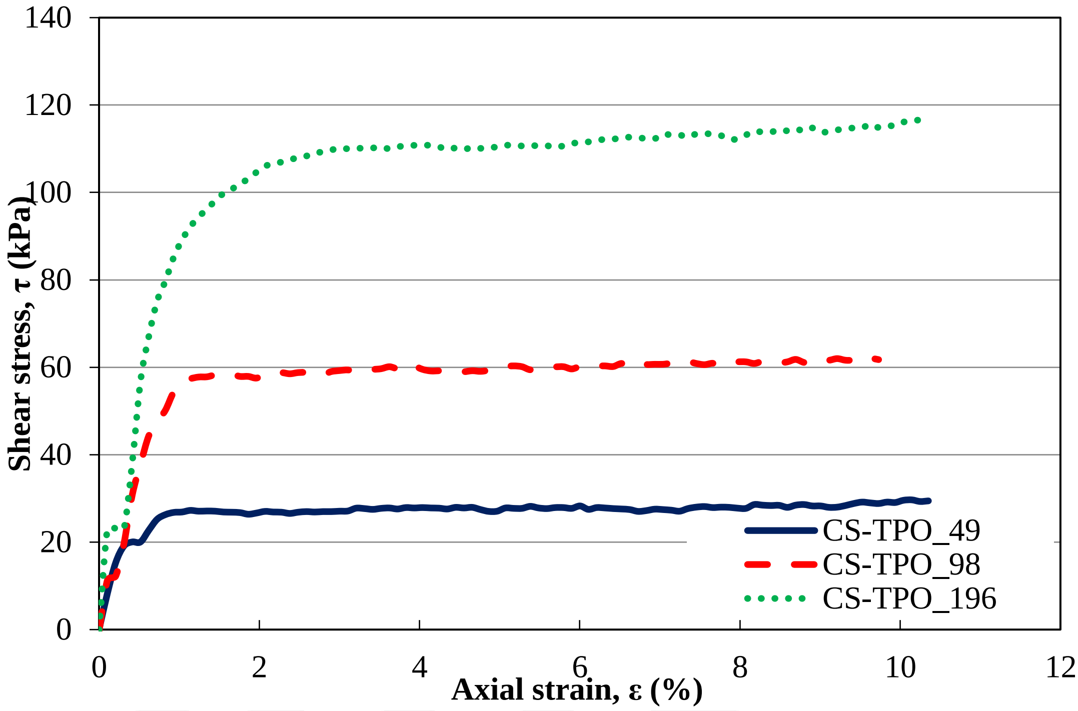

Figure A. 150: Shear stress (τ) – strain (ε) graphs of 16 months CCP cured TPO – CS interface

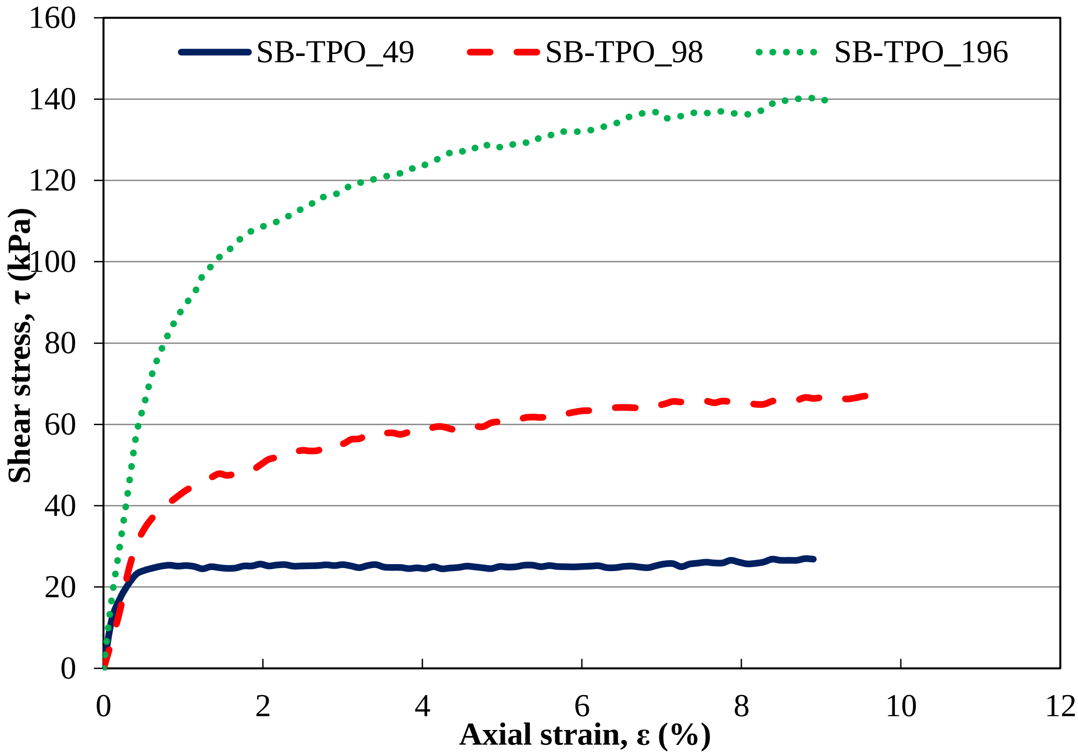

Figure A. 151: Shear stress (τ) – strain (ε) graphs of 16 months CCP cured TPO – SB interface

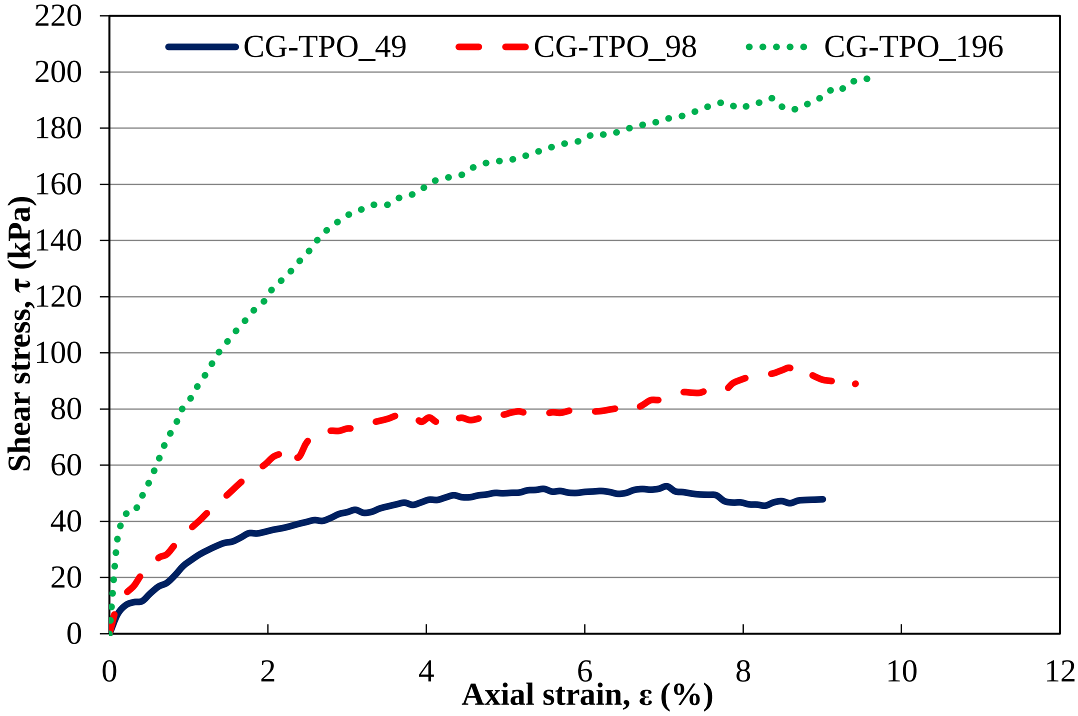

Figure A. 152: Shear stress (τ) – strain (ε) graphs of 16 months CCP cured TPO – CG interface

Interface Direct Shear Test Results for 16 Months MSW Curing

HDPE(S) – soil interfaces

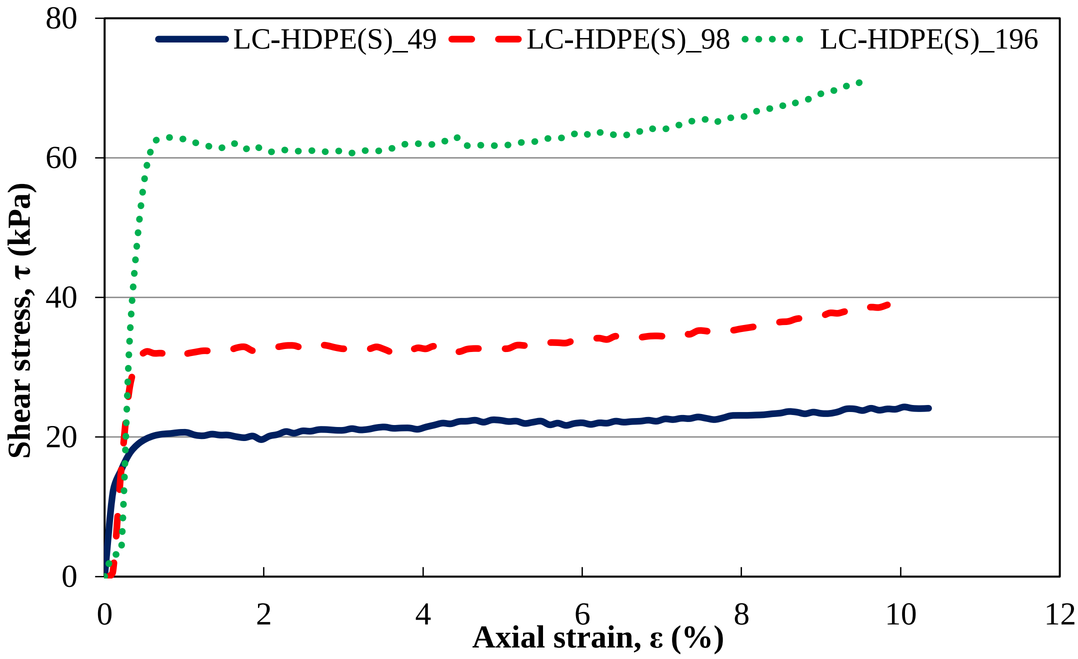

Figure A. 153: Shear stress (τ) – strain (ε) graphs of 16 months MSW cured HDPE(S) – LC interface

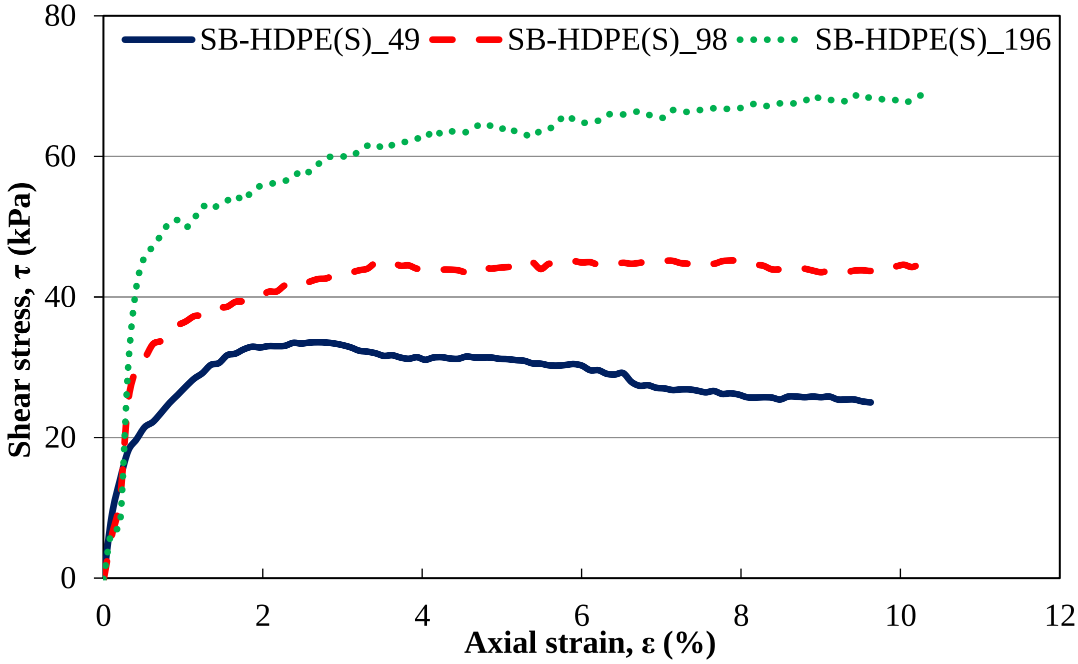

Figure A. 154: Shear stress (τ) – strain (ε) graphs of 16 months MSW cured HDPE(S) – SB interface

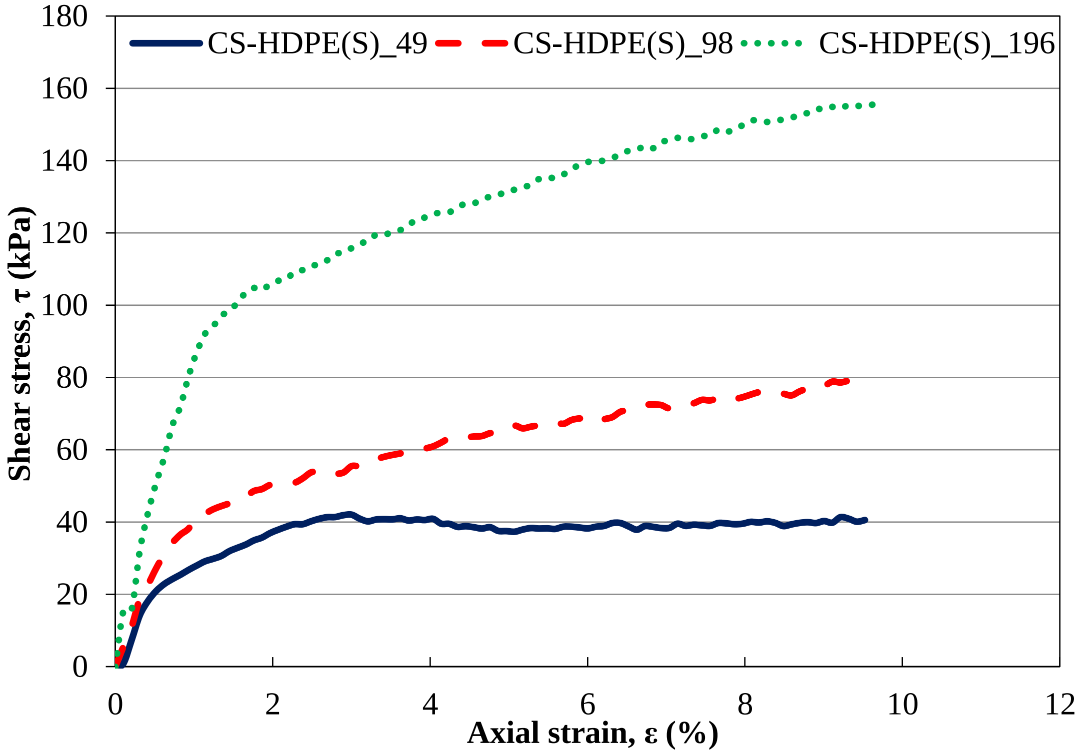

Figure A. 155 : Shear stress (τ) – strain (ε) graphs of 16 months MSW cured HDPE(S) – CS interface

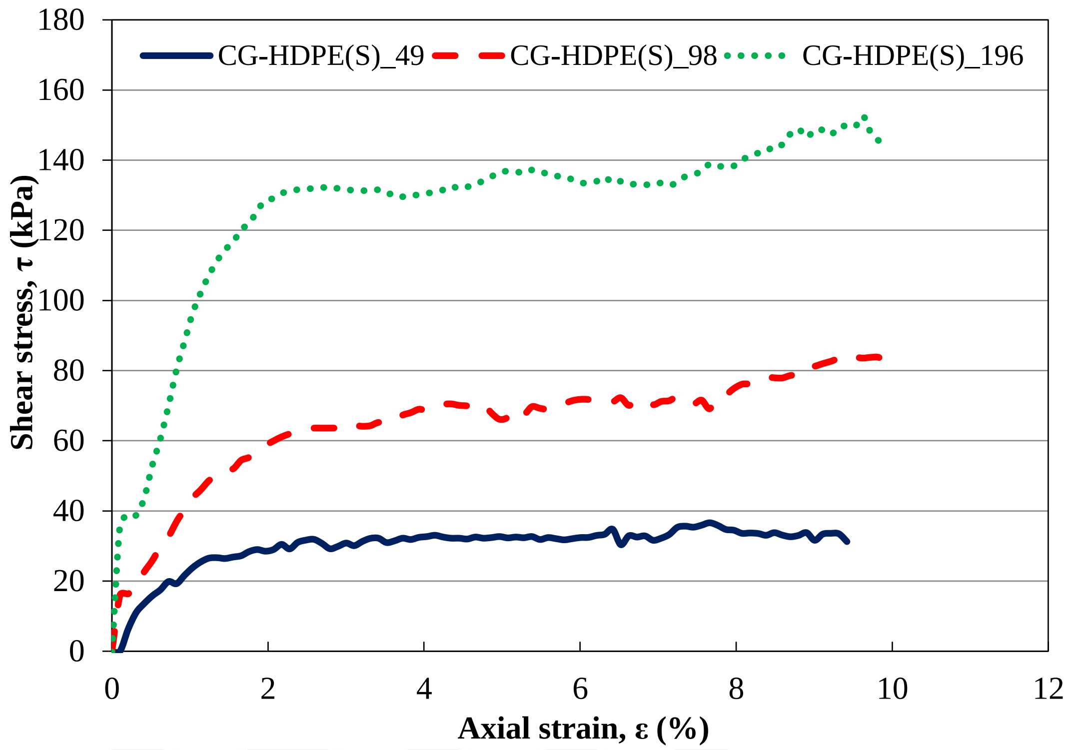

Figure A. 156: Shear stress (τ) – strain (ε) graphs of 16 months MSW cured HDPE(S) – CG interface

HDPE(T) – soil interfaces

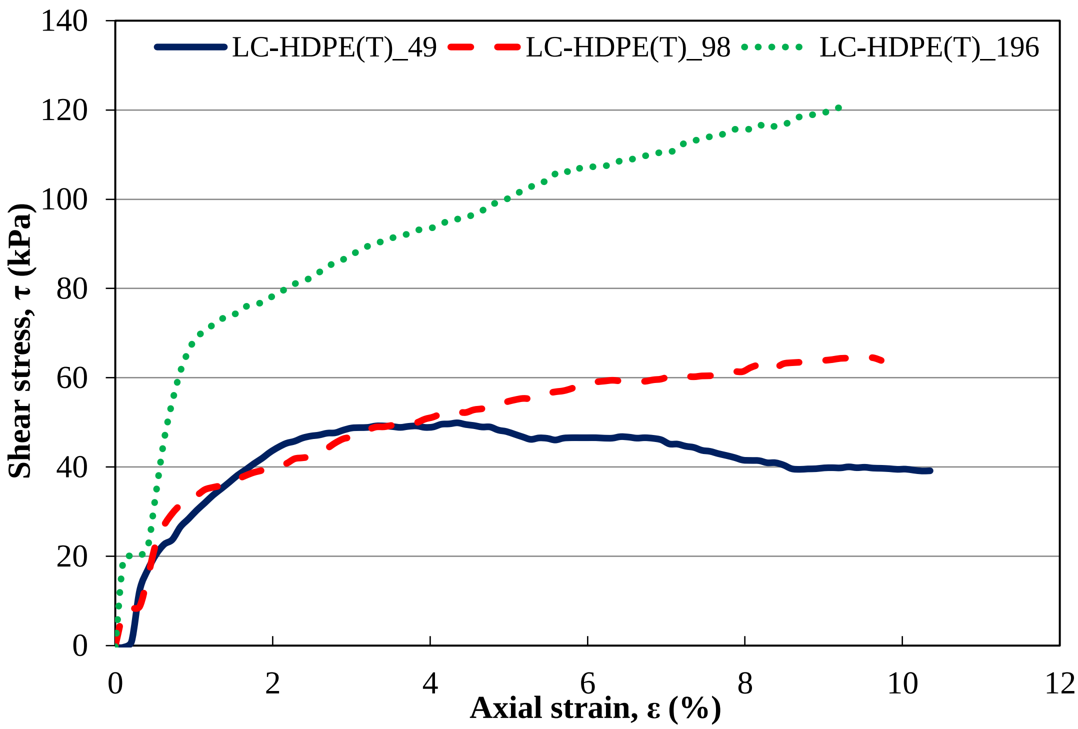

Figure A. 157 : Shear stress (τ) – strain (ε) graphs of 16 months MSW cured HDPE(T) – LC interface

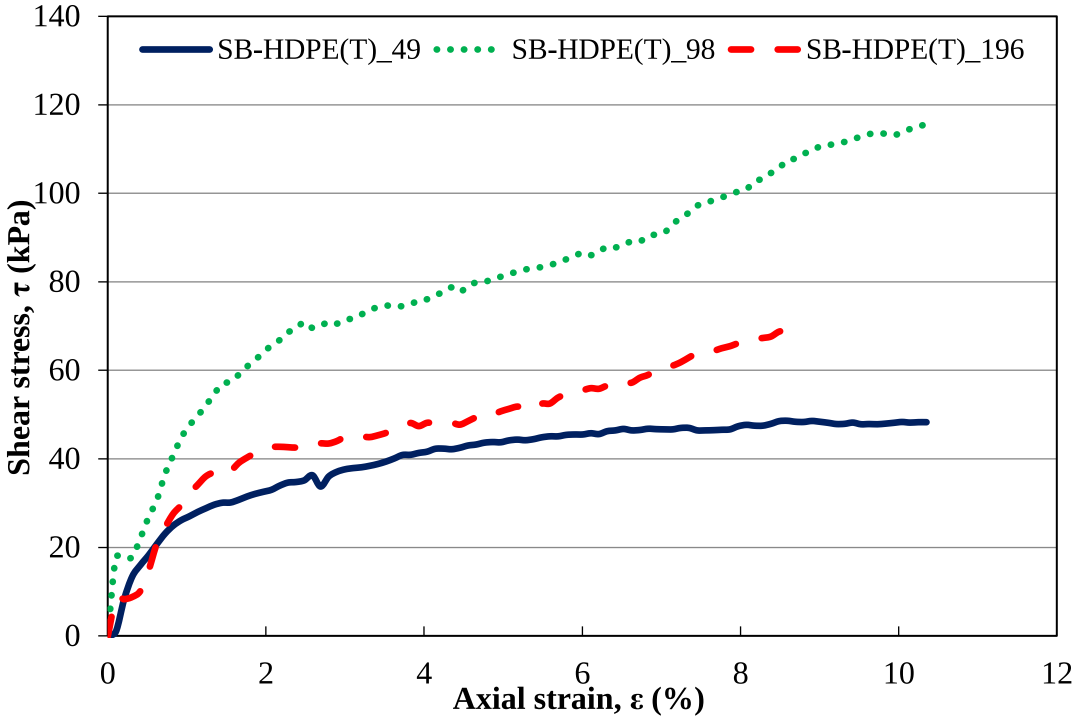

Figure A. 158: Shear stress (τ) – strain (ε) graphs of 16 months MSW cured HDPE(T) – SB interface

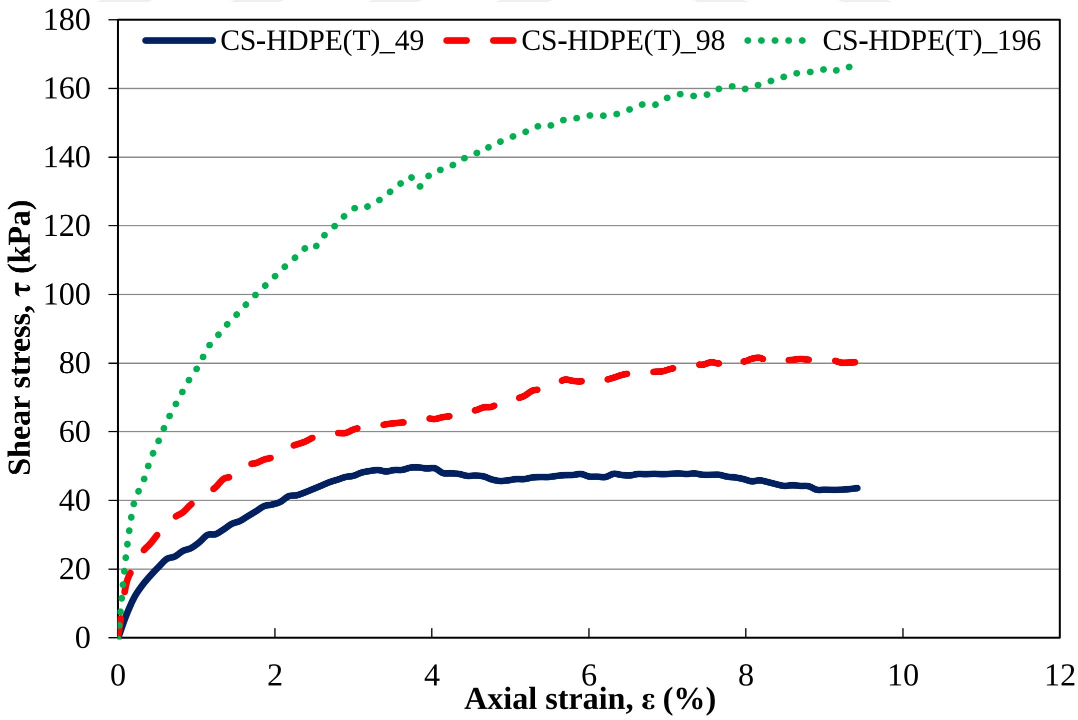

Figure A. 159: Shear stress (τ) – strain (ε) graphs of 16 months MSW cured HDPE(T) – CS interface

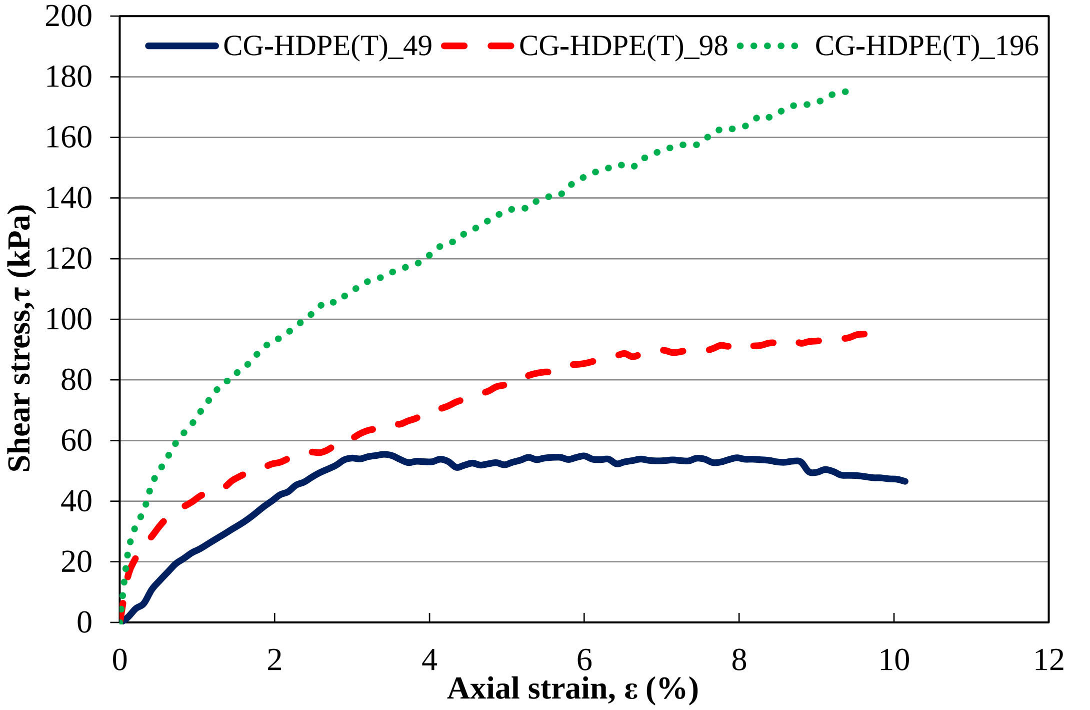

Figure A. 160: Figure A. 161: Shear stress (τ) – strain (ε) graphs of 16 months MSW cured HDPE(T) – CS interface

TPO – soil interfaces

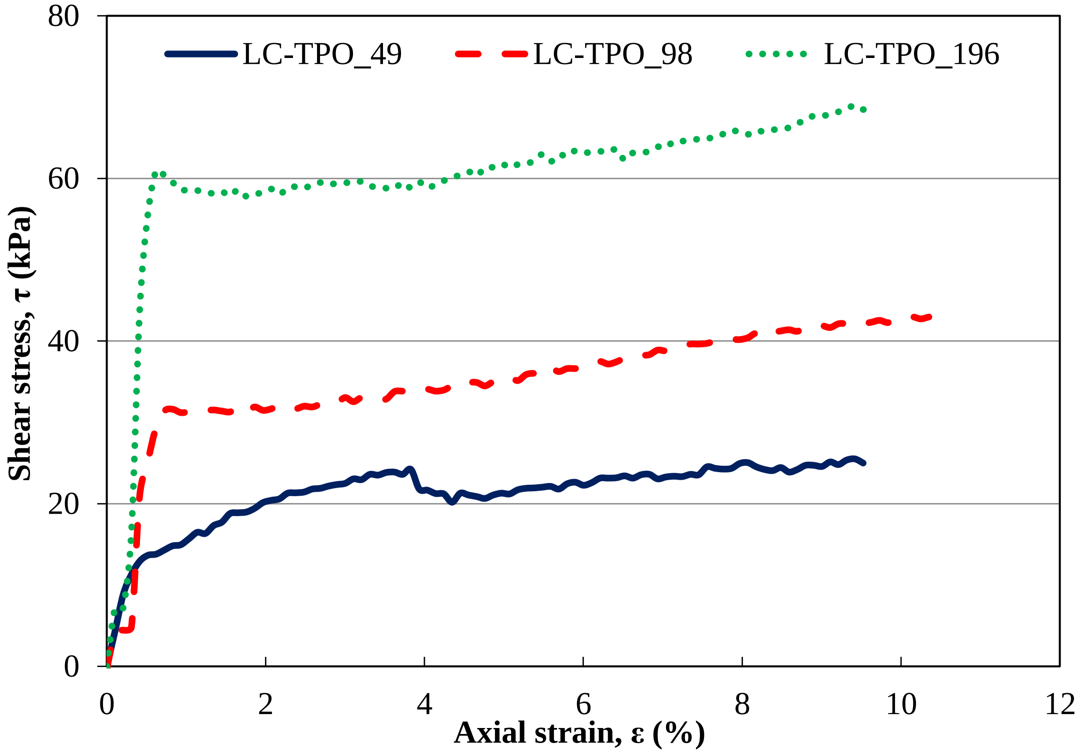

Figure A. 162: Shear stress (τ) – strain (ε) graphs of 16 months MSW cured TPO – LC interface

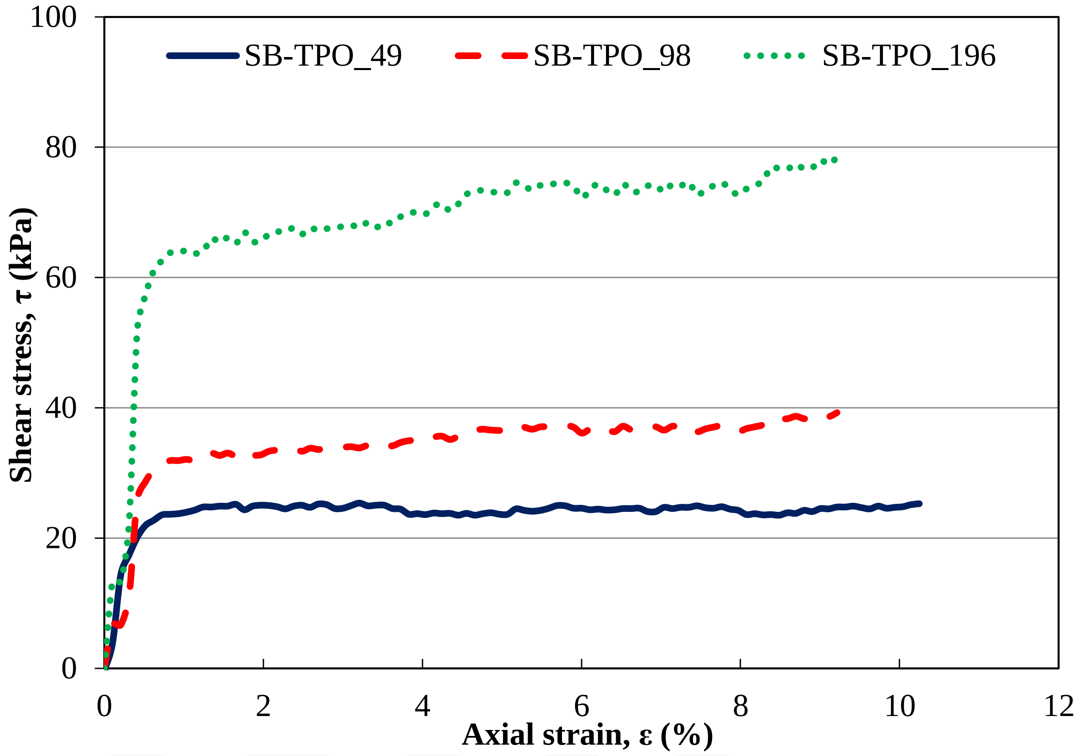

Figure A. 163: Shear stress (τ) – strain (ε) graphs of 16 months MSW cured TPO – SB interface

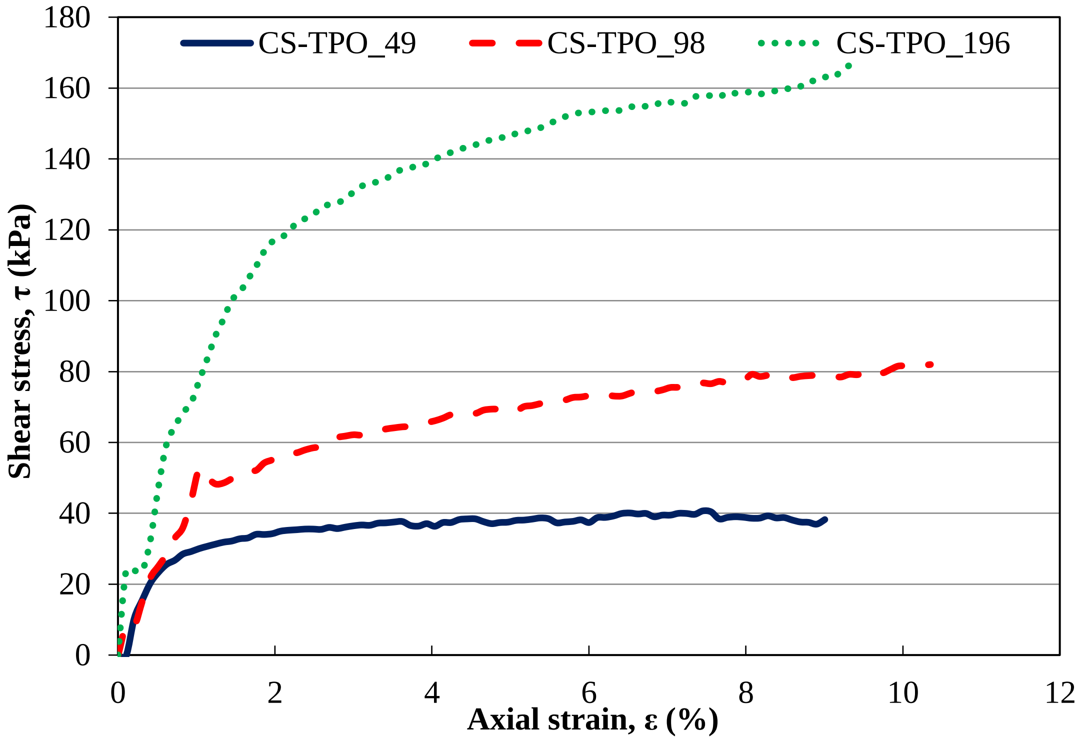

Figure A. 164: Shear stress (τ) – strain (ε) graphs of 16 months MSW cured TPO – CS interface

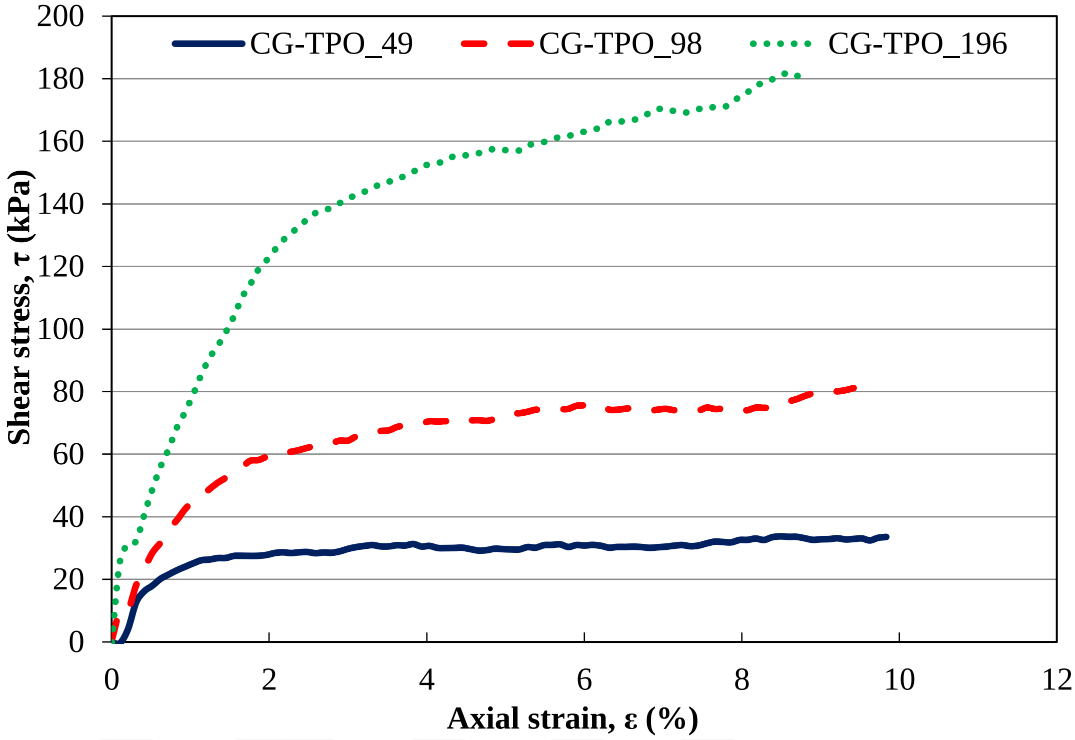

Figure A. 165: Shear stress (τ) – strain (ε) graphs of 16 months MSW cured TPO – CG interface

Appendix B

Publications from the Thesis

Conference Papers

1. Develioglu I., Pulat H.F. “Evaluation of Interface Shear Behavior Between Soil and PVC Geomembrane with Large Scale Direct Shear Test, 7^{th} Euroasia Congress on Scientific Researches and Recent Trends, 6-9 December 2020, Baku, AZERBAIJAN (Oral Presentation).

2. Develioglu I., Pulat H.F. “Zemin ve PVC geomembran arasındaki arayüzey kayma davranışının büyük ölçekli direk kesme deneyleri ile belirlenmesi”, 1^{st} International Congress on Engineering Science and Multidisciplinary Approaches, 23-24 February 2021, Istanbul, TURKIYE (Oral Presentation).

3. Develioglu I., Pulat H.F. “Determination of Interface Shear Behavior between Soil and Different Types of Geomembranes”, 14^{th} International Congress on Advances in Civil Engineering, 6-8 September 2021, Istanbul, TURKIYE (Oral Presentation).

4. Develioglu I., Pulat H.F. “Investigation of the Interface Shear Behavior of Geomembranes Used for Sealing in Foundations Under the Influence of Salt Water”, 10^{th} International Congress on Engineering, Architecture and Design, 24-26 December 2022, Istanbul, TURKIYE (Oral Presentation).

5. Develioglu I., Pulat H.F. “Effect of Grain Size, Angularity and Curing on Interfacial Shear Behavior Between Soil and Geomembrane”, 4^{th} International Göbeklitepe Scientific Research Congress, 7-8 October 2022, Sanliurfa, TURKIYE (Oral Presentation).

Journal Articles

1. Develioglu I., Pulat H.F. (2023). "Effects of Pore Fluid and Surface Roughness on Geomembrane-Soil Interface Behavior", Turkish Journal of Civil Engineering, 34(2), pp. 35 – 56. https://doi.org/10.18400/tjce.1224424.

2. Develioglu I., Pulat H.F. (2023). "Tuzlu Su Etkisindeki Geomembranların Ara Yüzey Kayma Davranışlarının İncelenmesi", Afyon Kocatepe Üniversitesi Fen ve Mühendislik Bilimleri Dergisi, 23(2), 448 – 458. https://doi.org/10.35414/akufemubid.1146658.

Projects

1. Zemin-geosentetik arayüzeyinin kayma mukavemeti davranışının belirlenmesi (Coordination Office of Scientific Research Projects through the Research Project 2020-TDR-FEBE-0006).

Curriculum Vitae

Name Surname : İnci Ertam

Education:

2009–2014 Dokuz Eylül University, Dept. of Civil Eng. (B.S.)

2015–2017 İzmir Kâtip Çelebi University, Dept. of Civil Eng. (M.S.)

Work Experience:

2015 – Present İzmir Kâtip Çelebi University, Research Assistant

Publications:

1. Takcı M., Develioglu I., Pulat H.F. (2023). "Laboratory modeling and analysis of slopes of different geometry under the effect of precipitation", Turkish Journal of Engineering, 7(4), pp. 349 – 357.

2. Develioglu I., Pulat H.F. (2023). "Tuzlu Su Etkisindeki Geomembranların Ara Yüzey Kayma Davranışlarının İncelenmesi", Afyon Kocatepe Üniversitesi Fen ve Mühendislik Bilimleri Dergisi.

3. Develioglu I., Pulat H.F. (2023). "Effects of Pore Fluid and Surface Roughness on Geomembrane-Soil Interface Behavior", Turkish Journal of Civil Engineering, 34(2), pp. 35 – 56. https://doi.org/10.18400/tjce.1224424.

4. Malikzada A., Arslan E., Develioglu I., Pulat H.F. (2022). "Determination of strength characteristics of natural and stabilized alluvial subgrades", Arabian Journal of Geoscience, 15(535), pp. 2 – 20. https://doi.org/10.1007/s12517-022-09829-2.

5. Develioglu I., Pulat H.F. (2021). "Shear strength of alluvial soils reinforced with PP fibers", Bulletin of Engineering Geology and the Environment, 80(12), pp. 9237 – 9248. https://doi.org/10.1007/s10064-021-02474-1.

6. Arslan E., Duzen I., Develioglu I., Pulat H.F. (2020). "Undrained shear strength of polypropylene fiber reinforced alluvial clay", Environmental Research and Technology, 4(3), pp. 219 – 229. https://doi.org/10.35208/ert.903408.

7. Develioglu I., Pulat H.F. (2020). "Experimental evaluation of compressibility parameters of lime and silica fume stabilized dredged soil", Environmental Research and Technology, 3(4), pp. 157 – 165. https://doi.org/10.35208/ert.782042.

8. Develioglu I., Pulat H.F. (2019). "Compressibility behaviour of natural and stabilized dredged soils in different organic matter contents", Construction and Building Materials, 228. https://doi.org/10.1016/j.conbuildmat.2019.116787.

9. Develioglu I., Pulat H.F. (2019). "Improvement of shear strength characteristics of İzmir Bay's dredged soil", Arabian Journal of Geoscience, 12(632), pp. 1 – 12. https://doi.org/10.1007/s12517-019-4825-y.

10. Pulat H.F., Develioglu I., Rassul A.Y. (2018). "Examination of Factors Affecting the Shear Strength of Granulated Blast Furnace Slag", Celal Bayar Üniversitesi Fen Bilimleri Dergisi, 14(3), pp. 291 – 295. https://doi.org/10.18466/cbayarfbe.423763.

11. Develioglu I., Pulat H.F. (2018). "Geotechnical characterization and bearing capacity performance of blast furnace slag", Građevinar, 70, pp. 571 – 579. https://doi.org/10.14256/JCE.2080.2017.

12. Semerci, B., Develioglu I., Pulat H.F. (2018). "Geotechnical Characterization of Alluvial Soil in Çiğli-Balatçık Region", Eurasian Journal of Civil Engineering and Architecture, 2(2), pp. 44 – 50.

13. Develioglu I., Pulat H.F. (2018). "Yüksek fırın cürufunun geoteknik özellikleri ve taşıma kapasitesi performansının incelenmesi", Pamukkale Üniversitesi Mühendislik Bilimleri Dergisi, 24(3), pp. 433 – 438. https://doi.org/10.5505/pajes.2017.82574.

14. Develioglu I., Pulat H.F. (2017). "Geotechnical Properties and Compressibility Behavior of Organic Dredged Soils", World Academy of Science, Engineering and Technology International Journal of Geotechnical and Geological Engineering, 11(2), pp. 204 – 208.